PNL-10359, VOL. 1
UC-721
2020

PROPERTY/COMPOSITION RELATIONSHIPS FOR HANFORD HIGH-LEVEL WASTE GLASSES MELTING AT 1150°C

Volume 1: Chapters 1 - 11

Principal Investigators and Authors
P. R. Hrma
G. F. Piepel

Other Significant Contributors and Authors
M. J. Schweiger
D. E. Smith
D.-S. Kim
P. E. Redgate
J. D. Vienna
C. A. LoPresti
D. B. Simpson
D. K. Peeler
M. H. Langowski

December 1994

Prepared for
the U.S. Department of Energy
under Contract DE-AC06-76RLO 1830

Pacific Northwest Laboratory
Richland, Washington 99352

DISCLAIMER

DISCLAIMER

Portions of this document may be illegible in electronic image products. Images are produced from the best available original document.

ABSTRACT

A Composition Variation Study (CVS) is being performed within the Pacific Northwest Laboratory[a] Vitrification Technology Development (PVTD) project in support of a future high-level nuclear waste vitrification plant at the Hanford site in Washington. From 1989 to 1994, over 120 nonradioactive glasses were melted and properties measured in five statistically-designed experimental phases. Glass composition is represented by the 10 components SiO_2, B_2O_3, Al_2O_3, Fe_2O_3, ZrO_2, Na_2O, Li_2O, CaO, MgO, and Others (all remaining components). The properties measured include viscosity (η), electrical conductivity (ϵ), glass transition temperature (T_g), thermal expansion of solid glass (α_s) and molten glass (α_m), crystallinity (quenched and canister centerline cooled glasses), liquidus temperature (T_L), durability based on normalized elemental releases from the Materials Characterization Center-1 28-day dissolution test (MCC-1, r_{Mi}) and the 7-day Product Consistency Test (PCT, r_{Pi}), and solution pHs from MCC-1 and PCT. Amorphous phase separation was also evaluated.

Empirical first- and second-order mixture models were fit using the CVS data to relate the various properties to glass composition. Equations for calculating the uncertainty associated with property values predicted by the models were also developed. The models were validated using both internal and external data. Other modeling approaches (e.g., non-bridging oxygen, free energy of hydration, phase-equilibria T_L) were investigated for specific properties. A preliminary Qualified Composition Region was developed to identify glass compositions with high confidence of being processable in a melter and meeting waste form acceptance criteria.

Models expressed in mass and mole fractions of the 10 components have similar goodness of fit (R^2) values. First- and second-order models fit the CVS data for: η and ϵ from 950 to 1250°C with R^2 from 0.93 to 0.98; T_g with R^2 from 0.88 to 0.97; α_s with R^2 from 0.87 to 0.93; α_m with R^2 from 0.43 to 0.75; r_{Pi} with R^2 from 0.73 to 0.92; r_{Mi} with R^2 from 0.60 to 0.83; T_L with

---

(a) Pacific Northwest Laboratory is operated by Battelle Memorial Institute for the U.S. Department of Energy under Contract DE-AC06-76RLO 1830.

R^2 = 0.90 for clinopyroxene, R^2 = 0.64 for spinel, and R^2 = 0.79 for Zr-containing crystals. The other modeling approaches investigated did not fit the CVS data as well as the CVS first- and second-order models.

Within the composition range studied: Li_2O and Na_2O decrease η, T_g, T_L, and durability (MCC-1 and PCT), and increase ϵ. SiO_2 increases durability, η, and T_g and decreases ϵ. In addition, Al_2O_3 increases η and durability; ZrO_2 increases η, T_g, durability, and T_L for clinopyroxene and Zr-containing phases; MgO increases T_L and decreases durability; Fe_2O_3 increases T_L for Fe-containing phases; B_2O_3 decreases durability and T_L for spinel and clinopyroxene.

The crystalline phases observed in canister centerline cooled samples of CVS glasses were spinel, clinopyroxene, and Zr-containing phases (zircon, ZrO_2, and Na-Zr silicate), orthopyroxene, nepheline, olivine, $CaSiO_3$, and SiO_2 (cristobalite and quartz). Hematite, Li_2SiO_3, and $LiAlSi_2O_6$ crystallized less frequently. Durability appeared to be decreased by crystallization of nepheline, $LiAlSi_2O_6$, and cristobalite. A method for predicting amorphous phase separation in multicomponent glasses was applied to 123 CVS glasses. Nine glasses were predicted as prone to amorphous phase separation.

The results (both data and models) from the CVS so far constitute an important contribution to vitrification knowledge and technology. However, research and its interpretation will be required as new problems and needs arise.

SUMMARY

A Composition Variation Study (CVS) is being conducted by the Pacific Northwest Laboratory Vitrification Technology Development (PVTD) project to characterize the relationships between glass composition and glass and melt properties. The glass and melt properties measured include: viscosity, electrical conductivity, glass transition temperature, thermal expansion of solid and molten glass, crystallinity (quenched and canister centerline cooled glasses), liquidus temperature, and durability and solution pH based on the Materials Characterization Center-1 (MCC-1) 28-day dissolution test and the 7-day Product Consistency Test (PCT). The main objectives of the CVS are to: 1) prepare glasses within a wide composition region and measure properties of these glasses, 2) develop understanding of glass composition effects on properties, 3) develop models relating the glass and melt properties to composition, 4) develop uncertainty equations for model predictions, and 5) use these models and uncertainty equations to develop a Qualified Composition Region (QCR) that contains, with acceptable confidence, only glasses that are processable and comply with Waste Acceptance Product Specifications (WAPS) requirements (DOE 1993).

The results of the study (data, models, model uncertainty equations, and the QCR) will support feed pretreatment specifications, frit specifications, melter feed makeup activities, formulation of radioactive glasses, and the development of process and product models to be used in performing Waste Form Qualification (WFQ) activities and operating the high-level waste vitrification plant. However, these activities are not within the scope of the CVS. The focus/scope of the CVS is to produce "building block" results that can be applied to these other needs.

Experimental Design

The study was planned and conducted in two major parts (CVS-I and CVS-II) consisting of five experimental and data analysis phases. Each phase was planned and the resulting data analyzed using statistical experimental design and empirical modeling techniques for mixture experiments. Results of previous phases were used in planning subsequent phases.

In CVS-I, a glass composition experimental region was selected for testing based on the results of a previous series of scoping and solubility studies and on projections of glass compositions that might be made from the various waste types[a] to be processed by the high-level waste vitrification plant. The experimental region was chosen to include glasses with acceptable as well as "unacceptable but close-to-acceptable" properties, so as to provide a firm basis for developing property models and the QCR. The experimental region was defined in terms of 10 glass (waste or frit) components: SiO_2, B_2O_3, Al_2O_3, Fe_2O_3, ZrO_2, Na_2O, Li_2O, CaO, MgO, and Others (all remaining waste components). A 23-glass test matrix focusing mainly on the boundary of the experimental region was statistically designed and the resulting glass and melt property data were fitted to first-order mixture models. Although these models had statistically significant lack-of-fits, they fit well enough to ascertain that all 10 components should be retained for study in CVS-II, and to serve in revising the composition experimental region to be studied in CVS-II. A detailed discussion of CVS-I and its results are contained in a report by Piepel, Hrma, et al. (1993).

CVS-II was planned and conducted in four phases, with the strategy of collecting data on glasses on the boundary and the interior of the revised (based on CVS-I results) composition experimental region. CVS-II Phase 1 involved testing 19 glasses in an interior subregion of the revised experimental region. CVS-II Phase 2 involved testing a total of 39 glasses: 20 glasses on the boundary of the revised experimental region, 10 glasses in a subregion of acceptable compositions, two glasses tested in CVS-I and CVS-II Phase 1, two glasses with lower and higher levels of SiO_2, two glasses containing UO_2, and three glasses with Others mixes corresponding to the CC, PFP, and NCRW waste types. All other CVS-II Phase 2 glasses had Others mixes

---

(a) Initial plans were for the high-level waste vitrification plant to vitrify four pretreated double shell tank (DST) waste streams: Neutralized Current Acid Waste (NCAW), Neutralized Cladding Removal Waste (NCRW), Plutonium Finishing Plant (PFP) waste, and Complexant Concentrate (CC) waste. Subsequently, vitrifying single shell tank (SST) wastes was added to the high-level waste vitrification plant mission. At the time CVS-I was planned, most was known about NCAW, so it had the most influence on the design of the study.

corresponding to the NCAW waste type. CVS-II Phase 3 involved testing 43 glasses, including seven with NCAW, NCRW, CC, and PFP waste types and two variations of the Defense Waste Processing Facility (DWPF) Environmental Assessment (EA) glass. CVS-II Phase 4 involved 22 glasses including 20 one-component-at-a-time variations of selected components from the HW-39-4 glass composition. Only PCT and MCC-1 durability properties were measured for the CVS-II Phase 4 glasses.

Both first- and second-order mixture models were fitted to the combined CVS-I and CVS-II (Phases 1, 2, and 3) data for viscosity at 1150°C, electrical conductivity at 1150°C, 7-day PCT and 28-day MCC-1 normalized elemental releases (Si, B, Li, and Na), glass transition temperature, and thermal expansion of solid and molten glass. Preliminary first-order mixture models were fit to liquidus temperature data for three primary crystalline phases (clinopyroxene, spinel, and Zr-containing). Fulcher and Arrhenius equations, with coefficients expanded as first-order mixture models, were also fitted to the combined CVS-I and CVS-II data for viscosity (both Fulcher and Arrhenius) and electrical conductivity (Arrhenius). These models allow viscosity and electrical conductivity to be predicted as a function of temperature as well as glass composition. The PCT and MCC-1 durability data for CVS-II Phase 4 was obtained shortly before this report was completed, and time was insufficient to include it with the other data in fitting durability models. However, the data and preliminary analyses are included in this report (see Chapter 12).

Qualified Composition Region

A preliminary QCR identifying the subregion of the composition space studied in CVS that is predicted to satisfy processing and product property constraints (after accounting for uncertainties in property models) was constructed and is described in this report. The QCR is very preliminary at this time because of the poor quality of preliminary liquidus temperature models and on-going discussions about exactly what should be factored into the definition of the QCR. Only a single QCR is defined in this report, but it may eventually be necessary to construct several QCRs applicable to different subregions of glass composition space. Multiple QCRs may be necessary if

different glass property models are developed for different subregions of glass composition space (to improve model accuracy). Multiple QCRs may also be necessary if warranted by extension of the glass composition experimental region (e.g., if "arms" or disconnected areas are added).

CONCLUSIONS

The following conclusions are based on work and results up through CVS-II Phase 3 and preliminary CVS-II Phase 4 results. The conclusions are organized according to several topics.

Glass Property Models

- There was no advantage (for the CVS data) to using component mole fractions instead of mass fractions for fitting first- and second-order mixture models.

- First- and second-order mixture models using mass fractions of SiO_2, B_2O_3, Al_2O_3, Fe_2O_3, ZrO_2, Na_2O, Li_2O, CaO, MgO, and Others account for the following percentages of the variability in the property data: (a) 94 to 98% for viscosity at 1150°C; (b) 93 to 98% for electrical conductivity at 1150°C; (c) 88 to 97% for glass transition temperature; (d) 73 to 92% for PCT normalized boron, lithium, sodium, and silica releases; (e) 60 to 83% for MCC-1 normalized boron, lithium, sodium, and silica releases; (f) 90%, 64%, and 79% for first-order models fit to limited liquidus temperature data for clinopyroxene, spinel, and Zr-containing phases, respectively. Models cannot be expected to explain 100% of the variability in experimental data, because some of the experimental variability is due to experimental uncertainty (e.g., in batching and melting glasses and measuring glass properties). Estimates of experimental uncertainty for each glass property based on replicates are provided in Appendix F.

- Many of the first- and second-order property models have statistically significant lack-of-fits (LOFs) at higher than 90% confidence. This means that the differences between predicted and measured property values are larger than can be explained by long-term within-lab experimental and measurement uncertainty. However, such LOFs may or may not be of practical significance depending on the formulations and processing strategies eventually selected.

- The first- and second-order property models were fitted to data from a constrained composition region. The models for viscosity, electrical conductivity, transition temperature, and durability (PCT and MCC-1) have predictive performances for other compositions inside the constrained region comparable to those for the compositions used to fit the models. Predictive performance of the models when extrapolated

outside the constrained region depends on the property model and the nature and extent of the extrapolation.

Viscosity

- Fulcher and Arrhenius equations with their coefficients (A, B, and T_0 for Fulcher; A and B for Arrhenius) expanded in the forms of first-order mixture models fit CVS measured viscosity data in the 950 to 1250°C range quite well. The Fulcher-mixture model accounted for 94 to 98% of the variation in the data, while the Arrhenius-mixture model accounted for 97%. The Fulcher-mixture model was fitted with and without augmenting the measured data with a "data point" for each glass consisting of an approximate $10^{11.3}$ Pa·s viscosity value at its transition temperature.

- Based on the first-order mixture model, Li_2O and Na_2O are predicted to have the strongest effects decreasing viscosity, while SiO_2, Al_2O_3, and ZrO_2 are predicted to have the strongest effects increasing viscosity.

- For the CVS data, the CVS first- and second-order models for viscosity at 1150°C performed significantly better than a non-bridging oxygen modeling approach, and slightly better than an empirical modeling approach using oxide/SiO_2 ratios (both proposed in the literature, see Section 7.6).

Electrical Conductivity

- A model consisting of the Arrhenius equation with its coefficients (A and B) expanded in the forms of first-order mixture models accounted for 96% of the variation in the CVS measured electrical conductivity data in the 950 to 1250°C range.

- Based on the first-order mixture model, Li_2O and Na_2O are predicted to have the strongest effects increasing electrical conductivity, while SiO_2 is predicted to have the strongest effect decreasing electrical conductivity.

Glass Transition Temperature

- Based on the first-order mixture model, Li_2O and Na_2O are predicted to have the strongest effects decreasing glass transition temperature, while SiO_2 and ZrO_2 are predicted to have the strongest effects increasing glass transition temperature.

PCT and MCC-1 Durability of Quenched Glass

- Ranking the CVS glasses according to MCC-1 dissolution test results did not yield the same order as ranking according to PCT dissolution test results.

- Based on first-order PCT and MCC-1 normalized B release models fitted to CVS data, Li_2O, Na_2O, and B_2O_3 are predicted to have the strongest

effects increasing B release, while Al_2O_3, SiO_2, and ZrO_2 are predicted to have the strongest effects decreasing B release. MgO is also predicted to increase PCT normalized B release.

- Experimentally varying components one-at-a-time from their values in the HW-39-4 glass showed that the effects of most components on PCT and MCC-1 are roughly linear over the ranges studied. Nonlinearity was seen for SiO_2, Al_2O_3, and B_2O_3 (MCC-1 only)[a].

- Plots of natural logarithms of PCT and MCC-1 normalized boron release versus free energy of hydration show essentially no relationship for CVS data (or any subset thereof). Correcting free energy of hydration for pH effects does not improve the relationships.

Liquidus Temperature and Crystallinity

- The prevailing primary crystalline phases within the CVS composition region are spinel, clinopyroxene, and Zr-containing phases (zircon, ZrO_2, and Na-Zr silicate), followed by orthopyroxene, nepheline, olivine, $CaSiO_3$, and SiO_2. Less frequent are Li_2SiO_3, $LiAlSi_2O_6$, and hematite. Liquidus temperatures (T_L) of two-thirds of the CVS glasses lie within the 800 to 1000°C range. The crystalline phases with T_L > 1050°C were mainly limited to spinels and Zr-containing phases.

- Based on the first-order mixture models, Na_2O and Li_2O are predicted to decrease T_L of all three crystalline phases, with Li_2O always having the stronger effect. B_2O_3 is predicted to decrease T_L of clinopyroxene and spinel, but slightly increase T_L of Zr-containing crystals. MgO and Fe_2O_3 are predicted to be most effective in increasing T_L of clinopyroxene or spinel. The T_L of Zr-containing phases is predicted to be most strongly increased by ZrO_2 followed by MgO. The strong predicted effect of MgO in increasing T_L of all three crystalline phases suggests caution when using MgO as an additive component.

- The current version of the phase-equilibria liquidus temperature model (which considers composition only in terms of the nine major CVS components and the Others component) does not predict the CVS data very well. However, the model is expected to improve after it is updated to account for solid solutions and minor components. Also, whether the CVS data may be affected by kinetic and other factors is being investigated.

- Approximately one-half of the CVS-I and CVS-II Phase 1, 2, and 3 glasses exhibited crystallinity after canister centerline cooling (CCC) heat treatment. The crystalline phases occurring most frequently were spinel, Li_2SiO_3, and clinopyroxene, followed by olivine, SiO_2, hematite, zircon, orthopyroxene, and nepheline.

(a) Second-order models and data from the literature show the effect of B_2O_3 on PCT to be nonlinear over a broad composition region.

- Based on study of a limited number of glasses after CCC, it appears that: crystallization of nepheline and SiO_2 have a strong negative effect on glass durability, and crystallization of clinopyroxenes and zircon only slightly affected glass durability.

Amorphous Phase Separation

- Of the 123 CVS-I and CVS-II Phase 1, 2, and 3 glasses, only nine are prone to amorphous phase separation, as predicted by a modified Taylor model using Na_2O+Li_2O - B_2O_3 - SiO_2 (NLBS) and Na_2O equivalent - B_2O_3 - SiO_2 submixtures. Experimentally, amorphous phase separation has been observed in only three CCC glasses and one quenched glass by SEM/TEM analysis.

- The NLBS submixture also suggests a relationship between composition and durability for both quenched PCT and MCC-1 data. Based on MCC-1 data and SEM results, glasses within the immiscibility dome show low durability as a result of insufficient structural integrity, not the development of amorphous phase separation.

Different Others Compositions

- Based on limited testing, varying the composition of the Others component from that used in most of the CVS glasses (which corresponds to NCAW) seems to affect some properties and not others. Viscosity, MCC-1 and PCT releases, and liquidus temperature can be affected depending on the composition of the glass and the composition of Others. Electrical conductivity, glass transition temperature, and thermal expansion appear to be only slightly affected, if at all, by varying Others composition.

- The presence of higher levels of Cr_2O_3 in some Others mixes seems to be a possible explanation for some of the significant changes in property values.

Model Uncertainty and the Qualified Composition Region

- The QCR is a subregion of the composition region studied in CVS that satisfies, with high confidence, processability and WAPS constraints. The preliminary QCR discussed in this report was based on viscosity, electrical conductivity, liquidus temperature, and PCT durability constraints and single-component constraints corresponding to the CVS composition region.

- Statistical confidence intervals and confidence bands were used to account for uncertainty in the first-order property models used to construct preliminary QCRs. Using confidence intervals addresses whether a single composition in the QCR will have acceptable properties with a specified confidence (say 95%) for each property. Using confidence bands addresses whether all of the compositions in the QCR

will have acceptable properties with a specified confidence (say 95%) for each property.

- The preliminary QCR is a nine-dimensional composition region defined using matrix equations (having slightly different forms depending on whether confidence intervals or confidence bands are used), and is thus impossible to visualize directly. Using confidence intervals to account for the uncertainty in the property models used to construct the QCR resulted in 5 to 35% shrinkage of the acceptable region for all properties except liquidus temperature, for which up to 83% shrinkage occurred. Larger shrinkages occurred for all properties using confidence bands.

- The preliminary QCR presented in this report should be considered a demonstration effort and not relied upon, due to the very preliminary nature of the liquidus temperature models used. The PCT durability models also have more uncertainty than is desirable. However, what is important is that: 1) a well-defined and defensible approach for identifying acceptable glass compositions (given model uncertainties) is in place, and 2) it is very easy to update the QCR as glass property models are improved or glass processability and waste form qualification constraints are revised.

More detailed conclusions are given in Section 15.1.

The results (both data and models) from the CVS so far constitute an important contribution to vitrification knowledge and technology. However, the research and understanding effort will continue as new problems and needs will inevitably arise. Work is in-progress to investigate glasses that melt at higher temperatures than 1150°C and to investigate the effects of components not studied so far in CVS. A number of suggestions for future research are listed in Section 15.2.

ACKNOWLEDGMENTS

The CVS and this report are the result of teamwork by several scientists, engineers, and technicians from different fields. P. R. Hrma was responsible for the materials science and glass development aspects of the study as well as for cost account leadership. G. F. Piepel was responsible for the statistical experimental design, modeling, and data analysis aspects of the study as well as for leading the writing of this report. M. J. Schweiger and D. E. Smith performed glass preparation and physical measurements and took responsibility for compliance with PNL guidelines. D.-S. Kim was responsible for evaluation of glass crystallinity and liquidus temperature and made contributions in writing parts of this report. P. E. Redgate performed the majority of the statistical experimental design, model fitting, and other statistical data analyses and associated graphics in the report. J. D. Vienna made contributions in data analysis, project support, and writing portions of the report. C. A. LoPresti and D. B. Simpson also performed statistical data analyses and produced related graphics. C. A. LoPresti also improved and used the historical database of glass compositions and properties to validate CVS-developed glass property models for viscosity, electrical conductivity, and glass transition temperature. D. K. Peeler was responsible for the analysis of immiscibility in CVS glasses. M. H. Langowski helped coordinate contributions for this report from various authors, provided thorough technical review and comments on drafts of the report, and wrote various text additions and revisions.

The authors acknowledge the technical efforts and contributions of the following individuals: D. E. Larson for task leadership and programmatic guidance, H. C. Buchanan and S. E. Palmer for laboratory support and materials preparation, P. T. Fini for experimental work and reporting on liquidus temperature and maximum waste loading, N. R. Gordon and K. L. Simmons for glass transition temperature and coefficient of thermal expansion measurements, N. T. Saenz for optical microscopy, J. E. Coleman for scanning electron microscopy and EDX, D. E. McCready for X-ray diffraction analysis, and P. J. Titzler for preparation of laboratory data for statistical analysis and development of an electrical conductivity measurement technique. M. W.

Urie, D. R. Sanders, J. J. Wagner, S. I. Barsoum, N. C. Cleavenger, D. E. Faulk, and J. M. Robbins are acknowledged for chemical analyses of glass and dissolution test solution samples. D. J. Bates is acknowledged for originally compiling the historical database of glass compositions and properties used in validating CVS-developed glass property models.

We also acknowledge the efforts of N. D. Foote who provided editorial comments on the whole report and prepared it for printing. F. M. Ryan also provided editorial comments on part of the report.

Independent technical review comments by R. P. Colburn, J. W. Johnston, J. A. Carr, and J. H. Holbrook led to improvements in the report and are greatly appreciated.

CONTENTS--VOLUME 1

ABSTRACT iii

SUMMARY v

ACKNOWLEDGMENTS xiii

1.0 INTRODUCTION 1.1

1.1 BACKGROUND 1.1

1.2 CVS OVERVIEW 1.2

2.0 CVS OBJECTIVES 2.1

3.0 MELT AND GLASS PRODUCT REQUIREMENTS 3.1

3.1 VISCOSITY 3.1

3.2 ELECTRICAL CONDUCTIVITY 3.3

3.3 LIQUIDUS TEMPERATURE 3.4

3.4 TIME-TEMPERATURE-TRANSFORMATION 3.4

3.5 GLASS TRANSITION TEMPERATURE 3.6

3.6 THERMAL EXPANSION 3.6

3.7 DURABILITY 3.6

4.0 EXPERIMENTAL DESIGN 4.1

4.1 EXPERIMENTAL DESIGN STRATEGY AND METHODOLOGY 4.1

4.1.1 Experimental Design Strategy 4.1

4.1.2 Mixture and Optimal Experimental Design Methodology . 4.2

4.2 CVS-I COMPOSITION REGION AND TEST MATRIX 4.3

4.2.1 Glass Components Studied in CVS-I 4.4

4.2.2 CVS-I Composition Region 4.4

4.2.3 CVS-I Test Matrix 4.7

4.3 CVS-II PHASE 1 COMPOSITION REGION AND TEST MATRIX 4.10
4.3.1 CVS-II Phase 1 Composition Region 4.10
4.3.2 CVS-II Phase 1 Test Matrix 4.11
4.4 CVS-II PHASE 2 COMPOSITION REGION AND TEST MATRIX 4.16
4.4.1 CVS-II Phase 2 Composition Region 4.16
4.4.2 CVS-II Phase 2 Test Matrix 4.17
4.4.3 Glasses Made with CC, PFP, and NCRW Others Mixes 4.20
4.5 CVS-II PHASE 3 COMPOSITION REGION AND TEST MATRIX 4.22
4.5.1 CVS-II Phase 3 Composition Region 4.24
4.5.2 CVS-II Phase 3 Test Matrix 4.25
4.6 CVS-II PHASE 4 COMPOSITION REGION AND TEST MATRIX 4.30
4.6.1 CVS-II Phase 4 Composition Region 4.31
4.6.2 CVS-II Phase 4 Test Matrix 4.32
4.7 COMBINED CVS EXPERIMENTAL DESIGN IN MASS FRACTIONS 4.33
4.8 COMBINED CVS EXPERIMENTAL DESIGN IN MOLE FRACTIONS 4.40
5.0 GLASS FABRICATION AND PROPERTY MEASUREMENTS 5.1
5.1 GLASS FABRICATION AND CHEMICAL ANALYSIS 5.1
5.2 VISCOSITY 5.3
5.3 ELECTRICAL CONDUCTIVITY 5.5
5.4 LIQUIDUS TEMPERATURE 5.6
5.5 CANISTER CENTERLINE COOLING AND CRYSTALLINITY 5.7
5.6 GLASS TRANSITION TEMPERATURE 5.9
5.7 THERMAL EXPANSION 5.9
5.8 DURABILITY 5.10
5.9 ACCURACY, PRECISION, AND OVERCHECK TESTING 5.13

6.0 PROPERTY MODELING AND OTHER DATA ANALYSIS METHODS 6.1

6.1 EMPIRICAL MIXTURE MODELS 6.1

6.1.1 First- and Second-Order Mixture Models 6.1

6.1.2 Model Fitting 6.4

6.1.3 Pseudocomponent Transformations 6.7

6.1.4 Variable Selection for Second-Order Models 6.8

6.1.5 Model Evaluation 6.9

6.1.6 Model Validation 6.13

6.2 MODEL PREDICTION UNCERTAINTIES 6.15

6.3 COMPONENT EFFECTS 6.16

6.4 COMPARISONS TO OTHER MODELS 6.18

7.0 VISCOSITY RESULTS AND DISCUSSION 7.1

7.1 VISCOSITY MODELS AS FUNCTIONS OF COMPOSITION AND TEMPERATURE 7.2

7.2 FIRST-ORDER MODELS AND COMPONENT EFFECTS FOR VISCOSITY AT 1150°C 7.13

7.3 INVESTIGATION OF POTENTIAL BIASES IN VISCOSITY AT 1150°C DATA DUE TO CVS PHASES 7.18

7.4 SECOND-ORDER MODELS FOR VISCOSITY AT 1150°C 7.20

7.5 VALIDATION OF FIRST- AND SECOND-ORDER MODELS FOR VISCOSITY AT 1150°C 7.23

7.5.1 Validation with CVS-II Phase 3 Data 7.23

7.5.2 Validation with Historical Database 7.30

7.5.3 Summary of Viscosity at 1150°C Model Validation . . . 7.35

7.6 OTHER MODEL FORMS INVESTIGATED 7.37

7.6.1 DWPF Approach 7.37

7.6.2 Alfred University Approach 7.43

7.7 VISCOSITY DISCUSSION 7.47

8.0 ELECTRICAL CONDUCTIVITY RESULTS AND DISCUSSION 8.1

8.1 ELECTRICAL CONDUCTIVITY MODELS AS FUNCTIONS OF COMPOSITION AND TEMPERATURE 8.2

8.2 FIRST-ORDER MODELS AND COMPONENT EFFECTS FOR ELECTRICAL CONDUCTIVITY AT 1150°C 8.2

8.3 INVESTIGATION OF POTENTIAL BIASES IN ELECTRICAL CONDUCTIVITY AT 1150°C DATA DUE TO CVS PHASES 8.11

8.4 SECOND-ORDER MODELS FOR ELECTRICAL CONDUCTIVITY AT 1150°C 8.13

8.5 VALIDATION OF FIRST- AND SECOND-ORDER MODELS FOR ELECTRICAL CONDUCTIVITY AT 1150°C 8.15

8.5.1 Validation with CVS-II Phase 3 Data 8.15

8.5.2 Validation with Historical Database 8.23

8.5.3 Summary of Electrical Conductivity at 1150°C Model Validation 8.30

8.6 ELECTRICAL CONDUCTIVITY DISCUSSION 8.30

9.0 GLASS TRANSITION TEMPERATURE RESULTS AND DISCUSSION 9.1

9.1 FIRST-ORDER MODELS AND COMPONENT EFFECTS FOR GLASS TRANSITION TEMPERATURE 9.1

9.2 INVESTIGATION OF POTENTIAL BIASES IN GLASS TRANSITION TEMPERATURE DATA DUE TO CVS PHASES 9.8

9.3 SECOND-ORDER MODELS FOR GLASS TRANSITION TEMPERATURE 9.8

9.4 VALIDATION OF FIRST- AND SECOND-ORDER MODELS FOR GLASS TRANSITION TEMPERATURE 9.10

9.4.1 Validation with CVS-II Phase 3 Data 9.10

9.4.2 Validation with Historical Database 9.17

9.4.3 Summary of Transition Temperature Model Validation 9.28

9.5 GLASS TRANSITION TEMPERATURE DISCUSSION 9.29

10.0 THERMAL EXPANSION RESULTS AND DISCUSSION 10.1

10.1 FIRST-ORDER MODELS AND COMPONENT EFFECTS FOR THERMAL EXPANSION 10.1

10.2 SECOND-ORDER MODELS FOR THERMAL EXPANSION 10.14

10.3 THERMAL EXPANSION DISCUSSION 10.19

11.0 GLASS CRYSTALLIZATION AND LIQUIDUS TEMPERATURE RESULTS AND DISCUSSION 11.1

11.1 OVERVIEW OF CRYSTALLINE PHASES IDENTIFIED IN CVS GLASSES 11.2

11.2 CRYSTALLIZATION OF CVS-I AND CVS-II GLASSES 11.5

11.2.1 Crystallization of Canister Centerline Cooled Glasses 11.17

11.2.2 Effects of Different Others 11.20

11.3 PRELIMINARY LIQUIDUS TEMPERATURE STUDIES 11.21

11.3.1 Initial Liquidus Temperature Determination Efforts in CVS-I and CVS-II Phase 1 . . . . . 11.21

11.3.2 Preliminary Studies to Develop Liquidus Temperature Measurement Procedure 11.22

11.4 LIQUIDUS TEMPERATURES AND PRIMARY CRYSTALLINE PHASES . . . 11.25

11.4.1 Results by Primary Crystalline Phase 11.38

11.4.2 Results for Replicate Glasses 11.43

11.4.3 Effects of Different Others 11.43

11.5 CRYSTALLINITY AND LIQUIDUS TEMPERATURE DISCUSSION 11.44

11.6 LIQUIDUS TEMPERATURE AND MULTIPLE-COMPONENT CONSTRAINTS . . 11.49

11.7 LIQUIDUS TEMPERATURE FIRST-ORDER MIXTURE MODELS 11.56

11.8 PHASE-EQUILIBRIA LIQUIDUS TEMPERATURE MODEL 11.65

11.9 EVALUATION OF PHASE-EQUILIBRIA LIQUIDUS TEMPERATURE MODEL 11.66

FIGURES--VOLUME 1

7.1a Predicted Versus Measured Viscosity at Temperature Values for the Combined Fulcher First-Order Mixture Model in the Mass Fractions of the Component Oxides (from Table 7.1a) 7.6

7.1b Predicted Versus Measured Viscosity at Temperature Values for the Combined Fulcher First-Order Mixture Model in the Mole Fractions of the Component Oxides (from Table 7.1b) 7.7

7.2a Predicted Versus Measured Viscosity at Temperature Values for the Combined Arrhenius First-Order Mixture Model Using Mass Fractions of the Component Oxides (from Table 7.2a) 7.11

7.2b Predicted Versus Measured Viscosity at Temperature Values for the Combined Arrhenius First-Order Mixture Model Using Mole Fractions of the Component Oxides (from Table 7.2b) 7.12

7.3a Predicted Viscosity at 1150°C from the First-Order Mixture Model Using Mass Fractions (from Column 2 of Table 7.3) Versus Predicted Viscosity at 1150°C from the Fulcher Equation for Each Glass (from Table B.2) 7.16

7.3b Predicted Viscosity at 1150°C from the First-Order Mixture Model Using Mole Fractions (from Column 3 of Table 7.3) Versus Predicted Viscosity at 1150°C from the Fulcher Equation for Each Glass (from Table B.2) 7.17

7.4 Predicted Component Effects on Viscosity at 1150°C Relative to the HW-39-4 Composition, Based on the First-Order Mixture Model Using Mass Fractions (from Column 2 of Table 7.3) 7.19

7.5 Predicted Viscosity at 1150°C from the Second-Order Mixture Model #1 (from Table 7.4) Versus Predicted Viscosity at 1150°C from the Fulcher Equation for Each Glass (from Table B.2) 7.22

7.6 Predicted Viscosity at 1150°C from the First-Order Mixture Model After CVS-II Phase 2 (from Table 7.5) Versus Predicted Viscosity at 1150°C from the Fulcher Equation for Each Glass (from Table B.2) for the CVS-II Phase 3 Data 7.25

7.7a Predicted Viscosity at 1150°C from the Second-Order Mixture Model #1 After CVS-II Phase 2 (from Table 7.5) Versus Predicted Viscosity at 1150°C from the Fulcher Equation for Each Glass (from Table B.2) for the CVS-II Phase 3 Data 7.26

7.7b Predicted Viscosity at 1150°C from the Second-Order Mixture Model #2 After CVS-II Phase 2 (from Table 7.5) Versus Predicted Viscosity at 1150°C from the Fulcher Equation for Each Glass (from Table B.2) for the CVS-II Phase 3 Data 7.27

7.7c Predicted Viscosity at 1150°C from the Second-Order Mixture Model #3 After CVS-II Phase 2 (from Table 7.5) Versus Predicted Viscosity at 1150°C from the Fulcher Equation for Each Glass (from Table B.2) for the CVS-II Phase 3 Data 7.28

7.8 Predicted Viscosity at 1150°C from the First-Order Mixture Model After CVS-II Phase 2 (from Table 7.5) Versus "Measured" Viscosity at 1150°C for the Historical Data 7.31

7.9a Predicted Viscosity at 1150°C from the Second-Order Mixture Model #1 After CVS-II Phase 2 (from Table 7.5) Versus "Measured" Viscosity at 1150°C for the Historical Data 7.32

7.9b Predicted Viscosity at 1150°C from the Second-Order Mixture Model #2 After CVS-II Phase 2 (from Table 7.5) Versus "Measured" Viscosity at 1150°C for the Historical Data 7.33

7.9c Predicted Viscosity at 1150°C from the Second-Order Mixture Model #3 After CVS-II Phase 2 (from Table 7.5) Versus "Measured" Viscosity at 1150°C for the Historical Data 7.34

7.10 Predicted Viscosity at 1150°C from the Second-Order Mixture Model #3 After CVS-II Phase 2 (from Table 7.5) Versus "Measured" Viscosity at 1150°C for the Historical Data, with the Number of Relaxed Component Constraints Satisfied Used as the Plotting Symbol 7.36

7.11 Predicted Viscosity at 1150°C Using DWPF Model with DWPF Coefficients Versus the CVS Viscosity at 1150°C Data Values from Table B.2 for CVS-I and CVS-II Phases 1, 2, and 3 Glasses 7.39

7.12 CVS Viscosity at 1150°C Data Values Versus DWPF NBO Variable for CVS-I and CVS-II Phase 1, 2, and 3 Glasses 7.40

7.13 Predicted Viscosity at 1150°C Using the DWPF Model with CVS Coefficients Versus the CVS Viscosity at 1150°C Data Values for CVS-I and CVS-II Phase 1, 2, and 3 Glasses 7.41

FIGURES--VOLUME 1 (continued)

7.14a Predicted Viscosity at 1150°C from the Mass Fraction Version of the Alfred University "Ratio to SiO_2" Model Versus Predicted Viscosity at 1150°C from the Fulcher Equation for Each Glass 7.45

7.14b Predicted Viscosity at 1150°C from the Mole Fraction Version of the Alfred University "Ratio to SiO_2" Model Versus Predicted Viscosity at 1150°C from the Fulcher Equation for Each Glass 7.46

7.15 Viscosity of a Simple Glass (70 wt% SiO_2, 14 B_2O_3, 9 Na_2O, 5 Li_2O, 1 CaO, 1 MgO) over the Temperature Range from 950 to 1250°C 7.47

7.16 T_0 Coefficients for Each CVS Glass from Fulcher Equations Fitted With and Without T_g Data 7.49

7.17 Viscosity Predictions from Fulcher Equations Fitted With and Without T_g Data for Glasses with Varying Differences in Fulcher T_0 Coefficients 7.49

8.1a Predicted Versus Measured Electrical Conductivity at Temperature Values for the Combined Arrhenius First-Order Mixture Model in the Mass Fractions of the Component Oxides (from Table 8.1a) 8.5

8.1b Predicted Versus Measured Electrical Conductivity at Temperature Values for the Combined Arrhenius First-Order Mixture Model in the Mole Fractions of the Component Oxides (from Table 8.1b) 8.6

8.2a Predicted Electrical Conductivity at 1150°C from the First-Order Mixture Model Using Mass Fractions (from Column 2 of Table 8.2) Versus Predicted Electrical Conductivity at 1150°C from the Arrhenius Equation for Each Glass (from Table C.3) 8.9

8.2b Predicted Electrical Conductivity at 1150°C from the First-Order Mixture Model Using Mole Fractions (from Column 3 of Table 8.2) Versus Predicted Electrical Conductivity at 1150°C from the Arrhenius Equation for Each Glass (from Table C.3) 8.10

8.3 Predicted Component Effects on Electrical Conductivity at 1150°C Relative to the HW-39-4 Composition, Based on the First-Order Mixture Model Using Mass Fractions (in Column 2 of Table 8.2) 8.12

8.4 Predicted Electrical Conductivity at 1150°C from the Second-Order Mixture Model #2 (from Table 8.3) Versus Predicted Electrical Conductivity at 1150°C from the Arrhenius Equation for Each Glass (from Table C.3) 8.16

8.5 Predicted Electrical Conductivity at 1150°C from the First-Order Mixture Model (After CVS-II Phase 2) Versus Predicted Electrical Conductivity at 1150°C from the Arrhenius Equation for Each Glass (from Table C.3) for the CVS-II Phase 3 Data 8.18

8.6a Predicted Electrical Conductivity at 1150°C from the Second-Order Mixture Model #1 (After CVS-II Phase 2) Versus Predicted Electrical Conductivity at 1150°C from the Arrhenius Equation for Each Glass (from Table C.3) for the CVS-II Phase 3 Data 8.19

8.6b Predicted Electrical Conductivity at 1150°C from the Second-Order Mixture Model #2 (After CVS-II Phase 2) Versus Predicted Electrical Conductivity at 1150°C from the Arrhenius Equation for Each Glass (from Table C.3) for the CVS-II Phase 3 Data 8.20

8.6c Predicted Electrical Conductivity at 1150°C from the Second-Order Mixture Model #3 (After CVS-II Phase 2) Versus Predicted Electrical Conductivity at 1150°C from the Arrhenius Equation for Each Glass (from Table C.3) for the CVS-II Phase 3 Data 8.21

8.7 Predicted Electrical Conductivity at 1150°C from the First-Order Mixture Model (After CVS-II Phase 2) Versus Measured Electrical Conductivity at 1150°C for 206 Historical Data Points (143 of Which are Outside the CVS Composition Region) 8.24

8.8a Predicted Electrical Conductivity at 1150°C from the Second-Order Mixture Model #1 (After CVS-II Phase 2) Versus Measured Electrical Conductivity at 1150°C for 206 Historical Data Points (143 of Which are Outside the CVS Composition Region) 8.25

8.8b Predicted Electrical Conductivity at 1150°C from the Second-Order Mixture Model #2 (After CVS-II Phase 2) Versus Measured Electrical Conductivity at 1150°C for 206 Historical Data Points (143 of Which are Outside the CVS Composition Region) 8.26

FIGURES--VOLUME 1 (continued)

8.8c Predicted Electrical Conductivity at 1150°C from the Second-Order Mixture Model #3 (After CVS-II Phase 2) Versus Measured Electrical Conductivity at 1150°C for 206 Historical Data Points (143 of Which are Outside the CVS Composition Region) 8.27

8.9 Predicted Electrical Conductivity at 1150°C from the First-Order Mixture Model (After CVS-II Phase 2) Versus Measured Electrical Conductivity at 1150°C for the Historical Data, With the Number of Relaxed Component Constraints Satisfied Used as the Plotting Symbol 8.29

8.10 First-Order Mixture Model Coefficients for Viscosity at 1150°C Versus for Electrical Conductivity at 1150°C 8.31

9.1a Predicted Versus Measured Glass Transition Temperature Values for the First-Order Mixture Model Using Mass Fractions (from Column 2 of Table 9.2) 9.5

9.1b Predicted Versus Measured Glass Transition Temperature Values for the First-Order Mixture Model Using Mole Fractions (from Column 3 of Table 9.2) 9.6

9.2 Predicted Component Effects on Glass Transition Temperature Relative to the HW-39-4 Composition, Based on the First-Order Mixture Model Using Mass Fractions (in Column 2 of Table 9.2) 9.7

9.3 Predicted Versus Measured Glass Transition Temperature Values for the Second-Order Mixture Model #3 (from Table 9.3) 9.11

9.4 Predicted Glass Transition Temperature from the First-Order Mixture Model (After CVS-II Phase 2) Versus Measured Glass Transition Temperature (from Table 9.1) for the CVS-II Phase 3 Data 9.13

9.5a Predicted Glass Transition Temperature from the Second-Order Mixture Model #1 (After CVS-II Phase 2) Versus Measured Glass Transition Temperature (from Table 9.1) for the CVS-II Phase 3 Data 9.14

9.5b Predicted Glass Transition Temperature from the Second-Order Mixture Model #2 (After CVS-II Phase 2) Versus Measured Glass Transition Temperature (from Table 9.1) for the CVS-II Phase 3 Data 9.15

FIGURES--VOLUME 1 (continued)

9.5c Predicted Glass Transition Temperature from the Second-Order Mixture Model #3 (After CVS-II Phase 2) Versus Measured Glass Transition Temperature (from Table 9.1) for the CVS-II Phase 3 Data 9.16

9.6 Predicted Transition Temperature from the First-Order Mixture Model (After CVS-II Phase 2) Versus Measured Transition Temperature for 143 Historical Data Points (115 of Which are Outside the CVS Composition Region) 9.19

9.7a Predicted Transition Temperature from the Second-Order Mixture Model #1 (After CVS-II Phase 2) Versus Measured Transition Temperature for 143 Historical Data Points (115 of Which are Outside the CVS Composition Region) 9.20

9.7b Predicted Transition Temperature from the Second-Order Mixture Model #2 (After CVS-II Phase 2) Versus Measured Transition Temperature for 143 Historical Data Points (115 of Which are Outside the CVS Composition Region) 9.21

9.7c Predicted Transition Temperature from the Second-Order Mixture Model #3 (After CVS-II Phase 2) Versus Measured Transition Temperature for 143 Historical Data Points (115 of Which are Outside the CVS Composition Region) 9.22

9.8 Predicted Transition Temperature from the First-Order Mixture Model (After CVS-II Phase 2) Versus Measured Transition Temperature for the Historical Data, With the Number of Relaxed Component Constraints Satisfied Used as the Plotting Symbol 9.23

9.9 Predicted Transition Temperature from the First-Order Mixture Model (After CVS-II Phase 2) Versus Measured Transition Temperature for 28 of the 143 Historical Data Points Within Relaxed CVS Single-Component Constraints 9.24

9.10a Predicted Transition Temperature from the Second-Order Mixture Model #1 (After CVS-II Phase 2) Versus Measured Transition Temperature for 28 of the 143 Historical Data Points Within Relaxed CVS Single-Component Constraints 9.25

9.10b Predicted Transition Temperature from the Second-Order Mixture Model #2 (After CVS-II Phase 2) Versus Measured Transition Temperature for 28 of the 143 Historical Data Points Within Relaxed CVS Single-Component Constraints 9.26

9.10c Predicted Transition Temperature from the Second-Order Mixture Model #3 (After CVS-II Phase 2) Versus Measured Transition Temperature for 28 of the 143 Historical Data Points Within Relaxed CVS Single-Component Constraints 9.27

9.11 First-Order Mixture Model Coefficients for T_g (from Table 9.2) Versus Those for "B" from the Fulcher Equation Expressing Viscosity as a Function of Temperature and Glass Composition (from Table 7.1a) 9.30

9.12 First-Order Mixture Model Coefficients for T_g (From Table 9.2) Versus Those for T_0 from the Fulcher Equation Expressing Viscosity as a Function of Temperature and Glass Composition (from Table 7.1) 9.31

10.1a Predicted Versus Measured Solid Glass Coefficient of Thermal Expansion Values for the First-Order Mixture Model Using Mass Fractions (from Column 2 of Table 10.2) 10.7

10.1b Predicted Versus Measured Solid Glass Coefficient of Thermal Expansion Values for the First-Order Mixture Model Using Mole Fractions (from Column 4 of Table 10.2) 10.8

10.2a Predicted Versus Measured Molten Glass Coefficient of Thermal Expansion Values for the First-Order Mixture Model Using Mass Fractions (from Column 3 of Table 10.2) 10.10

10.2b Predicted Versus Measured Molten Glass Coefficient of Thermal Expansion Values for the First-Order Mixture Model Using Mole Fractions (from Column 5 of Table 10.2) 10.11

10.3 Predicted Component Effects on Thermal Expansion Coefficient for Solid Glass (α_s) Relative to the HW-39-4 Composition, Based on the First-Order Mixture Model Using Mass Fractions (in Column 2 of Table 10.2) 10.12

10.4 Predicted Component Effects on Thermal Expansion Coefficient for Molten Glass (α_m) Relative to the HW-39-4 Composition, Based on the First-Order Mixture Model Using Mass Fractions (in Column 3 of Table 10.2) 10.13

10.5 Predicted Versus Measured Solid Glass Coefficient of Thermal Expansion Values for the Second-Order Model #2 (from Table 10.3) 10.17

10.6 Predicted Versus Measured Molten Glass Coefficient of Thermal Expansion Values for the Second-Order Model #1 (from Table 10.4) 10.18

10.7 First-Order Mixture Model Coefficients for Thermal Expansion of Solid Glass Versus Those for Thermal Expansion of Molten Glass 10.20

11.1 System $FeO-Fe_2O_3-Cr_2O_3$ at 1300°C 11.3

11.2 System $NiO-MgO-Fe_2O_3$ in the Temperature Range 1040-1280°C 11.3

11.3 Conceptual View of Crystallization Front Motion in the Gradient Furnace in Initially Crystal-Free (Crystallization Line) and Pre-Crystallized (Dissolution Line) Samples 11.23

11.4 Effects of Time, Platinum Foil Cover, and Measurement Method on Liquidus Temperature for the CVS Internal Standard Glass 11.24

11.5 Number of CVS Glass Samples with Major Crystalline Phases Identified After Canister Centerline Cooling 11.46

11.6 Liquidus Temperatures of Major Crystalline Phases in CVS Glasses 11.49

11.7 Effect of (CaO + MgO) Concentration on the Liquidus Temperature of Crystalline Phases Identified in CVS Glasses 11.51

11.8 Effect of (Fe_2O_3 + Al_2O_3 + ZrO_2 + Others) Concentration on the Liquidus Temperature of Crystalline Phases Identified in CVS Glasses 11.52

11.9 Effect of (Al_2O_3 + ZrO_2) Concentration on the Liquidus Temperature of Crystalline Phases Identified in CVS Glasses 11.53

11.10 Effect of (CaO + MgO + ZrO_2) Concentration on the Liquidus Temperature of Crystalline Phases Identified in CVS Glasses 11.54

11.11 Effect of (SiO_2/Al_2O_3) Ratio on the Liquidus Temperature of Crystalline Phases Identified in CVS Glasses 11.55

11.12 Predicted Versus Measured Liquidus Temperature of Clinopyroxene for the First-Order Mixture Model 11.59

FIGURES--VOLUME 1 (continued)

11.13 Predicted Versus Measured Liquidus Temperature of Spinel for the First-Order Mixture Model 11.59

11.14 Predicted Versus Measured Liquidus Temperature of Zr-Containing Crystals for the First-Order Mixture Model 11.60

11.15 Predicted Component Effects on Liquidus Temperature of Clinopyroxene Relative to the HW-39-4 Composition, Based on the First-Order Mixture Model Using Mass Fractions (in Column 2 of Table 11.7) 11.62

11.16 Predicted Component Effects on Liquidus Temperature of Spinel Relative to the HW-39-4 Composition, Based on the First-Order Mixture Model Using Mass Fractions (in Column 3 of Table 11.7) 11.63

11.17 Predicted Component Effects on Liquidus Temperature of Zr-containing Crystals Relative to the HW-39-4 Composition, Based on the First-Order Mixture Model Using Mass Fractions (in Column 4 of Table 11.7) 11.64

11.18 Predicted Versus Measured Liquidus Temperature of Glasses for Which the Experimental Primary Phase Agreed with the First Phase Predicted by the Phase Equilibria Model (Group A) 11.68

11.19 Predicted Versus Measured Liquidus Temperature of Glasses for Which the Experimental Primary Phase Agreed with the Second or Third Phases Predicted by the Phase Equilibria Model (Group B) 11.70

11.20 Same as Figure 11.19, Except the T_L of the Predicted First Phase was Used in Plotting and Calculating R^2 Instead of the T_L of the Predicted Second or Third Phase 11.71

11.21 Predicted Versus Measured Liquidus Temperature of Glasses for Which the Experimental Primary Phase Did Not Agree with Any of the Phases Predicted by the Phase Equilibria Model (Group C) 11.72

11.22 Predicted Versus Measured Liquidus Temperature of Group A, B, and C Glasses for the Phase Equilibria Model 11.74

TABLES--VOLUME 1

3.1 Glass Property Acceptability Criteria for an 1150°C Melter 3.2

4.1 Composition of the Others Component for NCAW Waste 4.5

4.2 Composition Region Studied in CVS-I 4.6

4.3 DWPF and Preliminary Hanford HLW Vitrification Solubility Limits 4.6

4.4 Glass Compositions Tested in CVS-I 4.8

4.5 Pairwise Correlations Among Glass Components for CVS-I Glasses 4.9

4.6 Composition Subregions Studied During CVS-II 4.12

4.7 Glass Compositions Tested in CVS-II Phase 1 . . . . . 4.14

4.8 Mass Fraction Composition of the CVS Internal Standard Glass Compared to the Mass Fraction Composition of the HW-39-4 Glass 4.15

4.9 Glass Compositions Tested in CVS-II Phase 2 . . . . . 4.18

4.10 Composition of Others Mixes Representative of CC, PFP, and NCRW Wastes Used in Glasses CVS2-55, CVS2-56, and CVS2-57 . . . . . 4.20

4.11 Preliminary Estimated Compositions for Pretreated NCAW, NCRW, PFP, and CC Wastes 4.24

4.12 Glass Compositions Tested in CVS-II Phase 3 . . . . . 4.26

4.13 Compositions of Others for CVS2-64 to CVS2-70, CVS2-95, CVS2-99, CVS2-100, and CVS2-101 Glasses 4.28

4.14 Glass Compositions Tested in CVS-II Phase 4 . . . . . 4.32

4.15 As-Batched Mass Fraction Compositions for CVS-I and CVS-II Glasses 4.34

4.16 Pairwise Correlations Among Glass Components for CVS-I and CVS-II Glasses 4.39

4.17 Mole Fraction Compositions for CVS-I and CVS-II Glasses Assuming F and SO_3 Do Not Remain in the Glass 4.41

TABLES--VOLUME 1 (continued)

4.18 Calculated Molecular Weight of Others for Various Others Mixes Used in CVS Glasses Assuming: (a) All F and SO_3 Volatilize During Melting, and (b) All F and SO_3 Remain After Melting 4.45

4.19 Mole Fraction Compositions for CVS-I and CVS-II Glasses Assuming F and SO_3 Remain in the Glass 4.46

5.1 Simulated Canister-Centerline-Cooling Schedule 5.8

6.1 Property Transformations Used in Modeling 6.6

7.1a Fitted Viscosity Model in Which the Fulcher Equation Coefficients A, B, and T_0 are Expressed as First-Order Mixture Models in the Mass Fractions of the Oxide Components 7.3

7.1b Fitted Viscosity Model in Which the Fulcher Equation Coefficients A, B, and T_0 are Expressed as First-Order Mixture Models in the Mole Fractions of the Oxide Components 7.4

7.2a Fitted Viscosity Model in Which the Arrhenius Equation Coefficients A and B are Expressed as First-Order Mixture Models in the Mass Fractions of the Oxide Components 7.9

7.2b Fitted Viscosity Model in Which the Arrhenius Equation Coefficients A and B are Expressed as First-Order Mixture Models in the Mole Fractions of the Oxide Components 7.10

7.3 Coefficients and Goodness-of-Fit Statistics for First-Order Mixture Models Fitted to Natural Logarithm of Viscosity at 1150°C Using Mass and Mole Fractions of the Oxide Components 7.15

7.4 Candidate Scheffé Second-Order Models Using Mass Fractions for Viscosity at 1150°C 7.21

7.5 First-Order Model and Three Candidate Second-Order Models Using Mass Fractions for Viscosity at 1150°C Fitted to CVS-I and CVS-II Phase 1 and 2 Data 7.24

7.6 DWPF and CVS Coefficients for the DWPF Model Form $\log(\eta_{1150}) = a + b\ NBO$ 7.42

TABLES--VOLUME 1 (continued)

7.7 Comparison of R^2 Values for the DWPF Viscosity at 1150°C Models with DWPF and CVS Coefficients and for the CVS Viscosity at 1150°C Mixture Models from Table 7.5 . . . . . 7.42

7.8 Coefficients for Mass and Mole Fraction Versions of Alfred University "Ratio to SiO_2" Model for Viscosity at 1150°C . . . 7.44

7.9 R^2 Values for the Alfred University "Ratio to SiO_2" Model and the CVS First-Order Mixture Model for Viscosity at 1150°C Using Mass and Mole Fractions 7.44

7.10 Component Coefficients from First-Order Mass Fraction Mixture Models for Several Viscosity Related Values 7.51

8.1a Fitted Electrical Conductivity Model in Which the Arrhenius Equation Coefficients A and B are Expressed as First-Order Mixture Models in the Mass Fractions of the Oxide Components 8.3

8.1b Fitted Electrical Conductivity Model in Which the Arrhenius Equation Coefficients A and B are Expressed as First-Order Mixture Models in the Mole Fractions of the Oxide Components 8.4

8.2 Coefficients and Goodness-of-Fit Statistics for First-Order Mixture Models Fitted to Natural Logarithm of Electrical Conductivity at 1150°C Using Mass and Mole Fractions of the Oxide Components 8.8

8.3 Candidate Scheffé Second-Order Models Using Mass Fractions for Electrical Conductivity at 1150°C 8.14

8.4 First-Order Model and Three Candidate Second-Order Models Using Mass Fractions for Electrical Conductivity at 1150°C Fitted to CVS-I and CVS-II Phase 1 and 2 Data 8.17

9.1 Glass Transition Temperature (T_g) Data for CVS-I and CVS-II Phase 1, 2, and 3 Glasses 9.2

9.2 Coefficients and Goodness-of-Fit Statistics for First-Order Mixture Models Fitted to T_g Using Mass and Mole Fractions of the Oxide Components 9.4

9.3 Candidate Scheffé Second-Order Models Using Mass Fractions for Glass Transition Temperature 9.9

TABLES--VOLUME 1 (continued)

9.4 First-Order Model and Three Candidate Second-Order Models Using Mass Fractions for Glass Transition Temperature Fitted to CVS-I and CVS-II Phase 1 and 2 Data 9.12

10.1 Thermal Expansion Coefficient Data for Solid Glass (α_s) and Molten Glass (α_m) for CVS-I and CVS-II Phase 1, 2, and 3 Glasses 10.2

10.2 Coefficients and Goodness-of-Fit Statistics for First-Order Mixture Models Fitted to Thermal Expansion Coefficient Data for Solid Glass (α_s) and Molten Glass (α_m) Using Mass and Mole Fractions of the Oxide Components 10.6

10.3 Candidate Scheffé Second-Order Models Using Mass Fractions for Thermal Expansion of Solid Glass 10.15

10.4 Candidate Scheffé Second-Order Models Using Mass Fractions for Thermal Expansion of Molten Glass 10.16

11.1 Crystallinity Analysis of CVS-I Glasses 11.6

11.2 Crystallinity Analysis of CVS-II Glasses After Canister Centerline Cooling 11.10

11.3 Liquidus Temperature of Crystalline Phases in CVS-I Glasses 11.26

11.4 Liquidus Temperature of Crystalline Phases in CVS-II Glasses 11.29

11.5 Maximum/Minimum Single- or Multiple-Component Concentrations That Precipitated No Crystalline Phases and Minimum/Maximum Single- or Multiple-Component Concentrations That Precipitated at least One Type of Crystalline Phase During Canister Centerline Cooling (CCC) 11.47

11.6 List of Glass Data Points Used for Liquidus Temperature First-Order Mixture Models 11.57

11.7 Coefficients and Goodness-of-Fit Statistics for First-Order Mixture Models Using Mass Fractions Fitted to Liquidus Temperature (°C) Data for Three Primary Crystalline Phases . . 11.58

11.8 Summary of Comparing the Primary Phases and Their Liquidus Temperatures Predicted by the Phase-Equilibria Liquidus Temperature Model and Measured Experimentally 11.67

TABLES--VOLUME 1 (continued)

11.9 Predicted and Measured Liquidus Temperatures of Glasses for Which the Experimental Primary Phase Did Not Agree with Any of the Primary Phases Predicted by the Phase Equilibria Model, but the Glass Used a Modified Others (Group D) 11.75

11.10 Predicted (the Phase Equilibria Model) and Measured Liquidus Temperatures of Glasses with the Unidentified Experimental Primary Phase (Group E) 11.76

11.11 Predicted (the Phase Equilibria Model) Liquidus Temperatures of Glasses with No Experimentally Observed Crystalline Phase (Group F); Viscosity Data at 1150°C and at the Predicted Liquidus Temperature of the Predicted First Phase Are Also Shown 11.77

1.0 INTRODUCTION

1.1 BACKGROUND

A Hanford high-level waste (HLW) vitrification plant is planned to convert selected pretreated Hanford defense high-level and transuranic wastes to a vitrified form (borosilicate glass) for final disposal in a geologic repository. Various pretreated waste streams of different compositions are expected to be vitrified. Also, the feed delivered to a HLW vitrification plant for each specific waste type is expected to vary in composition due to incomplete mixing of storage tank contents and tank-to-tank differences. The resulting glass product composition will therefore vary for different waste types, and will vary around the nominal glass composition for a given waste type.

Changes in glass composition affect melt viscosity, electrical conductivity, and phase behavior. These properties determine the processability of the glass. Glass composition also affects chemical durability, thus impacting the acceptability of the glass product for isolation in a geologic repository.

The minimum requirements that waste forms must meet to be acceptable for disposal in a geologic repository are specified by the Waste Acceptance Product Specifications (WAPS). These specifications were originally prepared by the Waste Acceptance Committee (WAC) for the Defense Waste Processing Facility (DWPF) and by the U.S. Department of Energy (DOE) Office of Civilian Radioactive Waste Management for the West Valley Demonstration Project (WVDP) (DOE 1987 and 1988). A preliminary Waste Form Qualification (WFQ) Plan (Nelson 1988) based on the DWPF WAPS was used in preparing the initial test plan for this study. The current revision of the WAPS applicable to all waste glass producers was issued by the DOE Office of Environmental Restoration and Waste Management in February 1993 (DOE 1993).

Where possible, it is envisioned that compliance with the WAPS will be achieved in a Hanford HLW vitrification plant by process control and direct measurement of process or product variables. Direct measurements will be limited in scope due to the remote operation and shielding requirements related to the radioactive process and product. Where direct measurements are

not possible or limited (e.g., glass product composition), translation of available direct measurements (e.g., feed composition) to the required WAPS specifications will be achieved through process and product models integrated into the plant process/product control system. Applying process and product models to feed composition information will reduce the number of glass samples required to assure product compliance. Data from the Composition Variation Study (CVS) and other testing will be used to develop product and process models. These models and actual plant operating data will then be the basis for demonstrating product compliance with the WAPS requirements during cold verification and hot operation. Control of the process will be monitored by analyses of samples taken at various points in the process and evaluated using the product and process models.

1.2 CVS OVERVIEW

The CVS was originally structured to support the Hanford Waste Vitrification Plant (HWVP) concept, which was abandoned in the 1993 Tri-Party Agreement (TPA) revision (GAO 1993). The original concept was based on a melter operating at 1150°C and processing glass with 25-28% waste loading. Since the 1993 TPA revision, the CVS has been extended to include a broader range of conditions and waste glass compositions (see Section 15.2).

The goals of the portion of CVS discussed in this report were to: (1) develop glass and melt property models as functions of composition, (2) develop uncertainty equations for these models, and (3) use these models and their uncertainties to specify the region of glass compositions that will satisfy with high confidence the requirements on physical and chemical properties of the glass. This region of acceptable compositions will be referred to as the Qualified Composition Region (QCR), and the HLW vitrification plant will operate within the QCR in order to produce an acceptable waste form.

The CVS was planned and conducted in two major parts (CVS-I and CVS-II) consisting of a total of five experimental and data analysis phases (CVS-I and CVS-II Phases 1, 2, 3, and 4). This report mainly covers results through

CVS-II Phase 3, although CVS-II Phase 4 durability data and preliminary analyses thereof are included. CVS-II Phase 4 involved collecting only durability data, which became available shortly before this report was issued. Hence, most of the durability results and all of the results for other properties in this report are based only on data obtained through CVS-II Phase 3.

Each CVS phase was planned and the resulting data were analyzed using statistical experimental design and modeling techniques for mixture experiments[(a)]. Results of previous phases were used in planning subsequent phases. A total of 124 glasses were tested in CVS-I and CVS-II Phases 1, 2, and 3 with the following properties measured: viscosity, electrical conductivity, glass transition temperature, thermal expansion, crystallinity, and durability based on the Materials Characterization Center (MCC) 28-day dissolution test (MCC-1) and the 7-day Product Consistency Test (PCT). An additional 22 glasses were tested in CVS-II Phase 4, with only PCT and MCC-1 properties measured.

The overall CVS experimental strategy was to: (1) select a region of glass compositions that might be produced in the HLW vitrification plant, and that would have acceptable and "somewhat unacceptable" glass and melt properties, and (2) investigate glasses both on the exterior and interior of this region. This region was defined in terms of 10 glass (waste or frit) components: SiO_2, B_2O_3, Al_2O_3, Fe_2O_3, ZrO_2, Na_2O, Li_2O, CaO, MgO, and Others (all remaining waste components). The components and region were selected based on the four double shell tank (DST) waste types originally planned to be vitrified: Neutralized Current Acid Waste (NCAW), Neutralized Cladding Removal Waste (NCRW), Plutonium Finishing Plant (PFP) waste, and Complexant Concentrate (CC) waste.

(a) A mixture experiment is one in which two or more ingredients are combined in various proportions, one or more properties of the resulting mixtures are measured, and the resulting property data are modeled using special empirical models intended for mixtures. The book by Cornell (1990) covers the statistical experimental design and data modeling techniques that have been developed for mixture experiments since the seminal work in the late 1950s.

CVS-I involved testing 23 glasses (including 17 boundary points, 2 interior points, and 4 replicates) and fitting empirical first-order mixture experiment models to the resulting data. While these models had statistically significant lack of fits, they were adequate for determining that the number of components (10) could not be reduced in CVS-II and for refining the definition of the composition region to be studied. The report by Piepel, Hrma, et al. (1993) provides a detailed coverage of the CVS-I study.

CVS-II was planned and conducted in four phases, with the intent of generating sufficient data both on the exterior and interior of a refined (based on CVS-I results) composition region of interest to provide for fitting second-order mixture models to the property data. This report presents available results up through CVS-II Phase 3, and data and limited results from CVS-II Phase 4.

Although the scope of the CVS completed to date is fairly broad, some important (or potentially important) variables have not yet been studied. Four such variables that will be investigated as part of ongoing CVS work include: (1) solubility of minor components, (2) water content in glass, (3) oxygen potential, and (4) time-temperature history.[a] Additional explanations of these items are given in the following paragraphs.

Solubility of some minor components (Cr_2O_3, F, P_2O_5, SO_3) can substantially restrict waste loading for wastes rich in these components. This characteristic provides an economic incentive to investigate the solubility of these components as functions of composition and temperature. It is also important to determine whether excesses of these components beyond their solubility limits can be tolerated by the melter, and if so, how much.

(a) In CVS so far, minor components have been controlled as a group and make up no more than 10 wt% of any glass. This has generally kept individual components below their solubility limits. The time-temperature treatment has been the same for all glasses. Water content in glass and oxygen potential (plus redox) were not directly controlled. However, using the same batch chemicals, melting procedures, and time-temperature history for all glasses should have kept these factors within narrow limits. Further, glasses were melted and tested in random order, so that composition effects are not confounded with non-controlled variables.

Water is a minor component in glasses up to melting temperatures and may affect glass properties (glass durability and transition temperature) (Li and Tomozawa 1994). If the water content in glass produced by the melter will be different than the water content of CVS glasses, a question arises regarding the impact of this difference on glass properties. This question should be kept in mind for applications of CVS studies to the HLW vitrification plant.

Oxygen potential of the glass affects the redox state of transition metal oxides which constitute a significant portion of the waste. In particular, it affects glass crystallinity, through which it may impact glass durability. Although redox ratio was not included as a variable in this study, it should be studied in the future.

When poured into canisters, glass undergoes complex time-temperature history. Because some waste glasses partly crystalize during cooling, and crystallization may affect durability, the time-temperature history becomes an important factor determining the quality of such glasses.

The main outputs of the CVS (upon completion) will be glass and melt property data, glass and melt property models, and model uncertainty equations. These main outputs can then be used in designing glass and frit compositions for specified waste compositions, constructing/updating feed specifications, defining the QCR for a given melter type (and its operating conditions) and waste feed composition range, and developing plant operating and monitoring algorithms and software, and many other such applications. Preliminary CVS results have already been used to: (1) develop frits and glass compositions for various estimates of pretreated NCAW, NCRW, PFP, and CC wastes, (2) develop frits and glass compositions for glasses made from tank core samples, and (3) develop the Ternary Waste Envelope Assessment Tool (TWEAT). TWEAT is designed to visualize the compositional field of acceptable glasses on a ternary diagram with waste, recycle, and frit as components. For more information about TWEAT, refer to Robertus, Lambert, and Hrma (1993).

2.0 CVS OBJECTIVES

The general objective of the CVS is to conduct composition variation experiments and collect melt and glass property data to provide a basis for waste form qualification, product/process control activities, HLW vitrification plant feed specifications, and compliance with the WAPS. The related specific objectives are to:

- Define a glass composition region including glasses with acceptable as well as somewhat unacceptable property values to provide for identifying the boundary of acceptability.
- Determine the effects of the major glass components on glass and melt properties within the study region.
- Develop first- or second-order empirical mixture models as appropriate to express the glass and melt properties as functions of composition. Second-order mixture models can account for nonlinear blending effects (i.e., interactions and curvature) of the glass components on glass and melt properties that first-order models cannot account for.
- Develop equations expressing the uncertainties in property predictions made with the fitted first- and second-order property models.
- Develop a Qualified Composition Region (QCR) of glass compositions expected to satisfy melter processability constraints and WAPS requirements with acceptable confidence.
- Provide input for graphical display of properties of glass prepared by mixing HLW vitrification plant waste streams, recycle streams, and frits.
- Provide input to the HLW vitrification plant feed performance assessment for projected waste feeds.
- Provide bases for formulating optimum glass compositions (i.e., maximum waste loading within the QCR) for candidate waste feed compositions.

The experimental work and data analyses conducted to meet these objectives are discussed in detail in the remainder of this report.

3.0 MELT AND GLASS PRODUCT REQUIREMENTS

Two types of melt and glass property limitations are of concern in these studies: 1) those required for melter processability, and 2) those required by the WAPS (DOE 1993) for repository acceptance of the glass. Melter processing requirements on glass viscosity, electrical conductivity, and liquidus temperature were established for the previously planned Hanford Waste Vitrification Plant (HWVP) melter. The WAPS impose limitations on PCT durability and require that chemical and phase stability information be reported. The glass transition temperature and crystallization behavior are also required to be reported. The WAPS also specify that neither liquid-liquid phase separation nor excessively volatile or corrosive secondary phases should occur in the canister. The property limitations associated with WAPS requirements as well as the processability requirements for the previously planned HWVP melter are listed in Table 3.1 and are discussed in the following sections.

Other engineering properties of glasses and glass melts such as density, surface tension, and diffusion coefficients are also important. These properties are functions of both composition and temperature. They were not included in this study because they are not primary factors with regard to glass composition formulation or waste form acceptability.

3.1 VISCOSITY

At melter operating temperatures, industrial glasses typically have a viscosity of about 10 Pa·s [100 poise[a]]. This viscosity has been used for waste glass tests in pilot- and engineering-scale melters and is in keeping with considerable melter experience at PNL (Hagy et al. 1974, Chick et al. 1984, Goles and Nakaoka 1990, Cooper et al. 1994). The viscosity of the waste glass at the nominal melter operating temperature (1150°C) should be between 2 and 10 Pa·s for optimum operation. This viscosity range corresponds

---

(a) The Standard International unit for viscosity is Pa·s. The older unit, poise, is no longer accepted internationally (1 Pa·s = 10 poise).

TABLE 3.1. Glass Property Acceptability Criteria for an 1150°C Melter

Property	Acceptability Criteria
Viscosity at 1150°C	2 - 10 Pa·s[a]
Electrical conductivity at 1150°C	10 - 100 S/m[b]
Liquidus temperature	≤ 1050°C[c]
Phase separation	No liquid-liquid separation in the melter
Dissolution rate in deionized water[d]	
PCT (7-day, A/V = 2000 m^{-1})	≤ EA glass[e]
B normalized release	8.2 g/m^2
Li normalized release	4.8 g/m^2
Na normalized release	6.6 g/m^2
Glass transition temperature[f]	Descriptive
Devitrification during cooling[g]	Descriptive
Other processability aspects[h]	

(a) See discussion in Section 3.1.

(b) S/m = Siemens/m = Ohm^{-1}/m. Limits of 18 - 50 S/m were used in planning and conducting the CVS through CVS-II Phase 2. The rationale for the 10 - 100 S/m limits is given in Section 3.2.

(c) See discussion in Section 3.3.

(d) Earlier versions of the WAPS (DOE 1987, 1988) specified an upper limit of 1 $g/m^2 \cdot day$ on normalized releases of sodium, silicon, boron, cesium-137, and uranium-238 averaged over a 28-day MCC-1 dissolution test with A/V = 10 m^{-1}. The current WAPS (DOE 1993) specify that PCT normalized elemental releases of boron, lithium, and sodium be less than that of the DWPF Environmental Assessment (EA) glass. These criteria will be applied to both quenched and canister centerline cooled glasses for application to a Hanford HLW vitrification plant.

(e) The numerical values for the normalized boron, lithium, and sodium PCT releases of the DWPF Environmental Assessment (EA) glass are preliminary values taken from Table 2 of the DWPF Waste Form Qualification Report (WQR) Volume 5 (WSRC 1993) based on work reported by Jantzen et al. (1993). The values listed in these references are in units of g/L, which involves normalizing for the concentration of an element in the glass, but not for the A/V. For an assumed A/V = 2000 m^{-1} for the PCT, the conversion of units from g/L to g/m^2 involves dividing by two.

(f) The WAPS do not specify an acceptability limit for glass transition temperature (T_g), but they do require that it be reported and that glass producers certify that glass temperature does not exceed 400°C after initial cooldown.

(g) The WAPS do not set a limit on the amount of crystalline material in the glass, but do require that crystalline material expected to be present be characterized.

(h) Work outside the CVS will address other processability aspects, such as feed requirements to limit foaming and guarantee a stable cold cap that melts at an acceptable rate.

approximately to a range of 1050 to 1150°C on T_{10}, the temperature at which viscosity is 10 Pa·s.

If the viscosity at 1150°C is outside the range of 2 to 10 Pa·s, processing problems may be encountered in the melter. Glass with viscosity lower than 2 Pa·s tends to penetrate into the melter bricks and to excessively corrode melter walls. Glass with viscosity higher than 10 Pa·s causes slow melting rate, is difficult to pour from the melter, and may not form a consolidated monolith in the canisters.

3.2 ELECTRICAL CONDUCTIVITY

In joule-heated ceramic melters designed at PNL, the electrical conductivity of the glass melt should be in the range 18 to 50 S/m[(a)] at 1150°C (according to an 1984 unpublished monthly report by J.E. Minor). This range was used in planning the CVS up through CVS-II Phase 2. However, in the DWPF melter design (which was specified for the previously planned HWVP), the acceptable range for electrical conductivity at 1150°C was determined to be 36 to 111 S/m (Bickford et al. 1990). Subsequently, DWPF dropped this electrical conductivity requirement as being unnecessary for glasses they expect to make. However, because electrical conductivity has restricted the CVS composition region studied so far, electrical conductivity acceptability criteria are retained for the time being.

The electrical conductivity range acceptable for the previously planned HWVP was expanded from 18 - 50 S/m (which was used through CVS-II Phase 2) to 10 - 100 S/m. Glass must have electrical conductivity at melter operating temperature at least two orders of magnitude higher than the refractory material of the melter walls. These materials never have electrical conductivity at 1150°C higher than 0.1 S/m (Begley 1974, p. 435). Hence, 10 S/m is a safe and acceptable lower limit for electrical conductivity at 1150°C. The upper limit of 100 S/m is an order of magnitude higher than the lower limit and is in the vicinity of the 111 S/m value estimated by Bickford et al. (1990).

(a) S/m = Siemens/m = Ohm^{-1}/m.

A low electrical conductivity at the melting temperature would require a higher voltage across the electrodes resulting in conduction within the melter refractory. The glass-contact refractory proposed for the previously planned HWVP melter was Monofrax K3 (57% Al_2O_3, 6.1% MgO, 5.9% Fe_2O_3, 1.6% LiO_2, 0.3% Na_2O and 0.4% Other). The electrical conductivity of this material is 0.5 S/m at 1150°C and 1.0 S/m at 1250°C. Thus, the lower limit of 18 S/m for the melt provides a sufficient safety margin. A low electrical conductivity could also cause melter start-up difficulties unless undesirably large electrical power systems are supplied. If the electrical conductivity is too high, the current required to heat the glass will exceed the recommended maximum density for the melter electrodes.

3.3 LIQUIDUS TEMPERATURE

The temperature at which the melt is in equilibrium with the primary crystalline phase is called the liquidus temperature (T_L). The previously planned HWVP adopted the DWPF criterion for T_L, which specifies an upper limit of 1050°C. Only minor crystalline phases such as the insoluble noble metals or their oxides should be present at 1050°C or higher temperatures. In addition, no excessive crystallization or phase separation should occur in the glass melter. The presence of insoluble and residual solid phases may increase the rate at which a sludge forms on the bottom of the melter, clog areas within the melter, and possibly short the melter electrodes (if the phases are conductive). Radionuclides such as cesium may be concentrated in a separated melt phase such as an alkali-sulfate melt. Such a phase may exhibit excessive volatility causing off-gas system clogging, electrical shorting, and increased corrosion of melter walls and electrodes.

3.4 TIME-TEMPERATURE-TRANSFORMATION

Crystallization is a concern in nuclear waste glass because it may adversely effect the durability and strength of some glasses. For this reason, WAPS (1993) has specified that:

"A time-temperature-transformation (TTT) diagram that identifies the duration of exposure at any temperature that causes significant changes in either the phase structure or the phase compositions ... shall be provided ..."

This requirement is descriptive, not restrictive, in nature (i.e., there are no restrictions on the crystalline content of waste glass). In addition to TTT diagrams, WAPS requires that the test methods used to develop the diagrams be described.

For a given glass composition, crystallization depends on the temperature history of the glass. Theoretically, crystallization kinetics can be determined from the TTT diagrams. For practical purposes, TTT diagrams allow the effects of varied temperature histories during processing or accident scenarios (i.e., transportation fires) to be assessed.

To accurately describe crystallinity by TTT, two test methods (isothermal and non-isothermal) are combined (Cahn and Haasen 1983). Isothermal TTT diagrams are generated by heat treating a series of samples so that each sample is held at a single temperature for a predetermined time. Generally, the temperatures range from the glass transition temperature to the liquidus temperature. For non-isothermal TTT diagrams each sample is cooled at a constant rate and for a set time. The cooling rates range from quench rate to below canister centerline cooling rate. To complete the TTT diagram, constant heating rate tests must also be done. Constant heating tests are done in much the same manner as constant cooling tests. The non-isothermal method requires an increase in time and labor, but more closely represents the time temperature schedule of a waste glass and may yield more relevant results.

TTT diagrams will be developed in FY1994 for HW-39-4 glass. This testing will be conducted by both isothermal and non-isothermal methods and will be followed by direct measurement of the effect of crystallinity on glass durability (see Chapter 11 and Section 12.11).

3.5 GLASS TRANSITION TEMPERATURE

The glass transition temperature (T_g) characterizes the transformation from an equilibrated melt to a "frozen" glass structure. At the glass transition temperature, thermal expansion, heat capacity, and other properties change abruptly.

The WAPS does not currently specify any limitations on glass transition temperature. However, the WAPS does require that: (1) T_g be reported as a descriptive property and (2) glass producers certify that after initial cooldown the waste form temperature was maintained below 400°C.

3.6 THERMAL EXPANSION

Thermal expansion coefficients of solid (α_s) and molten (α_m) glass are obtained as by-products of the T_g measurement, and therefore are also obtained as part of CVS testing. Although the WAPS do not specify any limits on thermal expansion of solid and molten glass, thermal expansion coefficients are important for glass processing and product properties. Thermal expansion of molten glass causes natural convection in the melter, and thus is responsible for heat transfer from molten glass to the cold cap. Thermal expansion of solid glass can be used to estimate: (1) thermal stresses when blocks of glass are cooled, and (2) chemical stresses caused by crystallization. Stress affects glass cracking and may enhance glass corrosion rate to some extent.

3.7 DURABILITY

Initial versions of the WAPS (DOE 1987, 1988) required the waste form to be capable of limiting normalized elemental release rates for sodium, silicon, boron, cesium-137, and uranium-238 to less than a 1.0 $g/m^2 \cdot day$ averaged over a 28-day MCC-1 test (MCC 1983). In other words, the normalized elemental releases determined by the 28-day MCC-1 test should not exceed 28 g/m^2. However, the WAPS have been revised (DOE 1993), and now require that the normalized releases of boron, lithium, and sodium determined by the PCT be less than the releases of these elements from the DWPF Environmental Assessment (EA) glass (DOE 1982). The EA elemental release values are not specified in the revised WAPS and have not yet been formally established.

Preliminary normalized boron, lithium, and sodium release values for the EA glass have been determined and reported by the DWPF program (WSRC 1993, based on results in Jantzen et al. 1993). The normalized release values listed in these references are in units of g/L, which involves normalizing for the concentration of an element in the glass, but not for the surface area to volume ratio (A/V). For an assumed A/V = 2000 m^{-1} for the PCT, converting g/L to g/m^2 involves dividing by two. The values reported by WSRC (1993), except expressed in the g/m^2 units being used in the CVS, are listed in Table 3.1.

The 28-day MCC-1 normalized elemental release limit of 1.0 $g/(m^2 \cdot day)$ was used as one of the bases for determining the compositional region and glass compositions within it to be studied during CVS. PCT releases were also considered for purposes of planning CVS, although indirectly for CVS-I and CVS-II Phases 1 and 2 because of the absence of established limits for normalized releases of boron, lithium, and sodium from the EA glass. PCT releases and rough estimates of EA glass releases were directly used in planning CVS-II Phase 3 (see Table 4.6 and Section 4.4).

The MCC-1 dissolution test was issued by the Materials Characterization Center.[a] The PCT (Jantzen et al. 1992) was developed at the Savannah River Technology Center for use by DWPF. Testing CVS glasses with both the MCC-1 test and the PCT is expected to fulfill the durability information requirements of the WAPS. Because the MCC-1 test and PCT are standard tests used to evaluate the durability of waste glasses, the dissolution behavior of CVS glasses can be compared to glasses developed for the Savannah River and West Valley programs (that have been tested by MCC-1 and PCT).

(a) Operated by Pacific Northwest Laboratory, Richland, Washington.

4.0 EXPERIMENTAL DESIGN

The CVS was designed in five phases so that the results of previous phases could be used in planning later phases. The glasses tested in each of the CVS phases (CVS-I and CVS-II Phases 1, 2, 3, and 4) were selected according to an overall strategy using statistical experimental design methodology and software. The experimental design strategy, methodology, and software are discussed in Section 4.1. The specific composition subregions and glasses tested during each phase of CVS are discussed in Sections 4.2 through 4.6. Section 4.7 combines all five phases of the experimental design and investigates pairwise correlations among the 10 oxide components. Section 4.8 presents and discusses mole fraction compositions of the CVS glasses.

4.1 EXPERIMENTAL DESIGN STRATEGY AND METHODOLOGY

The general statistical experimental design strategy for the CVS is discussed in Section 4.1.1. The methodology used to implement the strategy is discussed in Section 4.1.2.

4.1.1 Experimental Design Strategy

The statistical experimental design strategy used in the CVS involved defining a glass composition region expected to contain glasses that might be made from various waste types expected to be processed by the previously planned HWVP, and then selecting specific compositions for study so as to appropriately cover this region (referred to as the "experimental region"). Compositions on the exterior of the experimental region provide for identifying the boundary between acceptable and unacceptable glasses, and also have the greatest impact in reducing the imprecision of predictions made with models fitted to the data. However, it is also necessary to test glasses on the interior of the experimental region to assure that the fitted models will accurately predict glass properties there. Exterior and interior compositions were tested during the various CVS experimental phases so as to provide a basis for developing accurate and precise property prediction models.

This general strategy was implemented in the CVS by defining several subregions of the overall composition experimental region, and selecting points on the boundaries and interiors of these subregions so that a good coverage of the overall region was obtained. The initial overall experimental region used in CVS-I (discussed in Section 4.2) and the various subregions used in the four phases of CVS-II were defined using two types of constraints. Single-component constraints consist of lower and upper limits on each of the 10 glass components. Multiple-component constraints consist of lower and/or upper limits on ratios or linear combinations of glass components. In general, the experimental region and subregions defined by single- and multiple-component constraints in CVS are polyhedrons in nine dimensions (one less than the number of components, because of the restriction that the component mass or mole fractions must sum to one). Details about the constraints for the regions used in the CVS experimental design are presented in Sections 4.2 through 4.6.

4.1.2 Mixture and Optimal Experimental Design Methodology

Statistical mixture experiment design and optimal experimental design methods and software were used to select the glasses tested during CVS-I and CVS-II Phases 1, 2, 3, and 4. A mixture experiment is one in which two or more ingredients are mixed together in various proportions (which must sum to one) and one or more properties of the resulting mixture are measured. Special methods for the statistical design and analysis of mixture experiments have been developed and published since 1955, and are summarized in the book by Cornell (1990).

Optimal experimental design (OED) is a general term referring to a wide variety of techniques used in selecting experimental points so as to optimize various statistical properties of the resulting experimental designs (test matrices). The same basic OED implementation was used in CVS-I and CVS-II Phases 1, 2, and 3, and involved: (1) defining a subregion of the whole composition experimental region via upper and lower bounds on individual glass components and on linear combinations of glass components, (2) generating the vertices of the subregion using the CONVRT (Piepel 1988) or MIXSOFT™ (Piepel

1992) software, (3) choosing a statistical experimental design optimality criterion, and (4) selecting a subset of the vertices using the DETMAX (Mitchell 1974) or ACED (Welch 1987) software so as to optimize (or nearly optimize) the statistical criterion chosen. The two optimality criteria considered were D-optimality (minimizing the determinant of the matrix $(X'X)^{-1}$, where X is the test matrix expanded in the form of the property model to be fitted) and G-optimality (minimizing the maximum prediction variance of the fitted property model). Both criteria tend to select design points that evenly cover the boundary of the subregion, and typically designs that are "good" (optimal or nearly optimal) for one criterion are "good" for the other. (Appendix I further discusses model uncertainty, which depends on the $(X'X)^{-1}$ matrix, and hence the experimental design in matrix X.)

The glasses tested in CVS-II Phase 4 were selected by varying selected components one-at-a-time (within the mixture experiment framework). Varying components one-at-a-time is a non-optimum experimental approach when it is the only approach used, but can be very informative when used in conjunction with studying many-at-a-time changes in the components (as was done in phases prior to CVS-II Phase 4).

As noted earlier, in order to satisfy the overall strategy of selecting both exterior and interior points of the composition experimental region, various subregions were defined so that the vertices of the subregions lie in desired exterior or interior portions of the experimental region. Then, the subset of points (vertices) optimally selected for each subregion successfully covers that subregion, and the collection of all such subsets of points covers the whole composition experimental region (provided the subregions are appropriately chosen). The subregions chosen and test matrices selected for each phase of the CVS are discussed in the following sections.

4.2 CVS-I COMPOSITION REGION AND TEST MATRIX

A detailed discussion of the CVS-I composition experimental region and test matrix is given in the report by Piepel, Hrma, et al. (1993). A brief version of that discussion is given here to provide the appropriate background for the CVS-II phases discussed in the succeeding subsections.

4.2.1 Glass Components Studied in CVS-I

Based on results of previously completed scoping studies (from several unpublished project reports from 1985-1987), preliminary information on estimated waste feed compositions for the four waste types that were to be processed by HWVP (NCAW, NCRW, PFP, and CC), feasible frit compositions, and expected CVS resources, the 10 glass components SiO_2, B_2O_3, Na_2O, Li_2O, CaO, MgO, Fe_2O_3, Al_2O_3, ZrO_2, and Others were selected for study in CVS-I. The first nine components comprise the possible frit constituents (SiO_2, B_2O_3, Na_2O, Li_2O, CaO, and MgO) and the major waste constituents (SiO_2, Na_2O, CaO, MgO, Fe_2O_3, Al_2O_3, and ZrO_2). They were also the nine components expected to most significantly affect glass properties when varied over their anticipated ranges.

The tenth component, Others, consists of the remaining waste constituents (except for those such as total organic carbon and NO_x that will not end up in the glass). The composition of the Others mix used in CVS-I was based on the NCAW-87 waste composition, and is shown as the "Substitute Others" column in Table 4.1. As indicated there, the radioactive component (U_3O_8), a highly toxic component (BeO), and some rare earth components (Eu_2O_3 and Pm_2O_3) were replaced by Nd_2O_3 or MgO. Substitutions were made on a molar basis. Some minor components ($\leq$ 0.4 wt% in the waste) and technetium (1.59 wt% in the waste) were deleted, and the remaining constituents were renormalized to 100%.

4.2.2 CVS-I Composition Region

The composition region studied during CVS-I is described in Table 4.2. The single component constraints (lower and upper bounds for each of the 10 components) were selected based on potential waste and glass variations and on the results of the scoping studies mentioned in Section 4.2.1. Multiple-component constraints were specified in an attempt (only partially successful) to eliminate compositions with poor melt or glass properties. Based on the scoping studies, constraints to eliminate high viscosity glasses and highly crystalline glasses were estimated and are shown in Table 4.2. The crystallinity constraints include magnesium silicate and calcium zircon silicate (the

TABLE 4.1. Composition of the Others Component for NCAW Waste

Oxide	NCAW-87 Normalized Others (wt%)	Substitute Others (a) (wt%)	Oxide	NCAW-87 Normalized Others (wt%)	Substitute Others (a) (wt%)
NiO	9.13	10.30	Sm_2O_3	0.79	0.90
La_2O_3	9.92	11.19	Y_2O_3	0.79	0.90
Nd_2O_3	7.94	22.09	BeO	0.40	SUB Mg
SO_3	4.37	4.93	NpO_2	0.40	DEL
F	4.76	5.37	TeO_2	0.40	DEL
MoO_3	4.76	5.37	K_2O	0.20	DEL
U_3O_8	18.65	SUB Nd	PbO_2	0.20	DEL
CeO_2	2.38	2.69	SeO_2	0.12	DEL
Cs_2O	2.38	2.69	Am_2O_3	0.08	DEL
CuO	2.38	2.69	CdO	11.90	13.43
MnO_2	2.38	2.69	Eu_2O_3	0.08	SUB Nd
RuO_2	2.38	2.69	P_2O_5	1.59	1.79
Cr_2O_3	1.98	2.24	PuO_2	0.08	DEL
BaO	1.59	1.79	SnO_2	0.16	DEL
Pr_6O_{11}	1.59	1.79	Ag_2O	0.04	DEL
SrO	1.59	1.79	Gd_2O_3	0.04	DEL
Tc_2O_7	1.59	DEL	Nb_2O_5	0.04	DEL
PdO	0.79	0.90	Pm_2O_3	0.40	SUB Nd
Rb_2O	0.79	0.90	Ta_2O_5	0.12	DEL
Rh_2O_3	0.79	0.90	TiO_2	0.04	DEL
				100.0	100.0

(a) DEL and SUB indicate the corresponding oxide was deleted or substituted for in the simulated waste used in CVS glasses. These deletions and substitutions are not expected to significantly affect glass properties.

TABLE 4.2. Composition Region (mass fractions) Studied in CVS-I

Single-Component Constraints

	HW-39-4	Lower Limit	Upper Limit
SiO_2	.5353	.42	.57
B_2O_3	.1053	.05	.20
Na_2O	.1125	.05	.20
Li_2O	.0375	.01	.07
CaO	.0083	0	.10
MgO	.0084	0	.08
Fe_2O_3	.0719	.02	.15
Al_2O_3	.0231	0	.15
ZrO_2	.0385	0	.13
Others	.0592	.01	.10

An implicit constraint on the components is that their mass fractions must sum to 1.0.

Multiple-Component Constraints	Lower Limit	Upper Limit
Viscosity:		
$(Na_2O + Li_2O)/(SiO_2 + Al_2O_3 + ZrO_2)$	0.152	0.342
Crystallinity:		
SiO_2 / Al_2O_3	3.0	-----
MgO + CaO	---	0.10
$Al_2O_3 + ZrO_2$	---	0.16
$Fe_2O_3 + Al_2O_3 + ZrO_2$ + Others	---	0.24

TABLE 4.3. DWPF and Preliminary Hanford HLW Vitrification Solubility Limits

Preliminary Hanford HLW Vitrification[a] Solubility Limits (mass fractions)	DWPF Solubility[b] Limits (mass fractions)
$Cr_2O_3 \leq 0.005$	$Cr_2O_3 \leq 0.003$
$P_2O_5 \leq 0.010$	$PO_4 \leq 0.03$
$SO_3 \leq 0.005$	$SO_4 \leq 0.004$
$F \leq 0.017$	$TiO_2 \leq 0.01$
Rh_2O_3, PdO, and $Ru_2O_3 \leq 0.025$	NaF ≤ 0.01
	NaCl ≤ 0.006

(a) Unpublished 1987 project report by S.O. Bates.

(b) Bickford et al. (1990).

second crystallinity constraint), zircon silicate (the third crystallinity constraint), and spinel (the fourth crystallinity constraint). No constraints were estimated for electrical conductivity or glass durability.

Solubility limits and liquid-liquid separation limits for Cr_2O_3, F, P_2O_5, SO_3, and noble metal oxides were previously determined in scoping studies predating the CVS. The effects of P_2O_5 concentration in borosilicate glasses were studied by Vogel (1971). The previously developed solubility and liquid-liquid separation limits are summarized in Table 4.3. However, these limits may not be generally applicable over the whole CVS composition experimental region, because: (1) they were determined from several small studies based on the HW-39 composition and (2) the constraints in some cases were based on one-at-a-time experimental methods. Hence, the constraints may be too small for some compositions in the CVS composition region under study and too large for others.

For comparison purposes, the DWPF solubility and liquid-liquid separation limits are also listed in Table 4.3. The differences between the preliminary Hanford HLW vitrification plant values and the DWPF values need to be evaluated. This evaluation will involve determining what was done to arrive at each set of values, and how robust the values are to variations in glass composition. Because solubility and liquid-liquid separation limits are expected to be dependent on glass composition, it may not be possible to specify a single set of values that applies to the whole composition experimental region. Experimentation may be necessary to resolve these questions.

4.2.3 CVS-I Test Matrix

The CVS-I test matrix is given in Table 4.4. It consists of seventeen vertices, two interior points, and four replicates corresponding to the composition region defined in Table 4.2. The 1820 vertices of the composition region were generated using the CONVRT software (Piepel 1988). The ACED (Welch 1987) software was then used to select 17 of the vertices to provide an even coverage of the boundary of the composition region and good support for fitting first-order mixture models. One of the interior points is the overall

TABLE 4.4. Glass Compositions (mass fractions) Tested in CVS-I

Glass[a]	Run[b] Order	SiO_2	B_2O_3	Na_2O	Li_2O	CaO	MgO	Fe_2O_3	Al_2O_3	ZrO_2	Others[c]
CVS1-1 (1)	4	.4801	.1142	.1003	.0376	.0275	.0363	.0568	.0636	.0429	.0407
CVS1-2	10	.5500	.0500	.0500	.0700	.1000	.0000	.0200	.1500	.0000	.0100
CVS1-3	17	.4200	.2000	.0500	.0700	.0000	.0800	.0200	.1400	.0100	.0100
CVS1-4 (2)	12	.5700	.2000	.0900	.0100	.0200	.0800	.0200	.0000	.0000	.0100
CVS1-5	3	.5700	.0500	.0700	.0700	.0000	.0000	.1500	.0800	.0000	.0100
CVS1-6	5	.4400	.2000	.0500	.0700	.0000	.0000	.0200	.0000	.1200	.1000
CVS1-7	7	.5700	.0500	.0964	.0100	.1000	.0000	.0336	.0000	.1300	.0100
CVS1-8 (3)	9	.5363	.0500	.0837	.0100	.0000	.0800	.1500	.0000	.0800	.0100
CVS1-9	15	.4200	.1962	.0538	.0100	.0000	.0800	.1400	.0000	.0000	.1000
CVS1-10	6	.5700	.0851	.0949	.0100	.0000	.0000	.0200	.1200	.0000	.1000
CVS1-11	8	.4200	.1549	.0751	.0100	.1000	.0000	.0200	.1400	.0000	.0800
CVS1-12	16	.4200	.1764	.0736	.0700	.1000	.0000	.1500	.0000	.0000	.0100
CVS1-13	14	.5700	.2000	.1862	.0100	.0000	.0000	.0200	.0038	.0000	.0100
CVS1-14	22	.4200	.2000	.1862	.0100	.0000	.0000	.0200	.0238	.1300	.0100
CVS1-15	11	.5589	.0500	.1211	.0700	.0000	.0800	.0200	.0000	.0000	.1000
CVS1-16	2	.4327	.0500	.1873	.0100	.0000	.0800	.0858	.1442	.0000	.0100
CVS1-17	19	.4545	.0500	.1455	.0100	.1000	.0000	.1400	.0000	.0000	.1000
CVS1-18	18	.4214	.0500	.1186	.0700	.0200	.0800	.0200	.0000	.1300	.0900
CVS1-19 (1)	13	.4801	.1142	.1003	.0376	.0275	.0363	.0568	.0636	.0429	.0407
CVS1-20 (1)	21	.4801	.1142	.1003	.0376	.0275	.0363	.0568	.0636	.0429	.0407
CVS1-21 (2)	1	.5700	.2000	.0900	.0100	.0200	.0800	.0200	.0000	.0000	.0100
CVS1-22 (3)	20	.5363	.0500	.0837	.0100	.0000	.0800	.1500	.0000	.0800	.0100
CVS1-23	23	.5153	.0956	.1052	.0375	.0289	.0084	.1179	.0456	.0063	.0393

(a) CVS1-1 is the center point and CVS1-2 to CVS1-18 are vertices of the CVS-1 experimental region defined in Table 4.2. CVS1-23 is the HW-39-2 glass composition. The numbers in parentheses following the glass name denote replicate sets of glasses.

(b) Glasses were fabricated and tested in this random run order.

(c) The composition of the Others component is given in the Substitute Others column of Table 4.1.

center point of the composition region, and the other is the HW-39-2 composition. Two replicates of the overall center point and single replicates of two different vertices were also included in the test matrix.

The test matrix includes 19 distinct compositions, while the first-order mixture model only has 10 terms, so a nine-degree-of-freedom estimate of model lack-of-fit can be obtained. The four replicate points provide for a four-degree-of-freedom estimate of experimental error to statistically test the significance of the first-order model lack-of-fit (for each property of interest). Although first-order (linear) mixture models do not provide for modeling nonlinear blending behavior of the components, such information is included in the property data because the test matrix involved varying all

components simultaneously.[a] Nonlinear blending behavior of the glass components is expected, and will contribute to the lack-of-fit of the first-order mixture models.

Table 4.5 contains pairwise Pearson correlation coefficients among the 10 CVS-I glass components. Pearson correlation coefficients take values between -1.0 and +1.0, and indicate the strength of the linear relationship between two variables (two glass components in this case). Correlations of -1.0 and +1.0 represent perfect linear relationships with negative and positive slopes, respectively. A correlation of 0.0 represents a total lack

TABLE 4.5. Pairwise Correlations[a] Among Glass Components[b] for CVS-I Glasses

	SiO_2	B_2O_3	Na_2O	Li_2O	CaO	MgO	Fe_2O_3	Al_2O_3	ZrO_2
B_2O_3	-0.286								
Na_2O	-0.033	-0.093							
Li_2O	-0.167	-0.093	-0.410						
CaO	-0.105	-0.166	-0.169	0.034					
MgO	-0.026	-0.026	-0.061	-0.075	-0.499				
Fe_2O_3	-0.089	-0.316	-0.119	-0.086	0.034	0.052			
Al_2O_3	-0.140	-0.142	-0.121	0.142	0.106	-0.165	-0.231		
ZrO_2	-0.186	-0.103	0.081	0.018	-0.103	-0.023	-0.152	-0.382	
Others	-0.288	-0.076	-0.101	0.101	-0.002	-0.059	-0.107	-0.099	-0.005

(a) Pearson correlation coefficients take values between -1.0 and +1.0, and indicate the strength of the linear relationship between a pair of variables. Correlations of -1.0 and +1.0 represent perfect linear relationships with negative and positive slopes, respectively. A correlation of 0.0 represents a total lack of a linear relationship. Underlined values are statistically significant at the 90% confidence level.

(b) As-batched compositions of the glasses listed in Table 4.4 were used.

(a) This experimental design strategy is in contrast to the common, but inefficient and potentially misleading, experimental strategy of varying components one-at-a-time. One-at-a-time experimentation is inefficient in that many experiments are required to learn about individual component effects only, and potentially misleading because information about interactive/nonlinear behavior of the components is not obtained.

of a linear relationship. Because glass mass fractions must sum to 1.0, both positive and negative correlations between pairs of components must exist. Correlations greater than 0.6 - 0.8 (in absolute value) indicate the presence of significant confounding between pairs of components. This means that the components tend to vary together rather strongly over the data set being investigated, and this can make it difficult or impossible for empirical mixture models fitted to the data set to properly separate the effect of one component from the effect of the other. Hence, correlation coefficients among pairs of components were investigated during test matrix development to make sure confounding of components was not unacceptably high.

Three correlations are identified as statistically significant (at 90% confidence level or higher) in Table 4.5: Li_2O with Na_2O (-0.410), MgO with CaO (-0.499), and ZrO_2 with Al_2O_3 (-0.382). These significant correlations are due to the multiple-component constraints used to define the experimental region, and hence were unavoidable. Although statistically significant, these correlations do not represent major confounding of component effects, and thus the impact on empirical mixture modeling should be minimal.

4.3 CVS-II PHASE 1 COMPOSITION REGION AND TEST MATRIX

The CVS-II Phase 1 composition subregion and test matrix are defined and discussed in Sections 4.3.1 and 4.3.2, respectively.

4.3.1 CVS-II Phase 1 Composition Region

Due to the unacceptable property values (mainly MCC-1 durability and crystallinity) obtained for several CVS-I glasses, it was clear that the CVS-I composition region was too large in some directions and needed to be reduced for CVS-II. However, because the CVS-I property model data analyses were not complete at the time Phase 1 of CVS-II was being planned, revision of the CVS-I composition region was postponed until CVS-II Phase 2. In CVS-II Phase 1, it was decided to test glasses on an "inner shell" of the CVS-I region that would probably have acceptable properties. This decision was in keeping with the overall CVS strategy of testing interior and exterior glasses in the composition experimental region.

The individual component lower and upper bounds for the CVS-II Phase 1 subregion were obtained by reducing by roughly one-third the distance between the HW-39-4 value for each component and the CVS-I lower and upper bounds. The lower and upper limits for the crystallinity multiple-component constraints were reduced sufficiently from CVS-I values with the plan of avoiding crystallinity. In addition, a new multiple-component crystallinity constraint involving the sum of MgO, CaO, and ZrO_2 was used.

Property constraints on viscosity at 1150°C, electrical conductivity at 1150°C, and normalized Li release (based on linear mixture models fitted to the CVS-I data) were also used to define the CVS-II Phase 1 composition subregion. The viscosity at 1150°C constraint replaced the multiple-component constraint used to indirectly restrict viscosity in CVS-I (see Table 4.2). The normalized Li release model was selected for use in the durability constraint because Li releases tended to be the largest elemental releases observed in the CVS-I results.

The CVS-II Phase 1 composition subregion is defined in the Phase 1 columns of Table 4.6. Table 4.6 also contains columns describing the composition subregions studied in CVS-II Phases 2 and 3, which are discussed in Sections 4.4 and 4.5.

4.3.2 CVS-II Phase 1 Test Matrix

In CVS-II Phase 1, 19 glasses were melted and tested. The test matrix for CVS-II Phase 1 is listed in Table 4.7, and consists of 15 vertices of the CVS-II Phase 1 composition subregion, three interior points, and a replicate point. The same NCAW-based Others mix as used in CVS-I (see Table 4.1) was used (except for the internal standard glass, see Table 4.8). The test matrix was developed as follows.

First, the 3312 vertices of the CVS-II Phase 1 composition subregion (as defined in Table 4.6) were generated using the MCCVRT routine from the MIXSOFT™ package (Piepel 1989). The MCCVRT routine is an updated and renamed version of the CONVRT routine (Piepel 1988) used to generate the vertices for CVS-I. The ACED (Welch 1987) software was then used to select 15 of the

TABLE 4.6. Composition Subregions Studied During CVS-II

Individual Component Lower and Upper Bounds (mass fractions)

Oxide	HW-39-4	Phase 1		Phase 2a[a]		Phase 2b[a]		Phase 3		Phase 4[b]	
		Lower Bound	Upper Bound	Lower Bound	Upper Bound	Lower Bound	Upper Bound	Lower Bound	Upper Bound	Lower Bound	Upper Bound
SiO_2	.5353	.46	.56	.42	.57	.46	.57	.44	.56	.41	.57
B_2O_3	.1053	.07	.17	.05	.20	.05	.15	.06	.16	.05	.20
Na_2O	.1125	.07	.17	.05	.20	.05	.15	.05	.18	.05	.20
Li_2O	.0375	.02	.06	.01	.07	.01	.07	.01	.07	.01	.07
CaO	.0083	0	.07	0	.10	.02	.05	.005	.04	.0072	.02
MgO	.0084	0	.05	0	.08	.02	.05	.005	.04	0	.02
Fe_2O_3	.0719	.04	.12	.02	.15	.02	.10	.005	.105	.0626	.0913
Al_2O_3	.0231	.01	.11	0	.15	.03	.10	.02	.17	0	.15
ZrO_2	.0385	.01	.10	0	.13	.02	.07	.005	.11	.0355	.0489
Others	.0592	.025	.08	.01	.10	.03	.07	.02	.09	.0515	.0752

Stand-In[c] Crystallinity Constraints

Oxide Ratio or Sum of Mass Fractions	Phase 1		Phase 2a		Phase 2b		Phase 3	
	Lower Bound	Upper Bound	Lower Bound	Upper Bound	Lower Bound	Upper Bound	Lower Bound	Upper Bound
SiO_2/Al_2O_3	4.5	---	3.0	---	---	---	---	---
MgO+CaO	---	.08	---	.08	---	.07	---	.045
$Fe_2O_3+Al_2O_3+ZrO_2+$Others	---	.21	---	.21(e)	---	.18	---	.225
$Al_2O_3+ZrO_2$	---	.14	---	.14	---	.12	---	.18
$MgO+CaO+ZrO_2$	---	.18(d)	---	.18(e)	---	.12	---	.12

(a) Glasses were selected for the test matrix of CVS-II Phase 2 from two regions of composition space. Region 2a is a revision of the CVS-I region containing glasses with good and not-too-bad property values, whereas Region 2b is an interior subregion of Region 2a.

(b) CVS-II Phase 4 involves varying selected components (SiO_2, B_2O_3, Na_2O, Li_2O, CaO, MgO, and Al_2O_3) one-at-a-time while keeping the other components in the same relative proportions as in the HW-39-4 glass. Of the seven listed components, all were varied from the lower to upper bounds shown, except for Ca which was not varied to zero. The components Fe_2O_3, ZrO_2, and Others were not varied one-at-a-time (see Section 4.6).

(c) In the absence of liquidus temperature or crystallinity data early in the CVS, these constraints based on engineering correlation work and experimental scoping studies were developed to use on a stand-in basis until constraints based on liquidus temperature models could be developed.

(d) For information only, since this bound is implied by other constraints.

(e) Some vertices of the region with $Fe_2O_3+Al_2O_3+ZrO_2+$Others= 0.21 and/or $MgO+CaO+ZrO_2$ = 0.18 were determined to have substantial crystallinity problems, and were replaced with vertices from a modified region with $Fe_2O_3+Al_2O_3+ZrO_2+$Others = 0.18 and $MgO+CaO+ZrO_2$ = 0.15.

TABLE 4.6. Composition Subregions Studied During CVS-II (continued)

CVS-II Property Constraints[f]

Property	Units	Accept. Range	Phase 1 Lower Bound	Phase 1 Upper Bound	Phase 2a Lower Bound	Phase 2a Upper Bound	Phase 2b Lower Bound	Phase 2b Upper Bound	Phase 3 Lower Bound	Phase 3 Upper Bound
T_{10} (g)	°C	1050-1150	---	--	---	--	1075	1125	---	---
V(1150°C)	Pa·s	2-10	4	8	1.5	12	4.5	7.5	.5	20
E(1150°C)	S/m	18-50 (l)	22	40	12	60	28	39	5	130
MCC-1 Li (h)	g/m^2	< 28	---	28	---	50	---	28	---	---
MCC-1 Li (i)	g/m^2	< 28	---	20	---	40	---	16	---	---
MCC-1 B (j)	g/m^2	< 28	---	--	---	--	---	--	2	90 (n)
PCT B (k)	g/m^2	< 8.2 (m)	---	--	---	--	---	--	.03	20 (n)

(f) Property models fitted to CVS data up through the prior phase were equated to the indicated lower and upper limits and used as constraints in defining a subregion.

(g) T_{10} denotes the temperature at which viscosity is 10 Pa·s.

(h) MCC-1 28-day normalized Li release model fitted to all CVS data up through the prior phase. The upper limits for this model were set somewhat higher than for the model described in (h) to compensate for the overprediction of Li releases with this "full data set" model.

(i) MCC-1 28-day normalized Li release model fitted to all CVS data up through the prior phase except that the six CVS-I data points with the largest Li releases were not used. This model yielded more accurate predictions for lower releases, but could not be used to predict higher releases.

(j) MCC-1 28-day normalized B release.

(k) PCT 7-day normalized B release.

(l) Until CVS-II Phase 3, the acceptable range for electrical conductivity was 18 - 50 S/m. However, before the DWPF dropped their constraint on resistivity, it corresponded to an acceptable range on electrical conductivity of 36 - 111 S/m. Hence, the upper limit on electrical conductivity was raised substantially in CVS-II Phase 3.

(m) This value is based on an average release value for the DWPF EA glass reported in Volume 5 of the DWPF Waste Form Qualification Report (WSRC 1993).

(n) These lower and upper limits on MCC-1 and PCT B release were chosen to obtain more glasses with releases in the vicinity of the lower and upper limits, so as to improve the accuracy of model predictions for glasses with low and moderately high releases.

vertices in order to provide optimal coverage of the CVS-II Phase 1 composition subregion for fitting first-order mixture models.

The three interior points in the test matrix are the HW-39-4 glass, the center point composition included in CVS-I, and an internal CVS standard glass with composition close to that of HW-39-4 (see Table 4.8). Including the

TABLE 4.7. Glass Compositions (mass fractions) Tested in CVS-II Phase 1

Glass[a]	Run[b] Order	SiO_2	B_2O_3	Na_2O	Li_2O	CaO	MgO	Fe_2O_3	Al_2O_3	ZrO_2	Others[c]
CVS2-1	4	.5226	.0874	.0700	.0600	.0000	.0500	.0400	.0800	.0100	.0800
CVS2-2	11	.5017	.0700	.0883	.0600	.0700	.0000	.0450	.1100	.0300	.0250
CVS2-3	17	.4645	.1320	.0700	.0435	.0700	.0100	.0450	.1032	.0368	.0250
CVS2-4	1	.5600	.1095	.0700	.0536	.0700	.0000	.0400	.0619	.0100	.0250
CVS2-5	10	.4751	.1590	.1010	.0200	.0348	.0000	.0400	.0800	.0100	.0800
CVS2-6	13	.5373	.0700	.0700	.0382	.0700	.0046	.1200	.0159	.0100	.0641
CVS2-7	15	.4814	.1700	.0700	.0591	.0094	.0000	.0400	.0953	.0100	.0648
CVS2-8	7	.5115	.0700	.0985	.0600	.0000	.0500	.1140	.0610	.0100	.0250
CVS2-9	5	.5431	.0944	.0924	.0600	.0000	.0000	.0712	.0138	.1000	.0250
CVS2-10	12	.4694	.1700	.1306	.0200	.0000	.0000	.0669	.1043	.0100	.0288
CVS2-11	2	.4915	.0751	.0833	.0600	.0700	.0100	.0400	.0100	.0935	.0665
CVS2-12	6	.4683	.1700	.0700	.0466	.0700	.0100	.0400	.0901	.0100	.0250
CVS2-13	18	.4937	.0700	.1692	.0225	.0300	.0500	.0400	.0896	.0100	.0250
CVS2-14	9	.4600	.1313	.0802	.0486	.0500	.0200	.0400	.0243	.1000	.0457
CVS2-15	16	.4729	.0700	.1700	.0214	.0601	.0000	.0400	.0756	.0100	.0800
CVS2-16 (4)	3	.5353	.1053	.1125	.0375	.0083	.0084	.0719	.0231	.0385	.0592
CVS2-17 (1)	8	.4801	.1142	.1003	.0376	.0275	.0363	.0568	.0636	.0429	.0407
CVS2-18 (4)	14	.5353	.1053	.1125	.0375	.0083	.0084	.0719	.0231	.0385	.0592
CVS2-19 (5)	19	.5328	.1048	.1129	.0373	.0082	.0084	.0733	.0235	.0392	.0596

(a) CVS2-1 to CVS2-15 are vertices of the CVS-II Phase 1 composition subregion defined in Table 4.6. CVS2-16 is the HW-39-4 glass composition. CVS2-17 is a replicate of the center point composition (CVS1-1) from CVS-I. CVS2-18 is a replicate of CVS2-16. CVS2-19 is the CVS internal standard glass, which was designed to have a composition close to HW-39-4 (CVS2-16). The numbers in parentheses following the glass name denote replicate sets of glasses (the numbering is continued from Table 4.4).

(b) Glasses were fabricated and tested in this random run order.

(c) The composition of Others is given in the Substitute Others column of Table 4.1.

CVS-I center point provides a minimal basis for verifying that results from CVS-II Phase 1 are not biased relative to results from CVS-I. The CVS internal standard glass was made in sufficient quantity to include it in all phases of CVS-II. Finally, a replicate of the HW-39-4 composition was included to provide a limited basis for assessing short-term experimental variation in CVS-II Phase 1. The 19 CVS-II Phase 1 tests were conducted in the randomized run order given in Table 4.7.

TABLE 4.8. Mass Fraction Composition of the CVS Internal Standard Glass (CVS2-19, -51, -97, and -123) Compared to the Mass Fraction Composition of the HW-39-4 Glass

Oxide	Internal Standard	HW-39-4
SiO_2	.5328	.5353
B_2O_3	.1048	.1053
Na_2O	.1129	.1125
Li_2O	.0373	.0375
CaO	.0082	.0083
MgO	.0084	.0084
Fe_2O_3	.0733	.0719
Al_2O_3	.0235	.0231
ZrO_2	.0392	.0385
Others		
La_2O_3	.0154	.0064
Nd_2O_3	.0057	.0127
CeO_2	.00017	.0015
Pr_6O_{11}	.00188	.0010
Sm_2O_3	.0000	.0005
CdO	.0065	.0077
NiO	.0060	.0059
SO_3	.0044	.0046
F	.0019	.0031
MoO_3	.0031	.0031
Cs_2O	.0015	.0015
CuO	.00158	.0015
MnO_2	.00158	.0015
RuO_2	.00151	.0015
Cr_2O_3	.00129	.0013
BaO	.00099	.0010
SrO	.0000	.0010
P_2O_5	.00099	.0010
PdO	.0000	.0005
Rb_2O	.0000	.0005
Rh_2O_3	.0000	.0005
Y_2O_3	.0000	.0005
ZnO	0.0049	.0000
	0.9998	0.9996

4.4 CVS-II PHASE 2 COMPOSITION REGION AND TEST MATRIX

The CVS-II Phase 2 composition subregion and test matrix are defined and discussed in Sections 4.4.1 and 4.4.2, respectively.

4.4.1 CVS-II Phase 2 Composition Region

As overviewed in Section 4.1, the overall CVS strategy is to study glasses in the vicinity of the boundary between acceptable and unacceptable compositions (exterior compositions) as well as glasses on the interior of the region of acceptable compositions (interior compositions). Some of the exterior compositions studied in CVS-I were too extreme with respect to certain properties (mainly MCC-1 durability and crystallinity), and so part of the CVS-II Phase 2 effort was directed at obtaining data in the vicinity of a better estimate of the boundary of the region of interest[(a)]. This part of CVS-II is referred to as Phase 2a. It was also decided to collect additional interior composition data in different parts of the interior of the composition experimental region than studied in CVS-II Phase 1. This part of CVS-II is referred to as Phase 2b. Note that both parts of Phase 2 were conducted at the same time; the Phase 2a and 2b terminology merely makes it easier to refer to the two different aspects.

Because modeling of CVS-II Phase 1 data was not complete by the time it was necessary to plan CVS-II Phase 2, only CVS-I models were used in defining the Phase 2a and 2b composition regions, which are defined in Table 4.6.

The Phase 2a region is a revision of the CVS-I region that eliminates portions of composition space that have excessive crystallinity and unacceptably low MCC-1 durability values. The individual glass component lower and upper bounds are the same as for CVS-I, but the crystallinity multiple-component constraint upper bounds were reduced from the values used in CVS-I. The crystallinity bounds were adjusted due to the presence of crystallinity in some CVS-I glasses and in several scoping glasses considered

---

(a) The region of interest includes glasses with unacceptable as well as acceptable property values. This is necessary in order to develop models that fit well and can be used to determine the QCR.

in developing the CVS-II Phase 2 test matrix. Specifically, the multiple-component crystallinity constraints listed in Table 4.6 for Phase 2a were the result of two iterations involving: (1) defining the region, (2) generating a test matrix, and (3) performing scoping tests on glasses likely to have the most crystallinity. Finally, the property constraint lower and upper bounds shown in Table 4.6 for the Phase 2a region were selected to encompass the range of acceptable values specified in Table 3.1 and go somewhat beyond it, so as to provide information on where the boundary of the region of acceptable glasses begins.

The Phase 2b region was defined to include glasses with less extreme individual component variations and property values in the center of desired ranges. In this way glasses interior with respect to both properties and composition would be obtained. Such glasses would complement the exterior glasses selected from the Phase 2a region and would be different than the interior glasses studied in CVS-II Phase 1.

4.4.2 CVS-II Phase 2 Test Matrix

The CVS-II Phase 2 test matrix is given in Table 4.9. The matrix consists of 20 vertices of the Phase 2a region defined in Table 4.6, 10 vertices of the Phase 2b region defined in Table 4.6 (which are actually interior points of the overall experimental region), and 9 miscellaneous glasses. The nine miscellaneous glasses include the centroid and CVS internal standard glasses tested previously in CVS-I and CVS-II Phase 1, two glasses with lower and higher levels of SiO_2 than are generally being considered in the CVS, two uranium-doped glasses (UO_2 replaces Nd_2O_3), and three glasses with Others mixes corresponding to CC, PFP, and NCRW wastes. The selection of the various glasses included in CVS-II Phase 2 are discussed in the following paragraphs.

Glasses CVS2-20 to CVS2-39 were selected in two stages. First, the 3081 vertices of the Phase 2a region defined in Table 4.6 were generated by the MCCVRT routine from the MIXSOFT™ Version 2.0 software (Piepel 1992). Then, the ACED (Welch 1987) software was used to select a subset of 20 vertices according to a criterion that minimizes the maximum prediction variance for a

TABLE 4.9. Glass Compositions (mass fractions) Tested in CVS-II Phase 2

Glass[a]	Run[b] Order	SiO_2	B_2O_3	Na_2O	Li_2O	CaO	MgO	Fe_2O_3	Al_2O_3	ZrO_2	Others[c]
CVS2-20	3	.5700	.0500	.1031	.0669	.0000	.0000	.0600	.0100	.1300	.0100
CVS2-21	15	.5700	.1314	.0500	.0700	.0000	.0800	.0200	.0686	.0000	.0100
CVS2-22	6	.5700	.0500	.0735	.0700	.0000	.0800	.0200	.0365	.0000	.1000
CVS2-23	11	.5700	.0522	.2000	.0100	.0800	.0000	.0200	.0578	.0000	.0100
CVS2-24	2	.4464	.2000	.0736	.0700	.0000	.0000	.0200	.0961	.0000	.0939
CVS2-25	10	.5059	.0500	.0841	.0700	.0800	.0000	.1500	.0033	.0000	.0567
CVS2-26	24	.4431	.2000	.0512	.0700	.0800	.0000	.0200	.0257	.1000	.0100
CVS2-27	4	.5463	.0500	.2000	.0155	.0000	.0800	.0200	.0782	.0000	.0100
CVS2-28	1	.5619	.0500	.2000	.0126	.0000	.0000	.0200	.0555	.0000	.1000
CVS2-29	14	.4391	.2000	.0675	.0100	.0800	.0000	.0200	.0000	.0834	.1000
CVS2-30	9	.5190	.2000	.0832	.0100	.0000	.0000	.1320	.0458	.0000	.0100
CVS2-31	19	.5700	.1843	.0500	.0331	.0800	.0000	.0200	.0526	.0000	.0100
CVS2-32	5	.5445	.0500	.2000	.0428	.0000	.0000	.0200	.0027	.1300	.0100
CVS2-33	25	.4200	.0544	.2000	.0364	.0000	.0800	.0200	.0892	.0000	.1000
CVS2-34 (6)	22	.4200	.1743	.2000	.0369	.0000	.0000	.0200	.1388	.0000	.0100
CVS2-35	7	.4200	.0500	.2000	.0428	.0800	.0000	.0632	.1340	.0000	.0100
CVS2-36	8	.5421	.0500	.0891	.0700	.0800	.0000	.1500	.0088	.0000	.0100
CVS2-37	12	.5700	.0839	.1061	.0700	.0000	.0000	.0200	.1400	.0000	.0100
CVS2-38	16	.5147	.1109	.1044	.0100	.0000	.0800	.1428	.0272	.0000	.0100
CVS2-39	13	.4838	.0500	.1362	.0700	.0000	.0800	.0742	.0258	.0700	.0100
CVS2-40	26	.5040	.0639	.1500	.0421	.0200	.0500	.0200	.1000	.0200	.0300
CVS2-41	21	.5325	.0694	.0781	.0700	.0500	.0200	.0300	.1000	.0200	.0300
CVS2-42	28	.5675	.0500	.0625	.0700	.0320	.0380	.1000	.0300	.0200	.0300
CVS2-43	17	.5070	.1477	.0500	.0653	.0200	.0300	.0300	.0500	.0700	.0300
CVS2-44	29	.5700	.1078	.0500	.0699	.0500	.0200	.0200	.0623	.0200	.0300
CVS2-45	30	.5299	.1106	.0500	.0595	.0200	.0500	.0308	.0592	.0200	.0700
CVS2-46	18	.5264	.1259	.0577	.0700	.0200	.0200	.0200	.0746	.0200	.0654
CVS2-47	23	.5294	.0500	.1277	.0429	.0500	.0200	.0200	.0400	.0500	.0700
CVS2-48	27	.4700	.1442	.0968	.0390	.0500	.0200	.0200	.0854	.0200	.0546
CVS2-49	20	.5073	.1357	.0957	.0413	.0200	.0200	.0515	.0785	.0200	.0300
CVS2-50 (1)	31	.4801	.1142	.1003	.0376	.0275	.0363	.0568	.0636	.0429	.0407
CVS2-51 (5)	32	.5328	.1048	.1129	.0373	.0082	.0084	.0733	.0235	.0392	.0596
CVS2-52	34	.6000	.0817	.0450	.0788	.0008	.0009	.0720	.0233	.0385	.0590
CVS2-53	38	.5226	.0874	.0700	.0600	.0000	.0500	.0400	.0800	.0100	.0800
CVS2-54	39	.5328	.1048	.1129	.0373	.0082	.0084	.0733	.0235	.0392	.0596
CVS2-55	35	.5328	.1048	.1129	.0373	.0082	.0084	.0733	.0235	.0392	.0596
CVS2-56	36	.5328	.1048	.1129	.0373	.0082	.0084	.0733	.0235	.0392	.0596
CVS2-57	37	.5328	.1048	.1129	.0373	.0082	.0084	.0733	.0235	.0392	.0596
CVS2-58	33	.3900	.2000	.0500	.0700	.0200	.0800	.0200	.1500	.0100	.0100

(a) CVS2-20 to CVS2-36 are vertices of the CVS-II Phase 2a region defined in Table 4.6. CVS2-37 to CVS2-39 are vertices of the Phase 2a region modified as described in the (e) footnote of Table 4.6. CVS2-40 to CVS2-49 are vertices of the Phase 2b region defined in Table 4.6. CVS2-50 is a replicate of the center point (CVS1-1) from CVS-I. CVS2-51 is a replicate of CVS2-19, the CVS internal standard glass. CVS2-52 and CVS2-58 are high and low SiO_2 glasses, respectively. CVS2-53 and CVS2-54 are versions of CVS2-1 and CVS2-51 with UO_2 replacing Nd_2O_3 on a mass basis. CVS2-55, CVS2-56, and CVS2-57 are versions of CVS2-51 with Others mixes related to the CC, PFP, and NCRW waste types, respectively. The numbers in parentheses following the glass name denote replicate sets of glasses (the numbering is continued from Tables 4.4 and 4.7).

(b) Glasses were fabricated and tested in this random run order.

(c) The composition of Others is given in Table 4.1 for all glasses except CVS2-19, CVS2-51, and CVS2-53 to CVS2-57. The Others composition for CVS2-19 and CVS2-51 can be inferred from Table 4.8. The Others compositions for CVS2-53 and CVS2-54 are the same as for CVS2-1 and CVS2-51, respectively, except that Nd_2O_3 was replaced with UO_2. The Others compositions for CVS2-55 to CVS2-57 are given in Table 4.10.

linear mixture model. The 20 vertices were selected so as to best augment 31 glasses from CVS-I and CVS-II Phase 1 considered to be within or close to the revised composition experimental region[a]. Based on preliminary investigation of these twenty compositions, three were identified as potentially having unacceptably high crystallinity. These three compositions were replaced by three vertices from a modification of the Phase 2a region [see footnote (e) in Table 4.6]. The modified Phase 2a region has 5844 vertices, and three were selected by ACED to best augment the 31 CVS-I and CVS-II Phase 1 glasses, as well as the 17 vertices from the unmodified Phase 2a region.

Glasses CVS2-40 to CVS2-49 were selected from the 1446 vertices of the Phase 2b region defined in Table 4.6. They were selected independently of the previous CVS-I, CVS-II Phase 1, and CVS-II Phase 2 glasses already selected so as to best cover[b] the boundary of the Phase 2b region. However, because the Phase 2b region is a subregion of the Phase 2a experimental region, the vertices of the Phase 2b region are actually interior points of the Phase 2a experimental region.

Glasses CVS2-50 to CVS2-58 were selected to satisfy various purposes. The centroid (CVS2-50) and internal standard (CVS2-51) glasses that were tested in CVS-I and CVS-II Phase 1 provide replicate results that can be used to assess longer-term biases and/or random variations in melting and testing glasses. The low (CVS2-58) and high (CVS2-52) SiO_2 glasses provide some information about whether such glasses have acceptable properties. The two uranium-doped glasses (CVS2-53 and CVS2-54) have the same compositions as two previously tested glasses, except depleted UO_2 replaced Nd_2O_3 on a mass basis. Thus, these glasses provide information as to whether uranium affects glass properties. Finally, the three glasses with Others mixes representing preliminary CC, PFP, and NCRW waste compositions (Kruger, Watrous, and Piepel

---

(a) Various CVS-I glasses had one or more property values so extreme that they are no longer inside the composition experimental region being explored in CVS-II. Such glasses were not used as a basis to select CVS-II Phase 2 glasses for exploring the revised composition experimental region.

(b) A criterion of minimizing the maximum prediction variance for a first-order mixture model was used, as has been the case for other CVS-II glasses selected via this approach.

1990) provided a first look at the impact of different Others mixes on glass properties.

4.4.3 Glasses Made With CC, PFP, and NCRW Others Mixes

The Others mixes used in CVS-II Phase 2 glasses CVS2-55, CVS2-56, and CVS2-57 to represent the CC, PFP, and NCRW wastes are given in Table 4.10. The NCAW Others mix given earlier in Table 4.1 was used for all remaining CVS-II Phase 2 glasses, except for the CVS internal standard glass (CVS2-19 and CVS2-51) and the UO_2 substituted version of this glass. The compositions given in Table 4.10 do not correspond directly to preliminary composition estimates of CC, PFP, and NCRW wastes (Kruger, Watrous, and Piepel 1990) because: (1) certain minor components were eliminated or substituted for, and (2) it was necessary to modify the relative proportions of some constituents.

Ignoring the waste constituents separated out for individual study in CVS, the CC, PFP, and NCRW waste streams were estimated (at the time CVS-II Phase 2 was planned early in FY 1991) to consist primarily of five constituents: Nd_2O_3, Cr_2O_3, MnO_2, SO_3, and F. Noble metals were estimated only at low concentrations in NCRW, and at such levels are not expected to affect glass properties, and so were not included in the Table 4.10 Others mixes. U_3O_8 was estimated to occur only in NCRW and was replaced by Nd_2O_3.

TABLE 4.10. Composition of Others Mixes Representative of CC, PFP, and NCRW Wastes Used in Glasses CVS2-55, CVS2-56, and CVS2-57 (a)

Oxide	CVS2-55 CC (wt%)	CVS2-56 PFP (wt%)	CVS2-57 NCRW (wt%)
Cr_2O_3	15	12	9
MnO_2	47	78	0
Nd_2O_3	28	0	86
SO_3	5	5	0
F	5	5	5
	100	100	100

(a) See discussion in Section 4.4.3 about how these Others mixes were chosen.

Because of the preliminary nature of the CC, PFP, and NCRW waste composition estimates, the actual number of constituents is probably higher. However, a precedent exists for reducing the number of minor constituents included in Others. The Others component for the NCAW stream consists of 40 chemical constituents (39 oxides and F) based on analytical and flowsheet results, and yet only 22 of these chemical constituents (21 oxides and F) were included in the NCAW Others mix. In general, very minor components in glass are not expected to have significant impacts on glass properties, and so eliminating them in the CC, PFP, and NCRW Others mixes is not expected to be of consequence.

The three CC, PFP, and NCRW Others mix glasses (CVS2-55, CVS2-56, and CVS2-57) have the same nominal composition as the CVS internal glass, except that the CC, PFP, and NCRW Others mixes in Table 4.10 were used. It was decided to maintain a constant 10-component composition with only the Others mix changing to give a direct comparison of the effects of different Others mixes. The CVS internal standard glass was chosen as the base composition because it was close to HW-39-4 in composition and because of existing knowledge about HW-39-4. In addition, this standard allows comparing differences in the Others mixes glass results to differences in results from HW-39-4 (CVS2-16 and CVS2-18) and the internal standard (CVS2-19 and CVS2-51).

The disadvantage of using the CVS internal standard glass as the basis for comparison is that it is not an ideal glass composition for the CC, PFP, and NCAW wastes. Specifically, the proportions of Cr_2O_3, SO_3, and F in preliminary estimates of CC, PFP, and NCRW Others compositions are such that the CVS internal standard glass Others mass fraction of .0596 takes these components outside the critical solubility limits given in Table 4.3. This may partly be an artifact of the incomplete data on CC, PFP, and NCRW waste compositions. If the content of more oxides were known, the actual fraction of Cr_2O_3, SO_3, and F would be lower. Therefore, lower than estimated proportions of these constituents are used in the modified Others mixes listed in Table 4.10. The contents of SO_3 and F were set at the same level for CVS2-55 and CVS2-56 to reduce the number of components varied. The Cr_2O_3 concentration in glass reaches 0.9 wt% when the CVS2-55 Others mix is used with the

internal standard glass composition. Note this value is somewhat higher than the 0.5 wt% Cr_2O_3 constraint.

Section 13.2 presents and discusses the effects of the preceding Others mix variations on glass properties. Although limited in number, the Others mix variations included in CVS-II Phase 2 indicate that some glass properties are affected (positively or negatively) while other properties are not affected. Because variation in Others compositions will occur over the range of waste streams to be vitrified by a HLW vitrification plant, additional variations of the Others mix are needed to better assess the effects. This need was addressed in CVS-II Phase 3, as discussed in Section 4.5.

4.5 CVS-II PHASE 3 COMPOSITION REGION AND TEST MATRIX

In planning CVS-II Phase 3, an assessment was made of the data and results up through CVS-II Phase 2 to determine where additional information was most needed. The general conclusions reached were that glasses should be tested with: (1) properties somewhat outside acceptable limits, (2) Others mixes corresponding to updated estimates of pre-treated NCAW, NCRW, CC, and PFP wastes, and (3) modified ranges of some oxide components. Consideration was also given to selecting additional glasses within a smaller acceptable region. However, it was decided that the information on interior glass compositions in CVS-II Phase 1 and part of Phase 2 was reasonably adequate and that more exterior points were required to better resolve models and the boundary between acceptable and unacceptable compositions.

It was decided to select additional glasses with properties somewhat outside acceptable limits due to a shortage of such data. Not only is such data required to adequately identify the boundary between glasses with acceptable and unacceptable properties, but it is also expected to provide a better basis for developing glass property models over the full composition region being studied in CVS. The ranges of property values outside of acceptable limits that were targeted for study included: viscosity between

0.50[a] and 1.25 Pa·s on the low side, electrical conductivity between 5 and 10 S/m on the low side and between 100 and 130 S/m on the high side[b], MCC-1 28-day normalized boron release between 2 and 6 g/m^2 on the low side and between 40 to 90 g/m^2 on the high side, and PCT 7-day normalized boron release between 0.03 and 0.10 g/m^2 on the low side. How glasses were selected to achieve these targeted goals and what actually was achieved are discussed in Section 4.5.2.

Another objective of Phase 3 was to further study the effect of different Others mixes corresponding to specific waste types. Since CVS-II Phase 2 was planned and conducted, updated estimates of NCAW, NCRW, CC, and PFP pretreated wastes became available (see Table 4.11). It was decided to test glasses tailored to seven of these eleven wastes, and to further test variations of five of the seven by substituting the Others mix used for the majority of the CVS glasses tested (as given in Table 4.1) in place of the Others mix corresponding to each type of pre-treated waste (presented in Table 4.13). Some of the nominally minor components (such as Nd_2O_3, Mn_2O_3, CdO, and Cr_2O_3) in the Others mixes corresponding to some wastes can have larger mass fractions than do some of the nine oxide components being studied in CVS (such as MgO or CaO). Further, some nominally minor components (such as NiO or Cr_2O_3) affect liquidus temperature if they enter the primary crystalline phase. Hence for several reasons, it was decided that additional glasses with different Others mixes should be tested.

The CVS-II Phase 3 composition region and test matrix are defined and discussed in Sections 4.5.1 and 4.5.2, respectively.

(a) A value of 0.50 Pa·s was not actually achievable given the other constraints on the oxide components. Only a value of approximately 0.75 Pa·s could be achieved.

(b) The DWPF melter lower limit on resistivity corresponds to an upper limit of 111 S/m on electrical conductivity. It has been estimated that conductivities as high as 130 S/m may be acceptable. Hence, it was decided to study some glasses with predicted electrical conductivities up to 130 S/m.

TABLE 4.11. Preliminary Estimated Compositions for Pretreated NCAW, NCRW, PFP, and CC Wastes[a]

	Mass Fraction of Total Nonvolatile Oxides										
Waste:[b]	NCAW	NCRW	NCRW	CC	CC	CC	CC	CC	CC	PFP	PFP
Treatment:[c]	WS	WS	TRUEX	WS	TRUEX	WS	TRUEX	WS	TRUEX	WS	TRUEX
Tank:				EAST	EAST	SY101	SY101	SY103	SY103		
Oxide											
SiO_2	.0040	.0366	.0658	.1754	.6907	.0000	.0000	.0169	.1540	.0190	.0470
B_2O_3	.0001	.0060	.0108	.0000	.0000	.0002	.0014	.0002	.0023	.0028	.0027
Na_2O	.2142	.2553	.0029	.2509	.0988	.2983	.2419	.2083	.1897	.1490	.0430
Li_2O	.0000	.0000	.0000	.0000	.0000	.0000	.0000	.0000	.0000	.0000	.0000
CaO	.0079	.0023	.0041	.0238	.0028	.0073	.0018	.0062	.0017	.0300	.0030
MgO	.0020	.0009	.0016	.0149	.0018	.0000	.0000	.0006	.0002	.0120	.0028
Fe_2O_3	.2821	.0032	.0058	.0957	.0113	.0000	.0000	.0466	.0127	.1270	.0320
Al_2O_3	.0904	.0651	.3517	.2900	.1142	.6541	.5304	.5398	.4919	.3090	.7530
ZrO_2	.1511	.5530	.4977	.0065	.0008	.0000	.0000	.0007	.0002	.0020	.0020
Other waste components	.2482	.0776	.0596	.1428	.0796	.0401	.2245	.1807	.1473	.3492	.1145

(a) From an unpublished 1992 Westinghouse Hanford project report by T.H. May and R.A. Watrous.

(b) NCAW = Neutralized Current Acid Waste
CC = Complexant Concentrate
PFP = Plutonium Finishing Plant
NCRW = Neutralized Cladding Removal Waste

(c) WS = Sludge Washing
TRUEX = Transuranic Extraction

4.5.1 CVS-II Phase 3 Composition Region

The composition region studied during CVS-II Phase 3 is given in Table 4.6. The lower and upper bounds for most of the oxide components were modified from the values used in CVS-I and CVS-II Phase 2a (see Tables 4.2 and 4.6). The general intent was to slightly increase the lower bounds and decrease the upper bounds so as to get glasses with somewhat less extreme compositions than previously obtained in an effort to better cover the overall region. However, it was decided to decrease the Fe_2O_3 lower bound and to increase the Al_2O_3 upper bound based on updated information regarding

potential pre-treated NCAW, NCRW, CC, and PFP waste compositions. Further, to achieve some of the targeted property ranges, it was necessary to leave the Li_2O lower and upper bounds and the Na_2O lower bound unchanged and to modify a few other bounds less than was originally desired.

Also shown in the last column of Table 4.6 are the CVS-II Phase 3 crystallinity and property constraints. Because liquidus temperature models were not available during the planning of CVS-II Phase 3, the stand-in crystallinity constraints previously used in CVS-II Phases 1 and 2 were retained, but with modified upper bounds. The MgO+CaO upper bound was lowered to 0.045 corresponding to the lowered upper bounds of 0.04 on each of MgO and CaO. The upper bounds on Fe_2O_3+Al_2O_3+ZrO_2+Others and Al_2O_3+ZrO_2 were increased to obtain more glasses with liquidus temperature above 1050°C, because preliminary liquidus temperature results indicated a potential shortage of such data.

The property constraints shown in the Phase 3 column of Table 4.6 are the overall ranges studied. As indicated previously, specific ranges of these property values were targeted. Updated first-order property models based on results up through CVS-II Phase 2 were used to implement the property constraints in the statistical experimental design approach used. Boron release models for the MCC-1 and PCT tests were used in applying the durability constraints in CVS-II Phase 3.

4.5.2 CVS-II Phase 3 Test Matrix

The CVS-II Phase 3 test matrix contains 43 glasses and is given in Table 4.12. A description of each glass or group of glasses is given in a footnote following the table. Glasses CVS2-59 through CVS2-62 were selected to achieve specified values of one or more properties, while CVS2-63 was selected to study a glass with even lower SiO_2 (0.3232 mass fraction) than previously studied in CVS-II Phase 2. Glasses CVS2-64 through CVS2-70 were selected to investigate glasses with desirable properties corresponding to seven of the eleven updated waste composition estimates for NCAW, NCRW, CC and PFP waste types given in Table 4.11. The Others mixes for glasses CVS2-64 through CVS2-70 are given in Table 4.13.

TABLE 4.12. Glass Compositions (mass fractions) Tested in CVS-II Phase 3

Glass[a]	Run[b] Order	SiO_2	B_2O_3	Na_2O	Li_2O	CaO	MgO	Fe_2O_3	Al_2O_3	ZrO_2	Others[c]
CVS2-59	5	.4380	.1718	.1268	.0727	.0375	.0005	.0200	.1150	.0075	.0102
CVS2-60	10	.5281	.0876	.1725	.0743	.0063	.0005	.0200	.0925	.0075	.0107
CVS2-61	2	.5281	.0664	.1200	.0730	.0000	.0000	.0200	.1625	.0175	.0125
CVS2-62	13	.5579	.1765	.1125	.0156	.0500	.0005	.0200	.0500	.0075	.0095
CVS2-63	4	.3232	.1717	.1900	.0051	.1000	.0000	.0200	.1800	.0000	.0100
CVS2-64	24	.5697	.0509	.0925	.0642	.0025	.0008	.0812	.0288	.0431	.0663
CVS2-65	30	.5344	.1128	.0860	.0697	.0007	.0004	.0013	.0196	.1548	.0203
CVS2-66	3	.5175	.0917	.1211	.0523	.0097	.0061	.0388	.1180	.0026	.0422
CVS2-67	21	.4596	.1587	.1086	.0583	.0024	.0001	.0004	.2043	.0000	.0076
CVS2-68	11	.5040	.1355	.0797	.0696	.0007	.0002	.0046	.1640	.0001	.0416
CVS2-69	19	.5660	.0781	.0664	.0713	.0079	.0032	.0334	.0816	.0005	.0916
CVS2-70	38	.4854	.1418	.0812	.0691	.0008	.0008	.0080	.1819	.0005	.0305
CVS2-71	6	.5697	.0509	.0925	.0642	.0025	.0008	.0812	.0288	.0431	.0663
CVS2-72	9	.5175	.0917	.1211	.0523	.0097	.0061	.0388	.1180	.0026	.0422
CVS2-73	1	.5040	.1355	.0797	.0696	.0007	.0002	.0046	.1640	.0001	.0416
CVS2-74	34	.5660	.0781	.0664	.0713	.0079	.0032	.0334	.0816	.0005	.0916
CVS2-75	7	.4854	.1418	.0812	.0691	.0008	.0008	.0080	.1819	.0005	.0305
CVS2-76	15	.5018	.0600	.1800	.0632	.0400	.0050	.1050	.0200	.0050	.0200
CVS2-77	29	.4550	.0600	.1800	.0700	.0050	.0050	.0050	.0200	.1100	.0900
CVS2-78	33	.5600	.1600	.0500	.0254	.0050	.0400	.0699	.0200	.0497	.0200
CVS2-79	35	.5479	.1600	.0500	.0121	.0050	.0050	.1050	.0200	.0050	.0900
CVS2-80	22	.5074	.1600	.0500	.0176	.0050	.0400	.1050	.0200	.0750	.0200
CVS2-81	12	.4400	.0600	.1734	.0700	.0050	.0400	.1050	.0200	.0050	.0816
CVS2-82	23	.5600	.0950	.1800	.0700	.0050	.0400	.0050	.0200	.0050	.0200
CVS2-83	28	.4900	.0951	.1800	.0699	.0400	.0050	.0050	.0200	.0050	.0900
CVS2-84	39	.4550	.0600	.1800	.0700	.0050	.0050	.1050	.0200	.0800	.0200
CVS2-85	16	.4400	.0600	.1800	.0700	.0050	.0200	.0050	.1700	.0050	.0450
CVS2-86	25	.4764	.0600	.1800	.0136	.0400	.0050	.0050	.1700	.0050	.0450
CVS2-87	8	.4983	.0800	.1800	.0180	.0137	.0050	.0250	.0987	.0613	.0200
CVS2-88	37	.4597	.0600	.1403	.0700	.0400	.0050	.0250	.1050	.0750	.0200
CVS2-89	26	.4400	.1171	.1800	.0100	.0400	.0050	.1050	.0200	.0629	.0200
CVS2-90	20	.5600	.1600	.0542	.0700	.0050	.0050	.1008	.0200	.0050	.0200
CVS2-91	32	.5600	.1600	.1050	.0100	.0050	.0400	.0050	.0200	.0050	.0900
CVS2-92	27	.4400	.1600	.1000	.0700	.0050	.0400	.0050	.0200	.0700	.0900
CVS2-93	14	.4400	.1337	.1279	.0700	.0098	.0050	.0986	.0200	.0050	.0900
CVS2-94	18	.4400	.1600	.1800	.0526	.0400	.0050	.0271	.0703	.0050	.0200

(a) CVS2-59 is a low viscosity glass. CVS2-60 is a high electrical conductivity glass. CVS2-61 is a low PCT release glass. CVS2-62 is a low electrical conductivity glass. CVS2-63 is a low SiO_2 glass.

CVS2-64 to CVS2-70 have Others mixes corresponding to updated estimates of NCAW, NCRW, CC, and PFP wastes (see Table 4.13). Glasses CVS2-71, -72, -73, -74, and -75 are the same 10 component compositions as CVS2-64, -66, -68, -69, and -70, respectively, except the Others mix corresponds to the NCAW-87 waste (see Table 4.1).

CVS2-76 to CVS2-94 were picked via MIXSOFT and ACED optimal design software, except that CVS2-87 was modified somewhat to avoid ZrO_2 solubility problems.

(b) Glasses were fabricated and tested in this random run order.

(c) The NCAW-87 Others mix (Table 4.1) was used for all glasses except CVS2-64 through CVS2-70, CVS2-95, CVS2-99, CVS2-100, and CVS2-101 (see Table 4.13) and CVS2-97 (see Table 4.8).

TABLE 4.12. Glass Compositions (mass fractions) Tested in CVS-II Phase 3 (continued)

Glass[a]	Run[b] Order	SiO_2	B_2O_3	Na_2O	Li_2O	CaO	MgO	Fe_2O_3	Al_2O_3	ZrO_2	Others[c]
CVS2-95 (7)	36	.4895	.1112	.1671	.0428	.0113	.0166	.0897	.0367	.0041	.0310 (d)
CVS2-96 (1)	40	.4801	.1142	.1003	.0376	.0275	.0363	.0568	.0636	.0429	.0407
CVS2-97 (5)	31	.5328	.1048	.1129	.0373	.0082	.0084	.0733	.0235	.0392	.0596
CVS2-98 (6)	17	.4200	.1743	.2000	.0369	.0000	.0000	.0200	.1388	.0000	.0100
CVS2-99	41	.5203	.0969	.0980	.0356	.0097	.0077	.1019	.0523	.0199	.0577
CVS2-100	42	.5329	.0740	.0626	.0596	.0035	.0012	.1229	.0286	.0443	.0704
CVS2-101(7)	43	.4895	.1112	.1671	.0428	.0113	.0166	.0897	.0367	.0041	.0310 (e)

(a) CVS2-95 is the DWPF EA "standard glass" batched at PNL according to the composition given in Table 1 of Jantzen et al. (1993). This composition varies slightly from the EA glass composition listed in Table 4-1 of DOE (1982) due to: (1) distribution of the Other Solids component to its oxide component parts, and (2) removal of U_3O_8 so that a nonradioactive standard could be produced in large quantity. CVS2-96 is a replicate of the center point CVS1-1 from CVS-I. CVS2-97 is a replicate of the CVS internal standard glass, which was designed to have a composition close to that of HW-39-4 (same as CVS2-19 and CVS2-51). CVS2-98 is a replicate of CVS2-34. CVS2-99 is a simulated 101-AZ Core 1 glass. CVS2-100 is a simulated 101-AZ Core 2 glass. CVS2-101 is the DWPF EA "standard glass" obtained from SRTC.

The numbers in parentheses following the glass name denote replicate sets of glasses (the numbering is continued from Tables 4.4, 4.7, and 4.9).

(b) Glasses were fabricated and tested in this random run order.

(c) The NCAW-87 Others mix (Table 4.1) was used for all glasses except CVS2-64 through CVS2-70, CVS2-95, CVS2-99, CVS2-100, and CVS2-101 (see Table 4.13) and CVS2-97 (see Table 4.8).

(d) Fe_2O_3 = .0897 represents the sum of FeO = .0089 and Fe_2O_3 = .0808.

(e) This is the nominal composition of the DWPF EA glass written in the 10-component CVS format. SRTC had Corning make a large quantity of EA glass using the nominal composition as a target. The composition obtained by averaging 30 replicate analyses (by Corning) of the resulting glass is (.4873, .1128, .1681, .0426, .0112, .0172, .0738, .0370, .0046, .0454).

Glasses CVS2-71 through CVS2-75 are the same as CVS2-64, -66, -68, -69, and -70, respectively, except that the Others mix corresponds to that used for the majority of glasses tested in CVS (based on the NCAW-87 estimate, see Table 4.1). This pairing of glasses provides for a direct comparison of results to ascertain the effects of varying the Others composition on the data as well as on the predictive ability of the property models.

Glasses CVS2-76 through CVS2-94 (19 glasses) were selected using the computer-aided statistical experimental design approach and software used in planning previous phases of the CVS. Vertices of several composition subregions corresponding to the general constraints given in the Phase 3

TABLE 4.13. Compositions of Others for CVS2-64 to CVS2-70, CVS2-95, CVS2-99, CVS2-100, and CVS2-101 Glasses

(a) Oxide	CVS2-64 NCAW WS (wt%)	CVS2-65 NCRW WS (wt%)	CVS2-66 CC WS EAST (wt%)	CVS2-67 CC (b) (wt%)	CVS2-68 CC TRUEX SY103 (wt%)	CVS2-69 PFP WS (wt%)	CVS2-70 PFP TRUEX (wt%)	CVS2-99 NCAW 101-AZ Core 1 (wt%)	CVS2-100 NCAW 101-AZ Core 2 (wt%)	CVS2-95 CVS2-101 DWPF EA (wt%)
Ag_2O								1.73	0.43	
Cr_2O_3	1.70	23.7	25.5	17.8	71.3	25.93	38.31	3.47	0.85	
F	0.50		1.5	16.9	13.6	1.20				
P_2O_5	5.60			65.0		35.54	2.19	9.53	12.50	
SrO								0.69	0.71	
SO_3	4.20			0.3	0.2	7.51	0.90	6.93	4.55	
PdO	0.80					1.50	4.49			
Rh_2O_3	0.70	0.7				0.70	2.19			
RuO_2	2.66					0.70	2.33		1.28	
As_2O_3							3.49			
BaO			1.2					0.87	0.99	
CdO	19.51					1.20	3.59	5.20	11.36	
CeO_2	3.90						4.29	2.43		
Co_2O_3								1.73		
Cs_2O	3.90									
CuO						2.00	5.39	0.35	0.43	
K_2O	1.30	43.0			3.9			36.74	23.30	1.29
La_2O_3	4.20	2.1	10.1				1.80	2.43	6.53	13.18
MnO										43.09
MnO_2			34.4		6.4	16.32	11.57	8.32	2.98	
MoO_3	3.60		14.9		1.7			0.17		
Nd_2O_3	22.01	30.5				1.90	1.80	7.97	20.60	
NiO	14.81		12.4				2.69	5.03	9.80	19.61
PbO	4.20					1.60		3.47	1.56	
Sb_2O_3							1.60			
SeO_2						3.90	11.57			
TeO_2							1.80		0.71	
TiO_2	4.20							2.08	1.14	22.83
ZnO	2.20				2.9			0.87	0.28	
	99.99	100.00	100.00	100.00	100.00	100.00	100.00	100.01	100.00	100.00

(a) The Others compositions for CVS2-64 to CVS2-70 are based on an unpublished 1992 WHC project report by May and Watrous. The NCAW Others composition for NCAW is different from the earlier NCAW composition (see Table 4.1) used for the Others mix of most CVS glass. CVS2-99 and CVS2-100 have compositions of simulated waste glasses based on the Core 1 and Core 2 samples from DST 101-AZ, respectively.

(b) Not based directly on one of the eleven pretreated wastes in Table 4.11.

column of Table 4.6 and the targeted property ranges given in Section 4.5 were generated using and MCCVRT routine from MIXSOFT (Piepel 1992) and joined together into one set of 7726 vertices. These vertices were then supplied as a candidate set to ACED (Welch 1987) and several 19-point subsets were generated so as to best augment the previous 81 glasses tested during CVS-I and CVS-II Phases 1 and 2. A full second-order mixture model was assumed and a criterion of minimizing the maximum prediction variance was used to select the subsets. Several 19-point subsets were chosen using ACED, since it does not guarantee the generation of the optimal subset for any given try[(a)]. Further, it was desired to have several subsets to choose from, where achievement of the targeted property ranges was to be the deciding basis for selecting a 19-point subset from among the several generated. After selecting a 19-point subset, it was necessary to modify the composition of one glass (CVS2-87) to correct a ZrO_2 solubility problem detected in scoping tests[(b)].

The following chart gives the numbers of points within each of the targeted property ranges for the 19-point subset selected, as well as for the entire 43-point CVS-II Phase 3 test matrix:

Property	Range	No. points, 19-pt subset	No. points, 43-pt matrix
Viscosity (Pa·s)	0.75 - 1.25	8	9
Electrical conductivity (S/m)	5 - 10	3	3
Electrical conductivity (S/m)	100 - 130	7	8
MCC-1 28-day B release (g/m^2)	2 - 6	3	9
MCC-1 28-day B release (g/m^2)	40 - 90	10	11
PCT 7-day B release (g/m^2)	.03 - .10	1	5

(a) Achieving the exact optimal subset for a given criterion is not necessary to have a good subset. For a large number of candidate points, typically several nearly-optimal subsets are found, any one of which is a good subset.

(b) The CVS2-87 ZrO_2 level was lowered from 0.1013 to 0.0613, which was offset by increasing the B_2O_3 level from 0.0600 to 0.0800 and increasing the Al_2O_3 level from 0.0787 to 0.0987.

Rounding out the CVS-II Phase 3 test matrix are glasses CVS2-95 to CVS2-101. CVS2-95 was fabricated at PNL using the DWPF Environmental Assessment (EA) "standard" glass formulation (Table 1 in Jantzen et al. 1993). CVS2-101 is a sample of the EA standard glass obtained from WSRC. CVS2-95 and CVS2-101 are nominally the same composition. However, minor differences could exist due to differences in batching CVS2-95 at PNL and differences in the sample from WSRC used for CVS2-101 compared to the bulk EA standard glass composition at WSRC. CVS2-96, CVS2-97, and CVS2-98 are replicates of CVS1-1, CVS2-19 (the CVS internal standard glass), and CVS2-34, respectively. CVS2-99 and CVS2-100 are two simulated waste glasses based on the compositions of the Double Shell Tank 101-AZ Core 1 and Core 2 samples. These two glasses were tested for (and funded by) the PVTD Radioactive Process/Product Laboratory Testing activity. They were added to the test matrix because they were to be tested at the same time as CVS-II Phase 3 glasses and could be used to validate (and then possibly fit) property models.

All CVS-II Phase 3 glasses except CVS2-64 to CVS2-70, CVS2-95, CVS2-97, CVS2-99, CVS2-100, and CVS2-101 were made with the Others mix used in the majority of the CVS glasses tested so far (based on NCAW-87, see Table 4.1). The Others mixes for these glasses are given in Table 4.13, except for CVS2-97 (a replicate of the CVS internal standard glass), which has the Others mix defined in Table 4.8. The Others mix corresponding to the NCAW-87 waste estimate (see Table 4.1) was used for the majority of CVS-II Phase 3 glasses to maintain consistency with previous phases of the CVS. The three glasses from CVS-II Phase 2 and the nine from CVS-II Phase 3 with different Others mixes provide a basis for assessing the effects of different Others mixes (see Section 13.2).

4.6 CVS-II PHASE 4 COMPOSITION REGION AND TEST MATRIX

The CVS-II Phase 4 composition subregion and test matrix are defined and discussed in Sections 4.6.1 and 4.6.2, respectively.

4.6.1 CVS-II Phase 4 Composition Region

The composition subregion investigated in CVS-II Phase 4 corresponds to selected one-at-a-time changes in the components from the HW-39-4 composition. It is described in the Phase 4 column of Table 4.6 in terms of the lower and upper component bounds between which each component was varied directly (one-at-a-time) or indirectly (to offset one-at-a-time changes in other components). In previous phases of CVS, a subregion of interest was defined and then glass compositions were selected within the subregion. For CVS-II Phase 4, the process was essentially reversed; one-at-a-time glass compositions were specified, which then implicitly define a subregion.

The impetus for the one-at-a-time component variations was to provide a direct basis for understanding how single components affect PCT and MCC-1 durability. Thus, only those two properties were measured for CVS-II Phase 4 glasses. PCT was measured for both quenched and canister centerline cooled samples, while MCC-1 was only measured for quenched samples.

Seven of the ten CVS components were selected for varying one-at-a-time: SiO_2, B_2O_3, Na_2O, Li_2O, CaO, MgO, and Al_2O_3. Anomalous durability behavior associated with B_2O_3 and its nonlinear effect on durability made it an essential component to investigate. The alkalis (Na_2O and Li_2O) also play a role in the "boron anomaly" and the mixed alkali effect, and thus were chosen for investigation. Understanding the effects of CaO and MgO on durability is important because these components have traditionally been added to glass in order to increase durability. However, the CVS durability models predict that MgO and CaO decrease durability over the ranges of 0-10 wt% for CaO and 0-8 wt% for MgO. Thus, it was decided to investigate the effects of CaO and MgO for low concentrations (less than 2 wt%), where they may have positive effects on durability. Finally, SiO_2 and Al_2O_3 were selected for one-at-a-time investigation because of their strong potential to increase durability.

The single-component-change study was limited to 20 glasses, which did not allow testing of more than seven components. The seven components (Al_2O_3, B_2O_3, CaO, Li_2O, MgO, Na_2O, and SiO_2) where chosen for the reasons described above. Effects of one-at-a-time variations of Fe_2O_3, ZrO_2, and Others where not tested.

4.6.2 CVS-II Phase 4 Test Matrix

The CVS-II Phase 4 test matrix, listed in Table 4.14, consists of a collection of one-component-at-a-time variations from the HW-39-4 glass composition and the internal standard glass. The components SiO_2, B_2O_3, Na_2O, Li_2O, CaO, MgO, and Al_2O_3 were varied one-at-a-time while keeping the other components in the same relative proportions as in the HW-39-4 glass (see Section 6.3). Of these seven components, five were varied over ranges equaling or slightly exceeding the ranges previously investigated in CVS: SiO_2 (41-57 wt%), B_2O_3 (5-20 wt%), Na_2O (5-20 wt%), Li_2O (1-7 wt%), and Al_2O_3 (0-15 wt%). MgO was varied between 0 to 2 wt%, while CaO was only directly varied (i.e., one-at-a-time) from the HW-39-4 value (0.83 wt%) to 2 wt%. Indirectly

TABLE 4.14. Glass Compositions (mass fractions) Tested in CVS-II Phase 4

Glass[a]	Run[b] Order	SiO_2	B_2O_3	Na_2O	Li_2O	CaO	MgO	Fe_2O_3	Al_2O_3	ZrO_2	Others[c]
CVS2-102 (4)	21	.5353	.1053	.1125	.0375	.0083	.0084	.0719	.0231	.0385	.0592
CVS2-103	3	.4100	.1337	.1428	.0476	.0105	.0107	.0913	.0293	.0489	.0752
CVS2-104	2	.4500	.1246	.1332	.0444	.0098	.0099	.0851	.0273	.0456	.0701
CVS2-105	6	.4900	.1156	.1235	.0412	.0091	.0092	.0789	.0254	.0423	.0650
CVS2-106	4	.5700	.0974	.1041	.0347	.0077	.0078	.0665	.0214	.0356	.0548
CVS2-107	7	.5684	.0500	.1195	.0398	.0088	.0089	.0763	.0245	.0409	.0629
CVS2-108	5	.5086	.1500	.1069	.0356	.0079	.0080	.0683	.0220	.0366	.0562
CVS2-109	8	.4786	.2000	.1006	.0335	.0074	.0075	.0643	.0207	.0344	.0529
CVS2-110	9	.5730	.1127	.0500	.0401	.0089	.0090	.0770	.0247	.0412	.0634
CVS2-111	10	.5127	.1009	.1500	.0359	.0080	.0081	.0689	.0221	.0369	.0567
CVS2-112	11	.4825	.0949	.2000	.0338	.0075	.0076	.0648	.0208	.0347	.0534
CVS2-113	12	.5506	.1083	.1157	.0100	.0085	.0086	.0740	.0238	.0396	.0609
CVS2-114	22	.5228	.1028	.1099	.0600	.0081	.0082	.0702	.0226	.0376	.0578
CVS2-115	13	.5172	.1017	.1087	.0700	.0080	.0081	.0695	.0223	.0372	.0572
CVS2-116	14	.5290	.1041	.1112	.0371	.0200	.0083	.0711	.0228	.0381	.0585
CVS2-117	15	.5398	.1062	.1135	.0378	.0084	.0000	.0725	.0233	.0388	.0597
CVS2-118	16	.5290	.1041	.1112	.0371	.0082	.0200	.0711	.0228	.0381	.0585
CVS2-119	17	.5480	.1078	.1152	.0384	.0085	.0086	.0736	.0000	.0394	.0606
CVS2-120	18	.5206	.1024	.1094	.0365	.0081	.0082	.0699	.0500	.0374	.0576
CVS2-121	19	.4932	.0970	.1036	.0346	.0077	.0077	.0662	.1000	.0355	.0545
CVS2-122	20	.4658	.0916	.0979	.0326	.0072	.0073	.0626	.1500	.0335	.0515
CVS2-123 (5)	1	.5328	.1048	.1129	.0373	.0082	.0084	.0733	.0235	.0392	.0596

(a) CVS2-102 is the HW-39-4 glass, which was previously tested as CVS2-16 and CVS2-18. CVS2-123 is the CVS internal standard glass, which was previously tested as CVS2-19, CVS2-51, and CVS2-97. CVS2-103 through CVS2-122 are the one-at-a-time variations of the HW-39-4 composition. The numbers in parentheses following the glass name denote replicate sets of glasses (the numbering is continued from Tables 4.4, 4.7, 4.9 and 4.12).

(b) Glasses were fabricated and tested in this non-random run order.

(c) The composition of Others is given in the Substitute Others column of Table 4.1 for all glasses except CVS2-123, whose Others composition is given in Table 4.8.

(to help offset one-at-a-time changes in other components), CaO was varied down to 0.72 wt%. The components Fe_2O_3, ZrO_2, and Others were not varied one-at-a-time and so their ranges explored in CVS-II Phase 4 are only those resulting from offsetting the one-at-a-time changes made in SiO_2, B_2O_3, Na_2O, Li_2O, CaO, MgO, and Al_2O_3. These ranges are 6.26 to 9.13 wt% for Fe_2O_3, 3.35 to 4.89 wt% for ZrO_2, and 5.15 to 7.52 wt% for Others. The values of the components varied one-at-a-time are printed in boldface in Table 4.14 to make it easier to see how each component was varied.

The strategy of varying components one-at-a-time to understand their effects is widely used. It is a non-optimum strategy if only one-at-a-time variations are investigated, because: (i) no information is obtained about interactions among the components, and (ii) the information about the effects of the components may only be valid relative to the single composition used as the basis for one-at-a-time changes (HW-39-4 in this case). However, in the CVS situation, a significant portion of the experimental effort has involved varying the components many-at-a-time. One-at-a-time variations in components performed in conjunction with many-at-a-time changes is a good experimental strategy (the well-known central composite design uses this strategy).

4.7 COMBINED CVS EXPERIMENTAL DESIGN IN MASS FRACTIONS

Table 4.15 contains a complete list of the "9 components plus Others" as-batched mass fraction compositions of all glasses tested in CVS-I and CVS-II. Table 4.15 is essentially a compilation of Tables 4.4, 4.7, 4.9, 4.12, and 4.14, with "ID #" and "PS" information added. "ID #" gives a sequential numbering of all CVS glasses tested, and "PS" assigns a plotting symbol to various groups of glasses tested during CVS. These plotting symbols are used in various plots of the data throughout this report.

As-batched compositions of CVS glasses with minor component information are listed and compared to chemical analysis compositions in Appendix A. Several differences between as-batched and analyzed compositions were discovered, but most were attributed to analytical biases or were not practically significant (see Appendix A). Hence, it was decided to use as-batched compositions in fitting property models and other data analyses.

TABLE 4.15. As-Batched Mass Fraction Compositions for CVS-I and CVS-II Glasses

Glass[a]	ID[b] #	PS[b]	Run[c] Order	SiO_2	B_2O_3	Na_2O	Li_2O	CaO	MgO	Fe_2O_3	Al_2O_3	ZrO_2	Others[d]
CVS1-1 (1)	1	M	4	.4801	.1142	.1003	.0376	.0275	.0363	.0568	.0636	.0429	.0407
CVS1-2	2	1	10	.5500	.0500	.0500	.0700	.1000	.0000	.0200	.1500	.0000	.0100
CVS1-3	3	1	17	.4200	.2000	.0500	.0700	.0000	.0800	.0200	.1400	.0100	.0100
CVS1-4 (2)	4	1	12	.5700	.2000	.0900	.0100	.0200	.0800	.0200	.0000	.0000	.0100
CVS1-5	5	1	3	.5700	.0500	.0700	.0700	.0000	.0000	.1500	.0800	.0000	.0100
CVS1-6	6	1	5	.4400	.2000	.0500	.0700	.0000	.0000	.0200	.0000	.1200	.1000
CVS1-7	7	1	7	.5700	.0500	.0964	.0100	.1000	.0000	.0336	.0000	.1300	.0100
CVS1-8 (3)	8	1	9	.5363	.0500	.0837	.0100	.0000	.0800	.1500	.0000	.0800	.0100
CVS1-9	9	1	15	.4200	.1962	.0538	.0100	.0000	.0800	.1400	.0000	.0000	.1000
CVS1-10	10	1	6	.5700	.0851	:0949	.0100	.0000	.0000	.0200	.1200	.0000	.1000
CVS1-11	11	1	8	.4200	.1549	.0751	.0100	.1000	.0000	.0200	.1400	.0000	.0800
CVS1-12	12	1	16	.4200	.1764	.0736	.0700	.1000	.0000	.1500	.0000	.0000	.0100
CVS1-13	13	1	14	.5700	.2000	.1862	.0100	.0000	.0000	.0200	.0038	.0000	.0100
CVS1-14	14	1	22	.4200	.2000	.1862	.0100	.0000	.0000	.0200	.0238	.1300	.0100
CVS1-15	15	1	11	.5589	.0500	.1211	.0700	.0000	.0800	.0200	.0000	.0000	.1000
CVS1-16	16	1	2	.4327	.0500	.1873	.0100	.0000	.0800	.0858	.1442	.0000	.0100
CVS1-17	17	1	19	.4545	.0500	.1455	.0100	.1000	.0000	.1400	.0000	.0000	.1000
CVS1-18	18	1	18	.4214	.0500	.1186	.0700	.0200	.0800	.0200	.0000	.1300	.0900
CVS1-19 (1)	19	M	13	.4801	.1142	.1003	.0376	.0275	.0363	.0568	.0636	.0429	.0407
CVS1-20 (1)	20	M	21	.4801	.1142	.1003	.0376	.0275	.0363	.0568	.0636	.0429	.0407
CVS1-21 (2)	21	1	1	.5700	.2000	.0900	.0100	.0200	.0800	.0200	.0000	.0000	.0100
CVS1-22 (3)	22	1	20	.5363	.0500	.0837	.0100	.0000	.0800	.1500	.0000	.0800	.0100
CVS1-23	23	M	23	.5153	.0956	.1052	.0375	.0289	.0084	.1179	.0456	.0063	.0393
CVS2-1	24	2	4	.5226	.0874	.0700	.0600	.0000	.0500	.0400	.0800	.0100	.0800
CVS2-2	25	2	11	.5017	.0700	.0883	.0600	.0700	.0000	.0450	.1100	.0300	.0250
CVS2-3	26	2	17	.4645	.1320	.0700	.0435	.0700	.0100	.0450	.1032	.0368	.0250
CVS2-4	27	2	1	.5600	.1095	.0700	.0536	.0700	.0000	.0400	.0619	.0100	.0250
CVS2-5	28	2	10	.4751	.1590	.1010	.0200	.0348	.0000	.0400	.0800	.0100	.0800
CVS2-6	29	2	13	.5373	.0700	.0700	.0382	.0700	.0046	.1200	.0159	.0100	.0641
CVS2-7	30	2	15	.4814	.1700	.0700	.0591	.0094	.0000	.0400	.0953	.0100	.0648
CVS2-8	31	2	7	.5115	.0700	.0985	.0600	.0000	.0500	.1140	.0610	.0100	.0250
CVS2-9	32	2	5	.5431	.0944.	.0924	.0600	.0000	.0000	.0712	.0138	.1000	.0250
CVS2-10	33	2	12	.4694	.1700	.1306	.0200	.0000	.0000	.0669	.1043	.0100	.0288
CVS2-11	34	2	2	.4915	.0751	.0833	.0600	.0700	.0100	.0400	.0100	.0935	.0665
CVS2-12	35	2	6	.4683	.1700	.0700	.0466	.0700	.0100	.0400	.0901	.0100	.0250
CVS2-13	36	2	18	.4937	.0700	.1692	.0225	.0300	.0500	.0400	.0896	.0100	.0250
CVS2-14	37	2	9	.4600	.1313	.0802	.0486	.0500	.0200	.0400	.0243	.1000	.0457
CVS2-15	38	2	16	.4729	.0700	.1700	.0214	.0601	.0000	.0400	.0756	.0100	.0800

(a) The numbers in parentheses denote replicate sets of glasses. See Sections 4.2 through 4.6 and Tables 4.4, 4.7, 4.9, 4.12, and 4.14 for descriptions of the glasses tested.

(b) PS is the plotting symbol used in plots associated with these data. ID# is a consecutive integer numbering of all CVS glasses.

(c) The run orders are numbered within each phase of testing: CVS-I (CVS1-1 to CVS1-23), CVS-II Phase 1 (CVS2-1 to CVS2-19), CVS-II Phase 2 (CVS2-20 to CVS2-58), CVS-II Phase 3 (CVS2-59 to CVS2-101), and CVS-II Phase 4 (CVS2-102 to CVS2-123).

(d) The composition of Others is given in Table 4.1 for all glasses except CVS2-19, CVS2-51, CVS2-53 to CVS2-57, CVS2-64 to CVS2-70, CVS2-95, CVS2-97, CVS2-99, CVS2-100, CVS2-101, and CVS2-123. The Others composition for CVS2-19, CVS2-51, CVS2-97, and CVS2-123 (replicates of the internal standard glass) can be found in Table 4.8. The Others compositions for CVS2-55 to CVS2-57 are given in Table 4.10. The Others compositions for CVS2-53 and CVS2-54 are the same as in Table 4.1 except that Nd_2O_3 was replaced by UO_2. The Others compositions for CVS2-64 to CVS2-70, CVS2-95, and CVS2-101 are given in Table 4.13.

TABLE 4.15. As-Batched Mass Fraction Compositions for CVS-I and CVS-II Glasses (continued)

Glass[a]	ID[b] #	PS[b]	Run[c] Order	SiO_2	B_2O_3	Na_2O	Li_2O	CaO	MgO	Fe_2O_3	Al_2O_3	ZrO_2	Others[d]
CVS2-16 (4)	39	M	3	.5353	.1053	.1125	.0375	.0083	.0084	.0719	.0231	.0385	.0592
CVS2-17 (1)	40	M	8	.4801	.1142	.1003	.0376	.0275	.0363	.0568	.0636	.0429	.0407
CVS2-18 (4)	41	M	14	.5353	.1053	.1125	.0375	.0083	.0084	.0719	.0231	.0385	.0592
CVS2-19 (5)	42	M	19	.5328	.1048	.1129	.0373	.0082	.0084	.0733	.0235	.0392	.0596
CVS2-20	43	3	3	.5700	.0500	.1031	.0669	.0000	.0000	.0600	.0100	.1300	.0100
CVS2-21	44	3	15	.5700	.1314	.0500	.0700	.0000	.0800	.0200	.0686	.0000	.0100
CVS2-22	45	3	6	.5700	.0500	.0735	.0700	.0000	.0800	.0200	.0365	.0000	.1000
CVS2-23	46	3	11	.5700	.0522	.2000	.0100	.0800	.0000	.0200	.0578	.0000	.0100
CVS2-24	47	3	2	.4464	.2000	.0736	.0700	.0000	.0000	.0200	.0961	.0000	.0939
CVS2-25	48	3	10	.5059	.0500	.0841	.0700	.0800	.0000	.1500	.0033	.0000	.0567
CVS2-26	49	3	24	.4431	.2000	.0512	.0700	.0800	.0000	.0200	.0257	.1000	.0100
CVS2-27	50	3	4	.5463	.0500	.2000	.0155	.0000	.0800	.0200	.0782	.0000	.0100
CVS2-28	51	3	1	.5619	.0500	.2000	.0126	.0000	.0000	.0200	.0555	.0000	.1000
CVS2-29	52	3	14	.4391	.2000	.0675	.0100	.0800	.0000	.0200	.0000	.0834	.1000
CVS2-30	53	3	9	.5190	.2000	.0832	.0100	.0000	.0000	.1320	.0458	.0000	.0100
CVS2-31	54	3	19	.5700	.1843	.0500	.0331	.0800	.0000	.0200	.0526	.0000	.0100
CVS2-32	55	3	5	.5445	.0500	.2000	.0428	.0000	.0000	.0200	.0027	.1300	.0100
CVS2-33	56	3	25	.4200	.0544	.2000	.0364	.0000	.0800	.0200	.0892	.0000	.1000
CVS2-34 (6)	57	3	22	.4200	.1743	.2000	.0369	.0000	.0000	.0200	.1388	.0000	.0100
CVS2-35	58	3	7	.4200	.0500	.2000	.0428	.0800	.0000	.0632	.1340	.0000	.0100
CVS2-36	59	3	8	.5421	.0500	.0891	.0700	.0800	.0000	.1500	.0088	.0000	.0100
CVS2-37	60	3	12	.5700	.0839	.1061	.0700	.0000	.0000	.0200	.1400	.0000	.0100
CVS2-38	61	3	16	.5147	.1109	.1044	.0100	.0000	.0800	.1428	.0272	.0000	.0100
CVS2-39	62	3	13	.4838	.0500	.1362	.0700	.0000	.0800	.0742	.0258	.0700	.0100
CVS2-40	63	4	26	.5040	.0639	.1500	.0421	.0200	.0500	.0200	.1000	.0200	.0300
CVS2-41	64	4	21	.5325	.0694	.0781	.0700	.0500	.0200	.0300	.1000	.0200	.0300
CVS2-42	65	4	28	.5675	.0500	.0625	.0700	.0320	.0380	.1000	.0300	.0200	.0300
CVS2-43	66	4	17	.5070	.1477	.0500	.0653	.0200	.0300	.0300	.0500	.0700	.0300
CVS2-44	67	4	29	.5700	.1078	.0500	.0699	.0500	.0200	.0200	.0623	.0200	.0300
CVS2-45	68	4	30	.5299	.1106	.0500	.0595	.0200	.0500	.0308	.0592	.0200	.0700
CVS2-46	69	4	18	.5264	.1259	.0577	.0700	.0200	.0200	.0200	.0746	.0200	.0654
CVS2-47	70	4	23	.5294	.0500	.1277	.0429	.0500	.0200	.0200	.0400	.0500	.0700
CVS2-48	71	4	27	.4700	.1442	.0968	.0390	.0500	.0200	.0200	.0854	.0200	.0546
CVS2-49	72	4	20	.5073	.1357	.0957	.0413	.0200	.0200	.0515	.0785	.0200	.0300
CVS2-50 (1)	73	M	31	.4801	.1142	.1003	.0376	.0275	.0363	.0568	.0636	.0429	.0407
CVS2-51 (5)	74	M	32	.5328	.1048	.1129	.0373	.0082	.0084	.0733	.0235	.0392	.0596
CVS2-52	75	4	34	.6000	.0817	.0450	.0788	.0008	.0009	.0720	.0233	.0385	.0590

(a) The numbers in parentheses denote replicate sets of glasses. See Sections 4.2 through 4.6 and Tables 4.4, 4.7, 4.9, 4.12, and 4.14 for descriptions of the glasses tested.

(b) PS is the plotting symbol used in plots associated with these data. ID# is a consecutive integer numbering of all CVS glasses.

(c) The run orders are numbered within each phase of testing: CVS-I (CVS1-1 to CVS1-23), CVS-II Phase 1 (CVS2-1 to CVS2-19), CVS-II Phase 2 (CVS2-20 to CVS2-58), CVS-II Phase 3 (CVS2-59 to CVS2-101), and CVS-II Phase 4 (CVS2-102 to CVS2-123).

(d) The composition of Others is given in Table 4.1 for all glasses except CVS2-19, CVS2-51, CVS2-53 to CVS2-57, CVS2-64 to CVS2-70, CVS2-95, CVS2-97, CVS2-99, CVS2-100, CVS2-101, and CVS2-123. The Others composition for CVS2-19, CVS2-51, CVS2-97, and CVS2-123 (replicates of the internal standard glass) can be found in Table 4.8. The Others compositions for CVS2-55 to CVS2-57 are given in Table 4.10. The Others compositions for CVS2-53 and CVS2-54 are the same as in Table 4.1 except that Nd_2O_3 was replaced by UO_2. The Others compositions for CVS2-64 to CVS2-70, CVS2-95, and CVS2-101 are given in Table 4.13.

TABLE 4.15. As-Batched Mass Fraction Compositions for CVS-I and CVS-II Glasses (continued)

Glass[a]	ID[b] #	PS[b]	Run[c] Order	SiO_2	B_2O_3	Na_2O	Li_2O	CaO	MgO	Fe_2O_3	Al_2O_3	ZrO_2	Others[d]
CVS2-53	76	4	38	.5226	.0874	.0700	.0600	.0000	.0500	.0400	.0800	.0100	.0800
CVS2-54	77	M	39	.5328	.1048	.1129	.0373	.0082	.0084	.0733	.0235	.0392	.0596
CVS2-55	78	0	35	.5328	.1048	.1129	.0373	.0082	.0084	.0733	.0235	.0392	.0596
CVS2-56	79	0	36	.5328	.1048	.1129	.0373	.0082	.0084	.0733	.0235	.0392	.0596
CVS2-57	80	0	37	.5328	.1048	.1129	.0373	.0082	.0084	.0733	.0235	.0392	.0596
CVS2-58	81	4	33	.3900	.2000	.0500	.0700	.0200	.0800	.0200	.1500	.0100	.0100
CVS2-59	82	5	5	.4380	.1718	.1268	.0727	.0375	.0005	.0200	.1150	.0075	.0102
CVS2-60	83	5	10	.5281	.0876	.1725	.0743	.0063	.0005	.0200	.0925	.0075	.0107
CVS2-61	84	5	2	.5281	.0664	.1200	.0730	.0000	.0000	.0200	.1625	.0175	.0125
CVS2-62	85	5	13	.5579	.1765	.1125	.0156	.0500	.0005	.0200	.0500	.0075	.0095
CVS2-63	86	5	4	.3232	.1717	.1900	.0051	.1000	.0000	.0200	.1800	.0000	.0100
CVS2-64	87	0	24	.5697	.0509	.0925	.0642	.0025	.0008	.0812	.0288	.0431	.0663
CVS2-65	88	0	30	.5344	.1128	.0860	.0697	.0007	.0004	.0013	.0196	.1548	.0203
CVS2-66	89	0	3	.5175	.0917	.1211	.0523	.0097	.0061	.0388	.1180	.0026	.0422
CVS2-67	90	0	21	.4596	.1587	.1086	.0583	.0024	.0001	.0004	.2043	.0000	.0076
CVS2-68	91	0	11	.5040	.1355	.0797	.0696	.0007	.0002	.0046	.1640	.0001	.0416
CVS2-69	92	0	19	.5660	.0781	.0664	.0713	.0079	.0032	.0334	.0816	.0005	.0916
CVS2-70	93	0	38	.4854	.1418	.0812	.0691	.0008	.0008	.0080	.1819	.0005	.0305
CVS2-71	94	5	6	.5697	.0509	.0925	.0642	.0025	.0008	.0812	.0288	.0431	.0663
CVS2-72	95	5	9	.5175	.0917	.1211	.0523	.0097	.0061	.0388	.1180	.0026	.0422
CVS2-73	96	5	1	.5040	.1355	.0797	.0696	.0007	.0002	.0046	.1640	.0001	.0416
CVS2-74	97	5	34	.5660	.0781	.0664	.0713	.0079	.0032	.0334	.0816	.0005	.0916
CVS2-75	98	5	7	.4854	.1418	.0812	.0691	.0008	.0008	.0080	.1819	.0005	.0305
CVS2-76	99	5	15	.5018	.0600	.1800	.0632	.0400	.0050	.1050	.0200	.0050	.0200
CVS2-77	100	5	29	.4550	.0600	.1800	.0700	.0050	.0050	.0050	.0200	.1100	.0900
CVS2-78	101	5	33	.5600	.1600	.0500	.0254	.0050	.0400	.0699	.0200	.0497	.0200
CVS2-79	102	5	35	.5479	.1600	.0500	.0121	.0050	.0050	.1050	.0200	.0050	.0900
CVS2-80	103	5	22	.5074	.1600	.0500	.0176	.0050	.0400	.1050	.0200	.0750	.0200
CVS2-81	104	5	12	.4400	.0600	.1734	.0700	.0050	.0400	.1050	.0200	.0050	.0816
CVS2-82	105	5	23	.5600	.0950	.1800	.0700	.0050	.0400	.0050	.0200	.0050	.0200
CVS2-83	106	5	28	.4900	.0951	.1800	.0699	.0400	.0050	.0050	.0200	.0050	.0900
CVS2-84	107	5	39	.4550	.0600	.1800	.0700	.0050	.0050	.1050	.0200	.0800	.0200
CVS2-85	108	5	16	.4400	.0600	.1800	.0700	.0050	.0200	.0050	.1700	.0050	.0450
CVS2-86	109	5	25	.4764	.0600	.1800	.0136	.0400	.0050	.0050	.1700	.0050	.0450
CVS2-87	110	5	8	.4983	.0800	.1800	.0180	.0137	.0050	.0250	.0987	.0613	.0200
CVS2-88	111	5	37	.4597	.0600	.1403	.0700	.0400	.0050	.0250	.1050	.0750	.0200
CVS2-89	112	5	26	.4400	.1171	.1800	.0100	.0400	.0050	.1050	.0200	.0629	.0200
CVS2-90	113	5	20	.5600	.1600	.0542	.0700	.0050	.0050	.1008	.0200	.0050	.0200

(a) The numbers in parentheses denote replicate sets of glasses. See Sections 4.2 through 4.6 and Tables 4.4, 4.7, 4.9, 4.12, and 4.14 for descriptions of the glasses tested.

(b) PS is the plotting symbol used in plots associated with these data. ID# is a consecutive integer numbering of all CVS glasses.

(c) The run orders are numbered within each phase of testing: CVS-I (CVS1-1 to CVS1-23), CVS-II Phase 1 (CVS2-1 to CVS2-19), CVS-II Phase 2 (CVS2-20 to CVS2-58), CVS-II Phase 3 (CVS2-59 to CVS2-101), and CVS-II Phase 4 (CVS2-102 to CVS2-123).

(d) The composition of Others is given in Table 4.1 for all glasses except CVS2-19, CVS2-51, CVS2-53 to CVS2-57, CVS2-64 to CVS2-70, CVS2-95, CVS2-97, CVS2-99, CVS2-100, CVS2-101, and CVS2-123. The Others composition for CVS2-19, CVS2-51, CVS2-97, and CVS2-123 (replicates of the internal standard glass) can be found in Table 4.8. The Others compositions for CVS2-55 to CVS2-57 are given in Table 4.10. The Others compositions for CVS2-53 and CVS2-54 are the same as in Table 4.1 except that Nd_2O_3 was replaced by UO_2. The Others compositions for CVS2-64 to CVS2-70, CVS2-95, and CVS2-101 are given in Table 4.13.

TABLE 4.15. As-Batched Mass Fraction Compositions for CVS-I and CVS-II Glasses (continued)

Glass[a]	ID[b] #	PS[b]	Run[c] Order	SiO_2	B_2O_3	Na_2O	Li_2O	CaO	MgO	Fe_2O_3	Al_2O_3	ZrO_2	Others[d]	
CVS2-91	114	5	32	.5600	.1600	.1050	.0100	.0050	.0400	.0050	.0200	.0050	.0900	
CVS2-92	115	5	27	.4400	.1600	.1000	.0700	.0050	.0400	.0050	.0200	.0700	.0900	
CVS2-93	116	5	14	.4400	.1337	.1279	.0700	.0098	.0050	.0986	.0200	.0050	.0900	
CVS2-94	117	5	18	.4400	.1600	.1800	.0526	.0400	.0050	.0271	.0703	.0050	.0200	
CVS2-95 (7)	118	A	36	.4895	.1112	.1671	.0428	.0113	.0166	.0897	.0367	.0041	.0310	(e)
CVS2-96 (1)	119	M	40	.4801	.1142	.1003	.0376	.0275	.0363	.0568	.0636	.0429	.0407	
CVS2-97 (5)	120	M	31	.5328	.1048	.1129	.0373	.0082	.0084	.0733	.0235	.0392	.0596	
CVS2-98 (6)	121	5	17	.4200	.1743	.2000	.0369	.0000	.0000	.0200	.1388	.0000	.0100	
CVS2-99	122	5	41	.5203	.0969	.0980	.0356	.0097	.0077	.1019	.0523	.0199	.0577	
CVS2-100	123	5	42	.5329	.0740	.0626	.0596	.0035	.0012	.1229	.0286	.0443	.0704	
CVS2-101(7)	124	A	43	.4895	.1112	.1671	.0428	.0113	.0166	.0897	.0367	.0041	.0310	(f)
CVS2-102(4)	125	M	21	.5353	.1053	.1125	.0375	.0083	.0084	.0719	.0231	.0385	.0592	
CVS2-103	126	6	3	.4100	.1337	.1428	.0476	.0105	.0107	.0913	.0293	.0489	.0752	
CVS2-104	127	6	2	.4500	.1246	.1332	.0444	.0098	.0099	.0851	.0273	.0456	.0701	
CVS2-105	128	6	6	.4900	.1156	.1235	.0412	.0091	.0092	.0789	.0254	.0423	.0650	
CVS2-106	129	6	4	.5700	.0974	.1041	.0347	.0077	.0078	.0665	.0214	.0356	.0548	
CVS2-107	130	6	7	.5684	.0500	.1195	.0398	.0088	.0089	.0763	.0245	.0409	.0629	
CVS2-108	131	6	5	.5086	.1500	.1069	.0356	.0079	.0080	.0683	.0220	.0366	.0562	
CVS2-109	132	6	8	.4786	.2000	.1006	.0335	.0074	.0075	.0643	.0207	.0344	.0529	
CVS2-110	133	6	9	.5730	.1127	.0500	.0401	.0089	.0090	.0770	.0247	.0412	.0634	
CVS2-111	134	6	10	.5127	.1009	.1500	.0359	.0080	.0081	.0689	.0221	.0369	.0567	
CVS2-112	135	6	11	.4825	.0949	.2000	.0338	.0075	.0076	.0648	.0208	.0347	.0534	
CVS2-113	136	6	12	.5506	.1083	.1157	.0100	.0085	.0086	.0740	.0238	.0396	.0609	
CVS2-114	137	6	22	.5228	.1028	.1099	.0600	.0081	.0082	.0702	.0226	.0376	.0578	
CVS2-115	138	6	13	.5172	.1017	.1087	.0700	.0080	.0081	.0695	.0223	.0372	.0572	
CVS2-116	139	6	14	.5290	.1041	.1112	.0371	.0200	.0083	.0711	.0228	.0381	.0585	
CVS2-117	140	6	15	.5398	.1062	.1135	.0378	.0084	.0000	.0725	.0233	.0388	.0597	
CVS2-118	141	6	16	.5290	.1041	.1112	.0371	.0082	.0200	.0711	.0228	.0381	.0585	
CVS2-119	142	6	17	.5480	.1078	.1152	.0384	.0085	.0086	.0736	.0000	.0394	.0606	
CVS2-120	143	6	18	.5206	.1024	.1094	.0365	.0081	.0082	.0699	.0500	.0374	.0576	
CVS2-121	144	6	19	.4932	.0970	.1036	.0346	.0077	.0077	.0662	.1000	.0355	.0545	
CVS2-122	145	6	20	.4658	.0916	.0979	.0326	.0072	.0073	.0626	.1500	.0335	.0515	
CVS2-123(5)	146	M	1	.5328	.1048	.1129	.0373	.0082	.0084	.0733	.0235	.0392	.0596	

(a) The numbers in parentheses denote replicate sets of glasses. See Sections 4.2 through 4.6 and Tables 4.4, 4.7, 4.9, 4.12, and 4.14 for descriptions of the glasses tested.

(b) PS is the plotting symbol used in plots associated with these data. ID# is a consecutive integer numbering of all CVS glasses.

(c) The run orders are numbered within each phase of testing: CVS-I (CVS1-1 to CVS1-23), CVS-II Phase 1 (CVS2-1 to CVS2-19), CVS-II Phase 2 (CVS2-20 to CVS2-58), CVS-II Phase 3 (CVS2-59 to CVS2-101), and CVS-II Phase 4 (CVS2-102 to CVS2-123).

(d) The composition of Others is given in Table 4.1 for all glasses except CVS2-19, CVS2-51, CVS2-53 to CVS2-57, CVS2-64 to CVS2-70, CVS2-95, CVS2-97, CVS2-99, CVS2-100, CVS2-101, and CVS2-123. The Others composition for CVS2-19, CVS2-51, CVS2-97, and CVS2-123 (replicates of the internal standard glass) can be found in Table 4.8. The Others compositions for CVS2-55 to CVS2-57 are given in Table 4.10. The Others compositions for CVS2-53 and CVS2-54 are the same as in Table 4.1 except that Nd_2O_3 was replaced by UO_2. The Others compositions for CVS2-64 to CVS2-70, CVS2-95, and CVS2-101 are given in Table 4.13.

(e) Fe_2O_3 = .0897 represents the sum of FeO = .0089 and Fe_2O_3 = .0808.

(f) This is the nominal composition of the DWPF EA glass written in the 10-component CVS format. SRTC had Corning make a large quantity of EA glass using the nominal composition as a target. The composition obtained by averaging 30 replicate analyses (by Corning) of the resulting glass is (.4873, .1128, .1681, .0426, .0112, .0172, .0738, .0370, .0046, .0454).

Table 4.16 contains the pairwise Pearson correlation coefficients among the 10 components for all of the CVS glasses listed in Table 4.15 as well as for all glasses except those from CVS-II Phase 4 (because only durability data were collected for those glasses). Pearson correlation coefficients take values between -1.0 and +1.0, and indicate the strength of the linear relationship between two variables (two glass components in this case). Correlations of -1.0 and +1.0 represent perfect linear relationships with negative and positive slopes, respectively. A correlation of 0.0 represents a total lack of a linear relationship. Because glass mass fractions must sum to 1.0, both positive and negative correlations must exist among pairs of components. Correlations greater than 0.6 - 0.8 (in absolute value) indicate the presence of significant confounding between pairs of components. This means that the components tend to vary together rather strongly over the data set being investigated, and this can make it difficult or impossible for empirical mixture models fitted to the data set to properly separate the effect of one confounded component from the effect of the other. Hence, correlation coefficients among pairs of components were investigated during test matrix development to make sure confounding of components was not unacceptably high.

Several correlations are identified as statistically significant (i.e., significantly different from zero at the 95% confidence level or higher) in both parts of Table 4.16. These statistically significant correlations are attributable to the single-component and multiple-component constraints used to define the experimental region, and hence were unavoidable. Although statistically significant, these correlations do not represent major confounding of component effects and thus the impact on empirical mixture modeling will be minimal.

TABLE 4.16. Pairwise Correlations[a] Among Glass Components[b] For CVS-I and CVS-II Glasses

All CVS Glasses Except CVS-II Phase 4 (N = 124)

	SiO_2	B_2O_3	Na_2O	Li_2O	CaO	MgO	Fe_2O_3	Al_2O_3	ZrO_2
B_2O_3	-0.338								
Na_2O	-0.294	-0.281							
Li_2O	0.018	-0.181	-0.262						
CaO	-0.209	-0.010	-0.071	-0.104					
MgO	-0.040	-0.063	-0.091	-0.081	-0.253				
Fe_2O_3	0.081	-0.201	-0.132	-0.157	-0.019	0.020			
Al_2O_3	-0.328	0.060	0.075	0.138	0.039	-0.102	-0.474		
ZrO_2	-0.045	-0.092	-0.048	0.027	-0.056	-0.061	-0.019	-0.445	
Others	-0.013	-0.107	-0.111	0.020	-0.147	-0.042	-0.006	-0.257	-0.012

All CVS Glasses (N = 146)

	SiO_2	B_2O_3	Na_2O	Li_2O	CaO	MgO	Fe_2O_3	Al_2O_3	ZrO_2
B_2O_3	-0.334								
Na_2O	-0.289	-0.292							
Li_2O	0.041	-0.188	-0.269						
CaO	-0.209	-0.010	-0.061	-0.134					
MgO	-0.028	-0.065	-0.086	-0.105	-0.295				
Fe_2O_3	0.080	-0.212	-0.158	-0.144	0.018	0.051			
Al_2O_3	-0.320	0.076	0.109	0.130	-0.001	-0.144	-0.462		
ZrO_2	-0.054	-0.095	-0.048	0.038	-0.041	-0.047	-0.035	-0.451	
Others	-0.025	-0.113	-0.126	0.043	-0.115	-0.010	-0.047	-0.228	-0.039

(a) Pearson correlation coefficients take values between -1.0 and +1.0, which represent perfect negative and positive pairwise linear correlations, respectively. A correlation of 0.0 represents a total lack of pairwise linear correlation. Underlined values are statistically significant (i.e., different from zero at the 95% confidence level).

(b) As-batched compositions of the glasses as listed in Table 4.15 were used.

4.8 COMBINED CVS EXPERIMENTAL DESIGN IN MOLE FRACTIONS

Table 4.17 contains a complete list of the "9 components plus Others" mole fraction compositions of all glasses tested in CVS-I and CVS-II. Table 4.17 has the same format and information as Table 4.15, except that mole fraction compositions rather than mass fraction compositions are listed.

The mole fraction compositions in Table 4.17 were obtained from the mass fraction compositions in Table 4.15 using:

$$x_i = \frac{g_i / M_i}{\sum_{j=1}^{10} g_j / M_j} \qquad (4.1)$$

where x_i, g_i, and M_i are the mole fraction, mass fraction and molecular mass of oxide component i, respectively. The average molecular weight of Others is given by:

$$M_O = \frac{1}{\sum_{Others} g_{Oi} / M_i} \qquad (4.2)$$

where g_{0i} is the mass fraction of oxide component i in Others and M_0 is the calculated molecular weight of the Others component. For those Others compositions (see Table 4.13) containing possibly volatile components such as F and SO_3, three possible options exist: 1) assume all volatile species are removed in melting, 2) assume all species remain in glass, or 3) measure volatile components in glass after melting and use true composition. The molecular weights of the Others component for the various Others mixes used in CVS are given in Table 4.18 using Methods 1) and 2). Method 3) is deemed inappropriate because of the effect on melting conditions of retention of SO_3 and F in the glass.

TABLE 4.17. Mole Fraction Compositions for CVS-I and CVS-II Glasses Assuming F and SO_3 Do Not Remain in the Glass

Glass[a]	ID[b] #	PS[b]	Run[c] Order	SiO_2	B_2O_3	Na_2O	Li_2O	CaO	MgO	Fe_2O_3	Al_2O_3	ZrO_2	Others
CVS1-1 (1)	1	M	4	.5169	.1061	.1047	.0814	.0317	.0582	.0230	.0403	.0225	.0151
CVS1-2	2	1	10	.5562	.0436	.0490	.1424	.1083	.0000	.0076	.0894	.0000	.0035
CVS1-3	3	1	17	.4202	.1727	.0485	.1409	.0000	.1193	.0075	.0825	.0049	.0034
CVS1-4 (2)	4	1	12	.5691	.1723	.0871	.0201	.0214	.1191	.0075	.0000	.0000	.0034
CVS1-5	5	1	3	.6137	.0465	.0731	.1516	.0000	.0000	.0608	.0508	.0000	.0037
CVS1-6	6	1	5	.4876	.1913	.0537	.1560	.0000	.0000	.0083	.0000	.0648	.0382
CVS1-7	7	1	7	.6241	.0472	.1023	.0220	.1173	.0000	.0138	.0000	.0694	.0038
CVS1-8 (3)	8	1	9	.5967	.0480	.0903	.0224	.0000	.1327	.0628	.0000	.0434	.0038
CVS1-9	9	1	15	.4839	.1951	.0601	.0232	.0000	.1374	.0607	.0000	.0000	.0397
CVS1-10	10	1	6	.6565	.0846	.1060	.0232	.0000	.0000	.0087	.0814	.0000	.0397
CVS1-11	11	1	8	.4820	.1534	.0836	.0231	.1230	.0000	.0086	.0947	.0000	.0316
CVS1-12	12	1	16	.4415	.1600	.0750	.1480	.1126	.0000	.0593	.0000	.0000	.0036
CVS1-13	13	1	14	.5960	.1805	.1887	.0210	.0000	.0000	.0079	.0023	.0000	.0036
CVS1-14	14	1	22	.4764	.1958	.2047	.0228	.0000	.0000	.0085	.0159	.0719	.0039
CVS1-15	15	1	11	.5472	.0422	.1149	.1378	.0000	.1167	.0074	.0000	.0000	.0337
CVS1-16	16	1	2	.4716	.0470	.1979	.0219	.0000	.1300	.0352	.0926	.0000	.0038
CVS1-17	17	1	19	.5328	.0506	.1653	.0236	.1256	.0000	.0617	.0000	.0000	.0404
CVS1-18	18	1	18	.4376	.0448	.1194	.1462	.0223	.1238	.0078	.0000	.0658	.0322
CVS1-19 (1)	19	M	13	.5169	.1061	.1047	.0814	.0317	.0582	.0230	.0403	.0225	.0151
CVS1-20 (1)	20	M	21	.5169	.1061	.1047	.0814	.0317	.0582	.0230	.0403	.0225	.0151
CVS1-21 (2)	21	1	1	.5691	.1723	.0871	.0201	.0214	.1191	.0075	.0000	.0000	.0034
CVS1-22 (3)	22	1	20	.5967	.0480	.0903	.0224	.0000	.1327	.0628	.0000	.0434	.0038
CVS1-23	23	M	23	.5684	.0910	.1125	.0832	.0342	.0138	.0489	.0296	.0034	.0149
CVS2-1	24	2	4	.5468	.0789	.0710	.1263	.0000	.0780	.0157	.0493	.0051	.0288
CVS2-2	25	2	11	.5290	.0637	.0903	.1272	.0791	.0000	.0179	.0684	.0154	.0091
CVS2-3	26	2	17	.5006	.1228	.0731	.0943	.0808	.0161	.0182	.0655	.0193	.0093
CVS2-4	27	2	1	.5772	.0974	.0699	.1111	.0773	.0000	.0155	.0376	.0050	.0089
CVS2-5	28	2	10	.5384	.1555	.1110	.0456	.0423	.0000	.0171	.0534	.0055	.0312
CVS2-6	29	2	13	.5932	.0667	.0749	.0848	.0828	.0076	.0499	.0103	.0054	.0244
CVS2-7	30	2	15	.5214	.1589	.0735	.1287	.0109	.0000	.0163	.0608	.0053	.0242
CVS2-8	31	2	7	.5356	.0633	.1000	.1264	.0000	.0780	.0449	.0376	.0051	.0090
CVS2-9	32	2	5	.5858	.0879	.0966	.1302	.0000	.0000	.0289	.0088	.0526	.0093
CVS2-10	33	2	12	.5308	.1659	.1432	.0455	.0000	.0000	.0285	.0695	.0055	.0112
CVS2-11	34	2	2	.5245	.0692	.0862	.1288	.0800	.0159	.0161	.0063	.0487	.0244
CVS2-12	35	2	6	.4939	.1547	.0716	.0988	.0791	.0157	.0159	.0560	.0051	.0091
CVS2-13	36	2	18	.5189	.0635	.1724	.0476	.0338	.0783	.0158	.0555	.0051	.0090
CVS2-14	37	2	9	.4967	.1224	.0840	.1055	.0578	.0322	.0163	.0155	.0527	.0170
CVS2-15	38	2	16	.5269	.0673	.1836	.0479	.0717	.0000	.0168	.0496	.0054	.0307

(a) The numbers in parentheses denote replicate sets of glasses. See Sections 4.2 through 4.6 and Tables 4.4, 4.7, 4.9, 4.12, and 4.14 for descriptions of the glasses tested.

(b) PS is the plotting symbol used in plots associated with these data. ID# is a consecutive integer numbering of all CVS glasses.

(c) The run orders are numbered within each phase of testing: CVS-I (CVS1-1 to CVS1-23), CVS-II Phase 1 (CVS2-1 to CVS2-19), CVS-II Phase 2 (CVS2-20 to CVS2-58), CVS-II Phase 3 (CVS2-59 to CVS2-101), and CVS-II Phase 4 (CVS2-102 to CVS2-123).

TABLE 4.17. Mole Fraction Compositions for CVS-I and CVS-II Glasses Assuming F and SO_3 Do Not Remain in the Glass (continued)

Glass[a]	ID[b] #	PS[b]	Run[c] Order	SiO_2	B_2O_3	Na_2O	Li_2O	CaO	MgO	Fe_2O_3	Al_2O_3	ZrO_2	Others
CVS2-16 (4)	39	M	3	.5870	.0997	.1196	.0827	.0098	.0137	.0297	.0149	.0206	.0224
CVS2-17 (1)	40	M	8	.5169	.1061	.1047	.0814	.0317	.0582	.0230	.0403	.0225	.0151
CVS2-18 (4)	41	M	14	.5870	.0997	.1196	.0827	.0098	.0137	.0297	.0149	.0206	.0224
CVS2-19 (5)	42	M	19	.5848	.0993	.1201	.0823	.0096	.0137	.0303	.0152	.0210	.0236
CVS2-20	43	3	3	.6045	.0458	.1060	.1427	.0000	.0000	.0239	.0062	.0672	.0037
CVS2-21	44	3	15	.5464	.1087	.0465	.1349	.0000	.1143	.0072	.0387	.0000	.0033
CVS2-22	45	3	6	.5655	.0428	.0707	.1397	.0000	.1183	.0075	.0213	.0000	.0342
CVS2-23	46	3	11	.5939	.0469	.2020	.0210	.0893	.0000	.0078	.0355	.0000	.0036
CVS2-24	47	3	2	.4812	.1861	.0769	.1518	.0000	.0000	.0081	.0611	.0000	.0349
CVS2-25	48	3	10	.5411	.0462	.0872	.1506	.0917	.0000	.0604	.0021	.0000	.0209
CVS2-26	49	3	24	.4584	.1786	.0513	.1456	.0887	.0000	.0078	.0157	.0504	.0036
CVS2-27	50	3	4	.5514	.0436	.1957	.0315	.0000	.1203	.0076	.0465	.0000	.0035
CVS2-28	51	3	1	.6251	.0480	.2157	.0282	.0000	.0000	.0084	.0364	.0000	.0383
CVS2-29	52	3	14	.5073	.1994	.0756	.0232	.0990	.0000	.0087	.0000	.0470	.0398
CVS2-30	53	3	9	.5949	.1978	.0924	.0230	.0000	.0000	.0569	.0309	.0000	.0039
CVS2-31	54	3	19	.5866	.1637	.0499	.0685	.0882	.0000	.0077	.0319	.0000	.0035
CVS2-32	55	3	5	.5771	.0457	.2055	.0912	.0000	.0000	.0080	.0017	.0672	.0036
CVS2-33	56	3	25	.4431	.0495	.2046	.0772	.0000	.1258	.0079	.0555	.0000	.0363
CVS2-34 (6)	57	3	22	.4510	.1615	.2082	.0797	.0000	.0000	.0081	.0878	.0000	.0037
CVS2-35	58	3	7	.4492	.0462	.2074	.0921	.0917	.0000	.0254	.0845	.0000	.0037
CVS2-36	59	3	8	.5628	.0448	.0897	.1462	.0890	.0000	.0586	.0054	.0000	.0036
CVS2-37	60	3	12	.5819	.0739	.1050	.1437	.0000	.0000	.0077	.0842	.0000	.0035
CVS2-38	61	3	16	.5569	.1036	.1095	.0218	.0000	.1290	.0581	.0173	.0000	.0037
CVS2-39	62	3	13	.4839	.0432	.1321	.1408	.0000	.1193	.0279	.0152	.0341	.0034
CVS2-40	63	4	26	.5187	.0568	.1496	.0871	.0221	.0767	.0077	.0606	.0100	.0106
CVS2-41	64	4	21	.5420	.0610	.0771	.1433	.0545	.0303	.0115	.0600	.0099	.0105
CVS2-42	65	4	28	.5801	.0441	.0619	.1439	.0350	.0579	.0385	.0181	.0100	.0106
CVS2-43	66	4	17	.5250	.1320	.0502	.1360	.0222	.0463	.0117	.0305	.0353	.0107
CVS2-44	67	4	29	.5701	.0931	.0485	.1406	.0536	.0298	.0075	.0367	.0098	.0103
CVS2-45	68	4	30	.5464	.0984	.0500	.1234	.0221	.0768	.0119	.0360	.0101	.0249
CVS2-46	69	4	18	.5445	.1124	.0579	.1456	.0222	.0308	.0078	.0455	.0101	.0233
CVS2-47	70	4	23	.5599	.0456	.1309	.0912	.0567	.0315	.0080	.0249	.0258	.0255
CVS2-48	71	4	27	.5019	.1329	.1002	.0837	.0572	.0318	.0080	.0537	.0104	.0201
CVS2-49	72	4	20	.5413	.1250	.0990	.0886	.0229	.0318	.0207	.0494	.0104	.0110
CVS2-50 (1)	73	M	31	.5169	.1061	.1047	.0814	.0317	.0582	.0230	.0403	.0225	.0151
CVS2-51 (5)	74	M	32	.5848	.0993	.1201	.0823	.0096	.0137	.0303	.0152	.0210	.0236
CVS2-52	75	4	34	.6285	.0739	.0457	.1660	.0009	.0014	.0284	.0144	.0197	.0213

(a) The numbers in parentheses denote replicate sets of glasses. See Sections 4.2 through 4.6 and Tables 4.4, 4.7, 4.9, 4.12, and 4.14 for descriptions of the glasses tested.

(b) PS is the plotting symbol used in plots associated with these data. ID# is a consecutive integer numbering of all CVS glasses.

(c) The run orders are numbered within each phase of testing: CVS-I (CVS1-1 to CVS1-23), CVS-II Phase 1 (CVS2-1 to CVS2-19), CVS-II Phase 2 (CVS2-20 to CVS2-58), CVS-II Phase 3 (CVS2-59 to CVS2-101), and CVS-II Phase 4 (CVS2-102 to CVS2-123).

TABLE 4.17. Mole Fraction Compositions for CVS-I and CVS-II Glasses Assuming F and SO_3 Do Not Remain in the Glass (continued)

Glass[a]	ID[b] #	PS[b]	Run[c] Order	SiO_2	B_2O_3	Na_2O	Li_2O	CaO	MgO	Fe_2O_3	Al_2O_3	ZrO_2	Others
CVS2-53	76	4	38	.5464	.0789	.0709	.1262	.0000	.0779	.0157	.0493	.0051	.0296
CVS2-54	77	M	39	.5851	.0993	.1202	.0824	.0096	.0137	.0303	.0152	.0210	.0232
CVS2-55	78	0	35	.5820	.0988	.1196	.0819	.0096	.0137	.0301	.0151	.0209	.0283
CVS2-56	79	0	36	.5763	.0978	.1184	.0811	.0095	.0135	.0298	.0150	.0207	.0378
CVS2-57	80	0	37	.5915	.1004	.1215	.0833	.0098	.0139	.0306	.0154	.0212	.0125
CVS2-58	81	4	33	.3913	.1732	.0486	.1412	.0215	.1196	.0075	.0887	.0049	.0035
CVS2-59	82	5	5	.4475	.1515	.1256	.1494	.0410	.0008	.0077	.0692	.0037	.0036
CVS2-60	83	5	10	.5296	.0758	.1677	.1498	.0068	.0007	.0075	.0547	.0037	.0037
CVS2-61	84	5	2	.5474	.0594	.1206	.1522	.0000	.0000	.0078	.0993	.0088	.0045
CVS2-62	85	5	13	.5879	.1605	.1149	.0331	.0565	.0008	.0079	.0311	.0039	.0034
CVS2-63	86	5	4	.3631	.1665	.2070	.0115	.1204	.0000	.0085	.1192	.0000	.0039
CVS2-64	87	0	24	.6113	.0471	.0962	.1385	.0029	.0013	.0328	.0182	.0226	.0292
CVS2-65	88	0	30	.5608	.1022	.0875	.1471	.0008	.0006	.0005	.0121	.0792	.0091
CVS2-66	89	0	3	.5469	.0836	.1241	.1112	.0110	.0096	.0154	.0735	.0013	.0234
CVS2-67	90	0	21	.4864	.1449	.1114	.1241	.0027	.0002	.0002	.1274	.0000	.0028
CVS2-68	91	0	11	.5286	.1227	.0810	.1468	.0008	.0003	.0018	.1014	.0001	.0166
CVS2-69	92	0	19	.5930	.0706	.0674	.1502	.0089	.0050	.0132	.0504	.0003	.0410
CVS2-70	93	0	38	.5098	.1285	.0827	.1460	.0009	.0013	.0032	.1126	.0003	.0148
CVS2-71	94	5	6	.6141	.0474	.0967	.1392	.0029	.0013	.0329	.0183	.0227	.0246
CVS2-72	95	5	9	.5513	.0843	.1251	.1121	.0111	.0097	.0156	.0741	.0014	.0155
CVS2-73	96	5	1	.5294	.1228	.0812	.1470	.0008	.0003	.0018	.1015	.0001	.0150
CVS2-74	97	5	34	.5978	.0712	.0680	.1514	.0089	.0050	.0133	.0508	.0003	.0333
CVS2-75	98	5	7	.5118	.1290	.0830	.1465	.0009	.0013	.0032	.1130	.0003	.0111
CVS2-76	99	5	15	.5194	.0536	.1806	.1316	.0444	.0077	.0409	.0122	.0025	.0071
CVS2-77	100	5	29	.4876	.0555	.1870	.1509	.0057	.0080	.0020	.0126	.0575	.0332
CVS2-78	101	5	33	.6010	.1482	.0520	.0548	.0057	.0640	.0282	.0126	.0260	.0074
CVS2-79	102	5	35	.6398	.1613	.0566	.0284	.0063	.0087	.0461	.0138	.0028	.0362
CVS2-80	103	5	22	.5707	.1553	.0545	.0398	.0060	.0671	.0444	.0133	.0411	.0077
CVS2-81	104	5	12	.4644	.0547	.1774	.1486	.0057	.0629	.0417	.0124	.0026	.0297
CVS2-82	105	5	23	.5358	.0784	.1669	.1347	.0051	.0570	.0018	.0113	.0023	.0066
CVS2-83	106	5	28	.4977	.0834	.1772	.1428	.0435	.0076	.0019	.0120	.0025	.0315
CVS2-84	107	5	39	.4882	.0556	.1872	.1510	.0057	.0080	.0424	.0126	.0419	.0074
CVS2-85	108	5	16	.4573	.0538	.1814	.1463	.0056	.0310	.0020	.1041	.0025	.0161
CVS2-86	109	5	25	.5291	.0575	.1938	.0304	.0476	.0083	.0021	.1113	.0027	.0172
CVS2-87	110	5	8	.5509	.0763	.1929	.0400	.0162	.0082	.0104	.0643	.0330	.0076
CVS2-88	111	5	37	.4822	.0543	.1427	.1477	.0450	.0078	.0099	.0649	.0384	.0072
CVS2-89	112	5	26	.5030	.1155	.1995	.0230	.0490	.0085	.0452	.0135	.0351	.0079
CVS2-90	113	5	20	.5814	.1434	.0545	.1461	.0056	.0077	.0394	.0122	.0025	.0071

(a) The numbers in parentheses denote replicate sets of glasses. See Sections 4.2 through 4.6 and Tables 4.4, 4.7, 4.9, 4.12, and 4.14 for descriptions of the glasses tested.

(b) PS is the plotting symbol used in plots associated with these data. ID# is a consecutive integer numbering of all CVS glasses.

(c) The run orders are numbered within each phase of testing: CVS-I (CVS1-1 to CVS1-23), CVS-II Phase 1 (CVS2-1 to CVS2-19), CVS-II Phase 2 (CVS2-20 to CVS2-58), CVS-II Phase 3 (CVS2-59 to CVS2-101), and CVS-II Phase 4 (CVS2-102 to CVS2-123).

TABLE 4.17. Mole Fraction Compositions for CVS-I and CVS-II Glasses Assuming F and SO_3 Do Not Remain in the Glass (continued)

Glass[a]	ID[b] #	PS[b]	Run[c] Order	SiO_2	B_2O_3	Na_2O	Li_2O	CaO	MgO	Fe_2O_3	Al_2O_3	ZrO_2	Others
CVS2-91	114	5	32	.6008	.1482	.1092	.0216	.0057	.0640	.0020	.0126	.0026	.0332
CVS2-92	115	5	27	.4585	.1439	.1010	.1467	.0056	.0621	.0020	.0123	.0356	.0323
CVS2-93	116	5	14	.4780	.1254	.1347	.1529	.0114	.0081	.0403	.0128	.0026	.0337
CVS2-94	117	5	18	.4538	.1424	.1800	.1091	.0442	.0077	.0105	.0427	.0025	.0071
CVS2-95 (7)	118	A	36	.5216	.1023	.1726	.0917	.0129	.0264	.0360	.0230	.0021	.0114
CVS2-96 (1)	119	M	40	.5169	.1061	.1047	.0814	.0317	.0582	.0230	.0403	.0225	.0151
CVS2-97 (5)	120	M	31	.5848	.0993	.1201	.0823	.0096	.0137	.0303	.0152	.0210	.0236
CVS2-98 (6)	121	5	17	.4510	.1615	.2082	.0797	.0000	.0000	.0081	.0878	.0000	.0037
CVS2-99	122	5	41	.5784	.0930	.1056	.0796	.0116	.0128	.0426	.0343	.0108	.0315
CVS2-100	123	5	42	.5930	.0711	.0675	.1334	.0042	.0020	.0515	.0188	.0240	.0346
CVS2-101(7)	124	A	43	mole fractions not computed for this glass--not used in modeling									
CVS2-102(4)	125	M	21										
CVS2-103	126	6	3										
CVS2-104	127	6	2										
CVS2-105	128	6	6										
CVS2-106	129	6	4										
CVS2-107	130	6	7										
CVS2-108	131	6	5										
CVS2-109	132	6	8										
CVS2-110	133	6	9										
CVS2-111	134	6	10	mole fractions not computed for these glasses--not used in modeling									
CVS2-112	135	6	11										
CVS2-113	136	6	12										
CVS2-114	137	6	22										
CVS2-115	138	6	13										
CVS2-116	139	6	14										
CVS2-117	140	6	15										
CVS2-118	141	6	16										
CVS2-119	142	6	17										
CVS2-120	143	6	18										
CVS2-121	144	6	19										
CVS2-122	145	6	20										
CVS2-123(5)	146	M	1										

(a) The numbers in parentheses denote replicate sets of glasses. See Sections 4.2 through 4.6 and Tables 4.4, 4.7, 4.9, 4.12, and 4.14 for descriptions of the glasses tested.

(b) PS is the plotting symbol used in plots associated with these data. ID# is a consecutive integer numbering of all CVS glasses.

(c) The run orders are numbered within each phase of testing: CVS-I (CVS1-1 to CVS1-23), CVS-II Phase 1 (CVS2-1 to CVS2-19), CVS-II Phase 2 (CVS2-20 to CVS2-58), CVS-II Phase 3 (CVS2-59 to CVS2-101), and CVS-II Phase 4 (CVS2-102 to CVS2-123).

TABLE 4.18. Calculated Molecular Weight of Others for Various Others Mixes Used in CVS Glasses Assuming: (a) All F and SO_3 Volatilize During Melting, and (b) All F and SO_3 Remain After Melting

Glass	(a) No F, SO_3	(b) All F, SO_3
STD NCAW	174.5	109.4
CVS2-19	166.5	116.2
CVS2-55	138.4	95.4
CVS2-56	102.5	76.8
CVS2-57	319.0	173.0
CVS2-64	146.6	131.4
CVS2-65	140.0	140.4
CVS2-66	114.5	105.2
CVS2-67	172.0	68.1
CVS2-68	158.0	74.1
CVS2-69	140.5	115.2
CVS2-70	129.8	128.1
CVS2-95	174.5	91.1
CVS2-99	122.5	110.7
CVS2-100	136.0	126.2

Method 1 was used to compute the mole fractions listed in Table 4.17, because it corresponds to the method used by SRTC to compute mole fractions from mass fractions as one of the steps in calculating free energy of hydration (see Appendix H). However, F and SO_3 are retained in CVS glasses during melting, which argues for using Method 2 in the future. Table 4.19 lists mole fraction compositions obtained by Method 2 for comparison to those listed in Table 4.17. The mole fractions in Table 4.17 were the ones used to develop the mole fraction glass property models presented and discussed in later chapters of the report.

TABLE 4.19. Mole Fraction Compositions for CVS-I and CVS-II Glasses Assuming F and SO_3 Remain in the Glass

Glass[a]	ID[b] #	PS[b]	Run[c] Order	SiO_2	B_2O_3	Na_2O	Li_2O	CaO	MgO	Fe_2O_3	Al_2O_3	ZrO_2	Others
CVS1-1 (1)	1	M	4	.5123	.1052	.1037	.0807	.0314	.0577	.0228	.0400	.0223	.0239
CVS1-2	2	1	10	.5550	.0435	.0489	.1420	.1081	.0000	.0076	.0892	.0000	.0055
CVS1-3	3	1	17	.4194	.1724	.0484	.1405	.0000	.1191	.0075	.0824	.0049	.0055
CVS1-4 (2)	4	1	12	.5679	.1720	.0869	.0200	.0213	.1188	.0075	.0000	.0000	.0055
CVS1-5	5	1	3	.6123	.0464	.0729	.1512	.0000	.0000	.0606	.0506	.0000	.0059
CVS1-6	6	1	5	.4768	.1870	.0525	.1525	.0000	.0000	.0082	.0000	.0634	.0595
CVS1-7	7	1	7	.6227	.0471	.1021	.0220	.1170	.0000	.0138	.0000	.0693	.0060
CVS1-8 (3)	8	1	9	.5953	.0479	.0901	.0223	.0000	.1324	.0626	.0000	.0433	.0061
CVS1-9	9	1	15	.4727	.1906	.0587	.0226	.0000	.1342	.0593	.0000	.0000	.0618
CVS1-10	10	1	6	.6414	.0826	.1035	.0226	.0000	.0000	.0085	.0796	.0000	.0618
CVS1-11	11	1	8	.4731	.1506	.0820	.0227	.1207	.0000	.0085	.0929	.0000	.0495
CVS1-12	12	1	16	.4405	.1597	.0748	.1476	.1124	.0000	.0592	.0000	.0000	.0058
CVS1-13	13	1	14	.5947	.1801	.1883	.0210	.0000	.0000	.0079	.0023	.0000	.0057
CVS1-14	14	1	22	.4753	.1953	.2043	.0228	.0000	.0000	.0085	.0159	.0717	.0062
CVS1-15	15	1	11	.5364	.0414	.1127	.1351	.0000	.1145	.0072	.0000	.0000	.0527
CVS1-16	16	1	2	.4706	.0469	.1975	.0219	.0000	.1297	.0351	.0924	.0000	.0060
CVS1-17	17	1	19	.5203	.0494	.1615	.0230	.1226	.0000	.0603	.0000	.0000	.0629
CVS1-18	18	1	18	.4294	.0440	.1172	.1434	.0218	.1215	.0077	.0000	.0646	.0504
CVS1-19 (1)	19	M	13	.5123	.1052	.1037	.0807	.0314	.0577	.0228	.0400	.0223	.0239
CVS1-20 (1)	20	M	21	.5123	.1052	.1037	.0807	.0314	.0577	.0228	.0400	.0223	.0239
CVS1-21 (2)	21	1	1	.5679	.1720	.0869	.0200	.0213	.1188	.0075	.0000	.0000	.0055
CVS1-22 (3)	22	1	20	.5953	.0479	.0901	.0223	.0000	.1324	.0626	.0000	.0433	.0061
CVS1-23	23	M	23	.5634	.0902	.1115	.0824	.0339	.0137	.0485	.0294	.0034	.0236
CVS2-1	24	2	4	.5376	.0776	.0698	.1241	.0000	.0767	.0155	.0485	.0050	.0452
CVS2-2	25	2	11	.5262	.0634	.0898	.1265	.0787	.0000	.0178	.0680	.0153	.0144
CVS2-3	26	2	17	.4978	.1221	.0727	.0937	.0804	.0160	.0181	.0652	.0192	.0147
CVS2-4	27	2	1	.5742	.0969	.0696	.1105	.0769	.0000	.0154	.0374	.0050	.0141
CVS2-5	28	2	10	.5287	.1527	.1089	.0447	.0415	.0000	.0167	.0524	.0054	.0489
CVS2-6	29	2	13	.5847	.0658	.0739	.0836	.0816	.0075	.0491	.0102	.0053	.0383
CVS2-7	30	2	15	.5140	.1567	.0725	.1269	.0108	.0000	.0161	.0600	.0052	.0380
CVS2-8	31	2	7	.5328	.0629	.0995	.1257	.0000	.0776	.0447	.0374	.0051	.0143
CVS2-9	32	2	5	.5826	.0874	.0961	.1294	.0000	.0000	.0287	.0087	.0523	.0147
CVS2-10	33	2	12	.5273	.1648	.1422	.0452	.0000	.0000	.0283	.0690	.0055	.0178
CVS2-11	34	2	2	.5170	.0682	.0849	.1269	.0789	.0157	.0158	.0062	.0480	.0384
CVS2-12	35	2	6	.4913	.1539	.0712	.0983	.0787	.0156	.0158	.0557	.0051	.0144
CVS2-13	36	2	18	.5161	.0632	.1715	.0473	.0336	.0779	.0157	.0552	.0051	.0144
CVS2-14	37	2	9	.4918	.1211	.0831	.1045	.0573	.0319	.0161	.0153	.0521	.0268
CVS2-15	38	2	16	.5174	.0661	.1803	.0471	.0705	.0000	.0165	.0487	.0053	.0481

(a) The numbers in parentheses denote replicate sets of glasses. See Sections 4.2 through 4.6 and Tables 4.4, 4.7, 4.9, 4.12, and 4.14 for descriptions of the glasses tested.

(b) PS is the plotting symbol used in plots associated with these data. ID# is a consecutive integer numbering of all CVS glasses.

(c) The run orders are numbered within each phase of testing: CVS-I (CVS1-1 to CVS1-23), CVS-II Phase 1 (CVS2-1 to CVS2-19), CVS-II Phase 2 (CVS2-20 to CVS2-58), CVS-II Phase 3 (CVS2-59 to CVS2-101), and CVS-II Phase 4 (CVS2-102 to CVS2-123).

TABLE 4.19. Mole Fraction Compositions for CVS-I and CVS-II Glasses Assuming F and SO_3 Remain in the Glass (continued)

Glass[a]	ID[b] #	PS[b]	Run[c] Order	SiO_2	B_2O_3	Na_2O	Li_2O	CaO	MgO	Fe_2O_3	Al_2O_3	ZrO_2	Others
CVS2-16 (4)	39	M	3	.5793	.0984	.1180	.0816	.0096	.0136	.0293	.0147	.0203	.0352
CVS2-17 (1)	40	M	8	.5123	.1052	.1037	.0807	.0314	.0577	.0228	.0400	.0223	.0239
CVS2-18 (4)	41	M	14	.5793	.0984	.1180	.0816	.0096	.0136	.0293	.0147	.0203	.0352
CVS2-19 (5)	42	M	19	.5789	.0983	.1189	.0815	.0095	.0136	.0300	.0150	.0208	.0335
CVS2-20	43	3	3	.6032	.0457	.1058	.1424	.0000	.0000	.0239	.0062	.0671	.0058
CVS2-21	44	3	15	.5453	.1085	.0464	.1346	.0000	.1141	.0072	.0387	.0000	.0053
CVS2-22	45	3	6	.5543	.0420	.0693	.1369	.0000	.1160	.0073	.0209	.0000	.0534
CVS2-23	46	3	11	.5926	.0468	.2016	.0209	.0891	.0000	.0078	.0354	.0000	.0057
CVS2-24	47	3	2	.4715	.1823	.0754	.1487	.0000	.0000	.0079	.0598	.0000	.0545
CVS2-25	48	3	10	.5344	.0456	.0861	.1487	.0905	.0000	.0596	.0021	.0000	.0329
CVS2-26	49	3	24	.4574	.1782	.0512	.1453	.0885	.0000	.0078	.0156	.0503	.0057
CVS2-27	50	3	4	.5502	.0435	.1953	.0314	.0000	.1201	.0076	.0464	.0000	.0055
CVS2-28	51	3	1	.6111	.0469	.2109	.0276	.0000	.0000	.0082	.0356	.0000	.0598
CVS2-29	52	3	14	.4955	.1948	.0738	.0227	.0967	.0000	.0085	.0000	.0459	.0620
CVS2-30	53	3	9	.5935	.1974	.0922	.0230	.0000	.0000	.0568	.0309	.0000	.0063
CVS2-31	54	3	19	.5853	.1633	.0498	.0683	.0880	.0000	.0077	.0318	.0000	.0056
CVS2-32	55	3	5	.5758	.0456	.2050	.0910	.0000	.0000	.0080	.0017	.0670	.0058
CVS2-33	56	3	25	.4337	.0485	.2002	.0756	.0000	.1232	.0078	.0543	.0000	.0567
CVS2-34 (6)	57	3	22	.4500	.1612	.2077	.0795	.0000	.0000	.0081	.0876	.0000	.0059
CVS2-35	58	3	7	.4482	.0461	.2069	.0918	.0915	.0000	.0254	.0843	.0000	.0059
CVS2-36	59	3	8	.5616	.0447	.0895	.1458	.0888	.0000	.0585	.0054	.0000	.0057
CVS2-37	60	3	12	.5807	.0738	.1048	.1434	.0000	.0000	.0077	.0841	.0000	.0056
CVS2-38	61	3	16	.5557	.1033	.1093	.0217	.0000	.1288	.0580	.0173	.0000	.0059
CVS2-39	62	3	13	.4830	.0431	.1318	.1405	.0000	.1191	.0279	.0152	.0341	.0055
CVS2-40	63	4	26	.5154	.0564	.1487	.0866	.0219	.0762	.0077	.0603	.0100	.0169
CVS2-41	64	4	21	.5386	.0606	.0766	.1424	.0542	.0302	.0114	.0596	.0099	.0167
CVS2-42	65	4	28	.5765	.0438	.0615	.1430	.0348	.0575	.0382	.0180	.0099	.0167
CVS2-43	66	4	17	.5217	.1312	.0499	.1351	.0221	.0460	.0116	.0303	.0351	.0170
CVS2-44	67	4	29	.5666	.0925	.0482	.1397	.0533	.0296	.0075	.0365	.0097	.0164
CVS2-45	68	4	30	.5385	.0970	.0493	.1216	.0218	.0757	.0118	.0354	.0099	.0391
CVS2-46	69	4	18	.5371	.1109	.0571	.1436	.0219	.0304	.0077	.0449	.0099	.0367
CVS2-47	70	4	23	.5515	.0450	.1290	.0899	.0558	.0311	.0078	.0246	.0254	.0401
CVS2-48	71	4	27	.4959	.1313	.0990	.0827	.0565	.0315	.0079	.0531	.0103	.0317
CVS2-49	72	4	20	.5378	.1242	.0983	.0880	.0227	.0316	.0205	.0490	.0103	.0175
CVS2-50 (1)	73	M	31	.5123	.1052	.1037	.0807	.0314	.0577	.0228	.0400	.0223	.0239
CVS2-51 (5)	74	M	32	.5777	.0981	.1187	.0813	.0095	.0136	.0299	.0150	.0207	.0355
CVS2-52	75	4	34	.6206	.0729	.0451	.1639	.0009	.0014	.0280	.0142	.0194	.0335

(a) The numbers in parentheses denote replicate sets of glasses. See Sections 4.2 through 4.6 and Tables 4.4, 4.7, 4.9, 4.12, and 4.14 for descriptions of the glasses tested.

(b) PS is the plotting symbol used in plots associated with these data. ID# is a consecutive integer numbering of all CVS glasses.

(c) The run orders are numbered within each phase of testing: CVS-I (CVS1-1 to CVS1-23), CVS-II Phase 1 (CVS2-1 to CVS2-19), CVS-II Phase 2 (CVS2-20 to CVS2-58), CVS-II Phase 3 (CVS2-59 to CVS2-101), and CVS-II Phase 4 (CVS2-102 to CVS2-123).

TABLE 4.19. Mole Fraction Compositions for CVS-I and CVS-II Glasses Assuming F and SO_3 Remain in the Glass (continued)

Glass[a]	ID[b] #	PS[b]	Run[c] Order	SiO_2	B_2O_3	Na_2O	Li_2O	CaO	MgO	Fe_2O_3	Al_2O_3	ZrO_2	Others
CVS2-53	76	4	38	.5376	.0776	.0698	.1241	.0000	.0767	.0155	.0485	.0050	.0452
CVS2-54	77	M	39	.5777	.0981	.1187	.0813	.0095	.0136	.0299	.0150	.0207	.0355
CVS2-55	78	0	35	.5747	.0976	.1181	.0809	.0095	.0135	.0297	.0149	.0206	.0405
CVS2-56	79	0	36	.5691	.0966	.1169	.0801	.0094	.0134	.0295	.0148	.0204	.0498
CVS2-57	80	0	37	.5853	.0994	.1202	.0824	.0097	.0138	.0303	.0152	.0210	.0227
CVS2-58	81	4	33	.3905	.1728	.0485	.1409	.0215	.1194	.0075	.0885	.0049	.0055
CVS2-59	82	5	5	.4465	.1512	.1253	.1490	.0410	.0008	.0077	.0691	.0037	.0057
CVS2-60	83	5	10	.5284	.0756	.1673	.1495	.0068	.0007	.0075	.0545	.0037	.0059
CVS2-61	84	5	2	.5460	.0592	.1203	.1518	.0000	.0000	.0078	.0990	.0088	.0071
CVS2-62	85	5	13	.5867	.1602	.1147	.0330	.0563	.0008	.0079	.0310	.0038	.0055
CVS2-63	86	5	4	.3623	.1661	.2065	.0115	.1201	.0000	.0084	.1189	.0000	.0062
CVS2-64	87	0	24	.6092	.0470	.0959	.1380	.0029	.0013	.0327	.0181	.0225	.0324
CVS2-65	88	0	30	.5609	.1022	.0875	.1471	.0008	.0006	.0005	.0121	.0792	.0091
CVS2-66	89	0	3	.5458	.0835	.1238	.1109	.0110	.0096	.0154	.0733	.0013	.0254
CVS2-67	90	0	21	.4843	.1443	.1109	.1235	.0027	.0002	.0002	.1269	.0000	.0071
CVS2-68	91	0	11	.5189	.1204	.0795	.1441	.0008	.0003	.0018	.0995	.0001	.0347
CVS2-69	92	0	19	.5877	.0700	.0668	.1489	.0088	.0050	.0130	.0499	.0003	.0496
CVS2-70	93	0	38	.5097	.1285	.0827	.1459	.0009	.0013	.0032	.1126	.0003	.0150
CVS2-71	94	5	6	.6053	.0467	.0953	.1372	.0028	.0013	.0325	.0180	.0223	.0387
CVS2-72	95	5	9	.5463	.0835	.1239	.1110	.0110	.0096	.0154	.0734	.0013	.0245
CVS2-73	96	5	1	.5247	.1218	.0804	.1457	.0008	.0003	.0018	.1006	.0001	.0238
CVS2-74	97	5	34	.5862	.0698	.0667	.1485	.0088	.0049	.0130	.0498	.0003	.0521
CVS2-75	98	5	7	.5084	.1282	.0825	.1455	.0009	.0012	.0032	.1123	.0003	.0176
CVS2-76	99	5	15	.5172	.0534	.1799	.1310	.0442	.0077	.0407	.0121	.0025	.0113
CVS2-77	100	5	29	.4781	.0544	.1834	.1479	.0056	.0078	.0020	.0124	.0564	.0520
CVS2-78	101	5	33	.5983	.1475	.0518	.0546	.0057	.0637	.0281	.0126	.0259	.0117
CVS2-79	102	5	35	.6263	.1579	.0554	.0278	.0061	.0085	.0452	.0135	.0028	.0565
CVS2-80	103	5	22	.5681	.1546	.0543	.0396	.0060	.0668	.0442	.0132	.0409	.0123
CVS2-81	104	5	12	.4563	.0537	.1743	.1460	.0056	.0618	.0410	.0122	.0025	.0465
CVS2-82	105	5	23	.5337	.0781	.1663	.1341	.0051	.0568	.0018	.0112	.0023	.0105
CVS2-83	106	5	28	.4885	.0818	.1740	.1401	.0427	.0074	.0019	.0118	.0024	.0493
CVS2-84	107	5	39	.4860	.0553	.1864	.1504	.0057	.0080	.0422	.0126	.0417	.0117
CVS2-85	108	5	16	.4529	.0533	.1796	.1449	.0055	.0307	.0019	.1031	.0025	.0255
CVS2-86	109	5	25	.5238	.0569	.1918	.0301	.0471	.0082	.0021	.1101	.0027	.0272
CVS2-87	110	5	8	.5484	.0760	.1920	.0398	.0162	.0082	.0104	.0640	.0329	.0121
CVS2-88	111	5	37	.4802	.0541	.1421	.1470	.0448	.0078	.0098	.0646	.0382	.0115
CVS2-89	112	5	26	.5006	.1150	.1985	.0229	.0488	.0085	.0449	.0134	.0349	.0125
CVS2-90	113	5	20	.5789	.1428	.0543	.1455	.0055	.0077	.0392	.0122	.0025	.0114

(a) The numbers in parentheses denote replicate sets of glasses. See Sections 4.2 through 4.6 and Tables 4.4, 4.7, 4.9, 4.12, and 4.14 for descriptions of the glasses tested.

(b) PS is the plotting symbol used in plots associated with these data. ID# is a consecutive integer numbering of all CVS glasses.

(c) The run orders are numbered within each phase of testing: CVS-I (CVS1-1 to CVS1-23), CVS-II Phase 1 (CVS2-1 to CVS2-19), CVS-II Phase 2 (CVS2-20 to CVS2-58), CVS-II Phase 3 (CVS2-59 to CVS2-101), and CVS-II Phase 4 (CVS2-102 to CVS2-123).

TABLE 4.19. Mole Fraction Compositions for CVS-I and CVS-II Glasses Assuming F and SO_3 Remain in the Glass (continued)

Glass[a]	ID[b] #	PS[b]	Run[c] Order	SiO_2	B_2O_3	Na_2O	Li_2O	CaO	MgO	Fe_2O_3	Al_2O_3	ZrO_2	Others
CVS2-91	114	5	32	.5891	.1453	.1071	.0212	.0056	.0627	.0020	.0124	.0026	.0520
CVS2-92	115	5	27	.4499	.1412	.0991	.1439	.0055	.0610	.0019	.0121	.0349	.0506
CVS2-93	116	5	14	.4687	.1229	.1321	.1499	.0112	.0079	.0395	.0126	.0026	.0527
CVS2-94	117	5	18	.4519	.1418	.1792	.1086	.0440	.0077	.0105	.0425	.0025	.0113
CVS2-95 (7)	118	A	36	.5162	.1012	.1708	.0908	.0128	.0261	.0356	.0228	.0021	.0216
CVS2-96 (1)	119	M	40	.5123	.1052	.1037	.0807	.0314	.0577	.0228	.0400	.0223	.0239
CVS2-97 (5)	120	M	31	.5777	.0981	.1187	.0813	.0095	.0136	.0299	.0150	.0207	.0355
CVS2-98 (6)	121	5	17	.4500	.1612	.2077	.0795	.0000	.0000	.0081	.0876	.0000	.0059
CVS2-99	122	5	41	.5765	.0927	.1053	.0793	.0115	.0127	.0425	.0341	.0108	.0347
CVS2-100	123	5	42	.5914	.0709	.0674	.1330	.0042	.0020	.0513	.0187	.0240	.0372
CVS2-101(7)	124	A	43	mole fractions not computed for this glass									
CVS2-102(4)	125	M	21										
CVS2-103	126	6	3										
CVS2-104	127	6	2										
CVS2-105	128	6	6										
CVS2-106	129	6	4										
CVS2-107	130	6	7										
CVS2-108	131	6	5										
CVS2-109	132	6	8										
CVS2-110	133	6	9										
CVS2-111	134	6	10	mole fractions not computed for these glasses									
CVS2-112	135	6	11										
CVS2-113	136	6	12										
CVS2-114	137	6	22										
CVS2-115	138	6	13										
CVS2-116	139	6	14										
CVS2-117	140	6	15										
CVS2-118	141	6	16										
CVS2-119	142	6	17										
CVS2-120	143	6	18										
CVS2-121	144	6	19										
CVS2-122	145	6	20										
CVS2-123(5)	146	M	1										

(a) The numbers in parentheses denote replicate sets of glasses. See Sections 4.2 through 4.6 and Tables 4.4, 4.7, 4.9, 4.12, and 4.14 for descriptions of the glasses tested.

(b) PS is the plotting symbol used in plots associated with these data. ID# is a consecutive integer numbering of all CVS glasses.

(c) The run orders are numbered within each phase of testing: CVS-I (CVS1-1 to CVS1-23), CVS-II Phase 1 (CVS2-1 to CVS2-19), CVS-II Phase 2 (CVS2-20 to CVS2-58), CVS-II Phase 3 (CVS2-59 to CVS2-101), and CVS-II Phase 4 (CVS2-102 to CVS2-123).

5.0 GLASS FABRICATION AND PROPERTY MEASUREMENTS

For each phase of the CVS, the glasses selected in the experimental design for that phase (see Section 4.0) were batched and melted. The following glass and melt properties were then measured or tests conducted for each glass composition:

- viscosity and electrical conductivity of the melt over the temperature range from 950 to 1250°C (CVS-I and CVS-II Phases 1, 2, and 3)
- liquidus temperature (CVS-I and CVS-II Phases 1, 2, and 3)
- composition and volume fraction of crystalline phases after 24-hour heat treatment at 1050°C (CVS-I only) and after simulated canister centerline cooling (CVS-I and CVS-II Phases 1, 2, and 3)
- durability by 28-day MCC-1 and 7-day PCT dissolution tests (all CVS glasses)
- glass transition temperature and thermal expansion of solid and molten glass (CVS-I and CVS-II Phases 1, 2, and 3).

Acceptability criteria for these properties were summarized in Table 3.1. Glass fabrication, property measurement procedures, and overcheck testing of glasses are described in the following sections. The results were recorded in designated laboratory notebooks (see Appendix J).

The measurement devices used in the Glass Development Laboratory in the 3720 building are listed on the CVS Measurement and Test Equipment (M&TE) List, which is reviewed quarterly. To ensure that measurements were accurate, the devices were calibrated in accordance with PAP-70-1201 (PNL-MA-70 1990). The viscosity and electrical conductivity units were calibrated with NBS-711 glass every three months or if any changes occurred in the equipment. Thermocouples, temperature readouts, balances, and other equipment were calibrated according to the timetable in the M&TE list.

5.1 GLASS FABRICATION AND CHEMICAL ANALYSIS

The test glasses were batched and melted according to procedure PSL-417-GBM (Procedure for Glass Batching and Melting, Rev. 0). For each glass, the nine major glass components to be varied were batched separately as

oxides or carbonates. The remaining components were batched together in constant proportions and treated as a single component, Others. An Others composition corresponding to the NCAW waste type (see Table 4.1) was used for all glasses except those designed to investigate the effect of composition variation of Others on glass properties. Glasses with different Others compositions are discussed in various subsections of Section 4.

A quantity (~500 g) of each glass was melted in a platinum crucible under a lid (to reduce volatilization) using an electrically-heated resistance furnace. The amount of glass was enough for the measurements of viscosity and electrical conductivity (150 g), glass transition temperature (50 g), durability (100 g), liquidus temperature (50 g), and crystallinity for canister centerline cooled samples (40g). At least 100 g of glass and all scrap from viscosity and electrical conductivity testing was archived under conditions specified by the applicable HWVP-801-SUPP procedure (Archival of Samples). For better homogeneity, the glass was removed from the furnace after one hour of melting, cooled, and crushed in a tungsten carbide disc mill and remelted under a lid. The last operation was not performed in CVS-I, but was included in the CVS-II glass fabrication procedure because homogeneity may affect glass crystallization.

Molten glass was poured in bars and annealed for 2 h at 500°C for MCC-1 durability, glass transition temperature, liquidus temperature, and archive purposes (200 g). The remaining glass was poured on a steel plate and air quenched.

Samples (4-5 g) of all glasses from CVS-I and CVS-II Phases 1 and 2, and selected glasses from CVS-II Phase 3, were sent for elemental analysis by inductively coupled plasma atomic emission spectroscopy (ICP) for comparison to the as-batched compositions. Appendix A lists as-batched and as-analyzed glass compositions for all CVS-I, CVS-II Phase 1, and CVS-II Phase 2 glasses and for selected CVS-II Phase 3 glasses. Several statistically significant differences between as-batched and as-analyzed compositions were detected. Some were due to round-off error for minor components or were otherwise determined not practically significant. The differences large enough to be practically significant appeared to be due to analytical biases or undissolved

material in some glasses. It was decided to use as-batched compositions in fitting property models and many other data analyses. However, because analyzed glass compositions will eventually need to be used in the models and composition uncertainties accounted for, analyzed compositions from replicate analyses of the same glass were used to estimate longer-term uncertainty in analyzed compositions. The results are reported in Appendix A.

As indicated previously, only selected CVS-II Phase 3 compositions were analyzed for composition to check the prior decision to use as-batched rather than as-analyzed compositions for modeling and other data analysis efforts. Six of the eleven Phase 3 glasses analyzed were selected randomly (CVS2-59, CVS2-69, CVS2-70, CVS2-74, CVS2-79, and CVS2-91). CVS2-96, CVS2-97, and CVS2-98 are replicates of CVS1-1, the CVS internal standard glass (CVS2-19 and CVS2-51), and CVS2-34, respectively. CVS2-95 (the PNL batched version of the DWPF EA standard glass) and CVS2-101 (a sample of the large batch of the DWPF EA standard glass fabricated for Savannah River Technology Center (SRTC) by Corning) were also analyzed. Although not CVS glasses, the ARM-1 and ARG-1 glasses were also analyzed during the same time period as the CVS-II Phase 3 glasses. The as-batched and as-analyzed compositions for these glasses are listed in Table A.3 of Appendix A. A subjective comparison of as-batched and as-analyzed compositions indicated it was reasonable to continue using as-batched compositions of CVS-II Phase 3 glasses in modeling and other data analysis efforts.

The redox state (Fe^{2+}/Fe ratio) was determined for six quenched CVS glasses and one canister centerline cooled glass. Analysis was performed using procedure #255 of PNL-ALO-599. The results are reported in Table A.11 and discussed in Section A.5 of Appendix A.

5.2 VISCOSITY

For CVS-II glasses, viscosity was measured by a rotating spindle technique and evaluated using standard viscosity measurement procedures GDL-VSC (Viscosity Spindle Calibration, Rev. 0) and GDL-VIS (Standard Viscosity Measurement, Rev. 0). Each glass sample was heated to 1150°C in a platinum crucible and maintained until thermal equilibrium was reached (approximately

30 minutes). A measurement was then taken at 1150°C and subsequent measurements were taken at nominal temperatures of 1100°C, 1050°C, 1100°C, 1150°C, 1200°C, 1250°C, 1150°C, 1000°C, and 950°C. Viscosity within the most important temperature range (from 1050°C to 1150°C, the temperature range expected in the previously planned HWVP melter) was measured first before the melt could be affected by volatilization at higher temperatures or crystallization at lower temperatures. Measurement at each set temperature began six minutes after the temperature was reached and took five minutes. This time-temperature schedule allowed the sample to reach thermal and mechanical equilibrium while alteration of the melt by volatilization or crystallization was minimized.

Note that the viscosity measurement within the temperature range 1050°C to 1150°C was taken twice -- first at decreasing and then increasing temperature -- to check that viscosity was independent of time. Because the chance that the glass could be altered by volatilization at higher temperatures was judged to be substantially lower than the chance that crystallization would affect viscosity at lower temperatures, viscosity was first measured at 1200°C and 1250°C and then at 1000°C and 950°C. Two replicate measurements were made at 1150°C to compare the data with the initial measurement at that temperature (i.e., three measurements at a nominal temperature of 1150°C were made in total).

The preceding procedure was different from the method used for CVS-I glasses. For CVS-I samples, the glass was heated in a platinum crucible to the upper temperature to be measured, which was 1200°C in most cases and up to 1500°C for several glasses. At successively lower temperatures of 75 to 100°C increments, measurements were taken until the viscosity of the melt exceeded the upper limit of the viscometer, approximately 300 Pa·s. Each viscosity measurement was taken for 23 minutes to assess melt stability. For some of the glass samples tested, the time rate of change in viscosity exceeded 1 mPa (mPa = milipascal) at the lower end of the temperature range of testing, which indicated crystallization. Crystallization that occurred at 1050°C or higher was confirmed on thin sections of glass by optical microscopy (see Section

11). All suspect data were eliminated from use in the property modeling and other data analyses.

For CVS-I glasses, viscosities at 1150°C and temperatures at η = 10 Pa·s were initially obtained graphically from curves fitted to ln η versus 1/T plots. However, this method was replaced for all CVS glasses by fitting the raw viscosity at temperature data for each glass to the Fulcher equation:

$$\ln \eta = A + B/(T - T_O), \tag{5.1}$$

where A, B, and T_0 are the Fulcher equation coefficients and T is temperature. Viscosities at 1150°C were then calculated from the Fulcher equation fits for each glass.

5.3 ELECTRICAL CONDUCTIVITY

For CVS-I, CVS-II Phases 1 and 2, and CVS2-99 and CVS2-100 in CVS-II Phase 3, electrical conductivity measurements were conducted by following procedures GDL-ECC (Electrical Conductivity Calibration Procedure, Rev. 0) and GDL-ELC (Electrical Conductivity Measurement Procedure, Rev. 0). Measurements were automated for CVS-II Phase 3 using a General Purpose Interface Board and an IBM PC to collect data. Procedures GDL-AECC, Rev. 0 and GDL-AEC, Rev. 0 (Automated Electrical Conductivity Calibration and Measurement Procedures for Molten Glass) were used for these measurements.

For all CVS electrical conductivity testing, a probe with two platinum-10% rhodium blades was inserted into the glass to a known depth and the resistance of the glass between the blades was determined by a resistance meter. For CVS-I, CVS-II Phases 1 and 2, and CVS2-99 and CVS2-100 in CVS-II Phase 3, a 1-kilohertz frequency was continuously passed through a glass sample during the 20-minute measurement period to determine resistance. Under the new automated procedures for CVS-II Phase 3 glasses, a single rotation through a programmed loop of current frequencies at 0.1, 1, 10, and 100 kilohertz rapidly passing the currents through the glass was used to measure resistance. (A frequency of 1 kilohertz was used to provide the data for

CVS-II Phase 3 glasses to be compatible with the 1-kilohertz frequency used in the earlier phases of CVS.) The series of measurements was taken once every 60 seconds after temperature stability had been reached in the furnace. Measurements continued for an established time at each temperature, and then the furnace would cool to the next designated temperature. Temperatures of 1250°C, 1150°C, 1050°C, and 950°C were used. Because electrical conductivity is generally less sensitive to glass alteration by volatilization or crystallization than viscosity, no replicate points were taken.

For CVS-I glasses, electrical conductivity at 1150°C was initially determined graphically from curves fitted to ln ϵ versus 1/T plots. However, this method was replaced for all CVS glasses by fitting the raw conductivity at temperature data for each glass to the Arrhenius equation:

$$\ln \epsilon = A + B/T, \tag{5.2}$$

where A and B are Arrhenius coefficients for electrical conductivity, and T is absolute temperature (K). Electrical conductivities at 1150°C were then calculated from the Arrhenius equation fits for each glass.

5.4 LIQUIDUS TEMPERATURE

Liquidus temperature can be determined by heat treating either crystal-free or precrystallized glasses in a gradient furnace. The crystallization front in initially crystal-free glasses lies below the liquidus temperature because of the nucleation threshold. If the threshold is relatively high (more than 5°C), the following procedure must be used: (1) the crystal-free glass is heat treated in the gradient furnace to determine the temperature of the crystallization front, (2) the test glass receives heat pretreatment at a temperature about 10°C below that of the crystallization front to produce a small fraction of tiny crystals throughout the sample volume, (3) the partly crystallized glass specimen is heat treated in the gradient furnace until phase equilibrium is reached in the liquidus temperature range, (4) the liquidus temperature is determined from the position of the dissolution front of the primary crystalline phase. More accurately, the liquidus temperature

is within the interval bounded by the temperatures associated with the crystallization front of growing crystals and the dissolution front of dissolving crystals.

The minimum time necessary to dissolve crystals at temperatures above (but close to) the liquidus temperature depends on the crystalline phases formed. The minimum time could be as long as five days, based on refractory data in glass (Tooley 1974, pp. 443-446). Because the required heat treatment time of crystal-free glasses is considerably shorter (1 day) and the nucleation threshold appears to be within an acceptable limit for CVS glasses, the liquidus temperature of these glasses is determined by treating them in the gradient furnace without previous crystallization.

Liquidus temperature measurements were conducted by the following procedures: GDL-GFC (Gradient Furnace Calibration Procedure, Rev. 0) and GDL-LQT (Liquidus Temperature Measurement Procedure, Rev. 0). To evaluate the type(s) of crystalline phases(s) in the glass, thin sections of the glass were observed using an optical microscope with reflected and transmitted light. The chemical composition of crystalline phases was semi-quantitatively determined by Scanning Electron Microscopy with Energy Dispersive Spectroscopy (SEM/EDS).

Measuring liquidus temperature was not part of the original work scope for CVS-I (although liquidus temperatures have since been measured for CVS-I glasses). Instead, each CVS-I glass was heat treated at 1050°C for 24 hours to determine whether its liquidus temperature was above or below 1050°C. Each glass was examined by X-ray diffraction (XRD), in addition to optical microscopy and SEM/EDS, to identify crystalline phases and to determine their semi-quantitative volume fractions. The analyses were conducted in accordance with approved procedures PNL-SP-2, Rev. 1 (X-Ray Diffraction Analysis) and PNL-SP-3 (Scanning Electron Microscopy/ Energy Dispersive Spectrometry).

5.5 CANISTER CENTERLINE COOLING AND CRYSTALLINITY

The thermal history of a canister cooled glass can be complex. Part of the glass is quenched due to immediate contact with canister walls, while a portion of the glass (located near the canister centerline) is cooled slowly.

Cooled glass can be reheated when it comes in contact with hot, freshly poured glass. The thermal history of a majority of glass in the canister falls in the range between quenched and centerline cooled. Canister centerline cooling (CCC) represents the lowest cooling rate whereas, quenching represents the highest cooling rate which is experienced by glass in a canister. The nature and quantity of crystalline phases in the glass canister can be roughly estimated by examination of crystallization in quenched and CCC glass samples.

The CCC time-temperature schedule for a DWPF-type canister shown in Table 5.1 was obtained by numerical simulation, based on work in an 1986 unpublished project report by M.L. Elmore. The CCC time-temperature schedule in Table 5.1 was used for heat treatment of glasses in CVS-I and CVS-II Phases 1 and 2. This curve was obtained with the assumption that molten glass enters a canister at the same temperature at which it leaves the furnace. Edwards (1987) has shown that the stream of glass cools down to approximately 900°C before entering the canister. The same result was obtained numerically by Lee (1989). The portion of the canister centerline curve presented in Table 5.1 for T < 900°C is in reasonable agreement with the measurements by Edwards (1987) and associated numerical simulation by Lee (1989). The portion of the

TABLE 5.1. Simulated Canister-Centerline-Cooling Schedule[a]

Time (hr)	Temp (°C)	Time (hr)	Temp (°C)	Time (hr)	Temp (°C)
1	1069	12	781	23	516
2	1069	13	752	24	499
3	1056	14	725	25	483
4	1035	15	698	26	467
5	1004	16	672	27	451
6	972	17	647	28	436
7	937	18	623	29	421
8	904	19	600	30	406
9	872	20	577	31	392
10	840	21	556	32	378
11	810	22	535	33	365

(a) The schedule shown was used for glasses in CVS-I and CVS-II Phases 1 and 2. For CVS-II Phase 3 glasses, only the portion of the schedule at and below 872°C was used, with time measured from 1 hr at 872°C. See text for more discussion.

cooling curve in Table 5.1 for $T \leq 872°C$ (glass stream temperature) was therefore used to match the SRTC cooling curves for glasses in CVS-II Phase 3. The temperature history the glass undergoes at temperatures above 900°C has little or no effect on crystallization behavior for most CVS compositions.

Crystallinity was determined for all CCC glasses (except the radioactive glasses CVS2-53 and CVS2-54). Premelted glass samples were heated in high purity alumina crucibles at 1150°C for 30 min. and then cooled according to the simulated CCC schedule (Table 5.1). This phase of testing was conducted using procedure WTC-007-15-GDL-HTR (Test Procedure for Glass Heat Treatment). Quenched samples were prepared according to procedure PSL-417-GBM. After CCC heat treatment, thin sections were prepared from the glass samples for optical microscopy and SEM. The analyses were conducted in accordance with procedures PNL-SP-2 and PNL-SP-3. In addition, samples were ground and analyzed by X-Ray diffraction (XRD) to determine semi-quantitative volume fractions of well-defined crystalline phases.

5.6 GLASS TRANSITION TEMPERATURE

The Perkin-Elmer TMS-2 Thermomechanical Analyzer was used to measure the glass transition temperature of each CVS glass. A glass monolith 6 x 6 x 12 mm was cut from a glass bar, which had been annealed at 500°C for 2 hr and furnace cooled to 23°C at a rate of $\leq 1°C/min$. The monolith was then heated to the glass softening point at a rate of 20°C/min while measuring the change in sample length versus temperature. The glass transition temperature was determined as the intersection of the two linear segments of the sample length versus temperature curve on either side of the transition portion of the curve. This test was conducted in accordance with approved procedure PSL-324-TE (Procedure for Determining Thermal Expansion of HWVP Glasses and Extracting Parameters from Expansion Data).

5.7 THERMAL EXPANSION

Thermal expansion coefficients of solid and molten glass were calculated for each CVS glass from the length versus temperature curve generated for the glass transition temperature measurement.

5.8 DURABILITY

The chemical durability of glasses was determined by two methods, MCC-1 and PCT (Product Consistency Test). The MCC-1 dissolution test was issued by the Materials Characterization Center (MCC)[a] and was performed by following PNL Technical Procedure PSL-417-LCH, Rev. 0 (Leach Testing Using MCC-1P and MCC-3S Methods). The PCT was developed at the Savannah River Technology Center for use by DWPF and adapted as PNL procedure MCC-TP-19 (Leaching Test Using the PCT Test Method, Rev. 0). The PCT procedure was modified slightly (Jantzen et al. 1992) during the course of the CVS, but the modifications were not adopted for CVS testing (to maintain consistency throughout the CVS). Thus, the version of the PCT procedure described in PNL procedure MCC-TP-19 has been used for all PCT tests during CVS.

The testing was conducted using deionized water instead of repository-relevant ground waters equilibrated with engineering barrier materials. Because the MCC-1 test and PCT are standard tests used to evaluate the durability of waste glasses, the dissolution behavior of the CVS glasses can be compared to glasses developed for the Savannah River and West Valley programs (that have been tested by MCC-1 and PCT).

Teflon containers were used as dissolution vessels for both methods. The containers were baked at 200°C for one week to drive off fluorine. These containers do not release measurable amounts of fluorine during the 28-day MCC-1 tests[b]. The amounts of fluorine released from containers would be negligible compared to the amount of fluorine released from the glass. The solution pH is above 8.0; therefore, no free HF was present.

For the 28-day MCC-1 static dissolution test, a monolith sample of glass was placed on a Teflon support grid in the center of a 40 mL volume of deionized water at 90°C for 28 days in a sealed 60 mL Teflon container. The ratio of the surface area of the sample to volume of leachant is nominally 10 m^{-1}. The

---

(a) Operated by Pacific Northwest Laboratory, Richland, Washington.

(b) C. M. Jantzen, Private communication.

initial and final pH values of the solution were obtained. The concentrations of the glass components in the solution were determined by ICP analysis.

The PCT requires crushed glass of a particle size between 75 and 150 μm (-100 to +200 mesh). The glass was ground in a tungsten carbide grinding chamber and then sieved through 100 and 200 mesh stainless steel sieves. The large particles remaining on the top of the 100 mesh sieve were repeatedly crushed until all glass passed through it. The crushed glass was cleaned by washing in deionized water and ethanol using an ultrasonic cleaner. It was then dried, weighed, and 4 g of glass was added to a 60 mL Teflon container filled with 40 mL of deionized water. Hence, the solution volume to glass mass ratio was 10 mL/g glass. The ratio of the surface area of the sample to leachant volume was approximately 2000 m^{-1}, which was confirmed by the Brunauer-Emmett-Teller (BET) technique. The Teflon container and its contents were heated (without agitation) at 90°C for seven days. The initial and final pH values of the solution were taken. Aliquots of the solution were filtered through a 0.45 μm filter and submitted for ICP analysis.

Results are reported as normalized elemental mass releases

$$r_i = \frac{C_i}{f_i\,(A/V)} \tag{5.3}$$

where r_i is the normalized mass release of element i (g/m^2), C_i is the concentration of element i in solution (g/m^3), f_i is mass fraction of element i in the glass (unitless), and A/V is the surface area to volume ratio (1/m). Values of A/V used were 2000 for PCT and 10 for MCC-1. The normalized mass release of boron or lithium, which are not a part of the solid reaction products, provides a measure of the glass dissolution progress. Further insight into the glass corrosion mechanism is gained by comparison of the normalized mass releases of elements which are and are not involved in the solid reaction products.

Heat treatment of waste glasses below the liquidus temperature can affect glass durability. Mendel and McElroy (1972, pp. 5.7-5.9) showed that durability of phosphate glasses can decrease by three orders of magnitude if heat treated at 620 - 650°C for 24 h or longer, but the effect was small when

a borosilicate glass received the same treatment. Additional testing by Mendel et al. (1977) and Malow et al. (1980), who used a Soxhlet leach test, showed that the decrease in durability was related to crystallization. The effect was dependent on heat treatment time and temperature and the nature of the crystalline phase.

Bickford and Jantzen (1984) and Jantzen and Bickford (1985) studied the effect of crystallization of high aluminum and high iron borosilicate glasses using MCC-1 and Corning Glass Works (CGW) tests (CGW is a 24-h test of powdered glass between 100 and 200 mesh; the effective ratio of sample surface to leachant volume is 430 m^{-1}). They concluded that formation of spinel and acmite increased glass dissolution one to three times. According to an unpublished 1989 project report by S.O. Bates, the maximum crystallization was observed after heat treatment at 700°C, while the normalized elemental release by MCC-3 test was maximum at 600°C (a temperature at which the amount of crystals was significantly lower than at 700°C). Preliminary CVS results (see Section 12.7) show that crystallinity can have anywhere from a negligible to significant effect on glass durability.

Crystallization changes the chemical composition of the glass matrix, introduces grain boundaries, produces mechanical stresses, and can lead to microcracking; all these effects can adversely affect durability. The effect of crystallinity on durability also depends on the nature of the crystals, the fraction of crystalline material in glass, and the temperature at which crystals were produced. Therefore, the PCT was performed for slow-cooled glasses as well as quenched glasses. The rate of cooling was chosen to simulate the canister centerline (see Section 5.5). MCC-1 was not applied because the MCC-1 data (from both Jantzen and Bickford (1985) and the unpublished 1989 project report by S.O. Bates) exhibit large scatter, which is probably caused by the inhomogeneous stress within the monoliths.

Additional tests were performed with selected CVS glasses to address two concerns. First, it is assumed that any uranium present in radioactive glasses has no significant effect on durability of these glasses. To check this assumption, the release rates of uranium and other elements (e.g., B, Li, and Na) were determined by PCT for two glasses where depleted uranium oxide

(UO_2) was added as the source of uranium (results are discussed in Section 13.2). Second, glasses that undergo liquid-liquid separation can exhibit nonlinear effects that would complicate model development. An attempt made to detect liquid-liquid separation in suspected glass samples using SEM indeed showed the occurrence of immiscibility. Therefore, a study was launched to predict the immiscibility gap in the CVS composition range using empirical rules and phase equilibria (see Section 12.11.4). Experimental detection of phase separation was undertaken to check the predictions.

5.9 ACCURACY, PRECISION, AND OVERCHECK TESTING

Accuracy of viscosity and electrical conductivity data was controlled by using National Institute of Standards and Technology (NIST) lead-silicate glass (NBS-711) for equipment calibration. Previous experience has demonstrated that viscosity and electrical conductivity measurements of the same glass by different laboratories typically have good agreement. Also, overcheck measurements of viscosity and electrical conductivity were made by Corning, Inc. on the CVS internal standard glass and compared to the CVS values. The results of the comparison are discussed in Section 13.3.1.

Durability testing of CVS glasses via the PCT and MCC-1 tests is performed in duplicate. Past experience has shown little variability in triplicate dissolution results when the replicate tests are performed at the same time and replicate solutions are analyzed at the same time. Hence, it was concluded that duplicate dissolution tests during CVS were sufficient. Appendix D contains the data and statistical analysis results for duplicate MCC-1 and PCT dissolution tests on CVS glasses.

Samples of several CVS glasses were sent to SRTC, Rensselaer Polytechnic Institute (RPI), and Argonne National Laboratory (ANL) for MCC-1 and PCT durability tests. Section 13.3.2 describes and compares the CVS, SRTC, RPI, and ANL dissolution test results on these glasses.

The CVS internal standard glass (CVS2-19) was included in each phase of CVS-II, and the CVS-I centroid glass (CVS1-1) was included in CVS-I as well as CVS-II Phases 1, 2, and 3, to provide internal overchecks on the test results for all properties. Replicate testing of these and other glasses provides for

quantifying the long-term within-lab variation in test and measurement procedures for all properties (see Appendix F). Long-term variation in the data will be taken into account in assessing the adequacy of glass property models fitted to the data.

Significant overcheck testing at other laboratories would have been required to adequately quantify lab-to-lab variation. Such testing was determined to be beyond the scope of CVS. Similarly, extensive testing of standard glasses with certified compositions and glass properties were not performed because of cost concerns. Instead, the decision was made to maintain equipment calibrated to approved standards and rely on internal and external overchecks for a small number of glasses. This latter course does not provide the ideal basis for detecting and correcting biases in data, but was judged a reasonable tradeoff in that many more glasses could be included in the CVS.

6.0 PROPERTY MODELING AND OTHER DATA ANALYSIS METHODS

The statistical approaches and methods used in modeling and analyzing glass property data are discussed in this section.

6.1 EMPIRICAL MIXTURE MODELS

One of the primary goals of the CVS is to develop models that can be used to predict glass property values over the range of glass compositions studied in the CVS. Well-developed and well-accepted physical or theoretical models relating glass properties to composition do not exist, so a statistical empirical modeling approach was adopted for CVS. This approach is based on the premise that the relationship between each response variable (glass properties) and the predictor variables (glass composition) can be adequately approximated by relatively simple empirical model forms. Specifically, empirical model forms for mixture experiments are employed, as discussed in the following subsection.

6.1.1 First- and Second-Order Mixture Models

A number of different empirical mixture experiment[(a)] models have been proposed in the statistics literature over the years since the pioneering work of Scheffé (1958). The book by Cornell (1990) discusses many of these empirical mixture model forms. Attention in CVS has focused on the first-order Scheffé model form

$$y = \sum_{I=1}^{10} b_I x_I \qquad (6.1)$$

and the second-order Scheffé model form

$$y = \sum_{I=1}^{10} b_I x_I + \sum_{I=1}^{9} \sum_{J=I+1}^{10} b_{IJ} x_I x_J. \qquad (6.2)$$

(a) A mixture experiment is one in which two or more ingredients are mixed and one or more properties of the mixture are measured.

In the above model forms, x_i is the mass fraction of i-th oxide component, b_i is the coefficient corresponding to the first-order term involving x_i, b_{ij} is the coefficient corresponding to the second-order term involving x_i and x_j, and y is a glass property value (possibly mathematically transformed). Other statistical assumptions and aspects of fitting these models and quantifying uncertainties are discussed later in this chapter and in Appendix I.

First-order mixture models of the form (6.1), with the x_i being either mass or mole fractions, were fitted to investigate whether one provided a better fit than the other. This had been done previously in CVS-I, and while differences were found in the relative magnitudes of the coefficients, the mass and mole fraction models seemed to fit the data equally well. However, it was decided to revisit using both mass fractions and mole fractions in first-order mixture models fitted using all CVS-I and CVS-II data.

To investigate whether there are any block effects[(a)] in the CVS data due to conducting the study in phases (CVS-I and CVS-II Phases 1, 2, and 3), a modified form of the first-order model (6.1) was used:

$$y = \sum_{j=1}^{4} a_j P_j + \sum_{i=1}^{10} b_i x_i \qquad (6.3)$$

where

P_j = 1 for a data point if it is from block j of CVS, or 0 otherwise (note that j=1 for CVS-I and j=2,3,4 for CVS-II Phases 1, 2, and 3, respectively),

a_j = coefficient corresponding to the effect of block j, where $a_1 + a_2 + a_3 + a_4 = 0$,

and x_i and b_i are as defined previously. Statistical tests of whether the a_j coefficients are significantly different from zero provide for assessing whether there are any block effects in the property data related to collecting the CVS data in phases. Statistically significant block effects could be due

---

(a) Portions of an experimental design (test matrix) performed at different times or under different sets of conditions are referred to as "blocks" in the statistical literature.

to biases in the property data for particular phases. Or, they could be due to differences in the composition subregions studied during the four CVS phases (CVS-I and CVS-II Phases 1, 2, and 3). Unfortunately, the study design does not provide a basis for clearly determining which of the two is the case. However, it is important to first determine whether block effects exist, and then determine (using the limited bases available) if biased data is a possible explanation.

The first-order mixture model (6.1) is sometimes referred to as a linear mixture model, because it is linear in the component mass fractions with respect to the property (or its mathematical transformation, if one was used). Note, however, that if a mathematical transformation is applied, the first-order mixture model is actually a nonlinear function of composition with respect to the untransformed property. The first-order mixture model does not, however, provide the ability to represent nonlinear blending behavior (interactions or curvature) of the glass components with respect to the properties. Second-order mixture models (such as Eq. (6.2)) do have such abilities, and were considered in CVS for that reason. Other empirical mixture models besides (6.2) exist that can account for nonlinear blending behavior of mixture components, but they were not investigated.

The first- and second-order mixture model forms above were used directly for viscosity at 1150°C, electrical conductivity at 1150°C, PCT and MCC-1 normalized elemental releases, coefficients of thermal expansion for solid and molten glass, and transition temperature data. First-order mixture model forms were used to model subsets of the liquidus temperature data (subsetted by primary crystalline phase). First-order mixture model forms were also combined with the Fulcher and Arrhenius equations to model viscosity and electrical conductivity at temperature data. Specifically, viscosity models of the form

$$\ln \eta = A(x) + B(x)/(T - T_0(x)), \qquad (6.4)$$

and viscosity and electrical conductivity models of the form

$$\ln \epsilon = A(x) + B(x)/T, \tag{6.5}$$

were investigated, where A(x), B(x), and $T_0(x)$ have the first-order mixture model form (6.1). It was determined infeasible to use second-order mixture model forms for these coefficients, and so second-order modeling of viscosity and electrical conductivity occurred only at 1150°C.

Modeling viscosity as a function of both temperature and glass composition represents a change in approach from that used in CVS-I. The CVS-I approach involved interpolating measured data to obtain viscosity and electrical conductivity values at 1150°C, and then fitting mixture models to the interpolated values. Modeling the viscosity and electrical conductivity data at various temperatures provides additional flexibility for predicting values of these properties at any temperature of interest (within the range of temperatures for which data were collected).

6.1.2 Model Fitting

The empirical mixture models discussed in the previous subsection are fitted to appropriately transformed glass property values via least squares regression techniques. The underlying assumptions of ordinary (unweighted) least squares regression are that: (i) the predictor variable values (mass or mole fractions of the 10 CVS glass components) are known or measured without error, or at least that the error is small relative to the error in response variable (glass property) values, and (ii) the testing and/or measurement errors for each response variable are independently and identically distributed (i.e., with the same mean and variance).

Regarding assumption (i), the true composition of each CVS glass is not known, and so any representation of glass composition selected will be subject to uncertainty. Appendix A discusses the glass composition options that were considered and the decision to use as-batched glass compositions for modeling glass properties. As discussed in Appendix A, as-batched compositions are expected to be reasonable representations of actual compositions. Some

consideration was given to using measurement error (sometimes also called "errors in variables") models (Fuller 1987), which account for errors in predictor variables. However, these methods require considerably more effort than ordinary least squares methods, and software is not widely available. Further, it was thought that any consequences to ignoring uncertainty in the predictor variables would be small compared to consequences of using first- and second-order empirical models to approximate the relationships between glass properties and glass composition. It may be reasonable to reconsider the use of measurement error model methods at some point in the future.

The portion of assumption (ii) having to do with the independence of errors in testing and measuring properties may not be completely satisfied due to conducting CVS in phases over a longer period of time. Conducting the CVS in phases has the potential for errors in testing and measuring properties to depend on the CVS phase. However, this is difficult to investigate based on how the study was conducted. Glasses were tested and measured in random order within each CVS phase to minimize the impact of any time-related effects. The identically distributed portion of assumption (ii) is not valid for some properties, since the variance of errors in testing and measurement of properties depends on the value of the property. For example, the variance of viscosity and durability results tends to increase as the values of these properties increase. In cases where the identically distributed (equal variance) assumption is violated, it can often be remedied by applying a mathematical transformation to the property values. Such transformations also often make an empirical model form more appropriate for fitting the (transformed) property values, hence yielding a better fit. Based on common practice and results of a statistical technique for selecting response variable transformations[a], the property transformations identified in Table

---

(a) Property transformations were selected according to a statistical procedure described by Box and Draper (1987). The procedure considered the class of power transformations $y = z^k$ (where z is a property and y its transformation) for each of the properties. A value of $k = 0$ corresponds to a logarithmic transformation. The transformations indicated by this statistical technique corresponded to those commonly used (e.g., log transformations of viscosity and durability).

6.1 were selected. Results in Appendix F support that these transformations stabilize the variances of measured property values.

In summary, although the assumptions of ordinary least squares may not be completely satisfied for the CVS data, ordinary least squares is still reasonable for use in fitting glass property models.

The REG and NLIN procedures in the statistical software package SAS (SAS 1990) were used to fit mixture models to the data for the various glass properties. NLIN is a nonlinear[(a)] regression routine that was used for fitting viscosity data to the Fulcher equation (or extensions in which the Fulcher coefficients were expressed as mixture models). The REG procedure was used to fit all other property models.

TABLE 6.1. Property Transformations Used in Modeling

Property	Description	Transformation
η	Viscosity (Pa·s) at temperatures (°C)	ln η
ϵ	Electrical conductivity (S/m) at temperatures (K)	ln ϵ
T_L	Liquidus temperature (°C)	none (a)
T_g	Glass transition temperature (°C)	none (a)
α_s	Thermal expansion coefficient, solid glass (10^{-6}/K)	none (a)
α_m	Thermal expansion coefficient, molten glass (10^{-6}/K)	none (a)
r_{Mi}	28-day MCC-1 normalized i-th element release (g/m²)	ln r_{Mi}
r_{Pi}	7-day PCT normalized i-th element release (g/m²)	ln r_{Pi}

(a) "None" means the property was not transformed.

(a) Here, nonlinear refers to the model being a nonlinear function of its coefficients. Such models require iterative algorithms to estimate the model coefficients (as opposed to the one-step solution algorithm for models linear in their coefficients).

6.1.3 Pseudocomponent Transformations

Mixture models in general, especially second- and higher-order ones, are prone to a phenomenon known as multicollinearity. This means that approximate linear relationships exist between the terms in the model being considered. The phenomenon can occur in any empirical or physical modeling situation, but is fairly likely for highly constrained mixture experiments having a larger number of components and where second-order or higher-order models are considered. Some reasons for this phenomenon are: (1) the mixture constraint that the component proportions (oxide mass or mole fractions) must sum to one induces correlations among the components, (2) single-component and multiple-component constraints induce further correlations among the components, and (3) model terms that are functions of other terms are correlated with the terms from which they were formed. The consequence of severe multicollinearity is ill-conditioning, which means the numerical estimation of model coefficients via least squares regression is subject to instability and may yield incorrect answers.

Moderate to severe multicollinearity/ill-conditioning occurred when fitting the full second-order mixture models to CVS glass property data. Two remedies were investigated, and it turned out that one of them, the L-pseudocomponent transformation, was sufficient to correct the problem. The L-pseudocomponent transformation is given by the equation

$$x_i' = \frac{x_i - L_i}{1 - \sum_{l=1}^{10} L_l} \qquad (6.6)$$

where x_i' denotes the pseudocomponent for component i and L_i denotes the single-component lower bound of component i. Hence, in the full second-order models for CVS glass property data, L-pseudocomponent versions of the 10 glass components were used in models in place of the untransformed mass fractions.

Eventually, reduced versions of the full second-order model were fitted (see Section 6.1.4), and these are the only ones discussed in Sections 7 - 12. It wasn't necessary to apply the L-pseudocomponent transformations for these

reduced models, since the multicollinearity was not as bad as for the full second-order models.

6.1.4. Variable Selection for Second-Order Models

In fitting second-order mixture models to glass property data, it was necessary to be concerned about overfitting the data. The second-order mixture model form (6.2) contains 10 first-order terms and 45 second-order terms. Using all 55 terms can lead to overfitting the data and cause the resulting models to yield poor predictions. Thus, statistical variable selection algorithms available in the SAS (1990) REG procedure were applied to select a subset of Scheffé second-order terms for inclusion in the model for each property. Basically, variable selection involves successively augmenting the first-order mixture model with second-order terms to improve the model's predictive ability, and then stopping when adding additional terms fails to add additional predictive ability and begins to overfit the data.

Determining where gain in predictive ability stops and overfitting begins is both science and art. One technique used was to submit to the variable selection algorithms variables consisting of uniform (0,1) random numbers in addition to the second-order model terms (see Miller 1990). This technique was tried several times for each glass property with different sets of "random number" variables. The stages of the procedure at which random number variables began to be selected for the model instead of second-order terms indicated potential stopping points (because obviously random number variables are not useful predictors of glass properties, and thus second-order terms selected after random number variables would also be suspect). Statistical model evaluation and validation techniques (see Sections 6.1.5 and 6.1.6) were also used to help choose between candidate models for each property.

The variable selection approach involves starting with the linear mixture terms in the model, and then allowing the SAS (1990) variable selection algorithms to select from both crossproduct terms ($x_i x_j$) and squared terms (x_i^2). In the full Scheffé second-order model (6.2), the squared terms are not included, because doing so would over-specify the model (the squared

terms can be rewritten as linear combinations of linear and crossproduct terms and absorbed into similar terms). However, if only some of the second-order terms are included in the model, both crossproduct and squared terms can be considered.

No physical interpretation can necessarily be attached to second-order terms selected for a given property model. For example, just because an Al_2O_3 x ZrO_2 crossproduct term is selected for a model does not necessarily mean that there is an interactive effect of Al_2O_3 and ZrO_2 on the property. Such an interactive effect may exist, or it may just be that Al_2O_3 x ZrO_2 is highly correlated with one or more other crossproduct terms that do have interactive effects. The many second-order terms to select from and the intercorrelations among them are such that the terms selected may not be physically or theoretically interpretable. While such interpretability is desirable, the primary goal of CVS is to obtain models with adequate predictive ability. Variable selection techniques in regression modeling have a long history of producing useful predictive models. Predictive ability of first-order and variable-selected second-order models was investigated via model evaluation and model validation techniques, as discussed in Sections 6.1.5 and 6.1.6.

6.1.5 Model Evaluation

The term model evaluation refers to the application of statistical techniques to determine: (1) how well a model fits the data it was fitted to, and (2) how well the least squares assumptions (see Section 6.1.2) are satisfied. Violation of assumptions, detection of outlying data points, or detection of model inadequacy lead to implementing various remedies until the problem(s) are corrected. When the model being evaluated acceptably fits the data being used to develop the model, then model validation is performed with data not used to fit the model (see Section 6.1.6).

Model evaluation techniques applied to the fitted CVS property models include: predicted versus measured property plots, residual plots, outlier diagnostics, R^2 statistics, and statistical lack-of-fit (LOF) tests.

- Predicted versus measured property plots show how well model predictions compare to the measured values for the various glasses.
- Residual plots display residuals (r_i, differences in predicted and measured property values) versus the various glass components (r_i versus x_i) and the predicted property values (r_i versus $\hat{y}$). Patterns in the r_i versus $\hat{y}$ plot can indicate a violation of the least squares assumptions and suggest a property transformation to remedy the situation. Patterns in the r_i versus x_i plots can indicate inadequacies of the model.
- Outlier diagnostics indicate data points that are outlying or influential with respect to property value or composition.
- R^2 statistics (three are used, as discussed later in this section) indicate the proportion of variation in the property values accounted for by the fitted model.
- A statistical LOF test checks whether the differences between measured and predicted property values from a fitted model are larger than expected based on the experimental and measurement uncertainty in the data. If the predicted versus measured differences are larger than data uncertainty at a high enough statistical confidence (e.g., greater than 90%), the model is said to have a statistically significant LOF.

Replicate data points containing all applicable sources of experimental and measurement uncertainty[(a)] are required to perform statistical LOF tests. In the CVS, replicate data points were collected at different times within the same CVS experimental phase and replicates were performed in different CVS experimental phases. Replicate data points within the same experimental phase were batched, melted, and

---

(a) To be appropriate replicate data points, two or more glass samples of the same composition must be batched and melted at different times, and have their properties measured at different times. It is insufficient, for example, to batch and melt a glass once, and measure its properties several times (because the batching and melting sources of uncertainty are not included in the data. Similarly, replicate samples should not be measured at the same time (or close in time) because all sources of measurement uncertainty will not be included in the data.

properties measured at different times (a random run order was used for all glasses within each experimental phase).

Even when a fitted model has a statistically significant LOF, the LOF may not be "practically significant". An example of such a situation is when a fitted model yields biased predictions for higher and/or lower values of a property or in a particular subregion of compositions, but the model will not be applied to such areas in practice. Another example is when the model fits the data very well (e.g., $R^2 > 0.95$) without bias over the model's region of validity, but the LOF was statistically significant because the experimental and measurement uncertainty is very small (e.g., because glasses can be batched, melted, and properties measured very reproducibly). Finally, a statistically significant LOF may not be practically significant if the uncertainty in model predictions is considerably smaller than uncertainty that can be tolerated.

The model evaluation techniques discussed in the preceding bullets are included in, or easily obtained from, the output of the SAS (1990) REG procedure output. See Draper and Smith (1981) for further discussion of the concepts.

Three different R^2 statistics were used in evaluating models fitted to the glass property data:

R^2 — The fraction of variability in the property data (transformed or untransformed) accounted for by the fitted model.

$$R^2 = 1 - \frac{\sum_{i=1}^{n} (y_i - \hat{y}_i)^2}{\sum_{i=1}^{n} (y_i - \bar{y})^2} \qquad (6.7)$$

R^2(ADJ) — The fraction of variability in the property data (transformed or untransformed) accounted for by the fitted model, adjusted for the number of parameters and number of data points used in fitting the model. R^2(ADJ) is also useful for comparing fitted models based on different numbers of parameters.

$$R^2(ADJ) = 1 - \frac{\sum_{i=1}^{n} (y_i - \hat{y}_i)^2/(n-p)}{\sum_{i=1}^{n} (y_i - \bar{y})^2/(n-1)} \qquad (6.8)$$

R^2(PRESS) The fraction of variability in the property data (transformed or untransformed) accounted for by the fitted model, where each data point is "left out of the fit" in evaluating how well the model predicts the property for that data point. R^2(PRESS) estimates the fraction of variability that would be explained in predicting new observations drawn from the same composition space.

$$R^2(PRESS) = 1 - \frac{\sum_{i=1}^{n} (y_i - \hat{y}_{(i)})^2}{\sum_{i=1}^{n} (y_i - \bar{y})^2} \qquad (6.9)$$

In the above R^2 definitions,

n = the number of data points used to fit the model,

p = the number of terms in the model,

y_i = the measured property value for the i^{th} data point,

$\hat{y}_i$ = the predicted property value for the i^{th} data point made using the model fitted to all n data points,

$\hat{y}_{(i)}$ = the predicted property value for the i^{th} data point made using a model fitted to all data points except the i^{th},

$\bar{y}$ = the average of the n measured property values y_i.

The numerator of the ratio in (6.10) is referred to as the PRESS statistic, where PRESS is an acronym that stands for PRedicted Error Sums of Squares.

Generally R^2 statistics take values between 0 and 1. However, R^2(ADJ) and R^2(PRESS) can take negative values for a poor fitting model, a model that contains many more terms than needed to fit the data, or a model fitted to data with one or more very influential data points. Amongst the three R^2 statistics, typically, $R^2 > R^2(ADJ) > R^2(PRESS)$. More than a minor difference

between R^2 and R^2(ADJ) indicates that the model may contain more terms than needed to achieve the same goodness of fit. A substantial difference between R^2 and R^2(PRESS) is indicative of one or more data points being very influential in determining the fit of the model. Some reduction from R^2 to R^2(PRESS) is expected because R^2 corresponds to using all data to fit the model, whereas R^2(PRESS) corresponds to leaving each data point out of the fit when evaluating the performance of the model for that point. In general, a model will tend to predict better for data used to fit it than for data not used to fit it. Because R^2(PRESS) technically uses data not used in fitting the model to evaluate model performance, it can be considered a "model validation" rather than a "model evaluation" technique.

6.1.6 Model Validation

The term model validation refers to techniques applied to assess how well a fitted model predicts property values for glasses not used in fitting the model. The glasses used for validation must be in the same composition region as the data used to fit the property models, since (in general) fitted empirical models should not be used to extrapolate. Also, ideally the validation data should be evenly distributed over the region of validity of the fitted models to properly assess predictive ability. However, this is difficult to achieve in practice because validation data is typically not designed but consists of whatever is available.

Validation of CVS property models was performed using two different sets of data.[(a)] Models fitted to data up through CVS-II Phase 2 and included in an earlier unpublished version of this report were validated using the CVS-II Phase 3 data. Also, data for viscosity at 1150°C, electrical conductivity at 1150°C, and glass transition temperature from a historical database were used in validating CVS glass property models (see Appendix G). Data were gathered from several readily available sources including data from past Hanford HLW

(a) It would also be possible to use CVS-II Phase 4 data to validate PCT and MCC-1 models developed from data up through CVS-II Phase 3. However, the CVS-II Phase 4 data were not available in time to include such validation work in the report.

vitrification work, data generated at PNL for other sites, and older databases constructed by the Materials Characterization Center. Table G.1 in Appendix G summarizes the number of glasses and property values of each type available in the current database. All data available from the various sources were collected, although not all of the glasses are inside the CVS composition experimental region. Descriptions of the validation work done using the CVS-II Phase 3 data and the data in Appendix G are given in Chapters 7, 8, 9, and 12.

Validation generally consists of using the fitted models to predict property values for a set of validation data, and then comparing the predicted property values to the measured values from the validation database. Assessment of these comparisons is aided by plotting the predicted versus the measured values for each property. Statistical comparisons of predicted and measured values is also useful to see if differences are larger than their expected uncertainties. One such comparison is validation R^2:

$R^2(VAL)$ The fraction of variability in the (transformed or untransformed) property validation data accounted for by the fitted model.

$$R^2(VAL) = 1 - \frac{\sum_{i=1}^{n} (y_i - \hat{y}_i)^2}{\sum_{i=1}^{n} (y_i - \bar{y})^2} \qquad (6.10)$$

Note that $R^2(VAL)$ is defined exactly the same as the ordinary R^2 discussed in Section 6.1.5, except that instead of assessing model predictive performance with the data used to fit the models, data not used to fit the models (validation data) are used. Hence, the y_i, $\hat{y}_i$, and $\bar{y}$ values in Equation (6.10) are those corresponding to the validation data.

Another useful statistical comparison that can be combined with the plot of predicted versus measured property values is to include 95% prediction interval (see Appendix I) error bars on the predicted values. Then, if the error bar for a given validation data point overlaps a 45° line superimposed on the plot, the model is validated for that data point.

6.2 MODEL PREDICTION UNCERTAINTIES

Predictions made with a fitted property model are always subject to uncertainty in the estimated (fitted) model coefficients. This uncertainty results from the random errors in property values introduced during testing and measurement, as well as minor lack-of-fit of the empirical model relative to the true relationship. The purpose of applying statistical model evaluation and validation techniques (as discussed in Section 6.1) is to demonstrate that the fitted model adequately approximates the true relationship and does not have a significant lack-of-fit.

An additional source of uncertainty occurs when model predictions are made for uncertain, estimated compositions. For example, composition uncertainties will exist in the waste vitrification process because compositions will be estimated via sampling and chemical analyses.

Least squares regression theory and variance propagation theory provide equations that can be used to quantify model and composition uncertainties in model predictions. Background least squares theory and these equations are presented in Appendix I. The uncertainty equations are valid for models linear in the coefficients[(a)], provided the fitted models do not have a significant lack-of-fit (i.e., that they do not yield significantly biased predictions over the composition experimental region).

A key part of the equation for model uncertainty given in Appendix I is the covariance matrix of the estimated model coefficients. Each coefficient in a fitted empirical model has a variance, and pairs of coefficients have covariances. The covariance matrices for selected property models discussed in Sections 7 through 12 are reported in Section I.2 of Appendix I.

(a) Linearity in the coefficients is different than linearity in the predictor variables. The first- and second-order empirical models discussed in Section 6.1.1 are linear in their coefficients, with the exception of viscosity models based on the Fulcher equation.

6.3 COMPONENT EFFECTS

In order to better understand the effects of the 10 CVS glass components on glass and melt properties and to assess whether certain components could be eliminated from the models for certain properties, component effects plots (Piepel 1982) were produced using the fitted first-order mixture models and selected second-order models.

In an effects plot for a given property, there is one effect curve for each component. Each effect curve displays how the property changes (as predicted by the fitted property model) as the associated component varies over its allowable range (as determined by the single- and multiple-component constraints for the Phase 2a region in Table 4.5). As the concentration of the component of interest varies, the concentrations of all other components are kept in constant relative proportions determined by a reference mixture. This procedure is equivalent to adding a component to, or removing a component from, the reference mixture. Mathematically, a Δ_i change to the i-th component of the reference mixture s

$$x_i = s_i + \Delta_i \tag{6.11}$$

is offset by changes in the remaining $j \neq i$ components

$$x_j = s_j - \frac{\Delta_i s_j}{1 - s_i} \tag{6.12}$$

Then, it can be shown that $x_j/x_k = s_j/s_k$ for j and $k \neq i$. This is what was meant by the statement above that other components are kept in constant relative proportions.

In component effects plots, the predicted property values for a component effect curve are plotted against the differences $x_{ij} - X_i$, where X_i is the mass fraction of the i^{th} component in a selected reference mixture and x_i is the concentration of the i^{th} component at various points (indexed by j) along the effect curve. As a result, the curves for all mixture components for a given property intersect at $x_{ij} = X_i$. The reference mixture was the HW-39-4 glass composition for plots in this report, but any composition within the composition experimental region could be used. The effects plots given in

Sections 7 through 10 and 12 were produced using the EFFPLT routine in the MIXSOFT™ software (Piepel 1992) and the graphics capabilities of the S-Plus software (StatSci 1991). Effects plots based on mixture models in mole fractions could have been produced, but were not. Mole fraction models did not fit the data any better than mass fraction models, and test effects plots based on mole fraction models did not yield different conclusions than did effects plots based on mass fraction models.

Another way of considering component effects is based on thermodynamic relationships. The linear coefficients of a fitted first-order mixture model [such as b_i in Eq. (6.1)] approximate the partial specific properties in thermodynamics (Truesdell 1969, Gurtin and Vargas 1971). The linear coefficients and partial specific properties become identical if at least one of the following conditions is met: (1) the composition range approaches zero or (2) the mixture is linear in the sense that its properties are represented exactly by first-order models on the composition range in question.

The partial specific properties express the effects of component mass fractions on mixture properties. If the i-th component replaces the n-th component, the property change is proportional to the difference between the related first-order model coefficients

$$\frac{\partial p(x)}{\partial x_i} = b_i - b_n \qquad (6.13)$$

where p(x) is the first-order property model (Gurtin and Vargas 1971).

No simple relationship between a component effect and first-order model coefficients exists if the i-th component is simply added to or removed from the mixture (instead of replacing another component). The effect of adding component i to a selected point $s = (s_1, s_2, \ldots, s_{10})$ in the composition space (while keeping all other components in the same relative proportions) can be

expressed by the formula (Cox 1971 and Hrma et al. 1993):

$$\left(\frac{\partial p(x)}{\partial x_i}\right)_{add} = \frac{b_i - p}{1 - s_i} \qquad (6.14)$$

where p(x) is a first-order mixture model for a glass property (possibly mathematically transformed by the natural logarithmic transformation) as a function of the composition x, p is the predicted or measured mixture property at the selected point s in the composition space, b_i is the first-order mixture model coefficient, and s_i is the proportion of component i in the selected point s. The partial derivative notation is used in (6.14) to indicate that the effect is the property change for an infintisimally small change in composition by adding component i. The result of (6.14) may be thought of as the slope of the planar property surface (given by the first-order mixture model) along the direction of addition of component i to the starting composition s. Hence, the component effects defined by (6.14) depend on the starting composition even if the mixture is linear. However, it is clear that increasing the proportion of component i increases the value of the (possibly transformed) property [that is, $(\partial P(x)/\partial x_i)_{add} > 0$] if $b_i > p$ and decreases it if $b_i < p$. Hence, the values of first-order mixture model coefficients should not be considered alone in judging the effects on a property that result from adding (or subtracting) components from a given composition, but the coefficients should be compared to the value of the property for the starting glass composition(s) s of interest.

6.4 COMPARISONS TO OTHER MODELS

In addition to investigating empirical first- and second-order mixture model forms for glass and melt properties, several property model forms suggested by other researchers in the high-level waste glass arena were also investigated. The other property models investigated fall into the general class of semi-empirical models. In semi-empirical models the predictor variable(s) are developed using theory or other subject matter knowledge, and then the property variable is regressed against the constructed predictor variable(s) using empirical data. Investigating such semi-empirical models

allows comparing them to empirical mixture models so that the best possible models are obtained.

Comparisons of the CVS empirical mixture model forms and other semi-empirical model forms are based on the CVS data. This is an important point, since the performance of various model forms can depend on the composition region covered by the data. Models developed by other researchers for their composition region and data may not work as well for the CVS data due to the relatively large composition region studied in CVS. Similarly, CVS empirical models may not perform well for other researcher's data if it is for a composition region different than studied in CVS. In particular, the empirical CVS models are generally not applicable for extrapolating outside the CVS composition region. Discussions of the semi-empirical model forms investigated and comparisons to the CVS empirical mixture models are included in Chapters 7 (viscosity) and 12 (PCT and MCC-1 durability).

7.0 VISCOSITY RESULTS AND DISCUSSION

As discussed in Section 5.2, viscosity was measured at various temperatures for each CVS glass. The resulting data are given in Table B.1 of Appendix B, and estimates of uncertainty in the data based on replicate glasses are given in Appendix F. Overcheck viscosity measurements of the CVS internal standard glass (close to HW-39-4 composition) by Corning Engineering Laboratory Services (CELS) yielded results that were in very close agreement with the CVS results (see Section 13.2.1).

Table B.2 of Appendix B contains the results of fitting the Fulcher equation to the data for each glass in CVS-I and CVS-II Phases 1, 2, and 3 (from Table B.1). Values of viscosity at 1150°C (η_{1150}) estimated from these Fulcher fits ranged from 0.4 to 83.8 Pa·s, which exceed both limits of the acceptable η_{1150} range of 2 to 10 Pa·s. Of the 122 CVS-I and CVS-II Phase 1, 2, and 3 glasses for which viscosity was measured, 20 had η_{1150} less than 2 Pa·s, while 25 had η_{1150} greater than 10 Pa·s. Some glasses with η_{1150} values somewhat beyond the acceptable range of 2 to 10 Pa·s were designed into the CVS study to provide for developing models valid over a wider property range. In this way, accurate predictions within the acceptable range can be made.

Models expressing viscosity as a function of composition and temperature are discussed in Section 7.1. First-order mixture models for viscosity at 1150°C and corresponding component effects plots are presented in Section 7.2. The question of whether the viscosity data contains any biases, due to being collected in four phases (CVS-I and CVS-II Phases 1, 2, and 3), is addressed in Section 7.3. Second-order mixture models for viscosity at 1150°C are presented in Section 7.4. Model validation results are discussed in Section 7.5. Other model forms that were investigated are discussed in Section 7.6. A discussion of the results is presented in Section 7.7.

In completing the QA requirements for this report, it was detected that a different composition for CVS2-101 than given in Table 4.15 was used for all viscosity models in this chapter. The composition used was SiO_2 = .4873, B_2O_3 = .1130, Na_2O = .1680, Li_2O = .0426, CaO = .0112, MgO = .0172, Fe_2O_3 = .0738,

Al_2O_3 = .0370, ZrO_2 = .0046, and Others = .0453.[a] This difference has negligible impact on the fitted viscosity models, so the models were not redone using the CVS2-101 composition in Table 4.15.

7.1 VISCOSITY MODELS AS FUNCTIONS OF COMPOSITION AND TEMPERATURE

Viscosity at temperature data were modeled as a simultaneous function of temperature and composition by expressing the three coefficients of the Fulcher equation as first-order mixture models:

$$\ln \eta = \sum_{i=1}^{10} A_i x_i + \sum_{i=1}^{10} B_i x_i / (T - \sum_{i=1}^{10} T_i x_i) \qquad (7.1)$$

where T is temperature in °C, x_i is the mass or mole fraction of the i-th oxide component, and A_i, B_i, and T_i are coefficients. [Note that the values of A_i and B_i are not affected whether T is expressed in °C or K.] Results of fitting this model to the viscosity at temperature data of Table B.1 yielded unusual or inappropriate estimates of the A_i, B_i, and T_i coefficients. For example, nearly all of the T_i coefficients were negative, and the A_i, B_i, and T_i coefficients did not combine (when evaluated at each CVS composition) to yield results similar to the A, B, and T_0 coefficients obtained from fitting the Fulcher equation to the data for each glass (in Table B.2 of Appendix B). In spite of the unusual estimated A_i, B_i, and T_i coefficients, together they still yielded reasonable predicted values for viscosity at 1150°C. However, it was decided to augment the viscosity at temperature data in Appendix B.1 with an additional data point for each glass, consisting of associating an approximate viscosity of $10^{11.3}$ Pa·s with the transition temperature for each glass (Moynihan 1993). The resulting models are given in Table 7.1a for mass fractions and Table 7.1b for mole fractions. Based on the summary statistics from Tables 7.1a and 7.1b, the Fulcher first-order mixture models for both mass and mole fractions appear to fit quite well. For both mass and mole fraction models, the 95% confidence intervals for several of the 30 coefficients (parameters) include zero. This result indicates that not all of

---

(a) This composition was given in the Rev. 0 version of Jantzen et al. (1993) as the average of 30 analyses of the EA glass fabricated by Corning.

TABLE 7.1a. Fitted Viscosity Model in Which the Fulcher Equation Coefficients A, B, and T_0 are Expressed as First-Order Mixture Models in the Mass Fractions of the Oxide Components

Non-Linear Least Squares Summary Statistics[a]

Source	Degrees of Freedom	Sum of Squares	Mean Square
Regression	30	85644.498183	2854.816606
Residual	1101	258.286020	0.234592
Uncorrected Total	1131	85902.784202	
			R^2 = 0.9958
(Corrected Total)	1130	62134.704577	R^2(ADJ) = 0.9957

Coefficient Estimates

Coefficient	Estimate	Asymptotic Std. Error	Asymptotic 95% Confidence Interval Lower	Upper
A1 (SiO2)	-10.5899	1.204894	-12.9541	-8.2258
A2 (B2O3)	-24.4127	2.332649	-28.9897	-19.8357
A3 (Na2O)	2.0200	2.503166	-2.8916	6.9316
A4 (Li2O)	5.4558	5.332489	-5.0074	15.9190
A5 (CaO)	3.9535	4.465014	-4.8075	12.7146
A6 (MgO)	5.3088	4.137470	-2.8095	13.4272
A7 (Fe2O3)	-13.6326	2.765302	-19.0586	-8.2067
A8 (Al2O3)	1.4998	2.711253	-3.8201	6.8197
A9 (ZrO2)	-0.3590	3.477132	-7.1817	6.4637
A10 (Others)	-2.3815	3.451650	-9.1542	4.3911
B1 (SiO2)	19236.3263	1367.657846	16552.7704	21919.8822
B2 (B2O3)	15922.8410	2629.001157	10764.3348	21081.3473
B3 (Na2O)	-12965.4177	2791.126781	-18442.0395	-7488.7960
B4 (Li2O)	-39177.2042	6055.813858	-51059.6461	-27294.7622
B5 (CaO)	-18671.4525	5009.517328	-28500.8991	-8842.0060
B6 (MgO)	-11943.9611	4723.333366	-21211.8706	-2676.0517
B7 (Fe2O3)	14559.3344	3185.762687	8308.3761	20810.2928
B8 (Al2O3)	9524.4388	3079.281230	3482.4135	15566.4649
B9 (ZrO2)	4618.1457	3914.300874	-3062.3171	12298.6084
B10 (Others)	1710.2061	3922.131430	-5985.6214	9406.0337
T1 (SiO2)	76.1127	31.703254	13.9061	138.3194
T2 (B2O3)	263.4849	60.591132	144.5958	382.3747
T3 (Na2O)	425.7163	66.584930	295.0663	556.3662
T4 (Li2O)	474.4299	142.226241	195.3600	753.4997
T5 (CaO)	1065.8248	116.685906	836.8690	1294.7805
T6 (MgO)	752.2421	110.970394	534.5010	969.9831
T7 (Fe2O3)	43.6384	73.773110	-101.1158	188.3927
T8 (Al2O3)	178.5252	73.292332	34.7143	322.3360
T9 (ZrO2)	540.5086	91.986894	360.0162	721.0011
T10 (Others)	270.7406	91.716097	90.7794	450.7017

(a) This table was adapted from the SAS (1990) nonlinear regression procedure (NLIN) output.

(b) The data used to fit this model consisted of the measured viscosity at temperature data from Table B.1 augmented with a data point for each glass consisting of an approximate $10^{11.3}$ Pa·s viscosity value at that glasses transition temperature.

TABLE 7.1b. Fitted Viscosity Model in Which the Fulcher Equation Coefficients A, B, and T_0 are Expressed as First-Order Mixture Models in the Mole Fractions of the Oxide Components

Non-Linear Least Squares Summary Statistics[a]

Source	Degrees of Freedom	Sum of Squares	Mean Square
Regression	30	85653.236167	2855.107872
Residual	1101	249.548036	0.226656
Uncorrected Total	1131	85902.784202	
			R^2 = 0.9960
(Corrected Total)	1130	62134.704577	R^2(ADJ) = 0.9959

Coefficient Estimates

Coefficient	Estimate	Asymptotic Std. Error	Asymptotic 95% Confidence Interval Lower	Upper
A1 (SiO2)	-9.6876	1.035155	-11.7188	-7.6565
A2 (B2O3)	-25.9668	2.252105	-30.3858	-21.5478
A3 (Na2O)	2.0388	2.245201	-2.3666	6.4443
A4 (Li2O)	0.3594	2.274203	-4.1029	4.8217
A5 (CaO)	5.1372	3.747196	-2.2153	12.4898
A6 (MgO)	3.6759	2.430264	-1.0927	8.4445
A7 (Fe2O3)	-33.5957	6.549050	-46.4460	-20.7455
A8 (Al2O3)	1.1846	4.094196	-6.8488	9.2180
A9 (ZrO2)	-2.8340	6.214503	-15.0278	9.3598
A10 (Others)	-2.1461	8.226683	-18.2882	13.9959
B1 (SiO2)	17820.2054	1173.174901	15518.2551	20122.1557
B2 (B2O3)	16663.4562	2540.290252	11679.0144	21647.8979
B3 (Na2O)	-12773.1803	2491.717037	-17662.3139	-7884.0467
B4 (Li2O)	-16048.0935	2573.340917	-21097.3857	-10998.8012
B5 (CaO)	-18486.2993	4199.185253	-26725.7492	-10246.8494
B6 (MgO)	-7984.1814	2757.182943	-13394.2001	-2574.1628
B7 (Fe2O3)	36719.9535	7520.568258	21963.4372	51476.4697
B8 (Al2O3)	16882.6462	4639.963808	7778.3207	25986.9717
B9 (ZrO2)	11475.6139	6996.478292	-2252.5569	25203.7847
B10 (Others)	-922.2853	9386.568069	-19340.1813	17495.6107
T1 (SiO2)	103.3801	27.317050	49.7799	156.9804
T2 (B2O3)	262.0836	58.649529	147.0041	377.1630
T3 (Na2O)	426.8439	59.807065	309.4932	544.1946
T4 (Li2O)	395.0973	60.710228	275.9744	514.2201
T5 (CaO)	1031.9600	97.804348	840.0528	1223.8673
T6 (MgO)	636.8100	65.269707	508.7408	764.8793
T7 (Fe2O3)	-523.9734	175.183615	-867.7107	-180.2361
T8 (Al2O3)	-1.4005	111.149721	-219.4934	216.6925
T9 (ZrO2)	590.5572	164.459057	267.8632	913.2513
T10 (Others)	144.4930	219.435652	-286.0737	575.0596

(a) This table was adapted from the SAS (1990) nonlinear regression procedure (NLIN) output.

(b) The data used to fit this model consisted of the measured viscosity at temperature data from Table B.1 augmented with a data point for each glass consisting of an approximate $10^{11.3}$ Pa·s viscosity value at the transition temperature of that glass.

the coefficients are needed, and that a model with fewer coefficients could be developed if desired.

Figures 7.1a and 7.1b show the predicted versus measured viscosity values for the combined Fulcher first-order mixture model using mass fractions and mole fractions, respectively. Although these plots show the models fit the data fairly well, it was determined that they do not fit as well as separate Fulcher equations for each glass. This determination indicates that the first-order mixture model expansion of the Fulcher equation coefficients may not be sufficient and that second-order terms may be beneficial. However, including second-order mixture terms was not attempted because of the large number of terms in such models and the difficulties in removing unneeded terms from such large nonlinear (in the coefficients) models.

Augmenting the measured viscosity at temperature data with (transition temperature, $10^{11.3}$ viscosity) data points yielded appropriate estimates of the A_i, B_i, and T_i coefficients. The resulting models in Tables 7.1a and 7.1b are expected to better predict viscosities over a wider temperature range (than considered in CVS) compared to models fitted to the unaugmented data set. Models fitted to the unaugmented data must be extrapolated to make predictions outside CVS data range of 950 to 1250°C. Improved prediction performance is expected using models fitted to the augmented data because extrapolation is avoided for temperatures between 950°C and transition temperatures. Although viscosity predictions above 1250°C will still be extrapolations, the wider temperature range of data used to fit the model is expected to improve the accuracy of such extrapolations.[(a)]

The consequence of using the augmented data set and improving viscosity model predictions over wider temperature ranges is that the models fitted to the augmented data do not predict CVS measured data (in the range 950 to 1250°C) as well. For example, the mass fraction version of the model (7.1) fitted to the unaugmented data yielded $R^2 = 0.9838$, whereas the model in Table 7.1a (fitted to the augmented data) only yielded $R^2 = 0.9374$ for the

---

(a) Results (to be reported outside this report) for glasses with higher melting temperatures support this expectation.

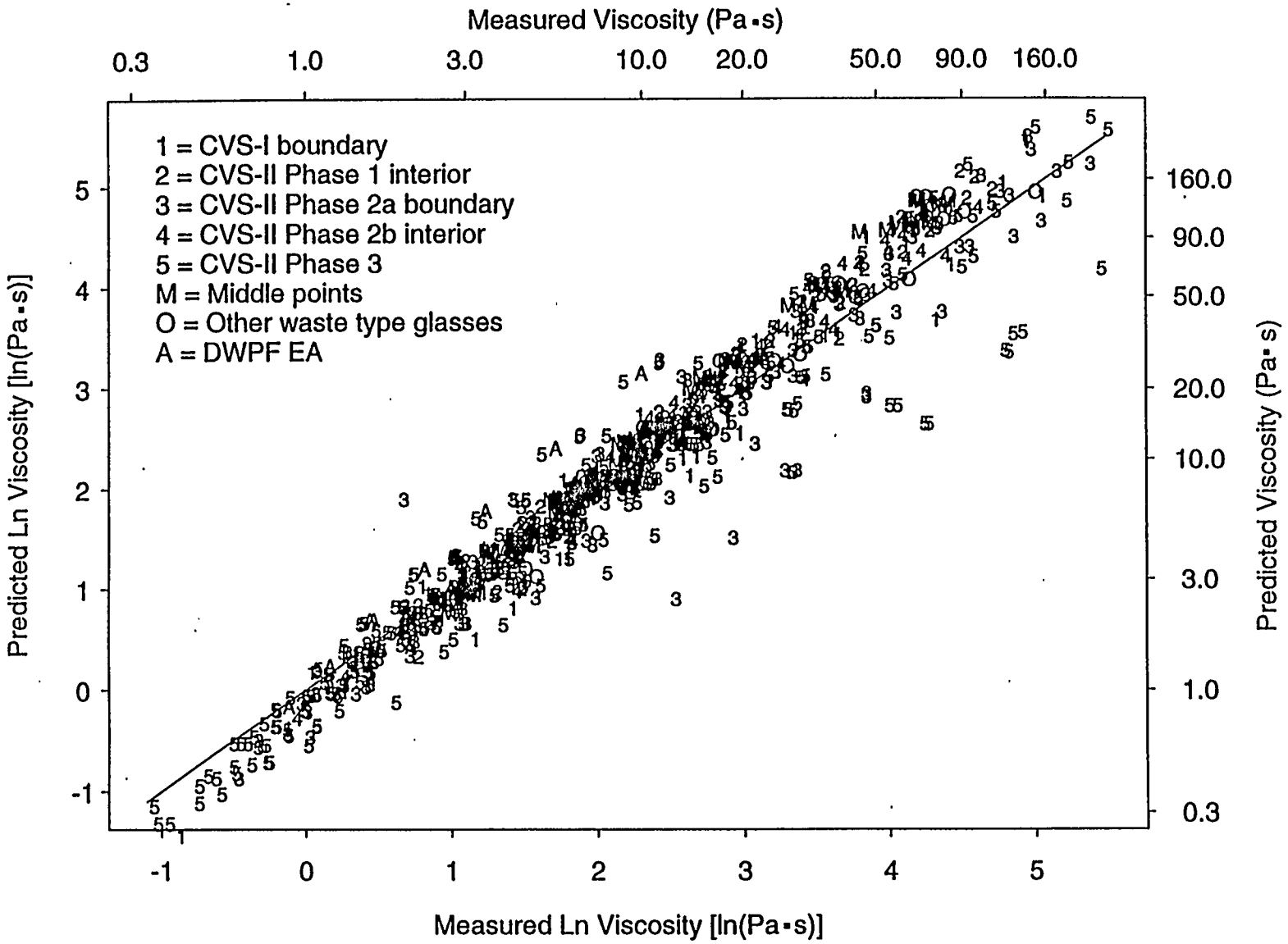

FIGURE 7.1a. Predicted Versus Measured Viscosity at Temperature Values for the Combined Fulcher First-Order Mixture Model in the Mass Fractions of the Component Oxides (from Table 7.1a)

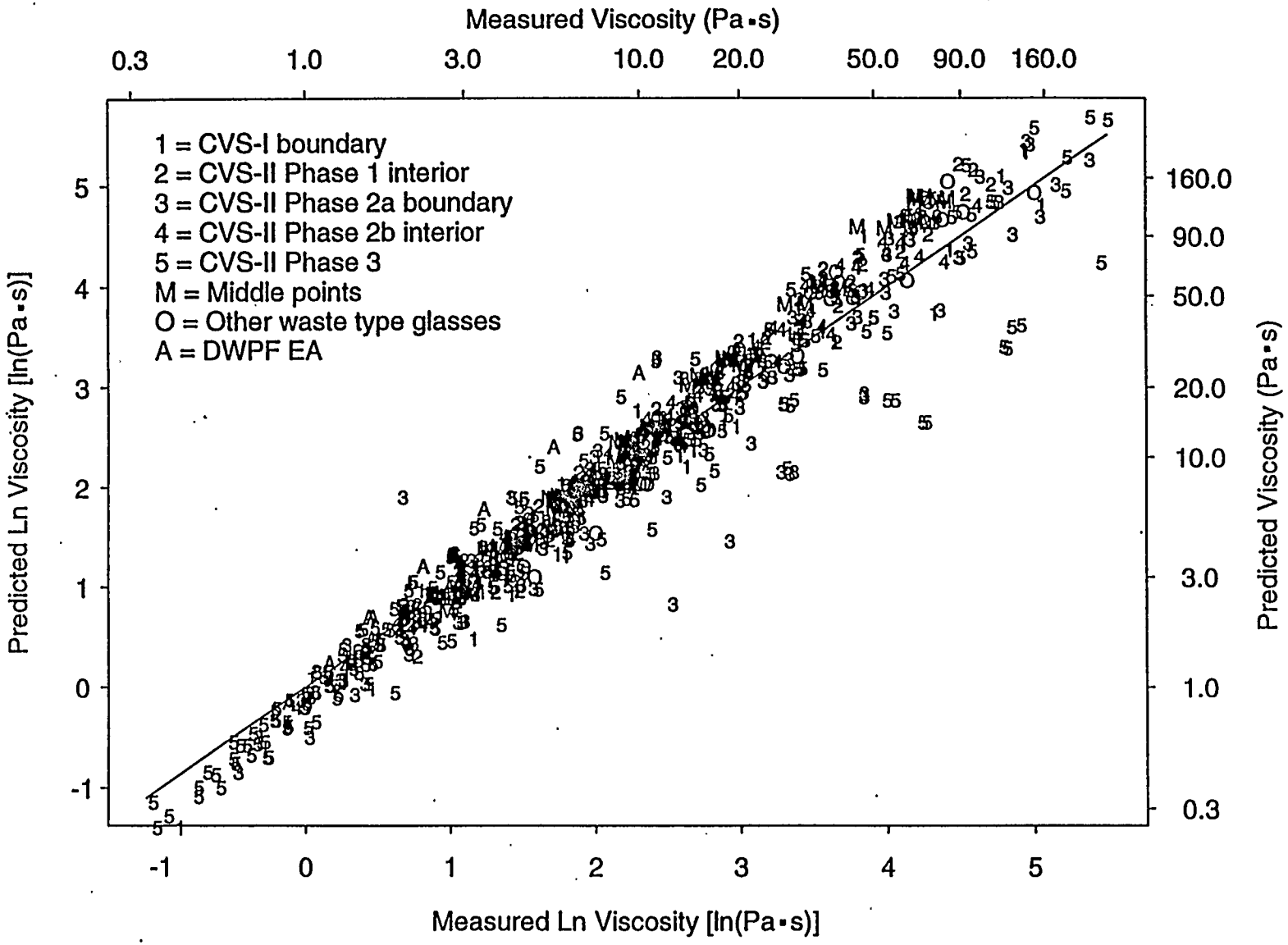

FIGURE 7.1b. Predicted Versus Measured Viscosity at Temperature Values for the Combined Fulcher First-Order Mixture Model in the Mole Fractions of the Component Oxides (from Table 7.1b)

unaugmented portion of the data. This reduction in prediction ability for the CVS viscosity data was expected, since the transition temperature data points have a strong influence on the overall fit of the model due to their much lower temperature values and very high viscosity values. In summary, predictions over wider temperature ranges are expected to be improved while predictions at 1150°C (and probably other temperatures in the range 950 to 1250°C) are somewhat degraded using the models fitted to the augmented data set. If predicting viscosity over a wide range of temperatures (including above and below the 950 to 1250°C range measured in CVS) is of interest, data should be collected over a wider temperature range to support fitting model (7.1).

Because the combined Fulcher first-order mixture model has 30 coefficients, requires nonlinear least squares regression, and is difficult to interpret physically, it was decided to also fit the Arrhenius equation:

$$\ln \eta = \sum_{i=1}^{10} A_i x_i + \sum_{i=1}^{10} B_i x_i / T \qquad (7.2)$$

obtained from (7.1) by dropping the temperature coefficient and expressing temperature (T) in Kelvin. The results for this model fitted to the unaugmented data set are given in Table 7.2a for mass fractions and Table 7.2b for mole fractions. The predicted versus measured viscosity at temperature plots are given in Figures 7.2a and 7.2b for the mass and mole fraction versions of the model, respectively.

A question of practical interest is whether the simpler Arrhenius first-order mixture model (with 20 coefficients) adequately predicts viscosity compared to the more complicated Fulcher first-order mixture model (with 30 coefficients). This question has two answers, depending on the temperature range over which predictions are desired. The Fulcher first-order mixture models in Tables 7.1a and 7.1b are expected to predict viscosity better at temperatures outside the CVS data range of 950 to 1250°C than the Arrhenius first-order mixture models in Tables 7.2a and 7.2b. This expectation follows from the additional flexibility of the Fulcher model over wider temperature ranges, and because the Fulcher first-order mixture models were fitted to the

TABLE 7.2a. Fitted Viscosity Model in Which the Arrhenius Equation Coefficients A and B are Expressed as First-Order Mixture Models in the Mass Fractions of the Oxide Components

Linear Least Squares Summary Statistics[a]

Source	Degrees of Freedom	Sum of Squares	Mean Square	F Value[b]	Prob>F[c]
Model	19	1555.79259	81.88382	1716.275	0.0001
Error	993	47.37624	0.04771		
C Total	1012	1603.16883			

Root Mean Square Error	0.21843	R^2	= 0.9704
Mean of Ln Viscosity	2.08735	R^2(ADJ)	= 0.9699
Coefficient of Variation	10.46429	R^2(PRESS)	= 0.9690

Coefficient Estimates

Variable	Degrees of Freedom	Coefficient Estimate	Standard Error	T-test for Coefficient=0 t-value	Prob > |T|[d]
SIO2	1	-11.084036	1.123630	-9.864	0.0001
B2O3	1	-13.658933	2.120677	-6.441	0.0001
NA2O	1	-9.603714	2.182123	-4.401	0.0001
LI2O	1	-4.514118	5.115170	-0.882	0.3777
CAO	1	-22.750189	3.755450	-6.058	0.0001
MGO	1	-21.104538	4.284975	-4.925	0.0001
FE2O3	1	-6.403733	2.944453	-2.175	0.0299
AL2O3	1	-4.088761	2.678404	-1.527	0.1272
ZRO2	1	-31.323104	3.314590	-9.450	0.0001
OTHERS	1	-17.017092	3.684877	-4.618	0.0001
SIO2/T	1	28539	1543.199176	18.493	0.0001
B2O3/T	1	10868	2912.153941	3.732	0.0002
NA2O/T	1	-1217.06	3000.369944	-0.406	0.6851
LI2O/T	1	-42288	7070.729522	-5.981	0.0001
CAO/T	1	21522	5159.543888	4.171	0.0001
MGO/T	1	25767	5903.376761	4.365	0.0001
FE2O3/T	1	8773.98	4064.628482	2.159	0.0311
AL2O3/T	1	21186	3687.292028	5.746	0.0001
ZRO2/T	1	54574	4555.969422	11.979	0.0001
OTHER/T	1	23027	5062.756413	4.548	0.0001

(a) This table was adapted from the SAS (1990) regression procedure (REG) output.

(b) F Value = Mean Square for Model / Mean Square for Error, the statistic for testing whether a significant portion of variation in the viscosity data is accounted for by the model.

(c) Probability that the model does not account for a significant portion of the variability in the data.

(d) Probability that the coefficient is significantly different than zero.

TABLE 7.2b. Fitted Viscosity Model in Which the Arrhenius Equation Coefficients A and B are Expressed as First-Order Mixture Models in the Mole Fractions of the Oxide Components

Linear Least Squares Summary Statistics[a]

Source	Degrees of Freedom	Sum of Squares	Mean Square	F Value[b]	Prob>F[c]
Model	19	1561.32884	82.17520	1950.286	0.0001
Error	993	41.83999	0.04213		
C Total	1012	1603.16883			

Root Mean Square Error	0.20527	R^2	= 0.9739
Mean of Ln Viscosity	2.08735	R^2(ADJ)	= 0.9734
Coefficient of Variation	9.83389	R^2(PRESS)	= 0.9725

Coefficient Estimates

Variable	Degrees of Freedom	Coefficient Estimate	Standard Error	T-test for Coefficient=0 t-value	Prob > |T|[d]
SIO2	1	-11.711204	0.993669	-11.786	0.0001
B2O3	1	-13.095657	2.161843	-6.058	0.0001
NA2O	1	-8.780435	1.999549	-4.391	0.0001
LI2O	1	-6.254821	2.234263	-2.800	0.0052
CAO	1	-20.768473	3.061976	-6.783	0.0001
MGO	1	-17.677246	2.584680	-6.839	0.0001
FE2O3	1	0.933899	6.893634	0.135	0.8923
AL2O3	1	-1.242356	4.061025	-0.306	0.7597
ZRO2	1	-51.385506	6.036688	-8.512	0.0001
OTHERS	1	-26.514879	8.905666	-2.977	0.0030
SIO2/T	1	28819	1365.569957	21.104	0.0001
B2O3/T	1	9054.08	2970.614626	3.048	0.0024
NA2O/T	1	-2002.31	2750.293569	-0.728	0.4668
LI2O/T	1	-12639	3090.010314	-4.090	0.0001
CAO/T	1	20359	4208.311504	4.838	0.0001
MGO/T	1	23268	3564.336321	6.528	0.0001
FE2O3/T	1	-5306.61	9519.422303	-0.557	0.5773
AL2O3/T	1	25113	5592.512476	4.491	0.0001
ZRO2/T	1	90415	8298.929436	10.895	0.0001
OTHER/T	1	29680	12238.49410	2.425	0.0155

(a) This table was adapted from the SAS (1990) regression procedure (REG) output.

(b) F Value = Mean Square for Model / Mean Square for Error, the statistic for testing whether a significant portion of variation in the viscosity data is accounted for by the model.

(c) Probability that the model does not account for a significant portion of the variability in the data.

(d) Probability that the coefficient is significantly different than zero.

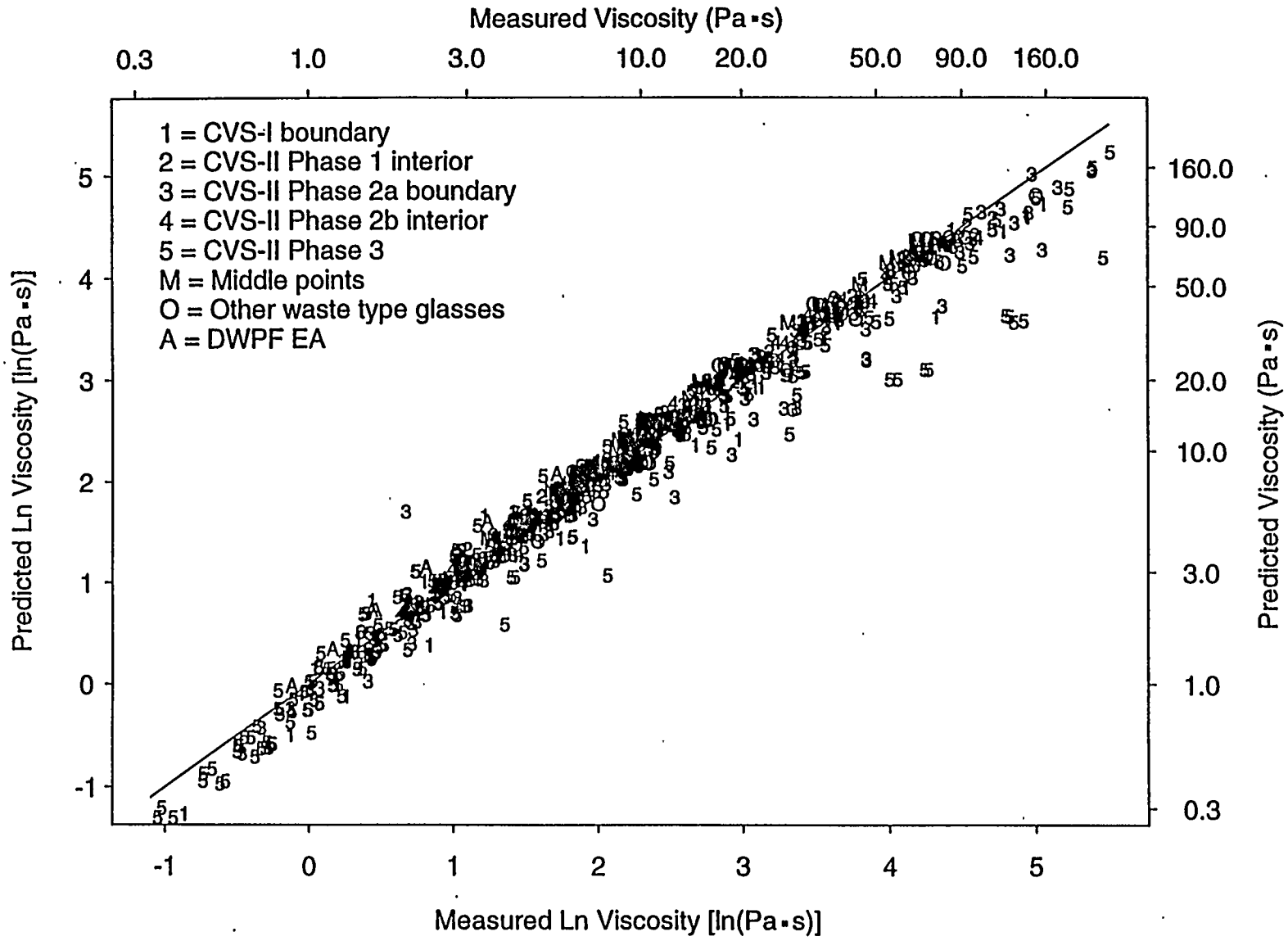

FIGURE 7.2a. Predicted Versus Measured Viscosity at Temperature Values for the Combined Arrhenius First-Order Mixture Model Using Mass Fractions of the Component Oxides (from Table 7.2a)

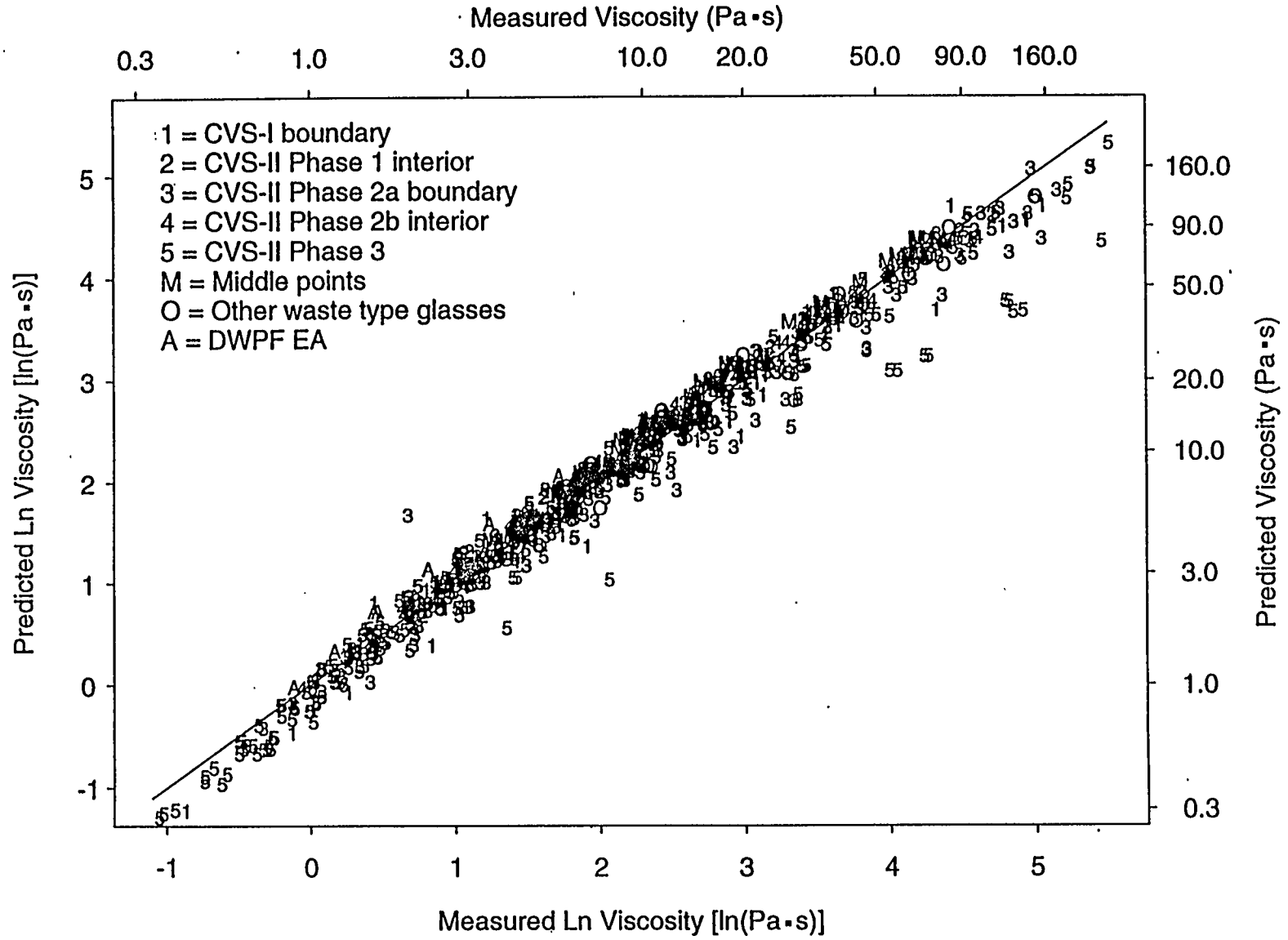

FIGURE 7.2b. Predicted Versus Measured Viscosity at Temperature Values for the Combined Arrhenius First-Order Mixture Model Using Mole Fractions of the Component Oxides (from Table 7.2b)

CVS data augmented by transition temperature data points. Based on comparison of R^2 values, the Arrhenius-mixture models in Tables 7.2a and 7.2b predict better than the Fulcher-mixture models in Tables 7.1a and 7.1b in the CVS data range of 950 to 1250°C. For example, the Arrhenius-mixture mass fraction model in Table 7.2a has $R^2 = 0.9704$ for the CVS 950 to 1250°C data, whereas the Fulcher-mixture mass fraction model in Table 7.1a has $R^2 = 0.9374$ for the CVS 950 to 1250°C data. However, the Fulcher-mixture models fitted to only the CVS measured data (these models are not included in this report) fitted the data better than the Arrhenius-mixture models. For example, the Fulcher-mixture mass fraction model has $R^2 = 0.9838$ for the CVS 950 to 1250°C data, whereas the Arrhenius-mixture mass fraction model in Table 7.2a has $R^2 = 0.9704$ for the CVS 950 to 1250°C data. Thus, whether limiting attention to the 950 to 1250°C measured data range, or an expanded temperature range, the Fulcher-mixture models appear to be preferable.

7.2 FIRST-ORDER MODELS AND COMPONENT EFFECTS FOR VISCOSITY AT 1150°C

Note that Equation (7.2) is linear in the coefficients, so that it is possible to factor it into the form:

$$\ln \eta = \sum_{i=1}^{10} (A_i + B_i/T)x_i . \tag{7.3}$$

Then

$$\ln \eta = \sum_{i=1}^{10} (A_i + B_i/1423)x_i . \tag{7.4}$$

provides a η_{1150} prediction equation that has the form of a first-order mixture model. It is also possible to use the η_{1150} values estimated from the individual Fulcher equation fits (from Table B.2 in Appendix B) as the

dependent variable in a first-order mixture model:

$$\ln \eta_{1150} = \sum_{i=1}^{10} b_i x_i . \qquad (7.5)$$

Previous results indicated a slight advantage to the Eq. (7.5) approach for predicting η_{1150}, so only those results are presented and discussed here.

The estimated coefficients from Equation (7.5) for mass and mole fractions of the oxide components are given in Table 7.3. The R^2 values in Table 7.3 indicate both models fit the data well, with a slight advantage to the mole fraction model. Figures 7.3a and 7.3b display the predicted η_{1150} values versus the η_{1150} values (from Table B.2 in Appendix B) for the first-order mixture models in mass and mole fractions from Table 7.3. These plots indicate that both models do a reasonable job of fitting the data without biases within the 1 to 15 Pa·s range. Both the mass and mole fraction models show a tendency to underpredict η_{1150} values above 15 to 20 Pa·s.

Although both models fit the data reasonably well, they have statistically significant LOFs with greater than 99% confidence. This result may be due to the first-order mixture model form being inadequate (e.g., components may have nonlinear or interactive effects), or to underestimation of the experimental variation in η_{1150} values used in performing the LOF tests. Predicted η_{1150} values (from the Fulcher equations fit to each glass) corresponding to replicates were used to estimate the experimental variation in η_{1150}. Because such values are from a fitted curve, they may yield an underestimate of the actual experimental variation in η_{1150}. Estimating the experimental variability from measured viscosity at temperature data could be investigated as an alternative. However, this may slightly overestimate the actual experimental variation due to temperature fluctuations around the nominal temperatures at which measurements were made.

TABLE 7.3. Coefficients and Goodness-of-Fit Statistics for First-Order Mixture Models Fitted to Natural Logarithm of Viscosity at 1150°C Using Mass and Mole Fractions of the Oxide Components

	Mass Fractions	Mole Fractions
SiO_2	8.967982	8.498225
B_2O_3	-6.204318	-6.841920
Na_2O	-11.016616	-10.685670
Li_2O	-34.239274	-15.030348
CaO	-7.466158	-6.279251
MgO	-2.776217	-1.198498
Fe_2O_3	-0.036918	-2.524915
Al_2O_3	11.306471	17.088329
ZrO_2	7.433982	12.810639
Others	-0.155959	-3.560768
# points[a]	124	124
R^2[b]	0.9391	0.9447
R^2(ADJ)[b]	0.9343	0.9404
R^2(PRESS)[b]	0.9260	0.9324
LOF?[c]	Yes (>99%)[d]	Yes (>99%)[d]

(a) Both models were fitted using the 124 viscosity at 1150°C values given in Table B.2 of Appendix B (including CVS2-9A and CVS2-16A). Viscosity was not measured for the radioactive glasses CVS2-53 and CVS2-54, and so those points were not included.

(b) R^2, R^2(ADJ), and R^2(PRESS) statistics take values between 0.0 and 1.0, and provide different measures of the proportion of variation in the property data accounted for by a fitted model. See Section 6.1.5 for the definitions of these statistics.

(c) A statistical F-test for lack-of-fit (LOF) was performed using the estimates of experimental variation obtained from replicate tests. "Yes" and "No" entries indicate whether the LOF was statistically significant at a 90% confidence level. The actual confidence level at which a LOF can be declared significant is given in parentheses following the "Yes" or "No" for each model.

(d) LOF test used the pooled transformed property SD estimate in Table F.4, not including replicate set 3.

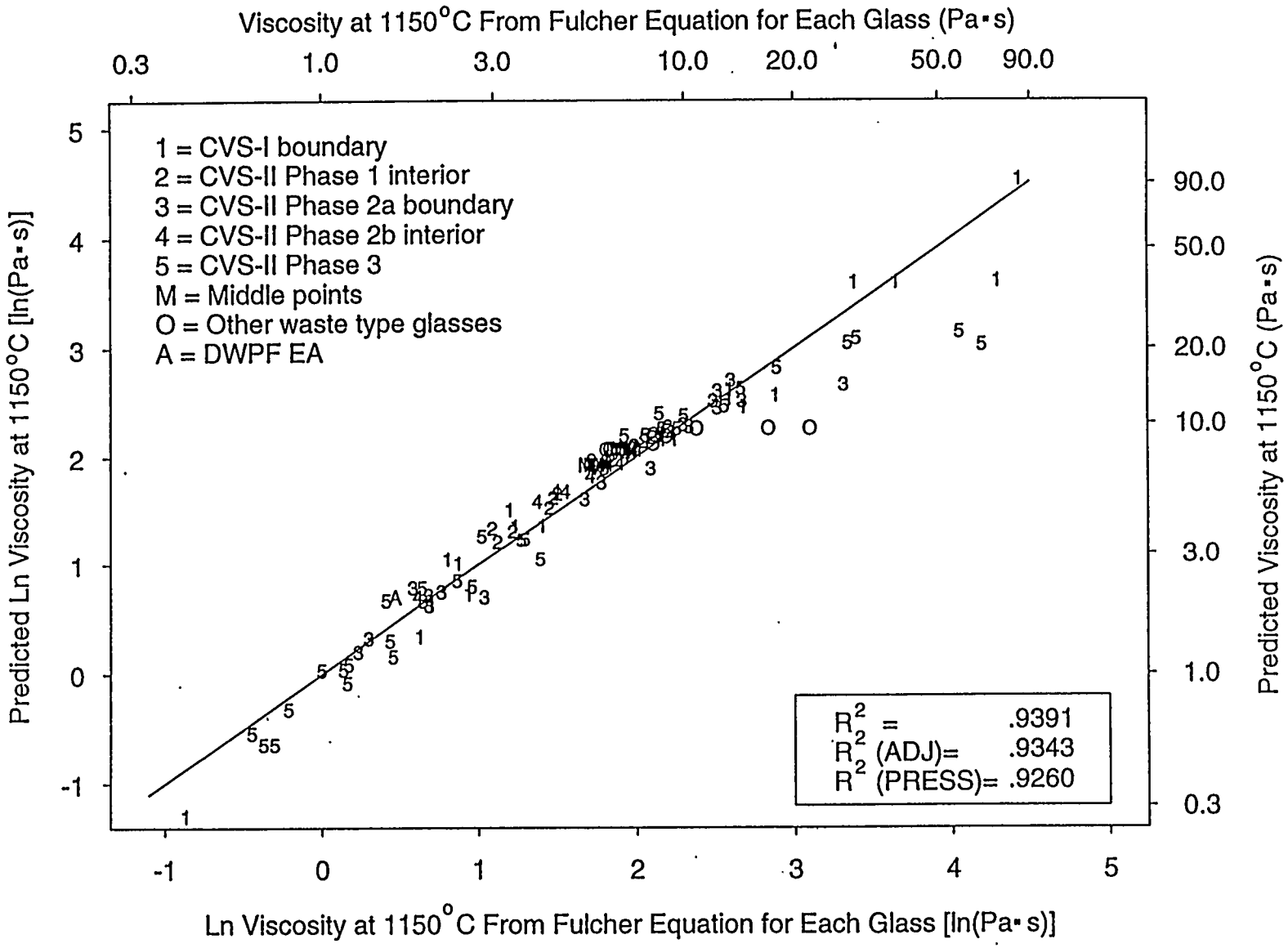

FIGURE 7.3a. Predicted Viscosity at 1150°C from the First-Order Mixture Model Using Mass Fractions (from Column 2 of Table 7.3) Versus Predicted Viscosity at 1150°C from the Fulcher Equation for Each Glass (from Table B.2)

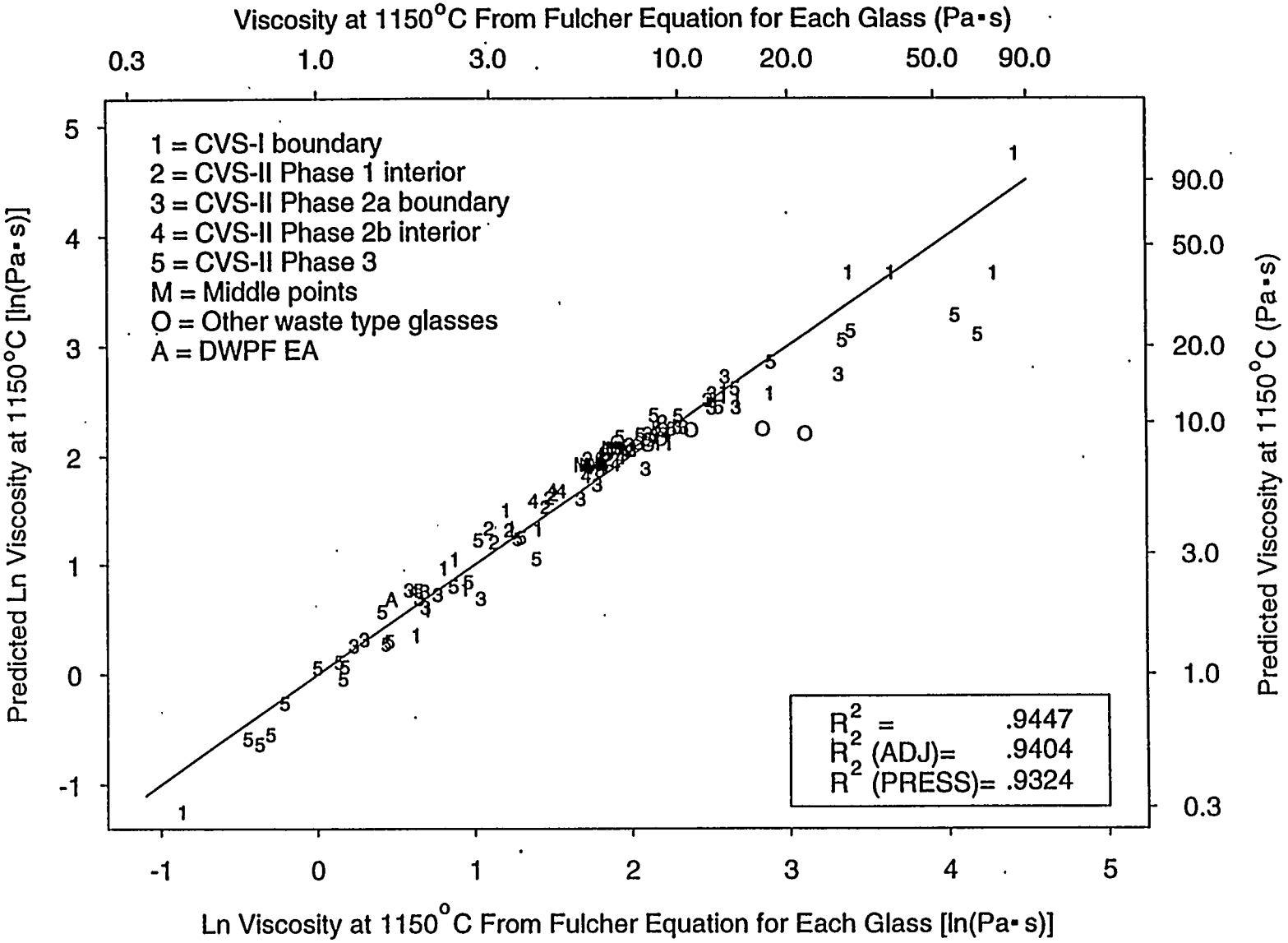

FIGURE 7.3b. Predicted Viscosity at 1150°C from the First-Order Mixture Model Using Mole Fractions (from Column 3 of Table 7.3) Versus Predicted Viscosity at 1150°C from the Fulcher Equation for Each Glass (from Table B.2)

The first-order mixture model using mass fractions given in Table 7.3 was used to produce a component effects plot (see Section 6.3) for η_{1150}, which is displayed in Figure 7.4. Only the single-component constraints and not the stand-in crystallinity constraints in Tables 4.2 and 4.6 were used to limit the effects plot (both were used in previous effects plots). As a result, effects are evaluated over wider ranges than in the past for several components involved in the stand-in constraints (most notably Al_2O_3 and SiO_2). The effects plot illustrates that η_{1150} of the HW-39-4 glass (used as the reference point in the plots) is predicted to be increased most (in order) by SiO_2, Al_2O_3, and ZrO_2. The effects plot also indicates that η_{1150} of HW-39-4 is predicted to be decreased most (in order) by Li_2O, Na_2O, and $CaO \approx B_2O_3$. The components MgO, Fe_2O_3, and Others are predicted to have mild reducing effects on viscosity, although due to the uncertainties in the fitted models they could have negligible or mild increasing effects. The effects plots and conclusions are quite similar to those from the CVS-I report (Piepel, Hrma, et al. 1993) and after previous phases of CVS-II.

7.3 INVESTIGATION OF POTENTIAL BIASES IN VISCOSITY AT 1150°C DATA DUE TO CVS PHASES

As discussed in Section 6.1.1, a model of the form (6.3) was fitted to the η_{1150} data for CVS-I and CVS-II Phases 1, 2, and 3 to ascertain whether any biases (block effects) exist in the η_{1150} data due to performing the CVS in phases. The mass fraction version of (6.3) yielded $R^2 = 0.9483$, which can be compared to $R^2 = 0.9391$ for the first-order mass fraction model (6.1) without the block effect terms (see Column 2 of Table 7.3). The mole fraction version of (6.3) yielded $R^2 = 0.9534$, which can be compared to $R^2 = 0.9447$ for the first-order mole fraction model (6.1) without the block effect terms (see Column 3 of Table 7.3).

Two statistically significant block effects were detected for both mass and mole fraction versions of the model (6.3) for η_{1150}. CVS-II Phase 1 was found to have a negative block effect on η_{1150}, while CVS-II Phase 3 was found to have a positive block effect on η_{1150}. This difference could be because the η_{1150} values were biased low for all or a substantial portion of the glasses in CVS-II Phase 1, and biased high for all or a substantial portion of the

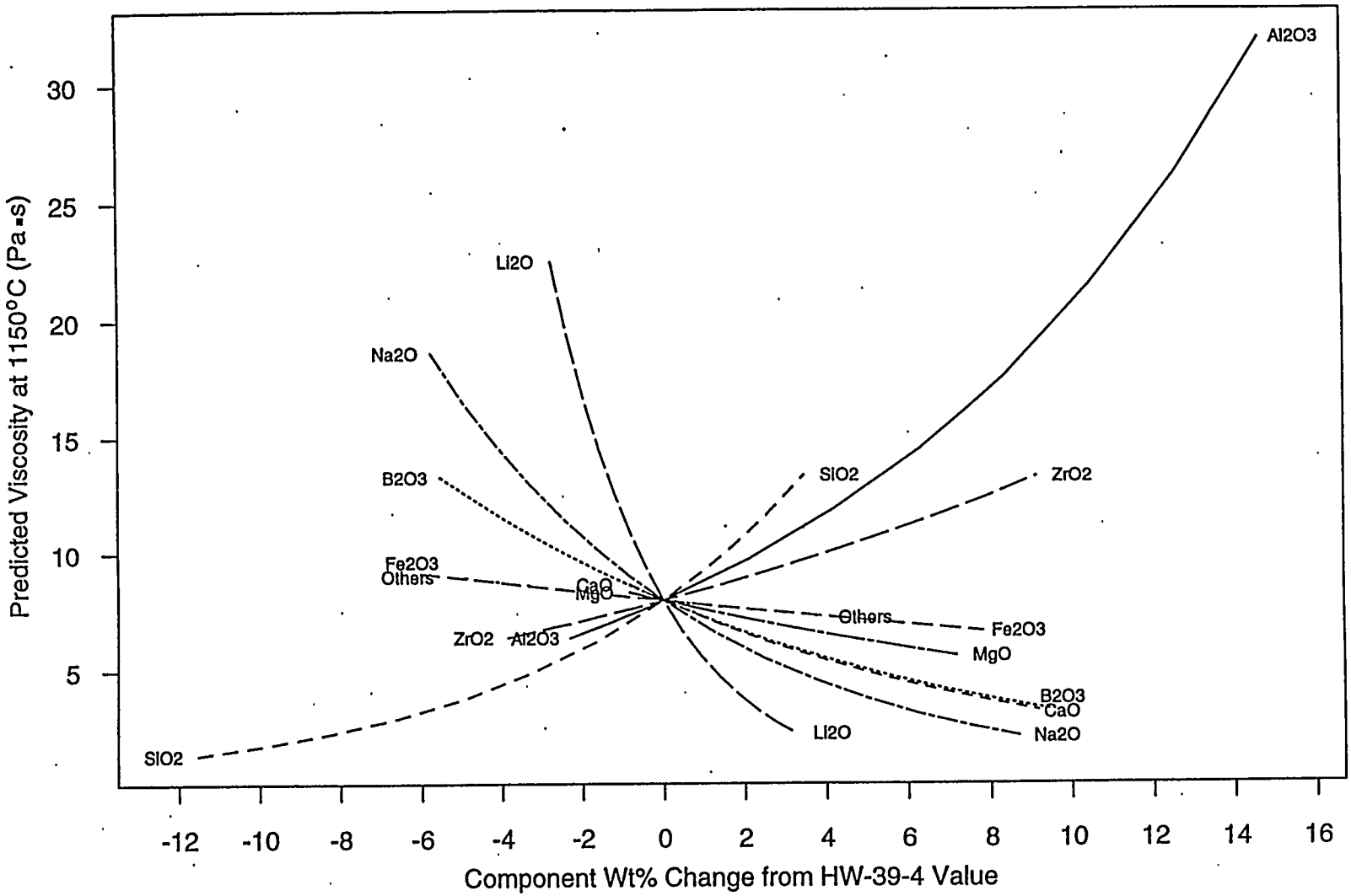

FIGURE 7.4. Predicted Component Effects on Viscosity at 1150°C Relative to the HW-39-4 Composition, Based on the First-Order Mixture Model Using Mass Fractions (from Column 2 of Table 7.3)

glasses in CVS-II Phase 3. Alternatively, it could be because CVS-II Phase 1 explored a reduced subregion of the full CVS composition experimental region, while CVS-II Phase 3 involved obtaining more extreme composition and property data than had been obtained in previous CVS phases. Data for replicate glasses in Table F.1 in Appendix F does not provide strong support for the "biased data" hypothesis.

Because of the uncertainty as to whether viscosity data for CVS-II Phases 1 and 3 are really biased, it was decided not to try to adjust the data and refit models.

7.4 SECOND-ORDER MODELS FOR VISCOSITY AT 1150°C

Expanding the three coefficients of the Fulcher equation and the two coefficients of the Arrhenius equation as second-order mixture models would result in full models with 165 and 110 coefficients, respectively. As seen in Section 7.1, even expanding the Fulcher and Arrhenius coefficients as first-order mixture models results in combined models with 30 and 20 coefficients, respectively. The much larger number of coefficients in the combined second-order models makes it difficult to fit these models (or reduced versions of them). Hence, it was decided to only fit second-order mixture models to the viscosity at 1150°C values obtained as predictions from the Fulcher equations fit to each glass (see Table B.2 in Appendix B). Further, because there was little difference in the fits of first-order mass and mole fraction models, second-order models were developed in terms of mass fractions only.

Three candidate Scheffé second-order mixture models for viscosity at 1150°C are given in Table 7.4. These models consist of the first-order mixture model terms and several second-order terms selected using statistical variable selection techniques (see Section 6.1.4). It was not necessary to apply the pseudocomponent transformation (see Section 6.1.3), so the usual glass oxide component mass fractions were used in fitting the models. Figure 7.5 displays the predicted η_{1150} values versus the η_{1150} values for Model #1 from Table 7.4.

TABLE 7.4. Candidate Scheffé Second-Order Models Using Mass Fractions for Viscosity at 1150°C[a]

Model #1		Model #2		Model #3 (b)	
Terms	Coefficients	Terms	Coefficients	Terms	Coefficients
SiO2	10.9874	SiO2	10.0943	SiO2	9.6667
B2O3	-6.1653	B2O3	-3.8943	B2O3	-3.4544
Na2O	-26.3877	Na2O	-21.0780	Na2O	-11.4798
Li2O	-75.8681	Li2O	-73.8599	Li2O	229.7322
CaO	-5.5719	CaO	-5.2809	CaO	-8.8883
MgO	-3.2329	MgO	-3.3056	MgO	-1.8798
Fe2O3	0.1485	Fe2O3	0.1254	Fe2O3	-1.0350
Al2O3	14.4910	Al2O3	14.5491	Al2O3	14.8627
ZrO2	10.1454	ZrO2	10.8893	ZrO2	12.1289
Others	-2.1192	Others	-14.9195	Others	-3.6879
B2O3 x Fe2O3	30.0977	B2O3 x Fe2O3	29.0862	SiO2 x Li2O	-299.3860
Na2O x Li2O	126.7491	Na2O x Li2O	122.6271	B2O3 x Li2O	-306.6521
Na2O x MgO	29.8751	Na2O x MgO	27.2706	Na2O x Li2O	-206.6521
Li2O x Others	78.9432	Li2O x Others	84.5019	CaO x Li2O	-257.3688
MgO x Fe2O3	-39.5274	MgO x Fe2O3	-33.9974	MgO x Li2O	-298.1902
Na2O x Na2O	43.5744	Na2O x Na2O	31.5975	Fe2O2 x Li2O	-306.7093
Li2O x Li2O	296.5902	Li2O x Li2O	279.6255	Al2O3 x Li2O	-332.4826
		SiO2 x Others	24.5186	ZrO2 x Li2O	-356.0579
		B2O3 x Na2O	-19.1042	Others x Li2O	-223.2521
		Al2O3 x ZrO2	-41.6230	B2O3 x Fe2O3	27.3838
				MgO x Fe2O3	-38.8460
				B2O3 x Na2O	-32.1617
				Al2O3 x ZrO2	-50.3898
R^2	= .9746	R^2	= .9783	R^2	= .9761
R^2(ADJ)	= .9708	R^2(ADJ)	= .9743	R^2(ADJ)	= .9709
R^2(PRESS)	= .9634	R^2(PRESS)	= .9678	R^2(PRESS)	= .9609
LOF?[c]	Yes (>99%)[d]		Yes (>99%)[d]		Yes (>99%)[d]

(a) These models were fitted using 124 CVS-I and CVS-II Phase 1, 2, and 3 viscosity at 1150°C values given in Table B.2 of Appendix B (including CVS2-9A and CVS2-16A). Viscosity was not measured for the radioactive glasses CVS2-53 and CVS2-54, and so those points were not included.

(b) This model was selected by first noting that all of the LiO_2 cross-product terms in the full second-order mixture were significantly different from zero. Thus, the linear terms and LiO_2 cross-product terms were forced into the model and then other second-order terms were added to the model using statistical variable selection methods.

(c) A statistical F-test for lack-of-fit (LOF) was performed using the estimates of experimental variation obtained from replicate tests. "Yes" and "No" entries indicate whether the LOF was statistically significant at a 90% confidence level. The actual confidence level at which a LOF can be declared significant is given in parentheses following the "Yes" or "No" for each model.

(d) LOF test used the pooled transformed property SD estimate in Table F.4, not including replicate set 3.

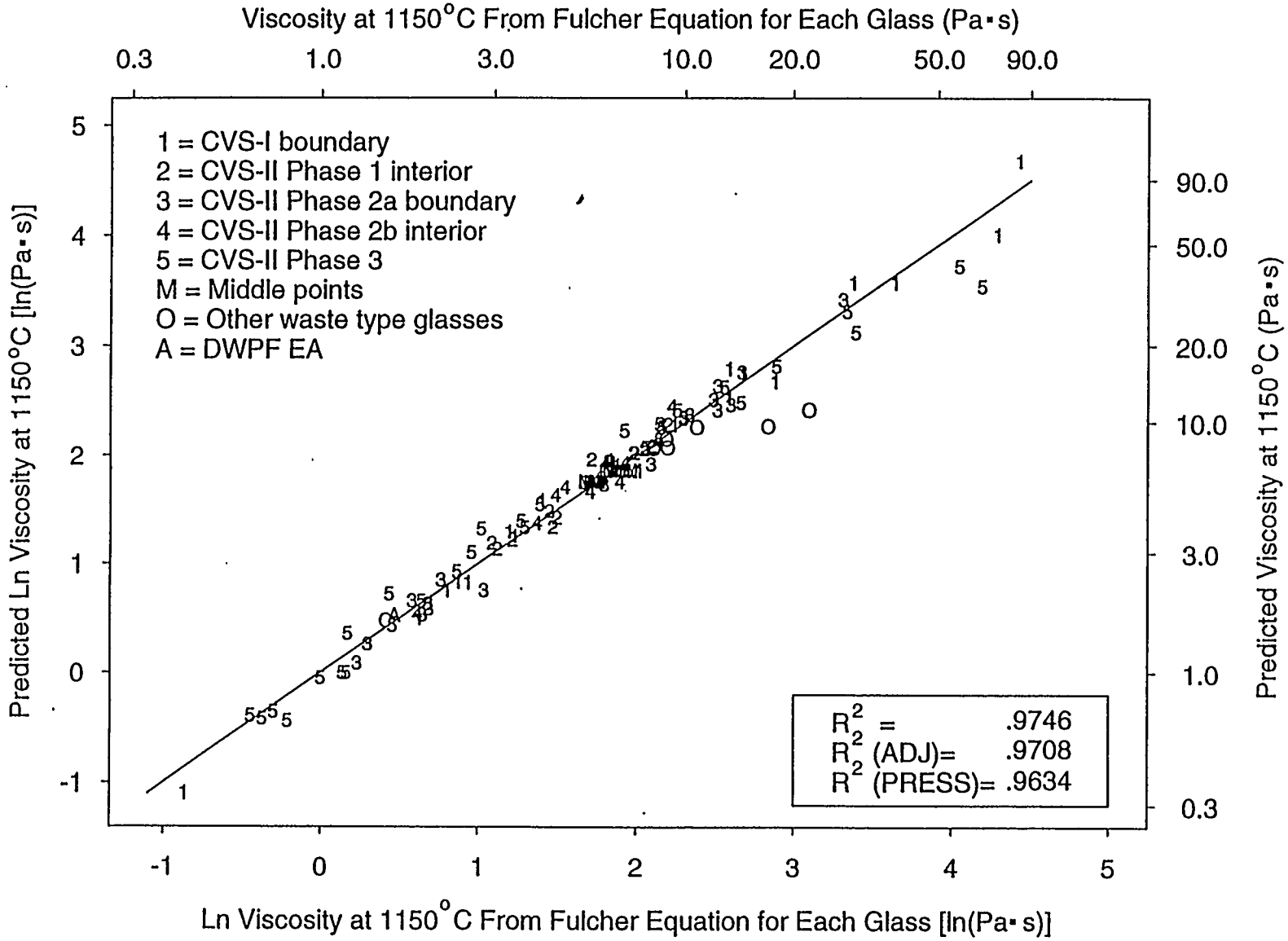

FIGURE 7.5. Predicted Viscosity at 1150°C from the Second-Order Mixture Model #1 (from Table 7.4) Versus Predicted Viscosity at 1150°C from the Fulcher Equation for Each Glass (from Table B.2)

The three candidate second-order mixture models in Table 7.4 provide a better fit than the first-order mass fraction mixture model in Table 7.3. This statement is based on comparing Figure 7.5 to Figure 7.3a, as well as on comparing the R^2 statistics for the models. However, the three candidate second-order models still have statistically significant LOFs at greater than 99% confidence (as indicated at the bottom of Table 7.4). This may be due to underestimation of the experimental variation in η_{1150} values used in performing the LOF test. Predicted η_{1150} values (from the Fulcher equations fit to each glass) corresponding to replicates were used to estimate the experimental variation in η_{1150}. Because such values are from a fitted curve, they may yield an underestimate of the actual experimental variation in η_{1150}. Estimating the experimental variability from measured viscosity at temperature data could be investigated as an alternative, although this may slightly overestimate the actual experimental variation due to temperature fluctuations around the nominal temperatures at which measurements were made.

7.5 VALIDATION OF FIRST- AND SECOND-ORDER MODELS FOR VISCOSITY AT 1150°C

The CVS-II Phase 3 data and a set of historical data were used to validate the first- and second-order Scheffé mixture models for viscosity at 1150°C developed using data up through CVS-II Phase 2. These models were reported in an earlier version of this report, but for convenience they are listed in Table 7.5. (Recall that validation involves using data not used to fit the models to assess their predictive performance--see Section 6.1.6.) The validation results for each of these data sets follow.

7.5.1 Validation with CVS-II Phase 3 Data

Figures 7.6, 7.7a, 7.7b, and 7.7c contain the validation results using the CVS-II Phase 3 data for the first-order and three candidate second-order mixture models (using mass fractions) for viscosity at 1150°C. These figures contain plots of the predicted versus "measured" η_{1150} values together with a superimposed 45° line that represents perfect prediction. The error bars on the plotted points represent 95% two-sided prediction intervals for the predicted η_{1150} values. If the error bars for a given point overlap the

TABLE 7.5. First-Order Model and Three Candidate Second-Order Models Using Mass Fractions for Viscosity at 1150°C Fitted to CVS-I and CVS-II Phase 1 and 2 Data[a]

First-Order Model		Three Candidate Second-Order Models					
		Model #1 (b)		Model #2		Model #3	
Terms	Coefficients	Terms	Coefficients	Terms	Coefficients	Terms	Coefficients
SiO2	8.7874	SiO2	10.6151	SiO2	9.4289	SiO2	9.4700
B2O3	-6.2771	B2O3	-16.4002	B2O3	-15.3360	B2O3	-14.5915
Na2O	-10.7199	Na2O	-15.0994	Na2O	-11.0827	Na2O	-11.0184
Li2O	-34.6126	Li2O	-33.1169	Li2O	-32.9541	Li2O	-33.6984
CaO	-6.2517	CaO	-5.0155	CaO	-3.6236	CaO	-5.3832
MgO	-1.8851	MgO	-6.3625	MgO	-2.0285	MgO	-1.5024
Fe2O3	0.0566	Fe2O3	-4.8618	Fe2O3	-1.1978	Fe2O3	-3.9269
Al2O3	11.0537	Al2O3 (b)	17.7692	Al2O3	11.9507	Al2O3	11.4124
ZrO2	7.8062	ZrO2	-0.1147	ZrO2	3.7870	ZrO2	9.9016
Others	-0.8167	Others	0.9946	Others	1.4450	Others	-0.3041
		B2O3 x Fe2O3	42.8450	B2O3 x Fe2O3	37.3363	B2O3 x Fe2O3	36.5869
		Li2O x CaO	-44.7237	Li2O x CaO	-55.4623	Fe2O3 x Al2O3	34.8765
		Fe2O3 x Others	-29.7983	Fe2O3 x Others	-42.0464	Al2O3 x ZrO2	-97.3354
		B2O3 x B2O3	34.9759	B2O3 x B2O3	31.4514	B2O3 x B2O3	29.4816
		ZrO2 x ZrO2	43.9507	ZrO2 x ZrO2	39.9708		
		SiO2 x Al2O3	-17.2148				
		Na2O x MgO	29.1101				
		Na2O x Fe2O3	24.8105				
		Na2O x Al2O3	22.7133				
		Na2O x ZrO2	22.6674				
		CaO x ZrO2	18.6650				
		MgO x ZrO2	22.0922				
R^2	= .9563	R^2	= .9939	R^2	= .9865	R^2	= .9864
R^2(ADJ)	= .9507	R^2(ADJ)	= .9918	R^2(ADJ)	= .9837	R^2(ADJ)	= .9838
R^2(PRESS)	= .9338	R^2(PRESS)	= .9849	R^2(PRESS)	= .9749	R^2(PRESS)	= .9742
LOF?[c]	Yes (>99%)[d]		Yes (98.7%)[d]		Yes (99.8%)[d]		Yes (99.8%)[d]

(a) Viscosity was not measured for the radioactive glasses CVS2-53 and CVS2-54, so they were not used to fit the models.

(b) In the previous version of this report, the coefficient for Al2O3 mistakenly had a negative sign.

(c) A statistical F-test for lack-of-fit (LOF) was performed using the estimates of experimental variation obtained from four replicate tests. "Yes" and "No" entries indicate whether the LOF was statistically significant at a 90% confidence level. The actual confidence level at which a LOF can be declared significant is given in parentheses following the "Yes" or "No" for each model.

(d) LOF test used a pooled transformed property SD estimate comparable to the one in Table F.4 not including replicate set 3, except only data through CVS-II Phase 2 were used.

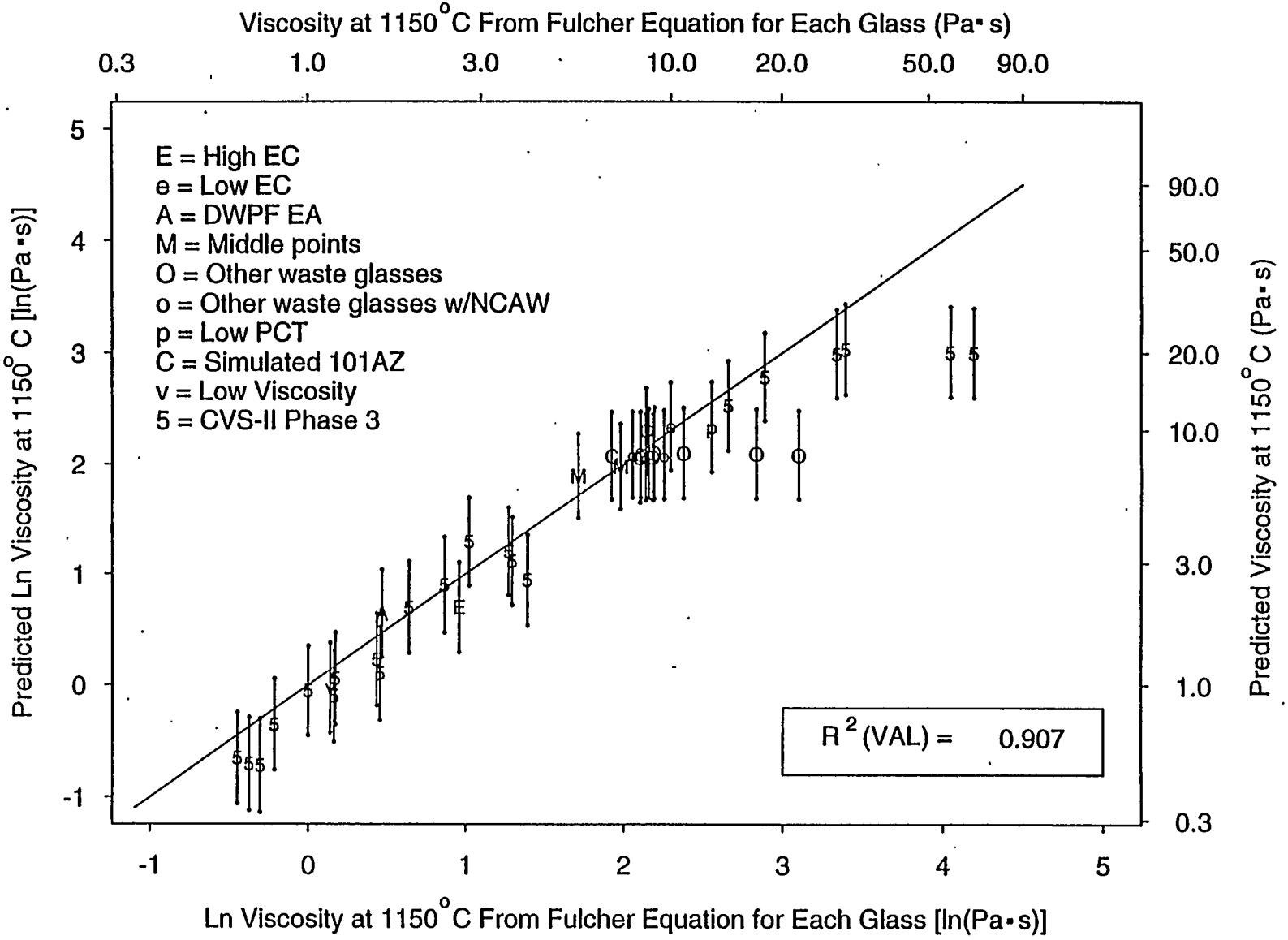

FIGURE 7.6. Predicted Viscosity at 1150°C from the First-Order Mixture Model After CVS-II Phase 2 (from Table 7.5) Versus Predicted Viscosity at 1150°C from the Fulcher Equation for Each Glass (from Table B.2) for the CVS-II Phase 3 Data

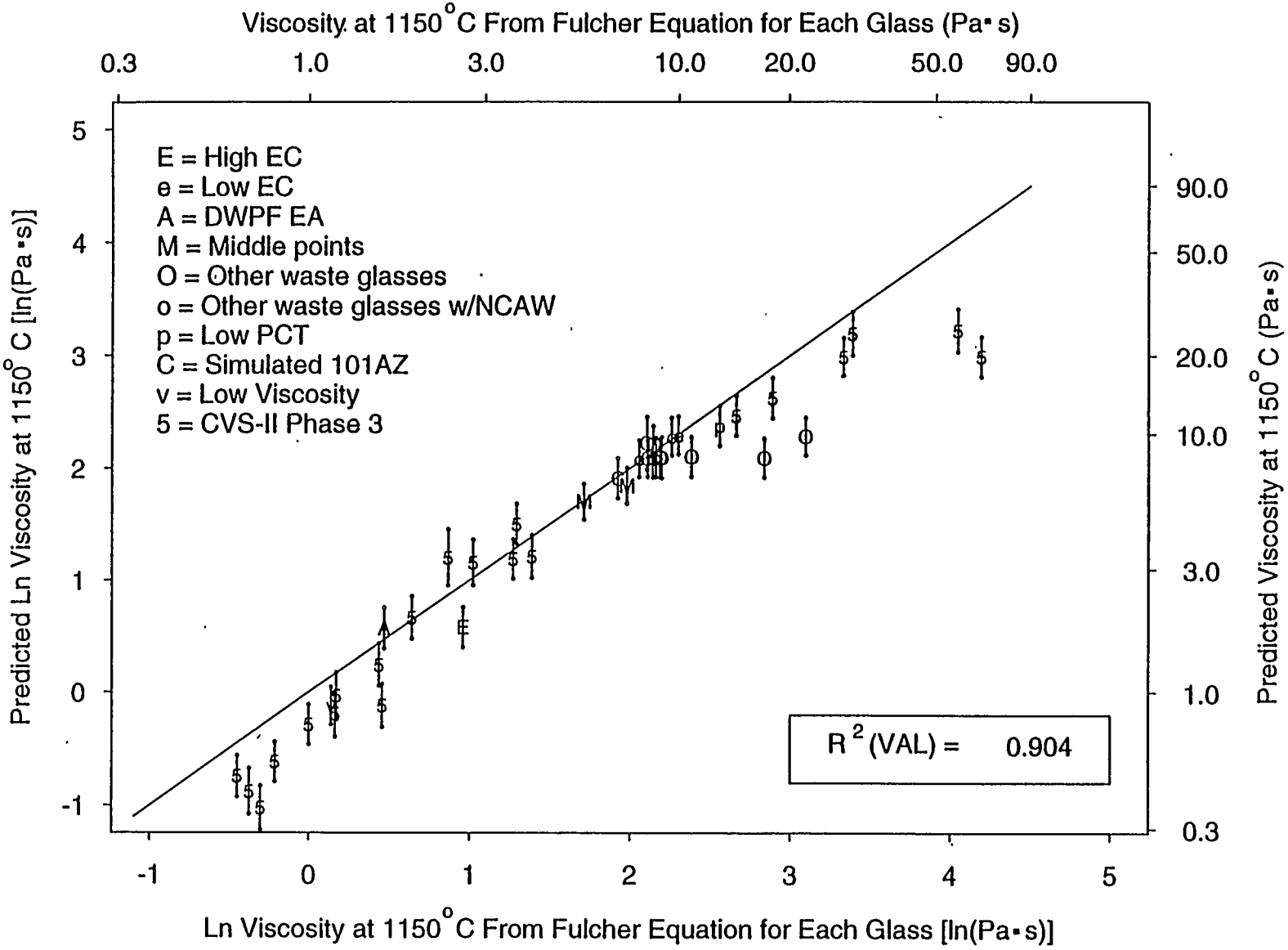

FIGURE 7.7a. Predicted Viscosity at 1150°C from the Second-Order Mixture Model #1 After CVS-II Phase 2 (from Table 7.5) Versus Predicted Viscosity at 1150°C from the Fulcher Equation for Each Glass (from Table B.2) for the CVS-II Phase 3 Data

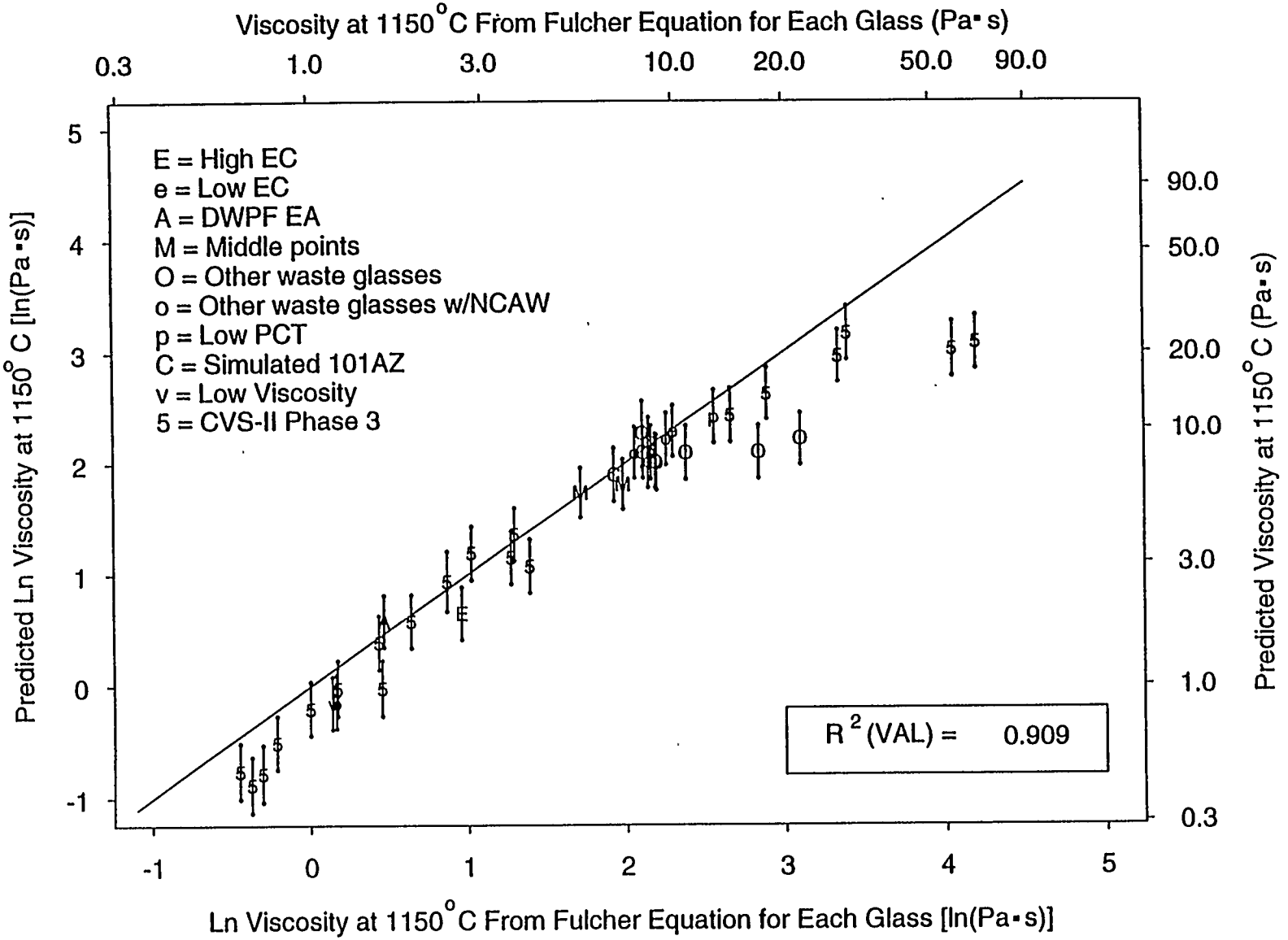

FIGURE 7.7b. Predicted Viscosity at 1150°C from the Second-Order Mixture Model #2 After CVS-II Phase 2 (from Table 7.5) Versus Predicted Viscosity at 1150°C from the Fulcher Equation for Each Glass (from Table B.2) for the CVS-II Phase 3 Data

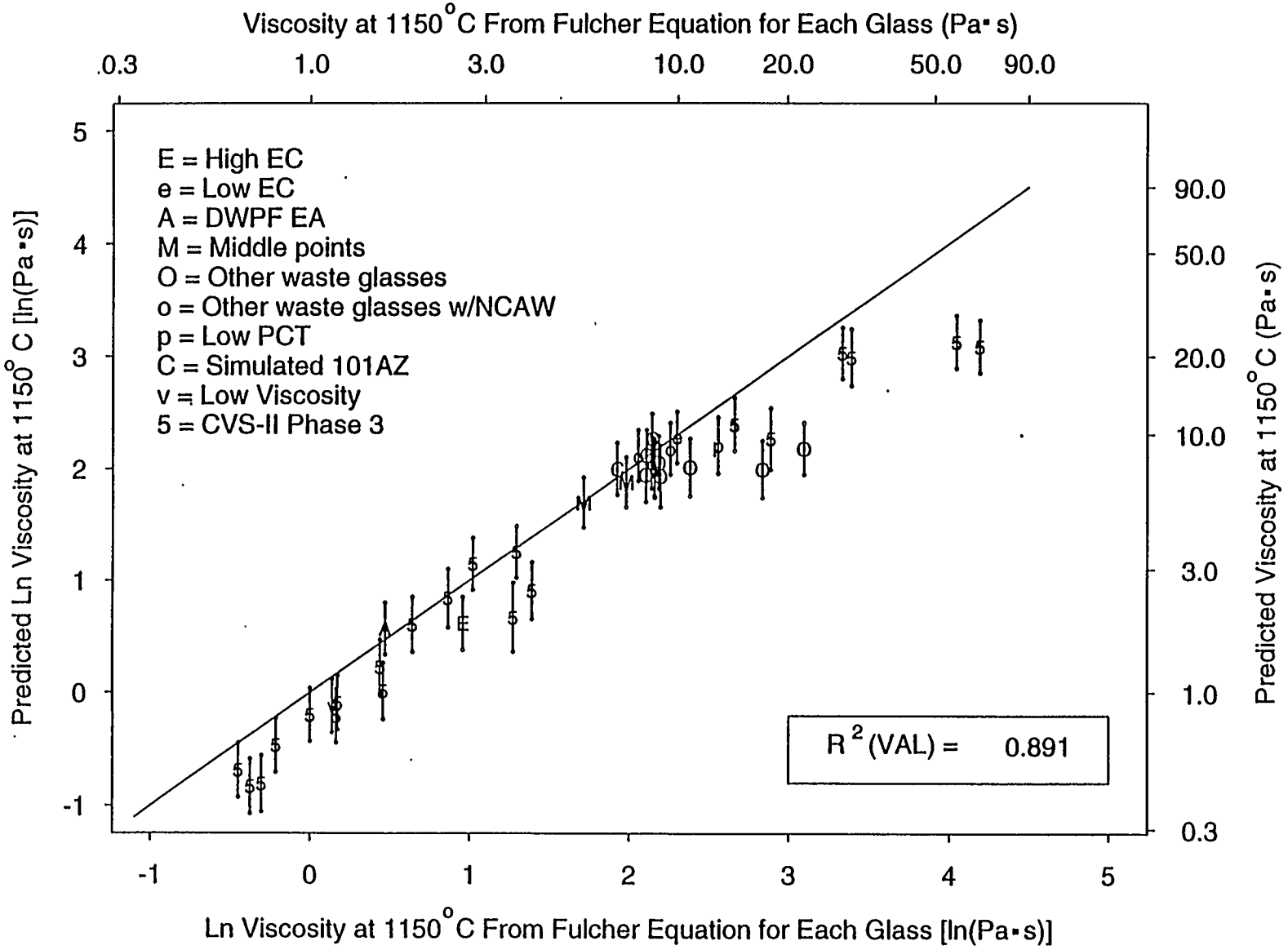

FIGURE 7.7c. Predicted Viscosity at 1150°C from the Second-Order Mixture Model #3 After CVS-II Phase 2 (from Table 7.5) Versus Predicted Viscosity at 1150°C from the Fulcher Equation for Each Glass (from Table B.2) for the CVS-II Phase 3 Data

45° line, the model is validated for that point, in the sense that no statistically significant difference exists between the predicted and "measured" values after accounting for their uncertainties. Various plotting symbols are used in Figures 7.6, 7.7a, 7.7b, and 7.7c to identify the specific nature of some of the CVS-II Phase 3 points. Points that are not otherwise specifically identified are plotted with a "5" as the plotting symbol.

Figure 7.6 shows that the first-order η_{1150} model is validated for nearly all of the CVS-II Phase 3 data points. Notable exceptions are two of the glasses with different Others mixes with plotting symbol "0" (CVS2-68 and CVS2-69), and two glasses on the right-hand side of the plot with plotting symbol "5" (CVS2-79 and CVS2-80). Problems were encountered in measuring the viscosity of these four glasses (see Appendix B), which also thus affected the fitted model in Table 7.5. These problems likely explain why there are differences between the predicted and measured values for these four glasses.

Figures 7.7a, 7.7b, and 7.7c show that the three candidate second-order models are not validated nearly as well as the first-order model for the CVS-II Phase 3 data, mainly because the second-order models have less uncertainty than the first-order model. Overlaying Figures 7.7a, 7.7b, and 7.7c on Figure 7.6 shows that the differences in predictions between the second-order models and the first-order model are small. The small differences are confirmed by the fact that the R^2(VAL) values (see Section 6.1.6) for the three second-order η_{1150} models are close to the R^2(VAL) value for the first-order η_{1150} model. These results suggest that the second-order models do not provide any better predictive performance than the first-order model, at least for the CVS-II Phase 3 data. It should be recalled that the CVS-II Phase 3 data is not an ideal validation data set, since it is not uniformly spread over the full CVS composition region. Part of the goal of CVS-II Phase 3 was to collect data for more extreme compositions and property values than had been obtained previously. The extreme nature of the CVS-II Phase 3 compositions is a potential reason why the second-order models did not predict any better than the first-order model for these data. However, the fact that the first-order model yielded R^2(VAL) = 0.907 in spite of these aspects of the CVS-II Phase 3 data indicates that it is a fairly good model.

7.5.2 Validation with Historical Database

The historical database gathered for purposes of validating CVS models is discussed in Appendix G. Although there were 680 glasses in the database, there were only 160 glasses for which viscosity at 1150°C could be obtained. For 138 of these glasses, measured viscosity values were available for either three or four temperatures (both above and below 1150°C, except in three cases) so that η_{1150} values were obtained as predictions (135 interpolations, 3 extrapolations) from Fulcher equations fitted for each glass. This general approach is how the η_{1150} values used to fit the models being validated were obtained, so it was the preferred approach for obtaining η_{1150} values for the historical data. This approach was not possible for the other 22 glasses, for which actual measurements at 1150°C (within ±3°C) were used. The η_{1150} values obtained for the 160 glasses ranged from approximately 1 to 400 Pa·s. By comparison, the 124 CVS-I and CVS-II Phase 1, 2, and 3 glasses had η_{1150} values ranging approximately from 0.4 to 84 Pa·s. The 160 historical database glass compositions (in the CVS 10-component form) and their viscosity at 1150°C values are given in Table G.3 of Appendix G.

Investigation of the 160 glass compositions for which η_{1150} values were obtained showed that only 44 of them were within slightly expanded versions of the lower and upper component bounds given in Table 4.2 (i.e., the region of compositions studied in CVS). (The slightly expanded composition region is defined in Table G.2 of Appendix G.) However, it was decided to proceed with validation using all 160 data points, and investigate whether the performance of the first- and second-order η_{1150} models from Table 7.5 depended on whether or not glass compositions were within the CVS region.

Figure 7.8 contains the plot of first-order model predicted versus "measured" η_{1150} values for all 160 data points. Figures 7.9a, 7.9b, and 7.9c contain similar plots for the three candidate second-order η_{1150} models. Error bars consisting of 95% prediction intervals on the predicted values are included in each plot. Figure 7.8 shows that the first-order model tends to underpredict η_{1150} values above 50 Pa·s, but that it does fairly well below that value. Figures 7.9a, 7.9b, and 7.9c show that the second-order models

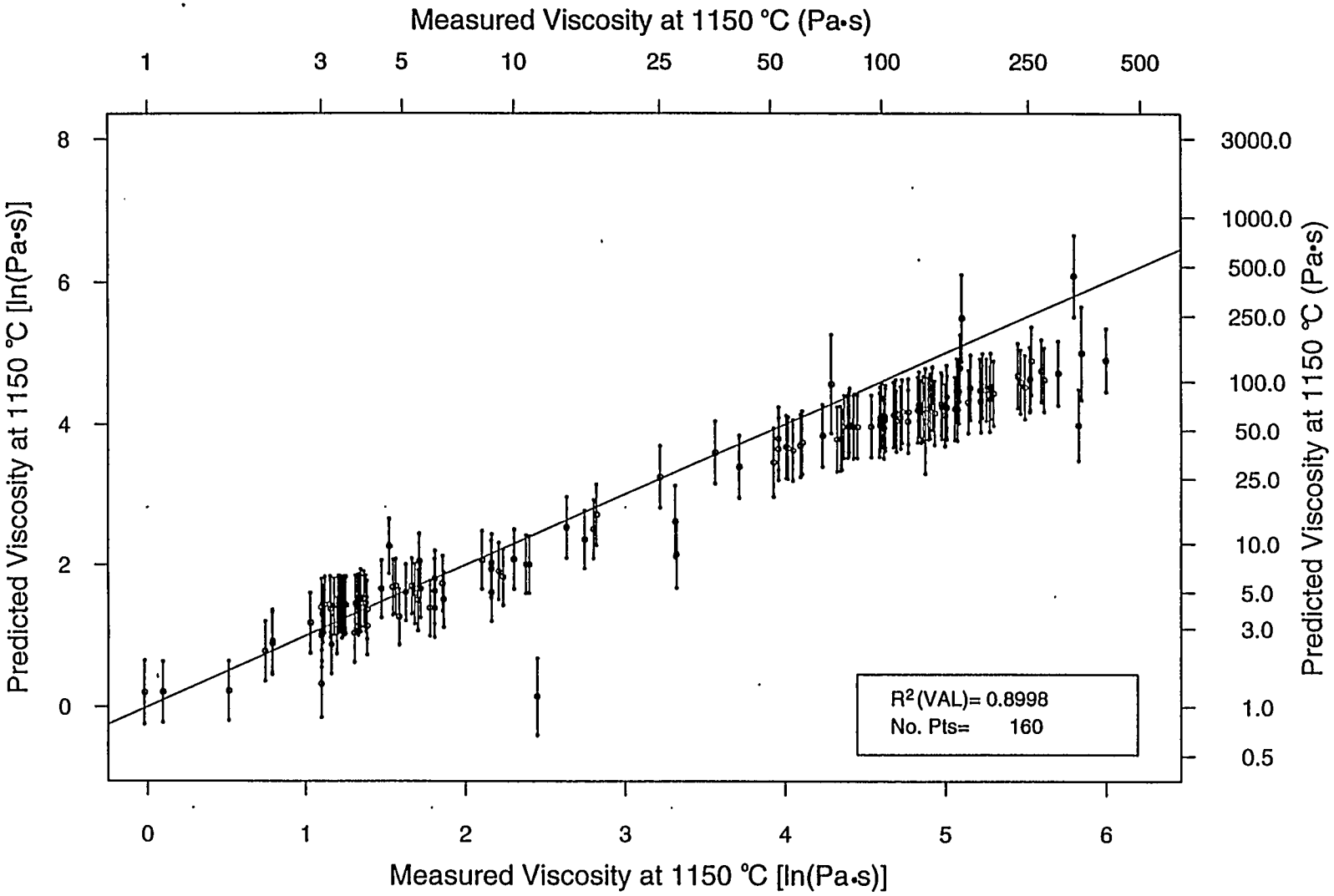

FIGURE 7.8. Predicted Viscosity at 1150°C from the First-Order Mixture Model After CVS-II Phase 2 (from Table 7.5) Versus "Measured" Viscosity at 1150°C for the Historical Data

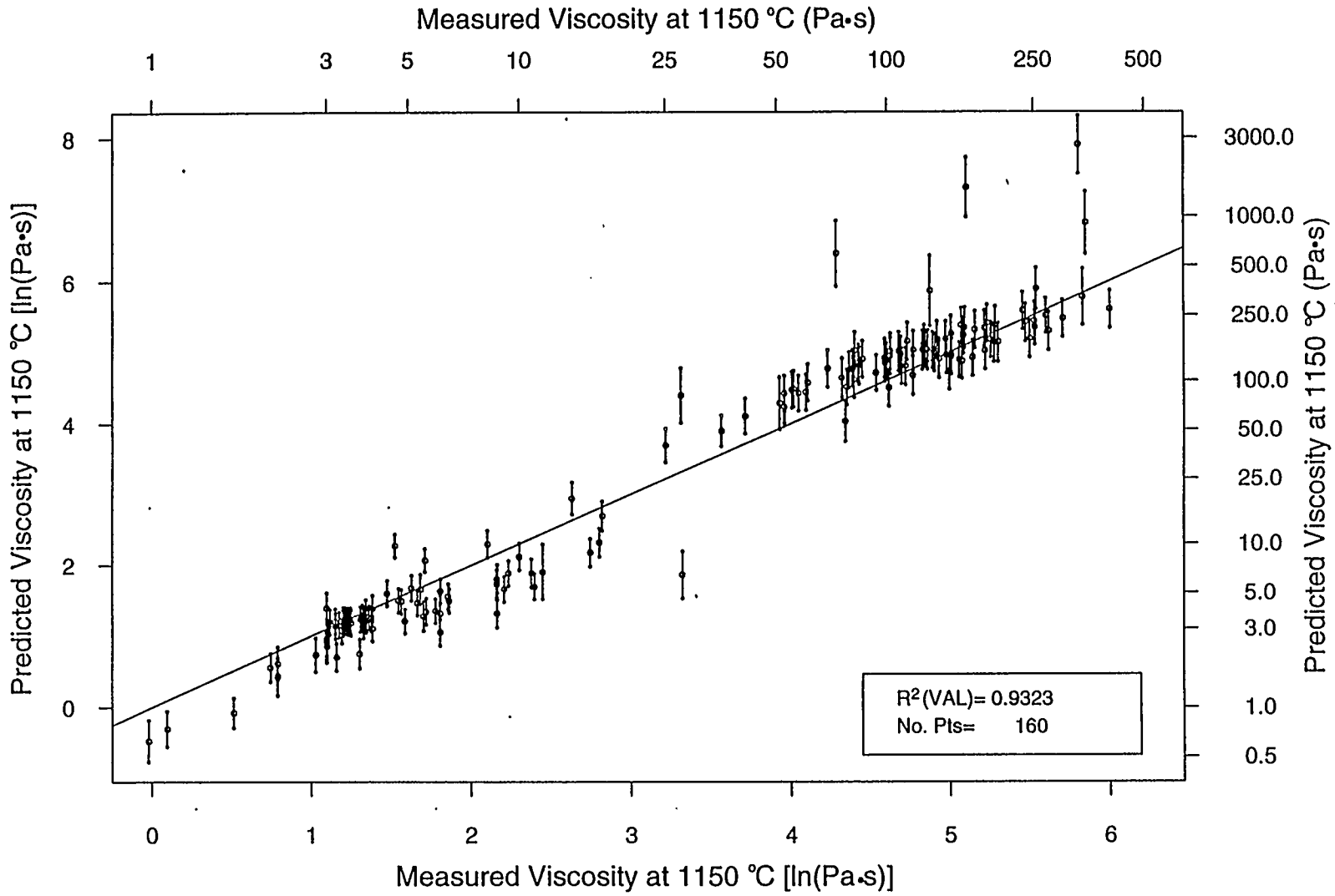

FIGURE 7.9a. Predicted Viscosity at 1150°C from the Second-Order Mixture Model #1 After CVS-II Phase 2 (from Table 7.5) Versus "Measured" Viscosity at 1150°C for the Historical Data

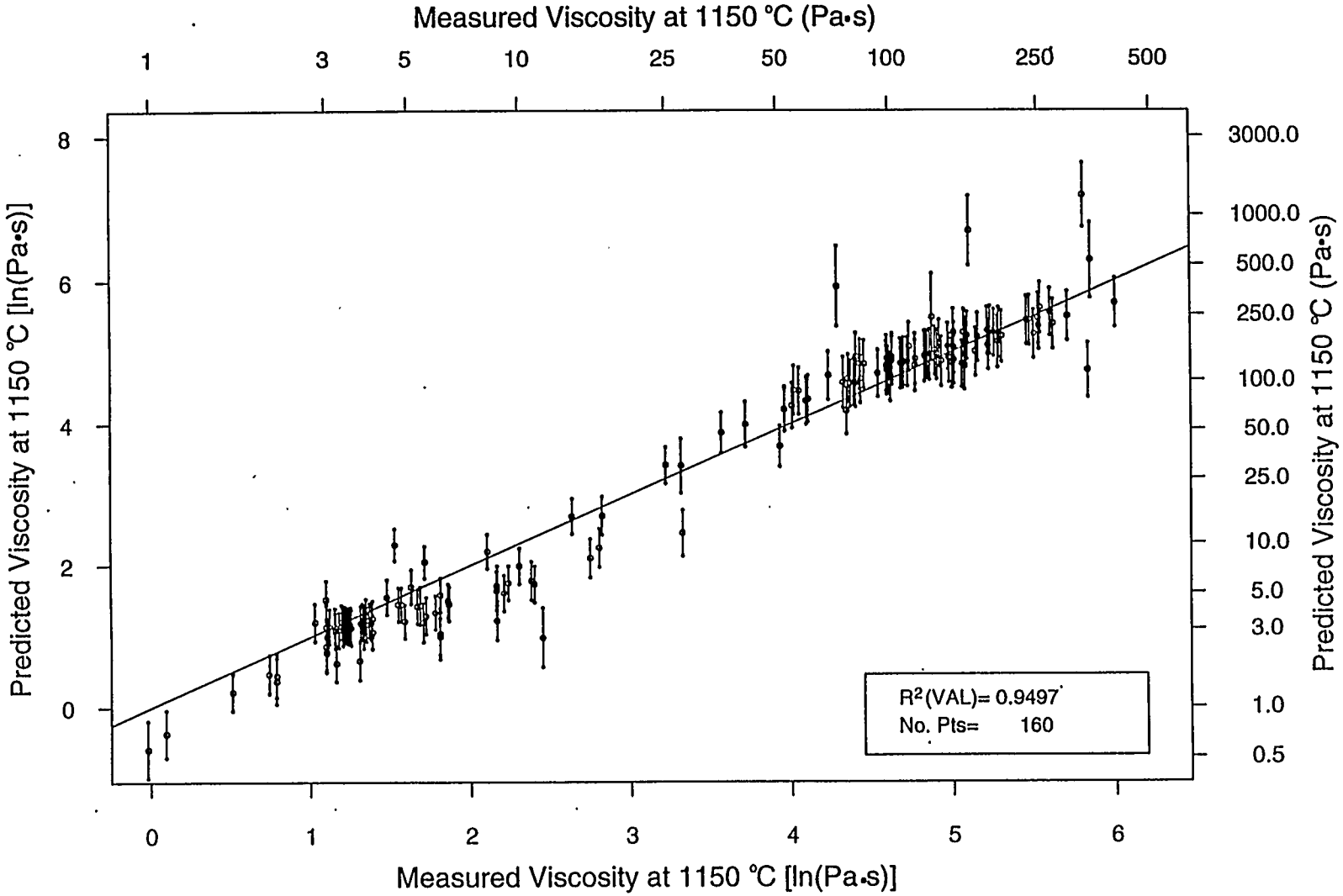

FIGURE 7.9b. Predicted Viscosity at 1150°C from the Second-Order Mixture Model #2 After CVS-II Phase 2 (from Table 7.5) Versus "Measured" Viscosity at 1150°C for the Historical Data

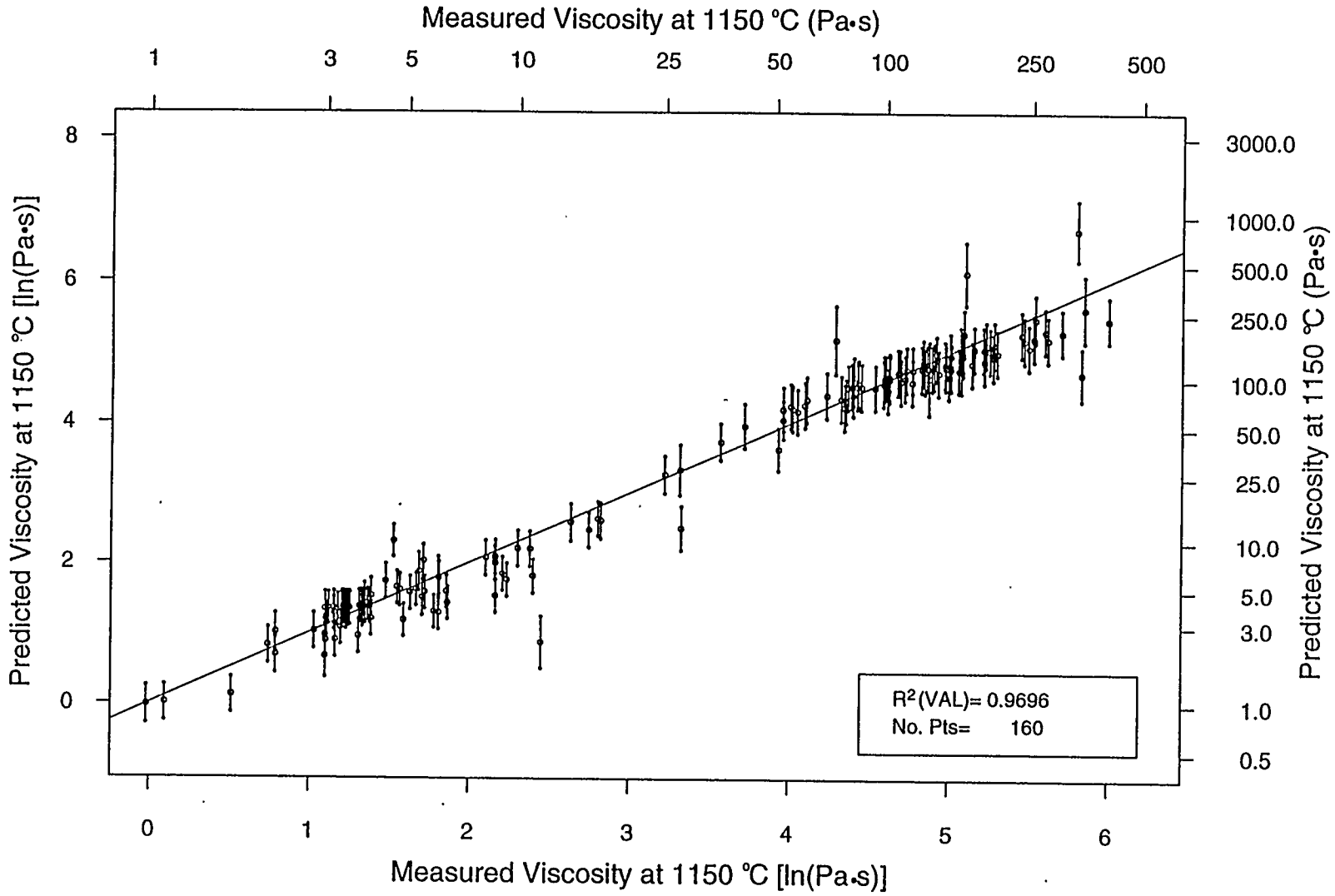

FIGURE 7.9c. Predicted Viscosity at 1150°C from the Second-Order Mixture Model #3 After CVS-II Phase 2 (from Table 7.5) Versus "Measured" Viscosity at 1150°C for the Historical Data

correct the tendency to underpredict η_{1150} values above 50 Pa·s. All three second-order models have $R^2(VAL)$ values larger than $R^2(VAL) = 0.8998$ for the first-order model, with second-order model #3 (the one with the fewest second-order terms) having the best value of $R^2(VAL) = 0.9696$. Overall, second-order model #3 appears to be the best second-order model, and avoids the biased prediction problems of the first-order model at higher η_{1150} values.

Figure 7.10 is a different version of Figure 7.9c, without the error bars, and with the number of single-component lower and upper bound constraints (out of 10, corresponding to the 10 CVS component) that are satisfied used as the plotting symbol for each glass. Figure 7.10 shows that many of the 160 data points only satisfy four to seven of the single-component constraints. Thus, the relatively good performance of the second-order model #3 is remarkable, given that it is being used to extrapolate outside the CVS region for many of these glasses.

7.5.3 Summary of Viscosity at 1150°C Model Validation

The validation work using the CVS-II Phase 3 and historical data sets focused on validating first- and second-order viscosity at 1150°C models developed from data up through CVS-II Phase 2 as presented in Table 7.5. Neither of these data sets were ideal validation data sets, because they do not evenly cover the CVS composition experimental region. However, both data sets indicated that either first-order models or second-order models with a few selected second-order terms provide quite good predictive performance, even beyond the composition region studied in CVS. Thus, the empirical mixture modeling approach appears to be adequate for predicting viscosity at 1150°C.

The first- and second-order viscosity at 1150°C models presented in Tables 7.4 and 7.5 of this report could be validated using the historical data, the CVS-II Phase 4 data, and any other data that subsequently becomes available. The models included in this report and the CVS-II Phase 4 data were not completed soon enough to enable validating them and reporting the results here.

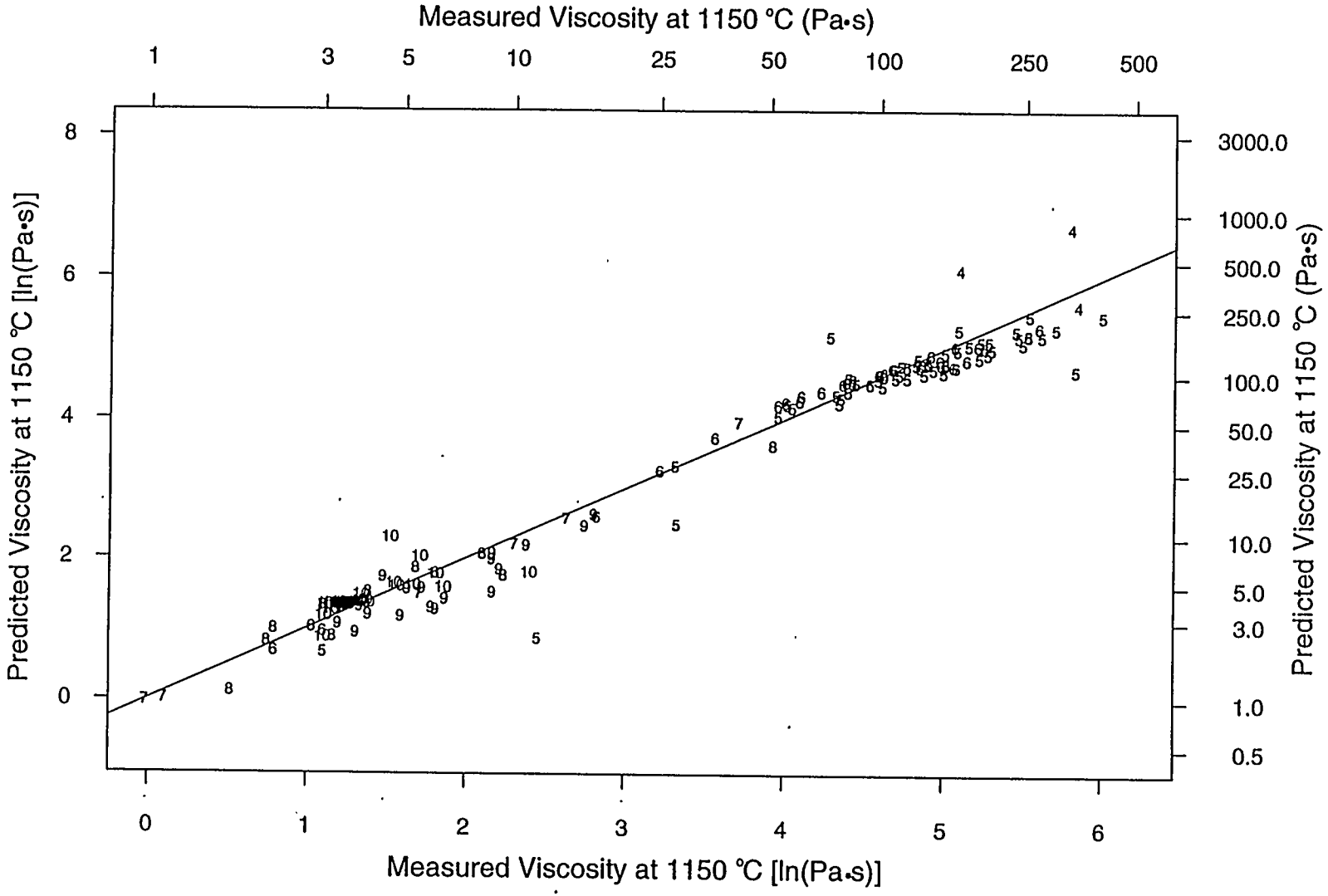

FIGURE 7.10. Predicted Viscosity at 1150°C from the Second-Order Mixture Model #3 After CVS-II Phase 2 (from Table 7.5) Versus "Measured" Viscosity at 1150°C for the Historical Data, with the Number of Relaxed Component Constraints Satisfied Used as the Plotting Symbol

7.6 OTHER MODEL FORMS INVESTIGATED

Two approaches for modeling viscosity proposed by other researchers are discussed and compared to CVS models in this section.

7.6.1 DWPF Approach

The viscosity model proposed for use in the Product Composition Control System (PCCS) of the Defense Waste Processing Facility (DWPF) from Jantzen and Brown (1993) is

$$\log_{10} \text{Viscosity} = -0.61 + [4472.45/T] - 1.534\ \text{NBO} \qquad (7.6)$$

where T is temperature in units of °C, viscosity is in units of poise, and

$$\text{NBO} = [2(K_2O+Cs_2O+Li_2O+Na_2O+Fe_2O_3-Al_2O_3)+B_2O_3]/SiO_2.$$

The glass oxide components, and thus NBO, are expressed in mole fractions. A simplified form of (7.6) for viscosity at 1150°C (η_{1150}) is

$$\log_{10}(\eta_{1150}) = 3.279 - 1.534\ \text{NBO}. \qquad (7.7)$$

Later this model is referred to as the "DWPF model with DWPF coefficients".

In order to evaluate the DWPF model in (7.7), the 124 CVS glass compositions from CVS-I and CVS-II Phases 1, 2, and 3 were converted from mass fraction to mole fraction compositions. Viscosity was not measured for two radioactive glasses studied in the CVS, but was measured by two different procedures for two other glasses. Hence, a total of 124 CVS composition and viscosity data points were used in the evaluations. The η_{1150} values were obtained from fitting a Fulcher equation to the viscosity at temperature data for each glass and predicting the viscosity at 1150°C. These η_{1150} values are contained in Table B.2[(a)], while the glass compositions (as-batched mass

---

(a) The η_{1150} values for CVS2-69, CVS2-79, and CVS2-80 in the main body of Table B.2 were used, not the ones in the corresponding footnotes.

fraction versions) are given in Table 4.15. Note that the CVS reports viscosity in Pa·s, whereas DWPF uses poise (10 poise = 1 Pa·s). Further, the CVS empirical mixture models for η_{1150} are based on $\log_e$ (ln) whereas the DWPF model is based on $\log_{10}$. These differences were accounted for in evaluating the performance of the DWPF model for CVS data.

The first evaluation of the DWPF modeling approach was simply to use (7.7) to predict $\log_{10}(\eta_{1150})$ values for all 124 CVS-I and CVS-II Phase 1, 2, and 3 data points. A plot of η_{1150} predicted values using the DWPF model with DWPF coefficients versus the CVS η_{1150} data values is given in Figure 7.11. The bulk of the data points (88 of 124) lie above the superimposed line of equality, which indicates that the DWPF model in (7.7) tends to overpredict viscosity at 1150°C for the CVS data. The R^2(VAL) value for the 124 data points was 0.697, confirming that the DWPF model with DWPF coefficients leaves considerable room for improvement in predicting CVS η_{1150} data values.

The second evaluation was to fit the DWPF model form to the CVS data. Figure 7.12 displays a plot of the CVS η_{1150} data versus the NBO constructed variable, with fitted lines corresponding to the DWPF model with DWPF coefficients and DWPF model with CVS coefficients superimposed. The DWPF model with CVS coefficients provides a slightly better fit (R^2 = 0.758), although considerable scatter is still present around the fitted line (especially at lower NBO values). Figure 7.13 contains a plot of η_{1150} values predicted by the DWPF model with CVS coefficients versus CVS η_{1150} data values. Figure 7.13 is analogous to Figure 7.11, except the DWPF model with CVS coefficients was used to calculate predicted η_{1150} values. Table 7.6 contains the DWPF and CVS coefficients for the DWPF viscosity at 1150°C model form as well as the corresponding R^2 values.

Table 7.7 compares the R^2 values for the two versions of the DWPF model (with DWPF and CVS coefficients) to the R^2 values for the empirical mixture models fitted to the CVS data given in Table 7.5. Both first- and second-order empirical mixture models perform much better for the CVS-I and CVS-II Phase 1, 2, and 3 data than either the DWPF model with DWPF coefficients or the DWPF model with CVS coefficients. Hence, the DWPF viscosity at 1150°C

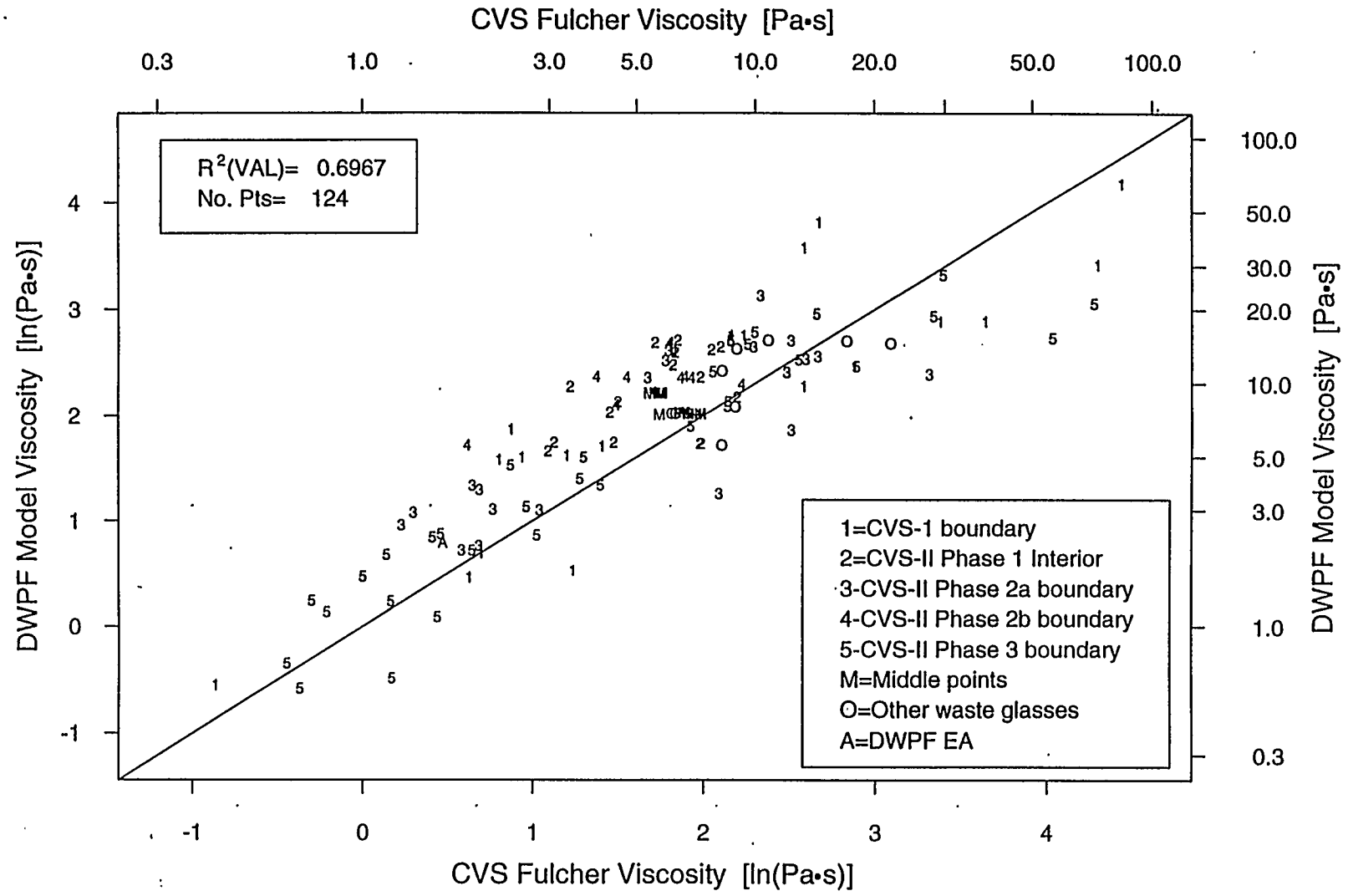

FIGURE 7.11. Predicted Viscosity at 1150°C Using DWPF Model with DWPF Coefficients Versus the CVS Viscosity at 1150°C Data Values from Table B.2 for CVS-I and CVS-II Phase 1, 2, and 3 Glasses

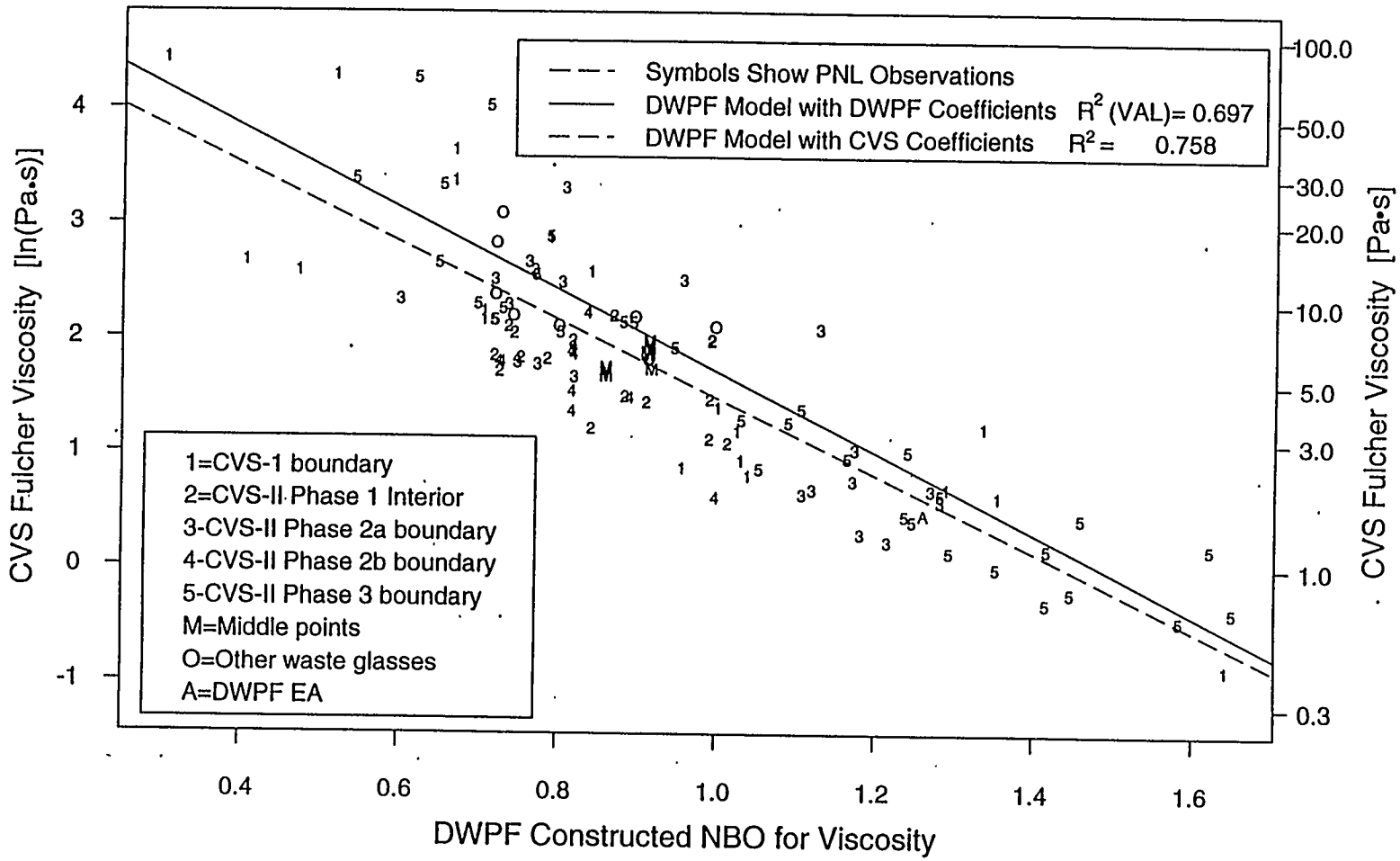

FIGURE 7.12. CVS Viscosity at 1150°C Data Values Versus DWPF NBO Variable for CVS-I and CVS-II Phase 1, 2, and 3 Glasses. DWPF models with DWPF and CVS coefficients are superimposed.

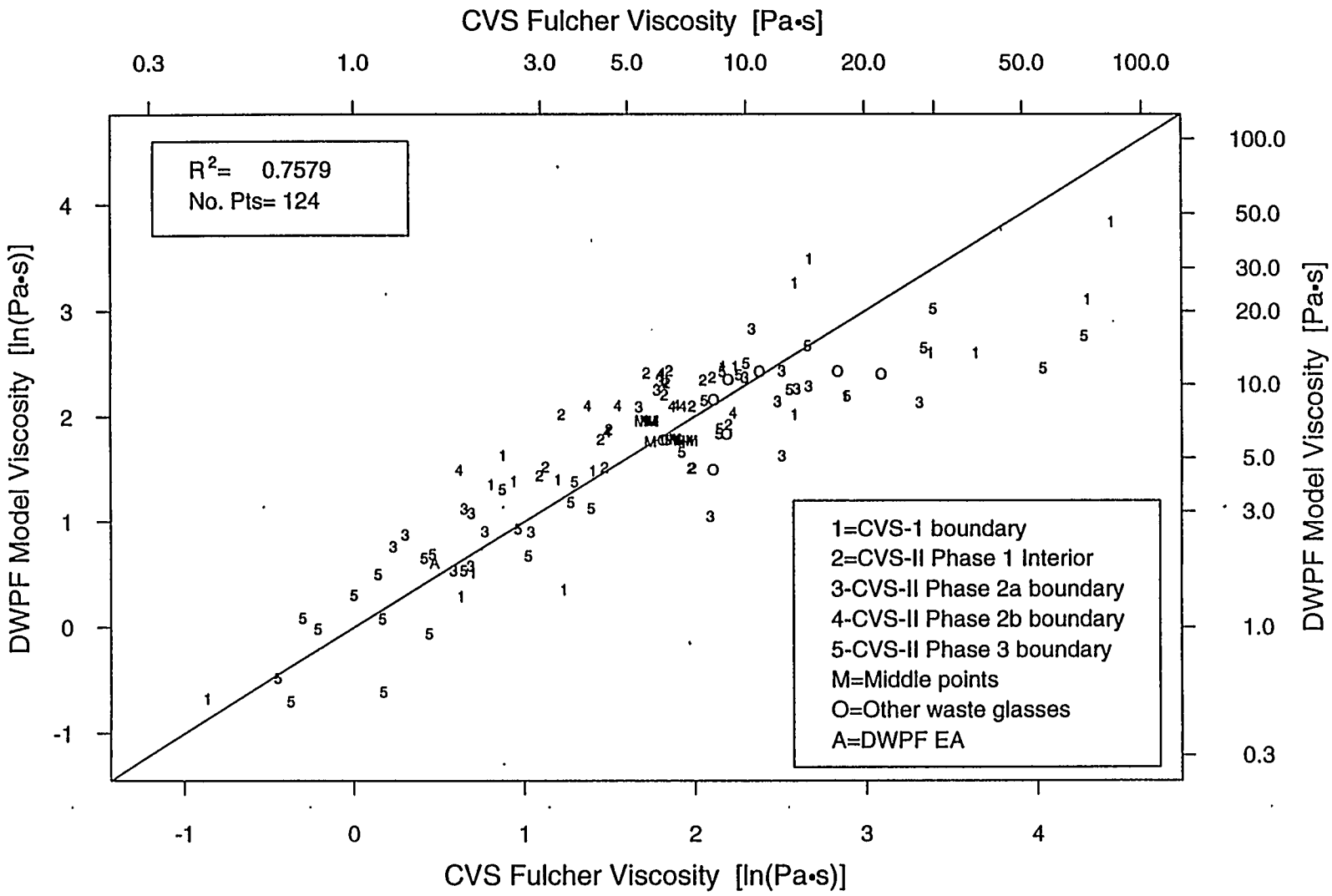

FIGURE 7.13. Predicted Viscosity at 1150°C Using the DWPF Model with CVS Coefficients Versus the CVS Viscosity at 1150°C Data Values for CVS-I and CVS-II Phase 1, 2, and 3 Glasses

TABLE 7.6. DWPF and CVS Coefficients for the DWPF Model Form $\log(\eta_{1150}) = a + b\ NBO$

Source of Model Coefficients	a	b	R^2 (a)
DWPF [ln(Pa·s)]	5.248	-3.532	0.697
CVS [ln(Pa·s)]	4.664	-3.249	0.758
DWPF [$\log_{10}$(poise)]	3.279	-1.534	0.697
CVS [$\log_{10}$(poise)]	3.025	-1.411	0.758

(a) The R^2 statistics are based on 124 data points from CVS-I and CVS-II Phases 1, 2, and 3.

TABLE 7.7. Comparison of R^2 Values for the DWPF Viscosity at 1150°C Models with DWPF and CVS Coefficients and for the CVS Viscosity at 1150°C Mixture Models from Table 7.5

Model	R^2
DWPF model form with DWPF coefficients	0.6966
DWPF model form with CVS coefficients	0.7579
CVS 1st-order mixture model (10 terms)	0.9391
CVS 2nd-order mixture model #1 (17 terms)	0.9746

model form, even when fitted to the CVS data, does not perform nearly as well for the CVS data as the empirical mixture models developed as part of the CVS.

7.6.2 Alfred University Approach

Another approach for modeling viscosity was included in an unpublished 1992 report, "Statistical Analysis of Viscosity Composition Data", submitted to the Savannah River Technical Center, by Dolun Oksoy of Alfred University. Based on this approach, a model for viscosity at 1150°C of the form

$$\ln(\eta_{1150}) = \sum_{i=1}^{9} b_i (x_i/SiO_2) + b_{10}(B_2O_3/SiO_2)^2 \qquad (7.8)$$

was investigated, where x_i is either the mass or mole fraction of the i-th oxide component (excluding SiO_2), b_i is the coefficient corresponding to the first-order term involving x_i/SiO_2, and b_{10} is the coefficient corresponding to the quadratic term $(B_2O_3/SiO_2)^2$.

Mass and mole fraction versions of model (7.8) were fitted to viscosity at 1150°C (Pa·s) values for 124 CVS-I and CVS-II Phases 1, 2, and 3 glasses. The model coefficients are given in Table 7.8. The predicted versus "measured" plots of η_{1150} for the mass and mole fraction versions of (7.8) are given in Figures 7.14a and 7.14b.

The R^2, R^2(ADJ), and R^2(PRESS) values for the mass and mole fraction versions of (7.8) are given in Table 7.9 along with the values for the mass and mole fraction versions of the first-order mixture model discussed earlier in Section 7.2. The predicted versus "measured" plots for the mass and mole fraction versions of (7.8) in Figures 7.14a and 7.14b may be compared to the corresponding first-order mixture model plots in Figures 7.3a and 7.3b. Comparison of these plots and the various R^2 values indicates that the model form (7.8) does not fit the CVS data any better than the first-order mixture model.

TABLE 7.8. Coefficients for Mass and Mole Fraction Versions of Alfred University "Ratio to SiO_2" Model for Viscosity at 1150°C

Variable	Mass Fractions	Mole Fractions
Intercept	5.5038	5.5050
B_2O_3/SiO_2	-6.2274	-7.1766
Na_2O_3/SiO_2	-6.1563	-6.3465
Li_2O/SiO_2	-17.4186	-8.6572
CaO/SiO_2	-4.5064	-4.2314
MgO/SiO_2	-2.3663	-1.6053
Fe_2O_3/SiO_2	-0.7201	-1.8795
Al_2O_3/SiO_2	4.6563	7.8988
ZrO_2/SiO_2	2.7749	5.6676
Others/SiO_2	-0.8348	-2.4617
$(B/SiO_2)^2$	4.8151	6.3704

TABLE 7.9. R^2 Values for the Alfred University "Ratio to SiO_2" Model and the CVS First-Order Mixture Model for Viscosity at 1150°C Using Mass and Mole Fractions

Model	Mass or Mole Fractions	R^2	R^2(ADJ)	R^2(PRESS)
Alfred Univ. "Ratio to SiO_2"	Mass	.9242	.9175	.9042
	Mole	.9247	.9418	.9047
First-Order Mixture	Mass	.9391	.9343	.9260
	Mole	.9447	.9404	.9324

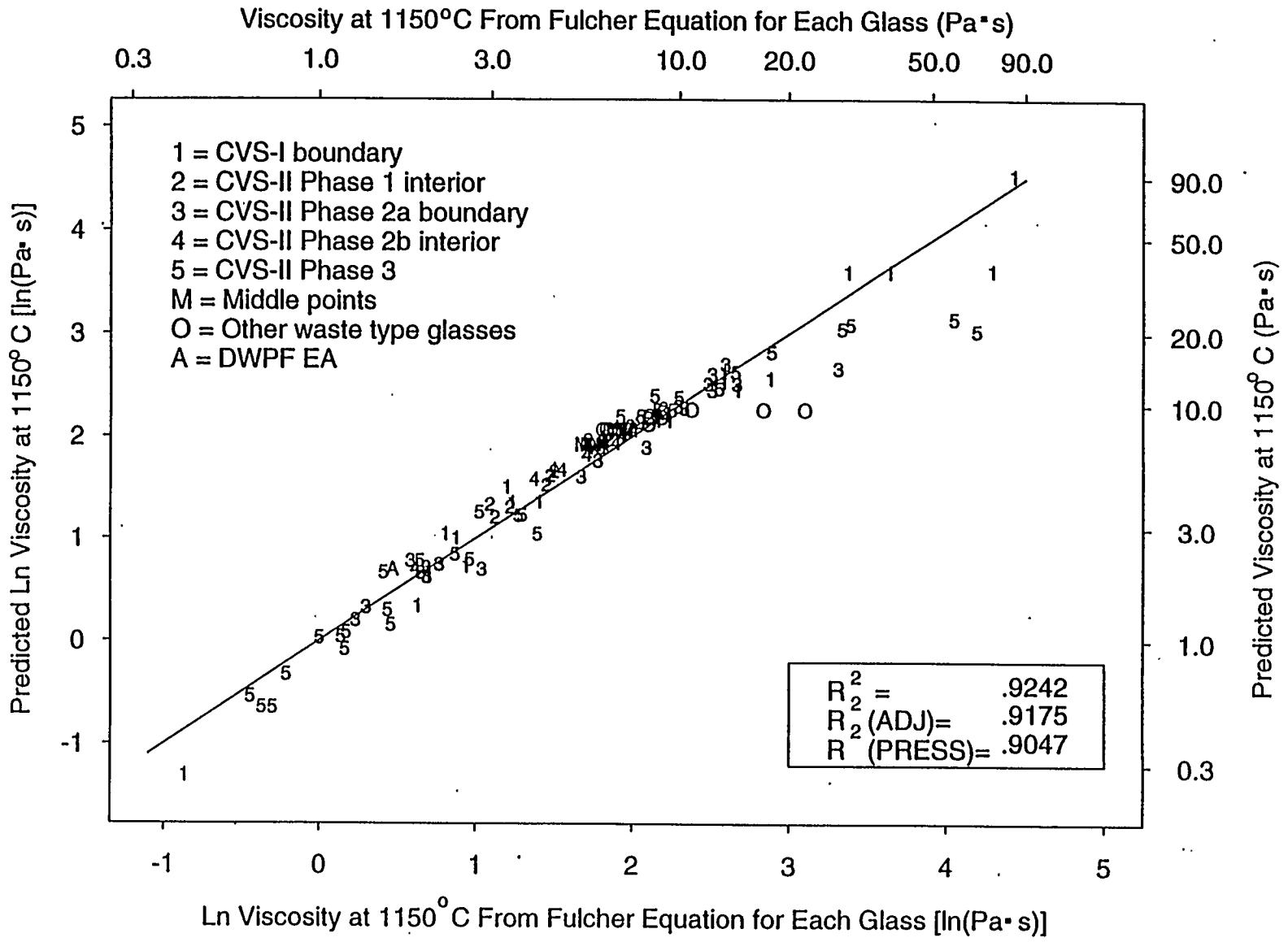

FIGURE 7.14a. Predicted Viscosity at 1150°C from the Mass Fraction Version of the Alfred University "Ratio to SiO_2" Model Versus Predicted Viscosity at 1150°C from the Fulcher Equation for Each Glass

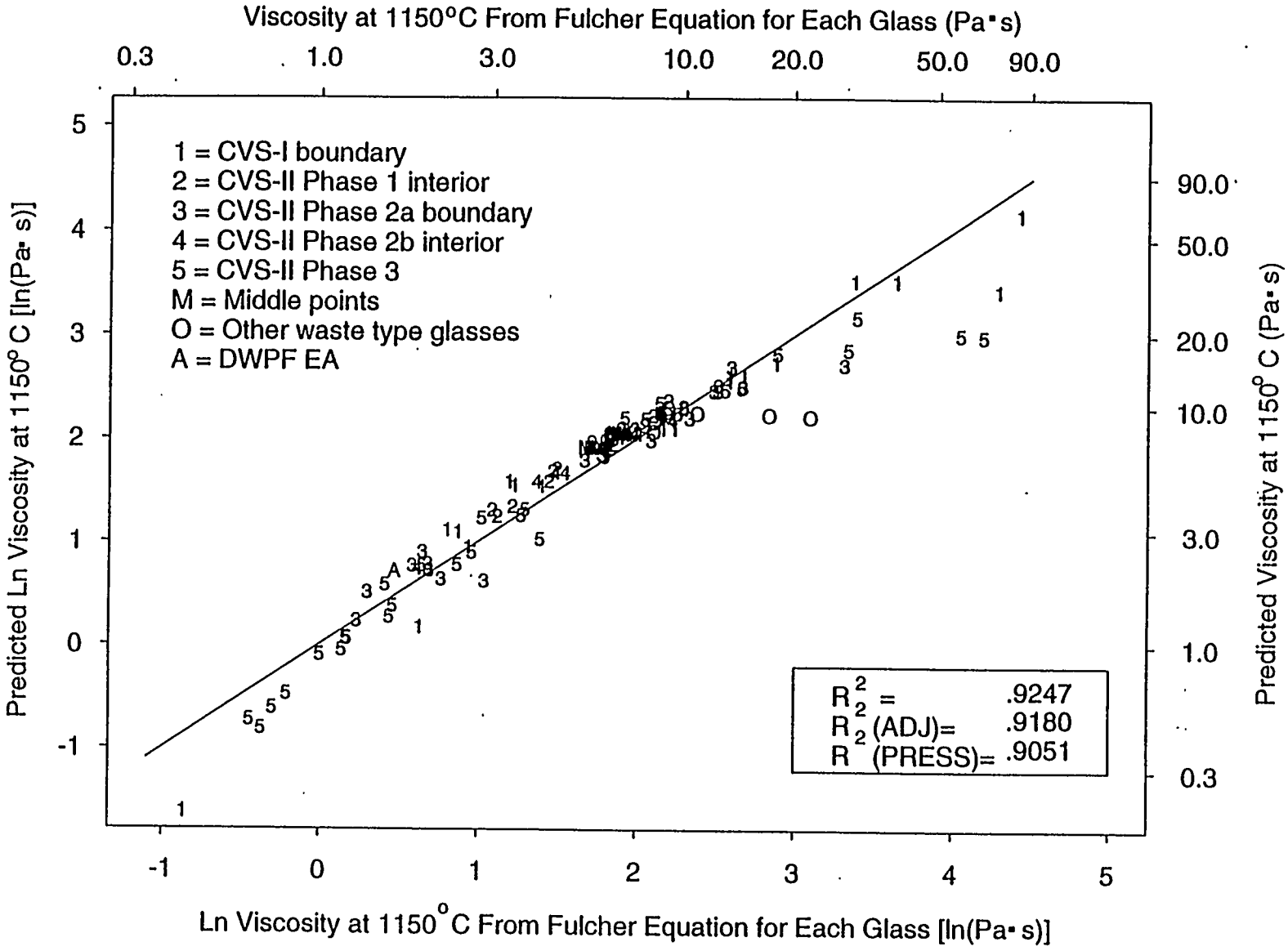

FIGURE 7.14b. Predicted Viscosity at 1150°C from the Mole Fraction Version of the Alfred University "Ratio to SiO_2" Model Versus Predicted Viscosity at 1150°C from the Fulcher Equation for Each Glass

7.7 VISCOSITY DISCUSSION

Viscosity data are fit to two equations in this chapter: (1) the Arrhenius equation $\ln \eta = A_A + B_A/T$ (Equation 7.2), and (2) the Fulcher equation $\ln \eta = A_F + B_F/(T-T_0)$ (Equation 7.1). The Fulcher equation differs from the Arrhenius equation by the coefficient T_0, which represents the temperature at which viscosity approaches infinity and thus glass theoretically becomes purely elastic. The Arrhenius equation assumes a linear relationship between ln viscosity and inverse temperature. The viscosity data for a simple glass are plotted in Figure 7.15 as a function of temperature. The nonlinearity of $\ln \eta$ versus 1/T shows that the Fulcher equation is more accurate than the Arrhenius equation even over the narrow temperature interval 950 to 1250°C. As the temperature interval increases, the estimation of viscosity by the Arrhenius equation becomes less accurate.

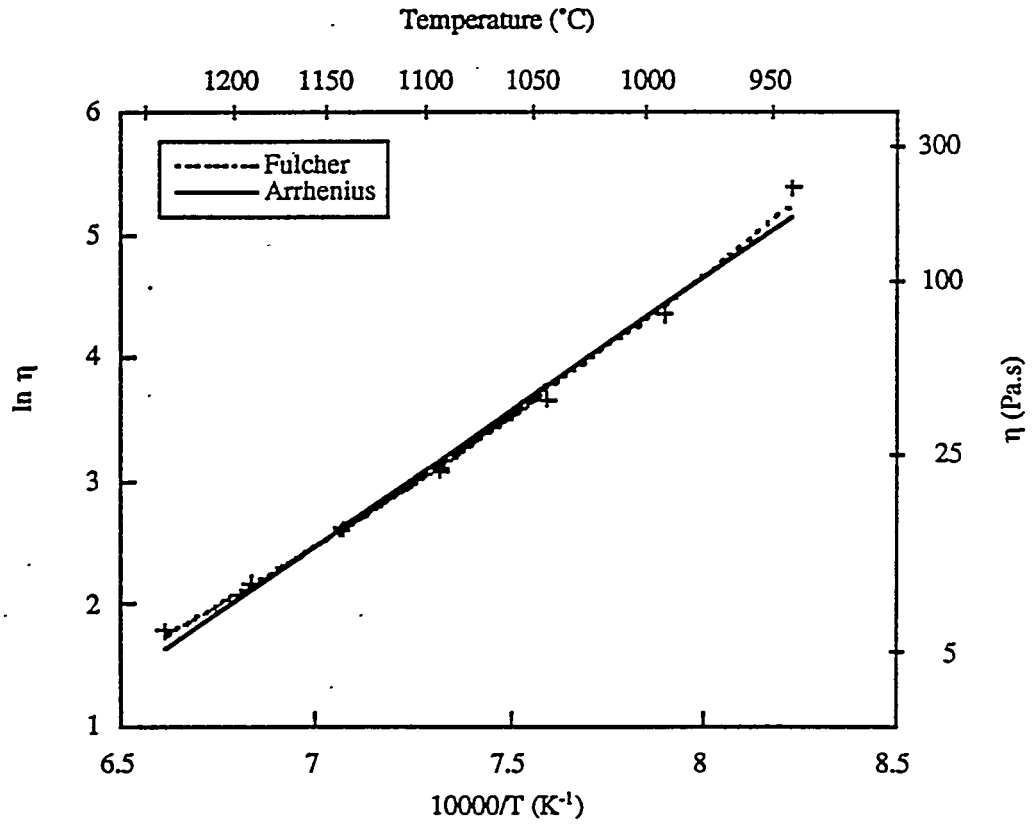

FIGURE 7.15. Viscosity of a Simple Glass (70 wt% SiO_2, 14 B_2O_3, 9 Na_2O, 5 Li_2O, 1 CaO, 1 MgO) over the Temperature Range from 950 to 1250°C

Hence, the Fulcher equation is more accurate for viscosity predictions over wide temperature intervals, while the Arrhenius equation is adequate over small temperature intervals. However, the Arrhenius equation is easier to fit because it is linear in its coefficients (requiring single-step linear least squares), whereas the Fulcher is more difficult to fit because it is nonlinear in its coefficients (requiring iterative nonlinear least squares).

The accuracy of the T_0 coefficient in the Fulcher equation can be negatively affected when the data used to fit the equation is in a narrow temperature interval far from the T_0 value. For most CVS glasses the T_0 values are in the 200 to 400°C range, whereas CVS viscosity data are in the 950 to 1250°C range. The difference in these temperature ranges means the T_0 values estimated in fitted Fulcher equations are large extrapolations of the data, and hence may not be very accurate. The accuracy of T_0 prediction, and hence low-temperature viscosity prediction, can be substantially improved by including T_g (in the 400 to 500°C range for CVS glasses) as an additional low-temperature data point to fit the Fulcher equation. Moynihan (1993) has shown that glass viscosity is $10^{11.3 \pm 0.4}$ Pa.s at T_g for many inorganic glasses of varied composition. Table 7.1 shows the coefficients for the Fulcher first-order mixture model (Equation 7.1) fit using measured CVS viscosity data along with the T_g data point for each CVS glass (from CVS-I and CVS-II Phases 1, 2, and 3). The relationship between T_0 and T_g is further discussed in Section 9.5.

Fulcher parameters (A_F, B_F, and T_0) were also fit to measured viscosity data (without the addition of the T_g data point) for individual glasses and are listed in Table B.2. Figure 7.16 compares T_0 coefficients obtained using T_g (from Table 7.1a) with those fit without T_g (from Table B.2). The extension of viscosity data to T_g has reduced the range in T_0 for CVS glasses from $0 < T_0 < 700$°C in Table B.2 to $100 < T_0 < 400$°C for T_0 calculated using Table 7.1a.[(a)] Figure 7.17 shows a comparison of viscosity curves using the

---

(a) The difference in T_0 ranges could also be due to differences between the bases for the two tables. Table B.2 values are based on separate Fulcher equations fitted to the data for each glass. Table 7.1a values are based on the assumption that the Fulcher coefficients (A_F, B_F, and T_0) dependence on composition is adequately represented by a first-order mixture model.

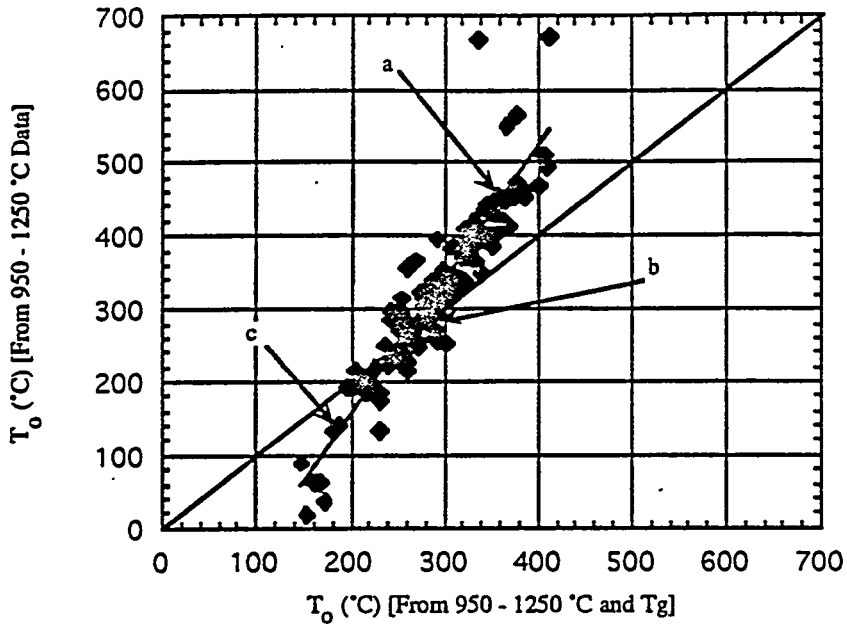

FIGURE 7.16. T_0 Coefficients for Each CVS Glass from Fulcher Equations Fitted With and Without T_g Data. Points a, b, and c are further examined in Figure 7.17.

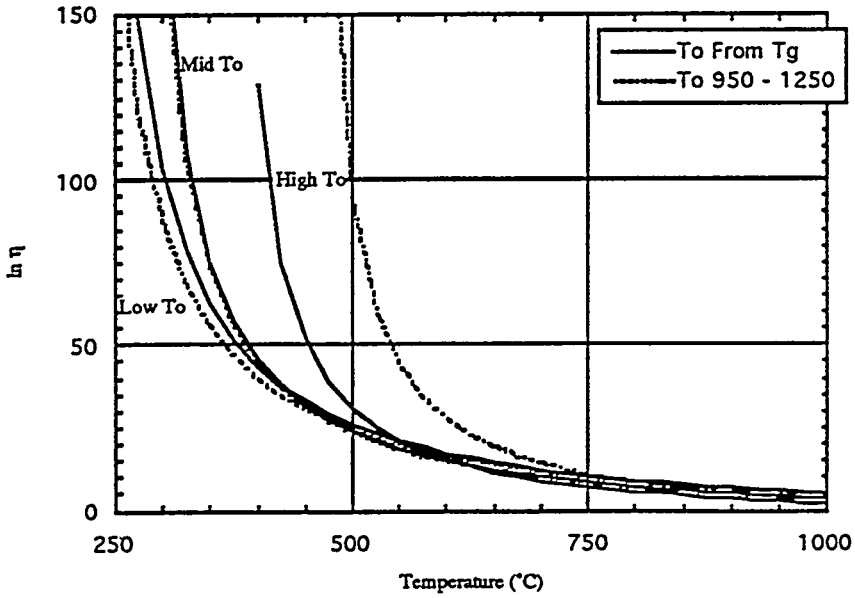

FIGURE 7.17. Viscosity Predictions from Fulcher Equations Fitted With and Without T_g Data for Glasses with Varying Differences in Fulcher T_0 Coefficients (a, b, and c in Figure 7.16)

two Fulcher fits. It can be seen that for glasses with high and low T_0 values, the viscosity curves from the two Fulcher fits differ more dramatically than for those with mid-range T_0 values. Figure 7.17 illustrates how the accuracy and precision of estimated T_0 values can be affected if extrapolated from a Fulcher equation fitted to viscosity data at higher temperatures (950 to 1250°C in CVS).

First-order mixture model coefficients corresponding to the A and B parameters of the Arrhenius-mixture model, and the A, B, and T_0 parameters of the Fulcher-mixture model fitted with T_g data (Table 7.1a), are displayed in Table 7.10. Also displayed in Table 7.10 are the coefficients of separate first-order mixture models fitted to the estimated A, B, and T_0 parameters for each glass given in Table B.2 of Appendix B.

The B coefficients (B_A and B_F for Arrhenius and Fulcher models) are related to activation energy for viscous flow in glass (E). Activation energy is defined as the first derivative of ln η with respect to inverse temperature. For the Arrhenius equation, activation energy is given by:

$$E = \frac{\partial(\ln \eta)}{\partial(1/T)} = B_A \tag{7.9}$$

For the Fulcher equation, activation energy is given by:

$$E = \frac{\partial(\ln \eta)}{\partial(1/T)} = \frac{B_F}{\left(1 - \frac{T_0}{T}\right)^2} \tag{7.10}$$

The glass length is a traditional expression for the working temperature range. Glasses that change viscosity only mildly with temperature are called "long" because they have a long working range. A glass blower could handle such a glass for a longer time compared to "short" glasses with a rapid change of viscosity with temperature. The glass length can be expressed by B_A in the working viscosity range ($10^3 \leq \eta \leq 10^{6.65}$ Pa·s). The value of E (the slope of the ln η versus inverse temperature curve) can be easily calculated at any temperature using (7.10). The effects of components on glass length are

TABLE 7.10. Component Coefficients from First-Order Mass Fraction Mixture Models for Several Viscosity Related Values

	SiO_2	B_2O_3	Na_2O	Li_2O	CaO	MgO	Fe_2O_3	Al_2O_3	ZrO_2	Others
Arrhenius A	-11.08	-13.65	-9.60	-4.51	-22.75	-21.10	-6.40	-4.08	-31.32	-17.01
Arrhenius B (K)	28539	10868	-1217	-42288	21522	25767	8774	21186	54574	23027
Fulcher A with T_g	-10.59	-24.41	2.02	5.45	3.95	5.30	-13.63	1.50	-0.35	-2.38
Fulcher B with T_g (K)	19236	15923	-12965	-39177	-18671	-11944	14559	9524	4618	1710
Fulcher To with T_g (°C)	76	263	425	474	1065	752	43	178	540	271
Fulcher A without T_g	-4.98	-2.46	-3.50	-9.06	-3.96	-15.82	-5.96	-6.31	-14.69	-7.60
Fulcher B without T_g (K)	11650	-9650	-6264	-8213	-8515	10232	4179	21899	22077	3618
Fulcher To without T_g (°C)	215	1110	661	-598	1163	280	383	-482	168	441

available only for the temperature range of measured viscosity (950 to 1250°C) because the Arrhenius model was only fitted using this data. For the temperature range of 950 to 1250°C, the relative effects of the components on E are roughly indicated by the first-order model coefficients for B_A in Table 7.10 (see Section 6.3). The alkali oxides (Li_2O and Na_2O) decrease the activation energy and hence lengthen the glass. The components with the strongest potential to shorten glass are SiO_2 and ZrO_2. All other components have little effect on glass length.

Considering the Fulcher model, at low temperatures (as T approaches T_0) E is dominated by the $(1 - T_0/T)^2$ term in (7.10). Hence, components which strongly affect T_0 also strongly affect the length of glass at low temperatures. Table 7.10 shows that alkaline earth oxides (CaO and MgO) will strongly decrease glass length at low temperatures because of their relatively large T_0 coefficients and large negative B_F coefficients. Table 7.10 also shows that SiO_2 will increase glass length.

8.0 ELECTRICAL CONDUCTIVITY RESULTS AND DISCUSSION

Electrical conductivity was measured at three to five temperatures for each glass as discussed in Section 5.3. The resulting data are given in Tables C.1 and C.2 of Appendix C, and estimates of uncertainty in the data based on replicate glasses are given in Appendix F. Overcheck electrical conductivity measurements of the CVS internal standard glass (close to HW-39-4 composition) by Corning Engineering Laboratory Services (CELS) yielded results that were in agreement with the CVS results (see Section 13.3.1).

The results of fitting the Arrhenius equation to the data for each glass are given in Table C.3 of Appendix C. Values of electrical conductivity at 1150°C (ϵ_{1150}) estimated from these Arrhenius fits ranged from 6.87 to 94.09 S/m. This range can be compared to the initial CVS acceptable electrical conductivity range of 18 to 50 S/m, and the subsequent revised acceptable range of 10 to 100 S/m (see Section 3.2). Of the 122 CVS-I and CVS-II Phase 1, 2, and 3 glasses for which electrical conductivity was measured, 17 had ϵ_{1150} less than 18 S/m, while 22 had ϵ_{1150} greater than 50 S/m. Glasses with more extreme values of ϵ_{1150} were designed into the CVS study to provide a basis for developing models valid over a wider property range so that accurate predictions within the acceptable range can be made.

Models expressing electrical conductivity as a function of composition and temperature are discussed in Section 8.1. First-order mixture models for electrical conductivity at 1150°C and corresponding component effects plots are presented in Section 8.2. The question of whether the electrical conductivity data contains any biases due to being collected in four phases (CVS-I and CVS-II Phases 1, 2, and 3) is addressed in Section 8.3. Second-order mixture models for electrical conductivity at 1150°C are presented in Section 8.4. Model validation results are discussed in Section 8.5, while other model forms that were investigated are discussed in Section 8.6. A discussion of the results is presented in Section 8.7.

8.1 ELECTRICAL CONDUCTIVITY MODELS AS FUNCTIONS OF COMPOSITION AND TEMPERATURE

Electrical conductivity at temperature data were modeled as a simultaneous function of temperature and composition by expressing the two Arrhenius equation coefficients as first-order mixture models:

$$\ln \epsilon = \sum_{i=1}^{10} A_i x_i + \sum_{i=1}^{10} B_i x_i / T. \qquad (8.1)$$

where temperature (T) is in Kelvin. Results of fitting this model to the electrical conductivity at temperature data of Tables C.1 and C.2 are given in Table 8.1a for mass fractions and Table 8.1b for mole fractions. The various R^2 values are approximately the same for the mass and mole fraction models. Note that most of the estimated coefficients are statistically different from zero, indicating that the models probably do not greatly overfit the data.

Figures 8.1a and 8.1b show the predicted versus measured electrical conductivity values for the combined Arrhenius first-order mixture model using mass fractions and mole fractions, respectively. Although these plots show the models fit the data fairly well, it was determined that they do not fit as well as separate Arrhenius equations for each glass. This fact indicates that the first-order mixture model expansion of the Arrhenius equation coefficients may not adequately account for composition effects, and that second-order terms may be beneficial. However, including second-order terms was not attempted because of the large number of terms in such models and the difficulties in removing unneeded terms from them.

8.2 FIRST-ORDER MODELS AND COMPONENT EFFECTS FOR ELECTRICAL CONDUCTIVITY AT 1150°C

Note that Equation (8.1) is linear in the coefficients, so that it is possible to factor it into the form:

$$\ln \epsilon = \sum_{i=1}^{10} (A_i + B_i/T) x_i. \qquad (8.2)$$

TABLE 8.1a. Fitted Electrical Conductivity Model in Which the Arrhenius Equation Coefficients A and B are Expressed as First-Order Mixture Models in the Mass Fractions of the Oxide Components

Linear Least Squares Summary Statistics[a]

Source	Degrees of Freedom (DF)	Sum of Squares	Mean Square	F Value[b]	Prob>F[c]
Model	19	270.57531	14.24081	557.677	0.0001
Error	462	11.79760	0.02554		
C Total	481	282.37292			

Root Mean Square Error	0.15980	R^2	= 0.9582
Mean of Viscosity	3.14785	R^2(ADJ)	= 0.9565
Coefficient of Variation	5.07647	R^2(PRESS)	= 0.9523

Parameter Estimates

Variable	DF	Parameter Estimate	Standard Error	T-test for Parameter=0 t-value	T-test for Parameter=0 Prob > |T|[d]
SiO2	1	8.12	0.85	9.58	0.0001
B2O3	1	12.82	1.58	8.09	0.0001
Na2O	1	6.05	1.87	3.24	0.0013
Li2O	1	7.47	3.68	2.03	0.0428
CaO	1	14.41	2.85	5.06	0.0001
MgO	1	10.39	3.15	3.30	0.0010
Fe2O3	1	9.94	2.25	4.41	0.0001
Al2O3	1	7.14	2.11	3.38	0.0008
ZrO2	1	7.93	2.55	3.11	0.0020
OTHERS	1	18.11	2.83	6.40	0.0001
SiO2/T	1	-10283.00	1146.15	-8.97	0.0001
B2O3/T	1	-15135.00	2138.82	-7.08	0.0001
Na2O/T	1	7089.48	2536.80	2.80	0.0054
Li2O/T	1	22484.00	5013.28	4.49	0.0001
CaO/T	1	-18769.00	3846.40	-4.88	0.0001
MgO/T	1	-13414.00	4250.43	-3.16	0.0017
Fe2O3/T	1	-10608.00	3059.21	-3.47	0.0006
Al2O3/T	1	-8227.18	2862.25	-2.87	0.0042
ZrO2/T	1	-9723.86	3463.42	-2.81	0.0052
OTHERS/T	1	-20653.00	3840.34	-5.38	0.0001

(a) This table was adapted from the SAS (1990) regression procedure (REG) output. The data for CVS2-81 were not used, since they were determined to be severe outliers.

(b) F Value = Mean Square for Model / Mean Square for Error, the statistic for testing whether a significant portion of variation in the electrical conductivity data is accounted for by the model.

(c) Probability that the model does not account for a significant portion of the variability in the data.

(d) Probability that the coefficient is significantly different than zero.

TABLE 8.1b. Fitted Electrical Conductivity Model in Which the Arrhenius Equation Coefficients A and B are Expressed as First-Order Mixture Models in the Mole Fractions of the Oxide Components

Linear Least Squares Summary Statistics[a]

Source	Degrees of Freedom (DF)	Sum of Squares	Mean Square	F Value[b]	Prob>F[c]
Model	19	271.52509	14.29079	608.633	0.0001
Error	462	10.84783	0.02348		
C Total	481	282.37292			

Root Mean Square Error	0.15323	R^2	= 0.9616
Mean of Viscosity	3.14785	R^2(ADJ)	= 0.9600
Coefficient of Variation	4.86784	R^2(PRESS)	= 0.9559

Parameter Estimates

Variable	DF	Parameter Estimate	Standard Error	T-test for Parameter=0 t-value	T-test for Parameter=0 Prob > |T|[d]
SiO2	1	8.41	0.78	10.91	0.0001
B2O3	1	12.96	1.64	7.88	0.0001
Na2O	1	5.82	1.75	3.34	0.0009
Li2O	1	7.77	1.63	4.76	0.0001
CaO	1	13.82	2.37	5.84	0.0001
MgO	1	9.97	1.93	5.17	0.0001
Fe2O3	1	10.87	5.40	2.01	0.0446
Al2O3	1	6.26	3.27	1.91	0.0564
ZrO2	1	7.31	4.76	1.54	0.1252
OTHERS	1	32.06	7.07	4.53	0.0001
SiO2/T	1	-10470.00	1043.45	-10.03	0.0001
B2O3/T	1	-15483.00	2223.54	-6.96	0.0001
Na2O/T	1	7157.78	2366.18	3.03	0.0026
Li2O/T	1	6863.36	2224.27	3.09	0.0022
CaO/T	1	-17621.00	3195.66	-5.51	0.0001
MgO/T	1	-11589.00	2608.41	-4.44	0.0001
Fe2O3/T	1	-13527.00	7331.81	-1.85	0.0657
Al2O3/T	1	-8646.92	4433.56	-1.95	0.0517
ZrO2/T	1	-11830.00	6458.29	-1.83	0.0676
OTHERS/T	1	-39574.00	9594.68	-4.13	0.0001

(a) This table was adapted from the SAS (1990) regression procedure (REG) output. The data for CVS2-81 were not used, since they were determined to be severe outliers.

(b) F Value = Mean Square for Model / Mean Square for Error, the statistic for testing whether a significant portion of variation in the electrical conductivity data is accounted for by the model.

(c) Probability that the model does not account for a significant portion of the variability in the data.

(d) Probability that the coefficient is significantly different than zero.

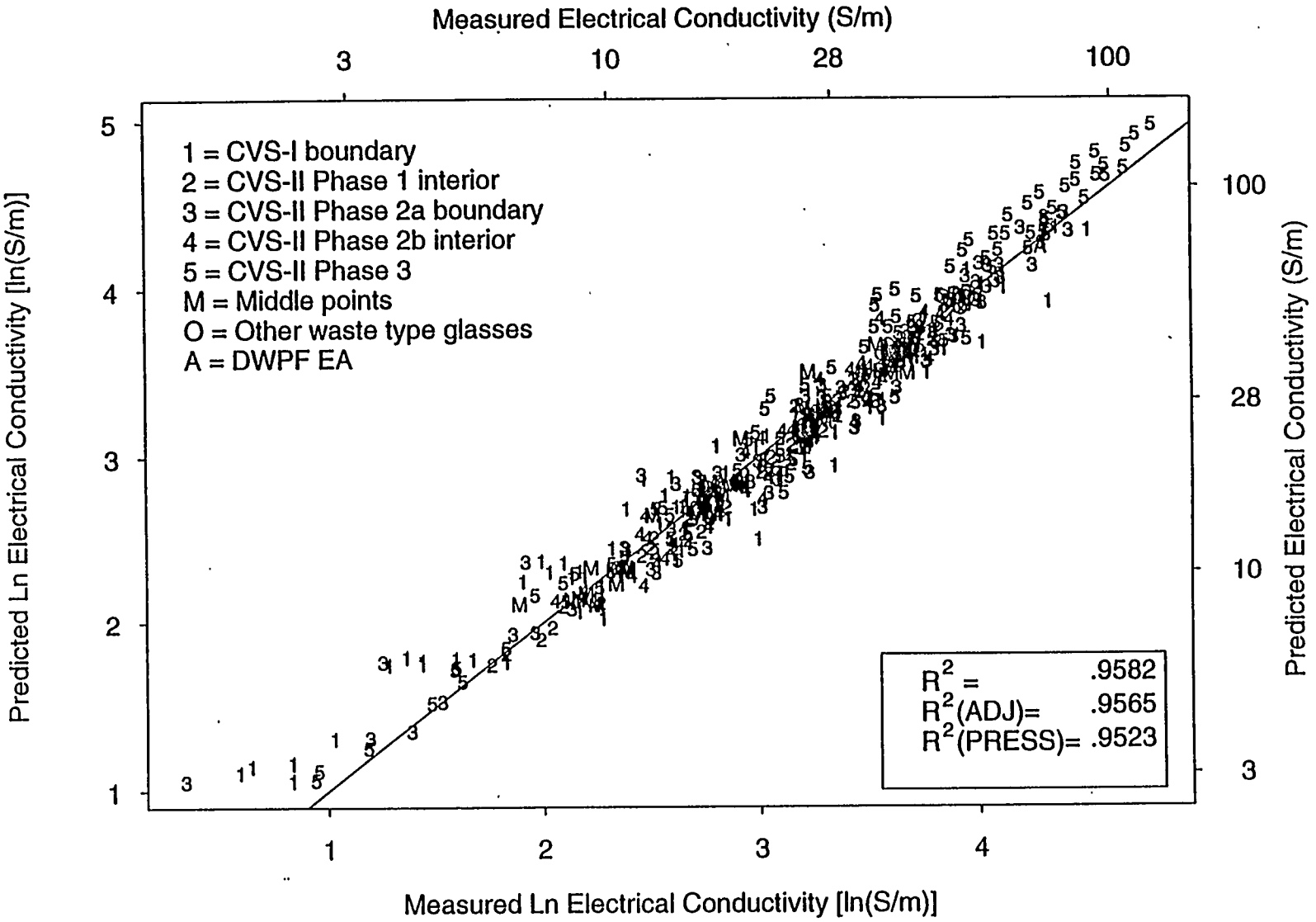

FIGURE 8.1a. Predicted Versus Measured Electrical Conductivity at Temperature Values for the Combined Arrhenius First-Order Mixture Model in the Mass Fractions of the Component Oxides (from Table 8.1a)

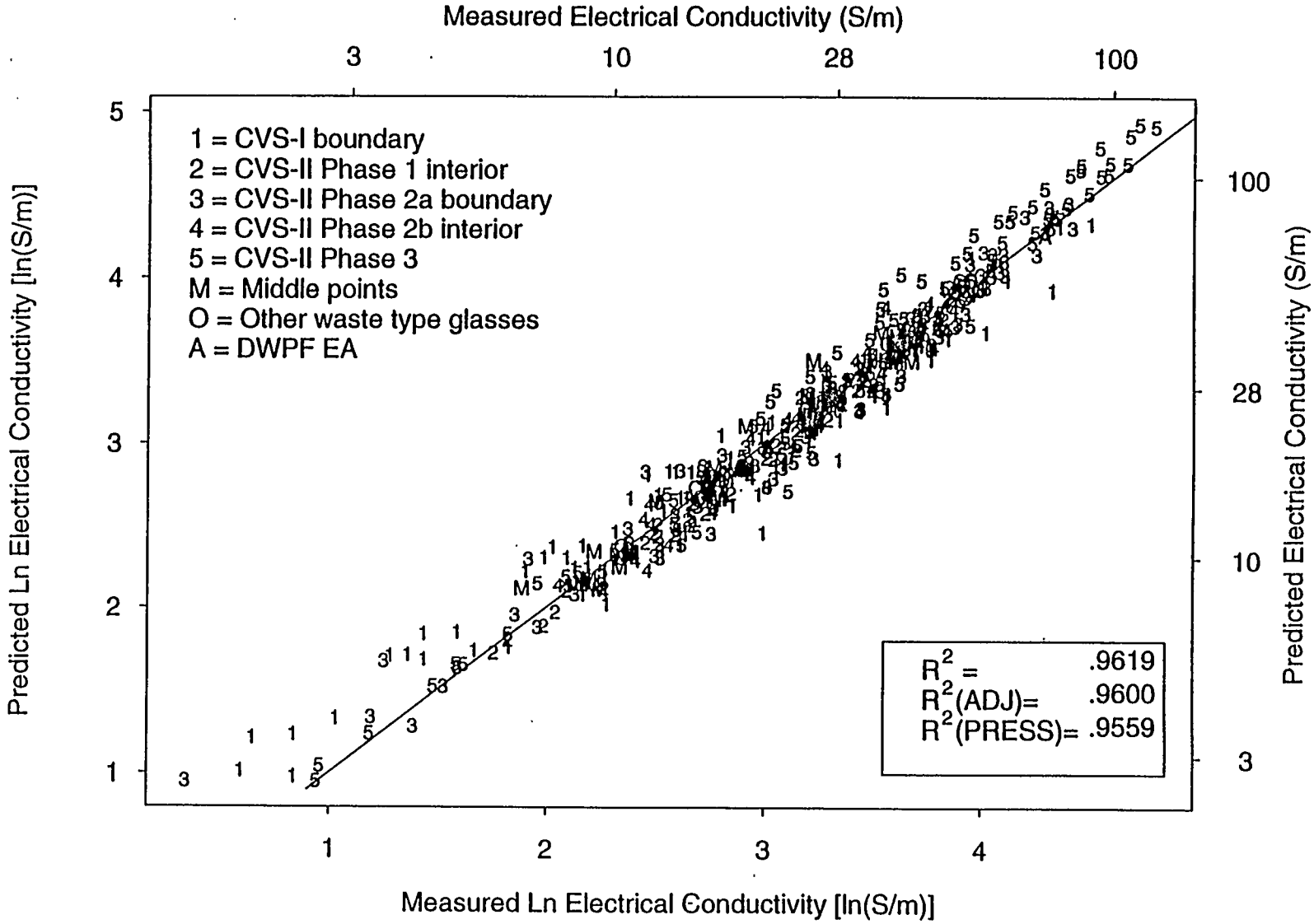

FIGURE 8.1b. Predicted Versus Measured Electrical Conductivity at Temperature Values for the Combined Arrhenius First-Order Mixture Model in the Mole Fractions of the Component Oxides (from Table 8.1b)

Then

$$\ln \epsilon_{1150} = \sum_{i=1}^{10} (A_i + B_i/1423) x_i. \qquad (8.3)$$

provides a ϵ_{1150} prediction equation that has the form of a first-order mixture model. It is also possible to use the ϵ_{1150} values estimated from the individual Arrhenius equation fits (from Table C.3 and also listed in Table 8.3) as the dependent variable in a first-order mixture model:

$$\ln \epsilon_{1150} = \sum_{i=1}^{10} b_i x_i. \qquad (8.4)$$

Previous results indicated there was a slight advantage to the Equation (8.4) approach for predicting ϵ_{1150}, so only those results are presented and discussed here.

The estimated coefficients from Equation (8.4) for mass and mole fractions of the oxide components are given in Table 8.2. The R^2 values in Table 8.2 indicate both models fit the data well, with a slight advantage to the mole fraction model. Figures 8.2a and 8.2b display the predicted ϵ_{1150} values versus the "measured" ϵ_{1150} values (from Table C.3 in Appendix C) for the first-order mixture models in mass and mole fractions from Table 8.2. These plots indicate that both models do a reasonably good job of fitting the data without biases within the 9 to 60 S/m range. Both the mass and mole fraction models show some tendency to overpredict ϵ_{1150} values below 9 S/m and above 60 S/m.

Although both models fit the data reasonably well, they have statistically significant LOFs with greater than 96% confidence. The LOFs may be due to the first-order mixture model form being inadequate (e.g., components may have nonlinear or interactive effects), or to underestimation of the experimental variation in ϵ_{1150} values used in performing the LOF tests. Predicted ϵ_{1150} values (from the Arrhenius equations fit to each glass) corresponding to replicates were used to estimate the experimental variation in ϵ_{1150}. Because such values are from a fitted curve, they may yield an underestimate of the actual experimental variation in ϵ_{1150}.

TABLE 8.2. Coefficients and Goodness-of-Fit Statistics for First-Order Mixture Models Fitted to Natural Logarithm of Electrical Conductivity at 1150°C Using Mass and Mole Fractions of the Oxide Components

	Mass Fractions	Mole Fractions
SiO_2	0.8471	0.9960
B_2O_3	2.2518	2.1530
Na_2O	11.0396	10.8435
Li_2O	23.5355	12.6937
CaO	1.4129	1.5996
MgO	1.0565	2.9739
Fe_2O_3	2.5863	1.7783
Al_2O_3	1.3108	0.1700
ZrO_2	1.1224	-0.8667
Others	3.4531	3.9422
# points[a]	120	120
R^2[b]	0.9314	0.9352
R^2(ADJ)[b]	0.9258	0.9299
R^2(PRESS)[b]	0.9100	0.9143
LOF?[c]	Yes (97.1%)[d]	Yes (96.4%)[d]

(a) Both models were fitted using the 120 electrical conductivity at 1150°C values given in Table C.3 of Appendix C. A total of 124 glasses are listed in Table C.3, but electrical conductivity was not measured for radioactive glasses CVS2-53 and CVS2-54, and the value for CVS2-81 was determined to be an outlier and thus was not used. The data point for CVS2-101 was not available at the time these models were developed, so it was not used.

(b) R^2, R^2(ADJ), and R^2(PRESS) statistics take values between 0.0 and 1.0, and provide different measures of the proportion of variation in the property data accounted for by a fitted model. See Section 6.1.5 for the definitions of these statistics.

(c) A statistical F-test for lack-of-fit (LOF) was performed using the estimates of experimental variation obtained from replicate tests. "Yes" and "No" entries indicate whether the LOF was statistically significant at a 90% confidence level. The actual confidence level at which a LOF can be declared significant is given in parentheses following the "Yes" or "No" for each model.

(d) LOF test used the pooled transformed property SD estimate in Table F.4.

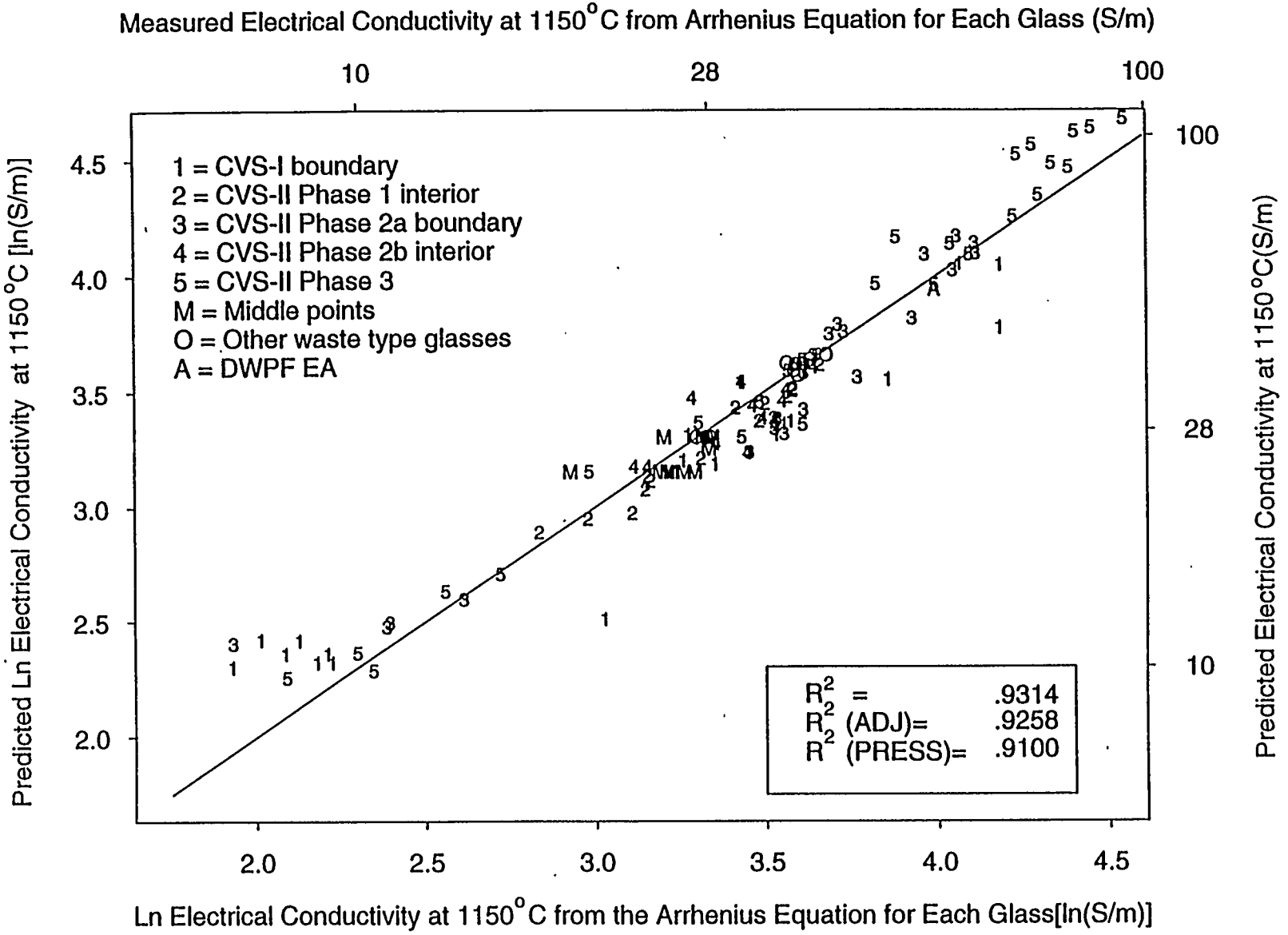

FIGURE 8.2a. Predicted Electrical Conductivity at 1150°C from the First-Order Mixture Model Using Mass Fractions (from Column 2 of Table 8.2) Versus Predicted Electrical Conductivity at 1150°C from the Arrhenius Equation for Each Glass (from Table C.3)

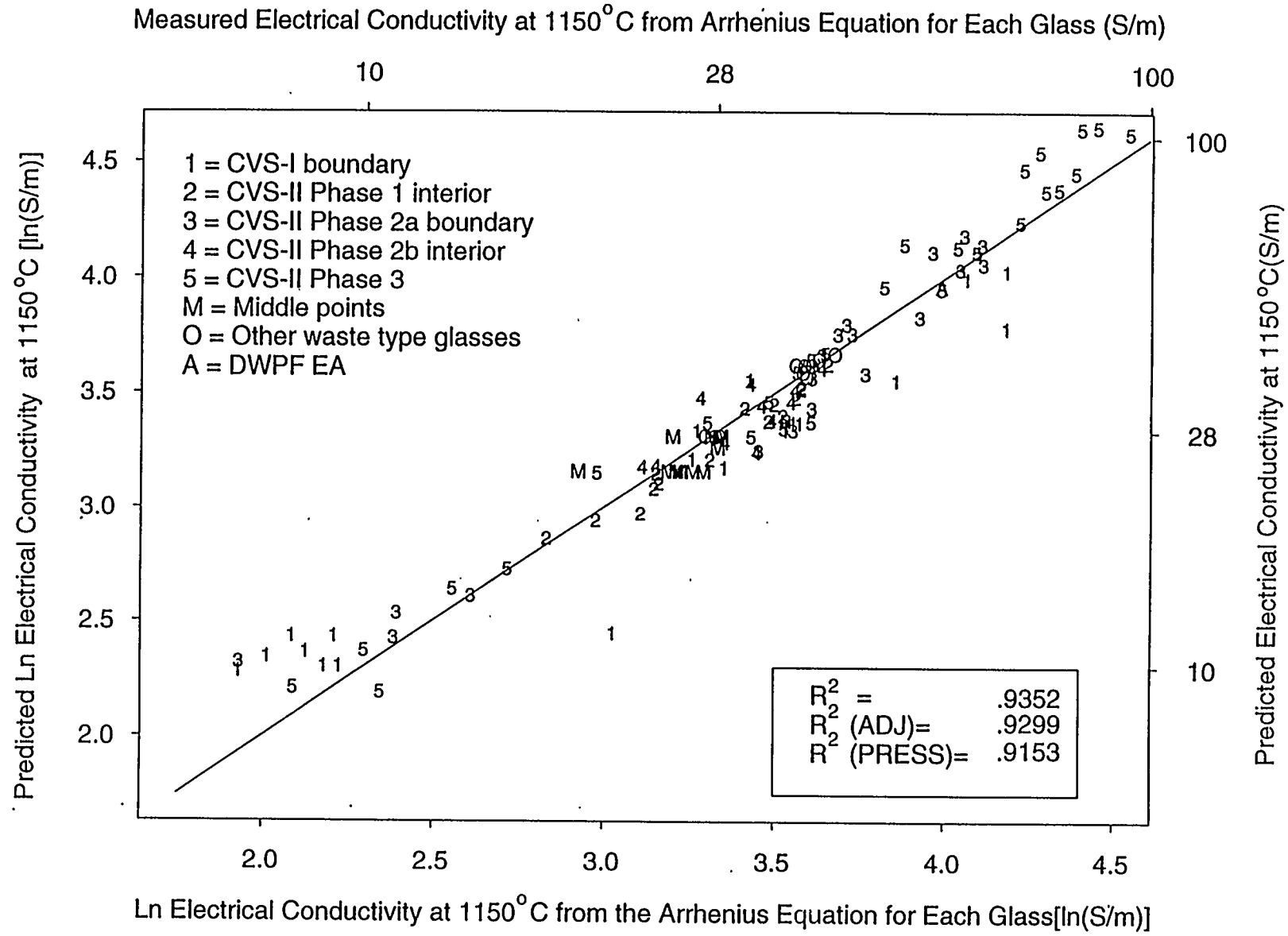

FIGURE 8.2b. Predicted Electrical Conductivity at 1150°C from the First-Order Mixture Model Using Mole Fractions (from Column 2 of Table 8.2) Versus Predicted Electrical Conductivity at 1150°C from the Arrhenius Equation for Each Glass (from Table C.3)

Estimating the experimental variability from measured electrical conductivity at temperature data could be investigated as an alternative, although this may slightly over-estimate the actual experimental variation due to temperature fluctuations around the nominal temperatures at which measurements were made.

The first-order mixture model using mass fractions given in Table 8.2 was used to produce a component effects plot (see Section 6.3) for ϵ_{1150}, which is displayed in Figure 8.3. Only the single-component constraints and not the stand-in crystallinity constraints in Tables 4.2 and 4.6 were used to limit the effects plot (both were used in previous effects plots). As a result, effects are evaluated over wider ranges than in the past for several components involved in the stand-in constraints (most notably Al_2O_3 and SiO_2). The effects plot illustrates that electrical conductivity at 1150°C of the HW-39-4 glass (used as the reference point in the plots) is predicted to be increased most by the two alkali oxide components (in order) Li_2O and Na_2O. Electrical conductivity at 1150°C is predicted to be reduced by SiO_2. The effects of the other components are mild or negligible. The effects plots and conclusions are quite similar to those from the CVS-I report (Piepel, Hrma, et al. 1993) and after previous phases of CVS-II.

8.3 INVESTIGATION OF POTENTIAL BIASES IN ELECTRICAL CONDUCTIVITY AT 1150°C DATA DUE TO CVS PHASES

As discussed in Section 6.1.1, a model of the form (6.3) was fitted to the ϵ_{1150} data for CVS-I and CVS-II Phases 1, 2, and 3 to ascertain whether any biases (block effects) were present in the ϵ_{1150} data due to performing the CVS in phases. The mass fraction version of (6.3) yielded $R^2 = 0.9363$, which can be compared to $R^2 = 0.9314$ for the first-order mass fraction model (6.1) without the block effect terms (see Column 2 of Table 8.2). The mole fraction version of (6.3) yielded $R^2 = 0.9392$, which can be compared to $R^2 = 0.9352$ for the first-order mole fraction model (6.1) without the block effect terms (see Column 3 of Table 8.2).

CVS-II Phase 3 was found to have a statistically significant negative block effect for both mass and mole fraction versions of the model (6.3) for ϵ_{1150}. This situation could occur because the ϵ_{1150} values were biased low for

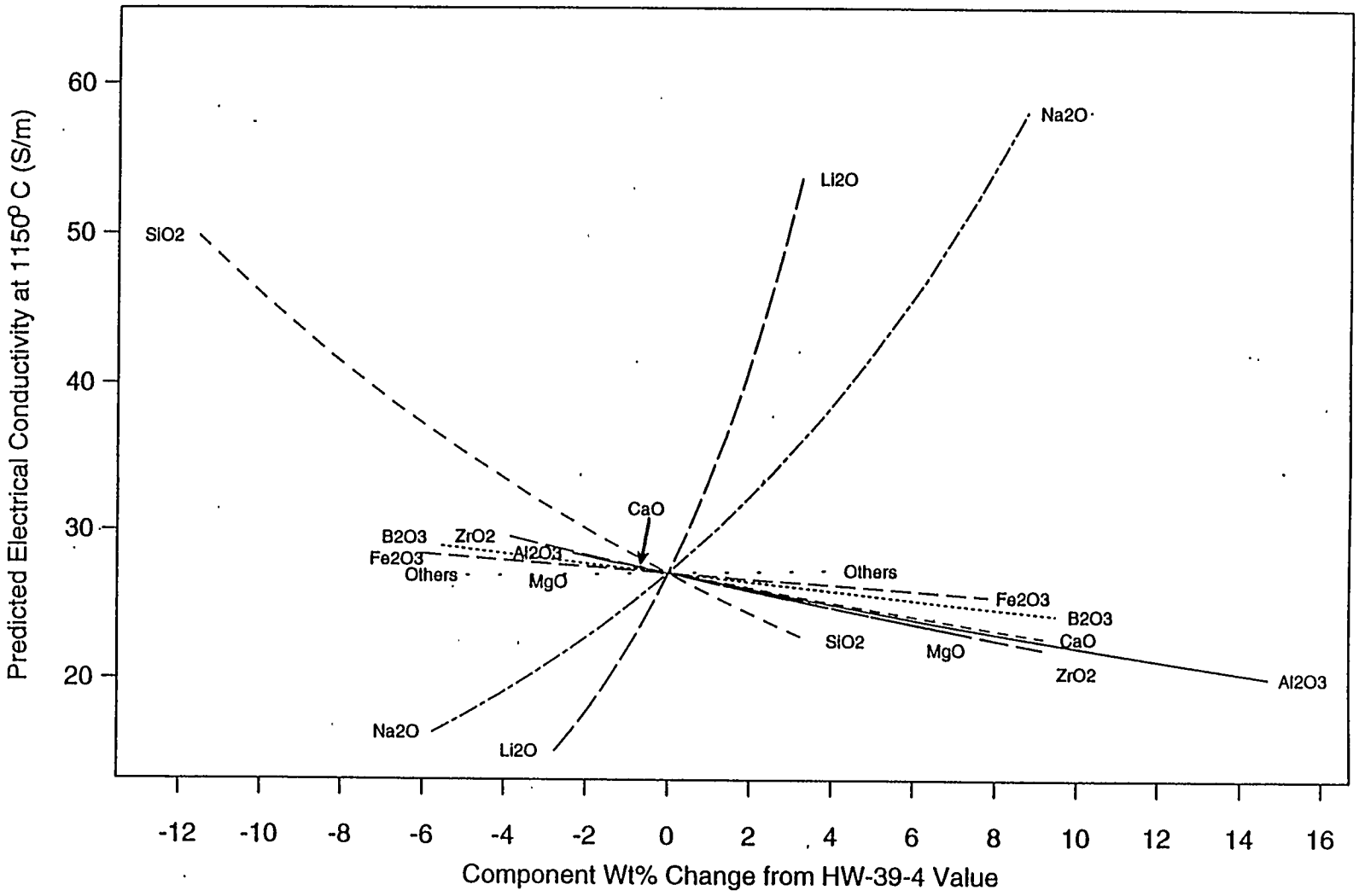

FIGURE 8.3. Predicted Component Effects on Electrical Conductivity at 1150°C Relative to the HW-39-4 Composition, Based on the First-Order Mixture Model Using Mass Fractions (in Column 2 of Table 8.2)

all or a substantial portion of the glasses in CVS-II Phase 3, or because CVS-II Phase 3 involved obtaining more extreme composition and property data than had been obtained in previous CVS phases. Data for replicate glasses in Table F.1 in Appendix F does not provide strong support for the "biased data" hypothesis.

Because of the uncertainty as to whether electrical conductivity data for CVS-II Phase 3 are really biased, it was decided not to try to adjust the data and refit models.

8.4 SECOND-ORDER MODELS FOR ELECTRICAL CONDUCTIVITY AT 1150°C

Expanding the two coefficients of the Arrhenius equation as second-order mixture models would result in a full Arrhenius second-order mixture model 110 coefficients. As seen in the previous section, even expanding the Arrhenius coefficients as first-order mixture models results in a combined model with 20 coefficients. The much larger number of coefficients in the Arrhenius second-order model makes it difficult to fit the model. Hence, it was decided to only fit second-order mixture models to the electrical conductivity at 1150°C data obtained as predictions from the Arrhenius equations fit to each glass (see Table C.3 in Appendix C). Further, because little difference was observed in the fits of first-order mass and mole fraction models, second-order models were developed in terms of mass fractions only.

Three candidate Scheffé second-order mixture models for electrical conductivity at 1150°C are given in Table 8.3. These models consist of the first-order mixture model terms and several second-order terms selected using statistical variable selection techniques (see Section 6.1.4). It was not necessary to apply the pseudocomponent transformation (see Section 6.1.3), so the usual glass oxide component mass fractions were used in fitting the models.

Candidate second-order mixture model #1 in Table 8.3 does not fit the data substantially better than the first-order mass fraction mixture model in Table 8.2, and like the first-order model has a statistically significant LOF. Candidate second-order mixture models #2 and #3 in Table 8.3 provide better fits to the data than the first-order mass fraction mixture model in Table 8.2, and do not have statistically significant LOFs. These conclusions are

TABLE 8.3. Candidate Scheffé Second-Order Models Using Mass Fractions for Electrical Conductivity at 1150°C[a]

Model #1		Model #2		Model #3	
Terms	Coefficients	Terms	Coefficients	Terms	Coefficients
SiO2	0.7881	SiO2	0.3033	SiO2	1.4795
B2O3	3.3795	B2O3	1.8778	B2O3	-2.4532
Na2O	11.0259	Na2O	14.5431	Na2O	6.7834
Li2O	23.4333	Li2O	31.6342	Li2O	5.7170
CaO	1.3776	CaO	-0.2232	CaO	2.7652
MgO	1.0767	MgO	0.7201	MgO	27.4889
Fe2O3	2.4592	Fe2O3	0.7712	Fe2O3	3.8165
Al2O3	1.2156	Al2O3	1.1045	Al2O3	2.4203
ZrO2	0.8230	ZrO2	-0.3288	ZrO2	-7.8377
Others	3.3734	Others	-5.2873	Others	5.4943
B2O3 x Fe2O3	1.5877	Na2O x Li2O	-84.8205	SiO2 x Na2O	4.8720
Fe2O3 x Al2O3	-3.5793	CaO x Fe2O3	28.3329	SiO2 x Li2O	17.7050
Al2O3 x ZrO2	13.5767	B2O3 x Fe2O3	12.0119	SiO2 x MgO	-24.9551
B2O3 x B2O3	-5.2255	MgO x ZrO2	25.7530	SiO2 x Fe2O3	-4.1074
		SiO2 x Others	17.2604	B2O3 x Na2O	23.7153
		Li2O x ZrO2	32.0439	B2O3 x Li2O	52.6655
				B2O3 X MgO	-37.7794
				B2O3 x Fe2O3	13.4238
				B2O3 x ZrO2	29.3642
				Na2O x MgO	-43.3936
				Na2O x ZrO2	22.1985
				Li2O x ZrO2	86.6763
				CaO x Fe2O3	31.7663
				CaO x Others	-46.9817
				MgO x Fe2O3	-37.3319
				MgO x Others	-41.2552
				ZrO2 x Fe2O3	13.6359
R^2	= .9327	R^2	= .9728	R^2	= .9778
R^2(ADJ)	= .9245	R^2(ADJ)	= .9689	R^2(ADJ)	= .9716
R^2(PRESS)	= .8995	R^2(PRESS)	= .9602	R^2(PRESS)	= .9537
LOF?[b]	Yes (97.4%)[c]		No (51.2%)[c]		No (42.2%)[c]

(a) These models were fitted using 120 CVS-I and CVS-II Phase 1, 2, and 3 electrical conductivity at 1150°C values given in Table C.3 of Appendix C. A total of 124 glasses are listed in Table C.3, but electrical conductivity was not measured for the radioactive glasses CVS2-53 and CVS2-54. CVS2-81 was omitted as being an extreme outlier. The data for CVS2-101 was not available at the time these models were fitted.

(b) A statistical F-test for lack-of-fit (LOF) was performed using the estimates of experimental variation obtained from replicate tests. "Yes" and "No" entries indicate whether the LOF was statistically significant at a 90% confidence level. The actual confidence level at which a LOF can be declared significant is given in parentheses following the "Yes" or "No" for each model.

(c) LOF test used the pooled transformed property SD estimate in Table F.4.

based on comparing the R^2 statistics, LOF test results, and predicted versus "measured" plots for the second-order models and the first-order model (both using mass fractions). Model #3 contains more terms than model #2, but this does not seem to add substantial predictive power. Figure 8.4 displays the predicted ϵ_{1150} values versus the ϵ_{1150} data values for model #2.

The experimental error variance estimate (from Table F.4) used in the statistical tests for model LOF may underestimate the experimental variation in ϵ_{1150} values. Predicted ϵ_{1150} values (from the Arrhenius equations fit to each glass) corresponding to replicate glasses were used to estimate the experimental variation in ϵ_{1150} values. Because the predicted ϵ_{1150} values are from a fitted curve, they may underestimate the actual experimental variation in ϵ_{1150}. Estimating the experimental variability from measured electrical conductivity at temperature data could be investigated as an alternative, although this may slightly overestimate the actual experimental variation due to temperature fluctuations around the nominal temperatures at which measurements were made.

8.5 VALIDATION OF FIRST- AND SECOND-ORDER MODELS FOR ELECTRICAL CONDUCTIVITY AT 1150°C

The CVS-II Phase 3 data and a set of historical data were used to validate the first- and second-order Scheffé mixture models for electrical conductivity at 1150°C developed using data up through CVS-II Phase 2. These models are listed in Table 8.4. (Recall that validation involves using data not used to fit the models to assess their predictive performance--see Section 6.1.6.) The validation results for each of these data sets follow.

8.5.1 Validation with CVS-II Phase 3 Data

Figures 8.5, 8.6a, 8.6b, and 8.6c contain the validation results using the CVS-II Phase 3 data for the first-order and three candidate second-order mixture models (using mass fractions) for electrical conductivity at 1150°C given in Table 8.4. These figures contain plots of the predicted versus "measured" ϵ_{1150} values along with a superimposed 45° line that represents

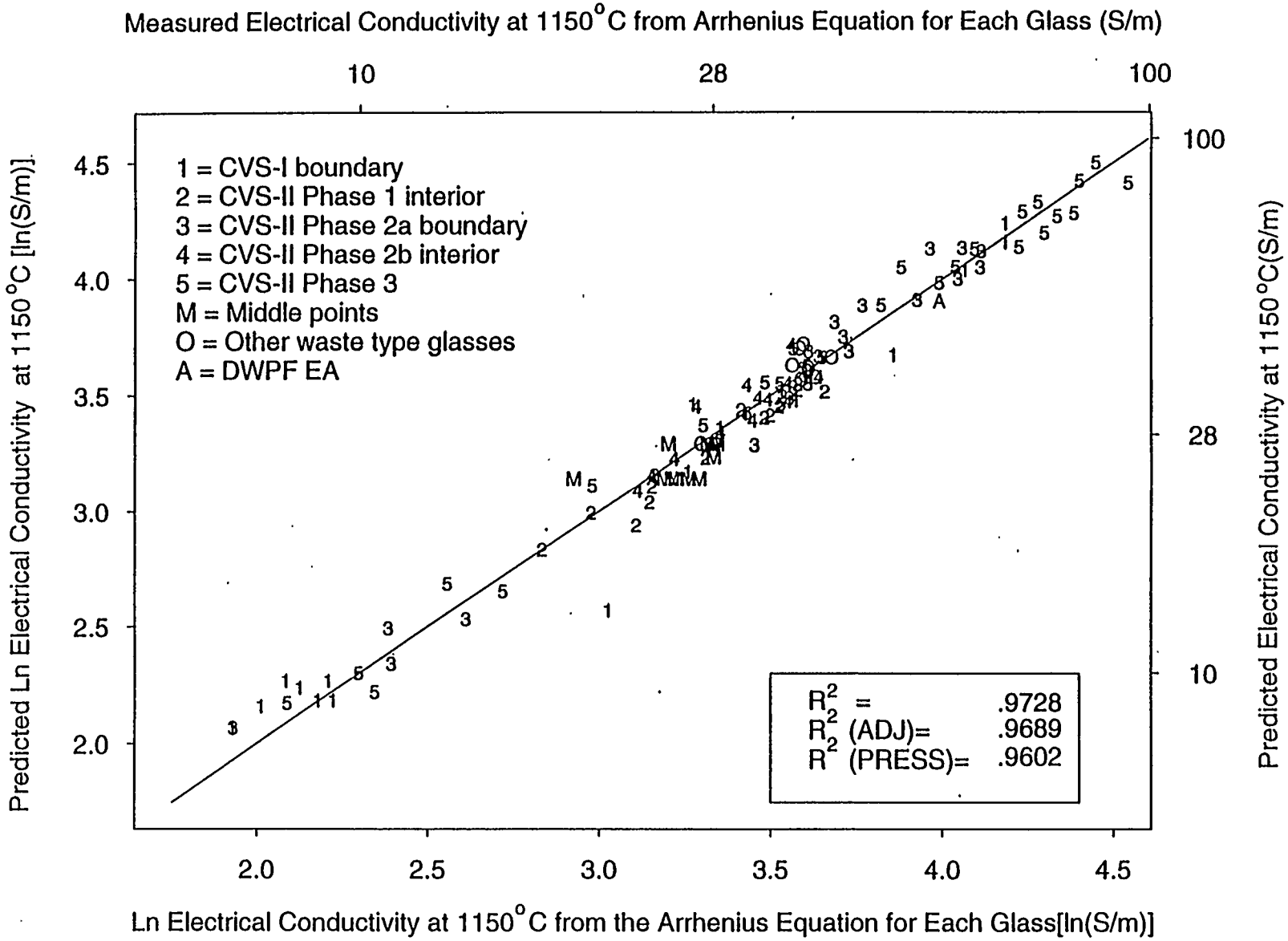

FIGURE 8.4. Predicted Electrical Conductivity at 1150°C from the Second-Order Mixture Model #2 (from Table 8.3) Versus Predicted Electrical Conductivity at 1150°C from the Arrhenius Equation for Each Glass (from Table C.3)

TABLE 8.4. First-Order Model and Three Candidate Second-Order Models Using Mass Fractions for Electrical Conductivity at 1150°C Fitted to CVS-I and CVS-II Phase 1 and 2 Data[a]

First-Order Model		Three Candidate Second-Order Models					
		Model #1 (b)		Model #2		Model #3	
Terms	Coefficients	Terms	Coefficients	Terms	Coefficients	Terms	Coefficients
SiO2	0.7115	SiO2	0.5584	SiO2	0.4497	SiO2	0.9121
B2O3	2.2649	B2O3	5.6371	B2O3	5.7214	B2O3	6.0920
Na2O	11.8930	Na2O	13.3040	Na2O	13.9836	Na2O	13.7875
Li2O	26.1298	Li2O	56.2542	Li2O	59.8837	Li2O	59.4912
CaO	0.5616	CaO	-3.5823	CaO	-0.4536	CaO	-0.9357
MgO	0.1883	MgO	0.0243	MgO	-0.1717	MgO	-0.9450
Fe2O3	2.3800	Fe2O3	1.2998	Fe2O3	1.8378	Fe2O3	1.3811
Al2O3	0.8256	Al2O3	-9.8791	Al2O3	-9.2953	Al2O3	-0.7546
ZrO2	0.5884	ZrO2	0.8074	ZrO2	-0.2126	ZrO2	-0.6340
Others	3.2929	Others	3.9906	Others	2.1740	Others	2.1391
		SiO2 x Li2O	-45.9115	SiO2 x Li2O	-49.4054	SiO2 x Li2O	-50.3716
		SiO2 x Al2O3	23.2258	SiO2 x Al2O3	21.4986	Na2O x Li2O	-101.2283
		B2O3 x Others	-15.6886	Na2O x Li2O	-90.0257	B2O3 x B2O3	-23.4896
		Na2O x Li2O	-84.2999	Li2O x Al2O3	-35.3055		
		Li2O x Al2O3	-33.2056	B2O3 x B2O3	-18.9119		
		CaO x Fe2O3	33.1730				
		CaO x Al2O3	21.1632				
		B2O3 x B2O3	-15.4522				
R^2	= .9234	R^2	= .9811	R^2	= .9712	R^2	= .9616
R^2(ADJ)	= .9134	R^2(ADJ)	= .9759	R^2(ADJ)	= .9661	R^2(ADJ)	= .9546
R^2(PRESS)	= .8817	R^2(PRESS)	= .9565	R^2(PRESS)	= .9396	R^2(PRESS)	= .9306
LOF?[b]	No (89.7%)[c]		No (8.9%)[c]		No (30.9%)[c]		No (54.7%)[c]

(a) Electrical conductivity was not measured for the radioactive glasses CVS2-53 and CVS2-54, so they were not used to fit the models.

(b) A statistical F-test for lack-of-fit (LOF) was performed using the estimates of experimental variation obtained from four replicate tests. "Yes" and "No" entries indicate whether the LOF was statistically significant LOF at a 90% confidence level. The actual confidence level at which a LOF can be declared significant is given in parentheses following the "Yes" or "No" for each model.

(c) LOF test used a pooled transformed property SD estimate comparable to the one in Table F.4, except only data through CVS-II Phase 2 were used.

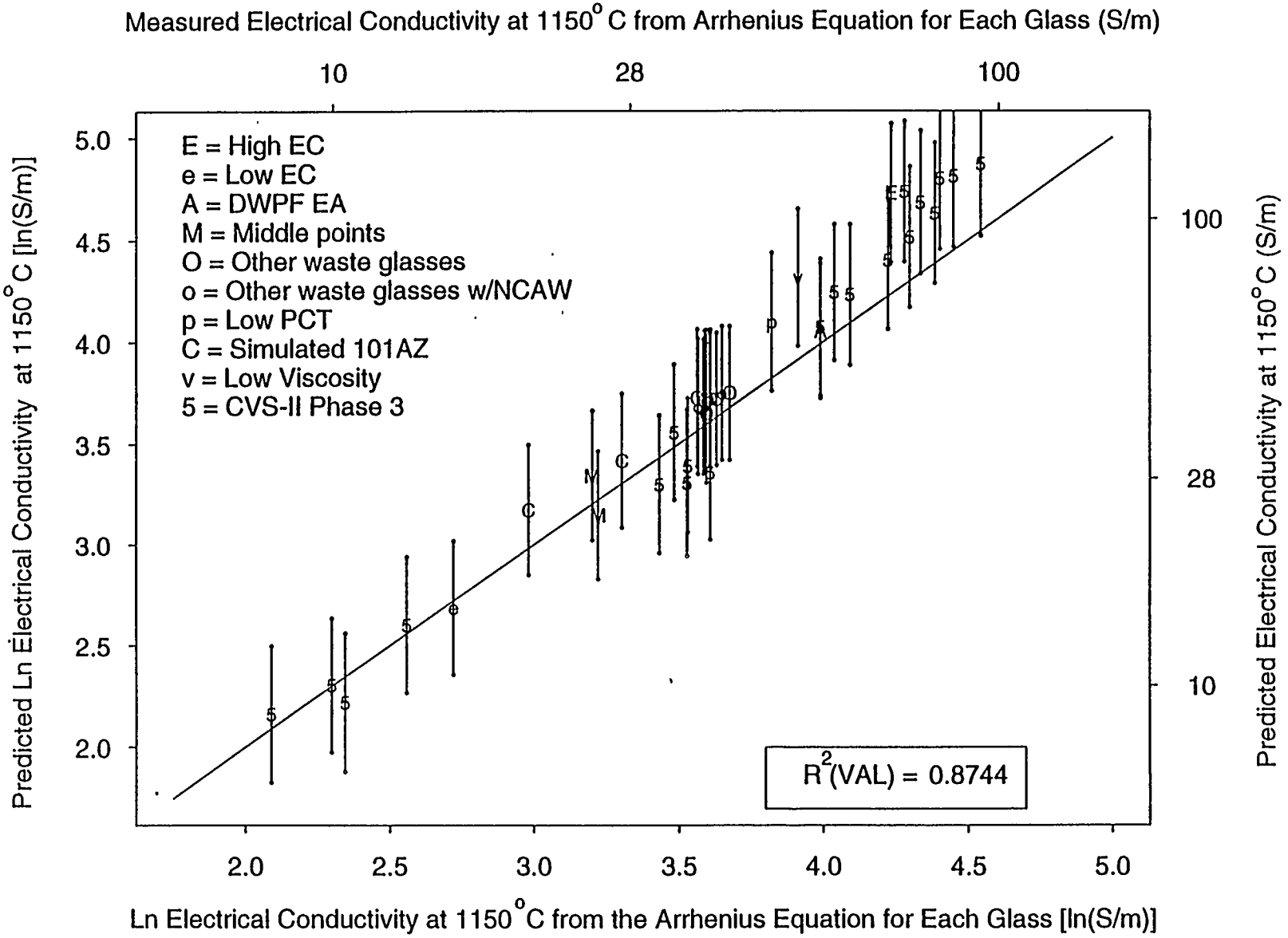

FIGURE 8.5. Predicted Electrical Conductivity at 1150°C from the First-Order Mixture Model (After CVS-II Phase 2) Versus Predicted Electrical Conductivity at 1150°C from the Arrhenius Equation for Each Glass (from Table C.3) for the CVS-II Phase 3 Data

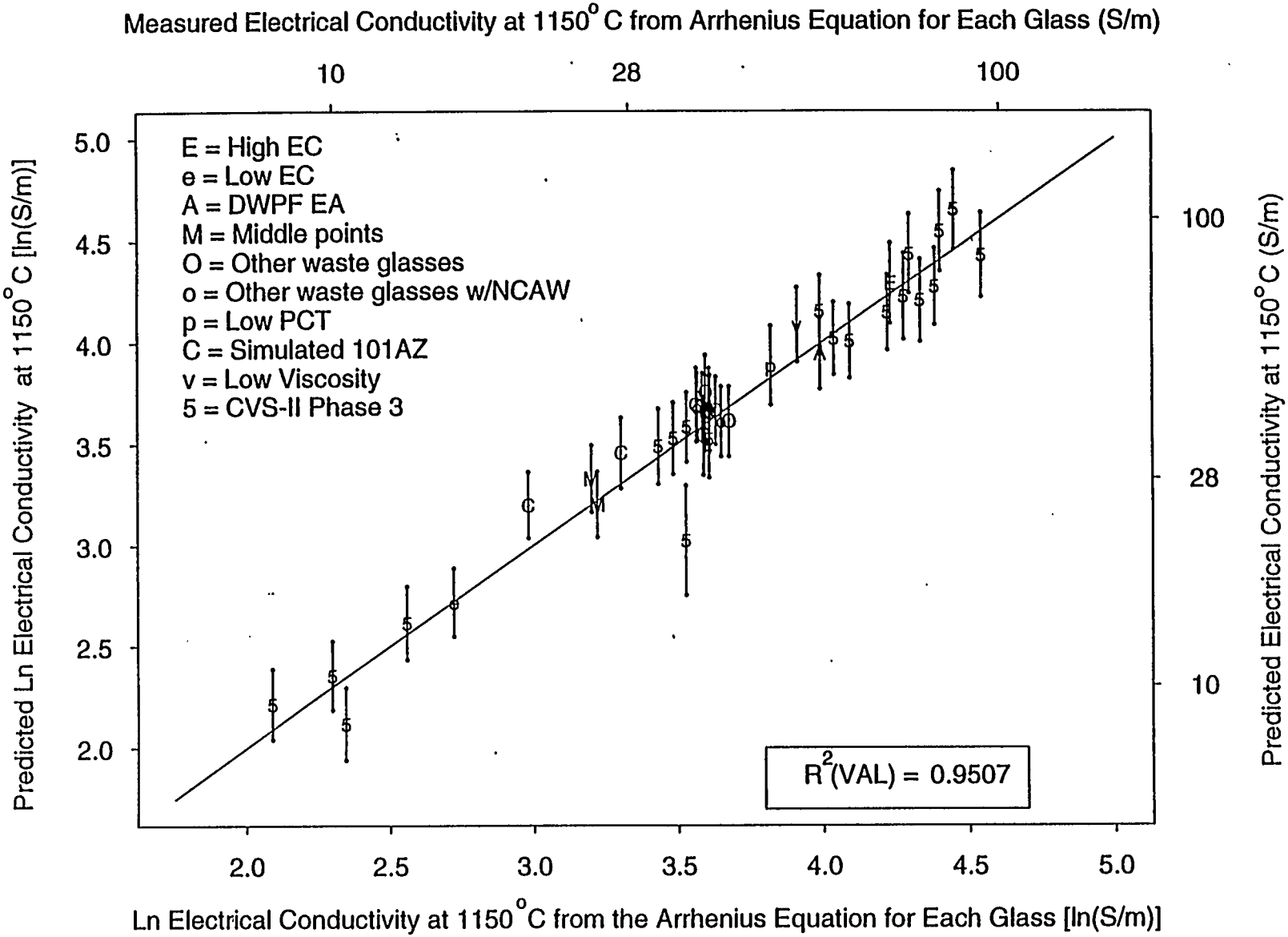

FIGURE 8.6a. Predicted Electrical Conductivity at 1150°C from the Second-Order Mixture Model #1 (After CVS-II Phase 2) Versus Predicted Electrical Conductivity at 1150°C from the Arrhenius Equation for Each Glass (from Table C.3) for the CVS-II Phase 3 Data

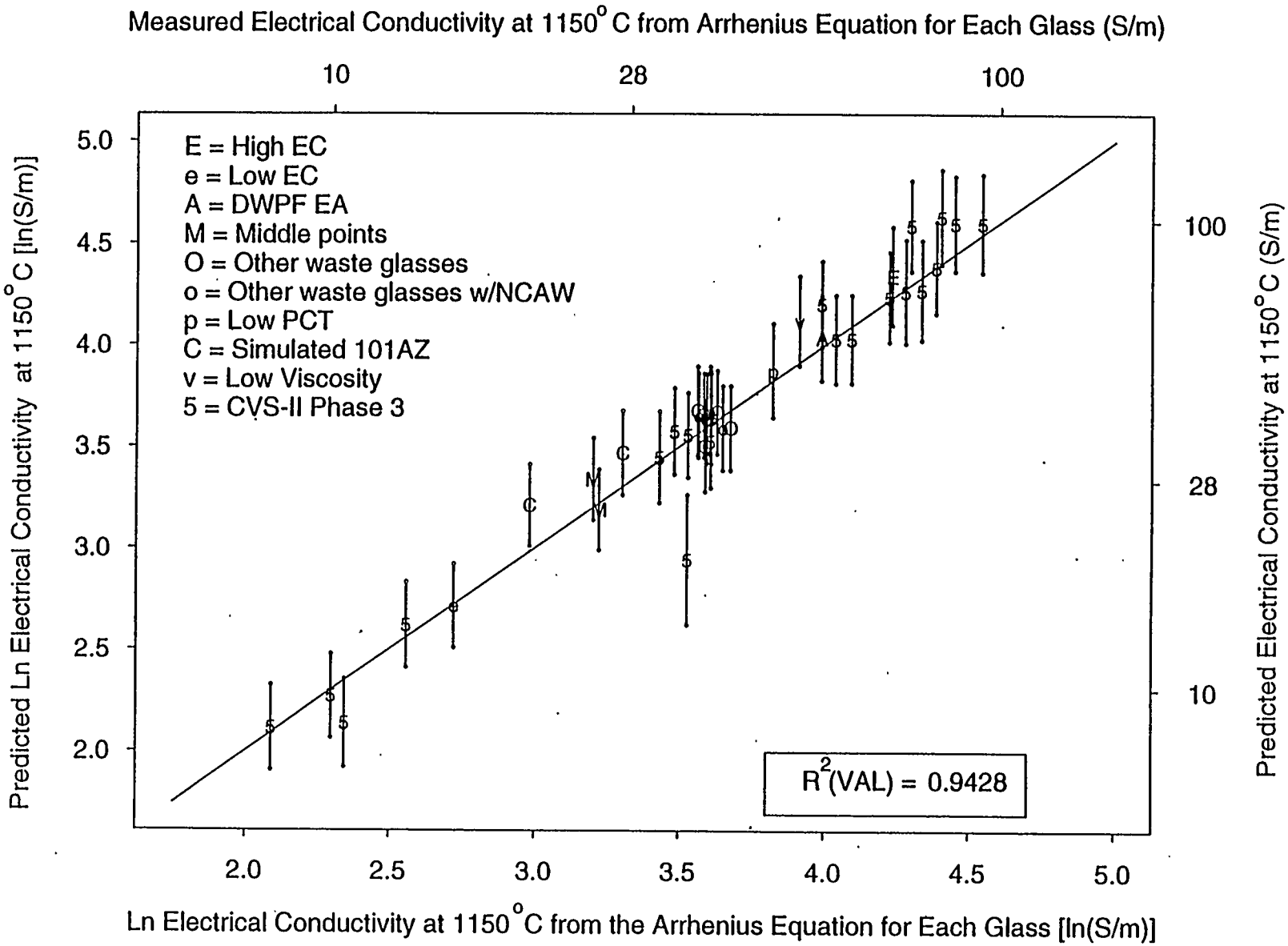

FIGURE 8.6b. Predicted Electrical Conductivity at 1150°C from the Second-Order Mixture Model #2 (After CVS-II Phase 2) Versus Predicted Electrical Conductivity at 1150°C from the Arrhenius Equation for Each Glass (from Table C.3) for the CVS-II Phase 3 Data

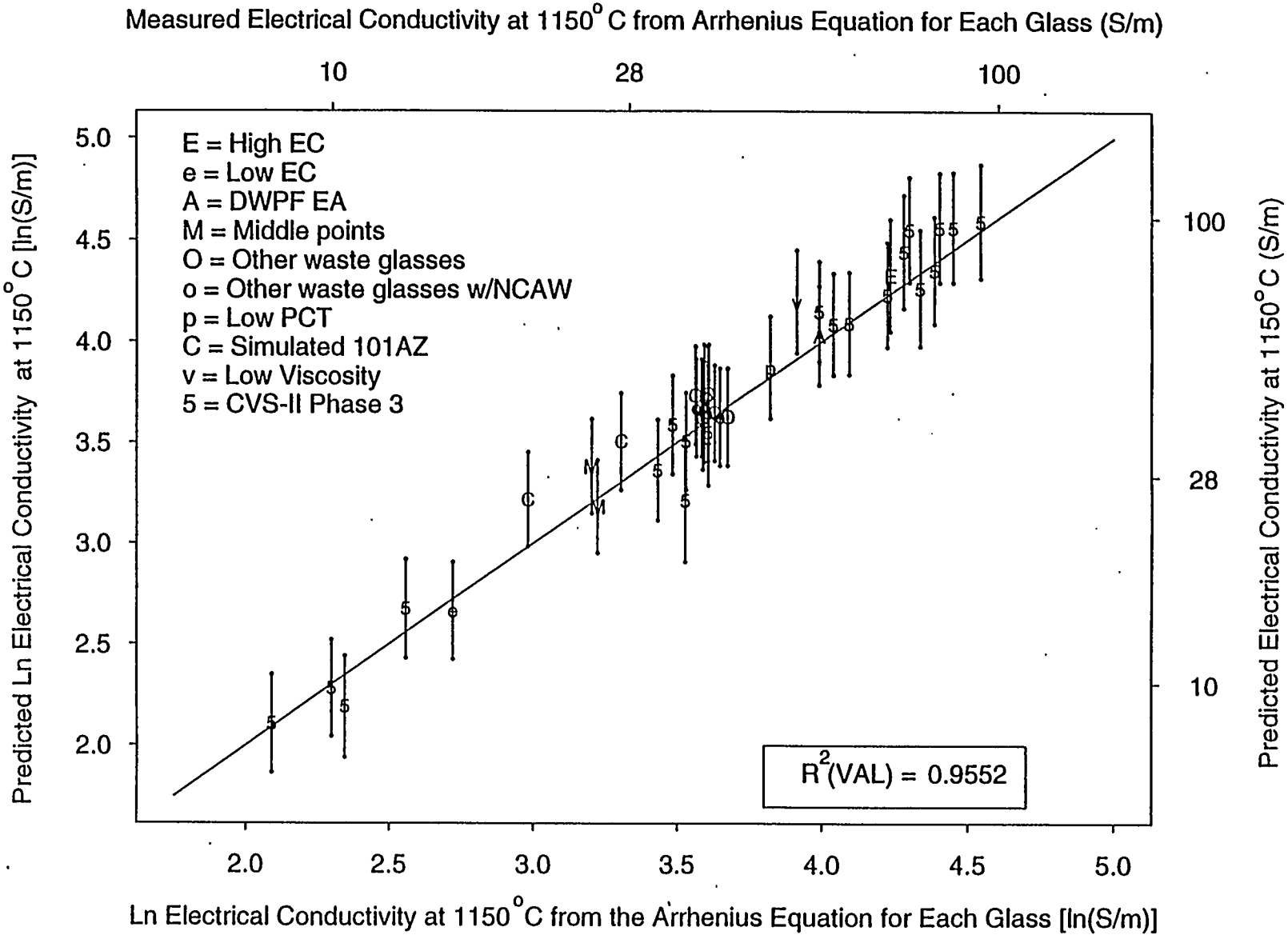

FIGURE 8.6c. Predicted Electrical Conductivity at 1150°C from the Second-Order Mixture Model #3 (After CVS-II Phase 2) Versus Predicted Electrical Conductivity at 1150°C from the Arrhenius Equation for Each Glass (from Table C.3) for the CVS-II Phase 3 Data

perfect prediction. The error bars on the plotted points represent 95% two-sided prediction intervals for the predicted ϵ_{1150} values. If the error bars for a given point overlap the 45° line, the model is validated for that point, in the sense that there is no statistically significant difference between the predicted and "measured" values after accounting for the uncertainties in the predicted and "measured" values. Various plotting symbols are used in Figures 8.5, 8.6a, 8.6b, and 8.6c to identify the specific nature of some of the CVS-II Phase 3 points. Points that are not otherwise specifically identified are plotted with a "5" as the plotting symbol.

Figure 8.5 shows that the first-order ϵ_{1150} model is validated for nearly all of the CVS-II Phase 3 data points. Notable exceptions are the points with the highest ϵ_{1150} values, which the first-order model tends to overpredict. The data point for CVS2-81 was a severe outlier and is not shown in Figure 8.5.

Figures 8.6a, 8.6b, and 8.6c show that the three candidate second-order models are also validated quite well for the CVS-II Phase 3 data, in spite of smaller prediction uncertainties than with the first-order model. The predicted versus "measured" ϵ_{1150} plots as well as the R^2(VAL) values (see Section 6.1.6) for the three second-order ϵ_{1150} models in Figures 8.6a, 8.6b, and 8.6c are better than those for the first-order model in Figure 8.5. The tendency of the first-order model to overpredict for the largest ϵ_{1150} is not seen with the second-order models. The second-order models do show an underprediction for the CVS2-63 data point, but otherwise the plots in Figures 8.6a, 8.6b, and 8.6c look quite good for data not used to fit the models. The R^2(VAL) values for the second-order models are all above 0.94, whereas the first-order model only achieves 0.8744. There does not appear to be much practical difference among the three candidate second-order models, in which case the one with the fewest number of second-order terms (Model #3 in Table 8.4) may be preferred.

These results suggest that the second-order models provide better predictive performance than the first-order model, at least for the CVS-II Phase 3 data. It should be recalled that the CVS-II Phase 3 data is not an ideal validation data set, because it is not uniformly spread over the full

CVS composition region. Part of the goal of CVS-II Phase 3 was to collect data for more extreme compositions and property values than had been obtained previously. Although the CVS-II Phase 3 data are not an ideal validation data set, they show that the first-order model does reasonably well and that the second-order models do even better.

8.5.2 Validation with Historical Database

The historical database gathered for purposes of validating CVS models is discussed in Appendix G. Although 739 glasses were available in the database, there were only 209 glasses for which electrical conductivity at 1150°C values could be obtained. For 205 of these glasses, ϵ_{1150} values were contained in the database and used directly. For the remaining four glasses, electrical conductivity values were available for at least three temperatures (both above and below 1150°C) so that ϵ_{1150} values were obtained as predictions (interpolations) from Arrhenius equations fitted for each glass. The 209 glass compositions (in the CVS 10-component form) and the corresponding ϵ_{1150} values are given in Table G.4 of Appendix G. The ϵ_{1150} values for the 209 glasses ranged from approximately 3 to 120 S/m. By comparison, the 124 CVS-I and CVS-II Phase 1, 2, and 3 glasses had ϵ_{1150} values ranging from approximately 7 to 94 S/m.

Investigation of the 209 glass compositions for which ϵ_{1150} values were obtained showed that only 63 of them were within slightly expanded versions of the lower and upper component bounds given in Table 4.2 (i.e., the region of compositions studied in CVS). (The slightly expanded component lower and upper bounds are given in Table G.2 of Appendix G.) However, it was decided to proceed with validation using all 209 data points, and investigate whether the performance of the first- and second-order ϵ_{1150} models in Table 8.4 depended on whether or not glass compositions were within the CVS region.

Figure 8.7 contains the plot of first-order model predicted versus "measured" ϵ_{1150} values for 206 of the 209 data points. Figures 8.8a, 8.8b, and 8.8c contain similar plots for the three candidate second-order ϵ_{1150} models. Error bars consisting of 95% prediction intervals on the predicted values are included in each plot. Three of the 209 data points were not used

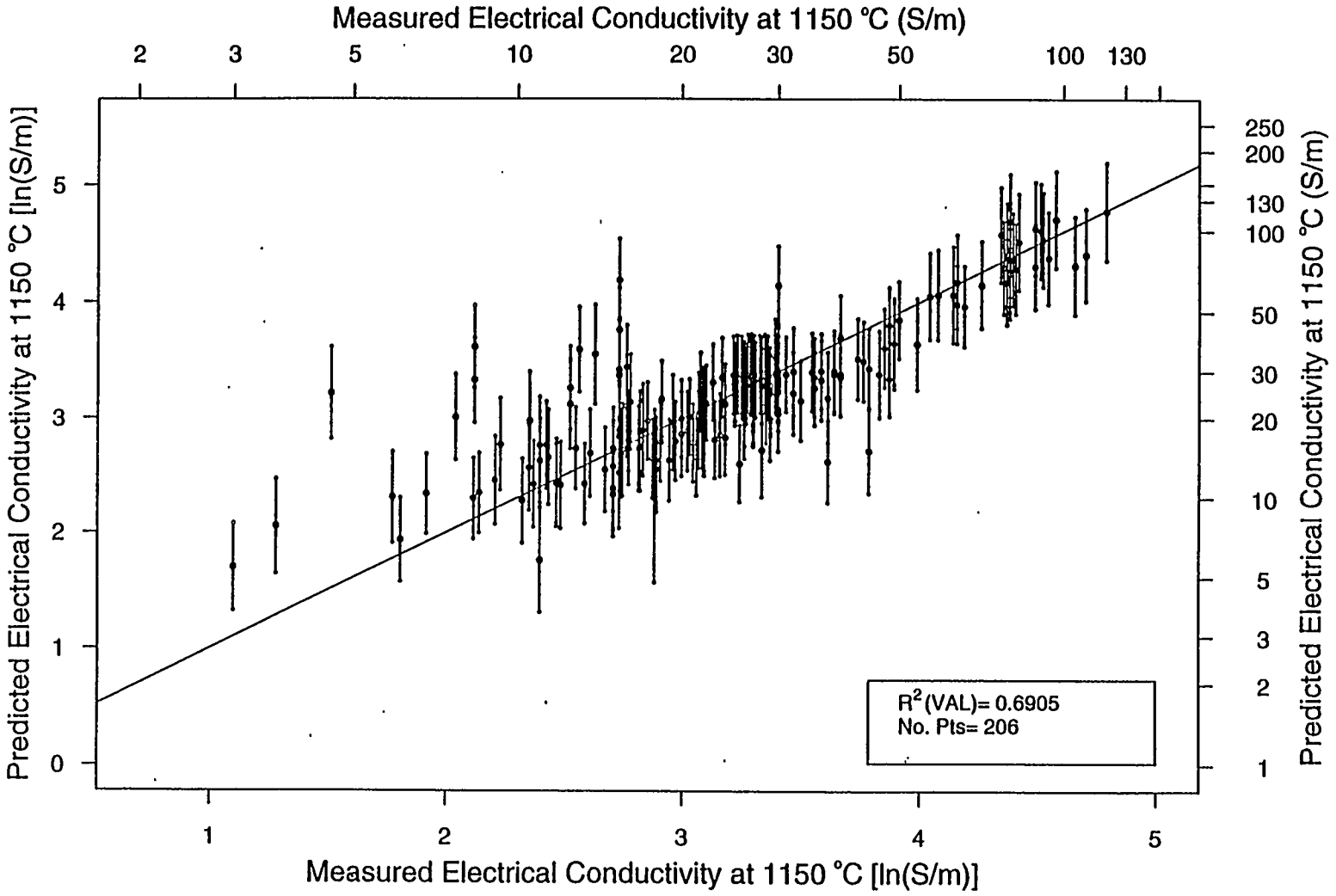

FIGURE 8.7. Predicted Electrical Conductivity at 1150°C from the First-Order Mixture Model (After CVS-II Phase 2) Versus Measured Electrical Conductivity at 1150°C for 206 Historical Data Points (143 of Which are Outside the CVS Composition Region)

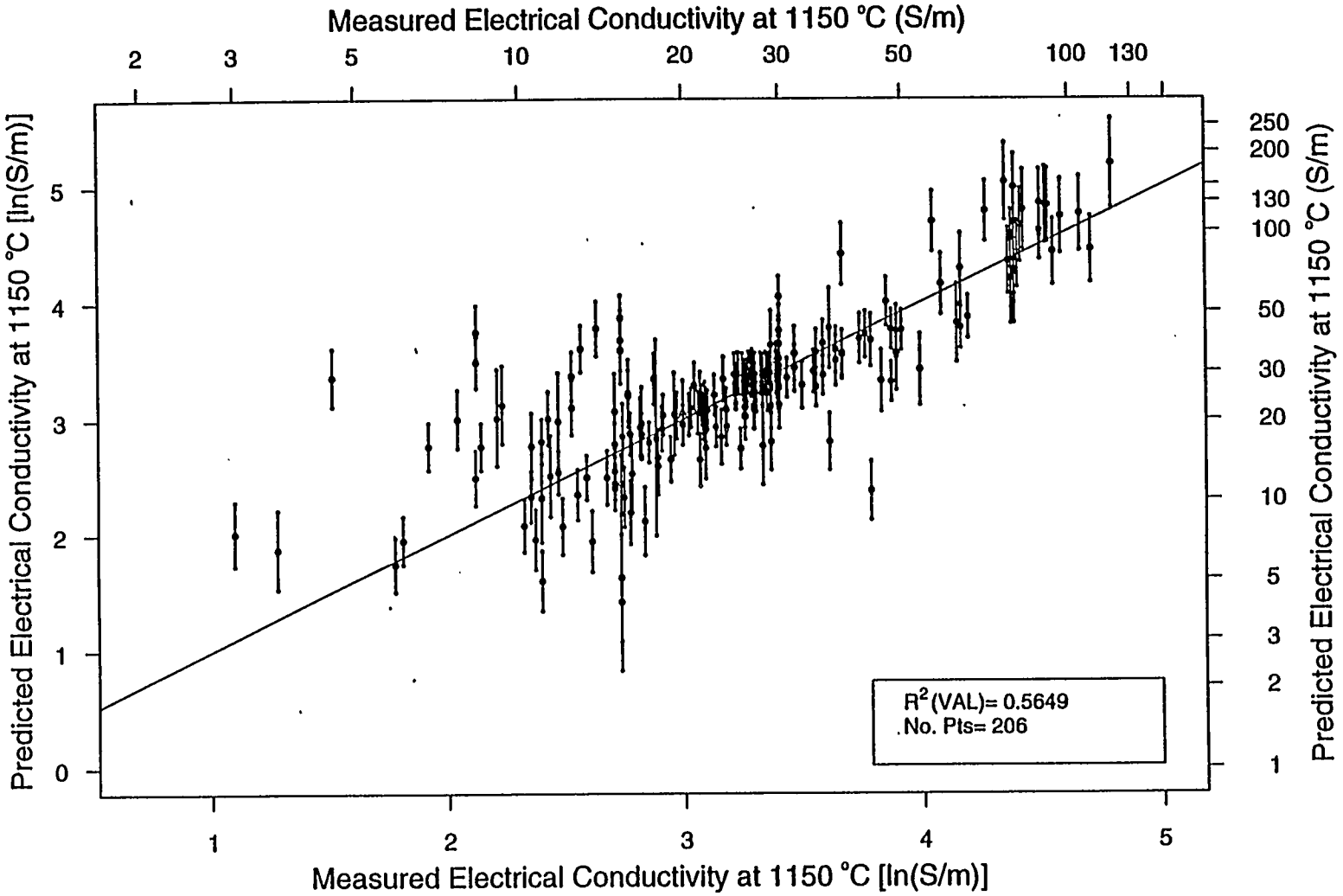

FIGURE 8.8a. Predicted Electrical Conductivity at 1150°C from the Second-Order Mixture Model #1 (After CVS-II Phase 2) Versus Measured Electrical Conductivity at 1150°C for 206 Historical Data Points (143 of Which are Outside the CVS Composition Region)

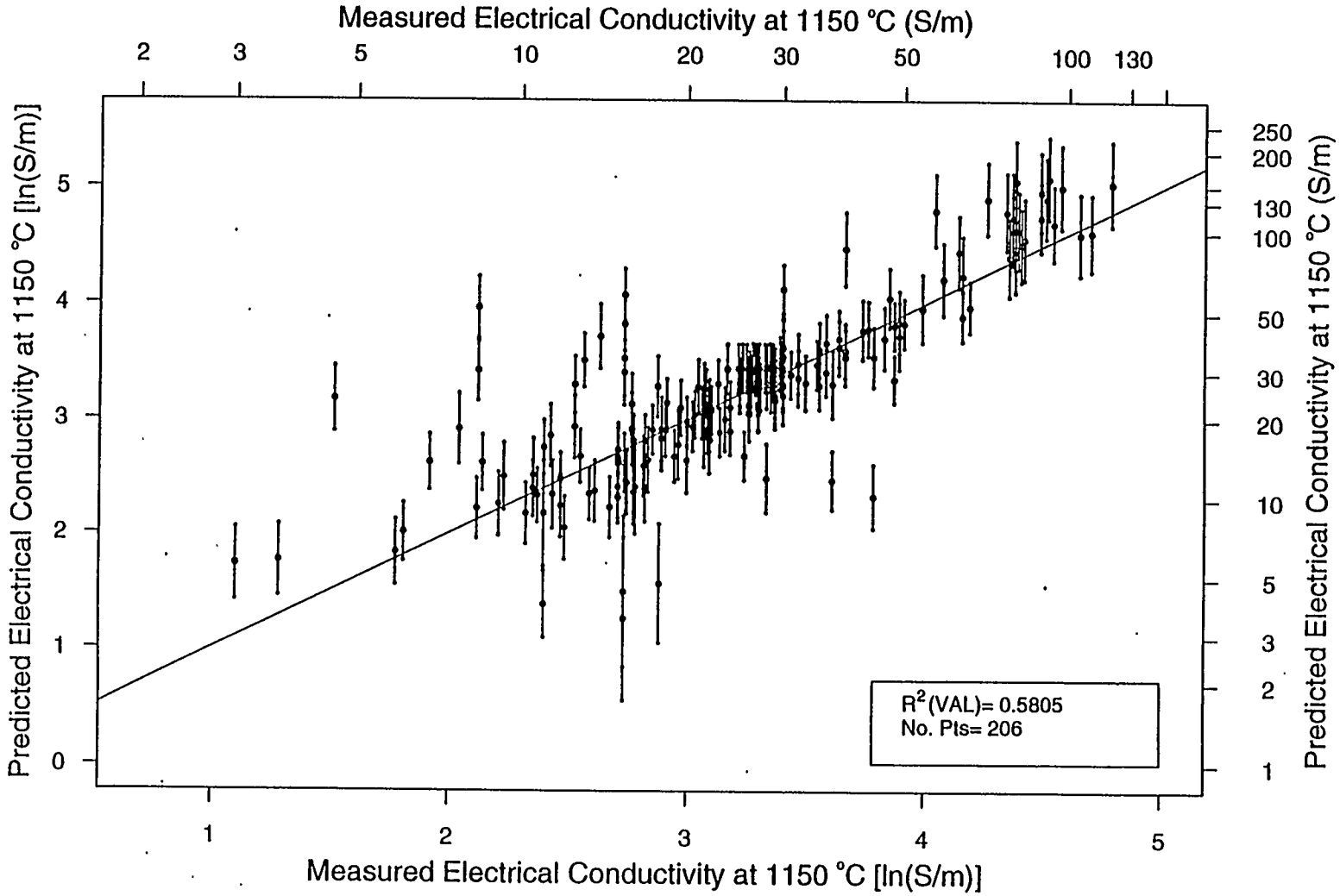

FIGURE 8.8b. Predicted Electrical Conductivity at 1150°C from the Second-Order Mixture Model #2 (After CVS-II Phase 2) Versus Measured Electrical Conductivity at 1150°C for 206 Historical Data Points (143 of Which are Outside the CVS Composition Region)

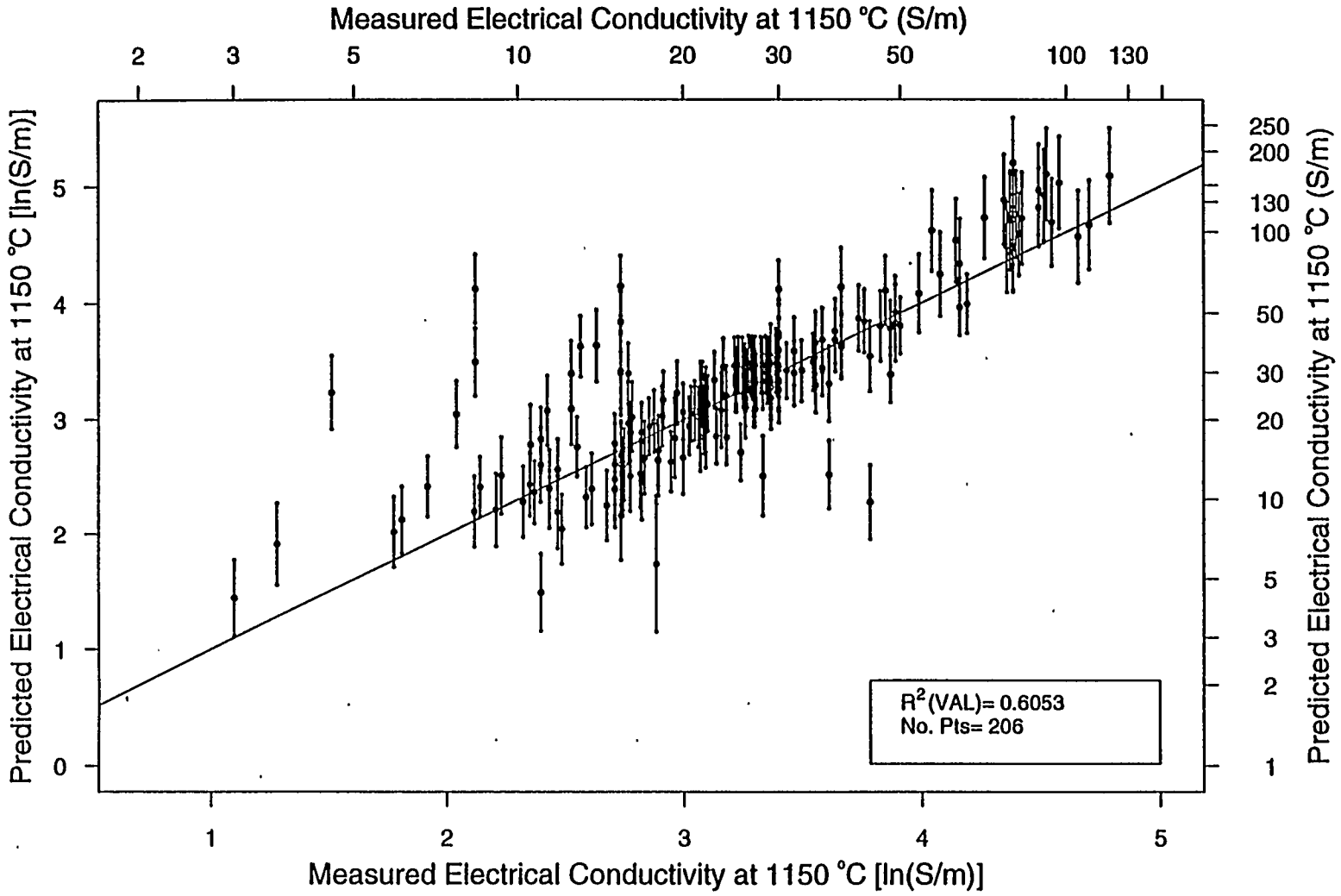

FIGURE 8.8c. Predicted Electrical Conductivity at 1150°C from the Second-Order Mixture Model #3 (After CVS-II Phase 2) Versus Measured Electrical Conductivity at 1150°C for 206 Historical Data Points (143 of Which are Outside the CVS Composition Region)

in the plots or in calculating R^2(VAL) values because they had large error bars indicating that they were outlying in composition space.

Figure 8.7 shows that the first-order model tends to predict ϵ_{1150} values fairly well for many of the points above 10 S/m, but a tendency exists to overpredict below 10 S/m. Several of the points in Figure 8.7 are well off the 45° line, which causes the R^2(VAL) = 0.6905 value to be considerably lower than what it would be without including such points.

Figures 8.8a, 8.8b, and 8.8c show that the second-order models have a similar range of prediction performance for the glasses in the historical database. R^2(VAL) values for the second-order models are 0.5649, 0.5805, and 0.6053, respectively, and the scatter of the points is similar. Thus, none of the second-order models appear to predict any more accurately than the first-order model for this data. However, 143 of the 206 data points are outside slightly expanded versions of the CVS component lower and upper bounds.

Figure 8.9 is a different version of Figure 8.7, without the error bars, and with the number of relaxed single-component constraints (out of the 10 CVS components, see Table G.2 of Appendix G) that are satisfied used as the plotting symbol for each glass. Figure 8.9 shows that many of the 206 data points only satisfy four to nine of the component constraints. The first- and second-order models perform fairly well for most of the points which satisfy all 10 constraints. They also perform well for many points satisfying fewer than 10 constraints, but rather poor prediction performance occurs for some points satisfying fewer than 10 constraints.

In using the historical database, some errors in the original database were discovered and corrected, and remaining errors may be present that could account for some of the lack of agreement between predicted and measured values. However, presumably many of the disagreements are due to the inadequacy of the first- and second-order models for extrapolating outside the CVS region.

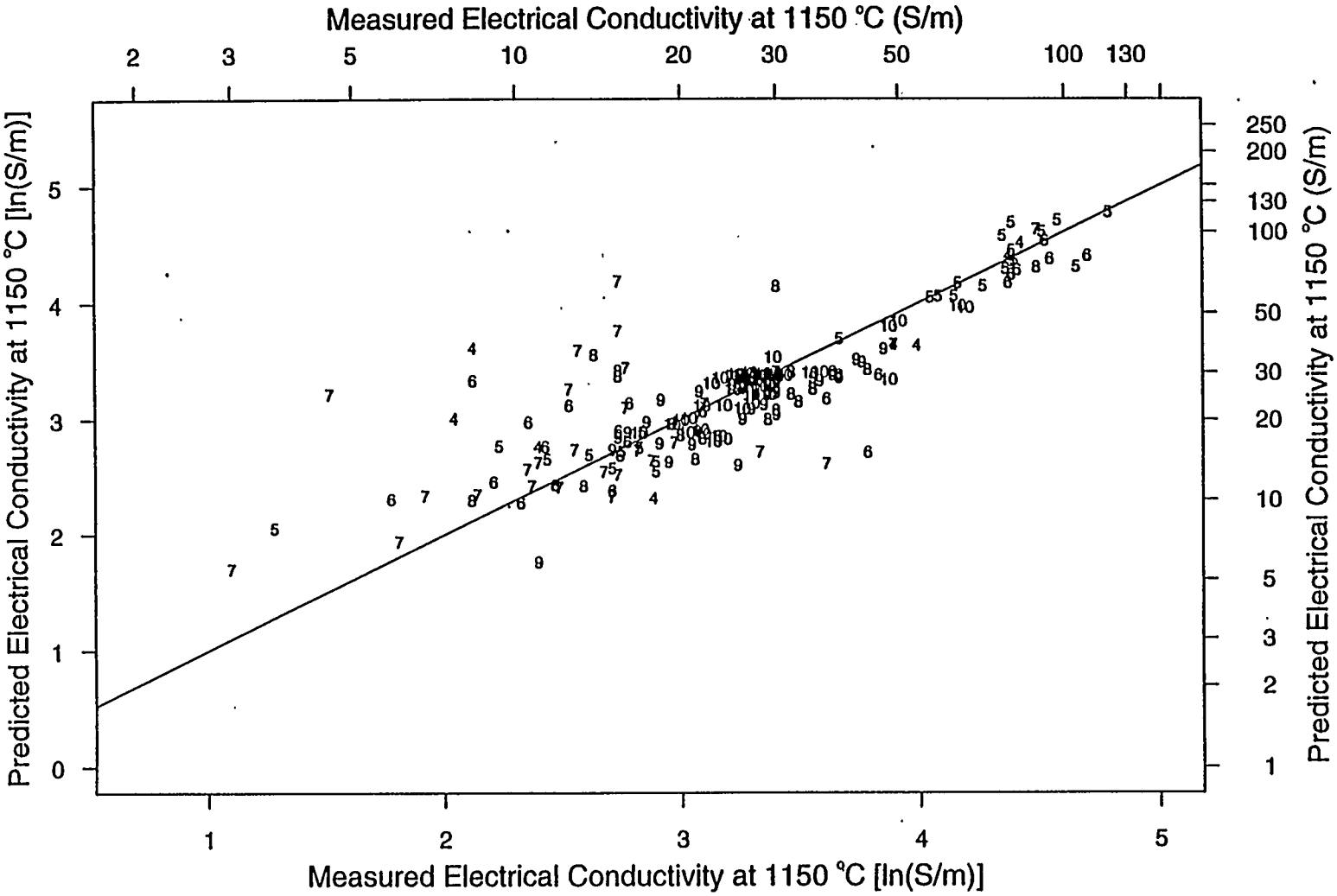

FIGURE 8.9. Predicted Electrical Conductivity at 1150°C from the First-Order Mixture Model (After CVS-II Phase 2) Versus Measured Electrical Conductivity at 1150°C for the Historical Data, With the Number of Relaxed Component Constraints Satisfied Used as the Plotting Symbol

8.5.3 Summary of Electrical Conductivity at 1150°C Model Validation

The validation work discussed above using the CVS-II Phase 3 and historical data sets focused on validating first- and second-order electrical conductivity at 1150°C models developed from data up through CVS-II Phase 2, as listed in Table 8.4. Neither of these data sets were ideal validation data sets, since they do not evenly cover the CVS composition region of interest. However, both data sets indicated that either first-order models or second-order models with a few selected second-order terms provide quite good predictive performance inside the CVS region, and have fairly good predictive ability outside this region for some compositions. Thus, the empirical mixture modeling approach appears to be adequate for predicting electrical conductivity at 1150°C.

The first- and second-order electrical conductivity at 1150°C models presented in Tables 8.2 and 8.3 of this report could be validated using the historical data, the CVS-II Phase 4 data, and any other data that subsequently becomes available. The models included in this report and the CVS-II Phase 4 data were not completed in time to enable validating them and reporting on it here.

8.6 ELECTRICAL CONDUCTIVITY DISCUSSION

Figure 8.10 plots the first-order mixture model component coefficients for electrical conductivity at 1150°C (from Column 2 of Table 8.2) against those for viscosity at 1150°C (from Column 2 of Table 7.3). The relative magnitudes of the coefficients for each property give an indication of the effects of the components. The plot of coefficients for the two properties displays whether components have similar or different relative effects for the two properties. Figure 8.10 shows that electrical conductivity at 1150°C is affected primarily by alkali oxides, Li_2O and Na_2O, while other components have little or no effect. Both Li_2O and Na_2O increase electrical conductivity at 1150°C, Li_2O considerably more strongly than Na_2O. Because viscosity and electrical conductivity at 1150°C are affected differently by components, no strong correlation exists between the first-order mixture model coefficients

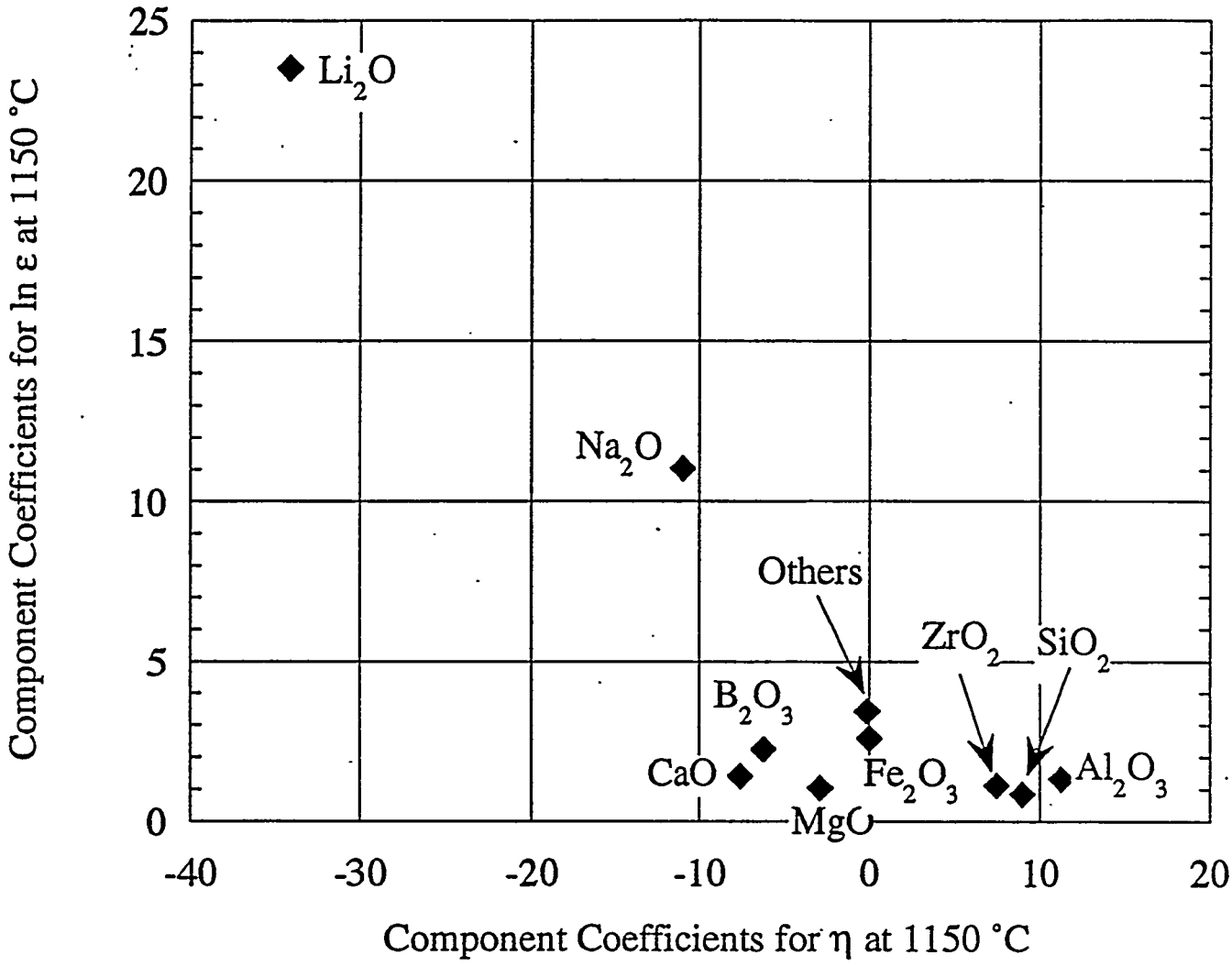

FIGURE 8.10. First-Order Mixture Model Coefficients for Viscosity at 1150°C Versus for Electrical Conductivity at 1150°C

for these properties (except that Li_2O and Na_2O have the strongest effects for both properties).

The differences between the Li_2O coefficients for viscosity and electrical conductivity and the Na_2O coefficients for the same properties confirm the observation made in the CVS-I report (Piepel, Hrma, et al. 1993) that it is beneficial for glass durability if Li_2O is used (to the maximum

practical extent) for adjusting electrical conductivity and viscosity of waste glasses instead of Na_2O. The reason is that the same change in viscosity and electrical conductivity can be achieved with a substantially smaller concentration (mass fraction) of alkali oxide if Li_2O is used rather than Na_2O. Then, since Li_2O and Na_2O affect durability in a similar manner, durability is less compromised. If the waste contains a large concentration of Na_2O, it may be worthwhile not to use Na_2O in frit at all.

9.0 GLASS TRANSITION TEMPERATURE RESULTS AND DISCUSSION

Glass transition temperature (T_g) values for CVS-I and CVS-II Phases 1, 2, and 3 glasses are included in Table 9.1, and range from 412.0 to 579.1°C. Estimates of uncertainties in the measured T_g values based on replicate glasses are given in Appendix F.

First-order mixture models for T_g and corresponding component effects plots are presented in Section 9.1. The question of whether the T_g data contains any biases due to being collected in four phases (CVS-I and CVS-II Phases 1, 2, and 3) is addressed in Section 9.2. Second-order mixture models for T_g are presented in Section 9.3. Model validation results are discussed in Section 9.4, while other model forms that were investigated are discussed in Section 9.5. A discussion of the results is given in Section 9.6.

9.1 FIRST-ORDER MODELS AND COMPONENT EFFECTS FOR GLASS TRANSITION TEMPERATURE

First-order mixture models of the form (6.1) using mass and mole fractions of the oxide components were fitted to the untransformed T_g values in Table 9.1, producing the coefficients given in Table 9.2. The evaluation statistics R^2 = 0.8865, R^2(ADJ) = 0.8773, and R^2(PRESS) = 0.8582 for the mass fraction model and R^2 = 0.8822, R^2(ADJ) = 0.8727, and R^2(PRESS) = 0.8521 for the mole fraction model indicate that the first-order mixture model form fits the transition temperature data fairly well, but with room for improvement. The plots of predicted versus measured glass transition temperature values in Figures 9.1a (mass fraction model) and 9.1b (mole fraction model) confirm this. Figures 9.1a and 9.1b show that the first-order mixture model form tends to overpredict small T_g and underpredict large T_g. Statistical tests for model lack-of-fit (LOF) (see Section 6.1.5) indicated that both mass and mole fraction first-order models have statistically significant LOFs with greater than 98% confidence (see Table 9.2).

The first-order mixture model using mass fractions given in Table 9.2 was used to produce a component effects plot (see Section 6.3) for T_g, which is displayed in Figure 9.2. Only the single-component constraints and not the

TABLE 9.1. Glass Transition Temperature (T_g) Data for CVS-I and CVS-II Phase 1, 2, and 3 Glasses

Glass [a]	ID[b] #	PS[c]	T_g (°C)	Glass [a]	ID[b] #	PS[c]	T_g (°C)
CVS1-1 (1)	1	M	486.2	CVS2-10	33	2	490.8
CVS1-2	2	1	487.6	CVS2-11	34	2	482.3
CVS1-3	3	1	486.3	CVS2-12	35	2	500.6
CVS1-4 (2)	4	1	524.6	CVS2-13	36	2	480.2
CVS1-5	5	1	450.9	CVS2-14	37	2	516.6
CVS1-6	6	1	490.5	CVS2-15	38	2	480.8
CVS1-7	7	1	579.1	CVS2-16 (4)	39	M	487.4
CVS1-8 (3)	8	1	547.0	CVS2-17 (1)	40	M	492.9
CVS1-9	9	1	516.9	CVS2-18 (4)	41	M	483.2
CVS1-10	10	1	519.4	CVS2-19 (5)	42	M	493.0
CVS1-11	11	1	537.1				
CVS1-12	12	1	469.3	CVS2-20	43	3	489.0
CVS1-13	13	1	526.7	CVS2-21	44	3	487.7
CVS1-14	14	1	520.4	CVS2-22	45	3	469.0
CVS1-15	15	1	429.6	CVS2-23	46	3	498.4
CVS1-16	16	1	488.5	CVS2-24	47	3	462.8
CVS1-17	17	1	490.4	CVS2-25	48	3	455.1
CVS1-18	18	1	429.3	CVS2-26	49	3	511.2
CVS1-19 (1)	19	M	491.3	CVS2-27	50	3	480.1
CVS1-20 (1)	20	M	496.3	CVS2-28	51	3	476.3
CVS1-21 (2)	21	1	543.5	CVS2-29	52	3	561.6
CVS1-22 (3)	22	1	559.9	CVS2-30	53	3	490.1
CVS1-23	23	M	486.5	CVS2-31	54	3	528.9
				CVS2-32	55	3	475.3
CVS2-1	24	2	474.5	CVS2-33	56	3	412.0
CVS2-2	25	2	479.8	CVS2-34 (6)	57	3	455.6
CVS2-3	26	2	522.1	CVS2-35	58	3	422.2
CVS2-4	27	2	497.6	CVS2-36	59	3	472.7
CVS2-5	28	2	519.3	CVS2-37	60	3	470.3
CVS2-6	29	2	497.7	CVS2-38	61	3	527.8
CVS2-7	30	2	475.5	CVS2-39	62	3	447.3
CVS2-8	31	2	465.4	CVS2-40	63	4	464.3
CVS2-9	32	2	483.6	CVS2-41	64	4	472.5

(a) The numbers in parentheses represent replicate sets of glasses.

(b) ID# is a consecutive integer numbering of all CVS glasses.

(c) PS is the plotting symbol used in plots associated with this data: 1 = CVS-I boundary, 2 = CVS-II Phase 1 interior, 3 = CVS-II Phase 2a boundary, 4 = CVS-II Phase 2b interior, 5 = CVS-II Phase 3 boundary, M = middle compositions, O = other than NCAW waste glasses, A = EA glass.

TABLE 9.1. Glass Transition Temperature (T_g) Data for CVS-I and CVS-II Phase 1, 2, and 3 Glasses (continued)

Glass [a]	ID[b] #	PS[c]	T_g (°C)
CVS2-42	65	4	477.9
CVS2-43	66	4	499.2
CVS2-44	67	4	483.8
CVS2-45	68	4	492.8
CVS2-46	69	4	480.1
CVS2-47	70	4	481.3
CVS2-48	71	4	489.5
CVS2-49	72	4	486.6
CVS2-50 (1)	73	M	491.2
CVS2-51 (5)	74	M	478.0
CVS2-52	75	4	479.0
CVS2-53	76	4	(d)
CVS2-54	77	M	(d)
CVS2-55	78	0	502.2
CVS2-56	79	0	496.6
CVS2-57	80	0	512.1
CVS2-58	81	4	499.1
CVS2-59	82	5	453.8
CVS2-60	83	5	432.0
CVS2-61	84	5	460.4
CVS2-62	85	5	537.2
CVS2-63	86	5	488.6
CVS2-64	87	0	471.8
CVS2-65	88	0	514.3
CVS2-66	89	0	470.1
CVS2-67	90	0	479.3
CVS2-68	91	0	465.7
CVS2-69	92	0	488.2
CVS2-70	93	0	484.2
CVS2-71	94	5	470.9
CVS2-72	95	5	462.7
CVS2-73	96	5	476.4
CVS2-74	97	5	470.3
CVS2-75	98	5	469.1
CVS2-76	99	5	428.9
CVS2-77	100	5	426.0
CVS2-78	101	5	519.4
CVS2-79	102	5	497.8
CVS2-80	103	5	530.4
CVS2-81	104	5	392.8
CVS2-82	105	5	438.5
CVS2-83	106	5	415.5
CVS2-84	107	5	418.8
CVS2-85	108	5	416.1
CVS2-86	109	5	510.2
CVS2-87	110	5	497.2
CVS2-88	111	5	441.7
CVS2-89	112	5	512.3
CVS2-90	113	5	486.1
CVS2-91	114	5	525.3
CVS2-92	115	5	467.8
CVS2-93	116	5	450.1
CVS2-94	117	5	454.4
CVS2-95 (7)	118	A	453.1
CVS2-96 (1)	119	M	494.0
CVS2-97 (5)	120	M	489.3
CVS2-98 (6)	121	5	461.1
CVS2-99	122	5	482.6
CVS2-100	123	5	476.4
CVS2-101(7)	124	A	(d)

(a) The numbers in parentheses represent replicate sets of glasses.

(b) ID# is a consecutive integer numbering of all CVS glasses.

(c) PS is the plotting symbol used in plots associated with this data: 1 = CVS-I boundary, 2 = CVS-II Phase 1 interior, 3 = CVS-II Phase 2a boundary, 4 = CVS-II Phase 2b interior, 5 = CVS-II Phase 3 boundary, M = middle compositions, 0 = other than NCAW waste glasses, A = EA glass.

(d) T_g not measured for radioactive glasses CVS2-53 and CVS2-54 and for the EA glass CVS2-101.

TABLE 9.2. Coefficients and Goodness-of-Fit Statistics for First-Order Mixture Models Fitted to T_g Using Mass and Mole Fractions of the Oxide Components

	Mass Fractions	Mole Fractions
SiO_2	622.973	614.822
B_2O_3	584.939	589.353
Na_2O	128.504	138.710
Li_2O	-571.109	-5.979
CaO	621.517	606.157
MgO	494.391	489.512
Fe_2O_3	427.129	331.466
Al_2O_3	544.451	579.255
ZrO_2	730.071	953.888
Others	363.637	162.318
# points[a]	121	121
R^2[b]	0.8865	0.8822
R^2(ADJ)[b]	0.8773	0.8727
R^2(PRESS)[b]	0.8582	0.8521
LOF?[c]	Yes (98.2%)[d]	Yes (98.5%)[d]

(a) Both models were fitted using the 121 T_g values given in Table 9.1. A total of 124 glasses are listed in Table 9.1, but T_g was not measured for the radioactive glasses CVS2-53 and CVS2-54 nor for the DWPF EA glass CVS2-101.

(b) R^2, R^2(ADJ), and R^2(PRESS) statistics take values between 0.0 and 1.0, and provide different measures of the proportion of variation in the property data accounted for by a fitted model. See Section 6.1.5 for the definitions of these statistics.

(c) A statistical F-test for lack-of-fit (LOF) was performed using the estimates of experimental variation obtained from replicate tests. "Yes" and "No" entries indicate whether the LOF was statistically significant at a 90% confidence level. The actual confidence level at which a LOF can be declared significant is given in parentheses following the "Yes" or "No" for each model.

(d) LOF test used the pooled SD estimate in Table F.4.

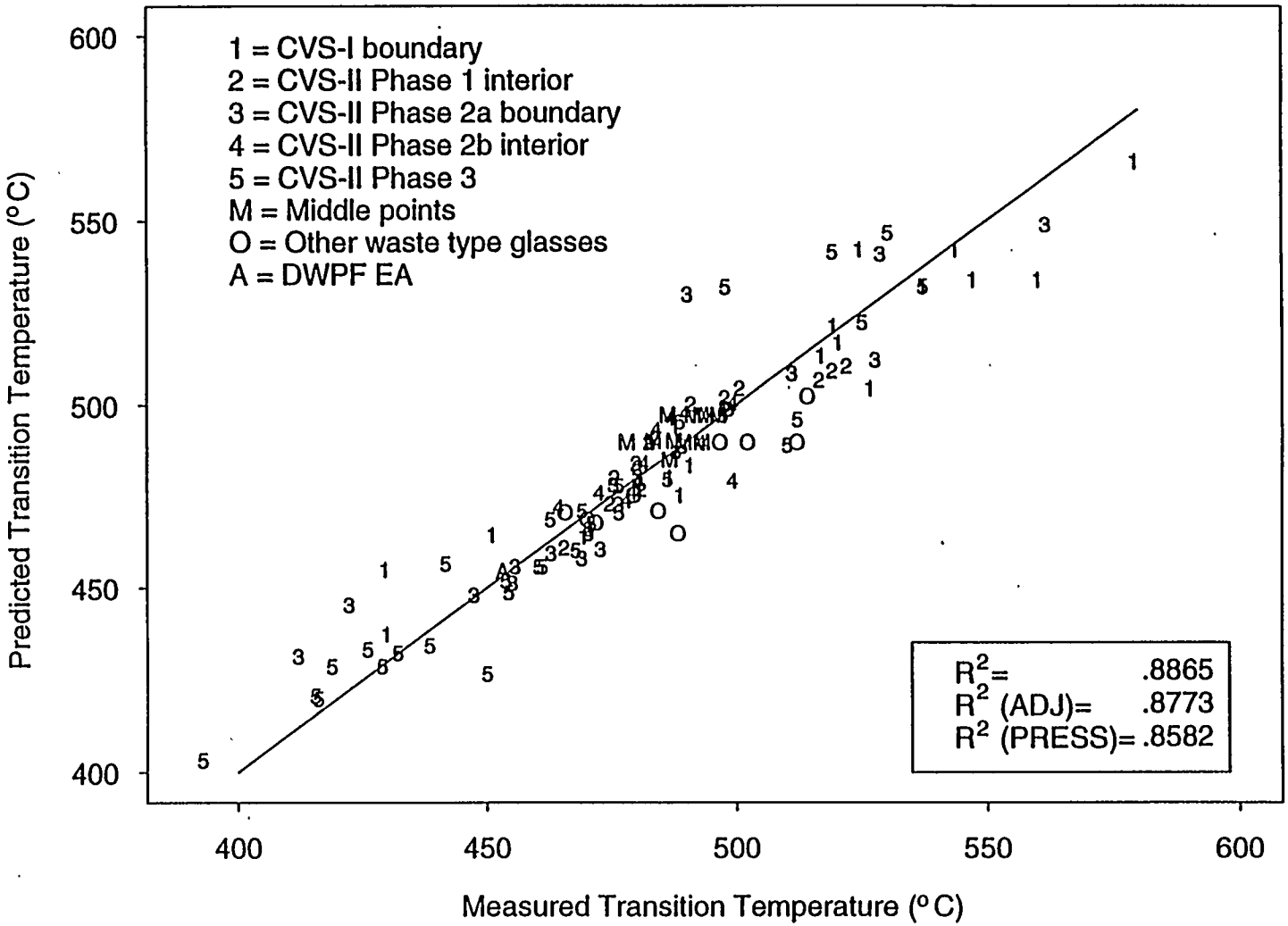

FIGURE 9.1a. Predicted Versus Measured Glass Transition Temperature Values for the First-Order Mixture Model Using Mass Fractions (from Column 2 of Table 9.2)

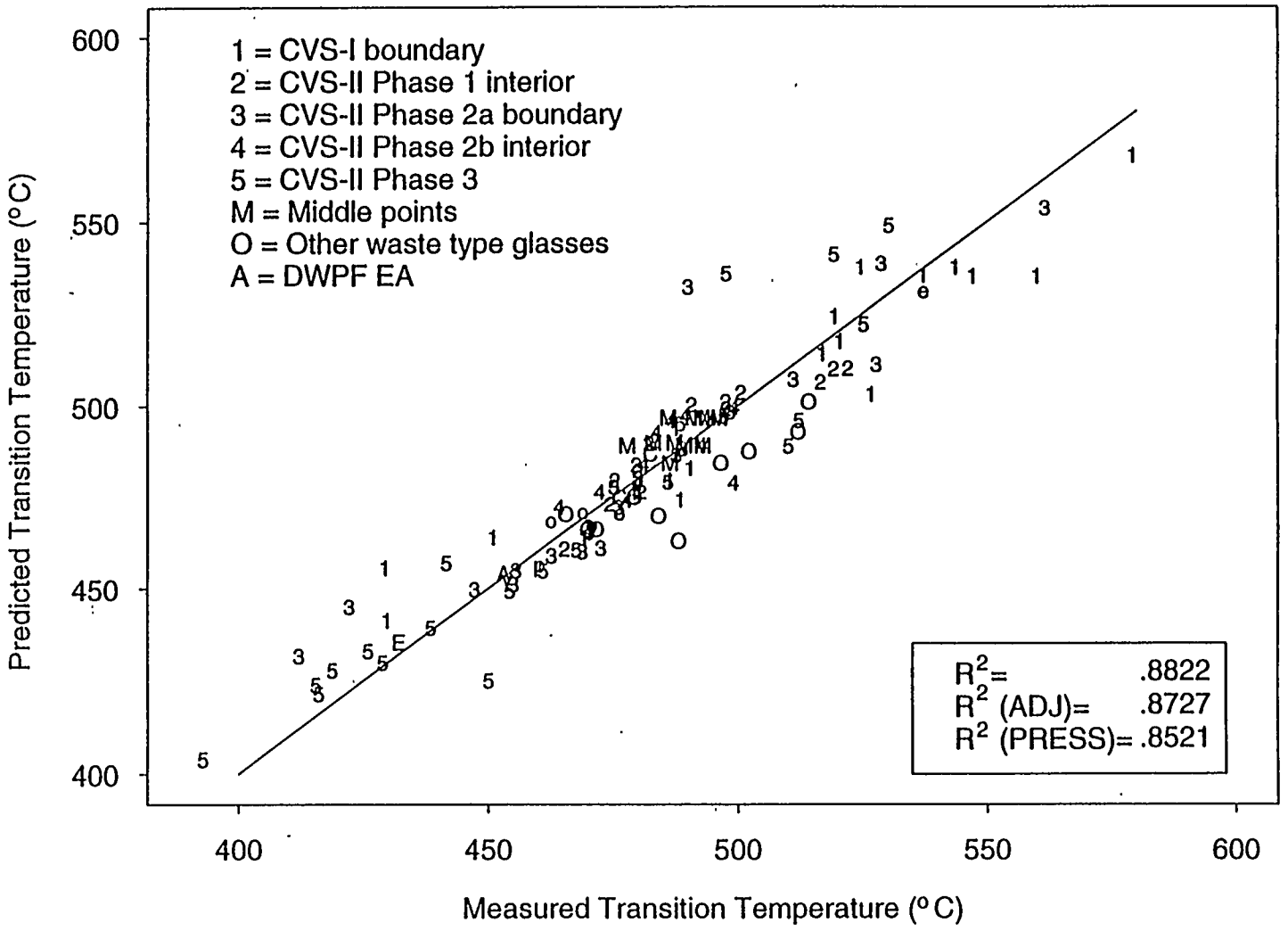

FIGURE 9.1b. Predicted Versus Measured Glass Transition Temperature Values for the First-Order Mixture Model Using Mole Fractions (from Column 2 of Table 9.2)

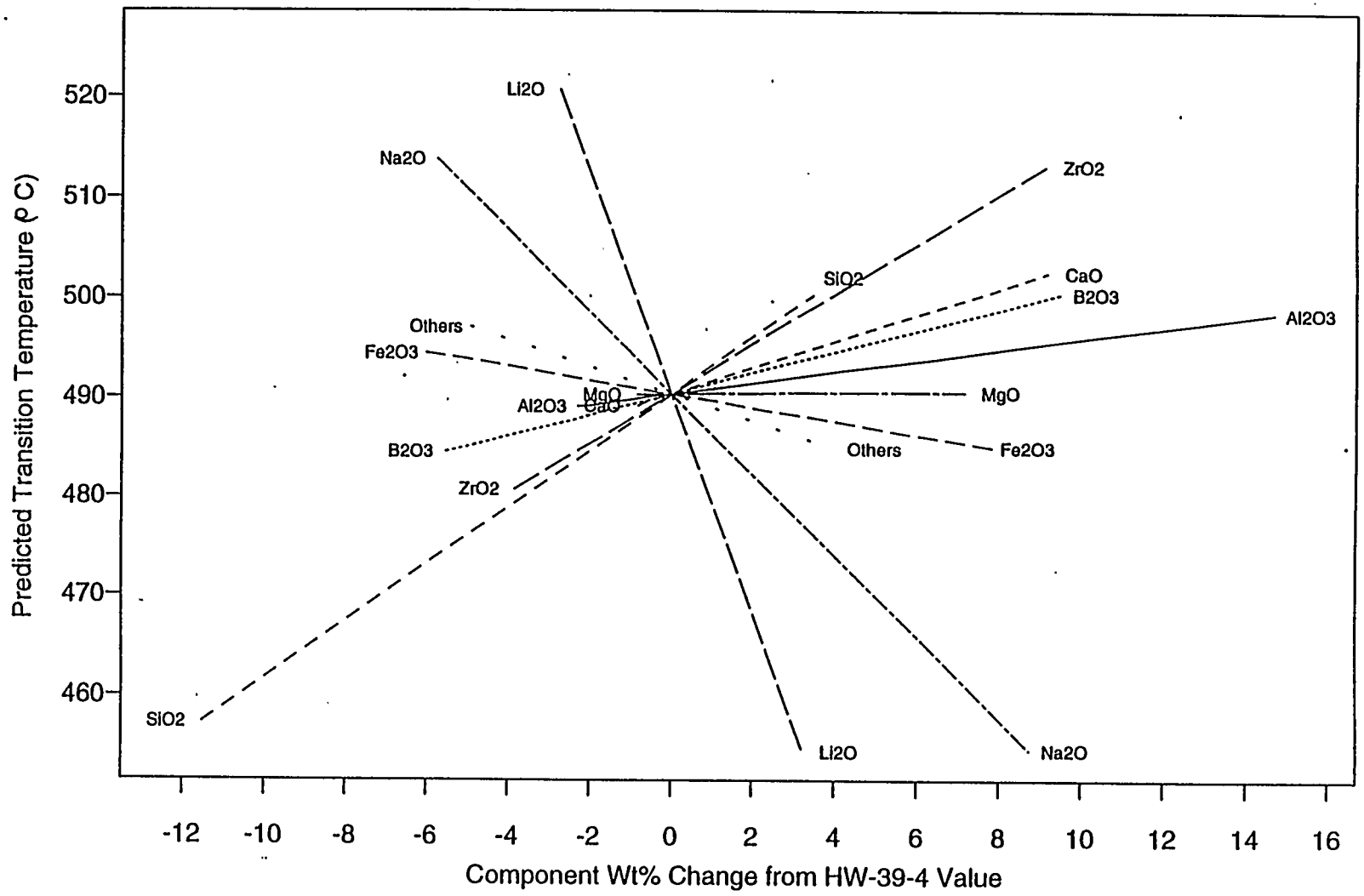

FIGURE 9.2. Predicted Component Effects on Glass Transition Temperature Relative to the HW-39-4 Composition, Based on the First-Order Mixture Model Using Mass Fractions (in Column 2 of Table 9.2)

stand-in crystallinity constraints in Tables 4.2 and 4.6 were used to limit the effects plot (both were used in previous effects plots). As a result, effects are evaluated over wider ranges than in the past for several components involved in the stand-in constraints (most notably Al_2O_3 and SiO_2). The effects plot illustrates that glass transition temperatures are predicted to be strongly decreased by Li_2O, and to a lesser extent (but still quite strongly) by Na_2O. SiO_2 and ZrO_2 are predicted to increase T_g, although not as strongly as Li_2O and Na_2O decrease it. CaO and B_2O_3 are also predicted to increase T_g, but not as much as SiO_2 and ZrO_2. All other components have moderate to negligible effects.

9.2 INVESTIGATION OF POTENTIAL BIASES IN GLASS TRANSITION TEMPERATURE DATA DUE TO CVS PHASES

As discussed in Section 6.1.1, a model of the form (6.3) was fitted to the T_g data for CVS-I and CVS-II Phases 1, 2, and 3 to ascertain whether any biases (block effects) are present in the T_g data because of performing the CVS in phases. The mass fraction version of (6.3) yielded $R^2 = 0.8871$, which can be compared to $R^2 = 0.8865$ for the first-order mass fraction model (6.1) without the block effect terms (see Column 2 of Table 9.2). The mole fraction version of (6.3) yielded $R^2 = 0.8827$, which can be compared to $R^2 = 0.8822$ for the first-order mole fraction model (6.1) without the block effect terms (see Column 3 of Table 7.4).

No statistically significant block effects were detected for either mass or mole fraction versions of the model (6.3) for T_g. This finding is consistent with the closeness of the R^2 values for first-order models (mass and mole fraction versions) with and without the block effect terms.

9.3 SECOND-ORDER MODELS FOR GLASS TRANSITION TEMPERATURE

Three candidate Scheffé second-order mixture models (using mass fractions of the oxide components) for glass transition temperature are given in Table 9.3. These models consist of the first-order mixture model terms and several second-order terms selected using statistical variable selection techniques (see Section 6.1.4). It was not necessary to apply the

TABLE 9.3. Candidate Scheffé Second-Order Models Using Mass Fractions for Glass Transition Temperature[a]

Model #1		Model #2		Model #3	
Terms	Coefficients	Terms	Coefficients	Terms	Coefficients
SiO2	631.8334	SiO2	627.7969	SiO2	619.9708
B2O3	986.3028	B2O3	908.8738	B2O3	265.8674
Na2O	567.1696	Na2O	647.3425	Na2O	-587.6421
Li2O	-195.6000	Li2O	-237.5252	Li2O	-270.0934
CaO	541.5698	CaO	534.3467	CaO	-5186.7255
MgO	246.9729	MgO	98.4273	MgO	356.3342
Fe2O3	349.1210	Fe2O3	378.5836	Fe2O3	1765.4182
Al2O3	394.9251	Al2O3	408.3860	Al2O3	1206.8501
ZrO2	582.9657	ZrO2	578.9085	ZrO2	758.0259
Others	286.4802	Others	288.1203	Others	505.1393
SiO2 x B2O3	-859.3591	SiO2 x B2O3	-700.7733	SiO2 x Na2O	1224.9516
B2O3 x Fe2O3	-1038.9664	B2O3 x Fe2O3	-991.1893	SiO2 x CaO	6740.7127
Na2O x Li2O	-3657.9119	Na2O x Li2O	-3345.5124	SiO2 x MgO	-1110.1644
MgO x Fe2O3	3245.1809	MgO x Fe2O3	3793.4438	SiO2 x Fe2O3	-2044.6131
Na2O x Na2O	-1406.1705	MgO x Al2O3	2321.2709	SiO2 x Al2O3	-1030.2442
		Al2O3 x Fe2O3	-1790.2632	B2O3 x Na2O	2540.1291
		Na2O x Na2O	-1765.1101	B2O3 x Li2O	1989.9948
				B2O3 x Ca2O	7369.2318
				B2O3 x Fe2O3	-1073.7580
				B2O3 x Al2O3	-1005.9577
				Na2O x Li2O	-2761.8014
				Na2O x CaO	4360.6795
				Na2O x MgO	-1974.7467
				Li2O x MgO	-3207.2766
				CaO x MgO	-5279.2824
				CaO x Fe2O3	6942.7194
				CaO x Al2O3	7500.8530
				CaO x ZrO2	8074.8011
				CaO x Others	6475.7321
				MgO x Others	-2242.5171
				Fe2O3 x Al2O3	-2658.8602
				Fe2O3 x ZrO2	-1704.2895
				Fe2O3 x Others	-1822.2821
R^2	= .9300	R^2	= .9415	R^2	= .9689
R^2(ADJ)	= .9207	R^2(ADJ)	= .9326	R^2(ADJ)	= .9576
R^2(PRESS)	= .9007	R^2(PRESS)	= .9176	R^2(PRESS)	= .9351
LOF?[b]	Yes (90.7%)[c]		No (84.2%)[c]		No (49.3%)[c]

(a) Second-order models were fitted to (untransformed) glass transition temperature using 121 data points in Table 9.1. A total of 124 glasses are listed there, but transition temperature was not measured for the radioactive glasses CVS2-53 and CVS2-54 nor for the EA glass CVS2-101.

(b) A statistical F-test for lack-of-fit (LOF) was performed using the estimates of experimental variation obtained from replicate tests. "Yes" and "No" entries indicate whether the LOF was statistically significant at a 90% confidence level. The actual confidence level at which a LOF can be declared significant is given in parentheses following the "Yes" or "No" for each model.

(c) LOF test used the pooled SD estimate in Table F.4.

pseudocomponent transformation (see Section 6.1.3), so the usual glass oxide component mass fractions were used in fitting the models. Figure 9.3 displays the predicted versus measured T_g values for the second-order mixture model #3 from Table 9.3.

The three candidate second-order mixture models in Table 9.3 provide a better fit than the first-order mass fraction mixture model considered in Section 9.1 (i.e., they have higher R^2 values). Candidate second-order mixture model #1 has a significant LOF at the 90% confidence level, but candidate second-order mixture models #2 and #3 do not (see Table 9.3).

9.4 VALIDATION OF FIRST- AND SECOND-ORDER MODELS FOR GLASS TRANSITION TEMPERATURE

The CVS-II Phase 3 data and a set of historical data were used to validate the first- and second-order Scheffé mixture models for glass transition temperature developed using data up through CVS-II Phase 2. These models are listed in Table 9.4. (Recall that validation involves using data not used to fit the models to assess their predictive performance--see Section 6.1.6.) The validation results for each of these data sets follow.

9.4.1 Validation with CVS-II Phase 3 Data

Figures 9.4, 9.5a, 9.5b, and 9.5c contain the validation results using the CVS-II Phase 3 data for the first-order and three candidate second-order mixture models (using mass fractions) for glass transition temperature given in Table 9.4. These figures contain plots of the predicted versus measured T_g values along with a superimposed 45° line that represents perfect prediction. The error bars on the plotted points represent 95% two-sided prediction intervals for the predicted T_g values. If the error bars for a given point overlap the 45° line, the model is validated for that point, in the sense that no statistically significant difference exists between the predicted and measured values after accounting for the uncertainties in the predicted and measured values. Various plotting symbols are used in Figures 9.4, 9.5a, 9.5b, and 9.5c to identify the specific nature of some of the CVS-II Phase 3

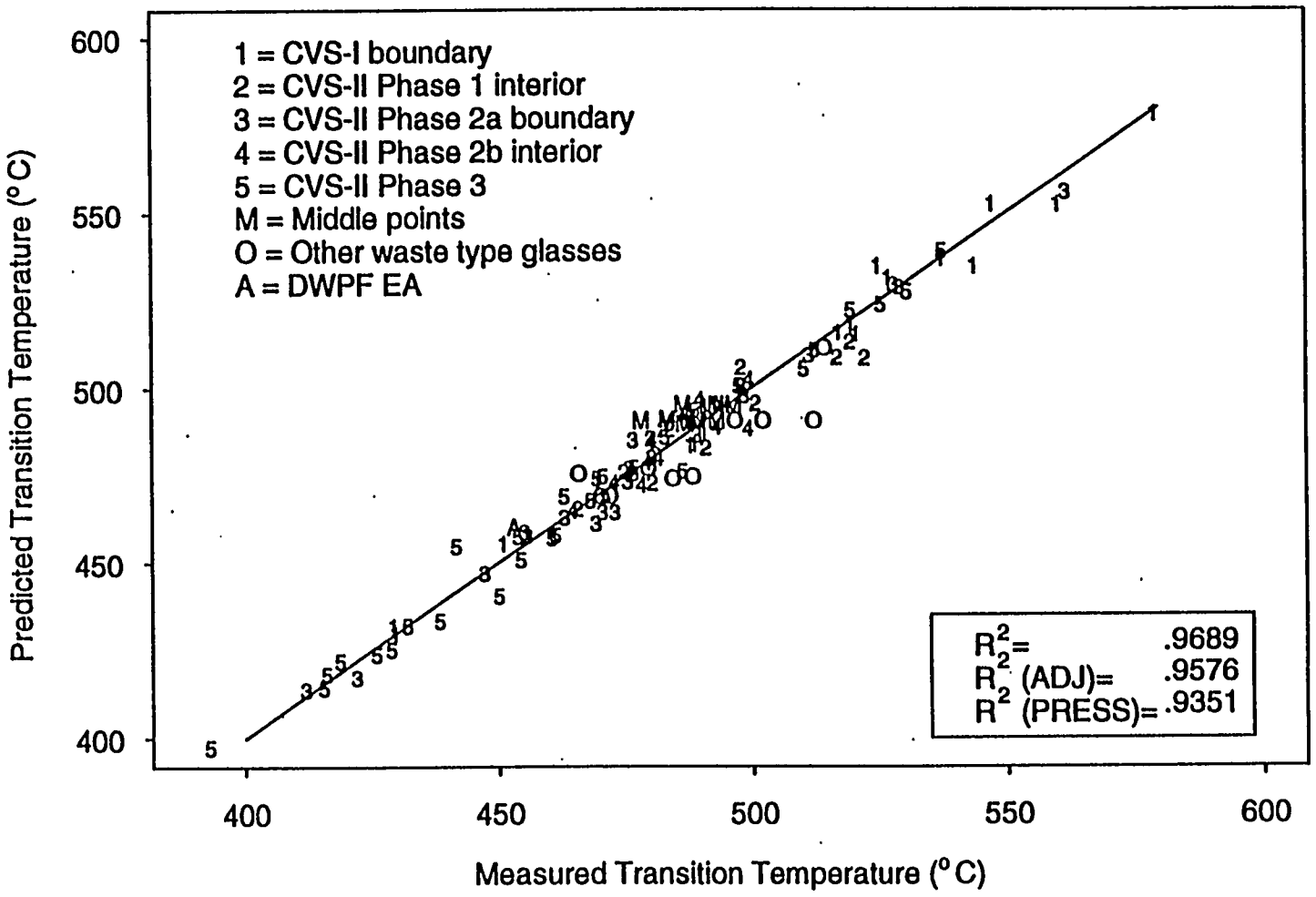

FIGURE 9.3. Predicted Versus Measured Glass Transition Temperature Values for the Second-Order Mixture Model #3 (from Table 9.3)

TABLE 9.4. First-Order Model and Three Candidate Second-Order Models Using Mass Fractions for Glass Transition Temperature Fitted to CVS-I and CVS-II Phase 1 and 2 Data[a]

First-Order Model		Three Candidate Second-Order Models					
		Model #1 (b)		Model #2		Model #3	
Terms	Coefficients	Terms	Coefficients	Terms	Coefficients	Terms	Coefficients
SiO2	627.927	SiO2	695.3893	SiO2	710.5035	SiO2	759.4372
B2O3	587.337	B2O3	1019.9283	B2O3	1126.7776	B2O3	1866.1371
Na2O	99.293	Na2O	-493.1412	Na2O	40.0712	Na2O	-58.6564
Li2O	-651.517	Li2O	-622.7228	Li2O	-705.7846	Li2O	-871.4920
CaO	630.344	CaO	1036.1026	CaO	466.4503	CaO	420.4993
MgO	525.403	MgO	203.0699	MgO	140.3864	MgO	356.3342
Fe2O3	457.179	Fe2O3	207.6430	Fe2O3	303.2076	Fe2O3	1566.5207
Al2O3	541.898	Al2O3	429.8970	Al2O3	389.7121	Al2O3	317.3691
ZrO2	755.760	ZrO2	661.7883	ZrO2	620,8412	ZrO2	533.4529
Others	366.096	Others	363.6871	Others	307.6615	Others	166.2236
		SiO2 x B2O3	-1088.1965	SiO2 x B2O3	-1093.0486	SiO2 x B2O3	-2059.2409
		SiO2 x Na2O	820.6809	B2O3 x Fe2O3	-1299.4416	SiO2 x Fe2O3	-2038.4574
		SiO2 x CaO	-937.2530	CaO x Fe2O3	2122.8726	B2O3 x Fe2O3	-2889.0687
		B2O3 x Na2O	1333.5071	MgO x Fe2O3	4177.9120	B2O3 x B2O3	-1279.3962
		B2O3 x Fe2O3	-1008.8133	MgO x Al2O3	2139.2115		
		Na2O x Fe2O3	1329.3493				
		CaO x Fe2O3	1621.2413				
		MgO x Fe2O3	4229.2039				
		MgO x Al2O3	2529.1344				
R^2	= .8754	R^2	= .9559	R^2	= .9415	R^2	= .9323
R^2(ADJ)	= .8592	R^2(ADJ)	= .9426	R^2(ADJ)	= .9287	R^2(ADJ)	= .9187
R^2(PRESS)	= .8189	R^2(PRESS)	= .9246	R^2(PRESS)	= .9037	R^2(PRESS)	= .8869
LOF?[b]	Yes (>99%)[c]		Yes (98.7%)[c]		Yes (99.9%)[c]		Yes (99.9%)[c]

(a) Glass transition temperature was not measured for the radioactive glasses CVS2-53 and CVS2-54, so they were not used to fit the models.

(b) A statistical F-test for lack-of-fit (LOF) was performed using the estimates of experimental variation obtained from four replicate tests. "Yes" and "No" entries indicate whether the LOF was statistically significant LOF at a 90% confidence level. The actual confidence level at which a LOF can be declared significant is given in parentheses following the "Yes" or "No" for each model.

(c) LOF test used a pooled SD estimate comparable to the one in Table F.4, except only data through CVS-II Phase 2 were used.

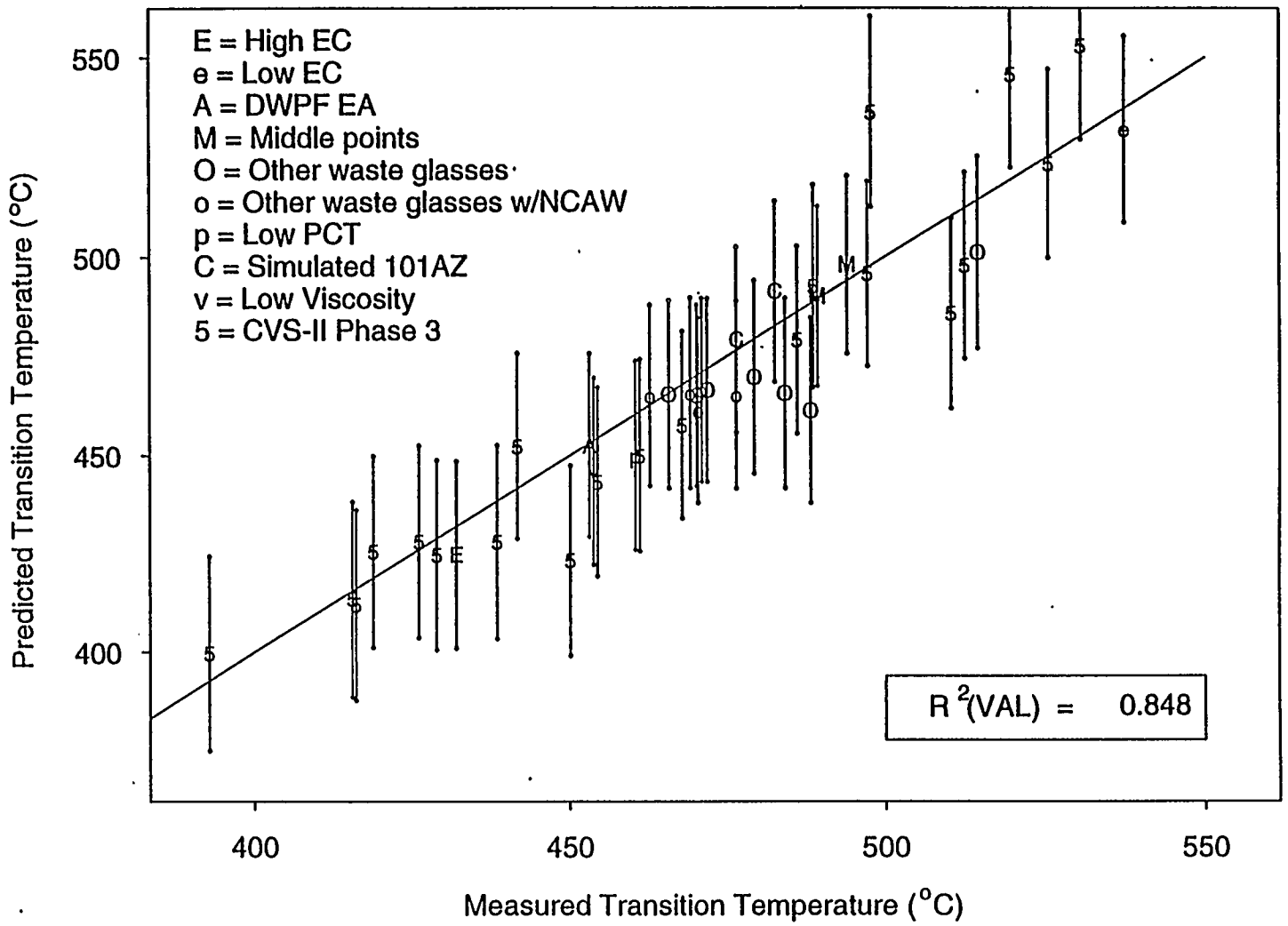

FIGURE 9.4. Predicted Glass Transition Temperature from the First-Order Mixture Model (After CVS-II Phase 2) Versus Measured Glass Transition Temperature (from Table 9.1) for the CVS-II Phase 3 Data

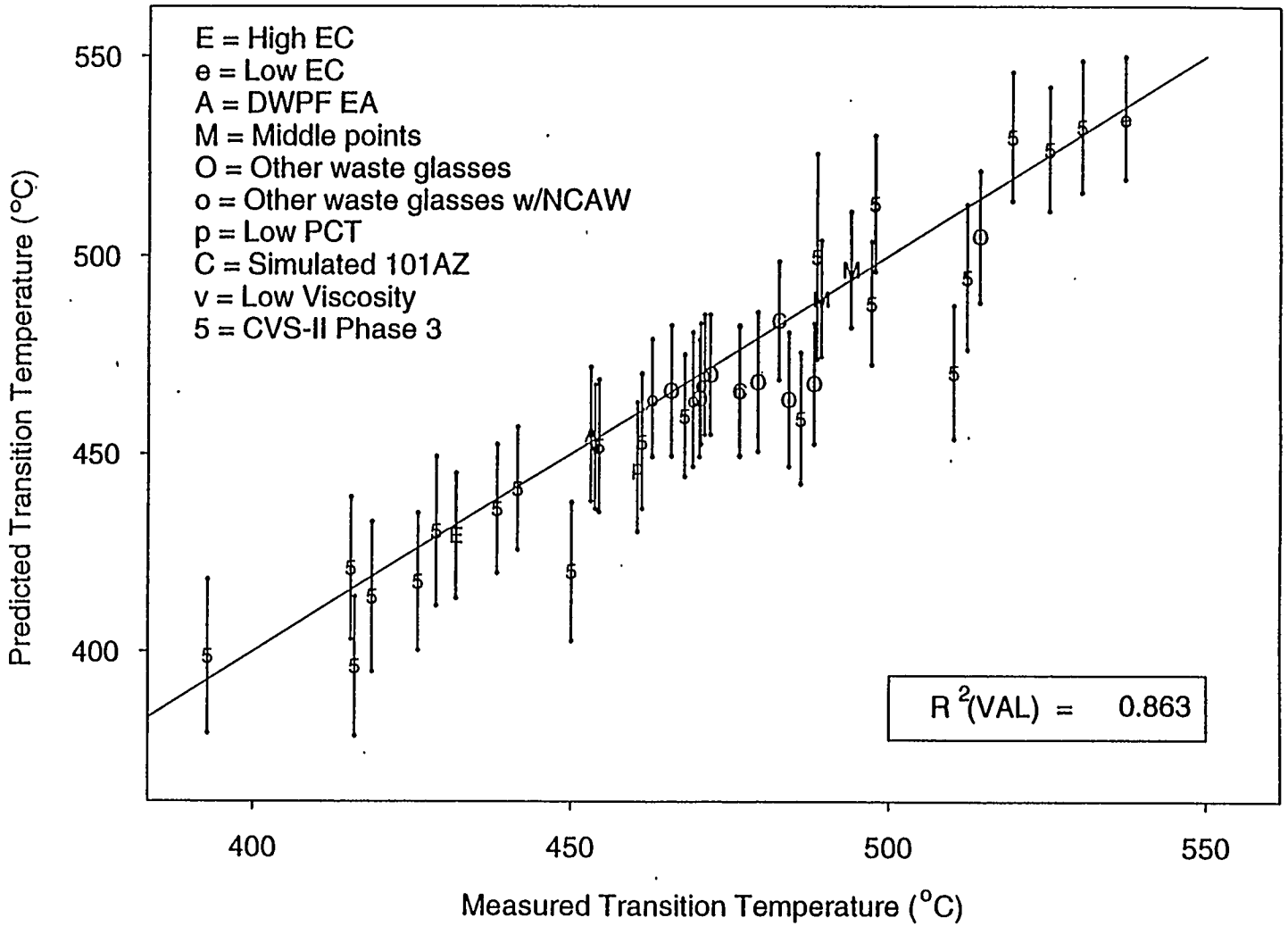

FIGURE 9.5a. Predicted Glass Transition Temperature from the Second-Order Mixture Model #1 (After CVS-II Phase 2) Versus Measured Glass Transition Temperature (from Table 9.1) for the CVS-II Phase 3 Data

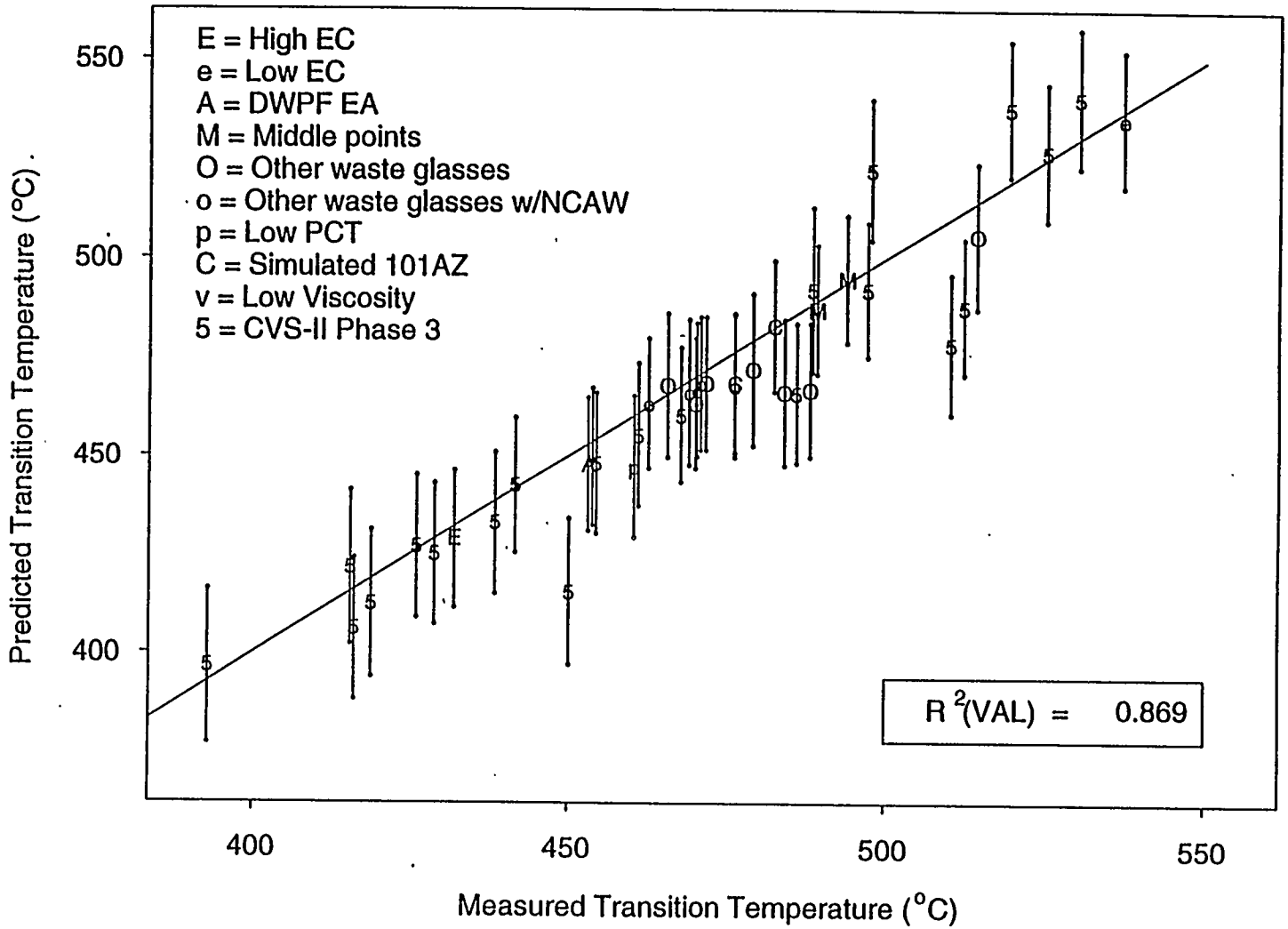

FIGURE 9.5b. Predicted Glass Transition Temperature from the Second-Order Mixture Model #2 (After CVS-II Phase 2) Versus Measured Glass Transition Temperature (from Table 9.1) for the CVS-II Phase 3 Data

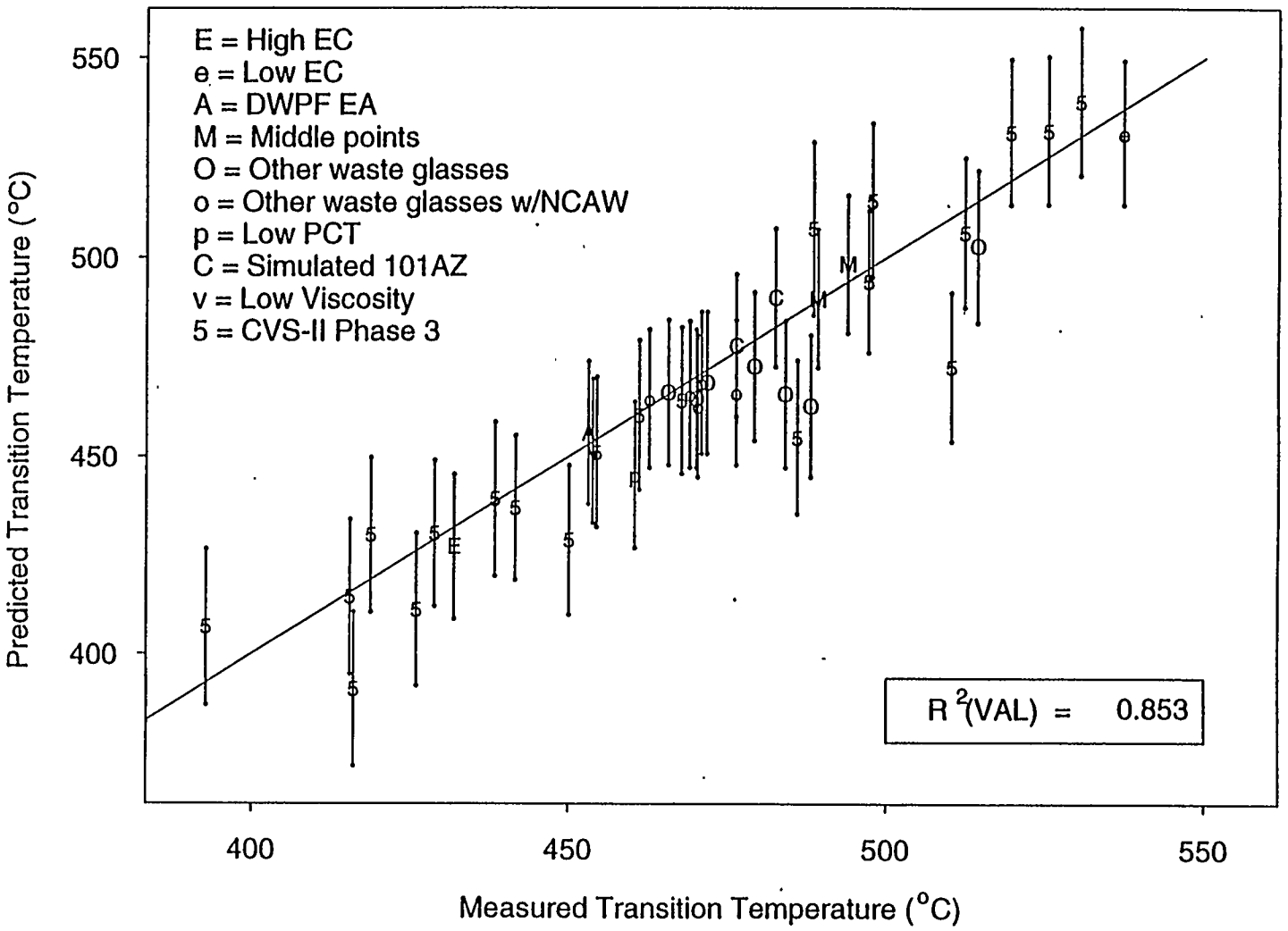

FIGURE 9.5c. Predicted Glass Transition Temperature from the Second-Order Mixture Model #3 (After CVS-II Phase 2) Versus Measured Glass Transition Temperature (from Table 9.1) for the CVS-II Phase 3 Data

points. Points that are not otherwise specifically identified are plotted with a "5" as the plotting symbol.

Figure 9.4 shows that the first-order T_g model is validated for nearly all of the CVS-II Phase 3 data points. No bias in predicted values is apparent for the CVS-II Phase 3 data.

Figures 9.5a, 9.5b, and 9.5c show that the three candidate second-order models are also validated reasonably well for the CVS-II Phase 3 data, in spite of smaller prediction uncertainties than with the first-order model. Overlaying Figures 9.5a, 9.5b, and 9.5c on Figure 9.4 shows that some predictions from the second-order models are better than those from the first-order model, some are worse, and many are only minimally changed. The R^2(VAL) values (see Section 6.1.6) for the three second-order T_g models are close to the R^2(VAL) for the first-order T_g model. These results suggest that the second-order models do not provide any better predictive performance than the first-order model, at least for the CVS-II Phase 3 data. It should be recalled that the CVS-II Phase 3 data is not an ideal validation data set, since it is not uniformly spread over the full CVS composition region. Part of the goal of CVS-II Phase 3 was to collect data for more extreme compositions and property values than had been obtained previously. The more extreme data is a potential reason why the second-order models did not predict any better than the first-order model for these data. However, the fact that the first-order model yielded R^2(VAL) = 0.848 in spite of these aspects of the CVS-II Phase 3 data indicates that it is a fairly good model.

9.4.2 Validation with Historical Database

The historical database gathered for purposes of validating CVS models is discussed in Appendix G. Although 680 glasses were listed in the database, T_g values could be obtained only 143 glasses. The 143 compositions (in 10-component CVS form) and the corresponding T_g values are given in Table G.5 of Appendix G. The T_g values for these 143 glasses ranged from approximately 280 to 690°C. By comparison, the 124 CVS-I and CVS-II Phase 1, 2, and 3 glasses had T_g values ranging from approximately 410 to 580°C. All but 16 of the 143 historical glass T_g values are in this range.

Investigation of the 143 glass compositions for which T_g values were obtained showed that only 28 of them were within slightly expanded versions of the lower and upper component bounds given in Table 4.2 (which defines the region of compositions studied in CVS). However, it was decided to proceed with validation using all 143 data points, and investigate whether the performance of the first- and second-order T_g models from Table 9.4 depended on whether or not glass compositions were within the CVS region.

Figure 9.6 contains the plot of first-order model predicted versus measured T_g values for all 143 data points. Figures 9.7a, 9.7b, and 9.7c contain similar plots for the three candidate second-order T_g models. Error bars consisting of 95% prediction intervals on the predicted values are included in each plot.

Figure 9.6 shows that the first-order model tends to underpredict T_g values above approximately 500°C, and overpredict below approximately 350-400°C. The plot and the low $R^2(VAL) = 0.3871$ value indicate that the first-order model does not predict well for this data. Figures 9.7a, 9.7b, and 9.7c show that the second-order models do not predict any better (and possibly worse) than the first-order model. The second-order models result in several points located far from the 45° line, which causes the $R^2(VAL)$ values to be lower than for the first-order model. The poor predictive performance of the first- and second-order models is likely due to the fact that 115 of the 143 glasses are outside the CVS composition experimental region, and thus the model predictions are extrapolations.

Figure 9.8 is a different version of Figure 9.6, without the error bars, and with the number of relaxed CVS single-component constraints that are satisfied (out of the 10 CVS components, see Table G.2 of Appendix G) used as the plotting symbol for each glass. Figure 9.8 shows that many of the 143 data points only satisfy four to nine of the component constraints.

Figure 9.9 contains the plot of first-order model predicted versus measured T_g values for the 28 data points within the relaxed set of CVS single component constraints (see Table G.2 of Appendix G). Figures 9.10a, 9.10b, and 9.10c contain similar plots for the three candidate second-order T_g

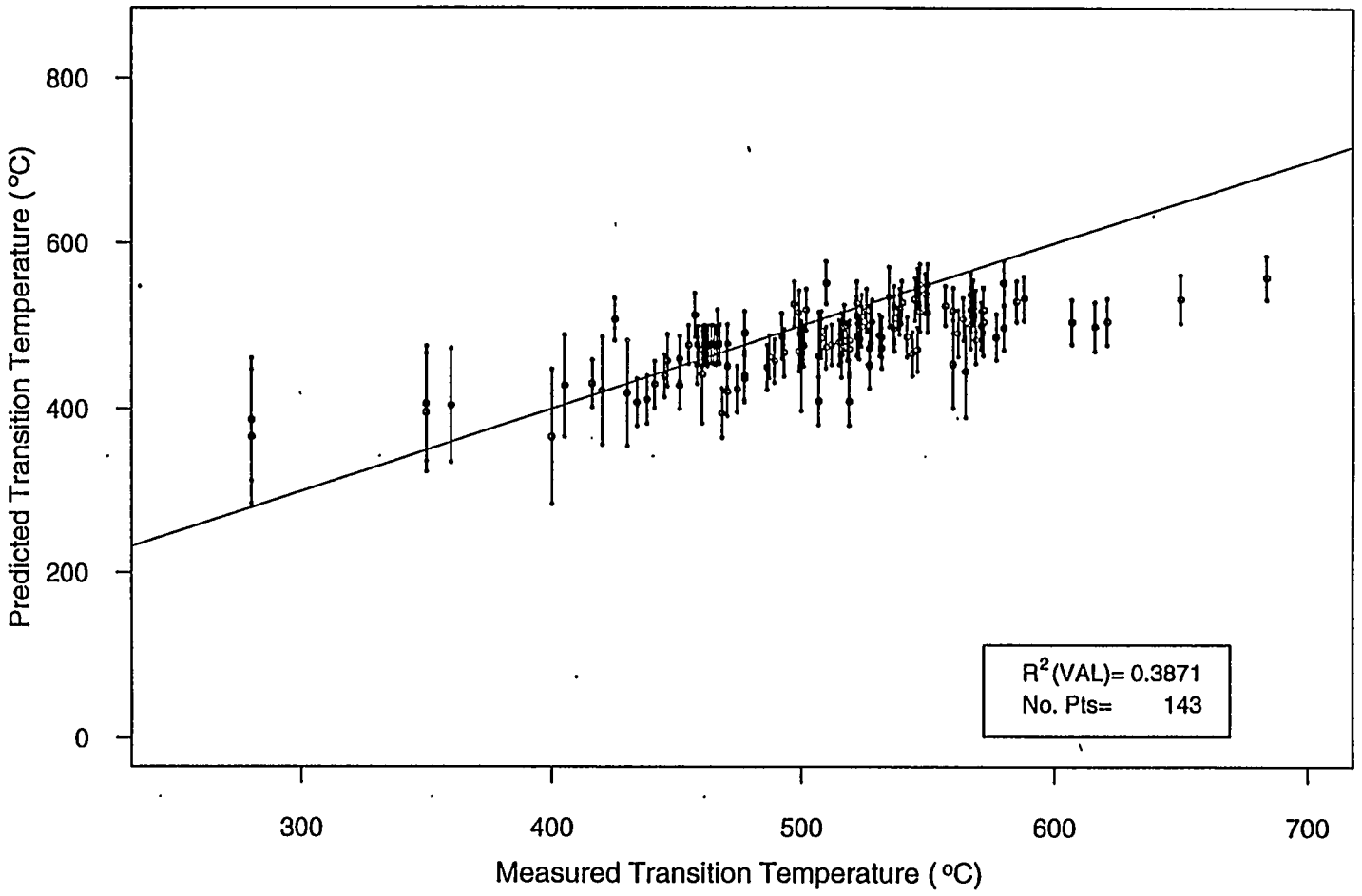

FIGURE 9.6. Predicted Transition Temperature from the First-Order Mixture Model (After CVS-II Phase 2) Versus Measured Transition Temperature for 143 Historical Data Points (115 of Which are Outside the CVS Composition Region)

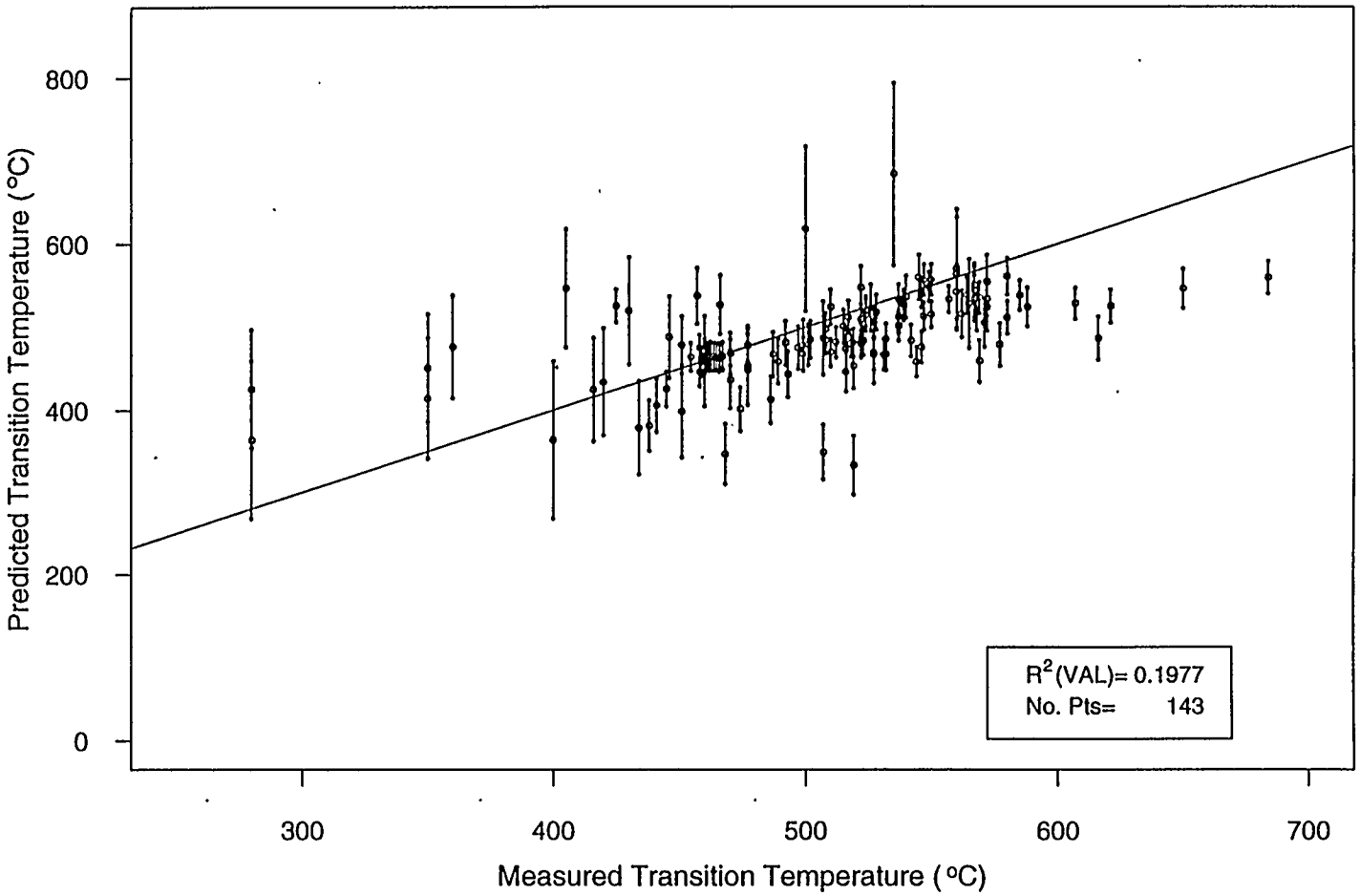

FIGURE 9.7a. Predicted Transition Temperature from the Second-Order Mixture Model #1 (After CVS-II Phase 2) Versus Measured Transition Temperature for 143 Historical Data Points (115 of Which are Outside the CVS Composition Region)

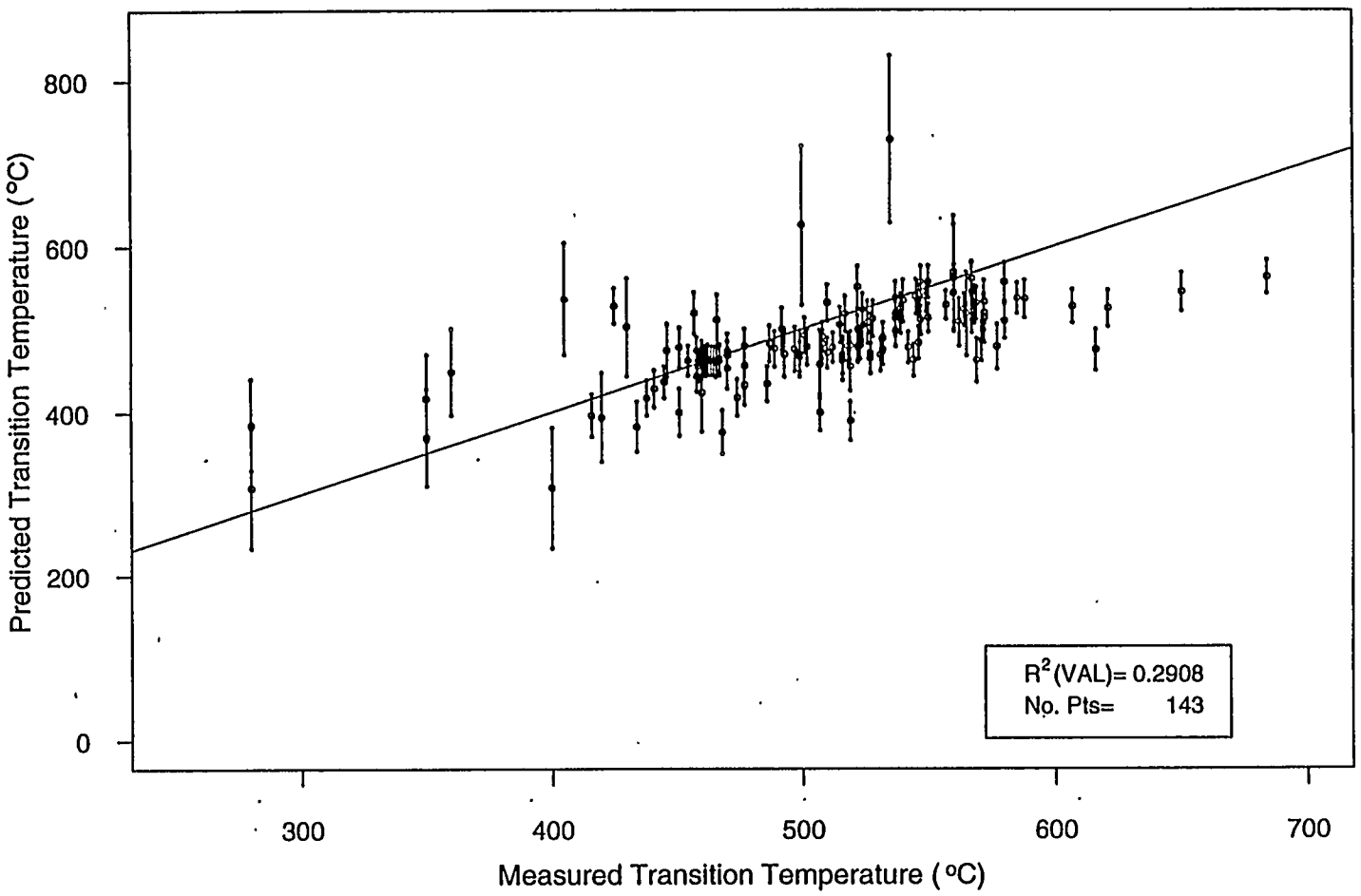

FIGURE 9.7b. Predicted Transition Temperature from the Second-Order Mixture Model #2 (After CVS-II Phase 2) Versus Measured Transition Temperature for 143 Historical Data Points (115 of Which are Outside the CVS Composition Region)

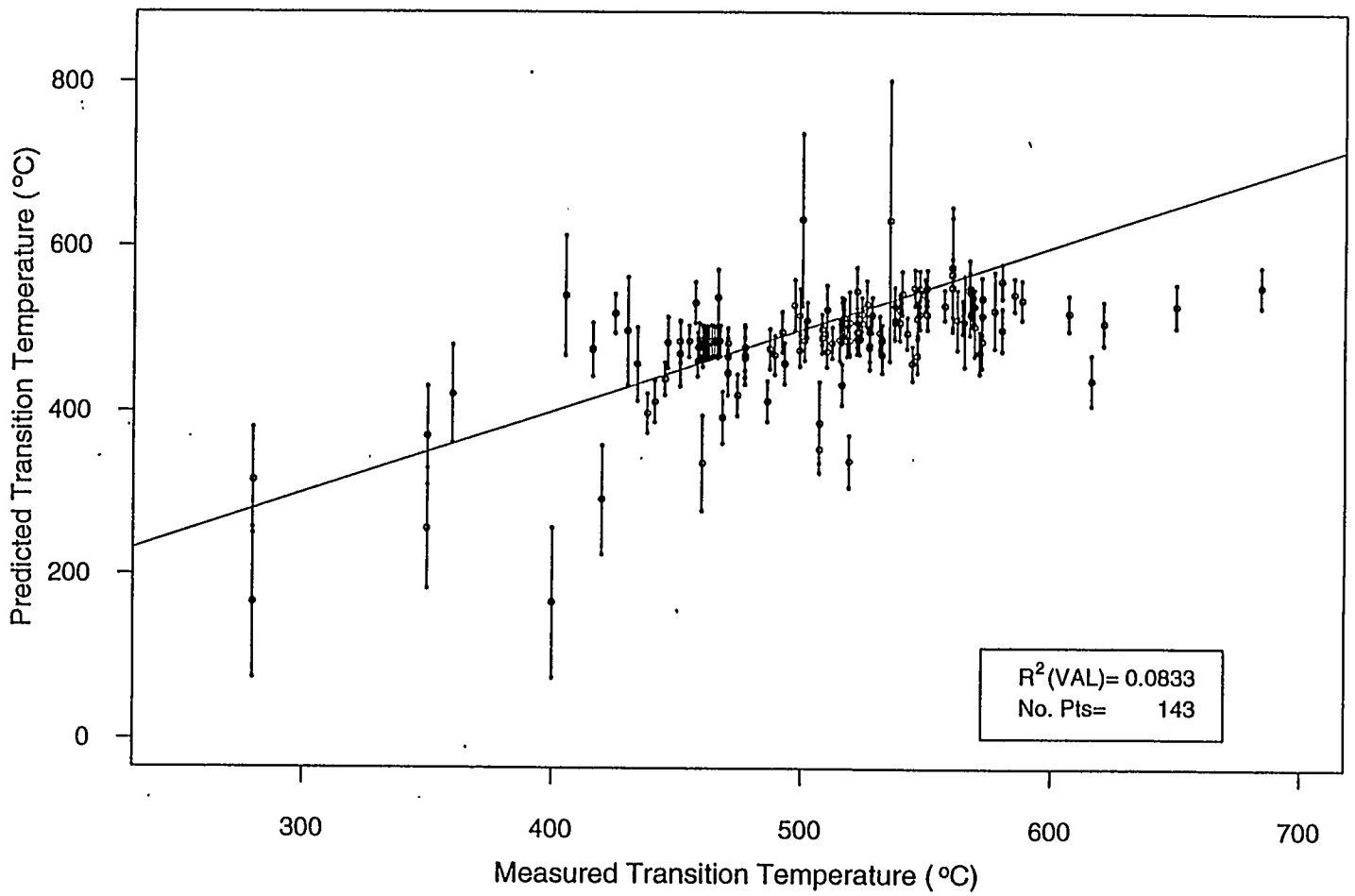

FIGURE 9.7c. Predicted Transition Temperature from the Second-Order Mixture Model #3 (After CVS-II Phase 2) Versus Measured Transition Temperature for 143 Historical Data Points (115 of Which are Outside the CVS Composition Region)

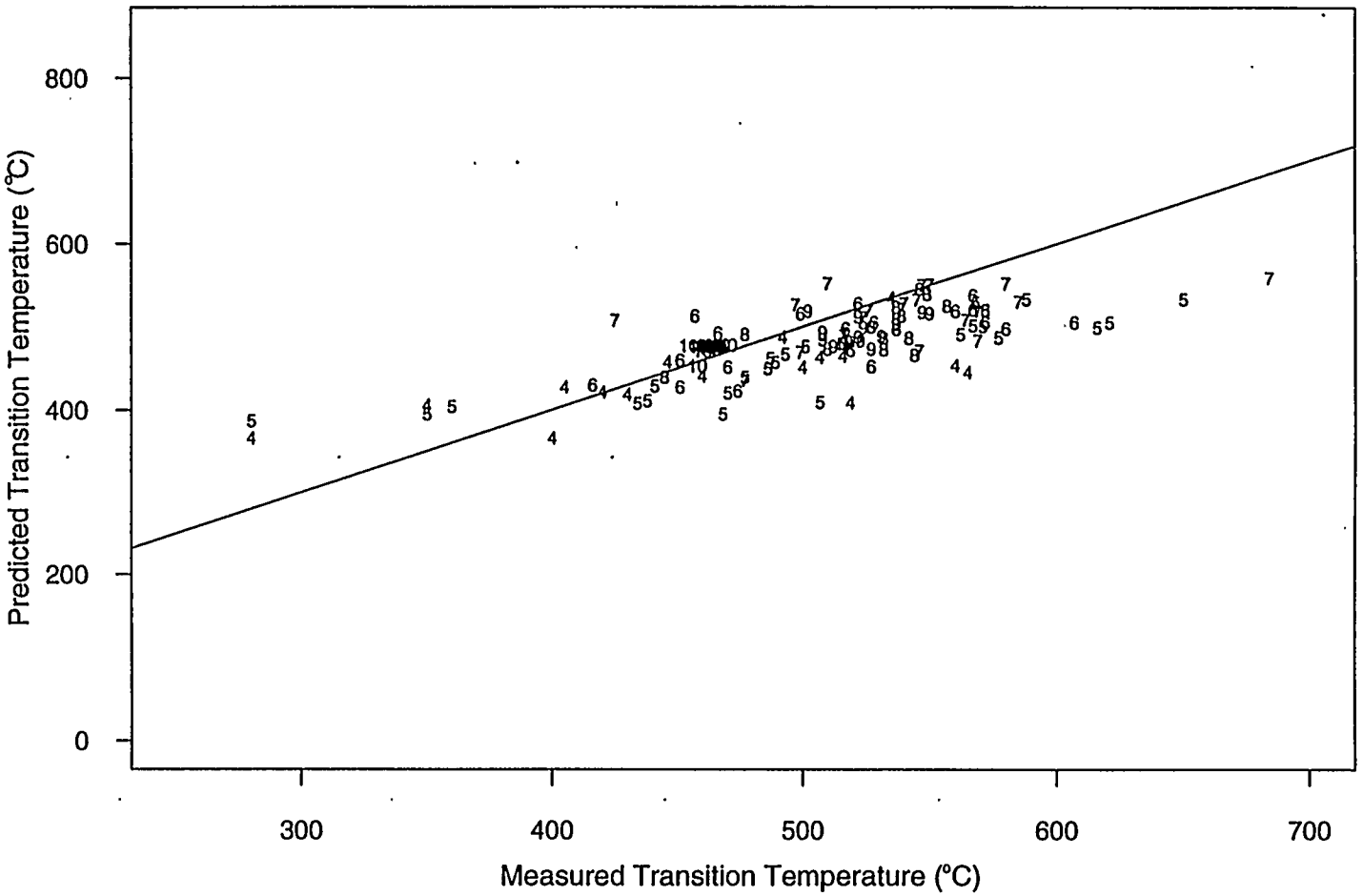

FIGURE 9.8. Predicted Transition Temperature from the First-Order Mixture Model (After CVS-II Phase 2) Versus Measured Transition Temperature for the Historical Data, With the Number of Relaxed Component Constraints Satisfied Used as the Plotting Symbol

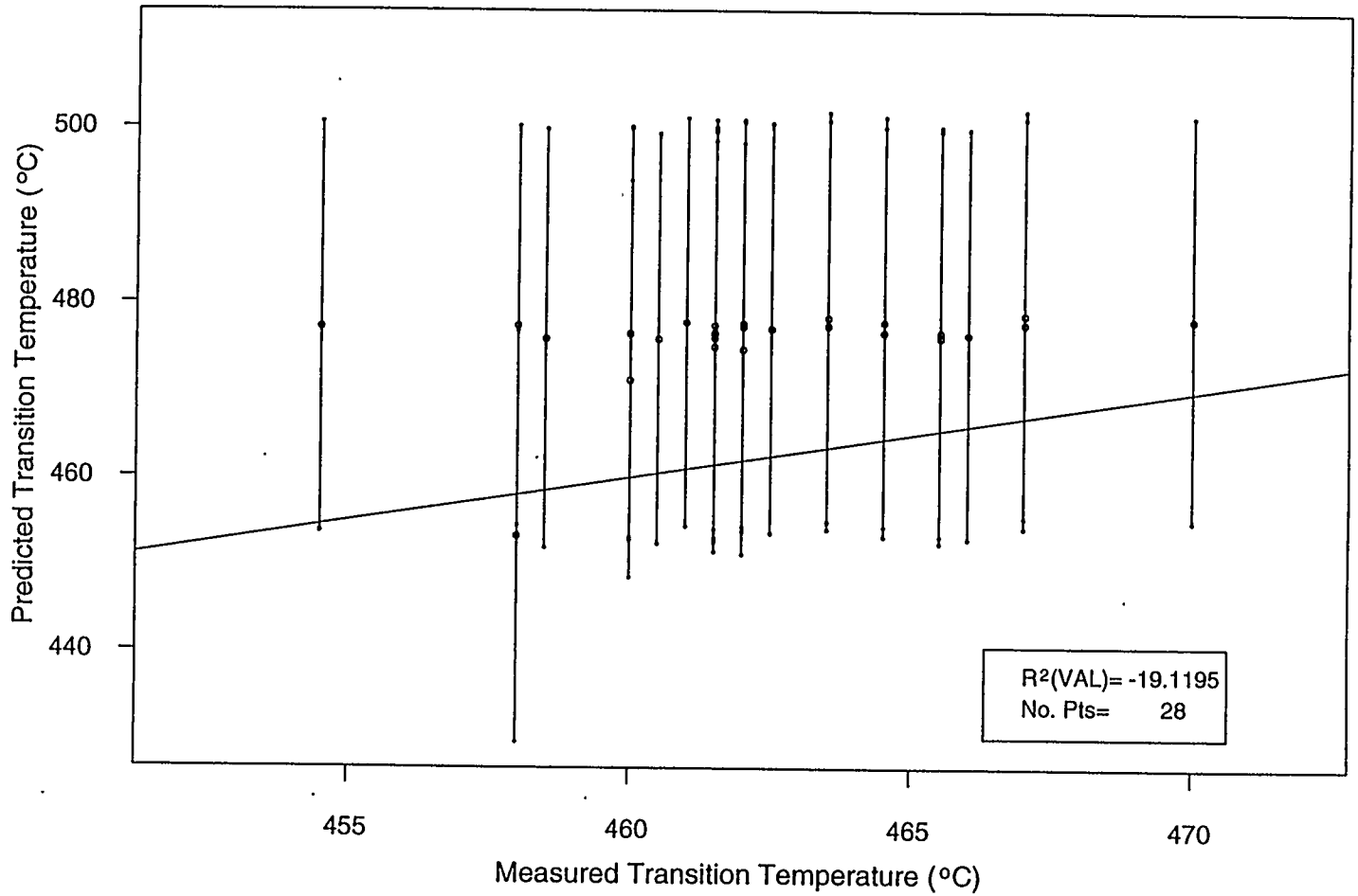

FIGURE 9.9. Predicted Transition Temperature from the First-Order Mixture Model (After CVS-II Phase 2) Versus Measured Transition Temperature for 28 of the 143 Historical Data Points Within Relaxed CVS Single-Component Constraints

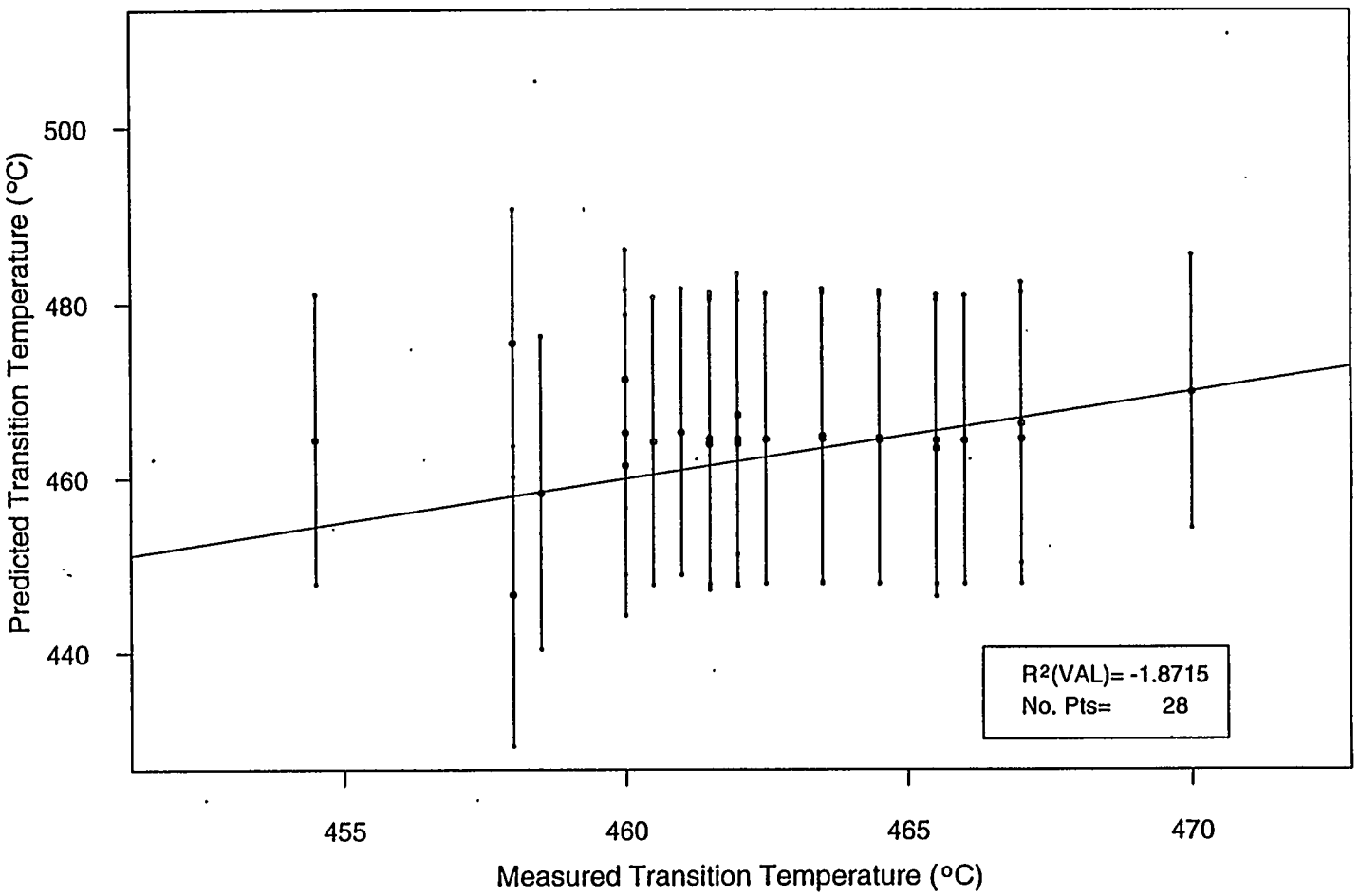

FIGURE 9.10a. Predicted Transition Temperature from the Second-Order Mixture Model #1 (After CVS-II Phase 2) Versus Measured Transition Temperature for 28 of the 143 Historical Data Points Within Relaxed CVS Single-Component Constraints

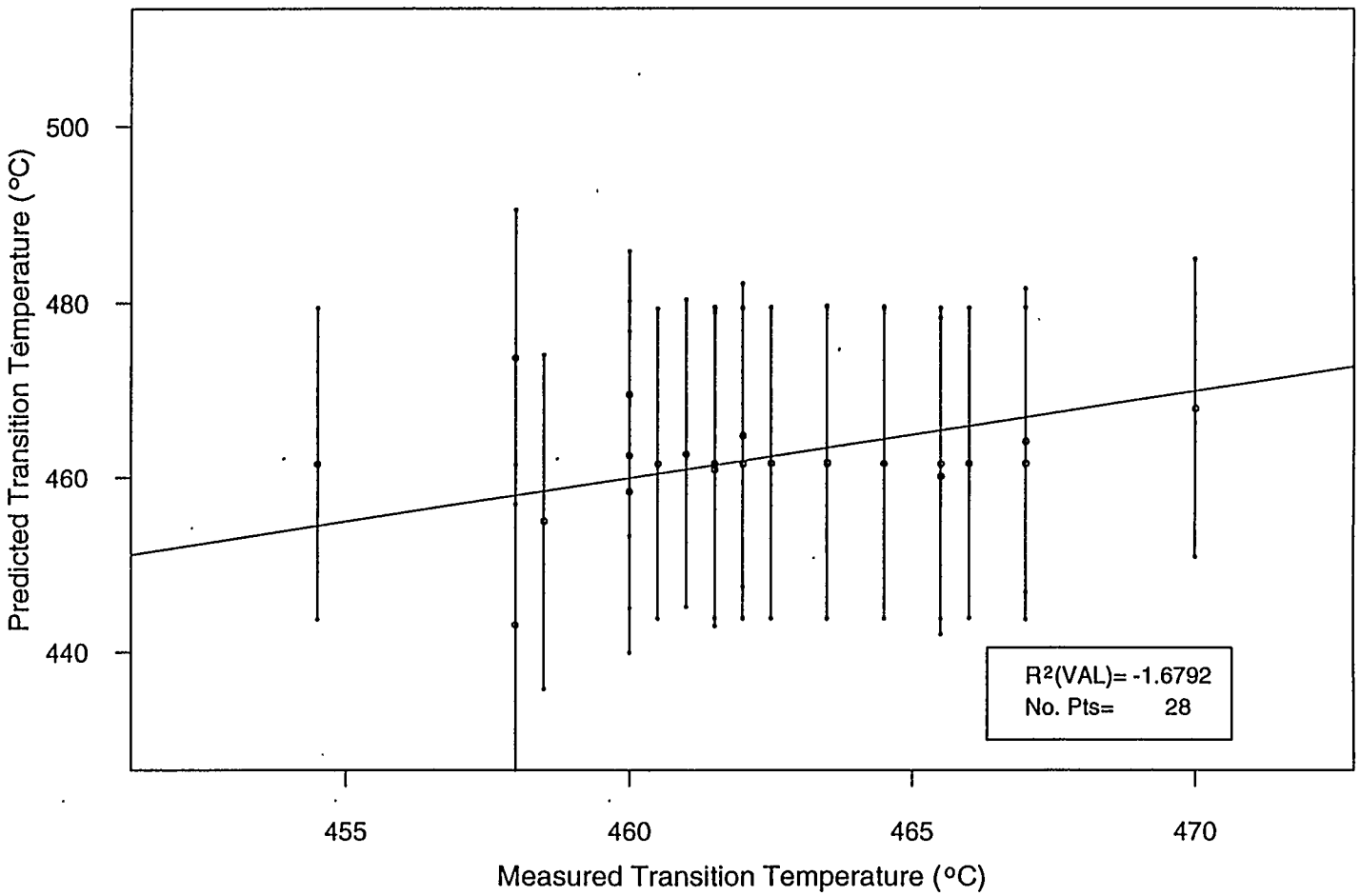

FIGURE 9.10b. Predicted Transition Temperature from the Second-Order Mixture Model #2 (After CVS-II Phase 2) Versus Measured Transition Temperature for 28 of the 143 Historical Data Points Within Relaxed CVS Single-Component Constraints

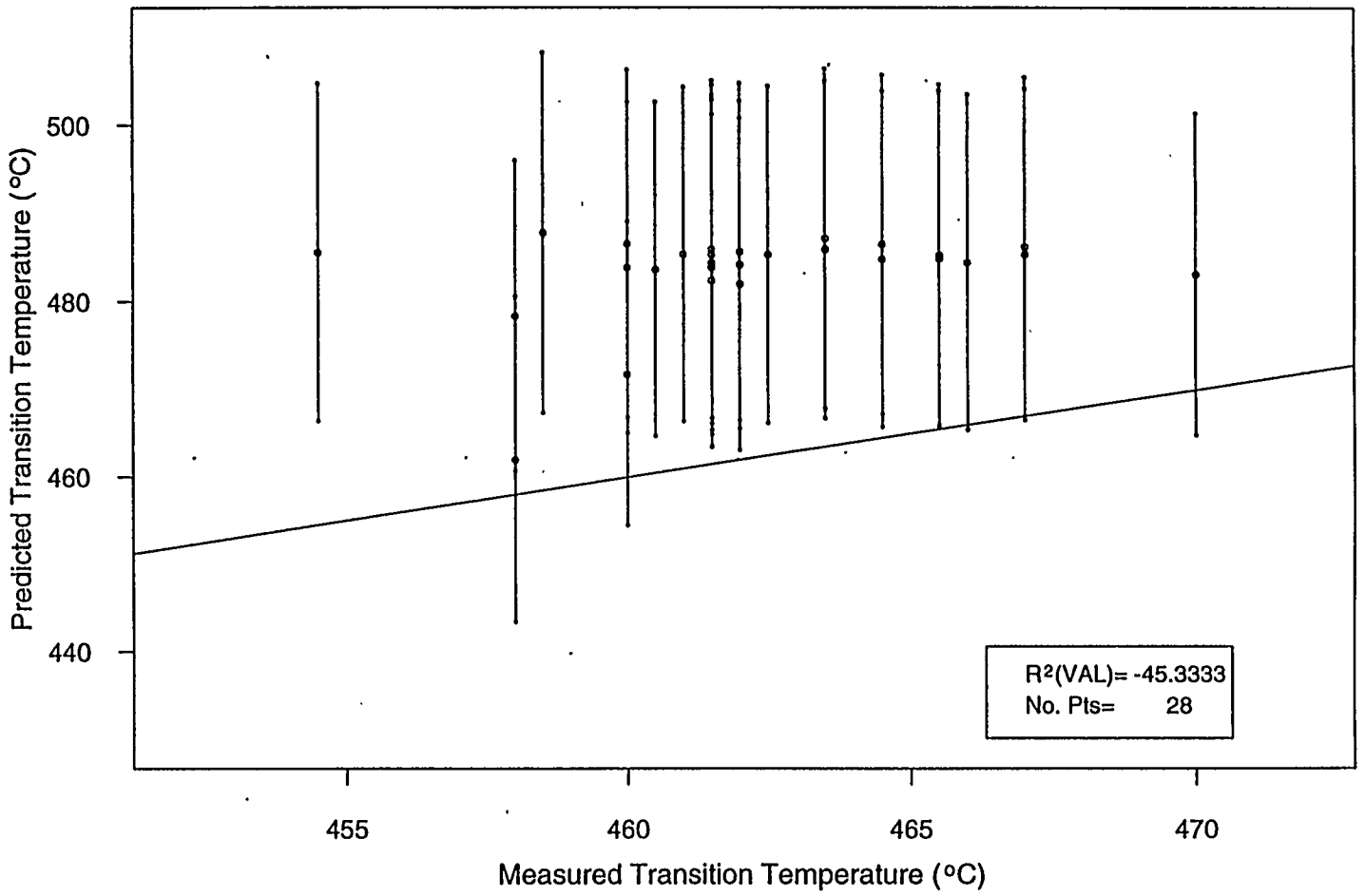

FIGURE 9.10c. Predicted Transition Temperature from the Second-Order Mixture Model #3 (After CVS-II Phase 2) Versus Measured Transition Temperature for 28 of the 143 Historical Data Points Within Relaxed CVS Single-Component Constraints

models. The first-order model (Figure 9.9) and second-order model #3 (Figure 9.10c) show a tendency to overpredict T_g. All four models/plots yield similar predicted values for most of the 28 points, which is partially due to the fact that 22 of the 28 points are essentially the same composition, and the variability in measured values probably is mainly measurement uncertainty. The error bars (95% prediction intervals) overlap the 45° line for all or nearly all points in Figures 9.9, 9.10a, and 9.10b, indicating that the corresponding models are validated for these data. However, this is not the case for second-order model #3 (Figure 9.10c), where only a few points have 95% prediction intervals that overlap the 45° line. Overall, selected first- and second-order models perform reasonably well for the small set of 28 points falling within or close to the CVS composition region over which the models were developed, but the 28 points occur in only a very small part of the CVS region. This fact and the resulting small range in measured T_g values caused the R^2(VAL) values to be negative, as shown in Figures 9.9 and 9.10a, 9.10b, and 9.10c. All in all, the historical data set was not representative of the CVS composition region, and did not prove very useful in validating the CVS models.

9.4.3 Summary of Transition Temperature Model Validation

The validation work discussed previously, using the CVS-II Phase 3 and historical data sets, focused on validating first- and second-order glass transition temperature models developed from data up through CVS-II Phase 2 as presented in Table 9.4. Neither of these data sets were ideal validation data sets, because they do not evenly cover the CVS composition experimental region. However, the CVS-II Phase 3 data set indicated that the first-order model provides reasonably good predictive performance inside the CVS region. The second-order models did not seem to improve the predictive ability inside the CVS region. The ability of the first- and second-order models to predict outside the CVS region was not particularly good, at least for the historical data set used. Thus, the empirical mixture modeling approach appears to show promise for predicting glass transition temperature inside (but possibly not outside) the CVS composition region.

The first- and second-order transition temperature models presented in Tables 9.2 and 9.3 of this report could be validated using the historical data, the CVS-II Phase 4 data, and any other data that subsequently becomes available. The models included in this report and the CVS-II Phase 4 data were not completed in time to enable validating them and reporting on it here.

9.5 GLASS TRANSITION TEMPERATURE DISCUSSION

Because glass transition temperature is strongly decreased by Li_2O and Na_2O the crystallization range of glasses with high Li_2O or Na_2O concentrations is expected to be extended to lower temperatures. Such a lower temperature limit for glass crystallization may enhance the precipitation of crystalline phases during cooling, but cannot produce crystallization during storage as long as the glass transition temperature is not exceeded. The WAPS (1993) require that the temperature of the canistered waste form remain below 400°C after initial cooldown. How much crystallinity will precipitate during cooling depends on the rate of crystal growth, which in turn is affected by both thermodynamic and kinetic factors. Only crystallization kinetics studies will provide sufficient evidence regarding the effects of Li_2O and Na_2O on glass crystallization.

Viscosity and glass transition temperature are highly related. The viscosity at the glass transition temperature is approximately $\eta = 10^{11.3}$ Pa·s, and these "data points" for each CVS glass were used in fitting combined Fulcher-mixture models to viscosity at temperature data (see Section 7.1). Short glasses tend to have high T_g values while long glasses have lower T_g (see Chapter 7.7 for discussion of glass length). Longer glasses have lower activation energy to viscous flow [related to the "B" parameter of Eq. (7.1)]. This in general means that the increase in viscosity is less for the same drop in temperature for a longer glass. Hence, a long glass is more fluid at low temperatures and has a lower T_g.

Figure 9.11 shows the relationship between component coefficients of first-order mixture models using mass fractions for T_g and B. The relative magnitudes of the component coefficients for T_g and B give an indication of the effects of the components on these properties. The plot of coefficients

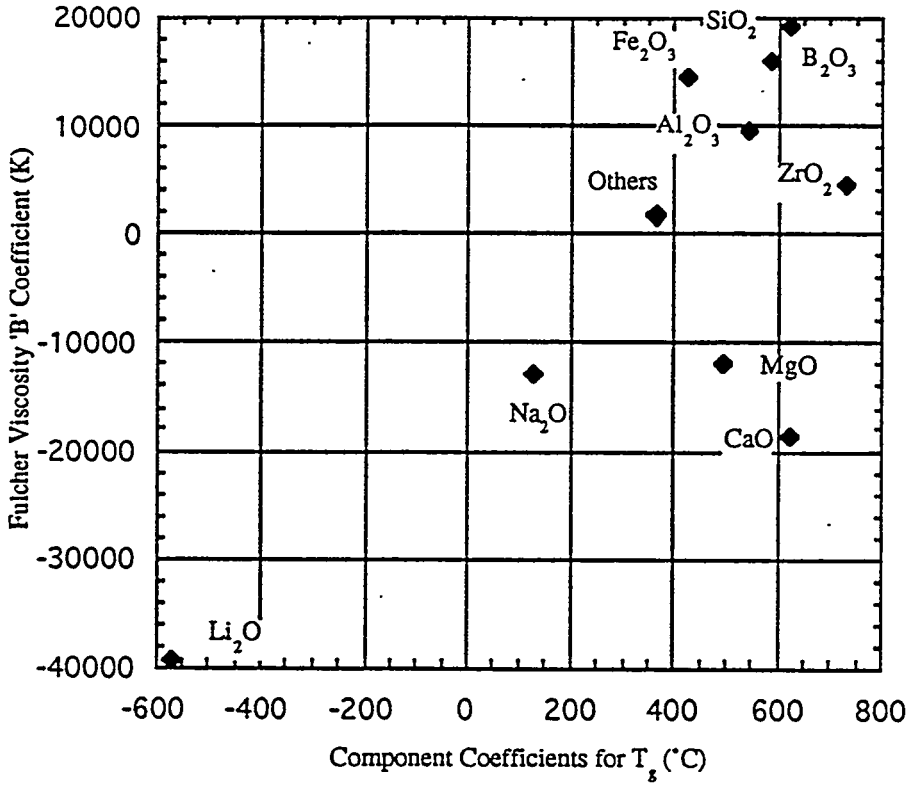

FIGURE 9.11. First-Order Mixture Model Coefficients for T_g (from Table 9.2) Versus Those for "B" from the Fulcher Equation Expressing Viscosity as a Function of Temperature and Glass Composition (from Table 7.1a)

for the two properties displays whether components have similar or different relative effects for the two properties. It is apparent from Figure 9.11 that those components that strongly decrease B (or increase glass length) also strongly decrease T_g.

The Fulcher coefficient T_0 can also be used for judging glass stability against structural changes. T_0 represents the temperature at which viscosity approaches infinity and thus glass becomes purely elastic. T_g characterizes glass transition with respect to volume expansion, whereas T_0 relates to the visco-elastic aspect of glass transition. Thus, T_g and T_0 express different

aspects of glass solidification, and it is interesting to compare them.

In Figure 9.12 the coefficients from the first-order mixture models for T_0 and T_g are plotted versus one another. The relative magnitudes of the component coefficients for T_0 and T_g give an indication of the effects of the components on these properties. The plot of coefficients for the two properties displays whether components have similar or different relative effects for the two properties. Figure 9.12 shows that CaO strongly increases T_0 and moderately increases T_g. Network-forming oxides (B_2O_3, Al_2O_3, SiO_2) reduce T_0 and increase T_g. Finally, ZrO_2 and Li_2O strongly influence T_g (increase and decrease, respectively) and mildly increase T_0.

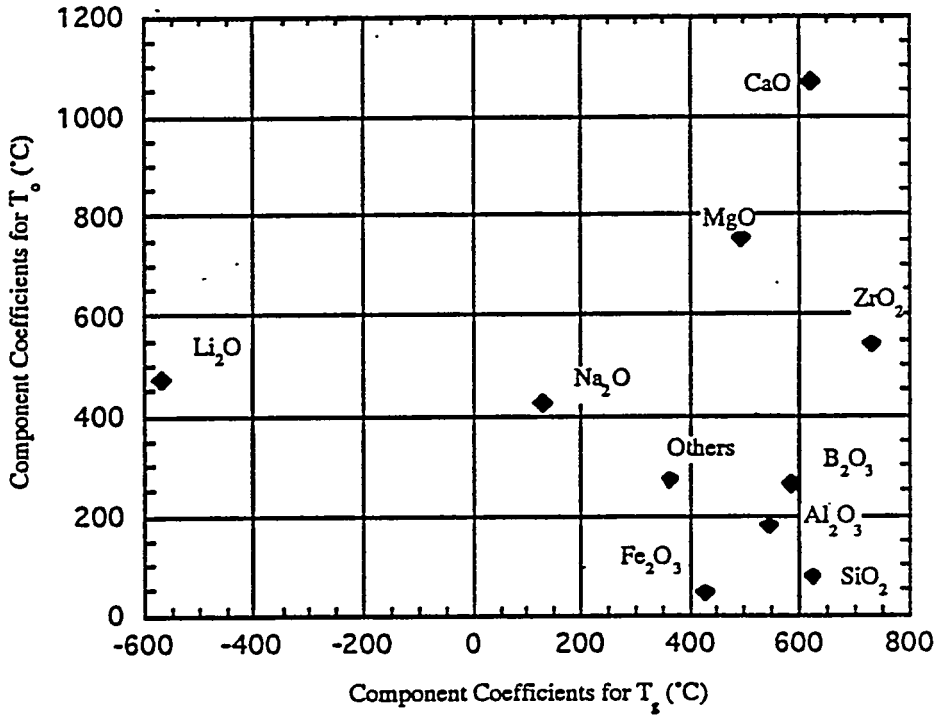

FIGURE 9.12. First-Order Mixture Model Coefficients for T_g (From Table 9.2) Versus Those for T_0 from the Fulcher Equation Expressing Viscosity as a Function of Temperature and Glass Composition (from Table 7.1)

10.0 THERMAL EXPANSION RESULTS AND DISCUSSION

The thermal expansion coefficient data for solid (α_s) and molten (α_m) glass are given in Table 10.1. Values for α_s ranged from 4.7 to 13.8 (10^{-6}/K), while values for α_m ranged from 49.2 to 151.4 (10^{-6}/K). Estimates of uncertainties in the measured α_s and α_m values based on replicate glasses are given in Appendix F.

10.1 FIRST-ORDER MODELS AND COMPONENT EFFECTS FOR THERMAL EXPANSION

First-order mixture models of the form (6.1) using both mass and mole fractions of the oxide components were fitted to the untransformed α_s and α_m values, producing the coefficients given in Table 10.2. The α_s data values for CVS2-7 and CVS2-15 and the α_m data value for CVS2-47 were deemed to be outliers based on initial fits to all the data in Table 10.1. No experimental reasons were found for why these points were outliers, but statistical methods clearly identified them as such. Thus, these data points were not used in fitting first-order models. Also not used were the α_s and α_m values for CVS2-75, which were obviously incorrect. The first-order models, fitted after eliminating the data points previously mentioned, are given in Table 10.2.

For thermal expansion of solid glass, the first-order mixture model evaluation statistics R^2 = 0.8709, R^2(ADJ) = 0.8601, and R^2(PRESS) = 0.8432 for mass fractions and R^2 = 0.8711, R^2(ADJ) = 0.8602, and R^2(PRESS) = 0.8439 for mole fractions indicate that the first-order mixture model fits the data fairly well, but with room for improvement. The similarity of these statistics for the mass and mole fraction versions of the first-order model indicates that neither version fits the data better than the other. The plots of predicted versus measured solid glass coefficient of thermal expansion values in Figure 10.1a (mass fractions) and Figure 10.1b (mole fractions) confirm these observations based on the general scatter about the 45° line. Further, the plots indicate that the first-order mixture model has a tendency to overpredict the lowest α_s values. A statistical test for model lack-of-fit (LOF) (see Section 6.1.5) indicates the α_s first-order mixture model does

TABLE 10.1. Thermal Expansion Coefficient Data for Solid Glass (α_s) and Molten Glass (α_m) for CVS-I and CVS-II Phase 1, 2, and 3 Glasses

Glass [a]	ID[b] #	PS[c]	α_s (10^{-6}/K)	α_m (10^{-6}/K)
CVS1-1 (1)	1	M	8.9	103.0
CVS1-2	2	1	9.4	72.0
CVS1-3	3	1	9.2	111.3
CVS1-4 (2)	4	1	6.9	69.7
CVS1-5	5	1	9.1	103.5
CVS1-6	6	1	8.6	96.5
CVS1-7	7	1	8.0	60.7
CVS1-8 (3)	8	1	8.1	79.8
CVS1-9	9	1	6.6	82.8
CVS1-10	10	1	6.6	53.7
CVS1-11	11	1	8.5	57.1
CVS1-12	12	1	10.3	132.3
CVS1-13	13	1	10.0	120.4
CVS1-14	14	1	9.4	95.1
CVS1-15	15	1	10.6	96.1
CVS1-16	16	1	10.9	58.6
CVS1-17	17	1	11.1	117.8
CVS1-18	18	1	12.4	75.7
CVS1-19 (1)	19	M	8.3	87.8
CVS1-20 (1)	20	M	9.5	91.6
CVS1-21 (2)	21	1	5.6	101.0
CVS1-22 (3)	22	1	7.1	49.2
CVS1-23	23	M	9.1	123.0
CVS2-1	24	2	8.8	114.2
CVS2-2	25	2	8.9	81.6
CVS2-3	26	2	9.1	81.5
CVS2-4	27	2	8.4	89.3
CVS2-5	28	2	7.9	59.3
CVS2-6	29	2	8.8	108.2
CVS2-7	30	2	11.2	88.4
CVS2-8	31	2	10.3	120.9
CVS2-9	32	2	9.0	83.3
CVS2-10	33	2	7.9	74.2

(a) The numbers in parentheses represent replicate sets of glasses.

(b) ID# is a consecutive integer numbering of all CVS glasses.

(c) PS is the plotting symbol used in plots associated with this data: 1 = CVS-I boundary, 2 = CVS-II Phase 1 interior, 3 = CVS-II Phase 2a boundary, 4 = CVS-II Phase 2b interior, 5 = CVS-II Phase 3 boundary, M = middle compositions, O = other than NCAW waste glasses, A = EA glass.

TABLE 10.1. Thermal Expansion Coefficient Data for Solid Glass (α_s) and Molten Glass (α_m) for CVS-I and CVS-II Phase 1, 2, and 3 Glasses (continued)

Glass [a]	ID[b] #	PS[c]	α_s (10^{-6}/K)	α_m (10^{-6}/K)
CVS2-11	34	2	9.5	83.7
CVS2-12	35	2	8.3	99.0
CVS2-13	36	2	10.7	77.8
CVS2-14	37	2	9.6	78.3
CVS2-15	38	2	8.3	88.1
CVS2-16 (4)	39	M	9.0	98.0
CVS2-17 (1)	40	M	8.6	97.7
CVS2-18 (4)	41	M	9.4	88.1
CVS2-19 (5)	42	M	9.8	99.3
CVS2-20	43	3	9.23	52.8
CVS2-21	44	3	8.38	93.2
CVS2-22	45	3	9.65	106.2
CVS2-23	46	3	11.32	68.8
CVS2-24	47	3	8.83	86.8
CVS2-25	48	3	10.95	107.0
CVS2-26	49	3	7.98	108.0
CVS2-27	50	3	10.99	69.1
CVS2-28	51	3	11.38	64.0
CVS2-29	52	3	6.28	94.3
CVS2-30	53	3	6.38	96.4
CVS2-31	54	3	6.52	72.4
CVS2-32	55	3	10.76	61.5
CVS2-33	56	3	12.19	72.4
CVS2-34 (6)	57	3	11.04	84.9
CVS2-35	58	3	13.13	60.1
CVS2-36	59	3	10.27	149.3
CVS2-37	60	3	10.59	63.0
CVS2-38	61	3	7.69	98.4
CVS2-39	62	3	11.83	81.8
CVS2-40	63	4	10.82	71.3
CVS2-41	64	4	9.15	97.8
CVS2-42	65	4	8.85	96.7
CVS2-43	66	4	8.23	92.8

(a) The numbers in parentheses represent replicate sets of glasses.

(b) ID# is a consecutive integer-numbering of all CVS glasses.

(c) PS is the plotting symbol used in plots associated with this data: 1 = CVS-I boundary, 2 = CVS-II Phase 1 interior, 3 = CVS-II Phase 2a boundary, 4 = CVS-II Phase 2b interior, 5 = CVS-II Phase 3 boundary, M = middle compositions, O = other than NCAW waste glasses, A = EA glass.

TABLE 10.1. Thermal Expansion Coefficient Data for Solid Glass (α_s) and Molten Glass (α_m) for CVS-I and CVS-II Phase 1, 2, and 3 Glasses (continued)

Glass [a]	ID[b] #	PS[c]	α_s (10^{-6}/K)	α_m (10^{-6}/K)
CVS2-44	67	4	8.41	78.4
CVS2-45	68	4	8.20	101.4
CVS2-46	69	4	7.09	82.3
CVS2-47	70	4	10.32	151.4
CVS2-48	71	4	8.70	99.7
CVS2-49	72	4	8.81	98.0
CVS2-50 (1)	73	M	8.72	80.6
CVS2-51 (5)	74	M	9.39	94.2
CVS2-52	75	4	8.39	91.8
CVS2-53	76	4	(d)	(d)
CVS2-54	77	M	(d)	(d)
CVS2-55	78	0	8.73	85.8
CVS2-56	79	0	9.05	98.9
CVS2-57	80	0	8.95	87.6
CVS2-58	81	4	7.98	96.7
CVS2-59	82	5	10.5	86.1
CVS2-60	83	5	9.7	71.8
CVS2-61	84	5	10.6	62.7
CVS2-62	85	5	8.0	112.3
CVS2-63	86	5	12.5	62.9
CVS2-64	87	0	10.0	80.9
CVS2-65	88	0	9.4	68.5
CVS2-66	89	0	8.8	79.3
CVS2-67	90	0	8.0	60.6
CVS2-68	91	0	7.7	74.0
CVS2-69	92	0	8.9	65.2
CVS2-70	93	0	8.4	94.0
CVS2-71	94	5	8.7	97.1
CVS2-72	95	5	8.4	76.3
CVS2-73	96	5	8.3	71.7
CVS2-74	97	5	8.8	83.3

(a) The numbers in parentheses represent replicate sets of glasses.

(b) ID# is a consecutive integer numbering of all CVS glasses.

(c) PS is the plotting symbol used in plots associated with this data: 1 = CVS-I boundary, 2 = CVS-II Phase 1 interior, 3 = CVS-II Phase 2a boundary, 4 = CVS-II Phase 2b interior, 5 = CVS-II Phase 3 boundary, M = middle compositions, 0 = other than NCAW waste glasses, A = EA glass.

(d) Properties not measured for radioactive glasses CVS2-53 and CVS2-54.

TABLE 10.1. Thermal Expansion Coefficient Data for Solid Glass (α_s) and Molten Glass (α_m) for CVS-I and CVS-II Phase 1, 2, and 3 Glasses (continued)

Glass [a]	ID[b] #	PS[c]	α_s (10^{-6}/K)	α_m (10^{-6}/K)
CVS2-75	98	5	77.1(e)	713.0(e)
CVS2-76	99	5	13.8	97.0
CVS2-77	100	5	11.7	76.1
CVS2-78	101	5	6.0	72.5
CVS2-79	102	5	4.7	56.1
CVS2-80	103	5	5.6	93.4
CVS2-81	104	5	13.7	79.5
CVS2-82	105	5	13.7	77.5
CVS2-83	106	5	13.4	73.1
CVS2-84	107	5	12.1	83.5
CVS2-85	108	5	8.4	64.0
CVS2-86	109	5	10.6	78.2
CVS2-87	110	5	8.7	59.5
CVS2-88	111	5	11.2	61.5
CVS2-89	112	5	10.4	101.7
CVS2-90	113	5	6.8	94.8
CVS2-91	114	5	7.0	90.8
CVS2-92	115	5	8.0	79.6
CVS2-93	116	5	12.3	105.4
CVS2-94	117	5	11.3	103.5
CVS2-95 (7)	118	A	11.3	90.3
CVS2-96 (1)	119	M	9.6	96.4
CVS2-97 (5)	120	M	10.1	104.1
CVS2-98 (6)	121	5	11.5	78.6
CVS2-99	122	5	8.6	74.0
CVS2-100	123	5	9.3	96.2
CVS2-101(7)	124	A	(f)	(f)

(a) The numbers in parentheses represent replicate sets of glasses.

(b) ID# is a consecutive integer numbering of all CVS glasses.

(c) PS is the plotting symbol used in plots associated with this data: 1 = CVS-I boundary, 2 = CVS-II Phase 1 interior, 3 = CVS-II Phase 2a boundary, 4 = CVS-II Phase 2b interior, 5 = CVS-II Phase 3 boundary, M = middle compositions, O = other than NCAW waste glasses, A = EA glass.

(e) These values appear to be erroneous and were not used in fitting models or other data analyses.

(f) Property not measured for this glass.

TABLE 10.2. Coefficients and Goodness-of-Fit Statistics for First-Order Mixture Models Fitted to Thermal Expansion Coefficient Data for Solid Glass (α_s) and Molten Glass (α_m) Using Mass and Mole Fractions of the Oxide Components

	Mass Fractions		Mole Fractions	
	α_s	α_m	α_s	α_m
SiO_2	1.634	56.866	2.067	59.726
B_2O_3	0.747	186.560	0.100	193.709
Na_2O	38.479	81.991	37.613	85.579
Li_2O	46.968	342.580	26.752	207.172
CaO	19.455	171.985	17.969	162.800
MgO	12.941	105.643	11.506	95.300
Fe_2O_3	10.170	194.435	12.042	339.871
Al_2O_3	3.990	-74.456	0.793	-176.043
ZrO_2	3.751	-71.236	-1.235	-219.155
Others	10.174	48.886	13.375	-23.416
# points[a]	117	119	117	119
R^2[b]	0.8709	0.4291	0.8711	0.4269
R^2(ADJ)[b]	0.8601	0.3820	0.8602	0.3795
R^2(PRESS)[b]	0.8432	0.2962	0.8439	0.2920
LOF?[c]	No (82.2%)[d]	Yes (99.0%)[e]	No (82.2%)[d]	Yes (99.0%)[e]

(a) There are 124 glasses listed in Table 10.1, but α_s and α_m were not measured for the radioactive glasses CVS2-53 and CVS2-54 or for CVS2-101, and the questionable data for CVS2-75 were not used in fitting the models. The CVS2-7, CVS2-15, and CVS2-85 data points for α_s and the CVS2-47 data point for α_m were determined to be outliers and thus were also omitted when fitting the models in this table.

(b) R^2, R^2(ADJ), and R^2(PRESS) statistics take values between 0.0 and 1.0, and provide different measures of the proportion of variation in the property data accounted for by a fitted model. See Section 6.1.5 for the definitions of these statistics.

(c) A statistical F-test for lack-of-fit (LOF) was performed using the estimates of experimental variation obtained from replicate tests. "Yes" and "No" entries indicate whether the LOF was statistically significant at a 90% confidence level. The actual confidence level at which a LOF can be declared significant is given in parentheses following the "Yes" or "No" for each model.

(d) LOF test used the pooled SD estimate in Table F.4.

(e) LOF test used the pooled SD estimate without replicate sets 2 and 3 in Table F.4.

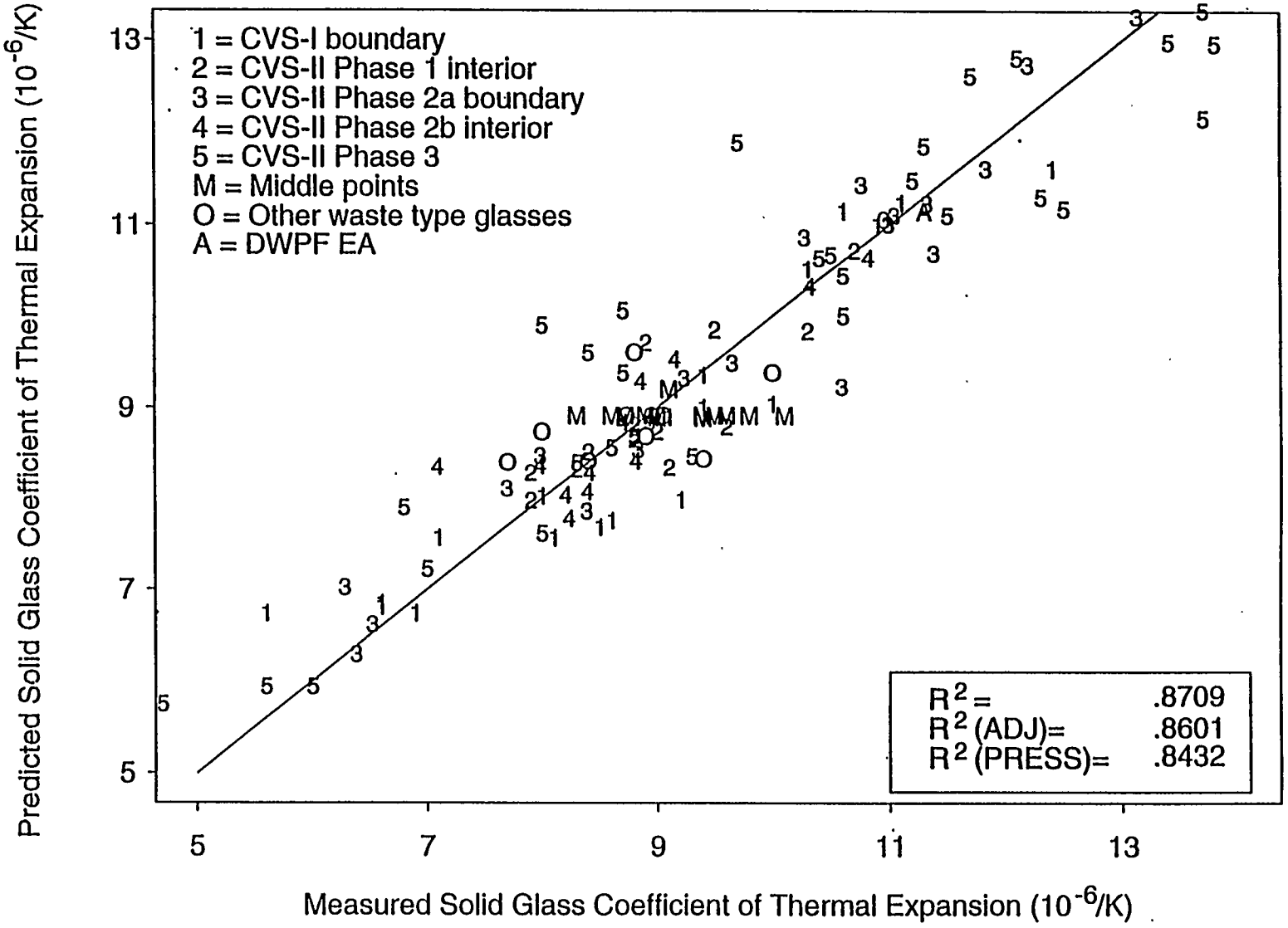

FIGURE 10.1a. Predicted Versus Measured Solid Glass Coefficient of Thermal Expansion Values for the First-Order Mixture Model Using Mass Fractions (from Column 2 of Table 10.2)

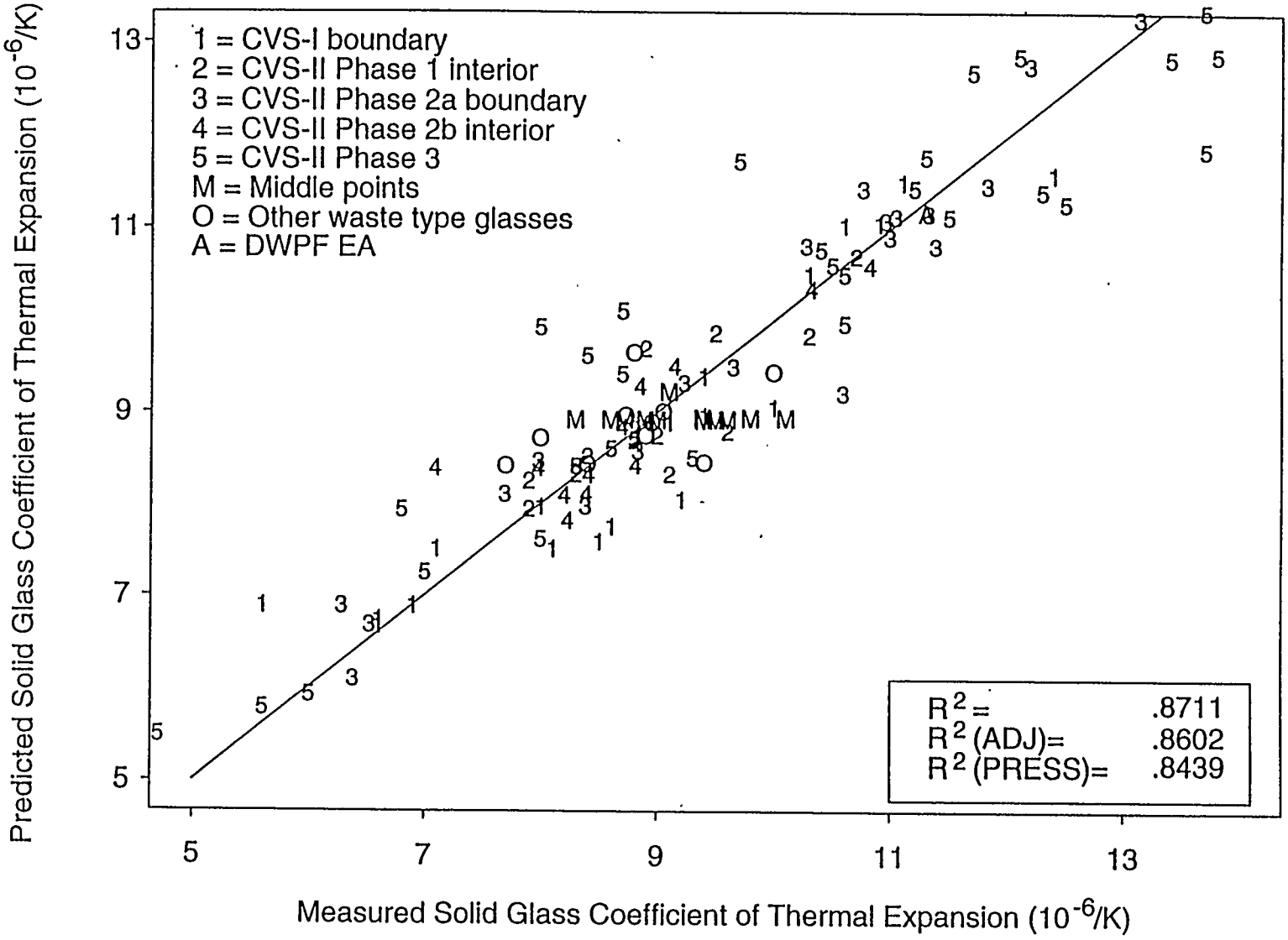

FIGURE 10.1b. Predicted Versus Measured Solid Glass Coefficient of Thermal Expansion Values for the First-Order Mixture Model Using Mole Fractions (from Column 4 of Table 10.2)

not have a statistically significant LOF at the 90% confidence level for either mass or mole fractions. This may seem somewhat surprising given that the various R^2 values for the α_m first-order (mass and mole fractions) models are in the 0.835 to 0.865 range. However, the estimate of experimental and measurement uncertainty (from Table F.4) used for the statistical LOF test is large enough that the lack of model performance is not significantly greater than this uncertainty at the 90% confidence level.

For thermal expansion of molten glass, the first-order mixture model evaluation statistics R^2 = 0.4291, R^2(ADJ) = 0.3820, and R^2(PRESS) = 0.2962 for mass fractions and R^2 = 0.4269, R^2(ADJ) = 0.3795, and R^2(PRESS) = 0.2920 for mole fractions indicate that the first-order mixture model does not fit the data very well for either mass or mole fractions. The plots of predicted versus measured molten glass coefficient of thermal expansion values in Figure 10.2a (mass fractions) and Figure 10.2b (mole fractions) confirm that the first-order mixture model does not fit very well. A statistical test for model lack-of-fit (LOF) (see Section 6.1.5) indicated that the α_m first-order mixture model has a statistically significant LOF at the 99% confidence level (see Table 10.2) for both mass and mole fraction versions of the model. Eliminating the data point in Figures 10.2a and 10.2b with the largest measured α_m (CVS2-36, which actually had the second-largest α_m overall before CVS2-47 was deleted) did not significantly improve the fit of the first-order models, so it was retained.

The component effects plots for solid and molten glass coefficients of thermal expansion (based on the first-order models using mass fractions) are given in Figures 10.3 and 10.4, respectively. Only the single-component constraints and not the stand-in crystallinity constraints in Tables 4.2 and 4.6 were used to limit the effects plot (both were used in previous effects plots). As a result, effects are evaluated over wider ranges than in the past for several components involved in the stand-in constraints (most notably Al_2O_3 and SiO_2). The effects plot in Figure 10.3 shows that alkali oxides (Li_2O more than Na_2O) are predicted to increase thermal expansion of solid glass, while SiO_2 and to a lesser extent B_2O_3 are predicted to decrease it. The remaining glass components are predicted to have mild or negligible

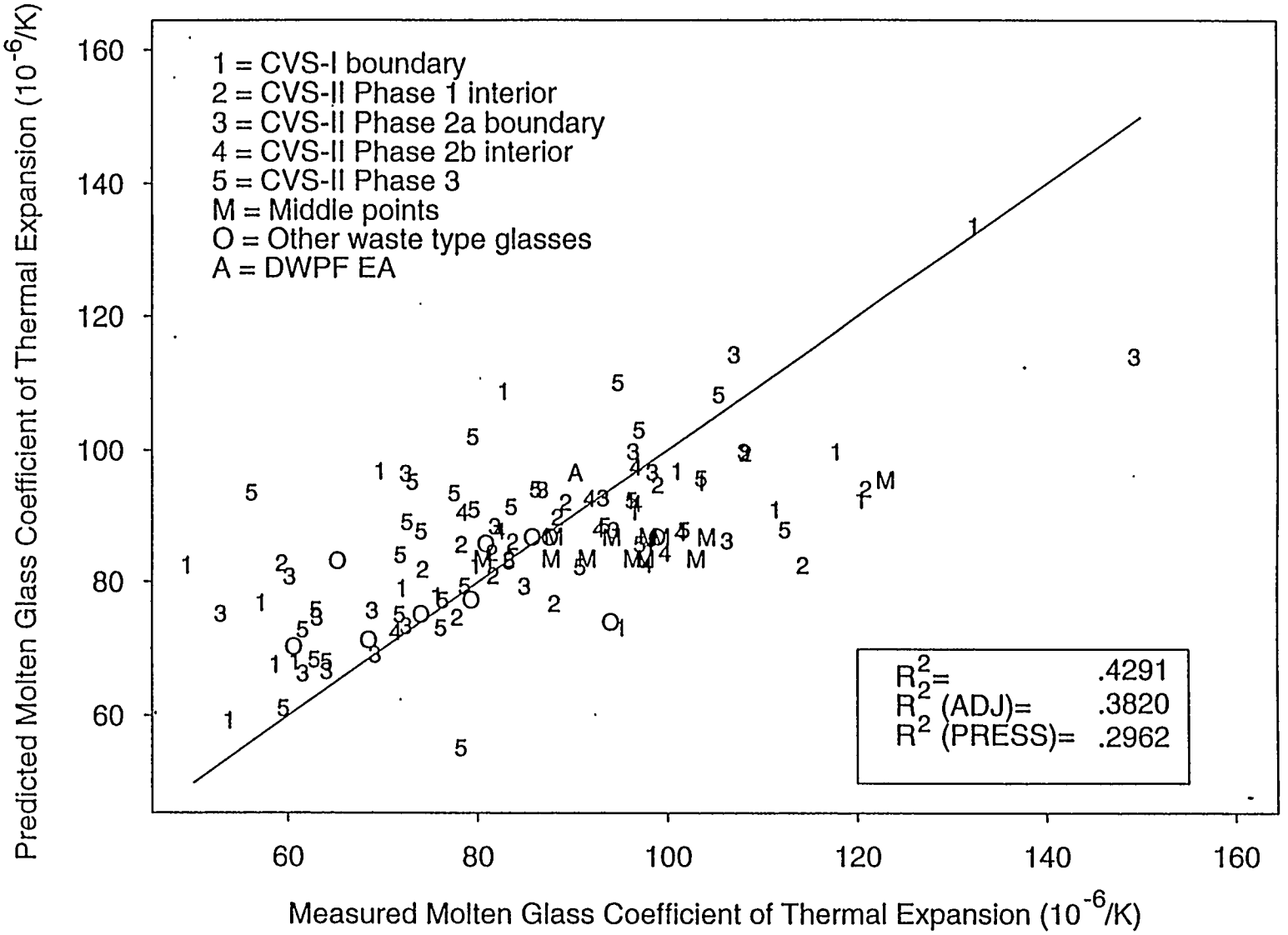

FIGURE 10.2a. Predicted Versus Measured Molten Glass Coefficient of Thermal Expansion Values for the First-Order Mixture Model Using Mass Fractions (from Column 3 of Table 10.2)

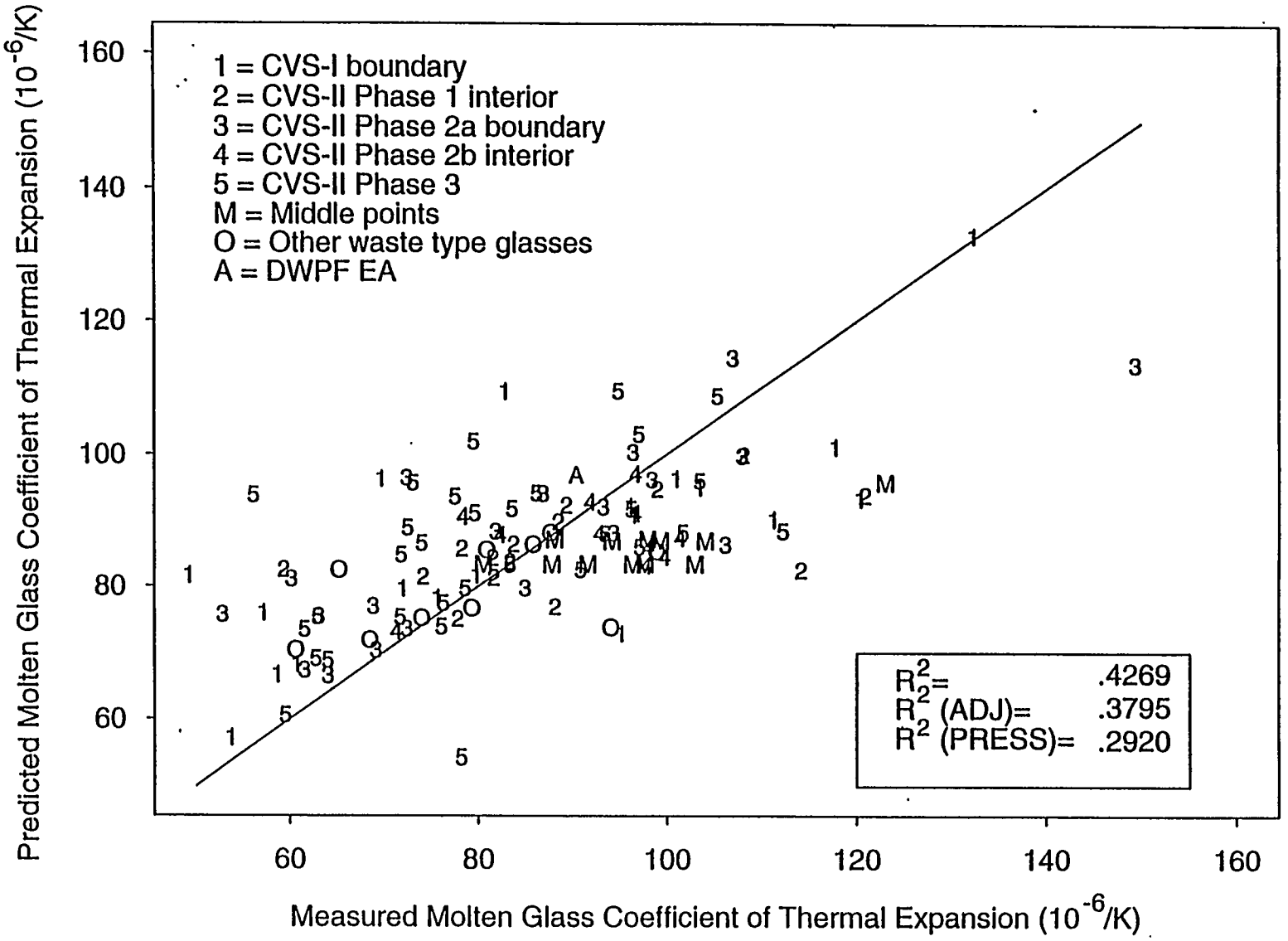

FIGURE 10.2b. Predicted Versus Measured Molten Glass Coefficient of Thermal Expansion Values for the First-Order Mixture Model Using Mole Fractions (from Column 5 of Table 10.2)

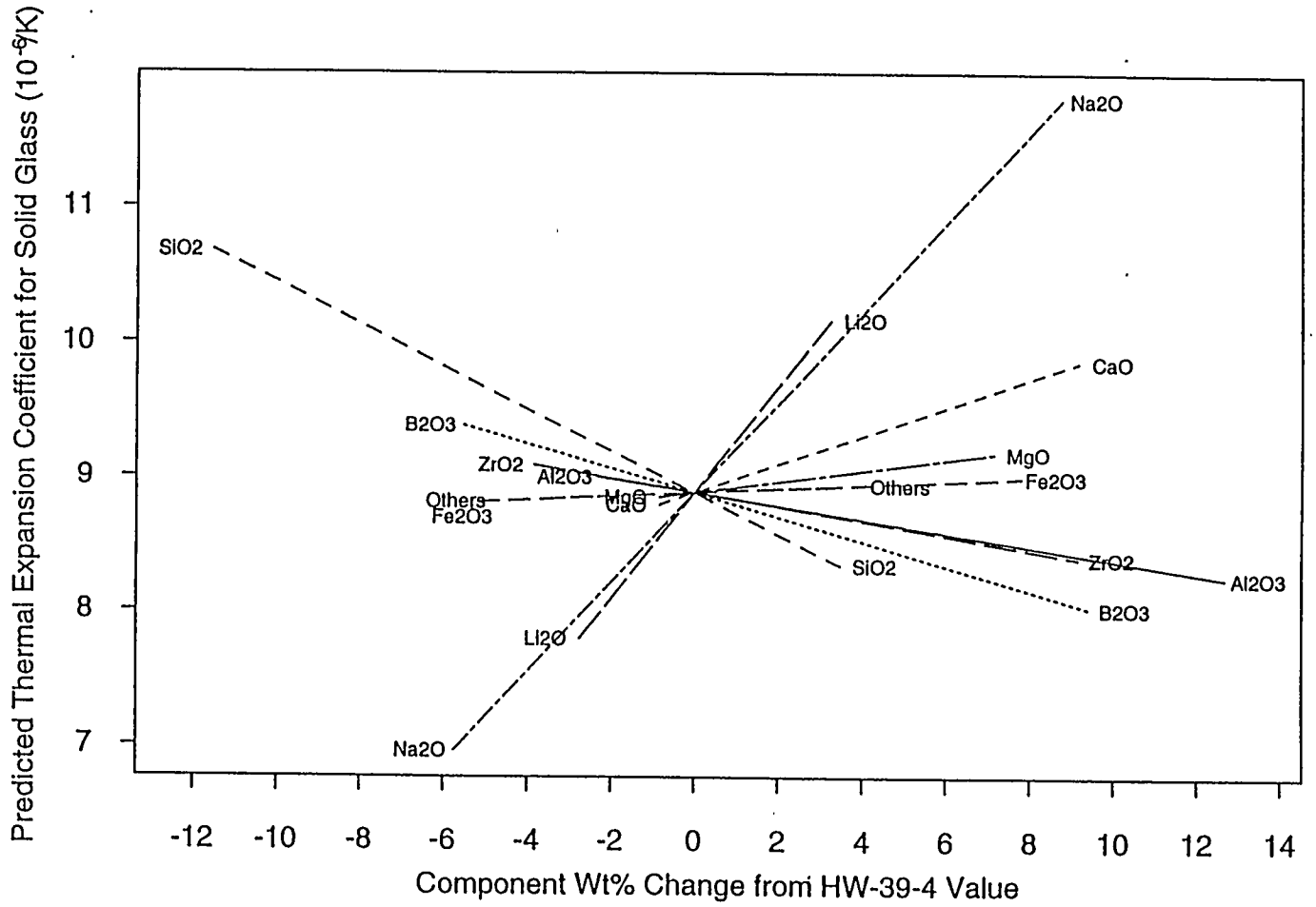

FIGURE 10.3. Predicted Component Effects on Thermal Expansion Coefficient for Solid Glass (α_s) Relative to the HW-39-4 Composition, Based on the First-Order Mixture Model Using Mass Fractions (in Column 2 of Table 10.2)

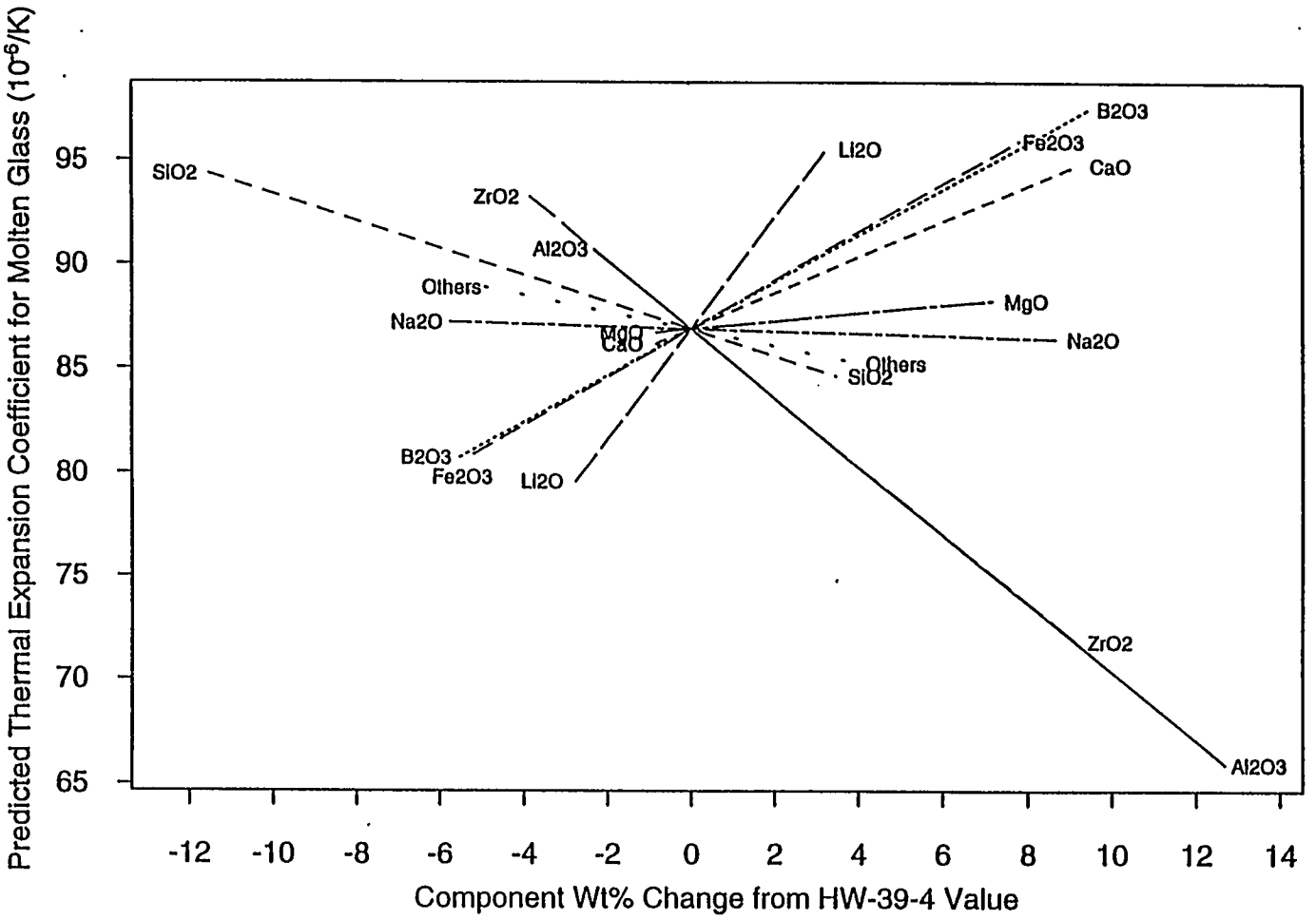

FIGURE 10.4. Predicted Component Effects on Thermal Expansion Coefficient for Molten Glass (α_m) Relative to the HW-39-4 Composition, Based on the First-Order Mixture Model Using Mass Fractions (in Column 3 of Table 10.2)

effects on the thermal expansion of solid glass. The effects plot in Figure 10.4 shows that the thermal expansion of molten glass is predicted to be increased (in order) by Li_2O, $B_2O_3 \approx Fe_2O_3$, and CaO, and is predicted to be decreased (in order) by $Al_2O_3 \approx ZrO_2$ and SiO_2. Others, MgO, and Na_2O are predicted to have mild or negligible effects on thermal expansion of molten glass. Due to the poor fit of the molten glass thermal expansion model, the preceding observations regarding the effects plot in Figure 10.4 should be considered with caution.

10.2 SECOND-ORDER MODELS FOR THERMAL EXPANSION

Three candidate Scheffé second-order mixture models for the coefficients of thermal expansion of solid and molten glass are given in Tables 10.3 and 10.4, respectively. These models were fitted to CVS-I and CVS-II Phase 1 and 2 data. Because no current need exists[(a)] for thermal expansion models, it was decided not to update the second-order models using CVS-II Phase 3 data due to the effort and time required to do so.

The candidate second-order models in Tables 10.3 and 10.4 consist of the first-order mixture model terms and several second-order terms selected using statistical variable selection techniques (see Section 6.1.4). It was not necessary to apply the pseudocomponent transformation (see Section 6.1.3), so the usual glass oxide component mass fractions were used in fitting the models. As was the case for the first-order models, the outlying data points corresponding to CVS2-7 and CVS2-15 for solid glass and CVS2-47 for molten glass were not used in fitting the second-order models. Figure 10.5 displays the predicted versus measured solid glass coefficient of thermal expansion values for Model #2 from Table 10.3. Figure 10.6 displays the predicted versus measured molten glass coefficient of thermal expansion values for Model #1 from Table 10.4.

The three candidate second-order mixture models in each of Tables 10.3 and 10.4 provide better fits than do the corresponding first-order mixture

---

(a) Thermal expansion data and models will be needed to address melter and waste form performance issues, as discussed in Section 3.6.

TABLE 10.3. Candidate Scheffé Second-Order Models Using Mass Fractions for Thermal Expansion of Solid Glass[a]

Model #1		Model #2		Model #3	
Terms	Coefficients	Terms	Coefficients	Terms	Coefficients
SiO2	0.6873	SiO2	0.2417	SiO2	2.2847
B2O3	2.1160	B2O3	2.7078	B2O3	1.6152
Na2O	21.2323	Na2O	17.3070	Na2O	37.6014
Li2O	48.7635	Li2O	76.7165	Li2O	48.1319
CaO	-10.8679	CaO	-3.0381	CaO	1.7832
MgO	10.9116	MgO	12.4311	MgO	7.5742
Fe2O3	9.3188	Fe2O3	9.3534	Fe2O3	8.2416
Al2O3	7.0671	Al2O3	6.3936	Al2O3	5.4872
ZrO2	27.0549	ZrO2	36.7550	ZrO2	2.0851
Others	33.8990	Others	25.7143	Others	10.1445
SiO2 x Na2O	35.4094	SiO2 x Na2O	41.0672	MgO x ZrO2	130.9577
SiO2 x ZrO2	-46.9326	SiO2 x ZrO2	-68.4574	CaO x CaO	157.8023
MgO x ZrO2	104.3144	B2O3 x CaO	-37.7174		
CaO x CaO	318.1517	Li2O x CaO	-150.1296		
Others x Others	-227.1140	Li2O x MgO	-45.3643		
		MgO x ZrO2	115.8343		
		Li2O x Li2O	-275.5161		
		CaO x CaO	388.2472		
		Others x Others	-163.6743		
R^2	= .9250	R^2	= .9332	R^2	= .9133
R^2(ADJ)	= .9081	R^2(ADJ)	= .9125	R^2(ADJ)	= .8986
R^2(PRESS)	= .8863	R^2(PRESS)	= .8857	R^2(PRESS)	= .8773
LOF?[b]	No (17.9%)[c]		No (14.8%)[c]		No (24.8%)[c]

(a) Second-order models were fitted to (untransformed) thermal expansion of solid glass using 77 data points from CVS-I and CVS-II Phases 1 and 2 glasses in Table 10.1. There are 81 glasses in CVS-I and CVS-II Phases 1 and 2, but thermal expansion was not measured for the radioactive glasses CVS2-53 and CVS2-54, and values for CVS2-7 and CVS2-15 were considered outliers and were not used.

(b) A statistical F-test for lack-of-fit (LOF) was performed using the estimates of experimental variation obtained from four replicate tests. "Yes" and "No" entries indicate whether the LOF was statistically significant LOF at a 90% confidence level. The actual confidence level at which a LOF can be declared significant is given in parentheses following the "Yes" or "No" for each model.

(c) LOF test used a pooled SD estimate comparable to the one in Table F.4, except only data through CVS-II Phase 2 were used.

TABLE 10.4. Candidate Scheffé Second-Order Models Using Mass Fractions for Thermal Expansion of Molten Glass[a]

Model #1		Model #2		Model #3	
Terms	Coefficients	Terms	Coefficients	Terms	Coefficients
SiO2	93.7085	SiO2	1242.1676	SiO2	1279.4253
B2O3	-63.0600	B2O3	-381.6395	B2O3	-412.1747
Na2O	-169.4463	Na2O	-459.4546	Na2O	-494.8162
Li2O	982.8040	Li2O	153.2389	Li2O	102.0646
CaO	10.0332	CaO	-164.3268	CaO	-194.7922
MgO	4.8287	MgO	-410.0952	MgO	-389.7173
Fe2O3	-89.8492	Fe2O3	-187.4042	Fe2O3	-164.4728
Al2O3	-168.5410	Al2O3	-591.5722	Al2O3	-579.7531
ZrO2	414.1691	ZrO2	-512.5587	ZrO2	-428.6971
Others	113.5136	Others	-245.2052	Others	-266.4116
B2O3 x Na2O	2634.2629	B2O3 x Na2O	2341.1349	B2O3 x Na2O	2394.5934
Na2O x CaO	1667.2894	MgO x Al2O3	4093.2549	MgO x Al2O3	3789.7642
MgO x Al2O3	3581.6694	SiO2 x SiO2	-1559.1295	SiO2 x SiO2	-1598.0825
Fe2O3 x ZrO2	-3530.6409			Fe2O3 x ZrO2	-1935.3779
Li2O x Li2O	-6580.0716				
Fe2O3 x Fe2O3	2194.0924				
ZrO2 x ZrO2	-3011.4624				
R^2	= .7485	R^2	= .7209	R^2	= .7357
R^2(ADJ)	= .6825	R^2(ADJ)	= .6694	R^2(ADJ)	= .6820
R^2(PRESS)	= .5759	R^2(PRESS)	= .5927	R^2(PRESS)	= .5905
LOF?[b]	No (80.9%)[c]		No (80.8%)[c]		No (82.3%)[c]

(a) Second-order models were fitted to (untransformed) thermal expansion of solid glass using 78 data points from CVS-I and CVS-II Phases 1 and 2 glasses in Table 10.1. There are 81 glasses in CVS-I and CVS-II Phases 1 and 2, but thermal expansion was not measured for the radioactive glasses CVS2-53 and CVS2-54, and the value for CVS2-47 was considered an outlier and was not used.

(b) A statistical F-test for lack-of-fit (LOF) was performed using the estimates of experimental variation obtained from four replicate tests. "Yes" and "No" entries indicate whether the LOF was statistically significant LOF at a 90% confidence level. The actual confidence level at which a LOF can be declared significant is given in parentheses following the "Yes" or "No" for each model.

(c) LOF test used a pooled SD estimate comparable to the one in Table F.4 without replicate sets 2 and 3, except only data through CVS-II Phase 2 were used.

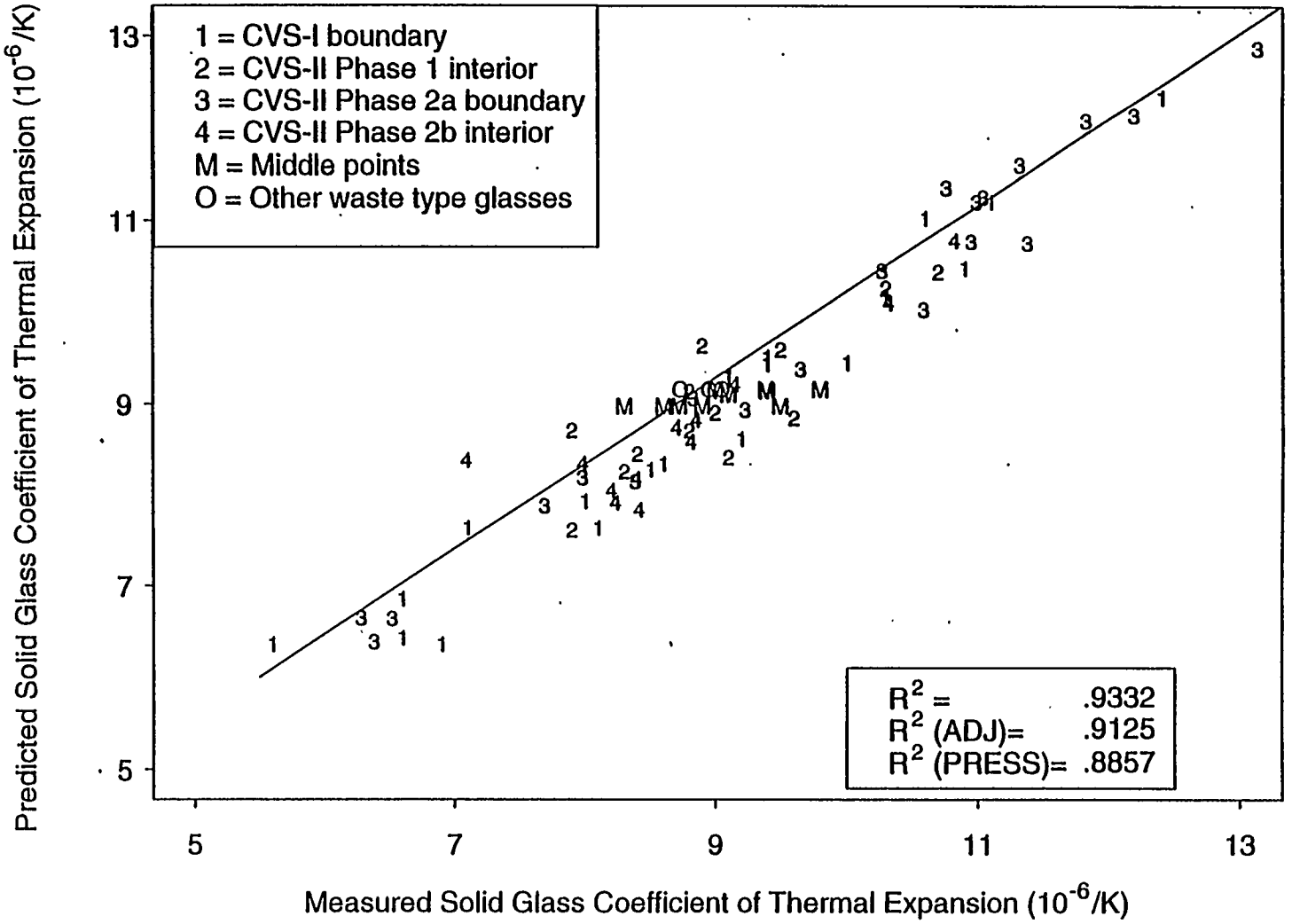

FIGURE 10.5. Predicted Versus Measured Solid Glass Coefficient of Thermal Expansion Values for the Second-Order Model #2 (from Table 10.3)

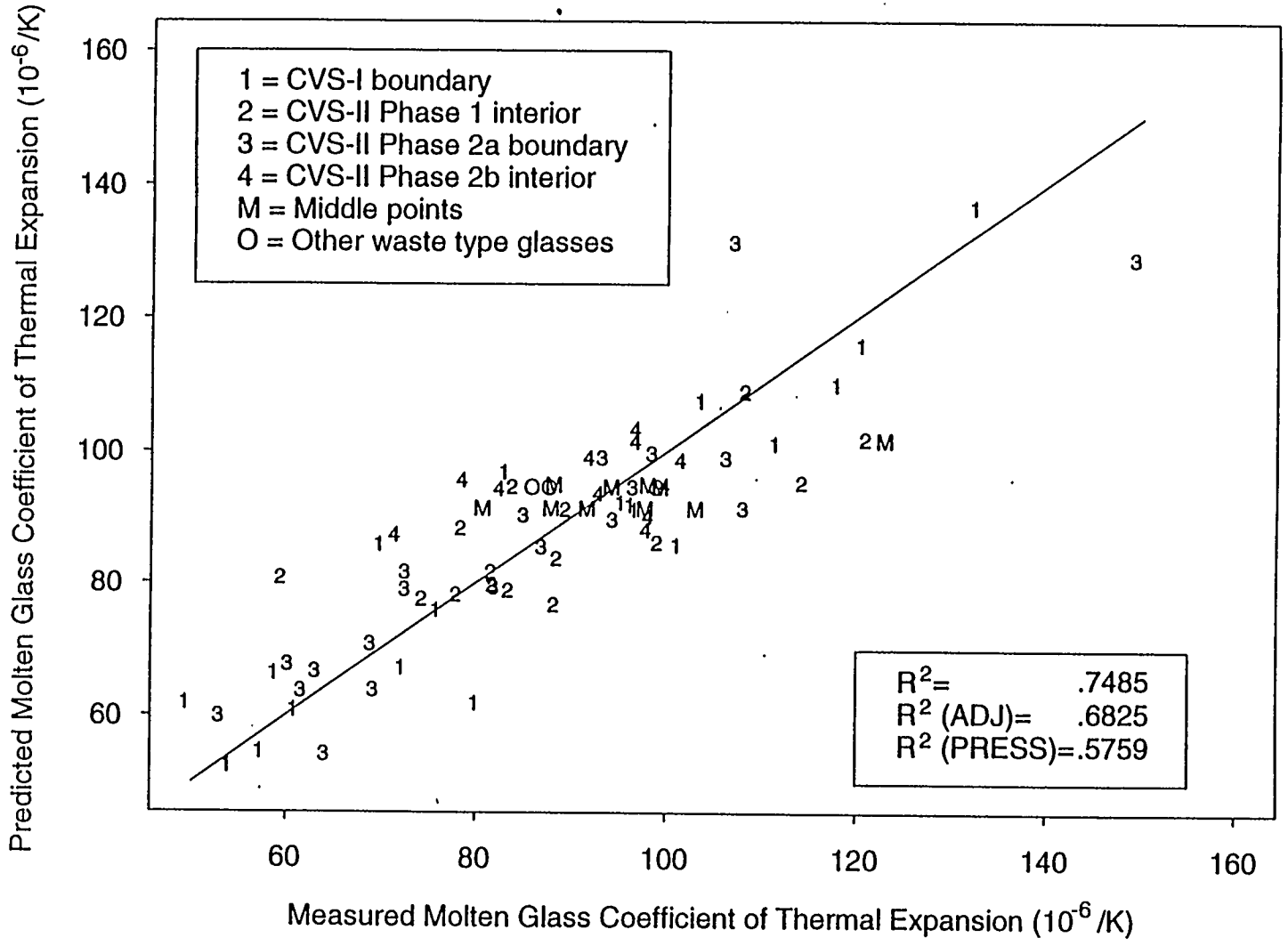

FIGURE 10.6. Predicted Versus Measured Molten Glass Coefficient of Thermal Expansion Values for the Second-Order Model #1 (from Table 10.4)

models fitted to the same data, and they do not have significant LOFs at the 90% confidence level. This statement is based on comparisons of R^2 and LOF statistics and predicted versus measured plots (not all presented here). It is not strictly appropriate to compare the updated first-order models given in Table 10.2 to the nonupdated second-order models in Tables 10.3 and 10.4, since the CVS-II Phase 3 data were used to obtain the former, but not the latter. However, it is expected that updated second-order models would fit the complete data set (including CVS-II Phase 3) better than the first-order models.

The thermal expansion of molten glass (α_m) is more difficult to measure than the thermal expansion of solid glass (α_s), which may account for the lesser fit of first- and second-order models to α_m data.

10.3 THERMAL EXPANSION DISCUSSION

Two sets of first-order mixture model coefficients are used for thermal expansion: for temperatures below T_g (solid glass) and temperatures above T_g (molten glass). These first-order model coefficients are listed in Table 10.2 and displayed in Figure 10.7. The relative magnitudes of the component coefficients for thermal expansion of solid and of molten glass give an indication of the effects of the components on these properties. The plot of coefficients for the two properties displays whether components have similar or different relative effects for the two properties. Figure 10.7 shows that thermal expansion of solid glass is predicted to be increased most by Li_2O and Na_2O and decreased most by SiO_2 and B_2O_3. Thermal expansion of molten glass is predicted to be increased most by Li_2O and decreased most by ZrO_2 and Al_2O_3. The observations for thermal expansion of molten glass should be considered with great caution however, since the first-order model does not fit very well (see Table 10.2).

If the effect of Li_2O (and to a smaller extent Na_2O) on thermal expansion remains strong at temperatures far above T_g, the presence of these components may enhance convection in the melter, which would contribute to higher melting rates. Free convection is determined by the Rayleigh number $Ra = \beta\Delta TgL^3/\nu\alpha$. Only β (thermal expansion), ν (kinematic viscosity), and α (heat diffusivity)

are glass properties. Viscosity will be kept in the range 2-10 Pa·s. It is not known how α is affected by Li_2O. However, if Li_2O affects Ra significantly by increasing β, convection will be enhanced by Li_2O addition. Because heat from the electrode region to the cold cap is convected, heat flux will increase with increasing Li_2O content. More heat means more feed melted, unless the melting rate is controlled by conversion rate, which is not certain.

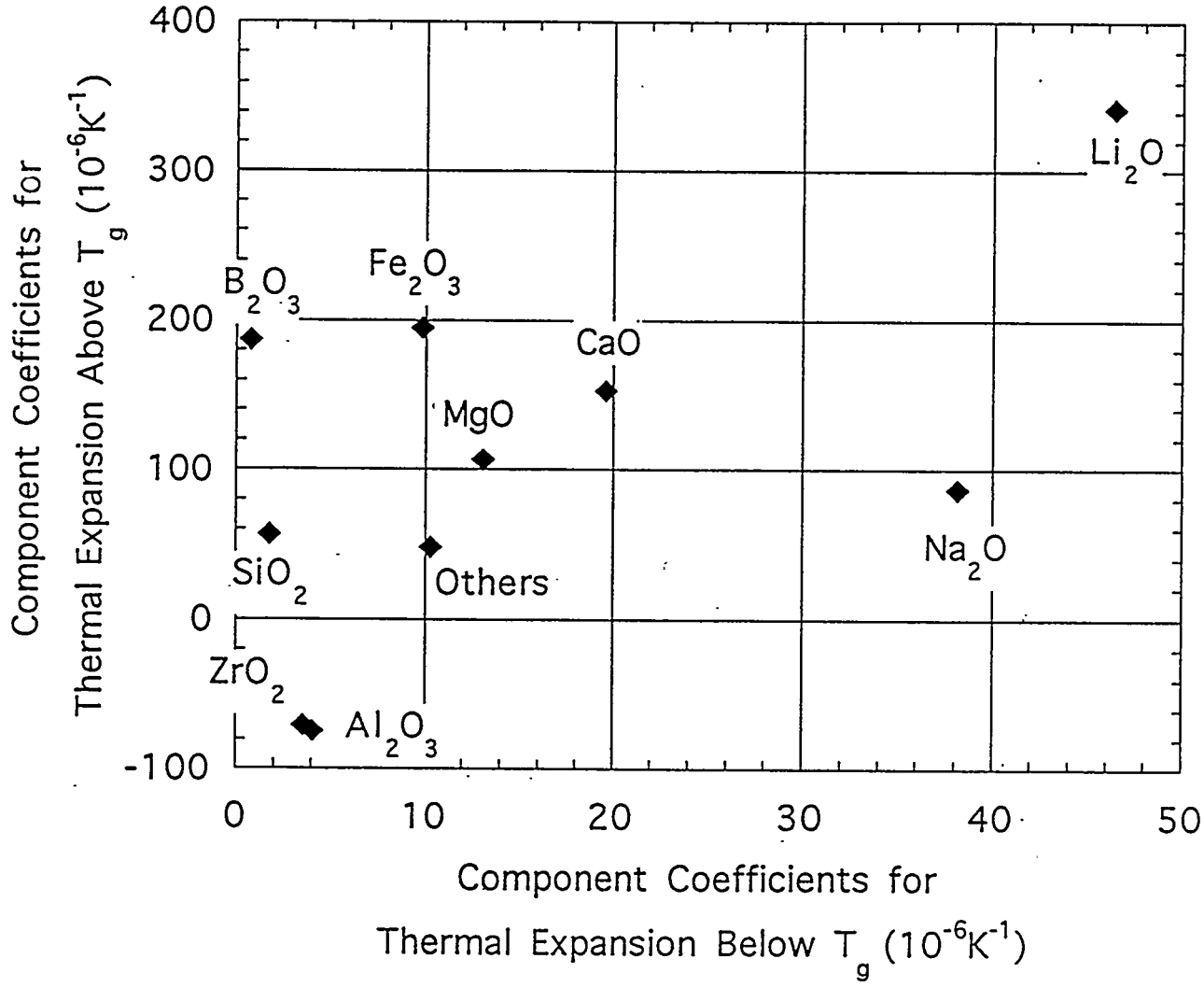

FIGURE 10.7. First-Order Mixture Model Coefficients for Thermal Expansion of Solid Glass Versus Those for Thermal Expansion of Molten Glass

11.0 GLASS CRYSTALLIZATION AND LIQUIDUS TEMPERATURE RESULTS AND DISCUSSION

In CVS-I, crystallinity after 24 hours heat treatment at 1050°C was determined to obtain guidance for improving the crystallinity constraints (see Section 5.4). These constraints served as a rough substitute for liquidus temperature models in planning CVS-II Phases 1, 2, and 3 of testing (see Sections 4.3.1, 4.4.1, and 4.5.1). Liquidus temperature data were subsequently obtained for all CVS-I and CVS-II Phase 1, 2, and 3 glasses except those with liquidus temperature beyond the temperature range of the gradient furnace (600-1150°C) and the radioactive glasses CVS2-53 and CVS2-54. Because the gradient furnace enables heat treatment within a wide temperature range in a single experiment, heat treatment for 24 hours at 1050°C was no longer needed after the gradient furnace was put in use.

Crystallinity was also evaluated for samples of all CVS-I and CVS-II Phase 1, 2, and 3 glasses heat-treated by following the canister centerline cooling (CCC) schedule presented in Table 5.1. The CCC schedule provides glasses with maximum amount of crystallinity within the canister volume. Quenched glasses and CCC glasses represent two extreme states (two extreme temperature histories) of canistered glass. The chemical durability of quenched and CCC glasses represents the durability range of the canister contents. Chemical durability results are discussed in Chapter 12.

The major crystalline phases identified in CVS glasses are summarized in Section 11.1. Crystallinity after CCC is discussed in Section 11.2, while liquidus temperature results are given in Sections 11.3 and 11.4. The CCC crystallinity and liquidus temperature results are discussed in Section 11.5.

The correlation between the stand-in crystallinity constraints used in defining the CVS experimental region (see Tables 4.2 and 4.6) and the experimental liquidus temperature was evaluated. The results are presented and discussed in Section 11.6. First-order liquidus temperature models for three crystalline phases for which a sufficient number of data points were available are presented in Section 11.7. A thermodynamic liquidus temperature model (Pelton et al. 1992) based on phase equilibria has been developed by

Ecole Polytechnique, Montreal, Canada. This model, discussed in Section 11.8, is a preliminary FY 1993 version that is currently being update and improved. The liquidus temperatures predicted by the preliminary thermodynamic model were compared with experimental data and the goodness-of-fit was evaluated. The evaluation results and discussion are given in Section 11.9.

11.1 OVERVIEW OF CRYSTALLINE PHASES IDENTIFIED IN CVS GLASSES

The major crystalline phases identified during the study of crystallinity in CVS glasses were oxides with spinel structure (spinels) and single-chain silicates (inosilicates). Orthosilicates (island silicates), disilicates (double island silicates or sorosilicates), and network silicates (tektosilicates) were also found in some glasses. More information about silicate phases can be found in books by Rumble (1976) and Deer, Howie, and Zussman (1978, 1982, 1986).

The spinel ($MgAl_2O_4$) structure is a cubic closest-packed array of oxygen ions with metal cations occupying a part of tetrahedral and octahedral interstitial sites. All oxide minerals with a spinel structure are called spinels. The spinel structure allows complete solid solutions between many different spinels (Figures 11.1 and 11.2). Spinels identified in CVS glasses were those containing Fe, Cr, and Ni (NiO and Cr_2O_3 are included in the Others component), namely magnetite (Fe_3O_4), chromite ($FeCr_2O_4$), and trevorite ($NiFe_2O_4$), which form solid solutions of the type $(Ni,Fe)(Fe,Cr)_2O_4$. Most common was magnetite (Fe_3O_4) with Ni and Cr as minor elements. Although Fe_2O_3 was used as a glass component, Fe^{2+} was produced by reduction at high temperatures (see Section A.4).

Hematite (Fe_2O_3) was the only iron oxide identified in CVS glasses other than spinels. Hematite (α-Fe_2O_3) has a corundum (α-Al_2O_3) structure in which the oxygens are in hexagonal closest packing with metal atoms in the octahedral sites. Other oxide phases identified were eskolaite, Cr_2O_3 (corundum structure), α-Al_2O_3, and ZrO_2. ZrO_2 has a distorted (monoclinic) fluorite (CaF_2) structure in which the anions are in simple cubic packing and the cations occupy the interstices at the center of every other cube.

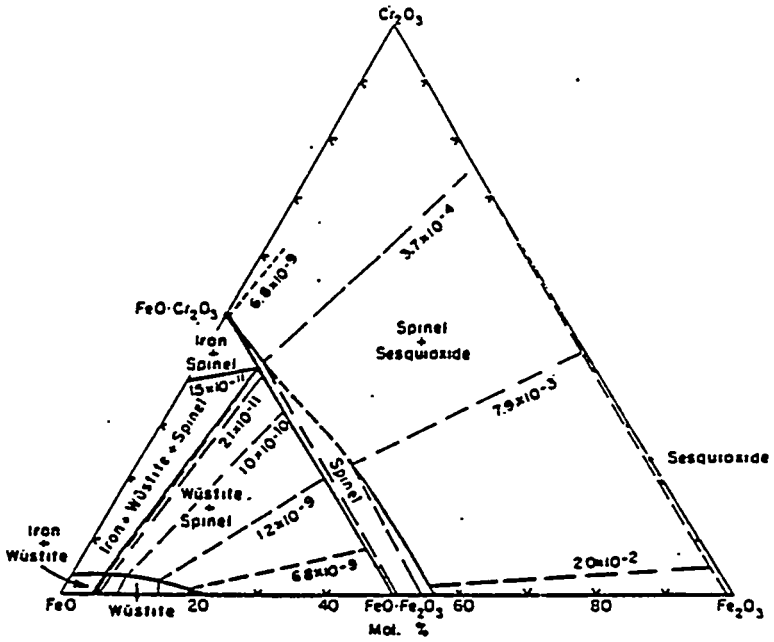

FIGURE 11.1. System $FeO-Fe_2O_3-Cr_2O_3$ at 1300°C (Katsura and Muan 1985)

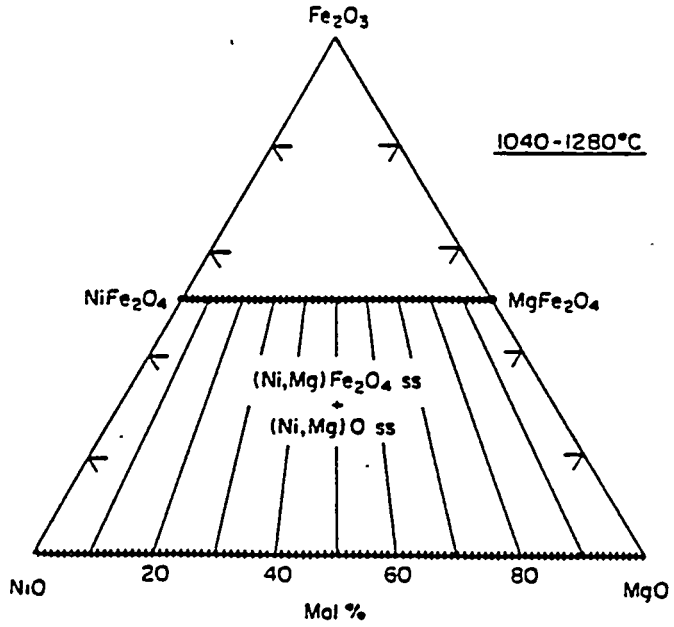

FIGURE 11.2. System $NiO-MgO-Fe_2O_3$ in the Temperature Range 1040-1280°C (Bashkirov and Bashkirova 1981)

In single-chain silicates, each $[SiO_4]^{4-}$ tetrahedron shares a corner with two other tetrahedra to form infinite $[SiO_3]^{2-}$ chains. A portion of the Si sites in the tetrahedra can be replaced by Al. The common single-chain silicates are pyroxenes, which consist of two sub-groups: clinopyroxenes (monoclinic) and orthopyroxenes (orthorhombic). In addition, silicates with single chains of $[SiO_4]^{4-}$ tetrahedra other than pyroxenes exist, which are referred to as non-pyroxene single-chain silicates.

The generalized chemical composition of clinopyroxenes may be written as $M_1M_2[Si_2O_6]$, where M_1 represents Na, Ca, or Li and M_2 represents Fe^{3+}, Fe^{2+}, Mg, Al, Mn, Ni, or Cr. In CVS glasses, diopside ($CaMgSi_2O_6$) and hedenbergite ($CaFe^{2+}Si_2O_6$) occurred most frequently although acmite (or aegirine, $NaFe^{3+}Si_2O_6$) was identified in some glasses. A wide range of cation substitutions is possible between clinopyroxene members to form a complete solid solution series. Many of the clinopyroxenes in CVS glasses were from the diopside-hedenbergite series; some contained Ni and/or Cr as a major or minor element.

Orthopyroxenes are represented by magnesium-iron pyroxenes (orthoenstatite-orthoferrosilite series), $(Mg,Fe)SiO_3$. In this series, the cations Mg and Fe are mutually replaceable, forming complete solid solutions over the whole composition range between end members of enstatite ($MgSiO_3$) and ferrosilite ($FeSiO_3$). In most of the orthopyroxenes identified in CVS glasses, Fe was the major element with Ni and Cr as possible minor components.

Non-pyroxene single-chain silicates identified in CVS glasses were lithium silicate (Li_2SiO_3), lithium-aluminum silicate ($LiAlSi_2O_6$), and krinovite ($NaMg_2CrSi_3O_9$).

In orthosilicates, no two tetrahedra share a corner, i.e., each tetrahedron is isolated from all others in the silicate structure. The orthosilicates identified in CVS glasses were forsterite (Mg_2SiO_4), which belongs to the olivine group, $(Mg,Fe)_2SiO_4$, and zircon ($ZrSiO_4$). Double island silicates (disilicates) consist of two tetrahedra sharing a corner. Gehlenite ($Ca_2Al_2SiO_7$), in which some of the Si^{4+} sites are replaced by Al^{3+}, was a double-island silicate identified in CVS glasses.

All the tetrahedra share their corners with others in an infinite three-dimensional network of SiO_2 (cristobalite and quartz) and nepheline ($NaAlSiO_4$), in which up to 50% of the tetrahedra are occupied by Al^{3+} instead of Si^{4+}. These three phases were also identified in CVS glasses.

Calcium silicate (possibly $CaSiO_3$) was identified only in liquidus temperature samples. Structural information and exact chemical composition of this crystal could not be obtained because XRD analysis was not performed for these samples.

The noble metals and their oxides, mostly RuO_2, were present as undissolved particles and sometimes as small needles that possibly crystallized from RuO_2 dissolved in the glass. In some glasses, spinels or other crystals were nucleated on RuO_2. Also, spinel crystals in some glasses provided nucleation sites for other crystals, such as clinopyroxenes, as observed previously in SRTC glasses by Bickford and Jantzen (1984, 1986).

11.2 CRYSTALLIZATION OF CVS-I AND CVS-II GLASSES

Table 11.1 contains a summary of the crystalline phases detected by XRD for CVS-I glasses after 24-hour heat treatment at 1050°C and after simulated CCC. Crystalline phases identified after CCC of CVS-II Phase 1, 2, and 3 glasses are summarized in Table 11.2. Crystalline phases making up less than four volume percent of the glass matrix and those forming solid solutions (e.g. spinels and clinopyroxenes) are difficult to identify by XRD alone. Therefore, selected glasses were investigated by SEM/EDS which allows detection of minor phases. All glasses were examined by optical microscopy. Results from SEM/EDS and optical microscopy are also included in Tables 11.1 and 11.2. In CVS-II Phase 3, glasses that were identified as crystal-free by optical microscopy were not tested by XRD or SEM/EDS. The radioactive glasses CVS2-53 and CVS2-54 and the EA glass received from SRTC (CVS2-101) were not investigated for crystallinity. Hence, 121 CVS-I and CVS-II Phases 1, 2, and 3 glasses were investigated for crystallinity.

TABLE 11.1. Crystallinity Analysis of CVS-I Glasses

A) Heat Treatment for 24 h at 1050°C

Glass	XRD Analysis Phase	XRD Analysis Est. vol%	SEM Analysis Phase	Optical Microscopy Phase
Center Point				
1	none	0	(Fe,Cr,Ni) undissolved ZrO_2 at crucible wall	none^#
Extreme Vertices				
2	unidentified	< 1	none	none^#
3	unidentified	< 1	not analyzed	none^#
4	unidentified	< 1	not analyzed	none^
5	none	0	(Fe; Cr,Ni)	spinel^§ RuO_2 needles
6	zircon $ZrSiO_4$	5-7	not analyzed	zircon + RuO_2 settled^#
7	$Ca_2ZrSi_4O_{12}$	4-6	(Ca,Zr,Si) (Zr,Si) undissolved ZrO_2 at crucible wall	$Ca_2ZrSi_4O_{12}$# zircon RuO_2 needles
8	zircon $ZrSiO_4$ orthopyroxene $(Mg,Fe)SiO_3$	12-15 3-4	not analyzed	zircon§#$ orthopyroxene spinel
9	unidentified	4-6	(Fe,Mg,Cr,Ni)	(?)^§
10	spinel	1-2	not analyzed	spinel§
11	unidentified	< 1	not analyzed	none^§
12	none	0	(Fe,Ni,Cr)	spinel§ hematite RuO_2 needles
13	unidentified	1	not analyzed	RuO_2 needles^
14	none	0	not analyzed	RuO_2 needles^#
15	unidentified	< 1	not analyzed	RuO_2 settled^§#
16	spinel olivine $(Mg,Fe)_2SiO_4$	1-2 1-2	(Fe; Mg,Cr,Ni) (Mg,Si; Fe)	spinel§# olivine
17	none	0	(Fe,Ni,Cr)	spinel^§#
18	ZrO_2	8-10	not analyzed	ZrO_2^# ZrO_2 + RuO_2 settled

^ Noble metal agglomerates were observed within glass volume and on crucible walls and bottom.
§ Spinel crystals were found within a boundary layer at crucible walls or bottom.
# Crystals other than spinel were found within a boundary layer at crucible walls or bottom.
$ Sample was almost totally crystallized and porous.
(?) Crystalline phase could not be determined, or was suspected.

TABLE 11.1. Crystallinity Analysis of CVS-I Glasses (continued)

A) Heat Treatment for 24 h at 1050°C (cont.)

Glass	XRD Analysis Phase	Est. vol%	SEM Analysis Phase	Optical Microscopy Phase
Center Point Replicates				
19	none	0	not analyzed	none^#
20	none	0	not analyzed	none^#
Replicates of CVS1-4 and -8				
21	unidentified	< 1	not analyzed	none^
22	zircon $ZrSiO_4$	12-15	not analyzed	zircon$
	orthopyroxene $(Mg,Fe)SiO_3$	3-4		orthopyroxene
				spinel
HW-39-2 Glass				
23	none	0	not analyzed	spinel^§#

B) Canister Centerline Cooling

Glass	XRD Analysis Phase	Est. vol%	SEM Analysis Phase	Optical Microscopy Phase
Center Point				
1	clinopyroxene	6-8	(Ca,Fe,Mg,Si; Zr)	clinopyroxene^§#+
	spinel		(Fe,Cr,Ni)	spinel
Extreme Vertices				
2	unidentified	< 1	not analyzed	none^
3	olivine $(Mg,Fe)_2SiO_4$	2-3	(Mg,Fe,Si; Ni,Zr)	olivine^#
4	unidentified	< 1	none	none^#
5	spinel	3-5	(Fe; Ni,Cr)	spinel^§#+
	Li_2SiO_3	1	(Si)	Li_2SiO_3
	unidentified	< 1	(Fe,Si)	(Fe,Si) phase growing from spinel
				hematite

^ Noble metal agglomerates were observed within glass volume and on crucible walls and bottom.
§ Spinel crystals were found within a boundary layer at crucible walls or bottom.
# Crystals other than spinel were found within a boundary layer at crucible walls or bottom.
+ Crystals were nucleation sites for another crystalline phase.
$ Sample was almost totally crystallized and porous.

TABLE 11.1. Crystallinity Analysis of CVS-I Glasses (continued)

B) Canister Centerline Cooling (cont.)

Glass	XRD Analysis Phase	Est. vol%	SEM Analysis Phase	Optical Microscopy Phase
Extreme Vertices (cont.)				
6	zircon $ZrSiO_4$	8-10	(Zr,Si)	zircon + RuO_2 settled^§#
	ZrO_2	< 1	(Zr)	ZrO_2
			(Ni,Fe,Cr)	high-Ni spinel(?)
7	$Ca_2ZrSi_4O_{12}$	3-5	(Ca,Zr,Si)	$Ca_2ZrSi_4O_{12}$#
				zircon
8	zircon $ZrSiO_4$	10-12	(Zr,Si)	zircon$
	orthopyroxene $(Mg,Fe)SiO_3$	2-4		
	clinopyroxene	3-5		
				spinel
				hematite
9	unidentified	5-7	(Fe; Mg,Ni,Cr)	large long crystals(?)^§$
	cristobalite SiO_2	< 1	(Si)	
	spinel	< 1		
10	spinel	1-2	(Fe,Ni,Cr)	spinel§
11	none	0	(Ni,Fe,Cr)	high-Ni spinel(?)^§
12	hematite α-Fe_2O_3	1-2	not analyzed	hematite§
	unidentified	2-3		unidentified
				spinel
				RuO_2 needles
13	none	0	none	RuO_2 needles^#
14	none	0	none	RuO_2 needles^#
15	Li_2SiO_3	2-3	(Si)	Li_2SiO_3^§#+
	olivine $(Mg,Fe)_2SiO_4$	< 1	(Mg,Fe,Ni,Si)	olivine
	clinopyroxene	< 2		clinopyroxene
16	nepheline $NaAlSiO_4$	15-18		nepheline§#
	spinel		(Fe; Ni,Cr)	spinel
17	maghemite γ-Fe_2O_3	1-2	(Fe,Ni,Cr)	spinel^
			(Ca,Fe,Si)	clinopyroxene
18	ZrO_2	12-13	(Zr)	ZrO_2^§#
	Li_2SiO_3	2-3	(Si)	Li_2SiO_3
			(Ca,Mg,Si; Fe,Ni)	clinopyroxene

^ Noble metal agglomerates were observed within glass volume and on crucible walls and bottom.
§ Spinel crystals were found within a boundary layer at crucible walls or bottom.
# Crystals other than spinel were found within a boundary layer at crucible walls or bottom.
+ Crystals were nucleation sites for another crystalline phase.
$ Sample was almost totally crystallized and porous.
(?) Crystalline phase could not be determined, or was suspected.

TABLE 11.1. Crystallinity Analysis of CVS-I Glasses (continued)

B). Canister Centerline Cooling (cont.)

Glass	XRD Analysis Phase	Est. vol%	SEM Analysis Phase	Optical Microscopy Phase
Center Point Replicates				
19	clinopyroxene	8-10	(Ca,Fe,Mg,Si; Zr) (Fe,Ni,Cr)	clinopyroxene^§#+ spinel
20	clinopyroxene	8-10	not analyzed	clinopyroxene^§#+ spinel
Replicates of CVS-I 4 and 8				
21	unidentified	< 1	none	none$
22	zircon $ZrSiO_4$	10-12	(Zr,Si)	zircon$
	orthopyroxene $(Mg,Fe)SiO_3$	2-4	(Mg,Fe,Si) (Fe,Si)	orthopyroxene
	clinopyroxene	2-3		clinopyroxene
				spinel
				hematite
HW-39-2 Glass				
23	clinopyroxene	2-3	(Ca,Fe,Si; Na,Al) (Fe,Ni,Cr)	clinopyroxene§#+ spinel

^ Noble metal agglomerates were observed within glass volume and on crucible walls and bottom.
§ Spinel crystals were found within a boundary layer at crucible walls or bottom.
# Crystals other than spinel were found within a boundary layer at crucible walls or bottom.
+ Crystals were nucleation sites for another crystalline phase.
$ Sample was almost totally crystallized and porous.

TABLE 11.2. Crystallinity Analysis of CVS-II Glasses After Canister Centerline Cooling

Glass	XRD Analysis Phase	Est. vol%	SEM Analysis Phase	Optical Microscopy Phase
Inner Shell Extreme Vertices (Phase 1)				
1	olivine $(Mg,Fe)_2SiO_4$	2-3	(Mg,Ni,Fe,Si)	olivine^§#+
	unidentified	< 1		
			(Cr,Fe,Ni)	spinel
2	none	0	not analyzed	none^#
3	none	0	not analyzed	oblong crystals(?)^§#
4	unidentified	< 1	not analyzed	none^§#
5	unidentified	1-2	(Ni,Fe,Cr)	high-Ni spinel(?)^§#
6	clinopyroxene	5	(Ca,Fe,Si; Ni,Mg)	clinopyroxene^§#+
			(Fe,Cr,Ni)	spinel
7	unidentified	2-3	(Ni,Fe,Cr)	high-Ni spinel(?)^§#
			(Fe,Cr,Ni)	spinel
8	spinel	3-4	(Fe,Ni,Cr)	spinel§#+
	orthopyroxene $(Mg,Fe)SiO_3$		(Mg,Fe,Si)	orthopyroxene
				hematite
9	none	0	none	ZrO_2 at bottom^§#
10	spinel	2	(Fe,Ni,Cr)	spinel§#
11	unidentified	< 2	none	none^§#
12	unidentified	< 2	none	none^§#
13	none	0	not analyzed	RuO_2 needles^#
14	none	0	not analyzed	none^#
15	unidentified	2-3	(Ni,Fe,Cr)	high-Ni spinel(?)^§#
			(Fe,Cr,Ni)	spinel
HW-39-4 Glass				
16	unidentified	< 1	not analyzed	none^§#
CVS-I Center Point Replicate				
17	clinopyroxene	10	(Ca,Fe,Mg,Si; Zr,Ni)	clinopyroxene^§#+
			(Fe,Cr,Ni)	spinel
HW-39-4 Glass Replicate				
18	not analyzed		not analyzed	none^#
CVS Internal Standard Glass				
19	none	0	not analyzed	clinopyroxene^§#

^ Noble metal agglomerates were observed within glass volume and on crucible walls and bottom.
§ Spinel crystals were found within a boundary layer at crucible walls or bottom.
# Crystals other than spinel were found within a boundary layer at crucible walls or bottom.
+ Crystals were nucleation sites for another crystalline phase.
(?) Crystalline phase could not be determined, or was suspected.

TABLE 11.2. Crystallinity Analysis of CVS-II Glasses After Canister Centerline Cooling (continued)

Glass	XRD Analysis Phase	Est. vol%	SEM Analysis Phase	Optical Microscopy Phase
Outer Shell Extreme Vertices (Phase 2a)				
20	none	0	not analyzed	undissolved ZrO_2^#
21	none	0	not analyzed	none^#
22	orthopyroxene $(Mg,Fe)SiO_3$	7	(Mg,Si; Fe,Ni)	orthopyroxene^§#
	Li_2SiO_3	7	(Si)	
	unidentified	2	(Mg,Ni,Si; Fe)	olivine
23	none	0	not analyzed	RuO_2 needles
24	unidentified	1-2	not analyzed	high Ni spinel(?)^§#
25	clinopyroxene	8	(Ca,Fe,Si; Na,Ni)	clinopyroxene§#+
	Li_2SiO_3	10	(Si)	Li_2SiO_3
	hematite α-Fe_2O_3	4		
			(Fe,Ni,Cr)	spinel
26	none	0	none	RuO_2 needles^#
27	none	0	none	RuO_2 needles^#
28	unidentified	1-2	not analyzed	none^
29	unidentified	< 1	none	none^§#
30	hematite α-Fe_2O_3	9	(Fe)	hematite§#
			(Fe,Ni,Cr)	spinel
	cristobalite SiO_2	2		
	quartze SiO_2	trace		
31	none	0	none	none^
32	none	0	not analyzed	undissolved ZrO_2
33	nepheline $NaAlSiO_4$	15	(Na,Al,Si; Fe,Mg)	nepheline^§#
	unidentified	2		
			(Mg,Ni,Si; Fe)	olivine
			(Ni,Cr,Fe)	high-Ni spinel(?)
34	none	0	not analyzed	RuO_2 needles^§#
35	nepheline $NaAlSiO_4$	10	(Na,Al,Si)	nepheline#
	gehlinite $Ca_2Al_2SiO_7$	7	(Ca,Al,Si)	gehlinite
	SiO_2(?)	2	(Si)	
36	clinopyroxene	5	(Ca,Fe,Si)	clinopyroxene§#
	Li_2SiO_3	2	(Si)	Li_2SiO_3
37	none	0	none	none^#

^ Noble metal agglomerates were observed within glass volume and on crucible walls and bottom.
§ Spinel crystals were found within a boundary layer at crucible walls or bottom.
# Crystals other than spinel were found within a boundary layer at crucible walls or bottom.
+ Crystals were nucleation sites for another crystalline phase.
(?) Crystalline phase could not be determined, or was suspected.

TABLE 11.2. Crystallinity Analysis of CVS-II Glasses After Canister Centerline Cooling (continued)

Glass	XRD Analysis Phase	XRD Analysis Est. vol%	SEM Analysis Phase	Optical Microscopy Phase
Outer Shell Extreme Vertices (Phase 2a) (cont.)				
38	spinel	7	(Fe;Ni,Cr)	spinel§#+
	krinovite $NaMg_2CrSi_3O_{10}$	2	(Fe,Mg,Na,Si)	star-like crystals growing from spinel
			(Mg,Fe,Si)	olivine
39	Li_2SiO_3	7	not analyzed	Li_2SiO_3§#
	Li_2MgSiO_4	3		RuO_2 needles
Inner Shell Extreme Vertices (Phase 2b)				
40	none	0	not analyzed	none^#
41	none	0	not analyzed	none^§#
42	clinopyroxene	20	(Ca,Fe,Mg,Si; Zr,Ni)	clinopyroxene^§#+
	Li_2SiO_3	10-15	(Si)	Li_2SiO_3
			(Fe,Cr,Ni)	spinel
43	none	0	none	none^#
44	none	0	not analyzed	none^#
45	clinopyroxene	9	(Ca,Mg,Fe,Ni,Si; Zr)	clinopyroxene^#+$
			(Fe,Cr,Ni)	spinel
46	none	0	none	none^§#
47	none	0	none	none^#
48	none	0	none	none^§#
49	none	0	not analyzed	none^§#
CVS-I Center Point Replicate				
50	clinopyroxene	12	(Ca,Fe,Mg,Si; Zr,Ni)	clinopyroxene^§#+
			(Fe,Ni,Cr)	spinel
CVS Internal Standard Glass Replicate				
51	none	0	not analyzed	clinopyroxene^§#
High SiO_2 (60 wt%) Glass				
52	none	0	not analyzed	clinopyroxene^§#
Glasses with Depleted Uranium				
53	not analyzed		not analyzed	not analyzed
54	not analyzed		not analyzed	not analyzed

^ Noble metal agglomerates were observed within glass volume and on crucible walls and bottom.
§ Spinel crystals were found within a boundary layer at crucible walls or bottom.
# Crystals other than spinel were found within a boundary layer at crucible walls or bottom.
+ Crystals were nucleation sites for another crystalline phase.
$ Sample was almost totally crystallized and porous.

TABLE 11.2. Crystallinity Analysis of CVS-II Glasses After Canister Centerline Cooling (continued)

Glass	XRD Analysis Phase	Est. vol%	SEM Analysis Phase	Optical Microscopy Phase
High Cr_2O_3 Glass (CC Waste Representant)				
55	none	0	(Cr,Fe)	Cr_2O_3§#
High MnO_2 Glass (PFP Waste Repesentant)				
56	none	0	none	none^§#
High Nd_2O_3 Glass (NCRW Representant)				
57	none	0	none	none§#
Low SiO_2 (39 wt%) Glass				
58	none	0	(Mg,Fe,Ni,Si; Zr)	olivine^#
CVS-II Phase 3 Low Viscosity Glass				
59	not analyzed		not analyzed	RuO_2 needles^§#
High Electrical Conductivity Glass				
60	none		none	RuO_2 needles^§#
Low PCT Release Glass				
61	none		none	none^§#
Low Electrical Conductivity Glass				
62	not analyzed		not analyzed	none^#
Low SiO_2 (32 wt%) Glass				
63	nepheline $NaAlSiO_4$	15	(Na,Al,Si)	nepheline^§#
			(Ca,Al,Si)	gehlinite
NCAW-91 Representative Glass with Modified "Others"				
64	unidentified		(Fe,Ni,Cr) (Fe,Si; Zr)	spinel^§#+ orthopyroxene
NCRW Representative Glass with Modified "Others"				
65	none		(Zr,Si)	zircon^#

^ Noble metal agglomerates were observed within glass volume and on crucible walls and bottom.
§ Spinel crystals were found within a boundary layer at crucible walls or bottom.
# Crystals other than spinel were found within a boundary layer at crucible walls or bottom.
+ Crystals were nucleation sites for another crystalline phase.

TABLE 11.2. Crystallinity Analysis of CVS-II Glasses After Canister Centerline Cooling (continued)

Glass	XRD Analysis Phase	Est. vol%	SEM Analysis Phase	Optical Microscopy Phase
CC Waste Representative Glass with Modified "Others"				
66	spinel	5	(Cr; Mn,Fe,Ni)	spinel§#
CC Waste Representative Glass with Modified "Others"				
67	none		none	none^#
CC Waste Representative Glass with Modified "Others"				
68	Li, Al silicate	8		Li, Al silicate^#
	eskolaite Cr_2O_3	2	(Cr)	Cr_2O_3
PFP Waste Representative Glass with Modified "Others"				
69	eskolaite Cr_2O_3	3	(Cr)	Cr_2O_3^#
	Li_3PO_4	2	(P)	Li_3PO_4
PFP Waste Representative Glass with Modified "Others"				
70	Li, Al silicate	10		Li, Al silicate^#
	eskolaite Cr_2O_3	<1	(Cr)	Cr_2O_3
CVS2-64 with NCAW-87 "Others"				
71	clinopyroxene(?)	<3	(Fe,Si)	orthopyroxene(?)^§#+
	spinel	<1	(Fe,Ni,Cr)	spinel
CVS2-66 with NCAW-87 "Others"				
72	not analyzed		not analyzed	none^§#
CVS2-68 with NCAW-87 "Others"				
73	not analyzed		not analyzed	none^#
CVS2-69 with NCAW-87 "Others"				
74	spinel	<5	(Cr,Fe,Ni)	spinel^§#+
CVS2-70 with NCAW-87 "Others"				
75	not analyzed		not analyzed	none^§#
Extreme Vertices (Phase 3)				
76	Li_2SiO_3	5	(Si)	Li_2SiO_3^§# RuO_2 needles

^ Noble metal agglomerates were observed within glass volume and on crucible walls and bottom.
§ Spinel crystals were found within a boundary layer at crucible walls or bottom.
# Crystals other than spinel were found within a boundary layer at crucible walls or bottom.
+ Crystals were nucleation sites for another crystalline phase.
(?) Crystalline phase could not be determined, or was suspected.

TABLE 11.2. Crystallinity Analysis of CVS-II Glasses After Canister Centerline Cooling (continued)

Glass	XRD Analysis Phase	Est. vol%	SEM Analysis Phase	Optical Microscopy Phase
Extreme Vertices (Phase 3) (cont.)				
77	cristobalite SiO_2	<2	(Si)	SiO_2^§
	unidentified		(Na,Zr,Si)	Na-Zr silicate
				RuO_2 needles
78	cristobalite SiO_2	22		SiO_2^§#$
	zircon $ZrSiO_4$	3	(Zr,Si)	zircon
	unidentified	3	(Fe,Mg,Si; Zr,Ni)	olivine
79	cristobalite SiO_2	20	(Si)	SiO_2§#
	spinel	5	(Fe; Ni,Cr)	spinel
	hematite Fe_2O_3	1	(Fe)	hematite
80	cristobalite SiO_2	15	(Si)	SiO_2§#
	zircon $ZrSiO_4$	9	(Zr,Si)	zircon
	unidentified	6	(Fe,Mg,Si; Ni)	olivine
81	spinel	5	(Fe,Ni,Cr)	spinel^§#
	Li_2SiO_3	4	(Si)	Li_2SiO_3
82	Li_2SiO_3	4	(Si)	Li_2SiO_3 ^#
				RuO_2 needles
83	none		none	RuO_2 needles^§#
84	Li_2SiO_3	5	(Si)	Li_2SiO_3^§#
				RuO_2 needles
85	nepheline	33	(Na,Al,Si)	nepheline^#
	Li_2SiO_3	30	(Si)	Li_2SiO_3
86	nepheline	5	(Na,Al,Si)	nepheline^#
87	not analyzed		not analyzed	none^#
88	not analyzed		not analyzed	RuO_2 needles^§#
89	not analyzed		not analyzed	RuO_2 needles^§#
90	cristobalite SiO_2	5	(Si)	SiO_2^§#
	spinel	< 1	(Fe,Ni)	spinel
	Li Al silicate (?)	< 1		
91	unidentified	<2	none	(?)^#
	cristobalite SiO_2	<1		
92	unidentified	<2	none	none^#
93	spinel	<4	(Fe,Cr,Ni)	spinel^§#
94	none		none	RuO_2 needles^§#
DWPF EA Glass				
95	none		none	none§#

^ Noble metal agglomerates were observed within glass volume and on crucible walls and bottom.
§ Spinel crystals were found within a boundary layer at crucible walls or bottom.
# Crystals other than spinel were found within a boundary layer at crucible walls or bottom.
+ Crystals were nucleation sites for another crystalline phase.
$ Sample was almost totally crystallized and porous.
(?) Crystalline phase could not be determined, or was suspected.

TABLE 11.2. Crystallinity Analysis of CVS-II Glasses After Canister Centerline Cooling (continued)

Glass	XRD Analysis Phase	Est. vol%	SEM Analysis Phase	Optical Microscopy Phase
CVS-I Center Point Replicate				
96	clinopyroxene	15	(Ca,Mg,Fe,Si)	clinopyroxene^§#+ spinel
CVS Internal Standard Glass Replicate				
97	none		(Ca,Fe,Si; Mg)	clinopyroxene^§#
Replicate of CVS2-34				
98	none		none	RuO_2 needles^§#
Simulated 101-AZ Core 1 Glass				
99	not analyzed		not analyzed	none§#
Simulated 101-AZ Core 2 Glass				
100	orthopyroxene	3	(Fe,Si)	orthopyroxene^§#+
	spinel	2	(Fe,Ni)	spinel

^ Noble metal agglomerates were observed within glass volume and on crucible walls and bottom.
§ Spinel crystals were found within a boundary layer at crucible walls or bottom.
# Crystals other than spinel were found within a boundary layer at crucible walls or bottom.
+ Crystals were nucleation sites for another crystalline phase.

Out of the 121 glasses investigated for crystallinity, 11 glasses were replicates of six different compositions and exhibited the same crystallinity as their replicated composition glasses after CCC. Out of the remaining 110 glasses (i.e., excluding the 11 replicates), 58 glasses precipitated at least one type of crystalline phase during CCC.

11.2.1 Crystallization of Canister Centerline Cooled Glasses

The effects of glass composition on the major crystalline phases in CCC glass are discussed in the following paragraphs.

Spinel and Hematite

All glasses with Fe_2O_3 > 11 wt% (13 glasses) formed at least one of the Fe-containing crystalline phases (spinel in 12 glasses and hematite in 6 glasses) and at least one other phase. Four out of five glasses with 15 wt% Fe_2O_3 (the maximum value) formed hematite. The lowest concentration of Fe_2O_3 that resulted in hematite precipitation was 10.5 wt% (CVS2-8 and CVS2-79). Spinel precipitated in 11 glasses out of 30 with 4 wt% < Fe_2O_3 ≤ 11 wt%, but only in 7 out of 67 with Fe_2O_3 ≤ 4 wt%. These seven glasses contained relatively high Al_2O_3 (≥ 6 wt%) and high Others [≥ 6.5 wt% except CVS2-66, which had modified Others with high Cr (see Table 4.13), which is sometimes a major element in spinels].

Overall, the chance of forming spinel crystals decreased as the concentration of Fe_2O_3 decreased, but spinel could precipitate at Fe_2O_3 concentration as low as 2 wt% (CVS1-10). Generally, for a given concentration of Fe_2O_3, the chance of spinel crystallization increased as the concentration of Al_2O_3 increased and the alkali (Na_2O and Li_2O) concentrations decreased. The Others mix, containing small amounts of Cr and Ni, seemed to promote spinel formation at low Fe_2O_3 concentrations. Among spinel crystals found in CVS glasses, magnetite ($Fe^{2+}Fe^{3+}{}_2O_4$) and chromite ($Fe^{2+}Cr_2O_4$) contain Fe^{2+}. This suggests that the glass oxidation state could also be an important factor in the crystallization of spinel.

Six glasses precipitated an unidentified (by XRD) crystalline phase, which consisted of Ni, Cr, and Fe by SEM/EDS. This phase was very small

in size (< 5 μm, similar to most spinels) and in crystal volume fraction (< 0.1%). This unidentified phase was designated (with a question mark) as high-Ni spinel in Tables 11.1 and 11.2. The major differences between spinel and the unidentified phase were their shape and chemical composition. Spinels always had a roughly cuboidal shape with an aspect ratio less than 2, whereas the unidentified phase had a bar shape with an aspect ratio approximately from 3 to 10. In most spinels, Fe was the major element with Ni and Cr as minor elements, but Ni was always the dominating element in the unidentified phase. All six glasses with this unidentified phase had relatively high concentrations of Others ($\geq$ 6.5 wt%) and low Fe_2O_3 ($\leq$ 4 wt%).

Clinopyroxene

Twelve glasses formed clinopyroxene crystals during CCC. Ten of these twelve glasses contained either relatively high Fe_2O_3 ($\geq$ 10 wt%) or high MgO (> 5 wt%), or both. Out of ten glasses with at least 0.8 wt% CaO (the remaining two glasses contained no CaO), hedenbergite was a major component in five glasses with $Fe_2O_3 \geq 12$ wt% and MgO < 1 wt%. Hedenbergite-diopside solid solution series was observed in four glasses with 3 wt% < $Fe_2O_3 \leq 10$ wt% and 1 wt% $\leq$ MgO < 5 wt%, and diopside was a major component in one glass with 2 wt% Fe_2O_3 and 8 wt% MgO. No glasses with B_2O_3 > 12 wt% precipitated clinopyroxenes, and seven out of twelve glasses with clinopyroxene had 5 wt% B_2O_3 (the minimum value). Accordingly, B_2O_3 seems to suppress formation of clinopyroxene crystals.

Orthopyroxene and Olivine

Fourteen glasses formed orthopyroxene or olivine crystals, which are both magnesium-iron silicates. These glasses contained either high Fe_2O_3 (> 8 wt%) or high MgO ($\geq$ 5 wt%), or both. Eight glasses formed olivine, five orthopyroxene, and one formed both. Among the 13 glasses which formed either orthopyroxene or olivine alone, high Fe_2O_3 (> 8 wt%) glasses tended to form orthopyroxene whereas high MgO (8 wt%, the maximum value) glasses tended to form olivine. Three glasses with 57 wt% SiO_2 formed orthopyroxene whereas three glasses with $SiO_2 \leq 42$ wt% formed olivine, which may be expected from

the fact that olivine, $(Mg,Fe)_2SiO_4$, needs less SiO_2 to crystallize than orthopyroxene, $(Mg,Fe)SiO_3$. All 14 glasses that formed orthopyroxene or olivine crystals had very low CaO concentrations (no CaO in eight glasses, $0.25 \leq CaO \leq 0.5$ wt% in five glasses, and 2 wt% CaO in one glass). However, nine out of twelve glasses that formed clinopyroxene had $CaO \geq 2$ wt%. This suggests that in glasses with high Fe_2O_3 and/or high MgO, orthopyroxene and olivine crystals tend to form if CaO concentration is low, but clinopyroxene tends to form if CaO is high.

Zirconium-Containing Crystals

No Zr-containing crystalline phases ($ZrSiO_4$, ZrO_2, $Ca_2ZrSi_4O_{12}$, or sodium-zirconium silicate) were found when the ZrO_2 concentration was < 5 wt%, but at least one Zr- containing crystalline phase was found in 7 out of 24 glasses with $ZrO_2 \geq 5$ wt%. The major phase in most of these glasses was zircon ($ZrSiO_4$). Crystallization of ZrO_2 was observed in two glasses with low SiO_2 (≤ 44 wt%). In one glass (CVS1-7), which contained a combination of maximum ZrO_2 (13 wt%) and maximum CaO (10 wt%), massive crystallization of $Ca_2ZrSi_4O_{12}$ along with small amount of zircon was observed. Sodium-zirconium silicate was suspected in one glass, but its structural information and exact composition could not be obtained because of very low volume fraction.

Aluminum-Containing Crystals

Six glasses precipitated nepheline ($NaAlSiO_4$) during CCC. All belonged to the group of eight glasses that contained high Al_2O_3 (≥ 9 wt%), high Na_2O (≥ 18 wt%), and relatively low SiO_2 (≤ 44 wt% in six glasses, and 48 and 50 wt% in the remaining two glasses). The remaining two glasses out of this group of eight glasses were crystal free. Two glasses with high CaO (≥ 8 wt%) as well as high Al_2O_3 and Na_2O crystallized gehlenite ($Ca_2Al_2SiO_7$) in addition to nepheline.

Lithium Silicate

Crystals of Li_2SiO_3 were identified in 13 CCC samples; 12 of them contained $Li_2O > 6$ wt% and $B_2O_3 \leq 6$ wt% and one had 9.5 wt% B_2O_3 along with

7 wt% Li_2O. Among 20 glasses with Li_2O > 7 wt% and B_2O_3 > 6 wt%, Li_2SiO_3 was found in only one glass. This might suggest that B_2O_3 suppresses Li_2SiO_3 crystallization in high Li_2O glasses.

Silicon Dioxide

Silicon dioxide (SiO_2), mostly cristobalite, was formed in nine glasses without any noticeable compositional dependence (e.g., SiO_2 concentration ranged from 42 to 56 wt%).

11.2.2 Effects of Different Others

Glasses CVS2-55, -56, and -57, had the same nominal composition as CVS2-19 (the CVS internal standard glass) but different Others mixes (see Tables 4.8 and 4.10). Among these glasses, only the glass with the highest Cr_2O_3 concentration (CVS2-55 with 0.89 wt% Cr_2O_3) precipitated Cr_2O_3. Glasses CVS2-19, -56, and -57 had 0.13 wt%, 0.72 wt%, and 0.54 wt% Cr_2O_3, respectively, and did not form any crystals. This suggests that the amount of Cr_2O_3 that can be added to the CVS internal standard glass composition without any Cr_2O_3 precipitation during CCC is between 0.72 and 0.89 wt%.

CVS2-64 and CVS2-71 had the same nominal composition, but CVS2-64 used updated NCAW-91 simulant for Others whereas CVS2-71 used the NCAW-87 simulant for Others. As can be seen by comparing the Others compositions in Table 4.1 (for CVS2-71) and Table 4.13 (for CVS2-64), the compositional change was very small and did not make any difference in crystallinity.

CVS2-66 and CVS2-72 had the same nominal composition, but CVS2-66 used a CC double shell tank waste simulant for Others (Table 4.13) whereas CVS2-72 used the NCAW-87 simulant (Table 4.1). CVS2-66 precipitated spinel, whereas CVS2-72 remained crystal-free. This may be due to the fact that the CVS2-66 Others had much higher Cr and slightly higher Ni concentrations than the CVS2-72 Others. Spinel group crystals identified in this study almost always contained Cr and Ni as minor or major elements.

Lithium-aluminum silicate was found in two glasses (CVS2-68 and CVS2-70) with Al_2O_3 > 16 wt%, 6.9 wt% Li_2O, and 2.97 or 1.17 wt% Cr_2O_3. They had Others

mixes with the highest Cr_2O_3 concentrations tested in CVS and also crystallized Cr_2O_3. However, CVS2-73 and CVS2-75 with the same nominal compositions as CVS2-68 and CVS2-70, but with NCAW-87 simulant for Others, were crystal-free. This suggests that small additions of insoluble oxides, such as Cr_2O_3, can cause precipitation of other crystalline phases.

CVS2-69 (which used a PFP Others mix given in Table 4.13) contained 2.38 wt% Cr_2O_3 and 3.26 wt% P_2O_5, and precipitated Cr_2O_3 and Li_3PO_4. CVS2-74 (which had the same nominal composition as CVS2-69 but used the NCAW-87 "Others mix given in Table 4.1) contained 0.21 wt% Cr_2O_3 and 0.16 wt% P_2O_5, and precipitated spinel.

CVS2-65 and CVS2-67 used different Others but did not have any counterparts of the same nominal compositions. CVS2-65 with high ZrO_2 content (15.5 wt%) crystallized zircon. CVS2-67, with high concentration of Al_2O_3 (20.4 wt%) but low concentrations of ZrO_2, Fe_2O_3, and MgO, was crystal-free.

11.3 PRELIMINARY LIQUIDUS TEMPERATURE STUDIES

Initial liquidus temperature determination efforts during CVS-I and CVS-II Phase 1 are briefly discussed in Section 11.3.1. Preliminary studies that led to the development of the liquidus temperature measurement procedure used in CVS are discussed in Section 11.3.2.

11.3.1 Initial Liquidus Temperature Determination Efforts in CVS-I and CVS-II Phase 1

Liquidus temperatures were not initially measured as part of CVS-I. Rather, the CVS-I glasses were heat treated for 24 hours at 1050°C and the presence or absence of crystals was assessed to determine whether the liquidus temperature was above or below 1050°C. The above/below 1050°C determination was based on XRD detection of a crystalline phase, with a detection limit of approximately 1-2 volume % of crystal (see Section 5.4). The above/below 1050°C data for the CVS-I glasses are given in Table E.1 in Appendix E.

Also included in Table E.1 are the results of liquidus temperature measurements for CVS-II Phase 1 glasses made by Corning. The Corning liquidus temperatures given in Table E.1 are substantially lower than T_L values

obtained at PNL (reported and discussed in Section 11.4). A more than two-times milder temperature gradient was used at PNL (~1.1 °C/mm) than was used at Corning (~2.4 °C/mm). With Corning's steeper temperature gradient and a resulting higher potential for thermal convection, it was more difficult for them to determine the crystallization front temperature accurately. Hence, only the PNL liquidus temperature data will be used in modeling and other data analysis efforts.

11.3.2 Preliminary Studies to Develop Liquidus Temperature Measurement Procedure

Figure 11.3 shows a schematic of the time change of the crystallization front in the two types of experimental approaches described in Section 5.4. If the glass was pre-crystallized, the crystals located in the gradient furnace above T_L (liquidus temperature) gradually dissolve and crystallization front moves toward the equilibrium position (the liquidus temperature) from the hot end. It is assumed that the process is not disturbed by volatilization or by flow. If a crystal-free sample is used, the crystallization front moves towards the liquidus from the cold end, but it can be prevented from reaching equilibrium by lack of nucleation.

Figure 11.4 displays the results of the preliminary study (for developing the T_L procedure) conducted with the CVS internal standard glass. It shows that in the crystallization test (starting with a crystal-free sample), the crystallization front moves towards the hot end during the first 24 hours of heat treatment and then, contrary to the illustration in Figure 11.3, moves back towards the cold end. This reverse motion is caused by flow within the sample. This flow is probably caused by a surface tension gradient produced by the temperature gradient. An attempt to prevent the flow was made by covering the glass with platinum foil, but this attempt was not successful. Therefore, 24 hours appears to be an optimum heat treatment time for the best value of T_L that can be achieved using the gradient furnace method. The effect of the 24-hour heat treatment time on T_L can be assessed when TTT diagrams are available. The expected effect is probably within 5°C.

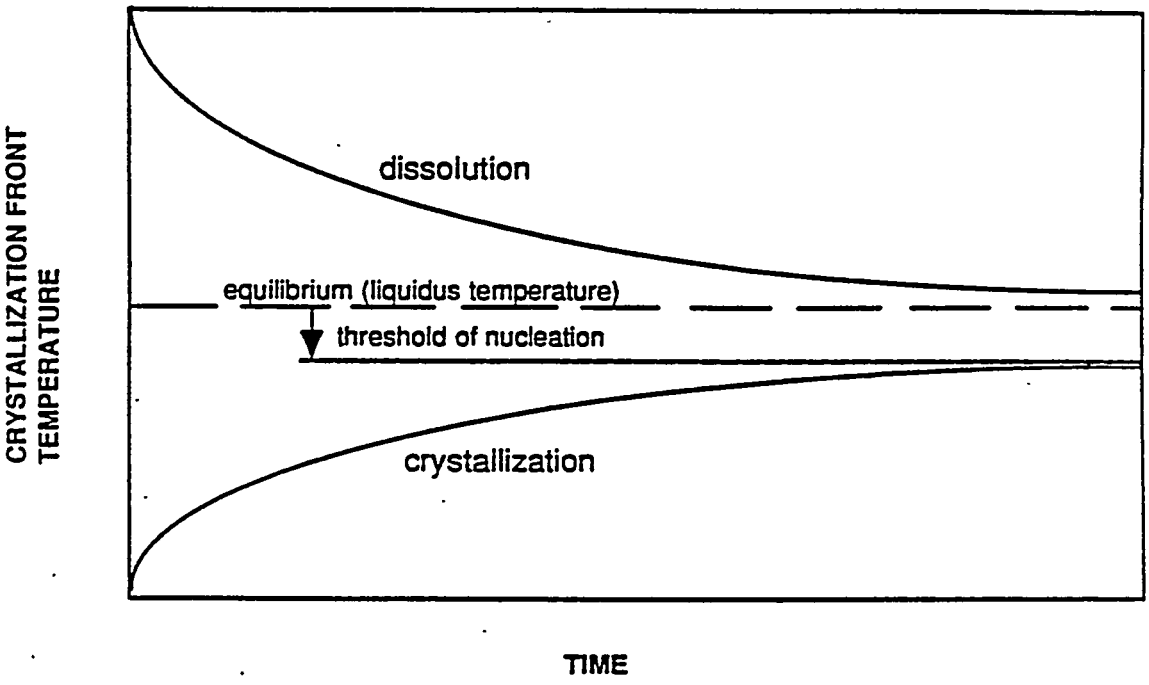

FIGURE 11.3. Conceptual View of Crystallization Front Motion in the Gradient Furnace in Initially Crystal-Free (Crystallization Line) and Pre-Crystallized (Dissolution Line) Samples

Results with pre-crystallized glass samples are also indicated by solid points in Figure 11.4. The results for the heat treatment for 24 hours or longer are indistinguishable from the data obtained by direct crystallization of samples that were crystal-free originally. This indicates that the nucleation threshold is negligible and that pre-crystallization is not necessary for the CVS internal standard glass. It was considered unlikely

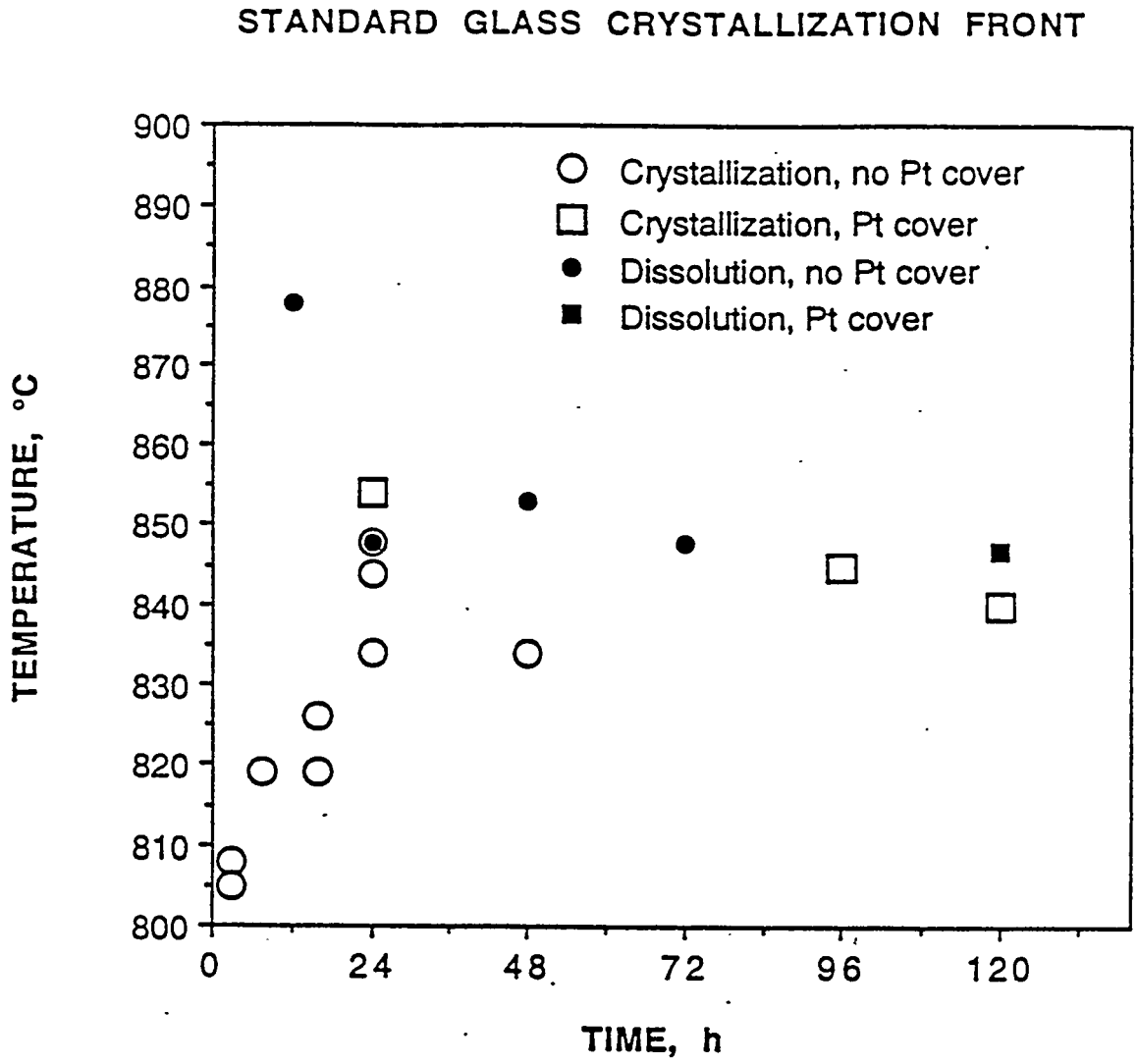

FIGURE 11.4. Effects of Time, Platinum Foil Cover, and Measurement Method on Liquidus Temperature for the CVS Internal Standard Glass

that the nucleation threshold would affect other CVS glasses. Therefore, liquidus temperature was measured for all CVS glasses using 24-hour heat treatment of crystal-free samples (see Section 5.4).

11.4 LIQUIDUS TEMPERATURES AND PRIMARY CRYSTALLINE PHASES

Tables 11.3 and 11.4 show liquidus temperature data for CVS-I and CVS-II Phase 1, 2, and 3 glasses obtained by using the procedure described in Section 5.4. The crystalline phases were identified by optical microscopic observation for all samples and by qualitative SEM/EDS for selected samples. In Tables 11.3 and 11.4, a list of elements identified in a given crystalline phase by SEM/EDS is shown in the parenthesis after the crystal name. For some crystalline phases, this list was divided into two groups of major and minor elements separated by a semicolon, with the first group representing the major elements. The results from XRD analysis of CCC samples were also used to help identify crystalline phases formed in liquidus temperature samples. For a few samples the amounts and sizes of crystalline phases were small. For such samples positive identification of each phase was very difficult or impossible, so the most probable phase was estimated and included in Tables 11.3 and 11.4 with a question mark.

The liquidus temperatures were obtained separately for crystalline phases other than spinel and for spinel-type crystals. Extremely small volume fractions (< 0.01%) of spinel-type crystals were observed in most samples, but this level of crystallinity is typical for air-quenched samples, probably a residue from melting reactions. The residual spinel had a characteristic appearance of dissolving crystals (round edges). The primary phase of crystallization was defined as the crystalline phase other than spinel with the highest liquidus temperature. If the liquidus temperature was outside the gradient furnace temperature range used for the sample, the gradient furnace measurement process was repeated until the crystallization front temperature of the primary phase was within the temperature range tested. However, no attempt was made to rerun the test if the hot-end temperature was $\geq$ 1110°C (included in Tables 11.3 and 11.4 as, e.g., > 1118°C) or cold-end temperature was $\leq$ 700°C (regarded as a crystal-free sample).

TABLE 11.3. Liquidus Temperature of Crystalline Phases in CVS-I Glasses

Glass	Crystals Other Than Spinel				Spinel Crystals	
	Liquidus T (°C)		Phase	Note*	Liquidus T (°C)	Note*
Center Point						
1	987	(SA)	zircon $ZrSiO_4$	A, G	~977	
	959	(CA)				
	913	(SA)	clinopyroxene	F1		
	903	(CA)				
Extreme Vertices						
2	942		Ca silicate-(Ca,Si))	B	none (891-1038)	
	~927	(DBT)				
	916		Li-Al silicate (Al,Si)	F1		
3	942		olivine (Mg,Si; Fe,Ni)	B	none (868-1038)	
	~929	(DBT)				
4	957		SiO_2 (Si)		none (927-1038)	
5	953	(SA)	orthopyroxene (Fe,Si)	A	~1035	
	939	(CA)				
6	≥1118		zircon $ZrSiO_4$	C1, D1	none (1014-1118)	
7	>1118		$Ca_2ZrSi_4O_{12}$	C2	none (1074-1118)	
	>1118		zircon $ZrSiO_4$	F1, C2		
8	>1118		zircon $ZrSiO_4$ (Zr,Si)	C2	>1118	C2
	>1118		orthopyroxene (Mg,Si)	F1, C2		
9	1097		(?) (Mg,Fe,Si; Cr,Ni)		>1118	C2
10	1052(?)		(?)		>1118	C2
	1026(?)		(?)	F1		
11	919		Ca silicate (Ca,Si; Nd,La)		~1035	
					~966 high-Ni spinel (?) (Ni,Cr,Fe)	F2
12	841	(SA)	orthopyroxene (Fe,Si)	A,B,D1	none (752-1038)	
	826	(CA)				
	~828	(DBT)				
13	<571		no crystals	C3	none (571-1038)	
14	<571		no crystals	C3	none (571-1038)	
15	880	(SA)	olivine (Mg,Ni,Si; Cr))	A	none (837-1118)	
	866	(CA)				
16	>1118		olivine (Mg,Si)	C2	>1118	C2

* General notes: see end of this Table
(SA) Surface area (see note A of this Table)
(CA) Center area (see note A of this Table)
(DBT) Dissolving boundary temperature (see note B of this Table)
(?) Liquidus temperature or crystalline phase could not be determined, or was suspceted.

TABLE 11.3. Liquidus Temperature of Crystalline Phases in CVS-I Glasses (continued)

Glass	Crystals Other Than Spinel			Spinel Crystals	
	Liquidus T (°C)	Phase	Note*	Liquidus T (°C)	Note*
Extreme Vertices (cont.)					
17	952 (SA) 943 (CA) 913	Ca silicate (Ca,Si) clinopyroxene (Ca,Fe,Si; Na,Ni)	A F1	~1000	
18	>1118	ZrO_2 (Zr)	C2, D2	none (1014-1118)	
Center Point Replicates					
19	916	zircon $ZrSiO_4$ clinopyroxene (Ca,Mg,Fe,Si; Ni,Cr)	 F3	~961	
20	913	zircon $ZrSiO_4$ clinopyroxene	 F3	~966	
Replicates of CVS-I 4 and 8					
21	957	SiO_2		none(927-1038)	
22	>1118 >1118	zircon $ZrSiO_4$ orthopyroxene	C2 F1, C2	>1118	C2
HW-39-2 Glass					
23	910 (SA) 858 (CA) ~880 (DBT)	clinopyroxene	A, B	~980	

General Notes in Table 11.3

A The front temperature (the highest temperature at which crystals were found) is higher at the glass top surface or crucible bottom than in the center area. The center front temperature is probably close to liquidus temperature unless dissolving crystals are observed (see note B).

B Crystals at high temperature region have rounded corners and edges characteristic for dissolution, probably because (1) crystals that initially formed in lower temperature region were transferred to higher temperature region by convection, or (2) crystals were formed at compositional inhomogeneities which later attenuated. The lowest temperature at which dissolving crystals become noticeable is indicated as DBT (dissolving boundary temperature). This temperature may be closer to the actual liquidus temperature than the front temperature.

C1 The highest temperature to which the sample was exposed appears close to the liquidus temperature.

C2 The highest temperature to which the sample was exposed is lower than the liquidus temperature.

C3 The lowest temperature to which the sample was exposed is higher than the liquidus temperature, or no crystals are formed in the sample at all.

TABLE 11.3. Liquidus Temperature of Crystalline Phases in CVS-I Glasses (continued)

General Notes in Table 11.3 (continued)

D1 Some crystals and RuO_2 agglomerates settled at the bottom. The estimated liquidus temperature may be inaccurate.

D2 Crystals and RuO_2 agglomerates are present only at the bottom half area of the crucible. The estimated liquidus temperature may be inaccurate.

F1 Another crystalline phase other than spinel.

F2 Another spinel type crystal.

F3 Two different crystals with a similar shape are present. It was not possible to distinguish each crystal in the area where the sample was heat treated at around liquidus temperature. Liquidus temperature of one crystal may be slightly lower (0 to ~20°C) than that of another.

G This glass had significantly different liquidus temperature with unknown reason. The data was not used for modeling and other data analysis purposes.

TABLE 11.4. Liquidus Temperature of Crystalline Phases in CVS-II Glasses

Glass	Crystals Other Than Spinel				Spinel Crystals	
	Liquidus T (°C)		Phase	Note*	Liquidus T (°C)	Note*
Inner Shell Extreme Vertices (Phase 1)						
1	929		olivine (Mg,Ni,Si; Fe,Cr)		~1048	C2
2	839		Ca silicate (Ca,Si)		none (826-928)	
	800		clinopyroxene (Ca,Fe,Ni,Si)	F1		
3	942	(SA)	zircon $ZrSiO_4$	A	none (782-1038)	
	931	(CA)				
	887		clinopyroxene	F1		
4	810		Ca silicate (Ca,Si)		none (702-812)	
	800		clinopyroxene (Ca,Fe,Ni,Si)	F1		
5	832		Ca silicate (Ca,Si)		~988	
					~993 high-Ni spinel (?)	F2
6	939		clinopyroxene (Ca,Fe,Si; Ni,Cr)		>1004	C2
7	819		clinopyroxene (Ca,Fe,Ni,Si)		~934	C2
8	880	(SA)	orthopyroxene	A,D3	≥1118	C1
	866	(CA)	(Fe,Si; Mg)			
9	1018		zircon $ZrSiO_4$	C2	none (735-1146)	
10	<585		no crystals	C3	>868	C2
11	1035		zircon $ZrSiO_4$ (Zr,Si)		none (927-1038)	
12	847	(SA)	clinopyroxene	A	none (826-918)	
	840	(CA)	(Ca,Fe,Mg,Si; Ni,Cr)			
13	909		clinopyroxene (Ca,Fe,Mg,Si)		none (826-911)	
14	>1118		zircon $ZrSiO_4$	C2,D1	none (1014-1118)	
15	<679		no crystal	C3	~956	C2
HW-39-4 Glass						
16	877		clinopyroxene		~906	
CVS-I Center Point Replicate						
17	925		zircon $ZrSiO_4$ (Zr,Si)		~971	
			clinopyroxene (Ca,Mg,Si; Fe)	F3		

* General notes: see end of this Table
(SA) Surface area (see note A of this Table)
(CA) Center area (see note A of this Table)
(?) Liquidus temperature or crystalline phase could not be determined, or was suspceted.

TABLE 11.4. Liquidus Temperature of Crystalline Phases in CVS-II Glasses (continued)

Glass	Crystals Other Than Spinel				Spinel Crystals	
	Liquidus T (°C)		Phase	Note*	Liquidus T (°C)	Note*
HW-39-4 Glass Replicate						
18	865		clinopyroxene (Ca,Fe,Si; Na,Cr,Ni)		~895	
CVS Internal Standard Glass						
19	862		clinopyroxene (Ca,Na,Fe,Si; Mg,Ni,Cr)		>883	C2
			Na·Zr silicate (Na,Zr,Si)	F3		
Outer Shell Extreme Vertices (Phase 2a)						
20	1087	(SA)	zircon $ZrSiO_4$ (Zr,Si)	A	none (1012-1115)	
	1081	(CA)				
21	911	(SA)	orthopyroxene (Mg,Si)	A	none (834-951)	
	904	(CA)				
22	989		olivine (Mg,Ni,Si)		~994	
23	887	(SA)	Ca silicate (Ca,Si)	A, B	none (807-1038)	
	858	(CA)				
	~873	(DBT)				
24	<714		no crystals	C3	~800	
					~934 high-Ni spinel (?)	F2
25	899		orthopyroxene (Fe,Si)	D1	>951	C2
26	1049		zircon $ZrSiO_4$		none (1012-1115)	
27	<642		no crystals	C3	none (642-1018)	
28	<642		no crystals	C3	none (642-872)	
29	1108		zircon $ZrSiO_4$ (Zr,Si)		none (1012-1115)	
30	~1070		hematite Fe_2O_3	E	~1090	
31	945	(SA)	SiO_2 (Si)	A	none (927-1038)	
	939	(CA)				
32	1089	(SA)	Na·Zr silicate (Na,Zr,Si)	A, B, D1	none (1008-1114)	
	1066	(CA)				
	~1054	(DBT)				
33	976	(SA)	olivine (Mg,Ni,Si)	A	>1038	C2
	967	(CA)				
	967		nepheline (Na,Al,Si)	F1		
34	736		nepheline (Na,Al,Si)		none (701-872)	
35	961		nepheline (Na,Al,Si)	B	none (895-1115)	
	~941	(DBT)				

* General notes: see end of this Table
(SA) Surface area (see note A of this Table)
(CA) Center area (see note A of this Table)
(DBT) Dissolving boundary temperature (see note B of this Table)
(?) Liquidus temperature or crystalline phase could not be determined, or was suspceted.

TABLE 11.4. Liquidus Temperature of Crystalline Phases in CVS-II Glasses (continued)

Glass	Crystals Other Than Spinel				Spinel Crystals	
	Liquidus T (°C)		Phase	Note*	Liquidus T (°C)	Note*
Outer Shell Extreme Vertices (Phase 2a) (cont.)						
36	887	(SA)	orthopyroxene	A, B	none (868-1038)	
	884	(CA)	(Fe,Si)			
	~877	(DBT)				
37	803		nepheline (Na,Al,Si)		none (752-1038)	
	774		Ca silicate	F1		
38	1059	(SA)	olivine (Mg,Si; Fe)	A, B	>1115	C2
	1042	(CA)				
	~1049	(DBT)				
39	1048		zircon $ZrSiO_4$	B	none (895-1115)	
	~1029					
Inner Shell Extreme Vertices (Phase 2b)						
40	862		clinopyroxene (Ca,Mg,Si; Cr)		none (826-928)	
41	887		clinopyroxene (Ca,Mg,Si; Fe,Ni,Cr)		none (854-936)	
42	969		clinopyroxene (Ca,Fe,Mg,Si)		~1093	
43	1113		zircon $ZrSiO_4$	B, D1	none (1012-1115)	
	~1090	(DBT)				
44	884		clinopyroxene (Ca,Mg,Si; Fe,Ni,Cr)		none (807-1038)	
45	911		clinopyroxene (Ca,Mg,Si; Fe,Ni,Cr)	B	>956	C2
	~894	(DBT)				
46	858		clinopyroxene (Ca,Cr,Fe,Mg,Ni,Si)		~1004	
					~854 high-Ni spinel (?)	F2
47	935	(SA)	clinopyroxene	A, B	none (807-1038)	
	877	(CA)	(Ca,Mg,Si; Na,Fe,Ni,Cr)			
	~919	(DBT)				
48	868		clinopyroxene (Ca,Mg,Si; Ni,Fe,Cr)		none (807-1038)	
49	847		clinopyroxene (Ca,Mg,Fe,Si; Ni,Cr)		~957	

---

* General notes: see end of this Table
(SA) Surface area (see note A of this Table)
(CA) Center area (see note A of this Table)
(DBT) Dissolving boundary temperature (see note B of this Table)
(?) Liquidus temperature or crystalline phase could not be determined, or was suspceted.

TABLE 11.4. Liquidus Temperature of Crystalline Phases in CVS-II Glasses (continued)

Glass	Crystals Other Than Spinel				Spinel Crystals	
	Liquidus T (°C)		Phase	Note*	Liquidus T (°C)	Note*
CVS-I Center Point Replicate						
50	922		zircon $ZrSiO_4$		~1025	
			clinopyroxene	F3		
CVS Internal Standard Glass Replicate						
51	856		clinopyroxene (Ca,Na,Fe,Si; Mg,Cr,Ni)		~899	
			Na·Zr silicate (Na,Zr,Si)	F3		
High SiO_2 (60 wt%) Glass						
52	973		orthopoyroxene (Fe,Cr,Si)		>1038	C2
Glasses with Depleted Uranium						
53			radioactive glass -- not measured			
54			radioactive glass -- not measured			
High Cr_2O_3 Glass (CC Waste Representant)						
55	944		Cr_2O_3	A, B	>1118	C2
	940	(SA)	clinopyroxene	A, B,F1		
	910	(CA)	(Na,Ca,Fe,Cr,Si)			
	~906	DBT				
High MnO_2 Glass (PFP Waste Repesentant)						
56	910	(SA)	clinopyroxene	A, B	~1117	
	880	(CA)	(Na,Ca,Fe,Cr,Si)			
	~884	(DBT)				
			Na·Zr silicate (Na,Zr,Si)	F3		
High Nd_2O_3 Glass (NCRW Representant)						
57	1036		Cr_2O_3 (Cr; Fe)		~953	
	945		clinopyroxene (Na,Ca,Fe,Cr,Si)	F1		

---

* General notes: see end of this Table
(SA) Surface area (see note A of this Table)
(CA) Center area (see note A of this Table)
(DBT) Dissolving boundary temperature (see note B of this Table)

TABLE 11.4. Liquidus Temperature of Crystalline Phases in CVS-II Glasses (continued)

Glass	Crystals Other Than Spinel			Spinel Crystals	
	Liquidus T (°C)	Phase	Note*	Liquidus T (°C)	Note*
Low SiO_2 (39 wt%) Glass					
58	921 (SA)	olivine (Mg,Si; Ni)	A		
	906 (CA)				
	908 (SA)	(?) (Mg)	A, F1		
	902 (CA)				
CVS-II Phase 3 Low Viscosity Glass					
59	715	SiO_2 (Si)		none (699-1038)	
High Electrical Conductivity Glass					
60	788	SiO_2 (Si)		none (752-966)	
Low PCT Release Glass					
61	792	SiO_2 (Si)		none (717-793)	
Low Electrical Conductivity Glass					
62	<554	no crystals	C3	none (554-1028)	
Low SiO_2 (32 wt%) Glass					
63	927	nepheline (Na,Al,Si)		none (868-1038)	
NCAW-91 Representative Glass with Modified "Others"					
64	895	orthopyroxene (Fe,Si; Cr,Ni)		~983	
NCRW Representative Glass with Modified "Others"					
65	>1114	zircon $ZrSiO_4$	C2	none (1066-1114)	
CC Waste Representative Glass with Modified "Others"					
66	799	nepheline (Na,Al,Si)		>1114	C2
CC Waste Representative Glass with Modified "Others"					
67	1022	Cr_2O_3 (Cr)		none (952-1066)	
CC Waste Representative Glass with Modified "Others"					
68	>1114	Cr_2O_3 (Cr)	C2	none (755-874)	

* General notes: see end of this Table
(SA) Surface area (see note A of this Table)
(CA) Center area (see note A of this Table)
(?) Liquidus temperature or crystalline phase could not be determined, or was suspceted.

TABLE 11.4. Liquidus Temperature of Crystalline Phases in CVS-II Glasses (continued)

Glass	Crystals Other Than Spinel				Spinel Crystals	
	Liquidus T (°C)		Phase	Note*	Liquidus T (°C)	Note*
PFP Waste Representative Glass with Modified "Others"						
69	>1114		Cr_2O_3 (Cr)	C2	>1114	C2
	992	(SA)	orthopyroxene	A		
	983	(CA)	(Cr,Fe,Si)			
PFP Waste Representative Glass with Modified "Others"						
70	>1114		Cr_2O_3	C2	none (642-931)	
	853	(SA)	Li·Al silicate (Al,Si)	A,F1		
	818	(CA)				
CVS2-64 with NCAW-87 "Others"						
71	890		orthopyroxene (Fe,Cr,Si)		~1004	
CVS2-66 with NCAW-87 "Others"						
72	794		nepheline		>868	C2
CVS2-68 with NCAW-87 "Others"						
73	840	(SA)	Li·Al silicate (Al,Si)	A	none (546-874)	
	816	(CA)				
CVS2-69 with NCAW-87 "Others"						
74	850		clinopyroxene (Ca,Fe,Si; Ni)		~1066	C2
CVS2-70 with NCAW-87 "Others"						
75	826	(SA)	Li·Al silicate (Al,Si)	A	none (807-1038)	
	815	(CA)				
Extreme Vertices (Phase 3)						
76	761		clinopyroxene (Ca,Fe,Si; Na)		none (712-924)	
	744		Li_2SiO_3 (Si)	F1		
77	1090	(SA)	Na·Zr silicate	A, B	none (967-1154)	
	1027	(CA)	(Na,Zr,Si)			
	~1055	(DBT)				
78	>1154		zircon $ZrSiO_4$	C2, B	none (1032-1154)	
	~1129	(DBT)				
79	949		SiO_2 (Si)		>1154	C2

* General notes: see end of this Table
(SA) Surface area (see note A of this Table)
(CA) Center area (see note A of this Table)
(DBT) Dissolving boundary temperature (see note B of this Table)

TABLE 11.4. Liquidus Temperature of Crystalline Phases in CVS-II Glasses (continued)

Glass	Crystals Other Than Spinel				Spinel Crystals	
	Liquidus T (°C)		Phase	Note*	Liquidus T (°C)	Note*
Extreme Vertices (Phase 3) (cont.)						
80	>1154		zircon $ZrSiO_4$ (Zr,Si)	C2	~1129	
81	>1154		Li_2SiO_3(?) (Si)	C2	~1013	
82	745		Li_2SiO_3 (Si)		none (693-924)	
83	741		Li_2SiO_3 (Si)		none (719-924)	
			Ca silicate (Ca,Si)	F3		
84	983	(SA)	Na-Zr silicate	A, B	none (869-1028)	
	975	(CA)	(Na,Zr,Si)			
	~966	(DBT)				
85	>1150		Li_2SiO_3(?) (Si)	C2	none (1042-1154)	
86	1015		nepheline (Na,Al,Si; S)		none (967-1154)	
87	<571		no crystals	C3	none (571-874)	
88	982	(SA)	ZrO_2	A	none (901-1152)	
	929	(CA)				
89	838		clinopyroxene (Ca,Fe,Si; Mg)		none (752-924)	
90	897		orthopyroxene (Fe,Si; Cr)		none (841-967)	
91	886		SiO_2 (Si)		>967	C2
92	897		zircon $ZrSiO_4$		~905 high-Ni, -Cr spinel (?)	
93	800	(SA)	clinopyroxene	A, B	>983	C2
	782	(CA)	(Na,Ca,Fe,Si)			
	~794	(DBT)				
94	663		Ca silicate (Ca,Si)		none (642-983)	
DWPF EA Glass						
95	804		clinopyroxene (Ca,Fe,Si; Na,Mg,Ti)		none (712-924)	
CVS-I Center Point Replicate						
96	946		zircon $ZrSiO_4$		~1010	
			clinopyroxene (Ca,Mg,Si; Fe)	F3		
CVS Internal Standard Glass Replicate						
97	858		clinopyroxene (Ca,Na,Fe,Si; Cr,Ni)		~887	
			Na-Zr silicate	F3		

* General notes: see end of this Table
(SA) Surface area (see note A of this Table)
(CA) Center area (see note A of this Table)
(DBT) Dissolving boundary temperature (see note B of this Table)
(?) Liquidus temperature or crystalline phase could not be determined, or was suspceted.

TABLE 11.4. Liquidus Temperature of Crystalline Phases in CVS-II Glasses (continued)

Glass	Crystals Other Than Spinel			Spinel Crystals	
	Liquidus T (°C)	Phase	Note*	Liquidus T (°C)	Note*
Replicate of CVS2-34					
98	740	nepheline		none (717-874)	
Simulated 101-AZ Core 1 Glass					
99	847	clinopyroxene (Ca,Fe,Si; Na)		~988	
Simulated 101-AZ Core 2 Glass					
100	924	orthopyroxene (Fe,Si)		~1030	

General Notes in 11.4

A The front temperature (the highest temperature at which crystals were found) is higher at the glass top surface or crucible bottom than in the center area. The center front temperature is probably close to liquidus temperature unless dissolving crystals are observed (see note B).

B Crystals at high temperature region have rounded corners and edges characteristic for dissolution, probably because (1) crystals that initially formed in lower temperature region were transferred to higher temperature region by convection, or (2) crystals were formed at compositional inhomogeneities which later attenuated. The lowest temperature at which dissolving crystals become noticeable is indicated as DBT (dissolving boundary temperature). This temperature may be closer to the actual liquidus temperature than the front temperature.

C1 The highest temperature to which the sample was exposed appears close to the liquidus temperature.

C2 The highest temperature to which the sample was exposed is lower than the liquidus temperature.

C3 The lowest temperature to which the sample was exposed is higher than the liquidus temperature, or no crystals are formed in the sample at all.

D1 Some crystals and RuO_2 agglomerates settled at the bottom. The estimated liquidus temperature may be inaccurate.

D3 RuO_2 agglomerates and very small spinel crystals (1 ~ 5 μm) are present mainly at the top and bottom areas of the crucible (more at the top area). Other crystals and larger spinel crystals (5 ~ 15 μm) are present mainly in the area where little RuO_2 agglomerates are present. The estimated liquidus temperature may be inaccurate.

E Crystals are difficult to distinguish among RuO_2 agglomerations or other small paricles.

F1 Another crystalline phase other than spinel.

F2 Another spinel type crystal.

F3 Two different crystals with a similar shape are present. It was not possible to distinguish each crystal in the area where the sample was heat treated at around liquidus temperature. Liquidus temperature of one crystal may be slightly lower (0 to ~20°C) than that of another.

When two or more crystalline phases other than spinel are found, the liquidus temperatures of the secondary phases were also obtained. It is possible that some glasses would crystallize secondary phases if they were heat treated at lower temperatures. The liquidus temperatures of the possible secondary phases and of spinel-type crystals were determined within the temperature range used to find the liquidus temperature of the primary phase: no attempt was made to rerun the tests after the liquidus temperature of the primary phase was obtained. For those samples without any spinel crystals, the temperature range in which the sample was tested is shown in the liquidus temperature column of spinel crystals in Tables 11.3 and 11.4. For example, the entry "none (891-1038)" means that this glass was tested between 891 and 1038°C, but no spinel crystals were found.

Crystals that occurred at temperatures close to T_L sometimes had rounded corners and edges characteristic of dissolution, probably because: (1) crystals that initially formed at temperatures lower than T_L were transferred to higher temperatures (close to T_L) by convection, or (2) crystals were formed at compositional inhomogeneities in the early melting which later attenuated. The lowest temperature at which dissolving crystals become noticeable (Dissolving Boundary Temperature, DBT in Tables 11.3 and 11.4) was used as a liquidus temperature. The temperature difference between the crystallization front temperature and DBT did not exceed 30°C except for one glass (42°C in CVS2-47). For some samples, the crystallization front temperature was higher at the glass top surface or at platinum boat bottom area (Surface Area, SA in Tables 11.3 and 11.4) than in the center (internal) area (CA in Tables 11.3 and 11.4). The temperature difference between the center-area front temperature and the surface-area front temperature was always 15°C or less except for one sample (63°C in CVS2-77). The center-area front temperature was used as the liquidus temperature. When the dissolving boundary temperature is obtained in addition to the center front temperature, the lower temperature was used as liquidus temperature in modeling and other data analysis efforts.

11.4.1 Results by Primary Crystalline Phase

Out of 110 glasses (excluding 11 replicates from the 121 glasses tested), six glasses did not precipitate any crystalline phases and three glasses precipitated only spinel (no precipitation of crystals other than spinel) during 24-hour gradient temperature heat treatment. In the following paragraphs of this section, the effect of glass composition on the primary crystalline phase and its liquidus temperature are discussed. The relations between the primary crystalline phases observed in the liquidus temperature samples and the phases identified after CCC are also presented in the following paragraphs when appropriate.

Spinel and Hematite

Even though the liquidus temperatures for spinel crystals were determined only within limited temperature ranges as mentioned earlier in this section, the high-end temperatures tested were at least 800°C or higher for almost all glasses identified as having no spinel crystallization. The spinel crystals in most of the samples are expected to be formed below the high-end temperatures tested if they were stable phases. Therefore, it may be assumed that these glasses do not precipitate any spinel crystals at all.

Out of 27 glasses with Fe_2O_3 > 8 wt%, 20 formed spinel during 24-hour gradient furnace heat treatment. The remaining seven glasses that did not form spinel were usually high in alkali oxides (Na_2O and Li_2O) and always low in Al_2O_3 (< 3.2 wt%). Spinel precipitated in 18 out of 36 glasses with 2 wt% < Fe_2O_3 < 8 wt%, but only in seven out of 47 glasses with $Fe_2O_3 \leq 2$ wt%. The latter glasses had low alkali and high Others concentrations. For example, CVS2-91 had the lowest Fe_2O_3 concentration (0.5 wt%), but had 11.5 wt% total alkali and 9 wt% Others, and formed spinel. The liquidus temperature of spinel was higher than 900°C in all glasses but one (T_L = 800°C for CVS2-24), and in some glasses reached above 1110°C, the hot-end temperature commonly used in the gradient furnace. Only one glass (CVS2-30) with 13.2 wt% Fe_2O_3 precipitated hematite as a primary phase with T_L = 1070°C and this glass also formed hematite during CCC.

The unidentified high-Ni phase (included as "high-Ni spinel (?)" in Tables 11.3 and 11.4) mentioned in Section 11.2 was formed in five glasses with the T_L ranging from 854 to 993°C. Spinel was also observed along with the unidentified phase in four out of these five glasses. All five of these glasses also formed the unidentified phase during CCC.

Clinopyroxene

Clinopyroxenes were formed as primary phases in 24 glasses, and their liquidus temperatures ranged from 761 to 969°C. Three glasses precipitated a Zr-containing phase along with clinopyroxene with almost identical T_L (within ~15°C). Glasses with Fe_2O_3 > 12 wt% did not form clinopyroxene as a primary phase, but usually formed orthopyroxene. When Fe_2O_3 > 7 wt% and CaO > 3 wt%, the clinopyroxene solid solutions contained hedenbergite ($CaFeSi_2O_6$) as a major component. Acmite ($NaFeSi_2O_6$) was found as a major phase only when Na_2O > 10 wt%. Most clinopyroxene phases found in glasses with Fe_2O_3 < 7 wt% were comprised of diopside ($CaMgSi_2O_6$) with hedenbergite as a minor phase.

Among 24 glasses that formed clinopyroxene as the primary phase, during CCC only six precipitated clinopyroxene, 17 did not precipitate any crystals other than spinel, and one precipitated lithium silicate. The first group of six glasses had relatively high T_L of clinopyroxene (all three glasses with T_L > 910°C belonged to this group). One glass (CVS2-76) that precipitated lithium silicate during CCC had the lowest T_L of clinopyroxene (761°C).

Orthopyroxene and Olivine

Twelve glasses precipitated orthopyroxene crystals as their primary phase with T_L ranging from 826 to 973°C for all but one sample (CVS1-8). This high ZrO_2 (8 wt%) glass formed $ZrSiO_4$ and orthopyroxene up to > 1118°C, which mostly settled at the bottom of the boat (the other 11 glasses contained ≤ 4.4 wt% ZrO_2). The orthopyroxene phase was close to $MgSiO_3$ composition in only two glasses, both containing 8 wt% MgO. One glass with 5 wt% MgO and 11.4 wt% Fe_2O_3 formed a solid solution of $FeSiO_3$ and $MgSiO_3$. The remaining nine glasses with Fe_2O_3 > 7 wt% and MgO < 1 wt% formed an orthopyroxene phase that was close to $FeSiO_3$ with Ni and Cr as minor elements.

Olivine was the primary phase in eight glasses, out of which seven had 8 wt% MgO and one had 5 wt% MgO. Fe_2O_3 was between 2 and 14 wt% for these eight glasses. The composition was close to Mg_2SiO_4 with Fe and Ni as minor components, with T_L ranging from 866 to 1042°C except in one glass (CVS1-16) with T_L > 1118°C.

Glasses with orthopyroxene crystals as the primary phase usually had high SiO_2 (> 50 wt% except one glass, CVS1-16) and low Al_2O_3 (≤ 0.08 wt%). In contrast, most glasses with olivine group crystals had relatively low SiO_2 (≤ 52 wt% in six out of the eight glasses) and high Al_2O_3 (≥ 8 wt% in five out of the eight glasses).

Among eight glasses with olivine as the primary phase, seven formed olivine during CCC. Interestingly, the single remaining glass had the highest T_L of olivine and formed nepheline instead of olivine during CCC. Out of 12 glasses with orthopyroxene as the primary phase, five formed orthopyroxene during CCC, five (with Fe_2O_3 > 8 wt%) formed various crystals (such as hematite, spinel, lithium silicate and clinopyroxene), and two (with Fe_2O_3 < 8 wt%) did not form any crystals.

Zirconium-Containing Crystals

Glasses that precipitated Zr-containing primary phases ($ZrSiO_4$, ZrO_2, $Ca_2ZrSi_4O_{12}$, or sodium-zirconium silicate) had at least 3.7 wt% ZrO_2. Out of 20 glasses with ZrO_2 ≥ 7 wt%, 19 glasses had one of the Zr-containing phases, mostly zircon ($ZrSiO_4$), as the primary phase with T_L > 1000°C in 16 glasses (T_L > 1110°C in seven). The remaining glass (CVS1-14), which contained 13 wt% ZrO_2, did not precipitate any crystals. Out of 15 glasses with 3.7 wt% ≤ ZrO_2 < 7 wt%, only five had a Zr-containing primary phase with a T_L ranging from 862 to 1129°C. In three of these five, clinopyroxene precipitated along with Zr-containing crystals with almost the same T_L as mentioned earlier in this section for clinopyroxene. In one glass, $Ca_2ZrSi_4O_{12}$ occurred along with a small amount of $ZrSiO_4$, with T_L > 1118°C for both. Sodium-zirconium silicate was found in five glasses with Na_2O > 11 wt% and T_L ranging from 862 to 1054°C. In one glass (CVS1-18) with a low concentration of SiO_2 (42.1 wt%), the primary phase was ZrO_2 with T_L > 1118°C. Overall, liquidus temperatures

of Zr-containing phases were usually higher (with most of them above 1000°C) than those of any crystalline phases other than spinel. In addition, T_L showed a general tendency to increase as ZrO_2 concentration increased and alkali concentrations decreased.

Among 24 glasses with at least one of the Zr-containing phases as the primary phase, a Zr-containing phase precipitated after CCC in seven out of eight glasses with T_L > 1110°C and in only one out of 16 glasses with T_L < 1110°C. This indicates that zircon crystallization was too slow to precipitate from glasses during CCC even with as much as 13 wt% ZrO_2 if T_L < 1110°C. One glass with 13 wt% ZrO_2 (CVS1-14) did not precipitate any crystals during CCC or during 24-hour isothermal heat treatment. This glass was high in both B_2O_3 (20 wt%) and Na_2O (19 wt%).

Aluminum-Containing Crystals

Nepheline ($NaAlSiO_4$) was the primary phase in eight glasses; its T_L range was between 736 and 1015°C. All these glasses were high in both Na_2O (> 10 wt%) and Al_2O_3 (≥ 9 wt%). The liquidus temperature seemed to decrease as the B_2O_3 concentration increased. Two glasses with 7 wt% Li_2O, 8 wt% Na_2O, and Al_2O_3 > 16 wt% formed lithium-aluminum silicate (a primary phase) with T_L = 815 and 816°C.

Among eight glasses with nepheline as the primary phase, four with T_L ≥ 927°C precipitated nepheline and four glasses with T_L ≤ 803°C did not form any crystals during CCC.

Lithium Silicate

Lithium silicate (Li_2SiO_3) was the primary phase in only four glasses; all contained 7 wt% Li_2O (the highest concentration used) and Na_2O > 17 wt%. The liquidus temperature was low (741 and 745°C) in two glasses and high (T_L > 1150°C) in the other two. The former had higher SiO_2 (≥ 49 wt%) and B_2O_3 (9.5 wt%) concentrations than the latter (44 wt% SiO_2 and 6 wt% B_2O_3).

Out of four glasses with Li_2SiO_3 as the primary phase, three precipitated Li_2SiO_3 during CCC (the remaining glass did not precipitate any crystals).

Calcium Silicate

Calcium silicate was the primary phase in eight glasses with T_L between 663 and 943°C. This phase was never observed in the CCC samples, and so structural information could not be obtained. Judging from the relative peaks of Ca and Si in the qualitative SEM/EDS spectra, it is likely that the composition was $CaSiO_3$. All eight glasses had $CaO \geq 3.5$ wt%, and six of them had $CaO \geq 7$ wt%. Interesting features in these eight glasses were low concentrations of MgO (≤ 0.5 wt%, zero in seven of them), Fe_2O_3 (≤ 4.5 wt%, except in one glass with 14 wt%), and ZrO_2 (≤ 1 wt%, except in one glass with 3 wt%).

Out of eight glasses with calcium silicate as the primary phase, one glass with 14 wt% Fe_2O_3 formed clinopyroxene during CCC and the other seven glasses with $Fe_2O_3 \leq 4.5$ wt% did not precipitate any crystals.

Silicon Dioxide

Silicon dioxide (SiO_2) was the primary phase in seven glasses with T_L from 715 to 957°C. These glasses contained high SiO_2 (≥ 52 wt% except in one glass with 44 wt%) and were generally low in Fe_2O_3 (≤ 2 wt%, except one glass with 10.5 wt%) and ZrO_2 (< 1.8 wt%). Generally, the liquidus temperature of SiO_2 increased as SiO_2 concentration increased and alkali (Na_2O and Li_2O) concentration decreased.

Out of seven glasses with silicon dioxide as the primary phase, only two glasses formed silicon dioxide after CCC and the other five glasses were crystal-free.

Crystal-Free Glasses (Except Spinel)

Nine glasses did not precipitate any crystalline phase other than spinel during 24-hour gradient furnace heat treatment. Generally these glasses showed a high sum of B_2O_3, Na_2O, and Li_2O concentrations and low concentrations of ZrO_2 and Fe_2O_3 (all had $Fe_2O_3 < 7$ wt% and six of them had $Fe_2O_3 \leq 2.5$ wt%). Spinel crystallized in three glasses (CVS2-10, CVS2-15, and CVS2-24). Two of these three glasses (CVS2-10 and CVS2-15) had higher Fe_2O_3 (6.7 and 4 wt%) and

had T_L > 868°C and T_L = 956°C. The other one (CVS2-24) had low Fe_2O_3 (2 wt%), and its T_L = 800°C was the lowest liquidus temperature of spinel observed in this study. As mentioned previously, the group of crystal-free glasses includes one glass with 13 wt% ZrO_2.

11.4.2 Results for Replicate Glasses

The 11 replicate CVS glasses had the same primary crystalline phase as their replicate counterpart glasses. A summary of liquidus temperatures of crystals other than spinel and of spinel crystals from replicate glasses is given in Table F.8 in Appendix F. Table F.8 also includes the means, standard deviations (SD), and percent relative standard deviations (%RSD) from each replicate set. The agreement of the liquidus temperature data for crystals other than spinel was very good with the maximum %RSD = 1.4, excluding CVS1-1. CVS1-1 had liquidus temperatures of 959°C for zircon and 903°C for clinopyroxene, while its five replicate samples had liquidus temperatures between 913 and 946°C for both zircon and clinopyroxene (see general notes F1 and F3 at the end of Table 11.4).

The liquidus temperature of spinel crystals also showed reasonably good agreement for replicate samples with determined T_L values. For replicate set 1 (except CVS1-1), the scatter of data was greater for spinels with %RSD = 2.9 than non-spinel crystals with %RSD = 1.4. This is understandable given the difficulties encountered during the crystallization front temperature determination for spinel crystals. Their small size and dark color (almost black) made it difficult to distinguish them from noble metal oxides, usually RuO_2 particles and agglomerations thereof.

11.4.3 Effects of Different Others

CVS2-55, -56, and -57 had the same nominal composition as the CVS internal standard glass (CVS2-19 and its replicates CVS2-51 and CVS2-97), but with different Others compositions (see Tables 4.8 and 4.10). The primary phase in CVS2-19 and CVS2-56 was clinopyroxene with T_L = 860°C (average value from three replicate glasses) and 880°C, respectively. CVS2-55 and CVS2-57 formed Cr_2O_3 as the primary phase with T_L = 944 and 1036°C, and clinopyroxene

as a secondary phase with T_L = 906 and 945°C. CVS2-55, -56, and -57 as well as the internal standard glass precipitated spinel and their liquidus temperatures increased as Cr_2O_3 concentration increased from 893°C (average value from CVS2-51 and CVS2-97) for the internal standard glass (with 0.13 wt% Cr_2O_3) up to > 1118°C in CVS2-55 (with 0.89 wt% Cr_2O_3).

CVS2-64 and CVS2-71 with the same nominal composition but slightly different Others (see Tables 4.13 and 4.1, respectively) had the same primary phase (orthopyroxene) with very close T_L values of 895 and 890°C. The liquidus temperature of spinel in these two glasses was also close with 983 and 1004°C.

Nepheline was the primary phase in CVS2-66 and CVS2-72 with the same nominal composition but different Others. CVS2-66 used Others with higher Cr_2O_3, MnO_2, and MoO_3 than Others in CVS2-72 but had almost the same T_L (799°C) as CVS2-72 (794°C). Spinel was formed in these two glasses, but the liquidus temperatures were not determined because they were higher than the hot-end temperatures used for both samples (1114 and 868°C, respectively).

CVS2-68, -69, and -70 used modified Others with high Cr_2O_3 (2.97, 2.38, and 1.17 wt% Cr_2O_3 in glass) and all formed Cr_2O_3 as the primary phase with T_L > 1114°C. Among CVS2-73, -74, and -75 with the same nominal composition as CVS2-68, -69, and -70 but with NCAW-87 Others, lithium-aluminum silicate was the primary phase in CVS2-73 and CVS2-75, and clinopyroxene in CVS2-74. Spinel was formed only in CVS2-69 and its counterpart with the same nominal composition, CVS2-74, with T_L > 1114°C and 1066°C, respectively. The higher T_L of spinel in CVS2-69 can be attributed to its higher Cr_2O_3 content than that of CVS2-74.

11.5 CRYSTALLINITY AND LIQUIDUS TEMPERATURE DISCUSSION

The primary crystalline phases identified in the liquidus temperature samples were generally found also in CCC samples, but this did not occur in some glasses. In these glasses, CCC either produced different crystalline phases, or the glasses remained free of crystals. Glasses with T_L < 1050°C are not expected to develop crystallinity in a 1150°C melter. Glasses with T_L > 1050°C may or may not devitrify in such a melter, dependent on kinetic

factors. These glasses may not even crystallize in the canister if their crystallization rate is slow. As discussed in Section 11.4, several glasses with T_L > 1050°C produced little or no crystallinity during CCC.

Some glasses produced unusually high crystallinity during CCC. CVS2-85 had the highest crystallinity of 60% (in volume), followed by CVS2-42 with 30-35%, CVS2-80 with 30%, CVS2-78 with 28%, CVS2-79 with 26%, CVS2-25 with 22%, and CVS1-8 with 15-21%. Such a high degree of crystallinity may impact product durability. The effect, discussed in Section 12.12, deserves a systematic study.

Out of 58 glasses that precipitated at least one type of crystal, 45 glasses produced more than 2 volume % crystallinity during CCC. If such glasses were produced and put in a canister, the spatial distribution of crystallinity within the canister could be determined based on the temperature history of the canister glass and TTT diagrams. As mentioned earlier, some crystal-free glasses after CCC had high liquidus temperatures (> 1110°C) and some glasses with unusually high crystallinity had liquidus temperature lower than 900°C. Hence, no clear correlation is apparent between liquidus temperature and the amount of crystallinity produced during CCC. The kinetic factors obviously play a decisive role.

Figure 11.5 shows the distribution of samples according to crystalline phases identified in canister centerline cooled CVS glasses. Figure 11.5 includes the crystalline phases that were formed in at least five glasses. Cr_2O_3 was formed in four glasses, all of which used modified Others components to simulate glasses that may be made from several types of wastes. Nine other minor crystalline phases were observed only in one or two glasses. The total number of glasses in Figure 11.5 exceeds 58 (the number of glasses that formed at least one type of crystalline phase during CCC, see Section 11.2) because some glasses formed two or more phases. As shown in Figure 11.5, spinel was found in the highest number of glasses (in 29), followed by lithium silicate (in 13) and clinopyroxene (in 12).

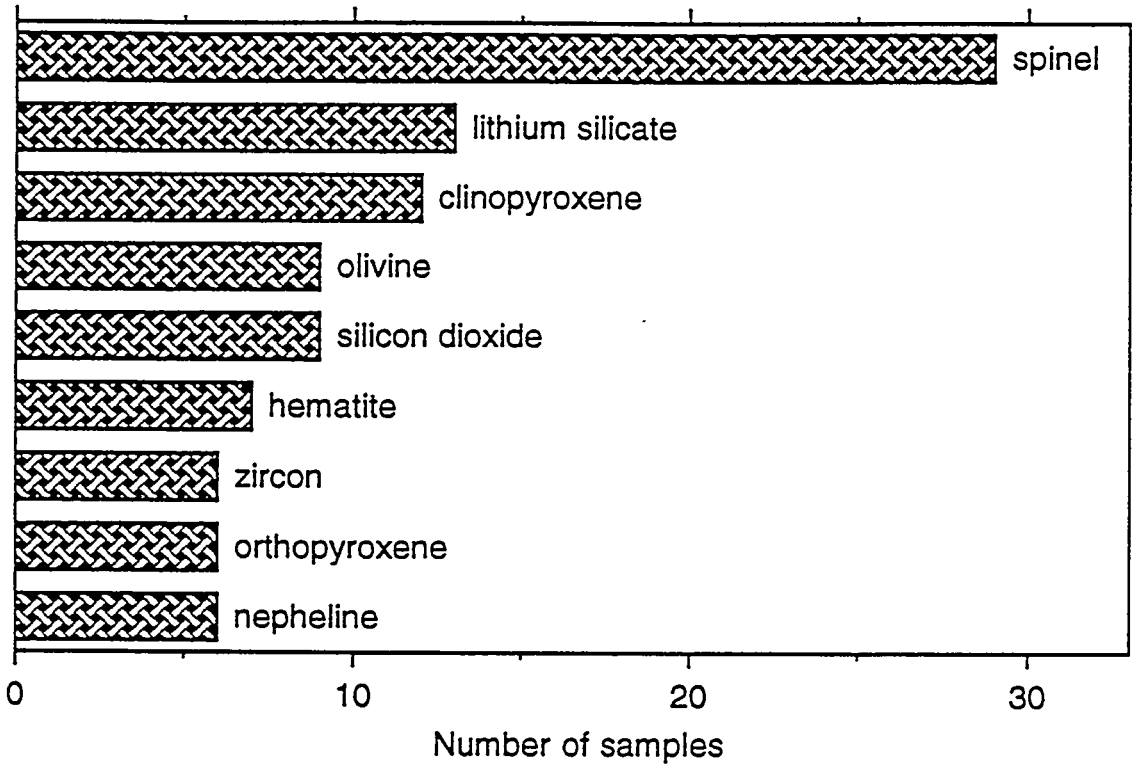

FIGURE 11.5. Number of CVS Glass Samples with Major Crystalline Phases Identified After Canister Centerline Cooling (some samples formed two or more phases)

Table 11.5 summarizes the effect of single- or multiple-component concentrations on the crystallization of CVS glasses during CCC. The maximum single- or multiple-component concentrations that existed in CVS glasses without precipitating any crystals are shown in the second column. For the SiO_2/Al_2O_3 ratio and the sums of $(B_2O_3 + Na_2O + Li_2O)$ and $(Na_2O + Li_2O)$, lower limits are given because these factors are expected to suppress crystallization. In the third column, the maximum or minimum single- or multiple-component concentrations that resulted in the precipitation of at least one type of crystalline phase are shown. The ranges of concentrations that were tested in CVS are given in the last two columns.

TABLE 11.5. Maximum/Minimum Single- or Multiple-Component Concentrations That Precipitated No Crystalline Phases and Minimum/Maximum Single- or Multiple-Component Concentrations That Precipitated at least One Type of Crystalline Phase During Canister Centerline Cooling (CCC). All concentrations are in wt%.

Crystallization Promoting Component(s)	No Crystals During CCC Upper Limit	Crystals During CCC Lower Limit	Range Tested in CVS (a) Lower Limit	Upper Limit
Fe_2O_3	10.5	0.13	0.04 (.5)	15.0 (15)
Al_2O_3	20.4	0	0 (0)	20.4 (17)
ZrO_2	13.0	0	0 (0)	15.5 (13)
Others	10.0	1.0	0.8 (1)	10.0 (10)
CaO + MgO (b)	10.0	0	0	10.0 (10)
Fe_2O_3 + Al_2O_3 + ZrO_2 + Others (b)	23.2	5.0	3.0	26.6 (24)
Al_2O_3 + ZrO_2 (b)	20.4	0	0	20.4 (18)
CaO + MgO + ZrO_2 (b)	18.0	0	0	23.0 (18)
CaO + MgO + Fe_2O_3 + Al_2O_3 + ZrO_2 + Others	29.0	9.5	3.4	34.0
CaO + MgO + Fe_2O_3	15.0	0.3	0.3	25.0
MgO + Fe_2O_3	11.0	0.2	0.1	23.0

Crystallization Suppressing Components	Lower Limit	Upper Limit		
SiO_2/Al_2O_3 (b)(c)	2.3	∞ [153]	1.8 (3)	∞ [202]
B_2O_3 + Na_2O + Li_2O	17.0	36.7	14.4	41.1
Na_2O + Li_2O	7.8	25.0	6.2	25.0

(a) CVS single- or multiple-component constraints are given in parentheses. Some glasses had compositions representative of several waste types that were not limited by the CVS single- or multiple-component constraints.

(b) Stand-in multiple-component constraints were used in CVS to indicate the possibility of higher crystallinity or liquidus temperature.

(c) The numbers in square brackets represent the maximum SiO_2/Al_2O_3 ratios when Al_2O_3 concentration is not zero.

As can be seen in Table 11.5, most of the single- or multiple-component concentrations that resulted in no crystallization during CCC extend (or are close) to the upper/lower limits tested in the CVS study. The results in Table 11.5 indicate that certain glasses with high concentrations of crystallization-promoting components and certain glasses with very low B_2O_3 or alkali can be crystal-free. The exceptions to the observation that crystal-free glasses exist over the full ranges of components studied in CVS were Fe_2O_3 among single components and the sums of (CaO + MgO + Fe_2O_3) and (MgO + Fe_2O_3) among multiple components. The worst case was the sum of (MgO + Fe_2O_3), where the maximum concentration of (MgO + Fe_2O_3) without crystallization was only 11 wt% compared to the maximum of 23 wt% tested in CVS.

All the lower concentration limits of crystallization-promoting component(s) that precipitated at least one type of crystal are very close to or the same as the lower limits tested in CVS. This is because, at low concentrations of given components, crystallization will depend on the concentrations of other crystallization-promoting components. The upper limits of crystallization-suppressing component(s) that precipitated at least one type of crystal are also very close to or the same as the upper limits tested in CVS. This suggests that certain glasses with very high concentrations of B_2O_3 and alkali can crystallize during CCC.

Figure 11.6 summarizes the liquidus temperatures of major crystalline phases identified in CVS glasses. As stated previously, glasses with $T_L \geq$ 1050°C can cause problems because they may precipitate crystals in the melter. Zirconium-containing crystals, spinel, and Cr_2O_3 are major crystalline phases that have strong possibilities of precipitating in the melter. Among these crystalline phases, Cr_2O_3 crystallization may be mainly dependent on the Cr_2O_3 concentration. Glasses with high Cr_2O_3 must be studied for other possible problems, such as phase separation, in addition to crystallization. Spinels usually grow as very small particles (< 5 μm) and may not affect melt processability if they are present in small quantities. As is shown in Section 11.6, the liquidus temperature of glass in general does not show strong dependence on the glass composition independent of crystalline phase,

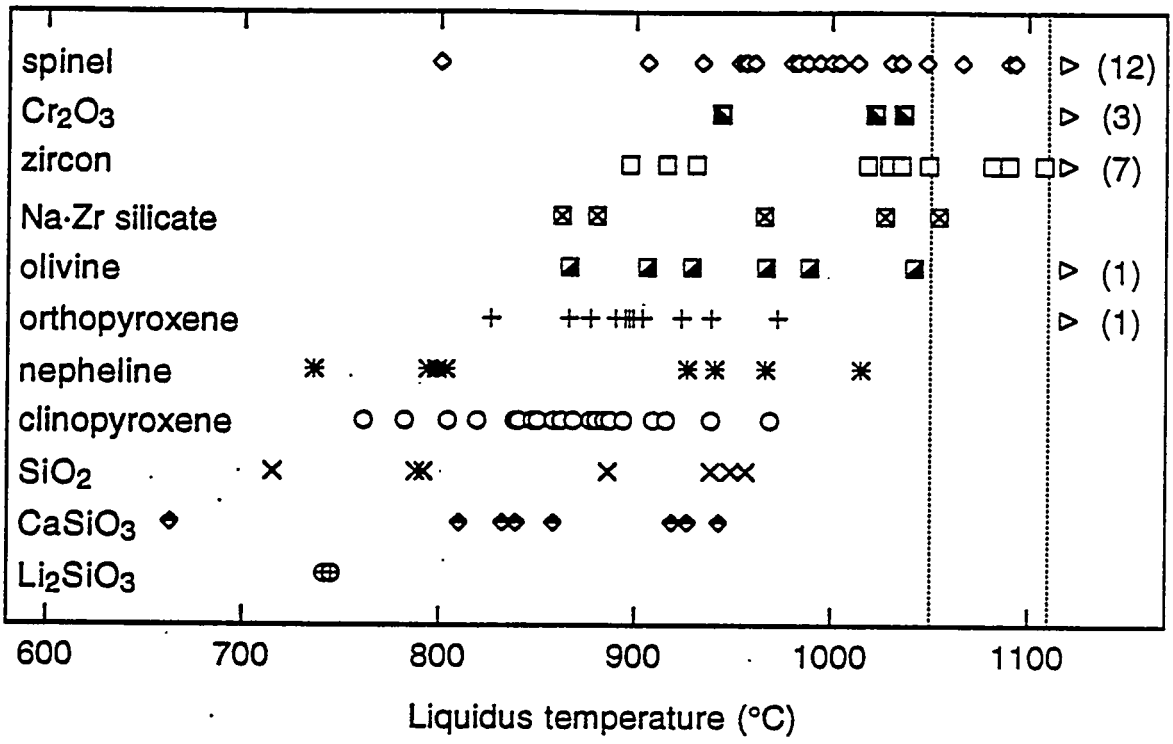

FIGURE 11.6. Liquidus Temperatures of Major Crystalline Phases in CVS Glasses. (The quantities in parentheses at the right of the figure represent the number of samples with $T_L \geq 1110°C$.)

because the compositional dependence of the liquidus temperature is different for different crystals. In Section 11.7, first-order mixture models for spinel and Zr-containing crystals are presented and the compositional dependence of the liquidus temperature of these crystals is discussed.

11.6 LIQUIDUS TEMPERATURE AND MULTIPLE-COMPONENT CONSTRAINTS

As mentioned in Section 4, multiple-component crystallinity constraints (see Tables 4.2 and 4.6) defining various composition subregions were used in developing the experimental designs for CVS-I and CVS-II Phases 1, 2, and 3. These constraints were originally (at the start of the CVS) intended to serve as indicators of the possibility of significant crystallinity and/or higher

liquidus temperatures. The multi-component expressions used in these constraints were not intended to correlate well with crystallinity or liquidus temperature. However, it was decided to investigate the relationships between the expressions used in the constraints and experimentally determined liquidus temperatures.

Figures 11.7 through 11.11 show the plots of liquidus temperature versus oxide ratio or sums used as multiple-component constraints. Different plotting symbols were used for different primary phases. For samples with "greater than" values for T_L, the hot-end temperatures were shown, but were not included in the calculation of R^2 values. The liquidus temperature data for Cr_2O_3 were not included in these plots: Cr_2O_3 was the primary phase only in glasses with modified Others component with high Cr_2O_3, and its liquidus temperature was not relevant to any multiple-component constraints.

As can be seen in Figures 11.7 through 11.11, none of the multiple-component constraints showed good correlation with liquidus temperature. The liquidus temperature had the strongest dependence (of all the multiple-component constraints used) on the sum of CaO, MgO, and ZrO_2 (Figure 11.10) with $R^2 = 0.314$. However, it should be noted that the maximum value of CaO and MgO sum was only 0.1 and, thus, the sum of CaO, MgO, and ZrO_2 at the higher end includes mainly high ZrO_2, which increases the liquidus temperatures of Zr-containing phases. In Figure 11.10, most glasses with CaO + MgO + ZrO_2 > 0.12 had Zr-containing crystals as the primary phase, which usually have higher liquidus temperatures than other primary phases. For the sum of Al_2O_3 and ZrO_2 (Figure 11.9), no correlation was found and $R^2 = 0$. The SiO_2/Al_2O_3 ratio was the only constraint with a lower limit, because it was expected that too low a value for this ratio would cause problems with excessive crystallinity or high liquidus temperature. It is not possible to confirm this expectation by use of Figure 11.11, due to lack of data below the lower limit.

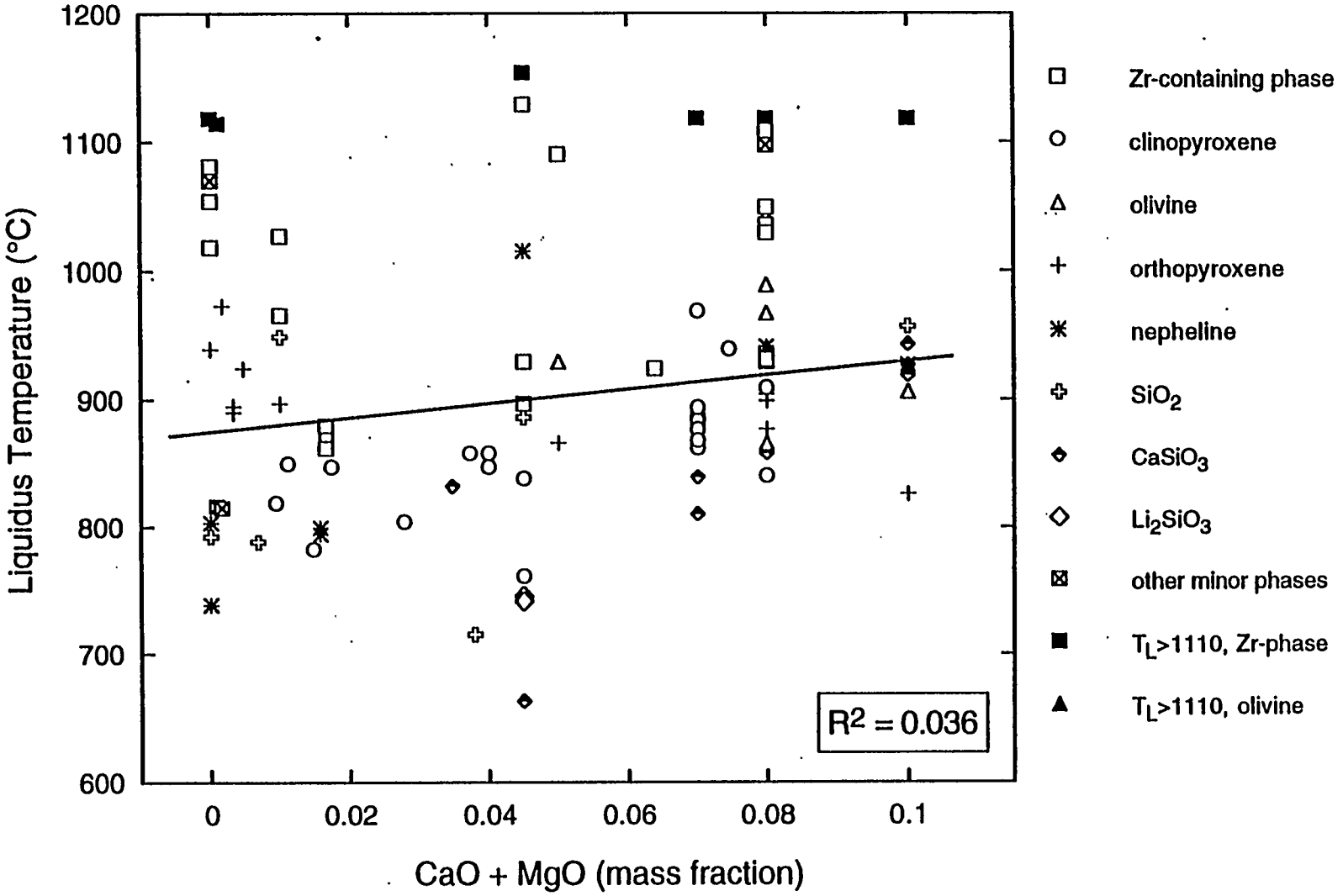

FIGURE 11.7. Effect of (CaO + MgO) Concentration on the Liquidus Temperature of Crystalline Phases Identified in CVS Glasses

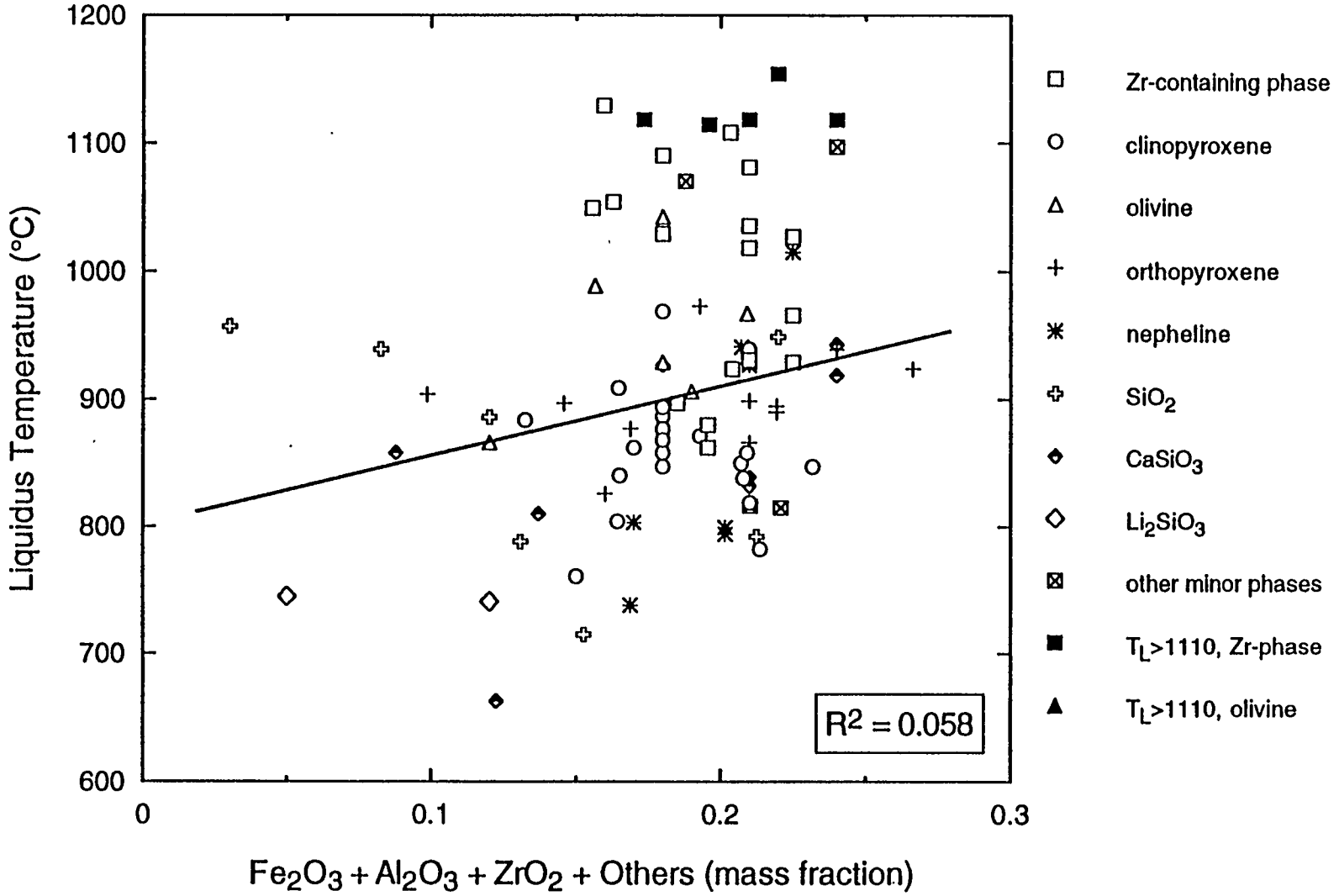

FIGURE 11.8. Effect of (Fe_2O_3 + Al_2O_3 + ZrO_2 + Others) Concentration on the Liquidus Temperature of Crystalline Phases Identified in CVS Glasses

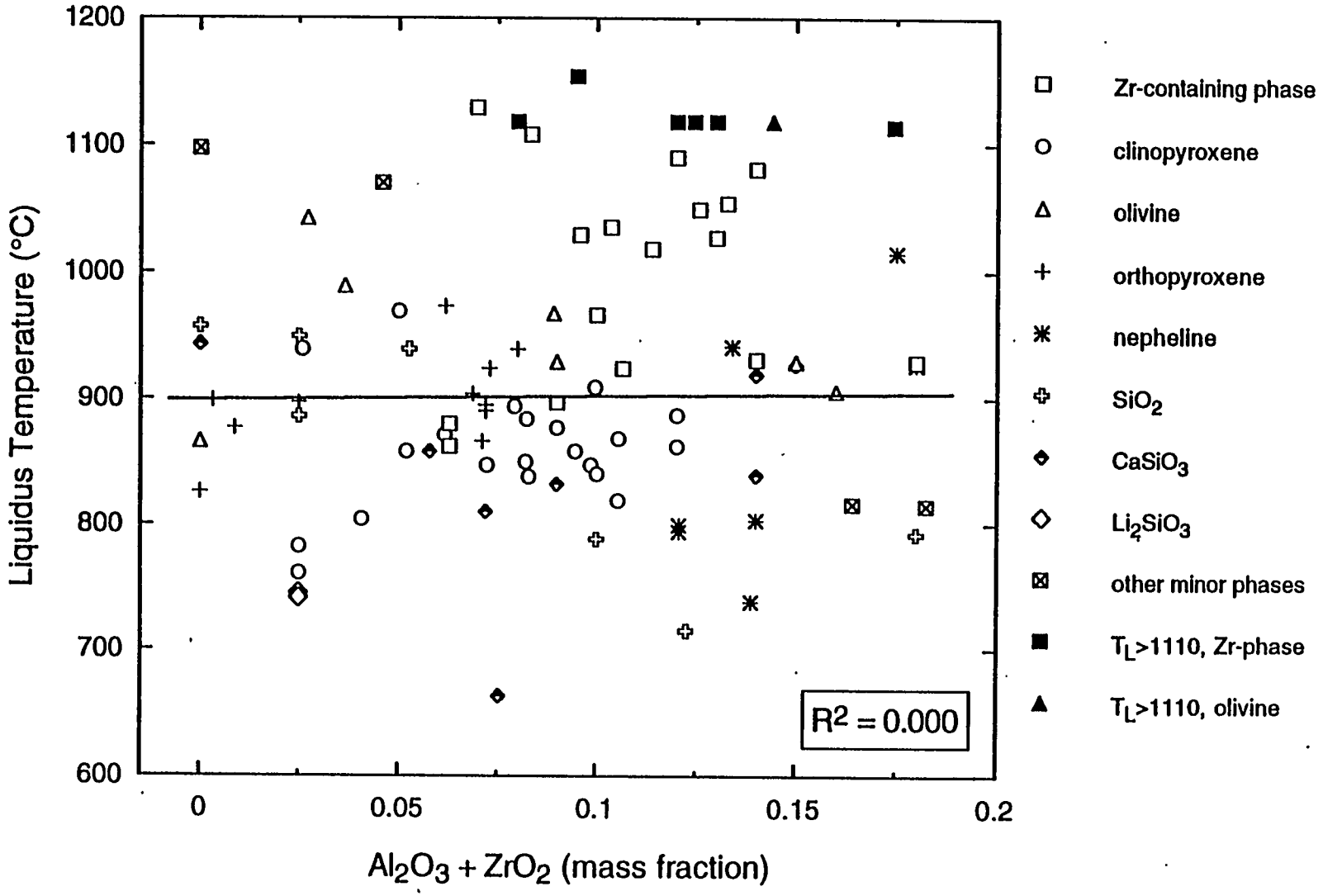

FIGURE 11.9. Effect of (Al_2O_3 + ZrO_2) Concentration on the Liquidus Temperature of Crystalline Phases Identified in CVS Glasses

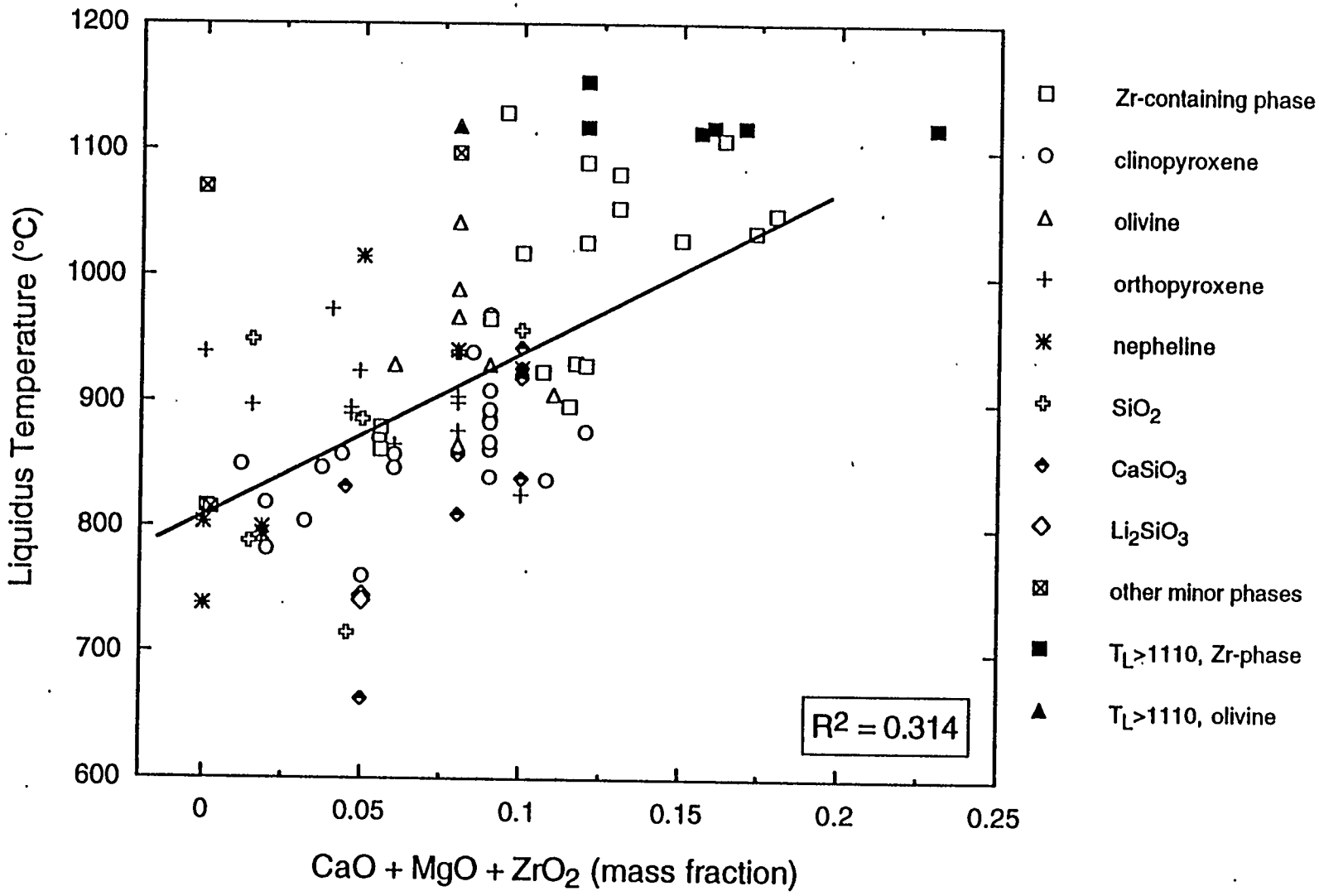

FIGURE 11.10. Effect of ($CaO + MgO + ZrO_2$) Concentration on the Liquidus Temperature of Crystalline Phases Identified in CVS Glasses

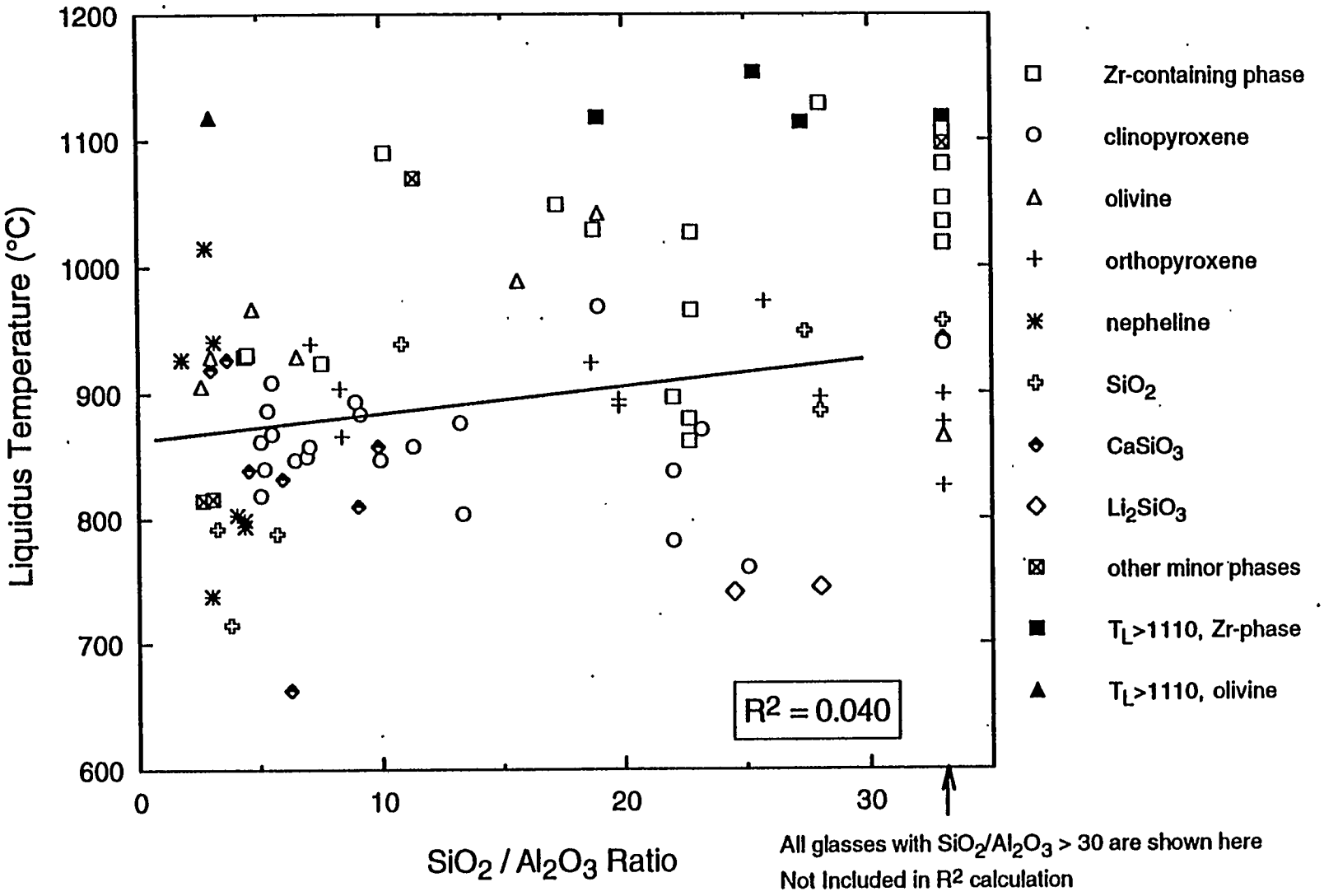

FIGURE 11.11. Effect of (SiO/Al_2O_3) Ratio on the Liquidus Temperature of Crystalline Phases Identified in CVS Glasses

Some of the oxide components used in the constraints are major components in many of the wastes. By limiting the concentrations of these components (through single- and multiple-component constraints) in the CVS glasses studied so far, the present CVS property models are applicable only over a glass composition region with limited waste loadings. To develop glasses with maximum waste loading, it will be necessary to expand the CVS composition range beyond these constraints, especially for those components that strongly increase the liquidus temperature of high-temperature crystals (such as spinel or Zr-containing phases).

11.7 LIQUIDUS TEMPERATURE FIRST-ORDER MIXTURE MODELS

The liquidus temperature data in Table 11.6 for CVS glasses with spinel, clinopyroxene, and zirconium-containing crystals were each fitted to the first-order mixture model of the form given by Equation (6.1) in Section 6.1.1. The number of data points for other crystalline phases was not large enough to fit the model. The first-order model coefficients and R^2 values for spinel, clinopyroxene, and zirconium-containing crystals are summarized in Table 11.7. Plots of predicted versus measured values are shown in Figures 11.12 to 11.14. Data from glasses with modified Others composition were not included in the calculation for spinel and clinopyroxene because Cr_2O_3 and NiO in the Others component affected the liquidus temperature. For Zr-containing crystals, the number of data points was large enough to fit the model only when all three different types of crystals (zircon, sodium-zirconium silicate, and ZrO_2) were treated together (Figure 11.14).

As shown in Table 11.7, the first-order model for clinopyroxene (Figure 11.12) showed the best fit of all these models with $R^2 = 0.906$, which is very good considering the differences in chemical compositions of clinopyroxenes identified in CVS glasses. The fit for the liquidus temperature of spinel (Figure 11.13) was poor. The fit for the liquidus temperature of Zr-containing crystals (Figure 11.14) was reasonably good although three different crystals were included in the model. It is expected that the fit would be better if the number of data points for each Zr-containing crystal was large enough to fit a separate model for each.

TABLE 11.6. List of Glass Data Points Used for Liquidus Temperature First-Order Mixture Models

Clinopyroxene

Glass (a)	T_L (°C)
CVS1-19 (1)	916
CVS1-20 (1)	913
CVS1-23	880
CVS2-6	939
CVS2-7	819
CVS2-12	840
CVS2-13	909
CVS2-16 (4)	877
CVS2-17 (1)	925
CVS2-18 (4)	865
CVS2-19 (5)	862
CVS2-40	862
CVS2-41	887
CVS2-42	969
CVS2-44	884
CVS2-45	894
CVS2-46	858
CVS2-47	919
CVS2-48	868
CVS2-49	847
CVS2-50 (1)	922
CVS2-51 (5)	856
CVS2-74	850
CVS2-76	761
CVS2-89	838
CVS2-93	794
CVS2-95	804
CVS2-96 (1)	946
CVS2-97 (5)	858

Spinel

Glass (a)	T_L (°C)
CVS1-5	1035
CVS1-11	1035
CVS1-17	1000
CVS1-19 (1)	961
CVS1-20 (1)	966
CVS1-23	980
CVS2-1	1048
CVS2-5	988
CVS2-7	934
CVS2-15	956
CVS2-16 (4)	906
CVS2-17 (1)	971
CVS2-18 (4)	895
CVS2-22	994
CVS2-24	800
CVS2-30	1090
CVS2-42	1093
CVS2-46	1004
CVS2-49	957
CVS2-50 (1)	1025
CVS2-51 (5)	899
CVS2-71	1004
CVS2-80	1129
CVS2-81	1013
CVS2-96 (1)	1010
CVS2-97 (5)	887
CVS2-99	988
CVS2-100	1030

Zr-containing Crystals

Glass (a)	T_L (°C)
CVS1-19 (1)	916
CVS1-20 (1)	913
CVS2-3	931
CVS2-9	1018
CVS2-11	1035
CVS2-17 (1)	925
CVS2-19 (5)	862
CVS2-20	1081
CVS2-26	1049
CVS2-29	1108
CVS2-32	1054
CVS2-39	1029
CVS2-43	1090
CVS2-50 (1)	922
CVS2-51 (5)	856
CVS2-77	1027
CVS2-78	1129
CVS2-84	966
CVS2-88	929
CVS2-92	897
CVS2-96 (1)	946
CVS2-97 (5)	858

T_L (Measured) > T_L (Max. tested) (b)

Spinel

Glass	T_L (°C)
CVS1-8 (3)	>1118
CVS1-9	>1118
CVS1-16	>1118
CVS1-22 (3)	>1118
CVS2-6	>1004
CVS2-8	>1118
CVS2-19	>883
CVS2-25	>951
CVS2-33	>1038
CVS2-38	>1115
CVS2-45	>956
CVS2-52	>1038
CVS2-72	>868
CVS2-79	>1154
CVS2-91	>967
CVS2-93	>983

Zr-containing Crystals

Glass	T_L (°C)
CVS1-6	>1118
CVS1-7	>1118
CVS1-8 (3)	>1118
CVS1-18	>1118
CVS1-22 (3)	>1118
CVS2-14	>1118
CVS2-65	>1114
CVS2-80	>1154

(a) Glasses with same number in parentheses are replicates.

(b) The measured T_L was higher than the hot-end temperature tested in the gradient furnace. These data were not included in the calculation of the model coefficients.

TABLE 11.7. Coefficients and Goodness-of-Fit Statistics for First-Order Mixture Models Using Mass Fractions Fitted to Liquidus Temperature (°C) Data for Three Primary Crystalline Phases

Component	Clinopyroxene	Spinel	Zr-containing Crystals
SiO_2	955.65	989.31	753.78
B_2O_3	314.72	666.42	1095.83
Na_2O	38.83	3.77	74.31
Li_2O	-207.05	-128.77	-956.39
CaO	1372.44	1366.21	886.76
MgO	2387.62	2830.58	2458.47
Fe_2O_3	1506.69	2256.00	1461.04
Al_2O_3	1319.78	1735.03	1138.06
ZrO_2	1844.50	928.11	4541.99
Others	1357.40	1005.56	657.99
# of data	29	28	22
Average T_L	874.55	985.64	979.17
R^2	0.9054	0.6433	0.7902
R^2(ADJ)	0.8605	0.4629	0.6328
R^2(PRESS)	0.6921	-0.8188[a]	0.3461

(a) The negative R^2(PRESS) value for the spinel model is due to three very influential data points (CVS1-11, CVS2-30, and CV2-81). Refitting the model without these three data points gave R^2 = 0.93, R^2(ADJ) = 0.89, and R^2(PRESS) = 0.74. However, the resulting model did not predict as well as the model reported here for the three data points or for the "greater than" liquidus temperature data listed at the bottom of Table 11.6.

For spinel and Zr-containing crystals with the measured T_L higher than the hot-end temperature tested in the gradient furnace, the plots of predicted liquidus temperature versus the hot-end temperature were overlaid in Figures 11.13 and 11.14. These data were not included in the calculation of the first-order mixture model coefficients. The overlaid plots of "greater than" T_L values can provide some information on the extrapolative values of the

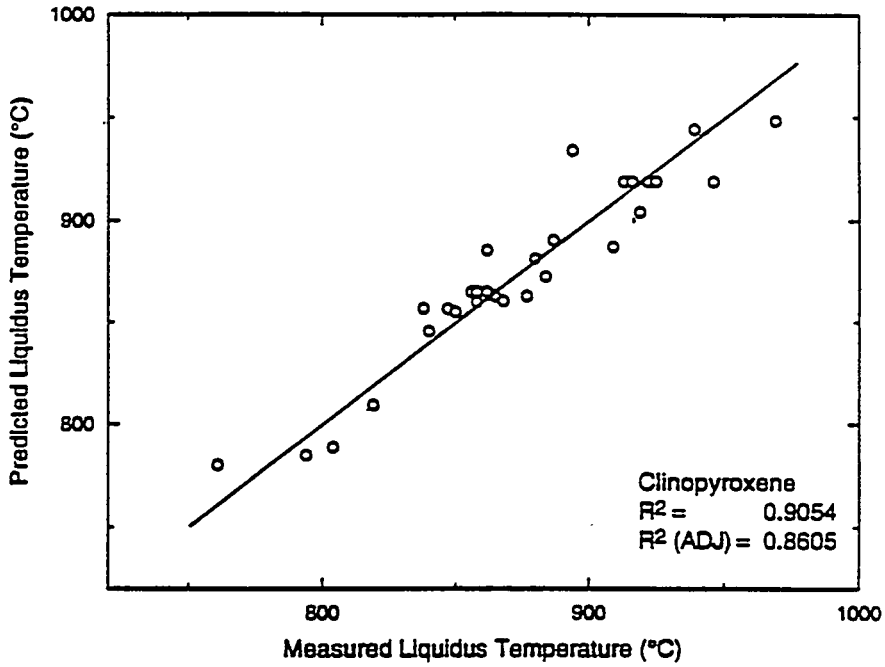

FIGURE 11.12. Predicted Versus Measured Liquidus Temperature of Clinopyroxene for the First-Order Mixture Model

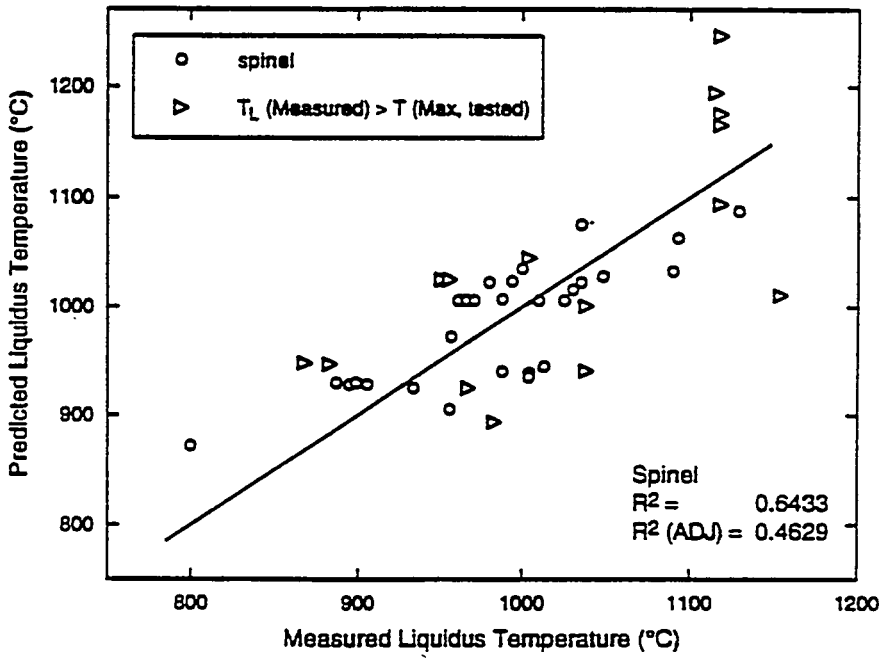

FIGURE 11.13. Predicted Versus Measured Liquidus Temperature of Spinel for the First-Order Mixture Model

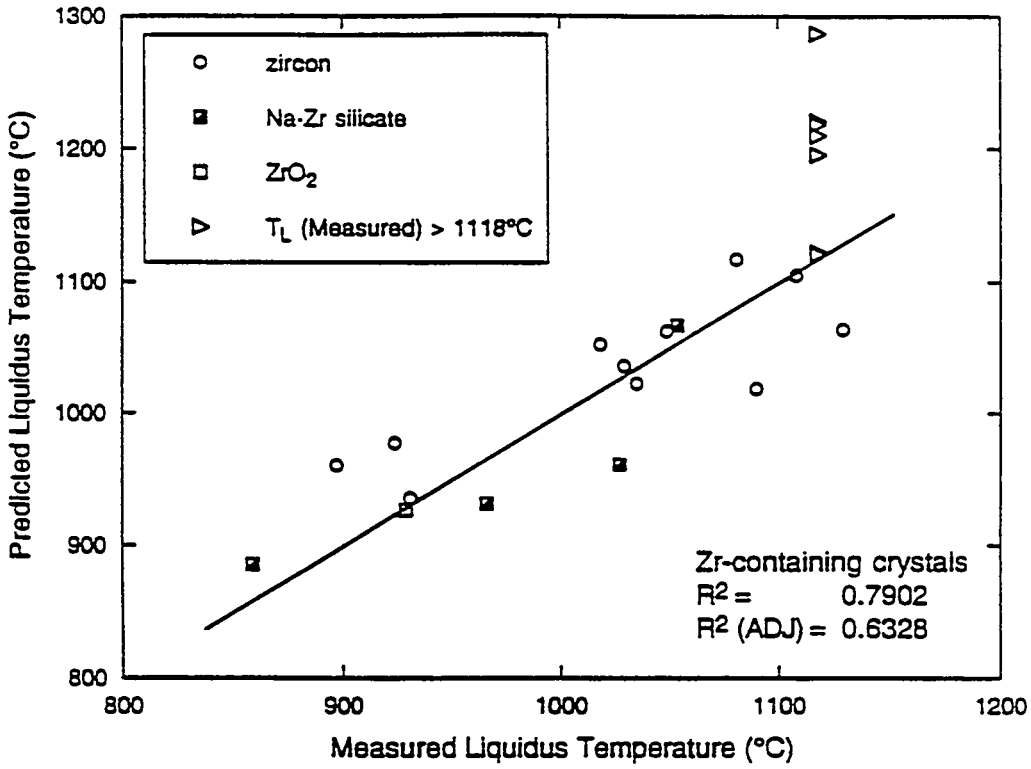

FIGURE 11.14. Predicted Versus Measured Liquidus Temperature of Zr-Containing Crystals for the First-Order Mixture Model

models. For Zr-containing crystals, the liquidus temperatures predicted by the first-order model were higher than the hot-end temperatures in all six glasses with "greater than" T_L values (see Figure 11.14). This suggests that the model may have some semi-quantitative predictive value for glasses with higher liquidus temperatures than the maximum temperature experimentally tested. Out of 15 glasses with "greater than" T_L values for spinel as the primary crystalline phase, the liquidus temperature was predicted to be higher than the "greater than" values for nine glasses and was predicted to be lower than the "greater than" values in six glasses (see Figure 11.13). This indicates the need for major improvement. The poor fit of the spinel model may be the result of redox reaction in glasses affecting the concentration of reduced iron oxide (FeO), which plays an important role in the precipitation of spinel.

Effects plots (see Section 6.3) with the HW-39-4 glass as the reference composition are shown for the first-order models of Table 11.7 in

Figures 11.15, 11.16, and 11.17. The effects of various components based on these effects plots and the relative magnitudes of the first-order model coefficients are discussed in the following paragraph. However, the somewhat lower R^2 values for the spinel and Zr-containing crystals liquidus temperature models suggests that the predicted effects based on these models be considered with some caution.

The relative magnitudes of the coefficients in Table 11.7 and the effects plots in Figures 11.15, 11.16, and 11.17 show that alkali oxides (Na_2O and Li_2O) are predicted to decrease the T_L of all three crystalline phases, Li_2O always having the stronger effect. B_2O_3 is predicted to decrease the T_L of clinopyroxene and spinel but is predicted to slightly increase that of Zr-containing crystals. MgO and Fe_2O_3 were predicted to increase the T_L of clinopyroxene, which can be expected from the observation that Mg and Fe were the major ingredients in most of the clinopyroxenes identified in CVS glasses. ZrO_2 was predicted as strongly increasing the T_L of clinopyroxene (with an effect between those of MgO and Fe_2O_3), although ZrO_2 was not a major component in clinopyroxenes. The T_L of spinel was predicted as most strongly increased by the presence of MgO and Fe_2O_3. It is surprising that MgO was predicted as having the strongest effect (even stronger than Fe_2O_3), because Mg was never detected in spinel crystals identified in CVS glasses. The low Others coefficient for spinel crystals in Table 11.7 and the effects plot in Figure 11.16 suggests Others has a negligible effect on T_L. However, experimental results seem to suggest that the Others component promotes the formation of spinel at low Fe_2O_3 concentrations (see Sections 11.2 and 11.4)[(a)]. As expected, ZrO_2 was predicted as most effective in increasing the T_L of Zr-containing crystals. MgO was also predicted as strongly increasing the T_L of Zr-containing crystals, although not as strongly as ZrO_2. This strong predicted effect of MgO is surprising (as it was for spinel crystals).

(a) This experimental observation suggests that the Others component may have an interactive effect with Fe_2O_3. However, the data in Table 11.6 were insufficient to consider fitting second-order mixture models, which provide for interactive (and curvature) effects of components.

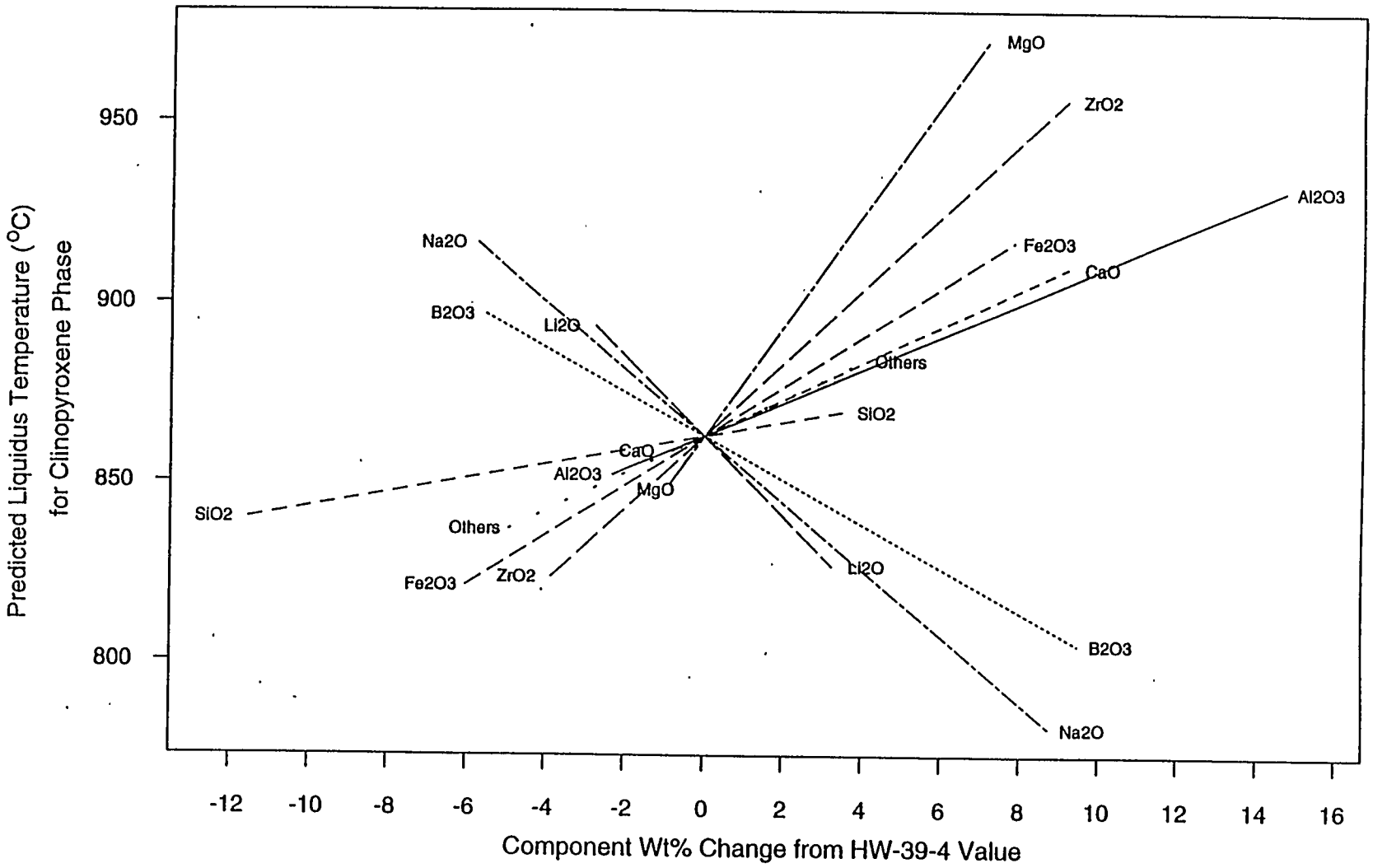

FIGURE 11.15. Predicted Component Effects on Liquidus Temperature of Clinopyroxene Relative to the HW-39-4 Composition, Based on the First-Order Mixture Model Using Mass Fractions (in Column 2 of Table 11.7)

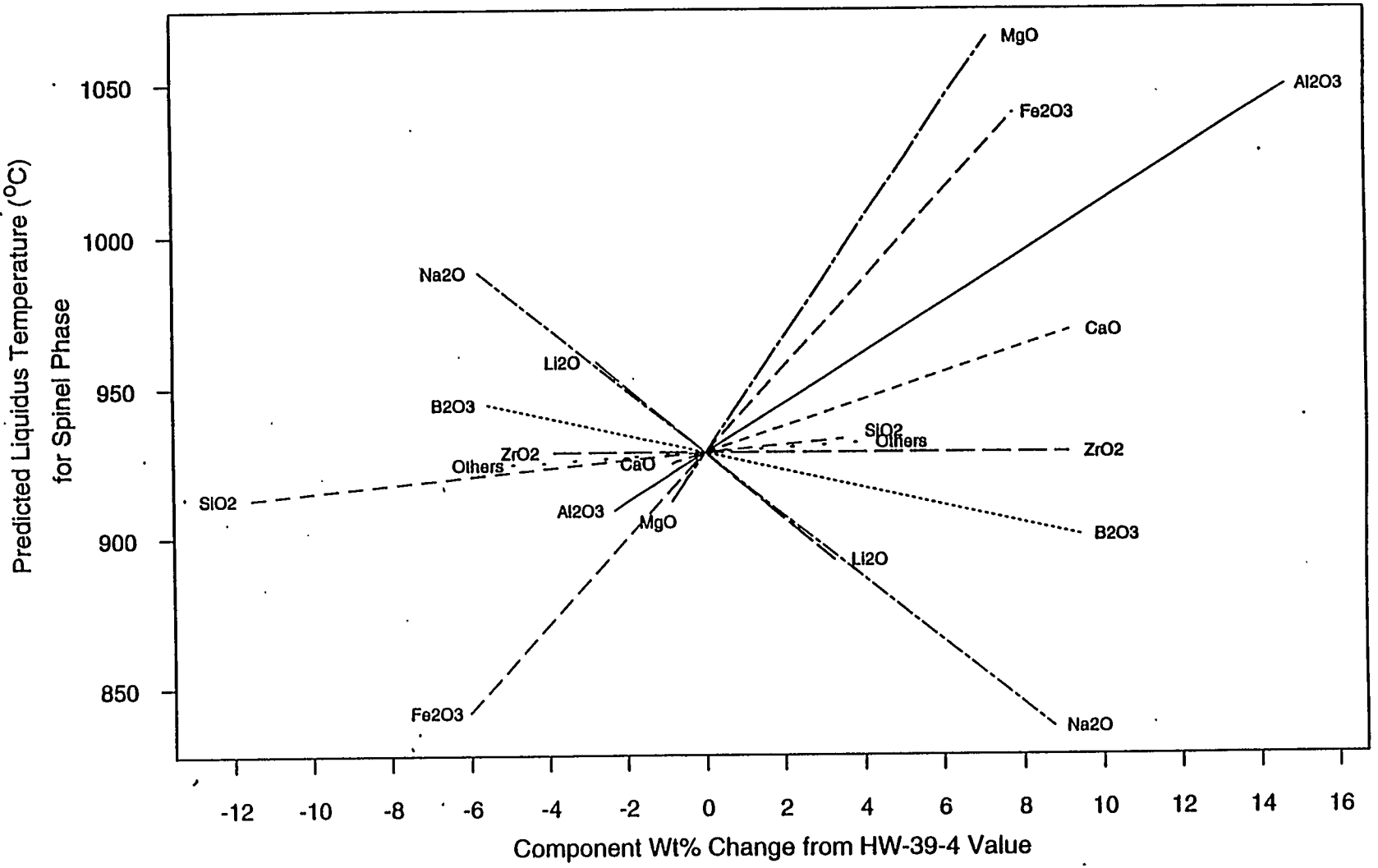

FIGURE 11.16. Predicted Component Effects on Liquidus Temperature of Spinel Relative to the HW-39-4 Composition, Based on the First-Order Mixture Model Using Mass Fractions (in Column 3 of Table 11.7)

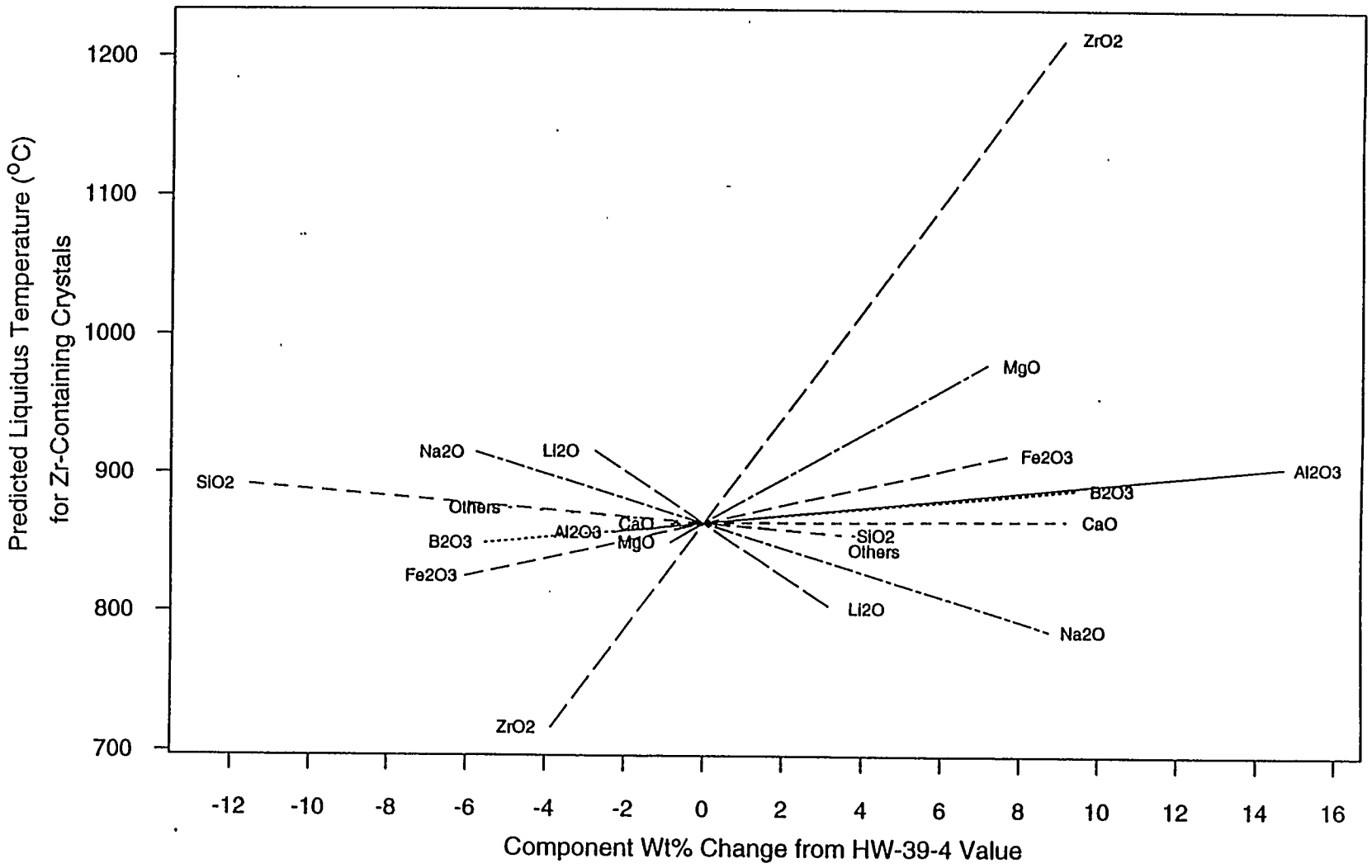

FIGURE 11.17. Predicted Component Effects on Liquidus Temperature of Zr-Containing Crystals Relative to the HW-39-4 Composition, Based on the First-Order Mixture Model Using Mass Fractions (in Column 4 of Table 11.7)

First-order (or other) mixture models are useful for predicting the liquidus temperature of glasses with known primary phases. The disadvantage of the first-order (or any other empirical) liquidus temperature model is that it cannot tell whether the phase with predicted liquidus temperature will precipitate or not. Even though the first-order models do not predict the primary phase directly, the primary phase can be estimated as the phase with the highest predicted liquidus temperature if reliable models are available for all major crystalline phases. The most frequently observed phases (within the CVS composition region) at temperatures higher than 1050°C are spinel and Zr-containing phases. Therefore, future efforts should be directed toward improving models for these phases.

Statistical empirical modeling techniques (such as logistic regression, binary tree regression, and discriminant analysis) exist for predicting categorical data (such as primary crystalline phase, or whether liquidus temperature is above or below a specific limit). However, such methods have not yet been applied to the CVS liquidus temperature data.

11.8 PHASE-EQUILIBRIA LIQUIDUS TEMPERATURE MODEL

Recent developments in computer modeling capabilities have made possible the thermodynamic modeling of multicomponent mixtures. A phase-equilibria liquidus temperature model has been developed by the Centre for Research in Computational Thermochemistry, Ecole Polytechnique, for PNL (Pelton et al. 1992). It applies Gibbs free energy minimization of a multicomponent liquid using optimized parameters derived from the phase equilibria and thermodynamic data for binary, ternary, and quaternary sub-systems. The output capability of the model includes the liquidus temperature and primary crystalline phase, metastable primary phase with T_L if the crystallization of the primary phase is suppressed, equilibrium crystallinity at temperatures below T_L (including fractions and activities of all crystalline phases considered), and composition of immiscible liquid phases, if desired. The model covers the entire composition range possible from the CVS nine major oxide components and Others, which is treated as a single pseudocomponent.

The current model considers the formation of most possible crystalline phases from the phase equilibria of the CVS nine major oxide components, but does not consider some crystalline phases such as spinels and clinopyroxene solid solutions, which have been observed in CVS glasses. The formation of spinels was not considered because the model's database did not contain data on systems containing Fe^{2+}, Ni, and Cr. However, the model is being updated to include spinel components (Fe^{2+}, Ni, and Cr) and clinopyroxene solid solutions.

11.9 EVALUATION OF PHASE-EQUILIBRIA LIQUIDUS TEMPERATURE MODEL

The primary phases and liquidus temperatures of CVS glasses predicted by the phase equilibria liquidus temperature model were compared with those measured experimentally (Tables 11.3 and 11.4). The model predicts one or more possible primary phases with their liquidus temperatures for a given glass (Pelton et al. 1992). The predicted first phase may not be observed experimentally because of kinetic reasons or when its equilibrium concentration is very low. Then, the second or third phase can be the primary phase observed experimentally. Phase-equilibria model predictions and experimentally observed values were compared for 110 glasses (excluding 11 replicates, two radioactive glasses, and one EA glass) of the 124 CVS glasses. As shown in Table 11.8, the 110 glasses were divided into six different groups based on the agreement between the experimental primary phase and predicted phases.

Acmite ($NaFeSi_2O_6$) was the only clinopyroxene crystal predicted as the possible primary phase by the model even though hedenbergite ($CaFeSi_2O_6$) and diopside ($CaMgSi_2O_6$) were also considered. As mentioned in Section 11.4, hedenbergite and diopside were major components in clinopyroxene solid solutions identified experimentally in CVS glasses.

Group A Glasses

The experimentally determined primary phase agreed with the predicted first phase in 31 out of 110 glasses. Figure 11.18 shows the plot of predicted versus measured liquidus temperatures for these Group A glasses. Different symbols were used for different primary phases determined

TABLE 11.8. Summary of Comparing the Primary Phases and Their Liquidus Temperatures Predicted by the Phase-Equilibria Liquidus Temperature Model and Measured Experimentally

Group	Description of Group	# of Glasses
A	Experimental primary phase agreed with predicted 1st phase	31
B	Experimental primary phase agreed with predicted 2nd or 3rd phase	20
C	Experimental primary phase did not agree with any of predicted phases	38
D	Experimental primary phase did not agree with any of predicted phases but modified Others was used	8
E	Experimental primary phase was unidentified	4
F	No crystallization was observed experimentally	9
	Total	110

experimentally. For the glasses with liquidus temperature higher than the hot-end temperature of the gradient furnace, the predicted temperatures were plotted against the hot-end temperatures with solid symbols. These data were not used for calculating the R^2(VAL) value given in Figure 11.18. See Equation (6.10) in Section 6.1.6 for the definition of R^2(VAL).

As shown in Figure 11.18, most Group A glasses had zircon or clinopyroxene as the primary phase. The liquidus temperature of zircon was predicted reasonably well by the model over the temperature range of the experimental liquidus temperatures. The model tended to predict clinopyroxene and lithium-aluminum silicate liquidus temperatures greater than the experimental values. The lesser experimental T_L could be caused by lack of crystal nucleation in glass as discussed in Section 11.3. Out of five glasses with T_L of zircon higher than 1110°C (the usual maximum hot-end temperature used in the gradient furnace), the model predicted the T_L greater than the hot-end temperature tested in four glasses, and underpredicted in one glass. Overall the model prediction for Group A glasses was fair with R^2(VAL) = 0.628.

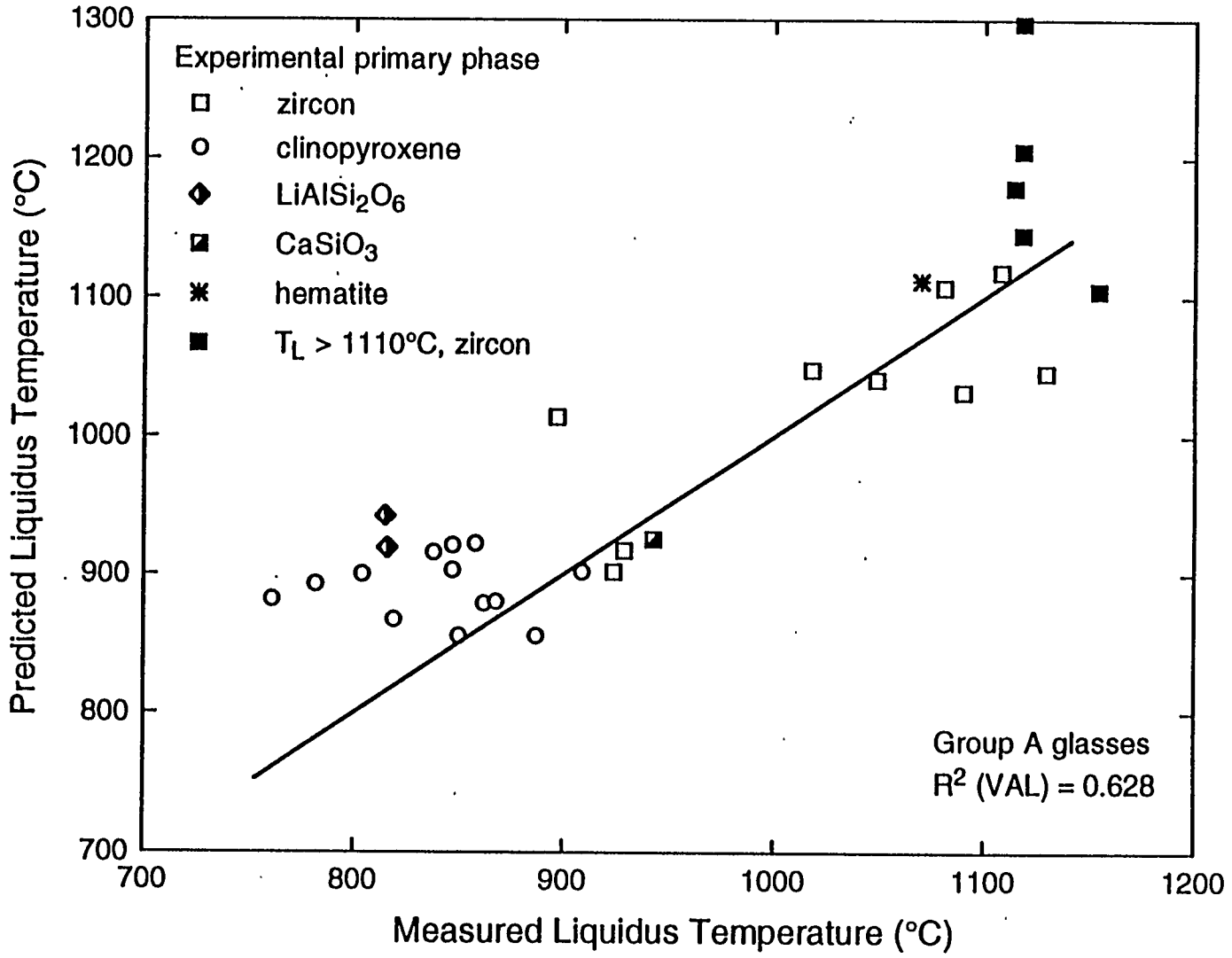

FIGURE 11.18. Predicted Versus Measured Liquidus Temperature of Glasses for Which the Experimental Primary Phase Agreed with the First Phase Predicted by the Phase Equilibria Model (Group A)

Group B Glasses

Figure 11.19 shows the plot of predicted versus measured liquidus temperatures of 20 Group B glasses for which the experimentally determined primary phase agreed with the predicted second or third phase instead of the predicted first phase. The liquidus temperature of the predicted second or third phase was generally lower than the experimental values, especially for nepheline and SiO_2 (and $CaSiO_3$ in one glass). Out of two glasses with T_L of zircon higher than 1110°C, the model predicted the T_L greater than the hot-end temperature tested in one glass, and underpredicted in the other glass. The negative R^2(VAL) value shown in Figure 11.19 is due to the nepheline and other points falling well off the 45° line.

Interestingly, as shown in Figure 11.20, when the T_L of the predicted first phase, which was not observed experimentally, was used instead of the T_L of the predicted second or third phase, the model fitted the experimental T_L slightly better with R^2(VAL) = 0.209. In the glasses with nepheline and SiO_2 as their experimental primary phase, the predicted liquidus temperatures were still lower than the experimental values. The higher experimental liquidus temperature of these glasses could be caused by compositional inhomogeneities.

Group C Glasses

The experimental primary phase did not agree with any of the model-predicted (first, second, or third) phases for 38 glasses. The liquidus temperature of the predicted first phase was plotted against the experimental T_L in Figure 11.21. The overall fit was poor with R^2(VAL) = 0.208. However, the model predictions for experimental phases of sodium-zirconium silicate, orthopyroxene, and olivine were relatively good, except for one glass. The model predicted higher liquidus temperatures than the experimental values for all glasses with $CaSiO_3$ and most glasses with nepheline and SiO_2 as their experimental primary phase.

Group C glasses do not include the glasses with clinopyroxene or zircon as their experimental primary phase (Figure 11.21). When clinopyroxene or zircon were observed experimentally, they were always predicted by the model as one of the possible primary phases (Figures 11.18 and 11.19). The model

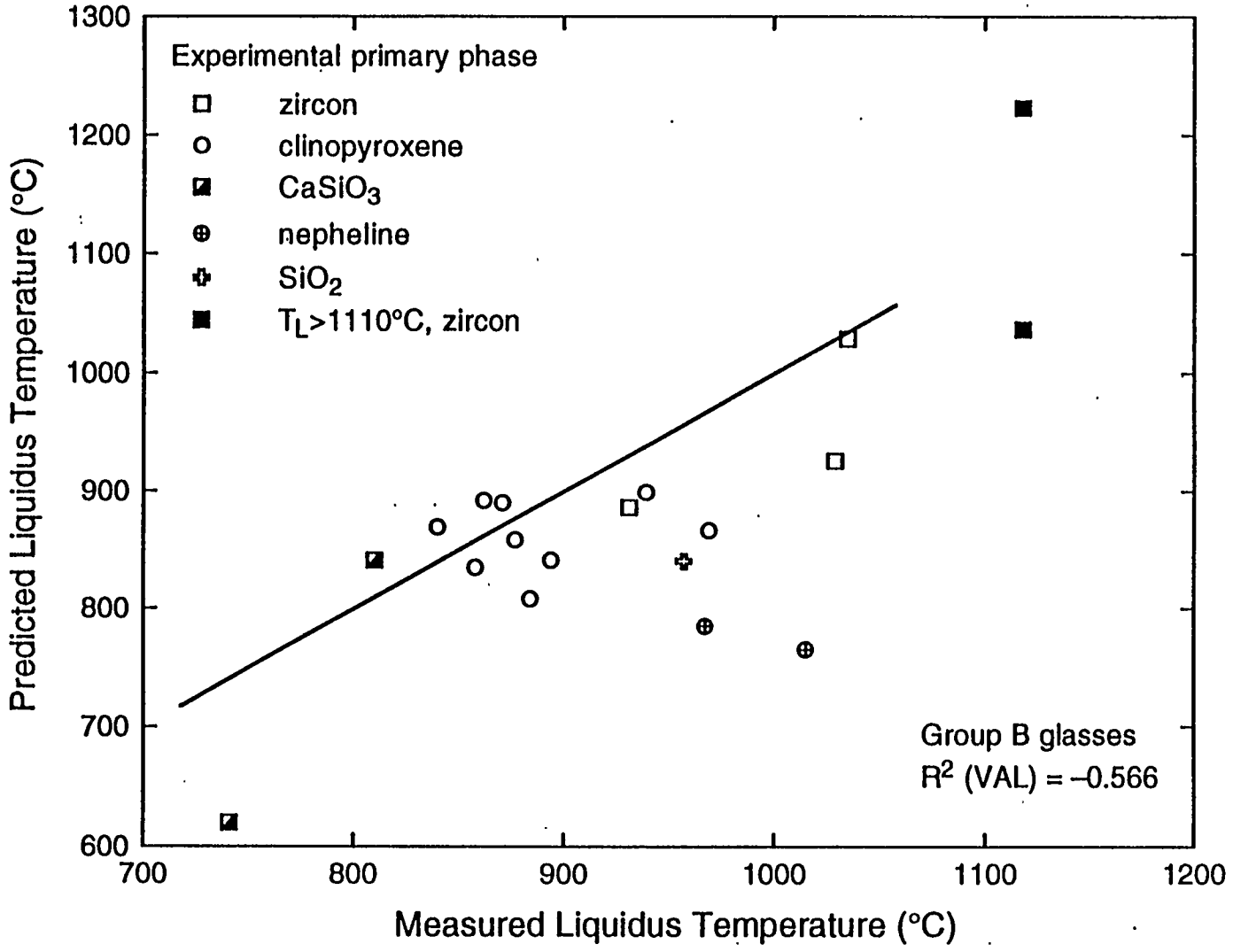

FIGURE 11.19. Predicted Versus Measured Liquidus Temperature of Glasses for Which the Experimental Primary Phase Agreed with the Second or Third Phases Predicted by the Phase Equilibria Model (Group B)

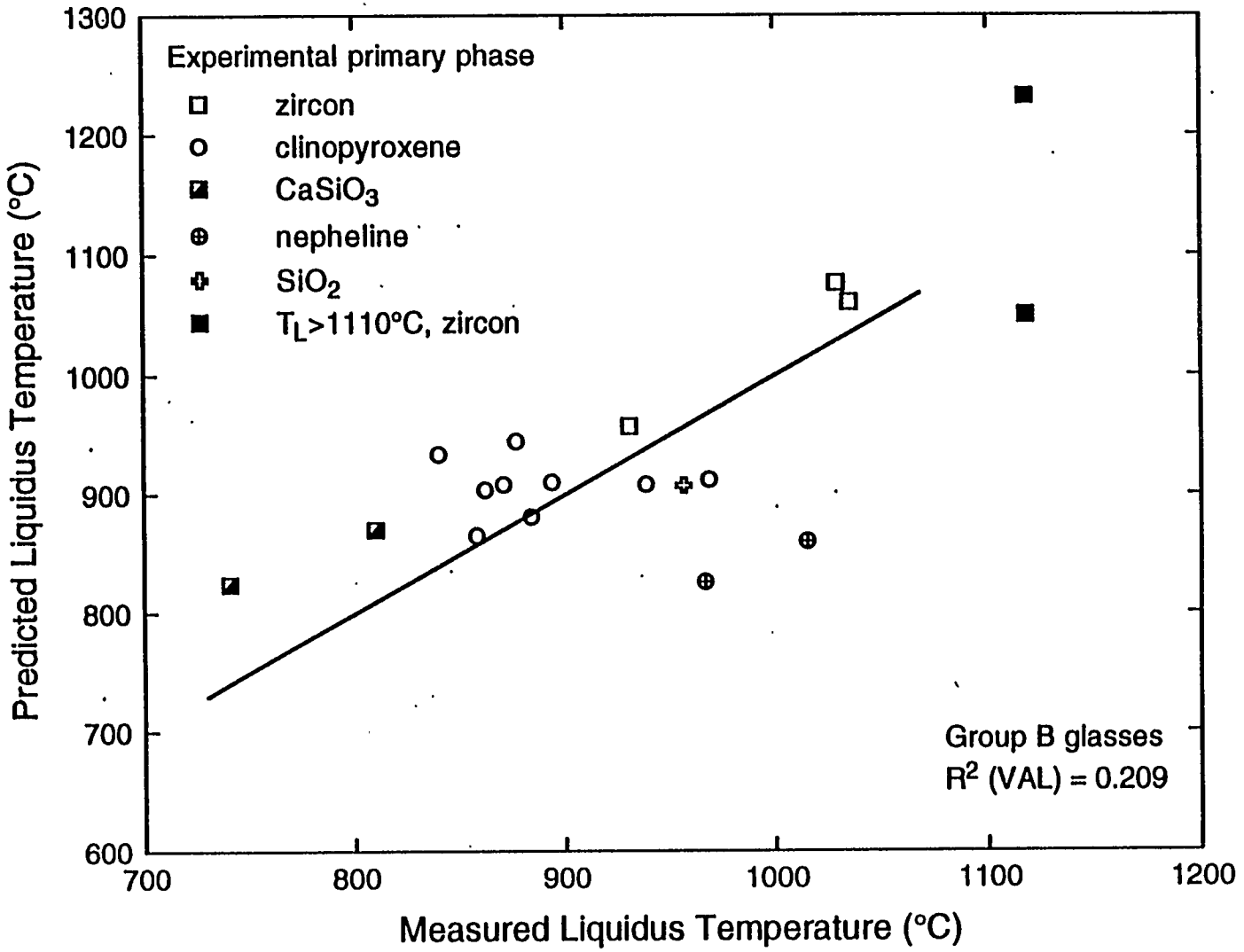

FIGURE 11.20. Same as Figure 11.19, Except the T_L of the Predicted First Phase was Used in Plotting and Calculating R^2 Instead of the T_L of the Predicted Second or Third Phase

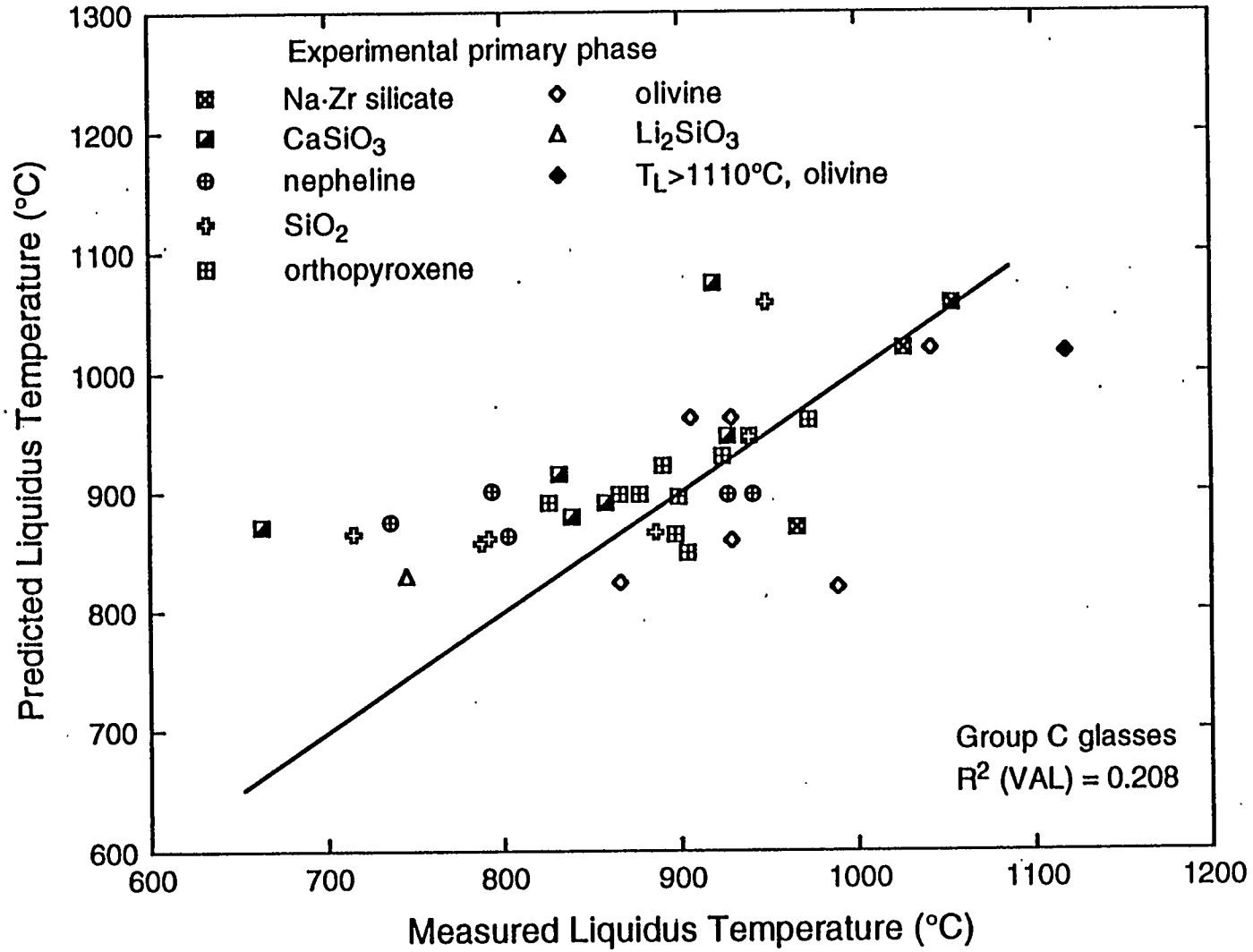

FIGURE 11.21. Predicted Versus Measured Liquidus Temperature of Glasses for Which the Experimental Primary Phase Did Not Agree with Any of the Phases Predicted by the Phase Equilibria Model (Group C)

never predicted sodium-zirconium silicate, olivine, and orthopyroxene as possible primary phases.

Figure 11.22 shows the plot of the predicted versus measured liquidus temperature for all glasses that belong to Groups A, B, and C. Figure 11.22 is the combination of Figures 11.18, 11.20, and 11.21 because the T_L of the predicted first primary phase was used as the model prediction regardless of primary phase agreement. The glasses are differentiated by their experimental primary phases using different symbols. The overall fit was not good, since $R^2(VAL) = 0.431$. As can be seen in Figure 11.22, the T_L prediction by the phase-equilibria model showed the greatest difference from the experimental T_L for some glasses with $CaSiO_3$, nepheline, and olivine as the experimental primary phase. Another notable feature of Figure 11.22 is that the phase-equilibria model predicts a much narrower range for T_L (roughly 825-950°C) than the corresponding measured values (650 to 1025°C) for many of the data points. This indicates the preliminary phase equilibria model does not provide a good basis for predicting T_L over the CVS composition region.

Group D Glasses

Eight glasses belonged to Group D, for which the experimental primary phase did not agree with any of the primary phases predicted by the model, but the glasses had a modified Others component (Table 11.9). Two more glasses with modified Others were not included in Group D because their experimental primary phases agreed with one of the predicted primary phases and Others in these glasses did not seem to affect the T_L significantly. As can be seen in Table 11.9, Cr_2O_3 was the primary phase in six out of eight glasses and these six glasses contained relatively high Cr_2O_3.

CVS2-55, CVS2-56, and CVS2-57 had the same nominal glass composition as CVS2-19 (the CVS internal standard glass) but had modified Others components. CVS2-56 belonged to Group B glasses with slightly higher T_L (880°C) than CVS2-19 (856 to 862°C). CVS2-55 and CVS2-57 had the experimental secondary phase (clinopyroxene) the same as the predicted second phase with T_L of 906 and 945°C, respectively, which are both higher than the T_L of CVS2-19. As

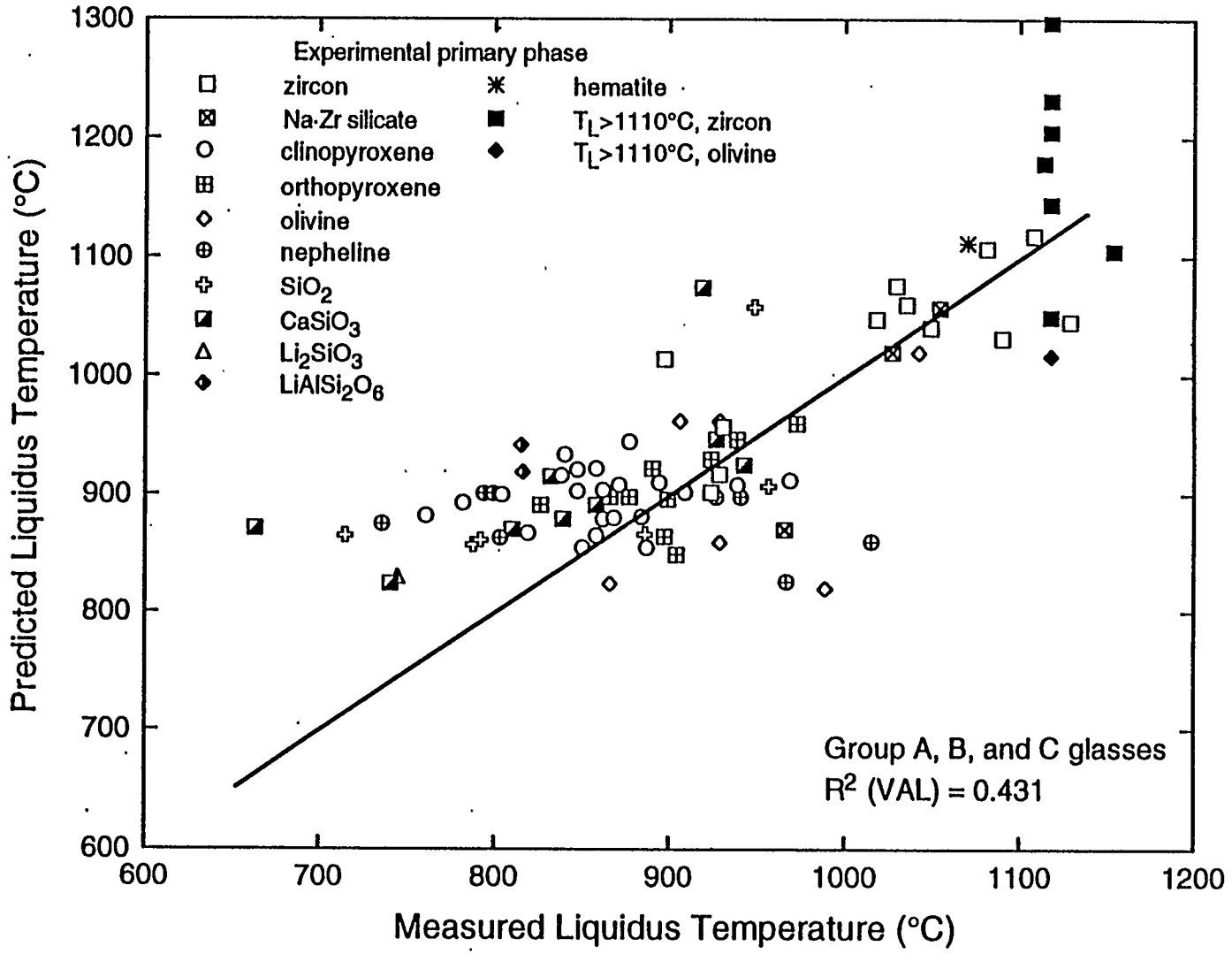

FIGURE 11.22. Predicted Versus Measured Liquidus Temperature of Group A, B, and C Glasses for the Phase Equilibria Model

TABLE 11.9. Predicted and Measured Liquidus Temperatures of Glasses for Which the Experimental Primary Phase Did Not Agree with Any of the Primary Phases Predicted by the Phase Equilibria Model, but the Glass Used a Modified Others (Group D)

Glass	Predicted First		Predicted Second		Experimentally Measured	
	T_L (°C)	Phase	T_L (°C)	Phase	T_L (°C)	Phase
CVS2-55	908	zircon	892	clinopyroxene	944	Cr_2O_3
					906	clinopyroxene
CVS2-57	908	zircon	892	clinopyroxene	1036	Cr_2O_3
					945	clinopyroxene
CVS2-64	922	zircon	882	clinopyroxene	895	orthopyroxene
CVS2-66	901	clinopyroxene	693	hematite	799	nepheline
CVS2-67	1036	Al_2O_3	911	mullite	1022	Cr_2O_3
CVS2-68	919	$LiAlSi_2O_6$	834	albite	>1114	Cr_2O_3
CVS2-69	855	clinopyroxene	605	$LiBO_2$	>1114	Cr_2O_3
					983	orthopyroxene
CVS2-70	942	$LiAlSi_2O_6$	848	albite	>1114	Cr_2O_3
					818	$LiAlSi_2O_6$

discussed previously, the liquidus temperatures of CVS2-55, CVS2-56, and CVS2-57 were affected by the different Others.

CVS2-64 and CVS2-66 had counterpart glasses (CVS2-71 and CVS2-72, Group C) with the same nominal composition but with NCAW-87 Others. CVS2-64 and CVS2-66 had the same primary phases as the counterpart glasses with very close T_L values. Therefore, for these two glasses (CVS2-64 and CVS2-66), the difference between experimental and predicted primary phases was not caused by different Others.

CVS2-69 formed orthopyroxene as the secondary phase whereas the same nominal composition glass (CVS2-74, Group A) with NCAW-87 Others formed clinopyroxene as the primary phase, which agreed with the predicted primary phase. CVS2-70 had $LiAlSi_2O_6$ as the experimental secondary phase, which was the experimental primary phase in the counterpart glass (CVS2-75, Group A) with NCAW-87 Others. The liquidus temperatures of $LiAlSi_2O_6$ in these two glasses were almost identical (818 and 815°C). This suggests that the different Others used in CVS2-70 did not affect the crystallization of

$LiAlSi_2O_6$. The predicted first phase in these glasses was also $LiAlSi_2O_6$, but with higher T_L (942°C) than experimental values.

Group E Glasses

Group E consists of four glasses for which the experimental primary phase could not be identified (Table 11.10). CVS1-9 showed massive crystallization of an unidentified (Mg, Fe, Si; Ni Cr) phase in CCC samples and liquidus temperature samples. The crystals in CVS2-81 and CVS2-85 were too small for positive identification with optical microscope and SEM/EDS. In CVS1-10, severe liquid-liquid phase separation and very small crystal size precluded the determination of the primary phase and liquidus temperature.

Group F glasses

As discussed in Section 11.4, nine glasses were crystal-free. Table 11.11 shows the predicted liquidus temperatures and primary phases of Group F glasses. The predicted first primary phase was clinopyroxene in seven glasses and Zr-containing crystal in two glasses. Considering the possible effect of the crystallization kinetics, the viscosity of these glasses at 1150°C and at the T_L of the predicted first primary phase were compared with the viscosity of Group A glasses. As Table 11.11 shows, the Group F glasses had a viscosity range similar to that of Group A glasses. This suggests that the viscosity was not a major factor in suppressing the crystallization in these glasses.

TABLE 11.10. Predicted (the Phase Equilibria Model) and Measured Liquidus Temperatures of Glasses with the Unidentified Experimental Primary Phase (Group E)

Glass	Predicted First		Predicted Second		Experimentally Measured	
	T_L (°C)	Phase	T_L (°C)	Phase	T_L (°C)	Phase
CVS1-9	1118	hematite	898	clinopyroxene	1097	unidentified
CVS1-10	939	albite	900	clinopyroxene	(a)	unidentified
CVS2-81	870	clinopyroxene	694	$CaSiO_3$	>1154	unidentified
CVS2-85	796	clinopyroxene	732	nepheline	>1150	unidentified

(a) The liquidus temperature of CVS1-10 could not be determined because of severe liquid-liquid phase separation.

TABLE 11.11. Predicted (the Phase Equilibria Model) Liquidus Temperatures of Glasses with No Experimentally Observed Crystalline Phase (Group F); Viscosity Data at 1150°C and at the Predicted Liquidus Temperature of the Predicted First Phase Are Also Shown

Glass	Predicted First		Predicted Second		Viscosity (Pa•s) (a)	
	T_L (°C)	Phase	T_L (°C)	Phase	at 1150°C	at T_L 1st
CVS1-13	857	clinopyroxene	778	SiO_2	3.3	178.8
CVS1-13	1107	zircon	1105	ZrO_2	3.4	5.8
CVS2-10	924	clinopyroxene	809	albite	9.0	130.6
CVS2-15	899	clinopyroxene	624	$NaBO_2$	4.5	86.8
CVS2-24	853	clinopyroxene	788	$LiBO_2$	2.0	30.1
CVS2-27	880	clinopyroxene	796	albite	14.4	433.2
CVS2-28	848	clinopyroxene	691	albite	13.4	196.9
CVS2-62	909	clinopyroxene	784	zircon	10.2	165.6
CVS2-87	890	ZrO_2	886	clinopyroxene	15.4	99.5

(a) For comparison, the viscosity of Group A glasses (Figure 11.18) was 1 to 23 Pa•s at 1150°C and 3 to 515 Pa•s at the T_L of the predicted 1st primary phase.

In summary, the overall ability of the phase-equilibria model to predict experimental results for the primary phase and liquidus temperature was not good. The poor prediction in some glasses may be improved after the model is updated to account for solid solutions and Fe^{2+}, Ni, and Cr. Using a gradient furnace to determine the liquidus temperature experimentally was very useful for a large number of samples but could also affect the measurement in some samples. The possible convection flow of glass within the platinum-gold boat used in the gradient furnace could cause inaccuracy in liquidus temperature measurement, and for some samples, the 24-hour heat treatment might not be long enough to reach equilibrium. Compositional inhomogeneities may also cause the precipitation of crystals above the T_L of compositionally homogeneous glass. It may be necessary to check the experimental data using isothermal heat treatment for more than 24 hours in a uniform-temperature furnace for those samples with a large difference between experimental and predicted liquidus temperatures.

DISTRIBUTION

No. of Copies

OFFSITE

12 DOE/Office of Scientific and Technical Information

S. M. Barnes
West Valley Nuclear Services
P. O. Box 191
West Valley, NY 14171

J. K. Bates
Argonne National Laboratory
9700 S. Cass Avenue
Argonne, IL 60439-4837

S. O. Bates
EG&G Idaho, Inc.
812 Dickson
Idaho Falls, ID 83402

N. E. Bibler
Westinghouse Savannah River Co.
P.O. Box 616
Aiken, SC 29802

D. F. Bickford
Westinghouse Savannah River Co.
P.O. Box 616
Aiken, SC 29802

R. R. Borisch
West Valley Nuclear Services
P. O. Box 191
West Valley, NY 14171

H. Brandt
DOE Savannah River Operations
P.O. Box A
Aiken, SC 29801

No. of Copies

K. G. Brown
Westinghouse Savannah River Co.
P.O. Box 616
Aiken, SC 29802

L. H. Cadoff
West Valley Nuclear Services
P. O. Box 191
West Valley, NY 14171

K. A. Chacey, EM-361
DOE Office of Environmental Management
19901 Germantown Road
Germantown, MD 20585

D. Clark
University of Florida
Advanced Materials Research
One Progress Blvd. #14
Alachua, FL 32615

J. A. Colemen, EM-35
DOE Office of Environmental Management
19901 Germantown Road
Germantown, MD 20585

C. R. Cooley, EM-55
DOE Office of Environmental Management
19901 Germantown Road
Germantown, MD 20585

A. R. Cooper
Case Western Reserve Univ.
Dept. Materials Science & Eng.
10900 Euclid Avenue
Cleveland, OH 44106

No. of
Copies

S. Cowan, EM-30
DOE Office of Environmental
Management
19901 Germantown Road
Germantown, MD 20585

D. E. Day
Univertiy of Missouri-Rolla
Materials Research Center
Rolla, MO 65401

I. J. Dempster
West Valley Nuclear Services
P. O. Box 191
West Valley, NY 14171

R. H. Doremus
Rensselaer Polytechnic Inst.
Materials Engineering Dept.
Troy, NY 12180-3950

D. Dreyfus, RW-1
DPE Office of Civilian
Radioactive Waste Management
1000 Independence Ave. S.W.
Washington, D.C. 20585

A. Drobot
West Valley Nuclear Services
P. O. Box 191
West Valley, NY 14171

W. Ebert
Argonne National Laboratory
9700 S. Cass Avenue
Argonne, IL 60439-4837

T. B. Edwards
Westinghouse Savannah River Co.
P.O. Box 616
Aiken, SC 29802

No. of
Copies

J. J. Einerson
EG&G Idaho, Inc.
2525 Fremont Avenue
Idaho Falls, ID 83415

A. Ellison
Argonne National Laboratory
9700 S. Cass Avenue
Argonne, IL 60439-4837

R. E. Ewing
University of New Mexico
Albuquerque, NM 87131

J. J. Fiore, EM-423
DOE Office of Environmental
Management
19901 Germantown Road
Germantown, MD 20585

C. Frank, EM-50
DOE Office of Environmental
Management
19901 Germantown Road
Germantown, MD 20585

M. Frei, EM-34
DOE Office of Environmental
Management
19901 Germantown Road
Germantown, MD 20585

T. Grumbly, EM-1
Assistant Secretary
DOE Office of Environmental
Management
1000 Independence Ave. S.W.
Washington, D.C. 20585

No. of
Copies

L. L. Hench
University of Florida
Advanced Materials Research
One Progress Blvd. #14
Alachua, FL 32615

J. Hennessey, EM-361
DOE Office of Environmental
Management
19901 Germantown Road
Germantown, MD 20585

E. W. Holtzscheiter
Westinghouse Savannah River Co.
P.O. Box 616
Aiken, SC 29802

N. D. Hudson
Westinghouse Savannah River Co.
P.O. Box 616
Aiken, SC 29802

V. J. Jain
West Valley Nuclear Services
P. O. Box 191
West Valley, NY 14171

C. M. Jantzen
Westinghouse Savannah River Co.
P.O. Box 616
Aiken, SC 29802

D. E. Karl
West Valley Nuclear Services
P. O. Box 191
West Valley, NY 14171

W. S. Ketola
DOE West Valley Project
P.O. Box 191
West Valley, NY 14171

No. of
Copies

R. B. King
Regents Professor of Chemistry
University of Georgia
1001 Cedar Street
Athens, GA 30602

J. R. Knight
Westinghouse Savannah River Co.
P.O. Box 616
Aiken, SC 29802

W. LaCourse
Alfred University
NYS College of Ceramics
Alfred, NY 14802

W. Lutze
Hahn-Meitner-Institut Berlin
D-1000
Berlin 39
Germany

J. E. Lytle, EM-30
DOE Office of Environmental
Management
19901 Germantown Road
Germantown, MD 20585

P. Macedo
Vitreous State Laboratory
Catholic University of Amierica
Washington, D.C. 20064

J. L. Mahoney
West Valley Nuclear Services
P. O. Box 191
West Valley, NY 14171

S. L. Marra
Westinghouse Savannah River Co.
P.O. Box 616
Aiken, SC 29802

No. of
Copies

L. B. McEwen
DOE Oakland Operations Office
1301 Clay Street
Oakland, CA 94612

T. W. McIntosh, EM-323
DOE Office of Environmental Management
19901 Germantown Road
Germantown, MD 20585

C. E. Miller, EM-323
DOE Office of Environmental Management
19901 Germantown Road
Germantown, MD 20585

R. A. Palmer
West Valley Nuclear Services
P. O. Box 191
West Valley, NY 14171

K. G. Picha, Jr., EM-323
DOE Office of Environmental Management
19901 Germantown Road
Germantown, MD 20585

M. J. Plodinec
Westinghouse Savannah River Co.
P.O. Box 616
Aiken, SC 29802

A. A. Ramsey
Westinghouse Savannah River Co.
P.O. Box 616
Aiken, SC 29802

No. of
Copies

W. G. Ramsey
Westinghouse Savannah River Co.
P.O. Box 616
Aiken, SC 29802

C. T. Randall
Westinghouse Savannah River Co.
P.O. Box 616
Aiken, SC 29802

C. P. Reeve
Westinghouse Savannah River Co.
P.O. Box 616
Aiken, SC 29802

J. L. Resce
Environmental Systems Eng.
Rich Environmental Res. Lab
Clemson Research Park
Clemson, SC 29634-0919

M. Smith
Westinghouse Savannah River Co.
P.O. Box 616
Aiken, SC 29802

J. F. Sproull
Westinghouse Savannah River Co.
P.O. Box 616
Aiken, SC 29802

M. Tomozawa
Rensselaer Polytechnic Inst.
Materials Engineering Dept.
Troy, NY 12180-3950

J. C. Tseng, EM-36
DOE Office of Environmental Management
19901 Germantown Road
Germantown, MD 20585

No. of Copies

D. R. Uhlmann
Arizona Materials Laboratory
University of Arizona
4715 E. Fort Lowell Road
Tucson, AZ 85712

A. K. Varshneya
Alfred University
NYS College of Ceramics
Alfred, NY 14802

H. F. Walter, EM-323
DOE Office of Environmental Management
19901 Germantown Road
Germantown, MD 20585

F. E. Woolley
Corning Incorporated
HP-ME-2-38-E6
Corning, NY 14831

R. G. Wymar
ORNL Consultant
188-A Outer Drive
Oak Ridge, TN 37830

ONSITE

9 DOE/Richland Operations Office

K. W. Bracken	S7-50
N. R. Brown	S7-53
S. T. Burnum	S7-53
M. Dev	S7-53
L. Erickson	S7-53
P. E. LaMont	S7-53
J. C. Peshcong	S7-53
G. H. Sanders	S7-53
T. R. Sheridan	S7-50

No. of Copies

25 Westinghouse Hanford Company

J. N. Appel	G3-21
A. L. Boldt	H5-49
K. D. Boomer	H5-49
R. B. Calmus	H5-27
R. P. Colburn	H5-27
T. W. Crawford	H5-49
J. S. Garfield	H5-49
R. L. Gibby	H5-27
J. W. Hales	H5-60
B. A. Higley	H5-27
J. O. Honeyman	S7-81
A. A. Kruger	H5-27
W. C. Miller	S4-55
R. M. Orme	H5-27
R. W. Powell	H4-14
E. H. Randklev	H5-27
P. S. Schaus	H4-14
R. G. Seymour	H5-27
G. E. Stegen	H5-27
D. J. Washenfelder	H5-27
R. A. Watrous	H5-27
E. T. Weber, III	H5-27
C. N. Wilson	H5-27
D. D. Wodrich	S7-84
G. Woodcock	H5-27

3 TDPO

J. A. Carr	K9-81
J. H. Holbrook	K9-81
G. B. Mellinger	K9-81

95 Pacific Northwest Laboratory

C. S. Amrine	P8-44
R. M. Bean	K9-76
G. H. Beeman	S7-71
W. F. Bonner	K9-14
M. F. Bryan	K5-12
C. C. Chapman	P7-41
J. M. Creer	K9-80
M. L. Elliott	P7-41

No. of Copies		
	X. D. Feng	P8-44
	N. D. Foote	K7-10
	W. K. Hahn	P8-44
	S. A. Hartley	K5-12
	L. K. Holton	P7-43
	M. Hoza	K7-22
	P. R. Hrma (20)	P8-37
	G. A. Jensen	P7-19
	B. M. Johnson	K1-78
	J. W. Johnston	K5-12
	D. S. Kim	P8-44
	M. H. Langowski	P8-44
	D. E. Larson (10)	K9-80
	H. Li	P8-44
	C. A. LoPresti	K5-12
	B. P. McGrail	K2-38
	P. J. Mellinger	K9-76
	E. V. Morrey	P7-19

No. of Copies		
	D. K. Peeler	P8-44
	J. M. Perez, Jr.	P7-41
	R. D. Peters	P7-41
	G. F. Piepel (20)	K5-12
	P. E. Redgate	K5-12
	R. J. Robertus	P8-38
	M. J. Schweiger	P8-37
	P. A. Scott	P7-43
	G. J. Sevigny	P7-33
	P. Sliva	P7-18
	D. E. Smith	P8-37
	P. A. Smith	P7-14
	D. M. Strachen	K2-44
	J. D. Vienna	P8-44
	J. H. Westsik, Jr.	P7-19
	K. D. Wiemers	P7-14
	Publishing Coordination	
	Technical Report Files (5)	